AD NUMBER

ADB004600

NEW LIMITATION CHANGE

TO

Approved for public release, distribution unlimited

FROM

Distribution authorized to U.S. Gov't. agencies only; Specific Authority; May 1975. Other requests shall be referred to AFFDL, Aero-Acoustics Branch, Wright-Patterson AFB, Ohio 45433.

AUTHORITY

st-a affdl notice, 29 aug 1977

AFFDL-TR-74-112

SONIC FATIGUE DESIGN GUIDE FOR MILITARY AIRCRAFT

ACOUSTIC & VIBRATION ASSOCIATES
A DIVISION OF
SCIENCE APPLICATIONS, INC.

TECHNICAL REPORT AFFDL—TR—74—112

MAY 1975

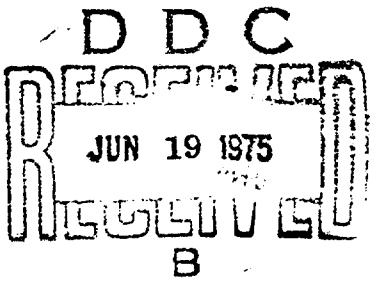

AIR FORCE FLIGHT DYNAMICS LABORATORY
AIR FORCE SYSTEMS COMMAND
WRIGHT—PATTERSON AIR FORCE BASE, OHIO 45433

NOTICE

When Government drawings, specifications, or other data are used for any purpose other than in connection with a definitely related Government procurement operation, the United States Government thereby incurs no responsibility nor any obligation whatsoever; and the fact that the government may have formulated, furnished, or in any way supplied the said drawings, specifications, or other data, is not to be regarded by implication or otherwise as in any manner licensing the holder or any other person or corporation, or conveying any rights or permission to manufacture, use, or sell any patented invention that may in any way be related thereto.

This technical report has been reviewed and is approved for publication.

FOR THE COMMANDER

Walter J. Mykytow

WALTER J. MYKYTOW
Ass't for Research and Technology
Vehicle Dynamics Division

Copies of this report should not be returned unless return is required by security considerations, contractual obligations, or notice on a specific document.

AIR FORCE/56780/4 June 1975 — 150

UNCLASSIFIED
SECURITY CLASSIFICATION OF THIS PAGE (When Data Entered)

REPORT DOCUMENTATION PAGE		READ INSTRUCTIONS BEFORE COMPLETING FORM
1. REPORT NUMBER AFFDL-TR-74-112	2. GOVT ACCESSION NO.	3. RECIPIENT'S CATALOG NUMBER
4. TITLE (and Subtitle) SONIC FATIGUE DESIGN GUIDE FOR MILITARY AIRCRAFT		5. TYPE OF REPORT & PERIOD COVERED Final Jun 73 to Mar 75
		6. PERFORMING ORG. REPORT NUMBER AVA/TR 73-280
7. AUTHOR(s) F. F. RUDDER, JR. H. E. PLUMBLEE, JR.		8. CONTRACT OR GRANT NUMBER(s) F33615-73-C-3124
9. PERFORMING ORGANIZATION NAME AND ADDRESS Acoustics & Vibration Associates, Division of Science Applications, Inc. Atlanta, Georgia		10. PROGRAM ELEMENT, PROJECT, TASK AREA & WORK UNIT NUMBERS 62201F 14710140
11. CONTROLLING OFFICE NAME AND ADDRESS Air Force Flight Dynamics Laboratory Aero-Acoustics Branch (FYA) Wright-Patterson AFB, Ohio 45433		12. REPORT DATE May 1975
		13. NUMBER OF PAGES 572
14. MONITORING AGENCY NAME & ADDRESS(if different from Controlling Office) Air Force Flight Dynamics Laboratory (same as above)		15. SECURITY CLASS. (of this report) Unclassified
		15a. DECLASSIFICATION/DOWNGRADING SCHEDULE

16. DISTRIBUTION STATEMENT (of this Report)

Distribution limited to U. S. Government agencies only: test and evaluation; statement applied 29 May 1975. Other requests for this document must be referred to AF Flight Dynamics Laboratory, (FY), Wright-Patterson AFB, Ohio 45433.

17. DISTRIBUTION STATEMENT (of the abstract entered in Block 20, if different from Report)

18. SUPPLEMENTARY NOTES

19. KEY WORDS (Continue on reverse side if necessary and identify by block number)

20. ABSTRACT (Continue on reverse side if necessary and identify by block number)

Accurate methods are presented for estimating the acoustic loading, structural response, and fatigue life of military aircraft structures. This report presents over sixty tables, 110 charts and nomographs, five computer programs and forty worked examples illustrating the use of the different methods. These results stem from a review and evaluation of over 300 references related to the various topics associated with sonic fatigue. This report is organized into independent sections with the subject classification allowing for ease of identification and future extension as required. Sufficient detail is (over)

DD FORM 1 JAN 73 1473 EDITION OF 1 NOV 65 IS OBSOLETE

UNCLASSIFIED
SECURITY CLASSIFICATION OF THIS PAGE (When Data Entered)

provided so that the entire handbook stands as an independent source of sonic fatigue design data.

FOREWORD

This report was prepared by Acoustics & Vibration Associates, Atlanta, Georgia, a Division of Science Applications, Inc., LaJolla, California, for the Aero-Acoustics Branch, Vehicle Dynamics Division, Air Force Flight Dynamics Laboratory, Wright-Patterson Air Force Base, Ohio, under Contract F33615-73-C-3124. The work described herein was conducted as Air Force System Command's exploratory development program. It establishes design methods and design criteria for sonic fatigue prevention for flight vehicles. This program was directed under Project 1471, "Aero-Acoustic Problems in Flight Vehicles," Task 147101, "Sonic Fatigue," and Work Unit 14710140, "Sonic Fatigue Design Handbook for Military Aircraft." Mr. R. C. W. van der Heyde was the engineer in charge of the work.

This report concludes the work on Contract F33615-73-C-3124, which covered the period from June 1973 to August 1974.

The authors of the report gratefully acknowledge the assistance rendered by R. H. Burrin, C. L. Balfour, and L. Densmore in developing and reproducing design nomographs and figures presented in the report. Special acknowledgement is given to Mrs. Peggy Weldon and Mrs. Margaret Clark for the meticulous typing of the manuscript. The Acoustics & Vibration Associates report identification number is AVA/TR 73-280.

The report was submitted for publication by the authors on 28 March 1975.

TABLE OF CONTENTS

TABLE OF CONTENTS

TABLE OF CONTENTS

TABLE OF CONTENTS

TABLE OF CONTENTS

TABLE OF CONTENTS

TABLE OF CONTENTS

LIST OF FIGURES

LIST OF FIGURES (Continued)

LIST OF FIGURES (Continued)

LIST OF FIGURES (Continued)

LIST OF FIGURES (Continued)

LIST OF FIGURES (Continued)

LIST OF FIGURES (Continued)

LIST OF FIGURES (Continued)

LIST OF FIGURES (Continued)

LIST OF FIGURES (Continued)

LIST OF FIGURES (Concluded)

LIST OF TABLES

LIST OF TABLES
(CONTINUED)

LIST OF TABLES
(CONTINUED)

LIST OF TABLES
(CONCLUDED)

SECTION I

INTRODUCTION

The consideration of acoustically induced fatigue failures in aircraft has been a design consideration for over 20 years. The problem was introduced with the advent of the turbojet engine and the resulting high intensity acoustic pressure levels experienced on the surfaces of aircraft. Since military aircraft have always been designed for performance, it is somewhat logical to see that acoustic fatigue design requirements have paralleled the requirements of the military and the evolution of high performance aircraft. Since the early investigations considering the development of sonic fatigue design criteria, it has been realized that such failures can substantially increase the maintenance burden and life cycle cost of the aircraft.

Sonic fatigue failures have resulted, however, in unacceptable maintenance and inspection burdens associated with the operation of the aircraft. In some instances, sonic fatigue failures have resulted in major redesign efforts of aircraft structural components. As with any topic of concern to the Air Force, much progress towards establishing acceptable prediction techniques and design methods was realized early in the investigations although some of the techniques tended to introduce conservatism into the designs. The conservatism was expressed, as is usual with aircraft design, in terms of increased weight.

The parallel development of improved testing techniques and data analysis capabilities has resulted in both prediction techniques and design methods that yield acceptable structural configurations in terms of weight, ease of manufacture, and cost. Hence, the designer is only faced, today, with applying these results to his particular aircraft requirements. The main problem facing the designer is simply accumulating and assessing the vast amount of data available that relates to sonic fatigue design. Hence, the designer is required to continually utilize bits and pieces of data resulting from both Government research and his own company's activity in the fields of acoustic excitation, structural response, and fatigue life estimation.

The diversity of the topics of near-field jet noise excitation, dynamic analysis of complex structural configurations, and assembly of material fatigue life data seems to almost preclude one individual from developing the detailed skills required to understand the interrelationships between the various aspects of sonic fatigue design. The objective of this program has been to compile a report for the development of sonic fatigue resistant structures for military aircraft. This report is aimed at enabling the designer to predict the acoustic loading and sonic fatigue life of aircraft structure. The development is to be in a consistent format describing the derivation and limitations of the data and to present examples of using the various techniques currently available.

1.1 SCOPE OF REPORT

The effort resulting in the development of this report was limited to the compilation, evaluation, and presentation of existing sonic fatigue design methods, charts, nomographs, and related computer programs to assist the designer in developing sonic fatigue resistant aircraft structure. Detailed analytical developments to extend the current state-of-the-art were not part of the effort.

The authors have attempted to consider the problem faced by the designer in his work. Namely, the designer must make decisions quickly and assess the significance of his problem within the budget limitations of the project. Undoubtedly, the designer can never spend his time either searching the references or developing analysis techniques. Hence, this report has evolved into both a source of related data supporting the methods and techniques described for predicting sonic fatigue life as well as the complete description of the particular design methods.

The data presented here has resulted from the review of over 300 technical reports, papers, journal publications, and text books. For each topic, a list of references has been presented so that the designer may go to the original source, as required, for additional detail. The use of these references is encouraged if the designer does not find a method or technique directly related to his problem. Hopefully, the supporting data presented in this report will allow the designer to utilize the contents as much as possible without acquiring a vast quantity of additional reference material.

The results of this effort has been to compile 65 tables, over 110 charts and nomographs, five computer programs, and to present over 40 worked examples illustrating the use of the data. The worked examples have been correlated as closely as possible between the various sections of the report so that not only will the designer understand the use of a particular result but he will also appreciate the interrelationships between the various sections.

Finally, it was understood at the beginning of the project that much relevant sonic fatigue design data was not available in the open literature and, hence, could not be utilized for the purposes of this effort. This consideration led to the concept of formulating the report into sections and subsections so that the designer could introduce his own data, analyses, and experience at any level. It is hoped that the designer will take advantage of this organization.

1.2 ORGANIZATION OF THE REPORT

This report is divided into five working subdivisions or sections. Section 2 represents basic design data for general acoustic and thermodynamic relationships. This data will assist the designer in utilizing the prediction methods for acoustic and aerodynamic loading of aircraft structure.

Section 3 presents a brief consideration of the topic of aircraft performance specifications and how they relate to establishing sonic fatigue design criteria for structural components. This section is brief because each aircraft design will require different detail considerations of the general

discussion presented, and the literature in this area is somewhat limited. Again, the section is organized so that the designer can augment the presentation with additional data as required.

Section 4 is devoted to the topic of loading actions or more specifically techniques found to be accurate and acceptable for predicting the nature of acoustic pressures acting on the aircraft structural components. Section 4 is further subdivided into methods related to propulsion system noise estimation and aerodynamic noise sources. References are presented sequentially within subdivisions at a logical level. This technique was adopted since it was understood that the designer might wish to inject future work at various levels in the presentation to maintain a current set of design methods.

Section 5 presents the broad topic of structural configurations and response. This section is the most lengthy section in the report and contains the data necessary to determine the response of structure to acoustic excitation. The section is divided into five subsections each devoted to one aspect of structural response. The first two subsections present data required to support and to extend the specific sonic fatigue design methods presented in Section 5.3, Built-Up Structure. Section 5.3 is the heart of the structural response discussion and contains, in a logical order, the many design charts and nomographs used by designers over the past few years. The last two sections are devoted to detail design considerations associated with structural joints and stress concentration factors.

Section 6 is devoted to the topic of fatigue and the general considerations and parameters describing the fatigue strength of various materials. Data scatter, cumulative damage theories, and random load fatigue curves are discussed. The final section is devoted to documented random load fatigue curves of aircraft materials. Here, the designer will most certainly want to maintain a continuous review of available data in order to extend his analysis capabilities.

1.3 USE OF THE REPORT

This report is organized so that each section stands as an independent unit. To quickly locate data in the report without searching the table of contents, all figures and equations are numbered at the third level of subdivision (i.e., Figure 3.2.2-3, etc.). This format was utilized since the grouping of the data and design methods suggested that the third level was the logical sequence to utilize. Due to this classification system, the extent of detail presented at a given level may vary from section to section. Since each subsection contains a brief description of the specific contents, it is possible to determine the detail presented at each level by reading a short paragraph.

Originally, the authors believed that a length of 250 pages would be optimum from the standpoint of convenience to the designer. However, the evolution of the various sections dictated a more thorough presentation in order to relieve the designer from accumulating additional references to utilize fully the contents of this report. Obviously, it would be possible to extend almost any subsection into a complete and independent volume. Hopefully, the contents are exactly what they were formulated to be - useful. Also, it is

hoped that the designer will extend the various topics suitable to his own requirements so that the data presented here will be refined further to improve the sonic fatigue design methods associated with military aircraft.

SECTION 2

BASIC DESIGN DATA

2.1 GENERAL ACOUSTIC AND THERMODYNAMIC RELATIONSHIPS

This section contains some useful conversion charts and other information to aid in the calculation of acoustic loads and in converting spectra from constant percentage bands, such as octave or 1/3 octave, to spectrum level. The first sub-section contains these acoustic conversion charts, while the second sub-section contains thermodynamic relationships and atmospheric charts.

2.1.1 GENERAL ACOUSTIC RELATIONSHIPS

Most of the noise prediction methods give results in terms of octave bands or 1/3 octave bands. Table 2.1.1-1 contains the center frequencies and band limits for standard octave and 1/3 octave filters.

If it is desired to convert sound pressure level (SPL) to spectrum level the general relationship is

$$L_{SL} = L - 10 \cdot \mathrm{Log}_{10}(\Delta f) \ , \qquad (2.1.1\text{-}1)$$

where L_{SL} is sound spectrum level in decibels and L is sound pressure level in a band Δf wide.

This difference, $L_{SL} - L$, is plotted in Figure 2.1.1-1 for octave bands, 1/3 octave bands and 7% filter bands.

Sound pressure loading is normally computed as a decibel quantity and is defined as

$$L = 10 \cdot \log_{10} (\overline{p}/p_{ref})^2 = 20 \cdot \log_{10} (\overline{p}/p_{ref}) \qquad (2.1.1\text{-}2)$$

where the reference pressure is,

$$p_{ref} = 0.00002 \ N/m^2 = 0.0002 \ \text{dynes/cm}^2 = 4.180 \times 10^{-7} \ \text{lbf/ft}^2$$
$$= 2.902 \times 10^{-9} \ \text{lbf/in}^2$$

The conversion from SPL to pressure in lbf/ft^2 and Newtons/meter^2 is given graphically in Figure 2.1.1-2.

2.1.2 THERMODYNAMIC RELATIONSHIPS

A general factor of confusion for structural engineers is the definition of the thermodynamic state of the exhaust gases at, for example, a jet engine exit. Generally, noise prediction methods require jet velocity and jet temperature as the control variables. However, the structural designer may have such diverse information as thrust and plenum temperature, with other parameters undefined.

In order to facilitate determination of the required parameters, a modification of a thermodynamic chart taken from Tanna, et al. (1), is given as Figure 2.1.2-1. The parameters included on the chart are plenum temperature ratio, jet temperature ratio, nozzle pressure ratio, Mach no., thrust, velocity ratio and jet density ratio. The chart is a multiple cross-plot of solutions of the thermodynamic equations for a perfect gas. These relationships are

$$M_j = \left[\frac{2}{\gamma-1}\left\{\left(\frac{P_R}{P_o}\right)^{\frac{\gamma-1}{\gamma}} - 1\right\}\right]^{1/2} \qquad (2.1.2\text{-}1)$$

$$\frac{T_j}{T_o} = \frac{T_R}{T_o}\left(\frac{P_R}{P_o}\right)^{-\left(\frac{\gamma-1}{\gamma}\right)} \qquad (2.1.2\text{-}2)$$

$$\frac{V_j}{a_o} = M_j\left(\frac{T_j}{T_o}\right)^{1/2} \qquad (2.1.2\text{-}3)$$

$$\frac{\rho_j}{\rho_o} = \left(\frac{T_j}{T_o}\right)^{-1} \qquad (2.1.2\text{-}4)$$

where the following definitions apply:

P = absolute pressure
T = absolute temperature

P_R	Stagnation (or Total or Reservoir or Plenum) pressure.
T_R	Stagnation (or Total or Reservoir or Plenum) temperature.
ρ_R	Reservoir or Plenum density.
P_o	Ambient pressure
T_o	Ambient temperature
ρ_o	Ambient density
a_o	Ambient speed of sound
P_j	Static pressure at Jet Exit Plane
T_j	Static temperature at Jet Exit Plane
ρ_j	Jet exit density
V_j	Jet exit velocity
a_j	Local speed of sound in the jet exit.
P_R/P_o	Stagnation Pressure Ratio
T_R/T_o	Stagnation (or Total) Temperature Ratio

T_j/T_o	Static (or Jet Exit) Temperature Ratio
ρ_j/ρ_o	Jet Exit Density Ratio
V_j/a_o	Jet Exit Velocity Ratio
M_j	Jet Exit Mach Number $(=V_j/a_j)$

Stagnation (or Total) = Static + Dynamic

Static: This is what is measured in the plenum

Dynamic: Since velocity of flow in plenum is very small, this is usually negligible compared to static

$\therefore$ In a perfect plenum (no flow), Stagnation (or Total) = static

T_j/T_o is always less than T_R/T_o

The ratio of specific heats, γ, appropriate for the stagnation temperature, was used in preparing the charts and is shown on Figure 2.1.2-1.

Since a velocity ratio results from part of the solution, it is necessary to determine the ambient speed of sound. Figures 2.1.2-2 and 2.1.2-3 give the speed of sound vs ambient temperature and the ICAO standard atmospheric properties vs attitude. This last figure includes graphs of speed of sound, temperature, pressure and density.

Example Problems:

1. Given an engine with a thrust of 20,000 lb., a diameter of 22" and a stagnation temperature of 1500°F, find the jet temperature and the jet velocity. Ambient temperature is assumed to be 70°F.

   a. The stagnation temperature ratio, T_R/T_o is

   $$\frac{T_R}{T_o} = \frac{1500 + 459.6}{70 + 459.6} = 3.700$$

   b. The equivalent thrust, T, for a 1" nozzle is

   $$T_{1"} = T\left(\frac{1}{22}\right)^2 = \frac{20,000}{(22)^2} = 41.3\#$$

   c. Entering Figure 2.1.2-1 with this information, one finds

$M_j = 1.60$ $\qquad$ $\rho_j/\rho_o = .382$

$P_R/P_o = 3.70$ $\qquad$ $V_j/a_o = 2.29$

$T_j/T_o = 2.61$

From Figure 2.1.2-2, the speed of sound for 70°F is

$$a_o = 1128 \text{ fps.}$$

Thus, $\qquad V_j = 2.29 \times 1128 = 2583 \text{ fps}$

and $\qquad T_j = 2.61 \times (70 + 459.6) = 1382°R = 923°F.$

2. Given an engine Mach no. of 1.2 and a jet density ρ_j/ρ_o of .4, find the jet temperature and velocity, for an ambient temperature of 40°F.

   a. The jet temperature ratio is the inverse of the density ratio, i.e.

   $$T_j/T_o = (\rho_j/\rho_o)^{-1} = 1/.4 = 2.5$$

   b. Entering the chart, we find

   $T_R/T_o = 3.1$ $\qquad$ $P_R/P_o = 2.40$

   $V_j/a_o = 1.95$

   Thrust (1" nozzle) = 23.5 lb.

From Figure 2.1.2-2, the speed of sound is

$$a_o = 1096 \text{ fps.}$$

Thus, $\qquad V_j = 1.95 \times 1096 = 2137 \text{ fps}$

and $\qquad T_j = 2.5 \times (40 + 459.6) = 1249°R = 789°F.$

REFERENCE FOR SECTION 2.1

(1) Tanna H. K., Fisher, J. J., and Dean, P. D., "Effect of Temperature on Supersonic Jet Noise," AIAA Paper 73-991, Oct. 1973.

TABLE 2.1.1-1

CENTER AND APPROXIMATE CUTOFF FREQUENCIES FOR STANDARD SET OF CONTIGUOUS-OCTAVE AND ONE-THIRD-OCTAVE BANDS COVERING THE AUDIO FREQUENCY RANGE

Band	Frequency, Hz					
	Octave			One-third octave		
	Lower band limit	Center	Upper band limit	Lower band limit	Center	Upper band limit
12	11	16	22	14.1	16	17.8
13				17.8	20	22.4
14				22.4	25	28.2
15	22	31.5	44	28.2	31.5	35.5
16				35.5	40	44.7
17				44.7	50	56.2
18	44	63	88	56.2	63	70.8
19				70.8	80	89.1
20				89.1	100	112
21	88	125	177	112	125	141
22				141	160	178
23				178	200	224
24	177	250	355	224	250	282
25				282	315	355
26				355	400	447
27	355	500	710	447	500	562
28				562	630	708
29				708	800	891
30	710	1,000	1,420	891	1,000	1,122
31				1,122	1,250	1,413
32				1,413	1,600	1,778
33	1,420	2,000	2,840	1,778	2,000	2,239
34				2,239	2,500	2,818
35				2,818	3,150	3,548
36	2,840	4,000	5,680	3,548	4,000	4,467
37				4,467	5,000	5,623
38				5,623	6,300	7,079
39	5,680	8,000	11,360	7,079	8,000	8,913
40				8,913	10,000	11,220
41				11,220	12,500	14,130
42	11,360	16,000	22,720	14,130	16,000	17,780
43				17,780	20,000	22,390

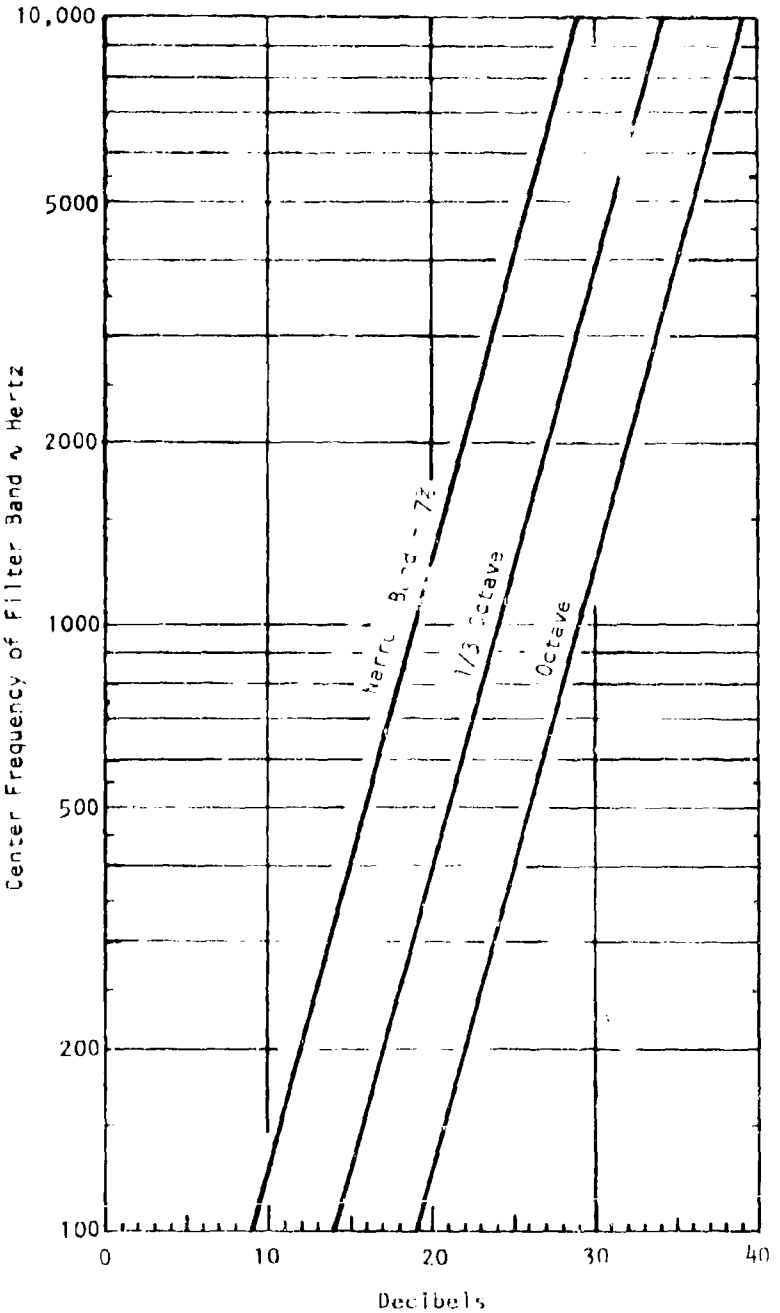

FIGURE 2.1.1-1 NUMBER OF DECIBELS TO BE SUBTRACTED FROM SOUND PRESSURE LEVEL READING TO CONVERT OCTAVE, 1/3 OCTAVE AND NARROW BAND (7%) TO SPECTRUM LEVEL IN DECIBELS.

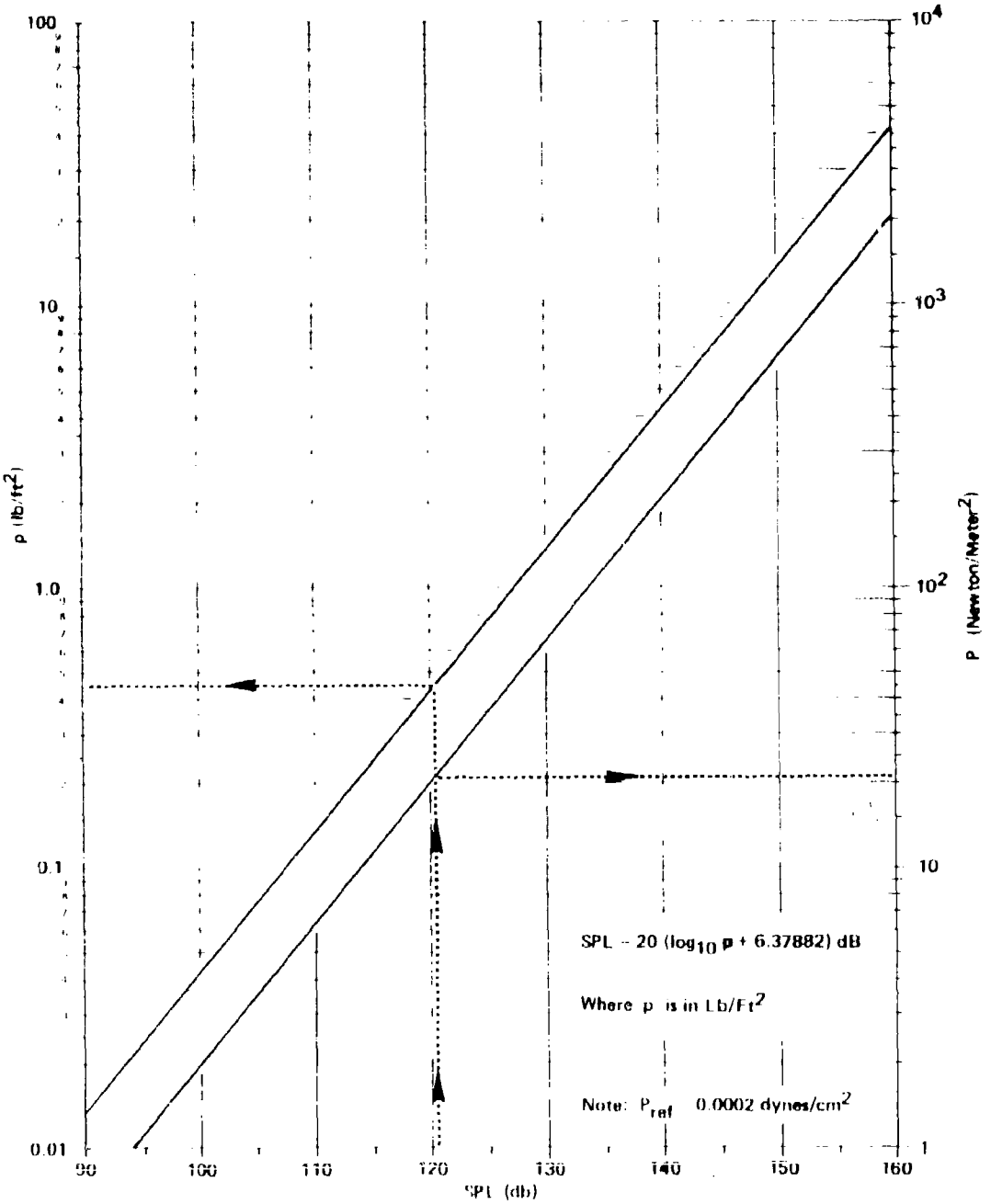

FIGURE 2.1.1-2 CONVERSION FROM SOUND PRESSURE LEVEL IN DECIBELS TO PRESSURE IN ENGLISH AND SI UNITS

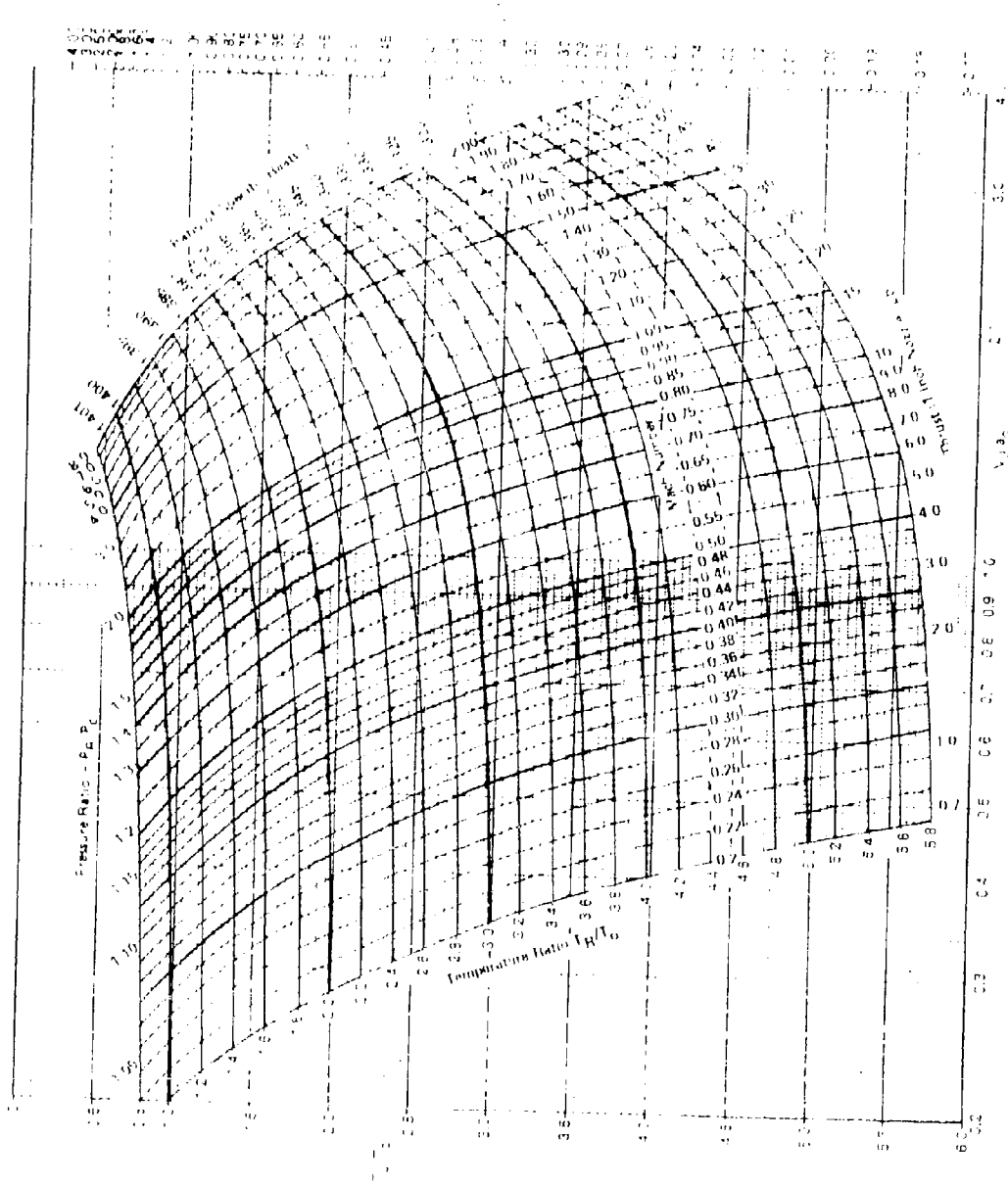

FIGURE 2.1.2-1 THERMODYNAMIC RELATIONSHIPS FOR A PERFECTLY EXPANDED ISENTROPIC FLOW

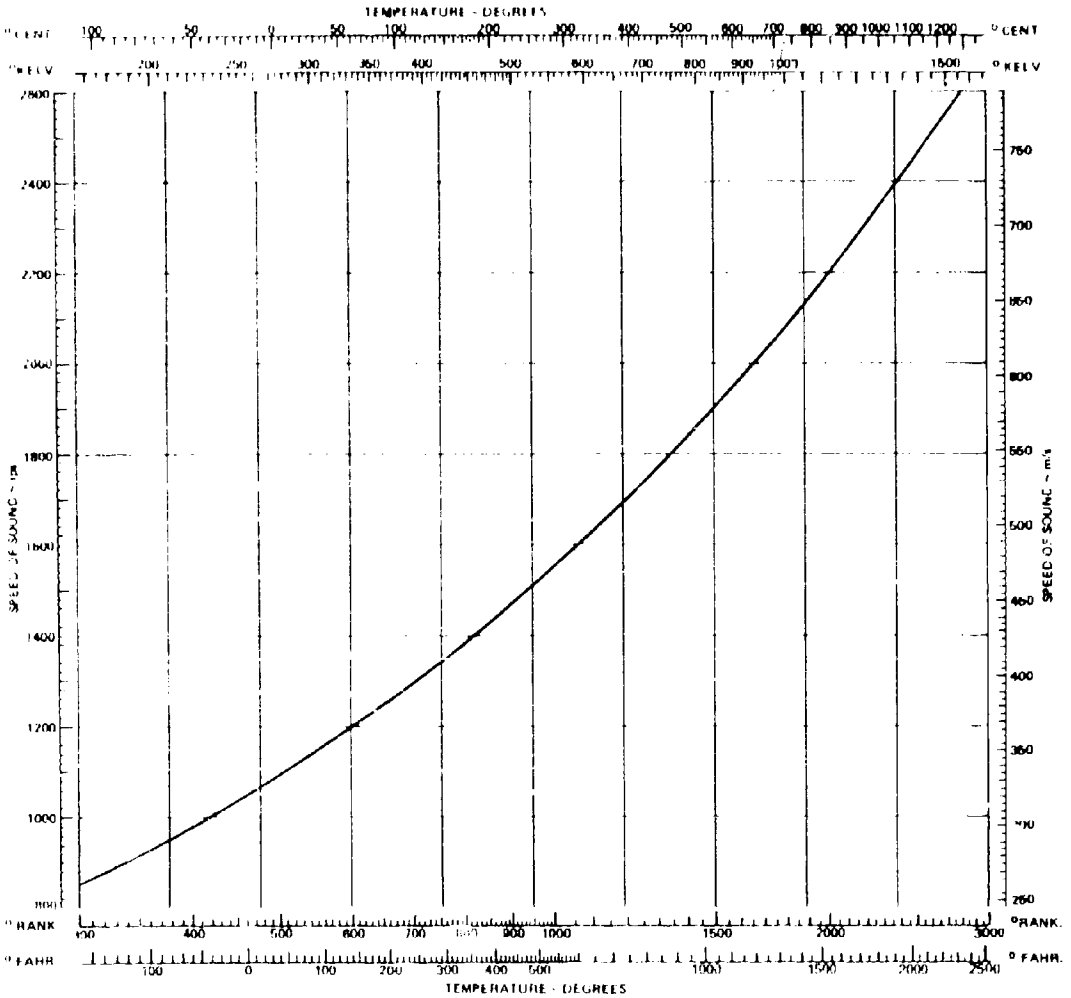

FIGURE 2.1.2 2 RELATIONSHIP BETWEEN SPEED OF SOUND AND TEMPERATURE FOR AIR

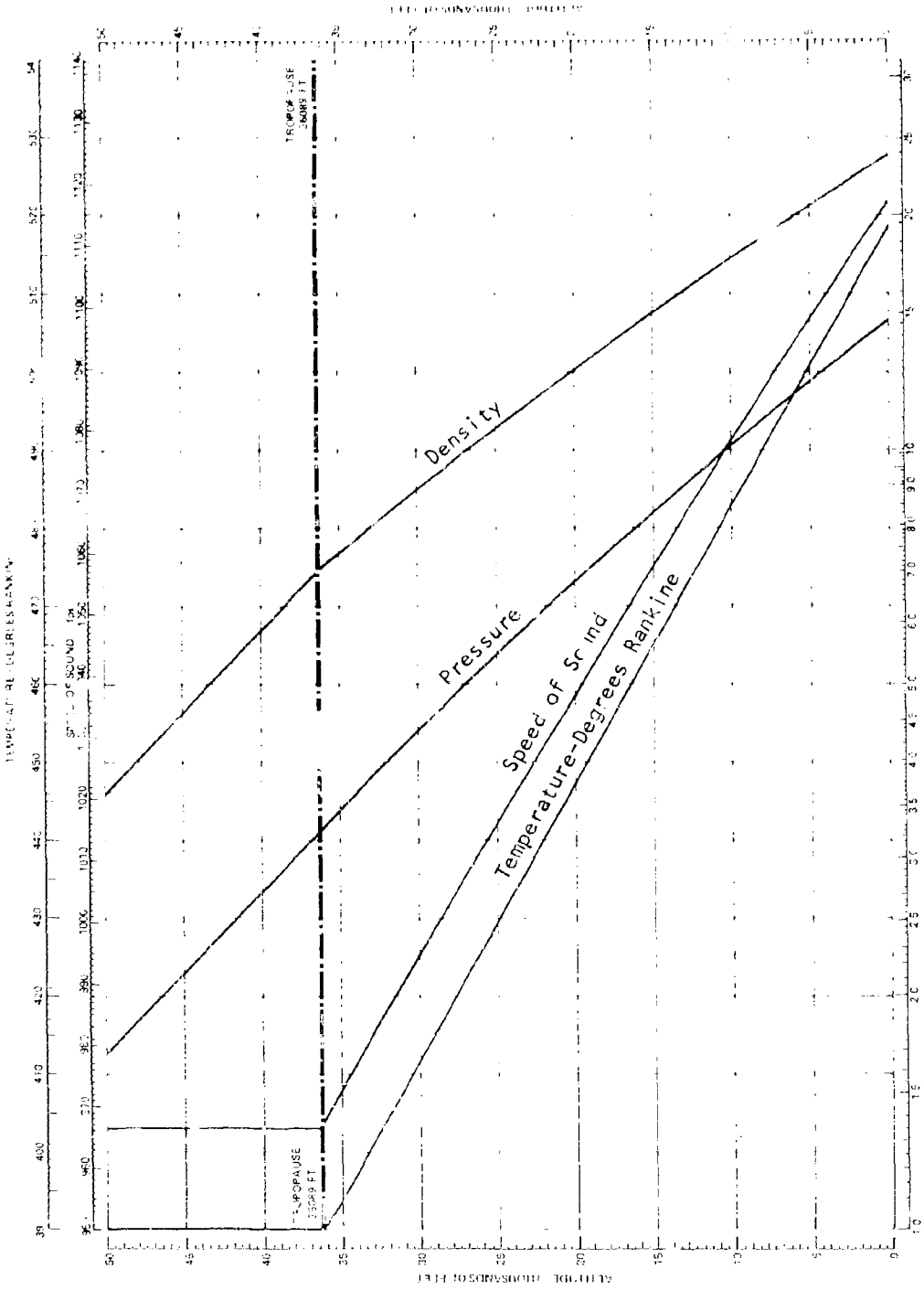

FIGURE 2.1.2-3 PROPERTIES OF ICAO STANDARD ATMOSPHERE

SECTION 3

EXPOSURE TIMES FOR STRUCTURAL COMPONENTS

This section presents guidance for defining the expected lifetime cumulative acoustic environment for various military aircraft design types. It must be recognized by the designer that the data presented here is only for guidance since the particular considerations related to an aircraft design specification must govern the design process. Determination of the service life of a structural component exposed to acoustic excitation requires the designer to estimate the acoustic environment for all service conditions and to relate the design life of the aircraft to the service life of the structural components. In order to relate the aircraft design life to the service life of the component, knowledge of the aircraft type, mission profiles, and mission mix is required. The various mission profiles are used to estimate the time that the structure is exposed to various levels of acoustic excitation. The designer is then concerned with relating specific segments of each aircraft mission with the associated acoustic environment and the resulting structural response. The total time experienced by the structural component for each level of acoustic excitation will then establish the required service life of the component.

The determination of the exposure time for a structural component is, in reality, only a proper accounting procedure wherein segments of exposure time at each sound pressure level are accumulated according to the efficiency of the acoustic excitation with regard to the level of structural response expected. That is, the designer must always realize that due to correlation of the acoustic pressures over the surface of the structure an accumulation of time at operating conditions experiencing similar levels of acoustic excitation is not the only consideration. Being an accounting procedure, the designer must include all segments or operating conditions expected to be encountered by the aircraft during the design life. References (1) through (4) present basic discussions of these topics.

3.1 BASIC CONSIDERATIONS

The significance of estimating the exposure time of structural components to determine the sonic fatigue design life is at best a weighted judgement by the designer. The designer must relate the aircraft mission characteristics to the acoustic environment. When determining the environment, it is necessary for the designer to understand the relationship between the acoustic parameters and the structural response. The basic parameters associated with the environment are the root mean square values of the acoustic pressure, the correlation of the acoustic pressures over the surface of the aircraft and the exposure time of the component to the acoustic excitation. If the pressures are highly correlated over an area the size of typical structural sections (an area typically the size of the frame and stringer spacing) and exhibit broad band frequency spectra, the designer can estimate the structural response parameters using the methods of Section 5. This situation corresponds to jet noise excitation of the structure with the acoustic environment being estimated using the techniques of Section 4. If the pressures are not highly correlated over the surface of the structure, such as is the case for boundary layer excitation, then the structural response is less than that experienced for jet noise for the same rms pressure level. Section 5 presents design guidance for estimating the structural response to boundary layer excitation, but due to the lengthy calculations involved specific techniques are beyond the scope of this report.

Generally speaking, when comparing two levels of acoustic excitation acting either simultaneously or for equivalent time spans, the designer can ignore the lower level if the difference between the two levels is 10 dB or greater (3). When comparing acoustic levels in dB, the designer must always be certain that the same reference pressure is used. A more certain procedure is to convert all acoustic levels, expressed in dB, to the rms value of the pressure level and sum the pressure levels squared to calculate the total rms pressure level. This statement implies that each of the pressures are uncorrelated and that the levels all correspond to the same filter band width. All of these considerations are explained in Section 4 and Section 5.

When the designer weighs the relative significance of the sonic fatigue damage resulting from equivalent exposure he must account for the exposure time of the component. Equivalence is used in the sense of comparing the rms acoustic pressures as described above.

3.2 AIRCRAFT TYPES

The classification of aircraft types in relation to the sonic fatigue design problem is logically dependent upon the performance characteristics and mission requirements of each type. These characteristics and requirements are of course stated in each aircraft design specification. The basic design parameter is the service life of the aircraft. The service life, for sonic fatigue design, comprises the total hours of aircraft utilization for all missions and must include estimates for aircraft ground operations. In particular, the ground operations must include maintenance activities requiring propulsion system operation (2).

High performance military aircraft generally are designed for structural lifetimes substantially less than that required for comparable civilian aircraft. Whereas, a fighter aircraft may be designed for a structural life of 4000 flying hours (4), it is quite likely that transport aircraft may be designed for 30,000 flying hours (1). Depending upon the design specification, a fighter may be required to perform several different missions during the design life, whereas, a bomber or transport aircraft may be required to perform only a relatively few missions that result in different acoustic exposure of the structure.

The aircraft configuration is almost totally related to the aircraft type. Conventional fighter configurations utilize engine placement in the fuselage resulting in only a small percentage of the total aircraft surface area being exposed to high level acoustic excitation from propulsion system noise. The high performance flight characteristics of fighters; however, require the designer to account for the possibility of significant aerodynamic noise sources when relating mission characteristics to sonic fatigue design requirements. Conventional transport or cargo aircraft configurations utilize engine placement on the wings and, hence, result in relatively large areas of the structure being exposed to significant levels of jet noise excitation. Aerodynamic noise sources for transport and cargo aircraft may not result in sonic fatigue design considerations due to the relatively low levels of excitation.

3.3 AIRCRAFT MISSION PROFILES

The definition of an aircraft mission profile is simply an attempt to define the aircraft operating conditions for each mission. Properly, the mission profile should include both ground operations and flight operations corresponding to the particular mission. The ground operations should include realistic estimates for both ground crew activities relating to engine operation and flight crew activities relating to taxi and apron holding operations. For all aircraft types and mission profiles, ground operation of the propulsion system either for maintenance or flight operations generally represents the most severe environment for the accumulation of sonic fatigue damage.

Typical mission profiles including estimates for maintenance activities are presented in the references for Section 3. Fitch (1) presents 16 mission profiles circa 1962 for intercept fighters, tactical fighters, strategic bombers, cargo aircraft, helicopters, and target drones. The engine ground operation summary derived by Fitch for various aircraft types and engine power setting is presented in Table 3.3.1-1. These values must be taken by the designer only as a representative classification system rather than for absolute values. The tabular form suggested by Fitch (1) for classifying the operational segments of mission profiles is presented in Tables 3.3.1-2 and 3.3.1-3 for two cargo aircraft missions. Again, this tabular form is presented only to provide design guidance so that the designer should understand the classification system rather than place emphasis on the specific times quoted in the tables. The flight operation segments of Tables 3.3.1-2 and 3.3.1-3 have been left intentionally blank so that the designer can proportion the flight segment to a particular specification with the only restriction being that the mission flight time be constrained to match the values indicated in the tables. The designer should note that all times in these tables have been "normalized" to operational hours per 1000 flight hours.

Ungar (4) presents estimates for both mission profiles and mission mix for fighter aircraft. The estimated mission profiles for an air superiority fighter, as presented by Ungar, is illustrated in Table 3.3.1-4. Ungar's approach is different from that used by Fitch (See Tables 3.3.1-2 and 3.3.1-3) in that ground operation time is considered as a lump sum quantity rather than prorated over each mission profile. As such, the ground operation time is only considered when accumulating total time for the aircraft service life.

For multi-engine aircraft, it is possible for routine maintenance activities and flight operations to result in one engine accumulating more operational time per flight hour than that experienced by the remaining engines. This consideration was realized by Tietzel (2) in the analysis of engine operational data of SAC aircraft during one year of flight operation. Smith (3) determined that this aspect of aircraft operation was significant from the standpoint of sonic fatigue accumu-

lation in that wing structure behind one engine experienced a significantly longer exposure time than structure behind other engines for KC-135 aircraft although this seems to be peculiar to SAC operations circa 1963. Smith also determined that consideration of only thrust augmented (water injection) takeoff operations resulted in only a 25% error which can be an acceptable margin depending upon the inaccuracies in estimating absolute sonic fatigue damage and any factors of safety included in the design.

TABLE 3.3.1-1

ENGINE GROUND RUN SUMMARY

HOURS PER 1000 FLIGHT HOURS
(REFERENCE 1)

Aircraft Classification	Power Setting				
	IDLE	80-90%	MILITARY	MAX (Static)	Takeoff
Intercept Fighter	267.33	27.71	6.63	5.91	7.26
Tactical Fighter	250.72	24.76	5.86	5.21	6.52
Strategic Attack	98.85	11.35	2.05	1.89	1.58
Tactical Attack	214.33	30.01	4.71	4.29	4.29
Cargo Transport	190.05	22.00	3.97	3.42	4.89
Helicopter	242.00	75.60	10.00	8.89	6.67

TABLE 3.3.1-2

CARGO TRANSPORT - MISSION A

SHORT LIFT
NORMAL OPERATIONAL CONFIGURATION

Oper No. (i)	Operation Description	Power Setting (Note 1.)	Operation Min/Mission (t_{ai})	Mean Alt	Mean A/S	Operation Hr/1000 Flt Hr (Note 2.)
1.	Engine Start	IDLE	1.5	S.L.	0	7.50
2.	Taxi out + Taxi In and Park	IDLE	14.0	S.L.	0	70.0
		80-90%	3.0	S.L.	0	15.00
3.	Power Check	MIL	0.05	S.L.	0	0.25
4.	Pre T.O. Interval	IDLE	3.0	S.L.	0	15.00
5.	Take off	MAX	0.8	S.L.		4.00
6.	Accelerate to Climb Speed	MIL				
7.	Climb to Best Cruise Altitude					
8.	Cruise	CRUISE				
9.	Descend for Landing	IDLE				
10.	Landing	IDLE				
11.	Maintenance	IDLE	.60	S.L.	0	63.00
		80-90%	0.60	S.L.	0	3.00
		MIL	0.60	S.L.	0	3.00
		MAX	0.60	S.L.	0	3.00
Mission A Flight Time ($T_{AF} = \sum_{5}^{10} t_{ai}$)			120			600
Mission A Total Operational Time ($T_{AO} = \sum_{1}^{11} t_{ai}$)			156.75			782

NOTES: 1. Max power settings within all operating limits
2. Operation hours per 1000 flight hours = (t_{ai}/T_{AF}) 600 hr = 5.00 (t_{ai})

TABLE 3.3.1-3

CARGO TRANSPORT - MISSION B

LONG RANGE LIFT
NORMAL OPERATIONAL CONFIGURATION

Oper No. (1)	Operation Description	Power Setting (Note 1.)	Operation Min/Mission (t_{bi})	Mean Alt	Mean A/S	Operation Hr/1000 Flt Hr (Note 2.)
1.	Engine Start	IDLE	1.50	S.L.	0	1.67
2.	Taxi out + Taxi In and Park	IDLE	14.00	S.L.	0	15.53
		80-90%	3.00	S.L.	0	3.33
3.	Powr Check	MIL	0.05	S.L.	0	0.06
4.	Pre T.O. Interval	IDLE	3.00	S.L.	0	3.33
5.	Take off	MAX	0.80	S.L.		0.89
6.	Accelerate to Climb Speed	MIL				
7.	Climb to Cruise	MIL				
8.	Cruise - Climb	CRUISE				
9.	Climb to Best Cruise Altitude	MIL				
10.	Cruise	CRUISE				
11.	Descend for Landing	IDLE				
12.	Landing	IDLE				
13	Maintenance	IDLE	12.60	S.L.	0	13.99
		80-90%	0.60	S.L.	0	0.67
		MIL	0.60	S.L.	0	0.67
		MAX	0.60	S.L.	0	0.67
Mission B Flight Time ($T_{BF} = \sum_{5}^{12} t_{bi}$)			360			400
Mission B Total Operational Time ($T_{BO} = \sum_{1}^{13} t_{bi}$)			396.75			440

NOTES: 1. Max power settings within all operating limits
2. Operation hours per 1000 flight hours = (t_{bi}/T_{BI}) 400 hr = 1.11 (t_{bi})

TABLE 3.3.1-4

AIR SUPERIORITY FIGHTER AIRCRAFT ESTIMATED MISSION PROFILES*

(REFERENCE 4)

Mission	Air-to-Air Combat	High Altitude Intercept	Low Altitude Ground Attack (Lo-Lo-Lo)	Low Altitude Ground Attack (Hi-Lo-Hi)	Miscellaneous Training, Ground Run[4]
Fraction	1/3	1/6	1/12	1/12	1/3
Takeoff[1]	3/-/0	3/-/0	3/-/0	3/-/0	3/-/0
Climb	3/0.8/-	3/0.8/-	---	1/0.8/-	3/-/-
Cruise	18/0.9/35	---	30/0.8/1	25/0.8/35	15/0.8/40
Acceleration	5/0.8-2.4/-	1/0.8-2.5/50	---	---	3/-/-
Descent	---	---	---	2/-/-	3/-/-
Combat[2]	5/2.4-1.5/40-10	10/2.5/50	5/0.85/1	5/0.85/1	---
Climb	3/0.8/-	---	---	1/0.8/-	3/-/-
Cruise	22/0.9/40	17/0.9/40	30/0.8/1	25/0.8/40	15/-/-
Descent	5/-/-	5/-/-	---	4/-/-	5/-/-
Loiter	3/0.4/3	3/0.4/3	3/0.4/3	3/0.4/3	10/0.4/3
Landing[3]	3/-/0	3/-/0	3/-/0	3/-/0	3/-/0
Total Time (min)	70	50	74	71	63

*Unless otherwise indicated, numbers represent: Time (min)/Mach number/Altitude (1000 ft). Dashes indicate data not applicable or defined.

1. Includes taxi, takeoff run, acceleration.
2. Includes gunfire and rocket release.
3. Includes approach, touchdown, landing roll, taxi.
4. 160 hrs of ground runup without afterburner and 40 hrs with afterburner are to be added to total exposure.

3.4 AIRCRAFT MISSION MIX

If an aircraft is designed to perform only a single mission, the aircraft mission profile relates directly to the cumulative exposure of the structure by a simple direct multiplication. If the aircraft is designed to perform several missions - one of which may be classified as a primary mission - then the total aircraft service life is prorated between the various missions. A typical fractional allocation of mission mix based upon the total flight time of the aircraft is presented in Table 3.4.1-1 for three types of fighter aircraft (4). The typical data presented in Tables 3.3.1-4 and 3.4.1-1 will be used to establish the estimate cumulative exposure time in the next section.

TABLE 3.4.1-1

FRACTIONAL DISTRIBUTION OF MISSION TIMES

(REFERENCE 4)

Mission	Aircraft Type		
	Air Superiority	Interdiction	Interception
Air-to-air combat	1/3*	1/6	-
High altitude intercept	1/6	1/6	1/2*
Low altitude ground attack (Lo-Lo-Lo) (Hi-Lo-Hi)	 1/12 1/12	1/3*	-
Miscellaneous (training, navigation, ground run)	1/3	1/3	1/2

*Primary mission

3.5 ACCUMULATION OF NOISE EXPOSURE

The accumulation of noise exposure for an aircraft service life defined in terms of the mission profiles and the mission mix can be approached from two standpoints by considering the total effect of the specified operating conditions. Each operating condition is usually defined in terms of the engine power setting, the aircraft speed, and the aircraft altitude. (Fitch (1) also considers weighing the service life in terms of ambient temperature to assess the sonic fatigue damage.)

The first approach considers each operating condition to be a static environment with all exposure time allocated to the maximum acoustic environment encountered during the operating condition. This approach is easy to apply since the number of conditions required to estimate the acoustic environment is minimized, but this approach also introduces an unknown amount of conservatism into the sonic fatigue design requirements.

The second, and more accurate technique, is to divide the time interval allocated to an operating condition into segments and redefining the operating conditions at the ends of each time interval. For example, the engine power setting for takeoff will be maximum or 100% for the total time interval allocated for takeoff, but the aircraft speed may vary between 0 and 300 knots during this time interval which will decrease the sound levels at a fixed location on the aircraft. In addition, the absence of ground reflection during perhaps 40% of the time allocated to the "takeoff" condition at maximum power can reduce the sound levels at a fixed location on the aircraft an additional amount. These two parameters alone may reduce the sound levels at a location on the aircraft by as much as 20 dB.

A method proposed by Smith (3) and based upon relative damage of the structure relates the time interval of a dynamic aircraft operational condition to the time interval allocated for static aircraft operations in terms of the difference in sound pressure levels between the static and dynamic conditions. Smith's relationship for conventional metallic aircraft structure is:

$$D_l/D_r = (t_l/t_r)\cdot 10^{-0.4(L_r-L_l)} \qquad (3.5.1\text{-}1)$$

where
- D denotes damage
- t denotes time allocated for the operation
- L denotes sound pressure level in dB
- l is a subscript denoting the dynamic condition
- r is a subscript denoting the static condition

To use this result, the designer must divide the total time allocated to the constant engine power setting into intervals, determine the sound pressure levels at the end of each interval by correcting the static levels for effects of aircraft motion and ground reflection, and assess the damage effect. An example will illustrate the point.

Example: Suppose that for a typical mission profile the maximum or 100% engine power setting is proportioned according to the following estimates: Power Check, 3 seconds; Takeoff, 48 seconds; Maintenance, 36 seconds. Determine the relative damage resulting from the Takeoff segment as compared to the static conditions of Power Check and Maintenance (39 seconds of maximum exposure at static conditions).

By estimating the aircraft acceleration during takeoff for, say, 6-second intervals; estimating the sound pressure levels at a location making corrections for aircraft motion and ground reflection, and allocating the highest sound levels to each 6 second interval suppose that the values presented in Table 3.5.1-1 are obtained (t_r = 39 seconds).

TABLE 3.5.1-1

DATA FOR EXAMPLE PROBLEM

Time from Brake Release, Sec.	$\Delta t = t_i$	$\Delta L = L_r - L_i$	D_i/D_r	$\sum_i D_i/D_r$
6	6	0	0.154	0.154
12	6	1	0.061	0.215
18	6	2	0.024	0.239
24	6	3	0.010	0.249
30	6	4	0.004	0.253
36	6	6	0.001	0.254
42	6	10	0.000	0.254
48	6	20	0.000	0.254

Hence, it is seen that the takeoff which represents over 50% of the total time at maximum power for the mission profile results in approximately 25% of the sonic fatigue damage relative to the damage associated with static ground operations. Hence, a more representative estimate (for sonic fatigue design) of the aircraft time at maximum power condition would be 1.25(39) = 49 sec. rather than 48 + 39 = 87 seconds.

To continue the example, suppose that the aircraft structure is required to survive 1000 operations as described above. Then, depending upon the degree of refinement, the sonic fatigue design life for the portion of structure considered in the example would be either 13.6 hours or 24.0 hours. If the structure is assumed to exhibit a resonant response at 300 Hz., then the sonic fatigue design life would be either 1.47×10^7 or 2.61×10^7 cycles to failure.

The designer must not maintain the position that ground operation of the engine(s) is the only condition to be considered or even that jet noise is the only acoustic source to be included for mission analysis related to acoustic fatigue design criteria. Many conditions that occur during flight can result in sonic fatigue failures (5), (6) or alter the estimation techniques normally used for sonic fatigue design methods (7).

From an overall standpoint, the designer must consider the total service life exposure of the aircraft and be assured that all operational conditions have been properly included in the mission analysis. Table 3.5.1-2 presents the estimated cumulative exposure time for an air superiority fighter with an estimated service life of 4000 hours (4). The mission profile for this aircraft is presented in Table 3.3.1-4 with the fractional mission mix presented in Table 3.4.1-1.

TABLE 3.5.1-2

AIR SUPERIORITY FIGHTER AIRCRAFT

ESTIMATED CUMULATIVE EXPOSURE TIMES

Flight Mode	Time		Altitude (1000 ft.)	Mach Numb.
	Percent	Hours		
Ground Runup (no AB)	4	160	0 to 0.5	0
(with AB)	1	40		
Takeoff	5	195	0.5 to 1	0 to 0.4
Climb (to 40,000 ft)	8	300	to 40	0.4 to 0.9
Cruise (500 ft)	6	250	1	0.8
(20,000 ft)	5	200	20	0.9
(40,000 ft)	40	1615	20	0.9
Acceleration	4	170	40 to 50	0.9 to 2.5
Combat (500 ft)	1	20	1	0.85
(5000 ft)		25	5	0.9
(10,000 - 40,000 ft)	2	100	10 to 40	1.5 to 2.5
(50,000 ft)	3	130	50	2.5
Descent	8	300	40 to 3	0.8
Loiter	8	300	3	0.4
Landing	5	195	3 to 0.5	

REFERENCES FOR SECTION 3

1. Fitch, G. E., et al.; "Establishment of the Approach to, and Development of, Interim Design Criteria for Sonic Fatigue," ASD-TDR-62-26, Air Force Flight Dynamics Laboratory, Wright-Patterson Air Force Base, Ohio, 1962.

2. Tietzel, F. A., et al.; "Time Histories of Ground Operations of B-52F and KC-135A Aircraft Engines," ASD-TDR-62-403, Air Force Flight Dynamics Laboratory, Wright-Patterson Air Force Base, Ohio, 1963.

3. Smith, D. L.; "The Effect of Operational Data on Sonic Fatigue Estimates," M.Sc. Thesis, School of Engineering, Air Force Institute of Technology, Air University, United States Air Force, Wright-Patterson Air Force Base, Ohio, August 1963.

4. Ungar, E. E., et al.; "A Guide for Predicting the Vibrations of Fighter Aircraft in the Preliminary Design Stages," AFFDL-TR-71-63, Air Force Flight Dynamics Laboratory, Wright-Patterson Air Force Base, Ohio, April 1973.

5. Roberts, W. H., and Willem, D. P.; "Simultaneous Application of Static and Dynamic Fatigue Test Articles," RTD-TDR-63-4201, Air Force Flight Dynamics Laboratory, Wright-Patterson Air Force Base, Ohio, 1964.

6. Hay, J. A.; "Shock Cell Noise: Aircraft Measurements," Paper D.1, Current Developments in Sonic Fatigue, A Conference, Institute of Sound and Vibration Research, University of Southampton, England, 1970.

7. Wang, A. P.; "Random Spectrum and Structural Probability of Failure," Journal of Sound and Vibration, Vol. 17, No. 3, 1971.

SECTION 4

LOADING ACTIONS

Prediction of acoustic (or fluctuating pressure) loads leading to possible sonic fatigue failure is first in the chain of four major tasks related to predicting sonic fatigue life and designing structures which are sonic fatigue resistant for a specified and predictable lifetime. The other three major items, of course, are (a) the prediction of structural response, in terms of stress amplitude, to a given acoustic load, (b) the prediction of stress concentration factors for a particular structural configuration and (c) the prediction of fatigue life for a particular structure, whatever its material composition, for a given stress distribution. These last three items can be complicated by numerous factors, including high temperature environments and multiple loading actions. These considerations are addressed in other sections of this report. This section, however, deals with methods for determining the acoustic loads on an aircraft structure due to the many possible sources of high sound levels.

It is impossible to set "a priori" a specific value on the sound pressure level at which a designer should begin to worry about the possibility of sonic fatigue failure in a structure. Air Force experience shows that below an overall sound pressure level of 140 dB, sonic fatigue failures are not to be expected (MIL-A-883, para. 4.3.1, Reference 9). At levels in excess of 140 dB overall sound pressure level, the designer should include sonic fatigue considerations into his design. Factors decreasing the fatigue life of structures exposed to acoustic loading include (but are not limited to):

- sound pressure amplitude
- sound pressure frequency spectrum shape
- correlation area of acoustic excitation
- structural flexibility (or rigidity)
- structural damping
- structural configuration (e.g. curved, flat, skin/stringer, honeycomb)
- fastening methods (e.g. rivets, bonding, welding, etc.)
- stress concentrations
- environment (e.g. temperature, etc.)

Thus, because of the complex nature of the problem, this section is not intended as a simple rule-of-thumb guide on operational regions, engine types, etc. to avoid as a means of reducing sonic fatigue. This section is instead intended as a source of design data for the estimation of all the known aspects of a particular acoustic source as it relates to the prediction and/or prevention of sonic fatigue failures.

4.1 ACOUSTIC SOURCES

Numerous possible sources of acoustic loading of aircraft structure can be identified; however, these various sources logically are classified as to propulsion system noise sources and aerodynamic noise sources and are the topic of this section. Another category of acoustic sources is that related to the operation of external and internal equipment. Equipment, such as an auxiliary power unit, while noted for its annoyance to humans, is not a usual noise source for inducing sonic fatigue. Thus, equipment noise is not included as a consideration in this report.

Propulsion system noise sources include jet noise, fan noise, propeller noise, shock cell noise, etc. From the standpoint of sonic fatigue design, near-field jet noise is by far the most damaging to aircraft structure. Jet noise overall sound pressure levels in excess of 165 dB have been noted by various experimenters. The methods for predicting the acoustic loading resulting from propulsion system operation are presented in Section 4.2. Aerodynamic noise covers a very broad classification of sources including boundary layer noise, cavity noise, shock wave noise, noise resulting from separated flow, flow impingement noise, etc. Prediction methods relating to cavity noise and boundary layer noise are presented in Section 4.3.

There are several parameters which must be calculated prior to and during the actual prediction of acoustic loading using the methods of this section. It is necessary, for instance, to convert octave or 1/3 octave sound pressure level to a spectrum level as input to the stress prediction. Or, it is necessary to calculate engine operating conditions, such as jet temperature and exhaust velocity, when one is given the plenum temperature and nozzle pressure ratio. Or else, one might require the speed of sound when only the temperature is known. Section 2.0 of this report includes numerous charts and conversion factors which will be useful to the designer in establishing these quantities while using the acoustic loading prediction methods of Section 4.0.

4.2 PROPULSION SYSTEM NOISE

The majority of occurrences of acoustically induced fatigue have resulted from propulsion system noise, with the primary offender being near-field jet noise Because of its prominence as a structurally damaging noise source much more study has gone into the prediction of near-field jet noise than any other type of noise source (with reference to the purpose of eliminating sonic fatigue of structures). Immediately after a list of symbols and definitions, the second section (4.2.2) is devoted to prediction methods for near-field jet noise. Following that, prediction methods for near-field propeller noise are given. Some very sparse data for near-field (in-duct) fan noise is included and finally a section discusses the effects of ground reflection, structural reflections and forward speed.

4.2.1 SYMBOLS AND DEFINITIONS

The notation used in this section is as follows:

a - radius of fuselage (Section 4.2.5.2)

$a_{i,j}$ - empirical constants for Equations (4.2.2-3) and (4.2.2-4)

a_o - ambient speed of sound

B - number of blades

C - correlation coefficient between P_r and P_d

$Cf_{1/3}$ - 1/3 octave center frequency

C_i - empirical constant in Equation (4.2.2-1);

C_p - specific heat at constant pressure of fully expanded jet gasses

c - chord of downstream rotor or stator blade (Section 4.2.4.2)

D - jet nozzle exit plane diameter in Section 4.2.2
propeller diameter in Section 4.2.3

$D(0)$ - source directivity

d - separation distance between rotor and stator blades

f - frequency (in Hertz or cycles per second)

f_m - the m^{th} multiple of the fundamental blade passage frequency, f_1

H' - height of source above ground (Figure 4.2.5-1)

J_m - m^{th} order Bessel function of first kind

K - empirical constant in Equation (4.2.2-1);
also reference SPL in Section 4.2.4.1

K_1, K_2 - constants in Equation (4.2.4-1)

k - wave number, $2\pi f/a_o = 2\pi/\lambda$

L - Overall sound pressure level

L_n - normalized octave band level

L_o - datum overall sound pressure level

L_s - octave band level

L_V - correction to L due to change in jet velocity

L_1 - level of 1st harmonic

L_ρ - correction to L due to change in jet density

M - jet exit plane Mach number

M_h - propeller tip true Mach no. (including forward velocity effect)

M_t - propeller tip rotational Mach no.

N - propeller rotational speed

N_m - m^{th} order Bessel function of second kind

n - velocity exponent in Section 4.2.2 (determined from Figure 4.2.2-2 or Figure 4.2.2-7)
tip Mach No. exponent in Section 4.2.4.1

P_d - direct pressure at receiver

P_r - reflected pressure at receiver

p - ambient pressure

R - gas constant
distance from source to receiver (Figure 4.2.5-1)

R' - distance from image source to receiver (Figure 4.2.5-1)

r - distance to field point from center of jet exit plane (Section 4.2.2.3)

r_o - radial distance from nozzle lip to "source" location (Section 4.2.2.3)

r_s - distance from jet noise "source" to field point

St - Strouhal Number, fD/V

T - thrust developed by propeller

T_j - jet (static) exit plane temperature

T_o - ambient temperature

T_R - total (or stagnation) temperature at jet exit plane

V, V_j - jet exit velocity - number of stator vanes in Section 4.2.4.2

V_f - aircraft forward speed

V_o - datum velocity

V_t - propeller tip rotational speed

X - fore/aft distance from propeller tip to computation point

X_o - source axial location (Section 4.2.2-3)

(x,y) - rectangular Cartesian coordinates of point in near field, relative to center of nozzle exit plane

Z - radial distance from propeller tip to computation point

α - empirical constant in Equation (4.2.2-1)

$\Delta L^{(n)}$ - incremental levels in propeller noise prediction method

Δ_s - rotor-stator interaction level, decibels

θ - angle between field point and jet exhaust axis with the nozzle exit plane as the origin of coordinates

θ' - angle between the source-image source axis and the radius R' (Figure 4.2.5-1)

θ_s - angle between field point and jet exhaust axis with the source location as the origin of coordinates

λ - wave length a_o/f

ρ - datum density

ρ_a - local density

ρ_j - jet (static) exit plane density

ρ_o - ambient density

σ - hub-to-tip radius ratio for a duct

τ - time delay between direct and reflected signals

ψ - angle between field point and propeller plane with origin at center of propeller (see Figure 4.2.3-10)

4.2.2 NEAR-FIELD JET NOISE

Numerous studies of the near noise field of jet engines have been made in the past 20 years. All the work has been experimental in nature, with various empirical techniques applied to the experimental data in an effort to predict the noise for other operating conditions and engine types. The tests from which the prediction methods have been derived were on both full-scale and model (both cold and hot) jets. The model jet data seems to scale on frequency and jet diameter to a reasonable degree of accuracy. However, the accuracy limits for all the prediction methods seem to be no more than ±5 dB.

Of all the prediction methods studied, three have been selected for inclusion in this report. The methods are presented in order of increased complication and sophistication.

The first, adapted from Thomson (1), is relatively simple to use. The primary prediction result is overall SPL contours. Estimates of spectral shape are given in terms of Strouhal number, St.

The second method, from Cockburn and Jolly (2), is derived from the data and prediction method of Hermes and Smith (3), based on a series of J-57 near field noise tests. This method gives spectral shapes for 24 different regions in the near-field, based on a smoothing of the measured spectral information from Hermes and Smith (3). These spectral data, and consequently the prediction methods, have ground reflections inherent in the measurements. These same spectra were corrected for ground reflection by Sutherland and Brown (4), but were not included in this report since the proposed level variation with velocity was unjustified and seemed somewhat questionable. However a combination of the Cockburn and Jolly (2) method and the Sutherland and Brown (4) method would seem to be a step in the right direction. Also, neither of the first two methods has any experimental verification of effects of temperature on the near field noise. The first hypothesizes a p^2 dependance, after Lighthill (5), for the far-field. The second ignores temperature altogether.

A third method, developed by Plumblee (6), is based on a series of tests with a model jet for a wide variance in both temperature and exhaust velocity. The data were acquired from a free-field, vertically exhausting jet and were empirically correlated using the best available theoretical models. The data do not contain ground reflections, thus, if that effect is to be included, the image source method for a directional source should be used as described in Section 4.2.5.1.

4.2.2.1 Overall Near-field Jet Noise (With Spectral Estimation)

Introduction and Discussion: This method, derived by Thomson (1), is primarily intended to give an overall value of SPL. The accuracy is estimated, by Thomson, to be within ±5 dB for overall levels, for jets operating near 2000 fps and 1250°R. The accuracy spread could be somewhat greater at temperatures or velocities significantly higher than the datum (1252°R or 696°K and 2000 fps or 610 m/s).

The noise levels predicted by this method are free field values. The prediction is not valid within an angle of 15° from the jet axis. Reflection corrections should be included by means of the methods of Section 4.2.5. The method is inapplicable to the case of shock-cell noise which results when the jet operates in an "over-choked" condition, whether the nozzle is convergent or convergent-divergent.

Calculation Procedure: The following information is required as a basis for the computation of the sound pressure level at some point in the field:

jet nozzle diameter	D
co-ordinates of the point	(x,y)
mean fully expanded jet velocity	V
jet pipe total temperature	T_R .

(1) Evaluate x/D and y/D.

(2) From Figure 4.2.2-1, which shows the free field datum noise level contours, read off the datum overall sound pressure level L_o at the position (x/D, y/D).

(3) From Figure 4.2.2-2, which shows velocity index contours, read off the velocity index n at the position (x/D, y/D).

(4) Calculate the first part of the velocity correction term ΔL_{v1}, from

$$\Delta L_{v1} = 10n \cdot \log_{10}\left(\frac{V}{V_o}\right).$$

(5) Obtain the second part of the velocity correction term ΔL_{v2} from Figure 4.2.2-3, which shows ΔL_{v2} plotted against $\log_{10}(V/V_o)$ for different values of n.

(6) Calculate the total jet velocity correction L_v from

$$L_v = \Delta L_{v1} + \Delta L_{v2} .$$

(7) Calculate the density of the jet gases ρ_j, with the aid of Figure 2.1.2-1, where

$$\rho_j = \frac{p}{RT_j}$$

and $T_j = T_R - \frac{V^2}{2C_p}$ for all jet velocities.

(8) Calculate density correction L_ρ,

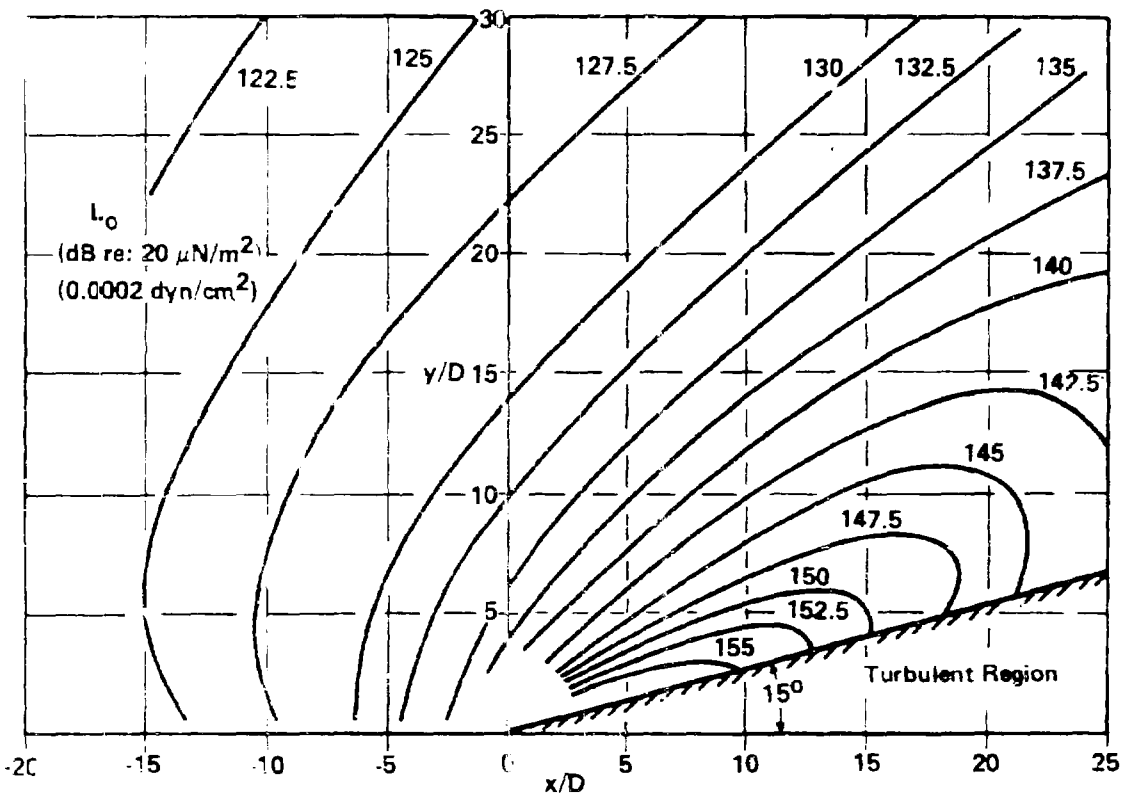

FIGURE 4.2.2-1 REFERENCE CONTOURS FOR JET NOISE OVERALL SOUND PRESSURE LEVEL PREDICTION

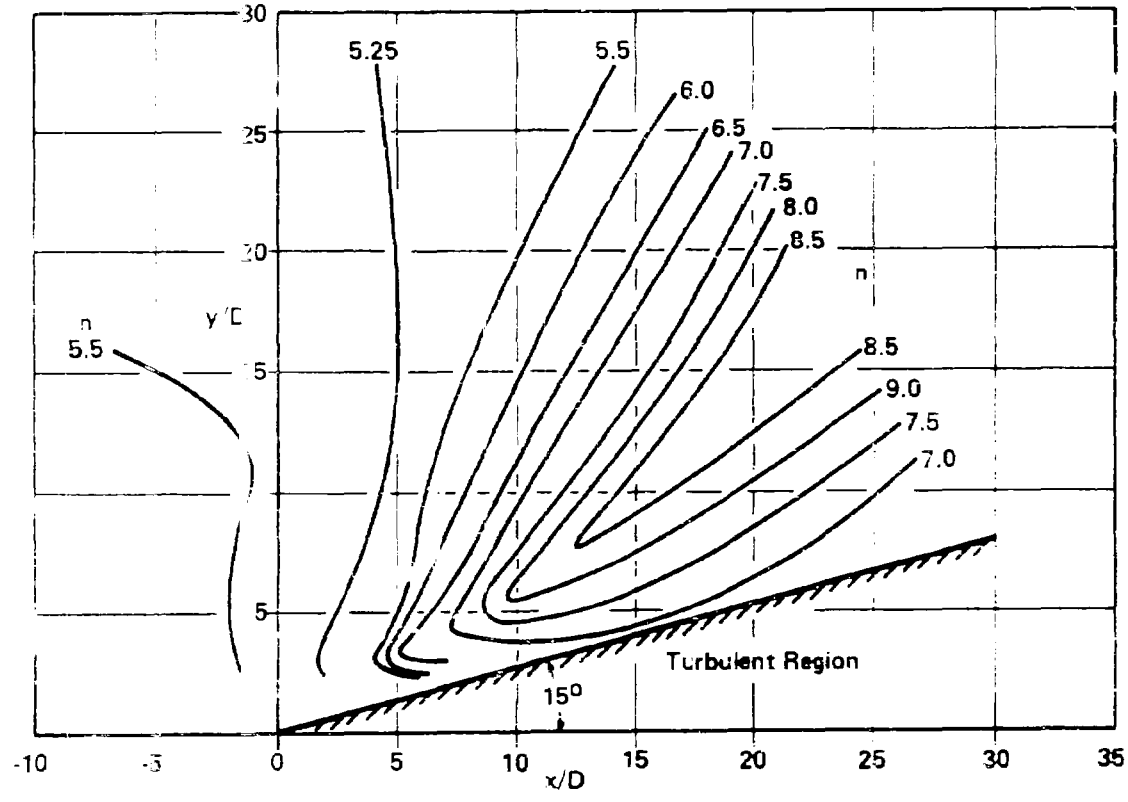

FIGURE 4.2.2-2 CONTOURS FOR JET VELOCITY EXPONENT, n, USED IN CALCULATING OVERALL JET NOISE

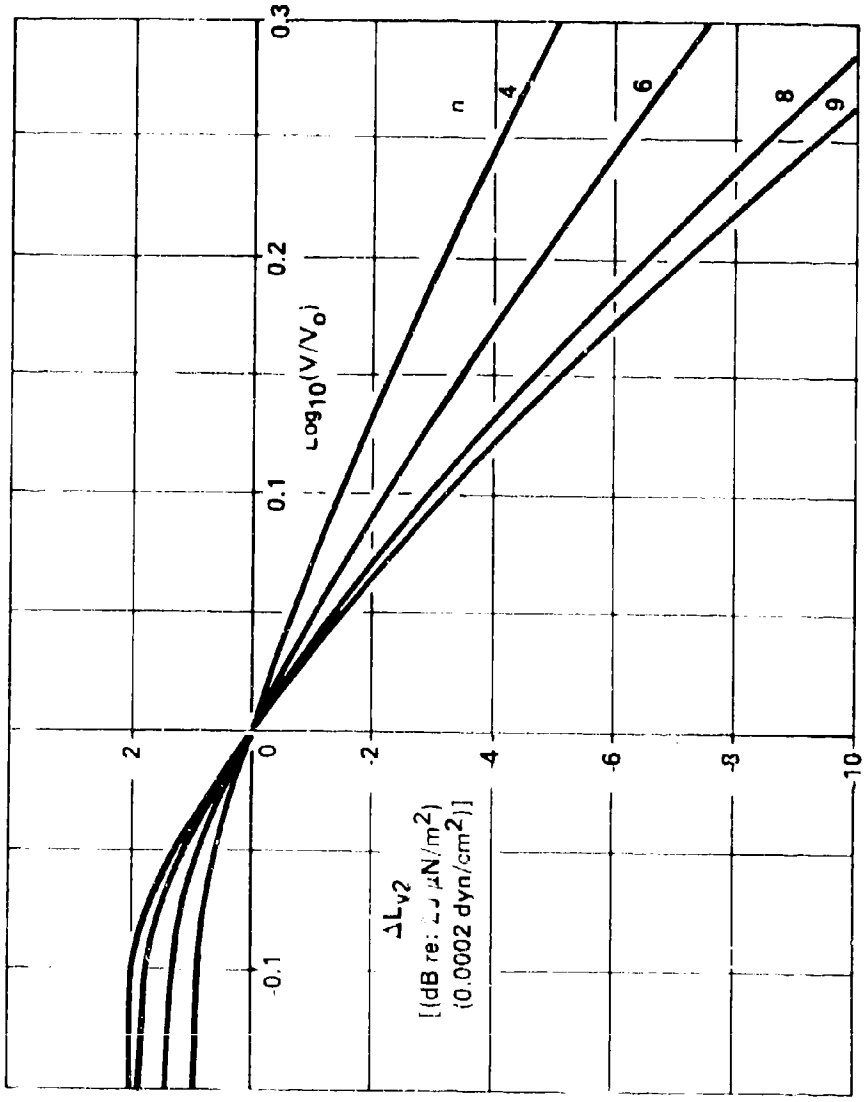

FIGURE 4.2.2-3 CORRECTION TO OVERALL SOUND PRESSURE LEVEL FOR CHANGES IN JET VELOCITY FOR VARIOUS VALUES OF THE VELOCITY EXPONENT n

where $L_\rho = 20 \cdot \log_{10}\left(\frac{\rho_j}{\rho_o}\right)$.

(9) Evaluate the overall sound pressure level (SPL) at the required point (x, y) as

$$L = L_o + L_v + L_\rho .$$

This level can be converted to a pressure loading by the use of the relation

$$\text{r.m.s. fluctuating pressure in } N/m^2 = 10^{(0.05L-4.699)},$$

or by use of Figure 2.1.1-2.

(10) For a given frequency the spectrum level in decibels relative to an arbitrary overall SPL may be read from Figure 4.2.2-4, after evaluating St = fD/V, and x/D. Alternatively, if the spectrum level is required in terms of pressure loading, this may be found using Figure 4.2.2-5. Taking values of St and x/D, the normalized spectral density in $(N/m^2)/Hz$, relative to 1 N/m^2 overall SPL, is read from the ordinate of Figure 4.2.2-5 and is then multiplied by the value of L obtained as a pressure loading in step (9). This gives the pressure spectral density for a specified frequency in $(N/m^2)/Hz$.

Use of Calculated Sound Pressure Levels: After the free field sound pressure levels have been estimated, corrections must be made for local effects, for example, reflection. When the wave fronts of this noise field strike a structure they are partially reflected, and the reflection process locally increases the pressure loading on the surface.

When the wave front strikes the surface at right angles (normal incidence) the pressure loading is doubled (a 6 dB increase on the calculated values). If the wave front moves parallel to the surface (grazing incidence) there is no increase in loading.

To allow for this reflection process, it is fairly general engineering practice to add a mean correction of 3 dB to the calculated free space levels (however, the method given in Section 4.2.5.2 can be used if more accurate corrections are required).

Further corrections must be made for the case of an aircraft in motion to allow for the effects of the aircraft velocity (see Section 4.2.5.3) and ambient speed of sound.

Example: Estimate the r.m.s. sound pressure level and the pressure spectral density at 300 Hz at a specific point, given the following conditions:

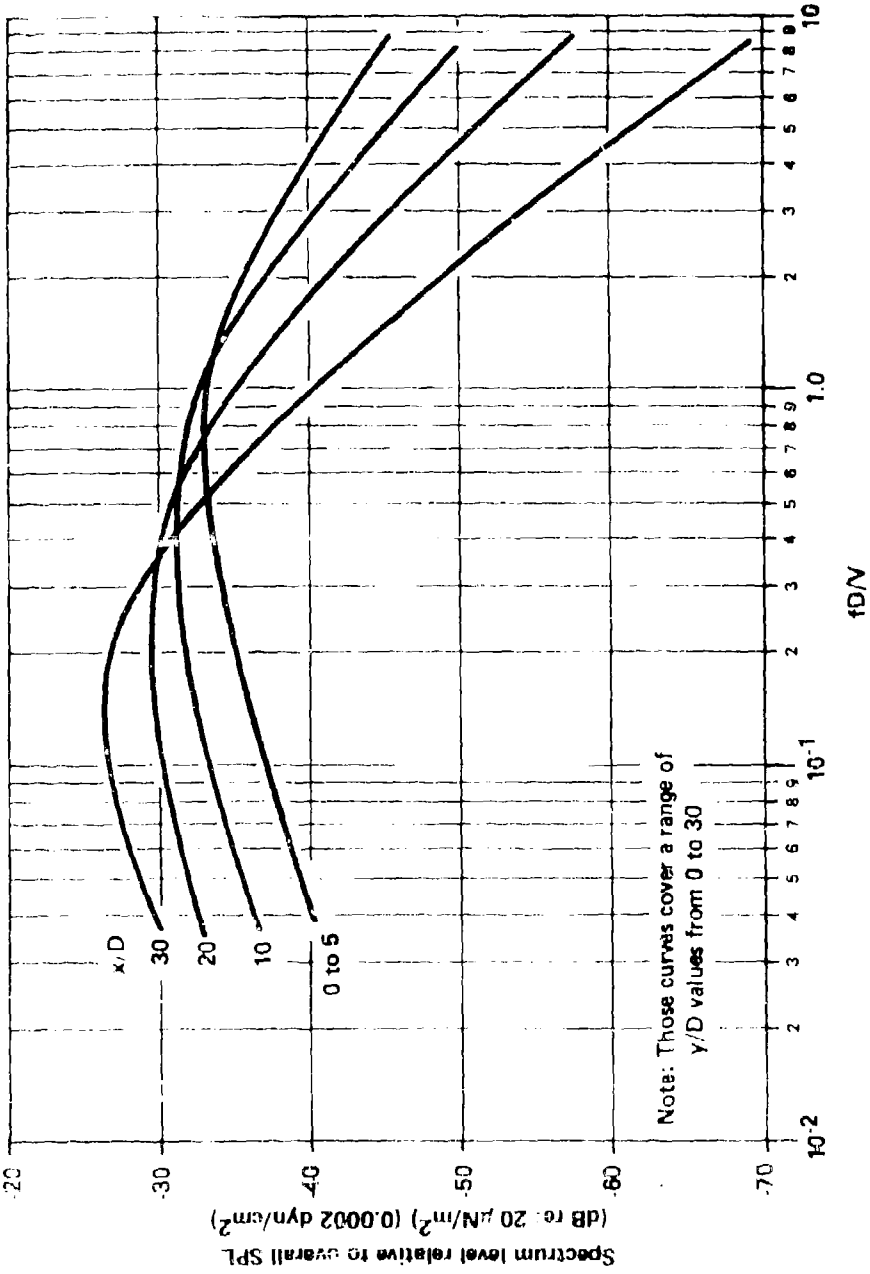

FIGURE 4.2.2-4 SPECTRAL ESTIMATION IN DECIBELS FOR VARIATION IN AXIAL DISTANCE FROM JET EXIT PLANE

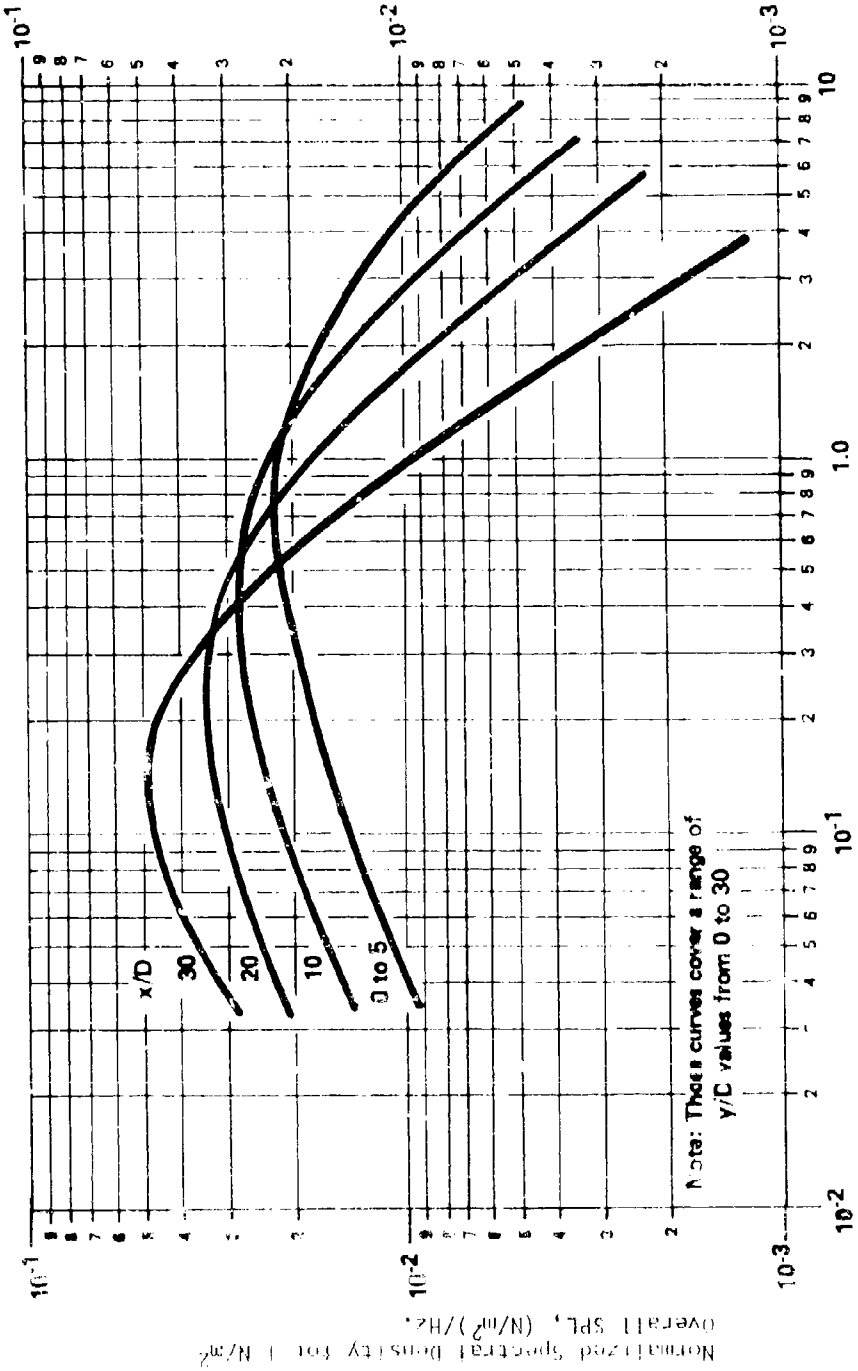

FIGURE 4.2.2-5 NORMALIZED PRESSURE SPECTRAL DENSITY ESTIMATION FOR VARIATION IN AXIAL DISTANCE FROM JET EXIT PLANE

$D = 0.61$ m, $x = 5.5$ m, $y = 6.7$ m,

$V = 670$ m/s, $T_R = 900$ K,

$V_o = 610$ m/s $\rho = 0.49$ kg/m^3 ,

$R = .287$ J/kgK $C_p = 1160$ J/kg K,

$p = 101 \times 10^3$ N/m^2 .

First,

$$\frac{x}{D} = \frac{5.5}{0.61} = 9.02 ,$$

and,

$$\frac{y}{D} = \frac{6.7}{0.61} = 11.0 .$$

From Figure 4.2.2-1,

$$L_o = 140 \text{ dB} ,$$

and, from Figure 4.2.2-2, by interpolation,

$$n = 6.2 .$$

Now,

$$\Delta L_{v1} = 10 \times 6.2 \log_{10}\left(\frac{670}{610}\right) = 2.5 \text{ dB},$$

and, from Figure 4.2.2-3, for $\log_{10}(V/V_j) = 0.0407$ and, interpolating for $n = 6.2$,

$$\Delta L_{v2} = -0.9 \text{ dB},$$

so that,

$$L_v = 2.5 - 0.9 = 1.6 \text{ dB} .$$

As

$$T_j = 900 - \frac{670^2}{2 \times 1160} = 707 \text{ K} ,$$

then

$$\rho_j = \frac{101 \times 10^3}{287 \times 707} = 0.498 \text{ kg/m}^3 .$$

Or alternatively,

$$\frac{V_j}{a_o} = \frac{2000}{1100} = 1.82$$

$$\frac{T_R}{T_o} = \frac{900 \times 9/5}{530} = 3.06$$

From Figure 2.1.2-1, we find $M = 1.14$, $T_j/T_o = 2.52$, $\rho_j/\rho_o = .397$. With $\rho_o = .002378$ slugs/ft^3, or 1.235 Kg/m^3, we have

$$\rho_j = 0.000944 \text{ slugs/ft}^3 \text{ or } 0.490 \text{ Kg/m}^3 ,$$

which is in close agreement with the computed value of 0.498 Kg/m^3.

Now $$L_\rho = 20 \cdot \log_{10} \left(\frac{0.498}{0.49}\right) = 0.14 \text{ dB}$$

and so, finally, $$L = 140 + 1.6 + 0.14 = 142 \text{ dB} .$$

To determine the corresponding normalized pressure spectral density for a frequency of 300 Hz, Figure 4.2.2-5 is used. The Strouhal frequency, St is

$$St = \frac{fD}{V} = \frac{300 \times 0.61}{670} = 0.273$$

and

$$\frac{x}{D} = 9.02 .$$

By interpolation, the normalized spectral density relative to an overall sound pressure level of 1 N/m^2 is found to be 0.026 (N/m^2)/Hz.

In this Example L = 142 dB, which from step (9) or Figure 2.1.1-2 is equivalent to 252 N/m^2.

So the pressure spectral density = $0.026 \times 252 = 6.55$ (N/m^2)/Hz.

4.2.2.2 Near Field Jet Noise Spectral Estimation

In the most comprehensive series of jet noise tests conducted to date on a full size jet engine, Hermes and Smith (3) conducted near field jet noise tests at exhaust velocities from 1250 fps to 2500 fps in five increments. The 1.85 foot diameter J57-P21 turbojet engine was tested at operational exhaust temperatures in the range of 800 to 1150°F.

From this extensive variation in jet exit velocity, Hermes and Smith formulated an 'n'-field contour chart similar to that presented in the previous section. This chart was, of course, to be used in conjunction with the measured spectra at each different position to predict the SPL at a given point in the near field. Cockburn and Jolly (2), armed with this data, smoothed and averaged the spectra in various regions in the near field and

developed a generalized prediction method which is relatively straightforward in implementation.

(1) Determine the non-dimensional location of the field point, (x,y) in terms of nozzle diameters, that is, (x/D, y/D).

(2) Determine the overall SPL, L_o, from Figure 4.2.2-6 at the desired field point (x/D, y/D), for the reference velocity of 1920 fps and the reference exit diameter of 1.85 feet (the approximate exit temperature, T_R, for the reference test was 1130°R).

(3) Based on at least two known exhaust gas conditions, use Figure 2.1.2-1 to determine exhaust velocity ratio V/a_o for the engine under consideration. Use Figure 2.1.2-2 or other sources to determine the ambient speed of sound, a_o, and then determine the velocity, V.

(4) Determine the value of the velocity exponent, n, from Figure 4.2.2-7 at the field point (x/D, y/D).

(5) The overall sound pressure level, L, at the point (x/D, y/D) for the new engine is

$$L = L_o + 10n[\log_{10}V - 3.283].$$

where n is the exponent determined in Step (4) above, and
V is the velocity determined in Step (3).

(6) To determine the correct octave spectrum shape, use Figure 4.2.2-8 to determine the spectral region number for the field point (x/D, y/D).

(7) From Figure 4.2.2-9, find the spectrum for the region number from (6) above.

(8) The octave spectrum levels, L_s, are determined by adding the overall SPL, L, to the normalized spectra, L_n, from Figure 4.2.2-9

$$L_s = L + L_n .$$

(9) The frequencies are determined from the relationship

$$f = \frac{St\,V}{D} .$$

To determine the standard octave levels (listed in Table 2.1.1-1, calculate the center frequency of the octave bands in terms of Strouhal number, St,

$$St = \frac{(CF)D}{V}$$

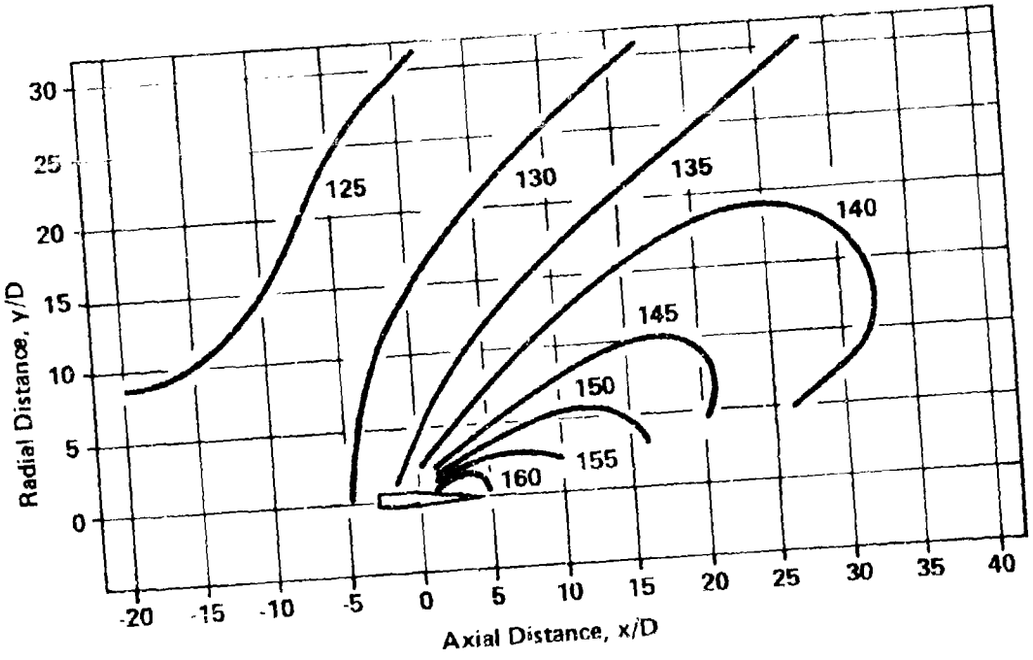

FIGURE 4.2.2-6 OVERALL JET NOISE FIELD SHAPE FOR REFERENCE CONDITIONS

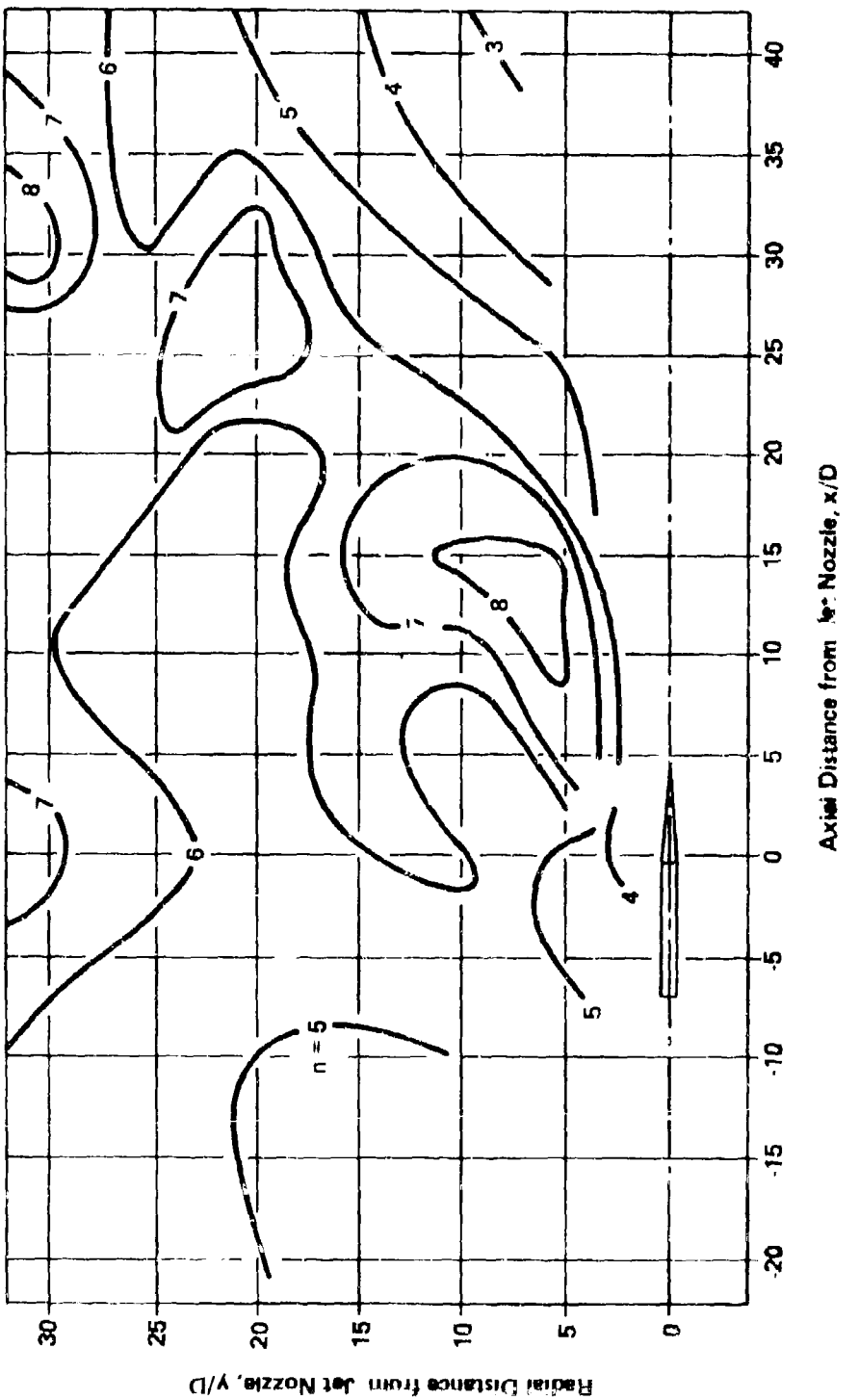

FIGURE 4.2.2-7 VELOCITY EXPONENT CONTOUR MAP FOR OVERALL SPL

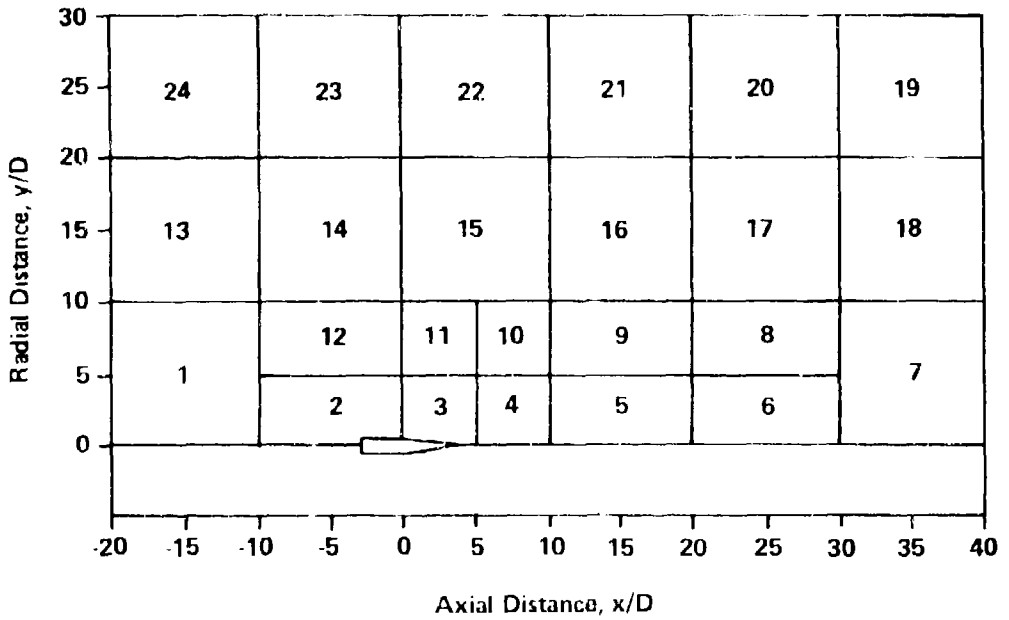

FIGURE 4.2.2-8 DEFINITION OF OCTAVE SPECTRAL REGIONS

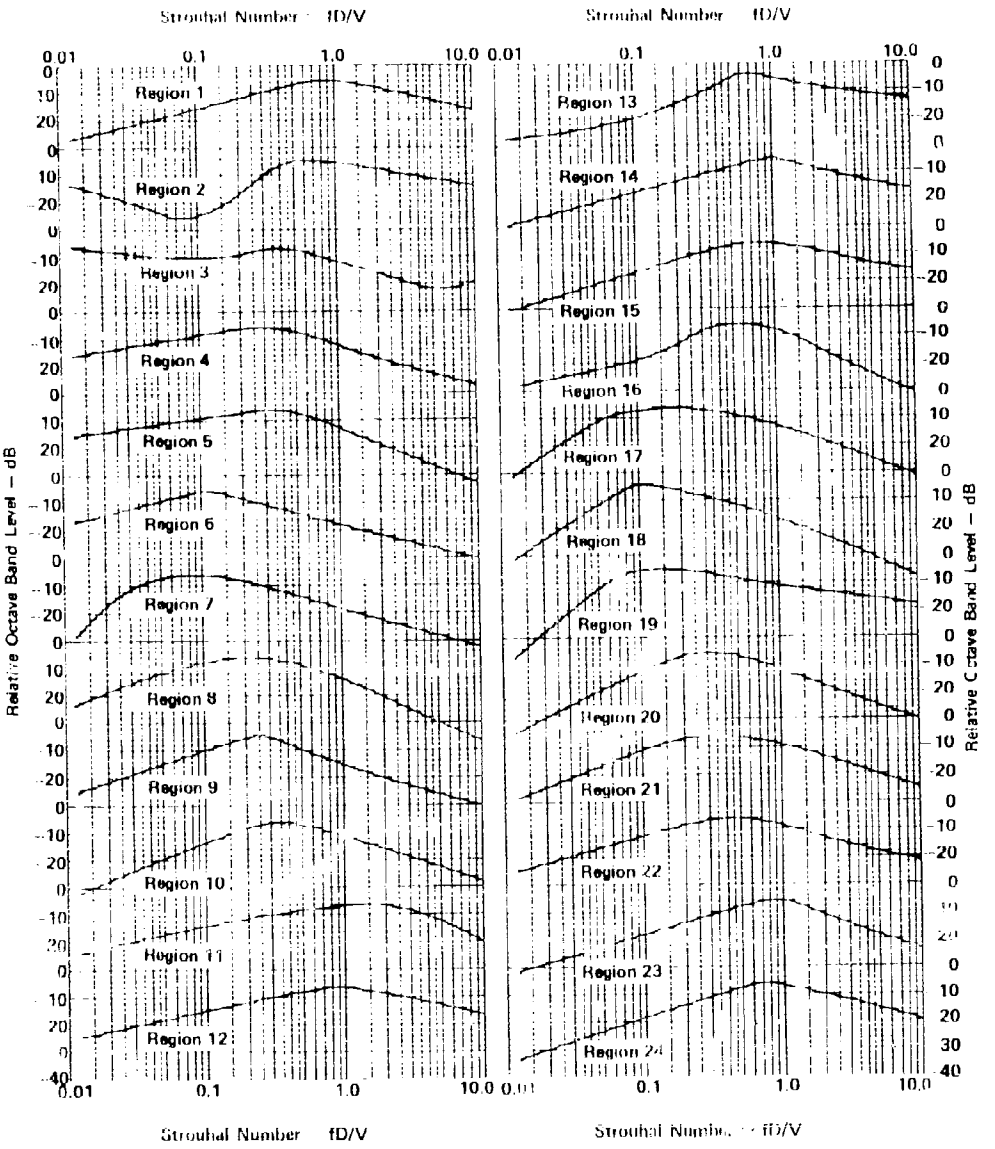

FIGURE 4.2.2-9 OCTAVE SPECTRAL SHAPES FOR EACH SPECTRAL REGION (DEFINED IN FIGURE 4.2.2-8)

Example: Assume a jet engine with a 1.85 foot diameter operating at 1250 fps. Determine the octave band near-field SPL contours for the octave band with 100 Hz center frequency.

(1) Read and tabulate the overall SPL at a sufficient number of field points from Figure 4.2.2-6 to facilitate later replotting of the octave band contours (see Table 4.2.2-1).

(2) Tabulate the spectral region for each field point from Figure 4.2.2-8.

(3) Tabulate the n value for each field point from Figure 4.2.2-7.

(4) Determine the non-dimensional Strouhal center frequency

$$St = \frac{(Cf)D}{V} = \frac{(100)\cdot(1.85)}{1250} = .148.$$

(5) Read and tabulate the relative octave band levels in each spectral region for the Strouhal frequency from Figure 4.2.2-9.

(6) Calculate the reduction in SPL due to reduction in velocity from the relationship

$$L_V = 10n[\log_{10} V - 3.283].$$

(7) Sum the data determined in steps (1), (5), and (6) to determine the octave band SPL at the specified field points.

(8) Plot the data on a field plot and estimate the position of contours of equal as shown in Figure 4.2.2-10.

(9) Use the method in Section 4.2.5.2 to modify the SPL for 'pressure doubling' at the structure surface.

(10) The data inherently have ground reflections. If removal or modification of ground reflection factors is desired refer to Section 4.2.5.1, in conjunction with the Smith & Hermes (3) report which gives details of the test set-up.

4.2.2.3 Effect of Temperature and High Velocity on Near Field Jet Noise

The two previous prediction methods for near-field jet noise were derived from data for engines operating at temperatures not exceeding 1150°F. No accounting for temperature on the contour shape modifications was made and in fact the level change was assumed to be a function of p_j^2 in the 4.2.2.1 method and was not accounted for at all in the 4.2.2.2 method.

If engines are to be used with operating conditions considerably removed from the conditions $1260 \leq T_j \leq 1660°R$ and $1200 \leq V_j \leq 2000$ fps, then the method presented below should be used. This method is based on a series of free-field high temperature subsonic and supersonic jet noise tests. The

TABLE 4.2.2-1. EXAMPLE CALCULATION OF OCTAVE BAND SPL FOR CONTOUR MAP (CONTINUED)

Field Point Coordinates		Reference SPL, L_c (From Fig. 4.2.2-6)	Spectral Region Number (From Fig. 4.2.2-8)	Velocity Exponent n (From Fig. 4.2.2-7)	$L_v = 10 \cdot n \cdot \text{Log}_{10} \frac{V}{1920}$	Octave Band Increment Below Overall Level, L_n (From Fig. 4.2.2-9)	Octave Band SPL $L = L_o + L_v + L_n$
X'D	Y'D						
1	1	155	3	4	-7.5	-10	138
1	3	161	3	4	-7.5	-10	144
1	5	160	3	4	-7.5	-10	143
2	[illegible]	150	3	4	-7.5	-10	133
2	3	159	3	4	-7.5	-10	142
2	5	158	3	5	-9.3	-10	139
2	[illegible]	157	4	5	-9.3	-7	141
[illegible]	10	156	4	5	-9.3	-7	140
[illegible]	[illegible]	135	[illegible]	4.8	-8.9	-10	116
[illegible]	[illegible]	141	[illegible]	6.3	-11.7	-10	119
[illegible]	[illegible]	145	[illegible]	7.2	-13.4	-10	122
5	[illegible]	149	4	7.6	-14.2	-7	128
[illegible]	10	151	4	8.0	-14.9	-7	129
[illegible]	15	150	5	7.6	-14.2	-8	128
[illegible]	20	145	5	5.4	-10.1	-8	127
[illegible]	25	141	6	4.8	-8.9	-7	125
[illegible]	0	134	11	5.2	-9.7	-12	112
[illegible]	3	138	11	5.6	-10.4	-12	116
[illegible]	5	141	11	6.0	-11.2	-12	118
[illegible]	[illegible]	145	10	7.0	-13.0	-10	122
[illegible]	[illegible]	148	10	7.8	-14.5	-10	124
[illegible]	[illegible]	148	9	8.0	-14.9	-7	126
[illegible]	20	146	9	5.9	-11.0	-7	128
[illegible]	25	142	8	5.2	-9.7	-6	126
[illegible]	0	132	11	6.0	-11.2	-12	109

TABLE 4.2.2-1. EXAMPLE CALCULATION OF OCTAVE BAND SPL FOR CONTOUR MAP (CONCLUDED)

Field Point Coordinates		Reference SPL L_o	Spectral Region Number	Velocity Exponent n	$L_V = 10 \cdot n \cdot \text{Log}_{10} \frac{V}{1920}$	Octave Band Increment Below Overall Level, L_n	Octave Band SPL $L = L_o + L_V + L_n$
X/D	Y/D	(From Fig. 4.2.2-6)	(From Fig. 4.2.2-8)	(From Fig. 4.2.2-7)		(From Fig. 4.2.2-9)	
10	5	137	11	5.7	-10.6	-12	114
10	10	142	10	6.6	-12.3	-10	120
10	15	145	9	8.0	-14.9	-7	123
10	20	145	9	7.0	-13.0	-7	125
10	25	143	8	5.6	-10.4	-6	127
15	0	130	15	6.0	-11.2	-14	105
15	5	133	15	6.3	-11.7	-14	107
15	10	137	15	6.7	-12.5	-14	111
15	15	141	16	7.1	-13.2	-16	112
15	20	142	16	6.5	-12.1	-16	114
15	25	142	17	6.1	-11.4	-7	124
20	0	128	15	5.8	-10.8	-14	103
20	5	130	15	5.8	-10.8	-14	105
20	10	133	15	5.8	-10.8	-14	108
20	15	136	16	5.8	-10.8	-16	109
20	20	138	16	5.9	-11.0	-16	111
20	25	139	17	7.2	-13.4	-7	119

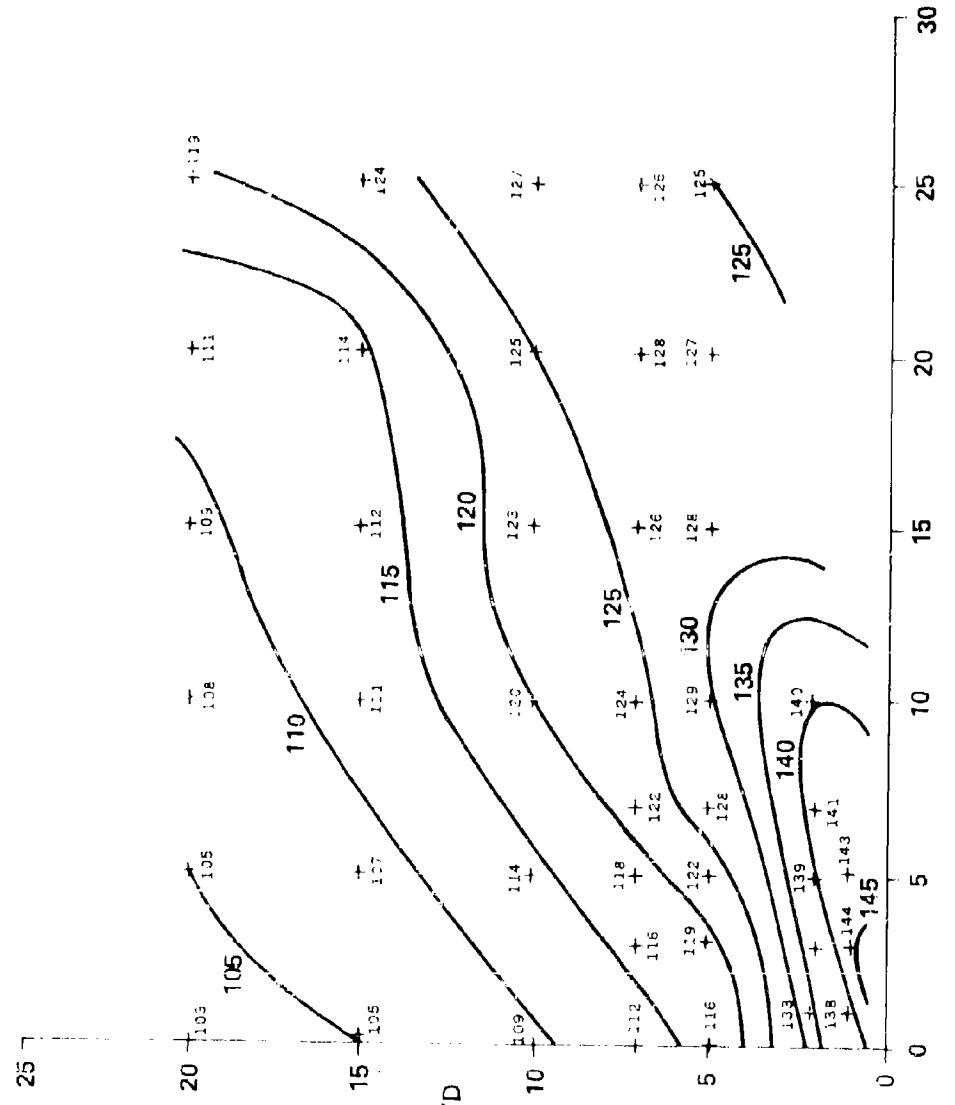

FIGURE 4.2.2-10 ESTIMATED OCTAVE BAND NEAR-FIELD NOISE CONTOUR SHAPE USING METHOD OF SECTION 4.2.2.2

data do not contain ground reflections. A ground reflection method is given in Section 4.2.5.1.

Derivation: This near field jet noise method is based on a systematic series of near field jet noise tests over the velocity range $885 \leq V_J \leq 3688$ fps and the temperature range $390 \leq T_J \leq 2740°R$. The data which were measured in the aft quadrant ($7.5 \leq \theta \leq 97.5°$), were empirically correlated, making use of available theoretical models. For a complete discussion of the correlation, see Plumblee (6, 7).

Design Equations: The sound pressure at a point in the near field, with the source point being the origin of coordinates, as shown in Figure 4.2.2-11, is given by the following equation:

$$\frac{P^2}{} = \frac{KT_R^s M^n (1 + \alpha^2 M^2)^{5/2} (1 + \cos^4 \theta_s) \left(\frac{C_1}{r_s^2} + \frac{C_2}{r_s^4} + \frac{C_3}{r_s^6} \right)}{\left[\left(1 - \frac{M \cos \theta_s}{1 + C_6 e^{-C_7 r_s}} \right)^2 + \alpha^2 M^2 \right]^{5/2} \left(1 + \frac{C_4 e^{-C_5 \theta_s}}{1 + C_6 e^{-C_7 r_s/4}} \right)} \quad (psi)^2 \qquad (4.2.2\text{-}1)$$

The parameters in Equation 4.2.2-1 are functions of Mach number, temperature and frequency (although each parameter is not necessarily a function of all variables). The temperature parameter used in the correlation was total rather than jet (or static) temperature. The equations defining the parameters are given below. The parameters which are independent of frequency are:

$$C_1 = M^{2.34}$$

$$C_2 = 10.65 \left(\frac{T_R}{T_o} \right)^{0.93}$$

$$C_3 = -15.18 \left(\frac{T_R}{T_o} \right)^{1.11} M^{0.89} \qquad (4.2.2\text{-}2)$$

$$C_6 = 17.5 \left(\frac{T_R}{3000} \right)^{0.890 (M^2 - 1)}$$

$$C_7 = 0.41 \left(\frac{T_R}{3600} \right)^{0.566 (M^2 - 1)}$$

The parameters which are dependent on frequency are (where the subscript i refers to the frequency band).

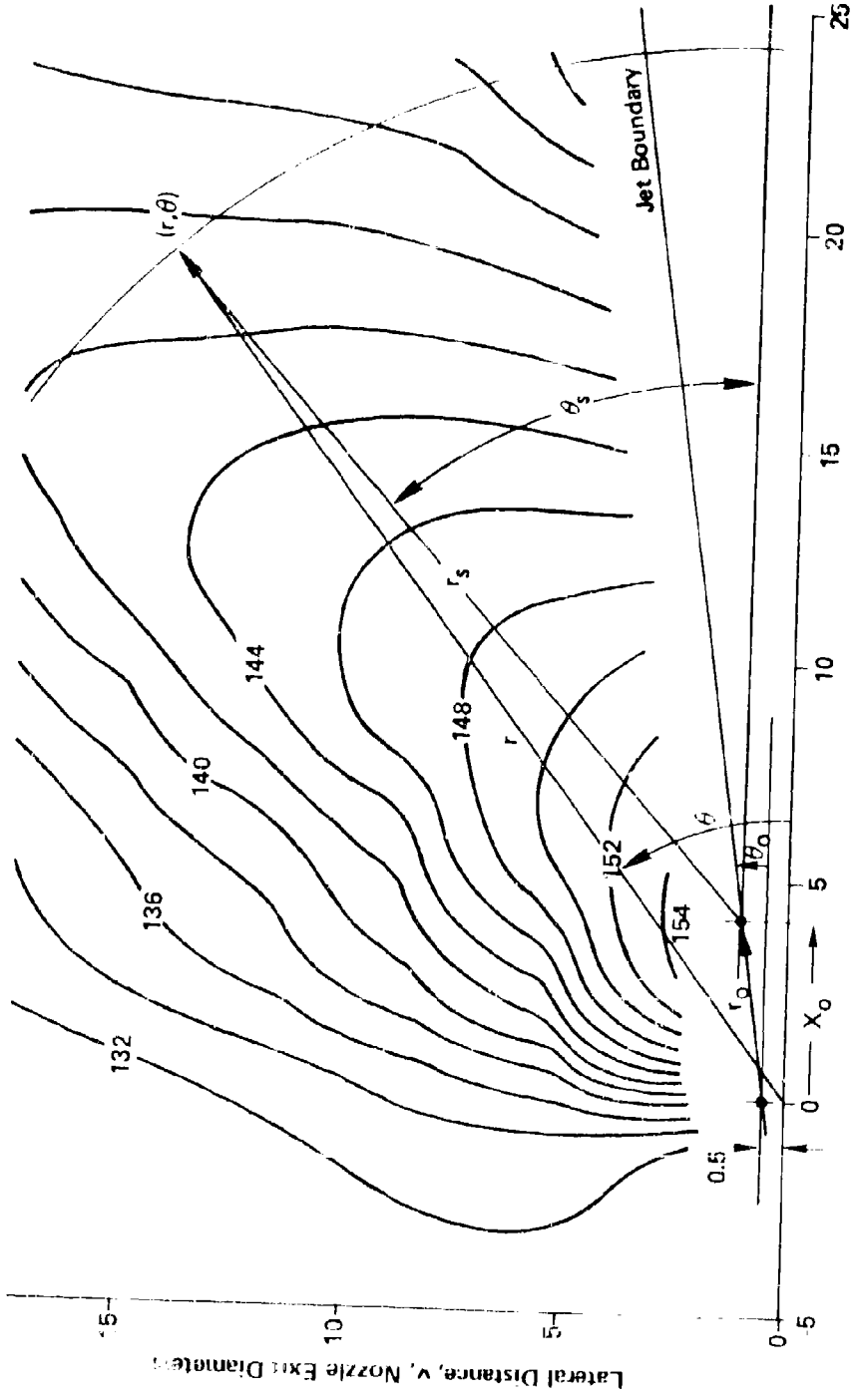

FIGURE 4.2.2-11 DEFINITION OF COORDINATE SYSTEM FOR SECTION 4.2.2.3

$$
\begin{aligned}
\alpha^2 &= a_{i,1} M^{a_{i,2}} (T_R/1000)^{a_{i,3}+a_{i,4}M} \\
C_4 &= a_{i,5} M^{a_{i,6}} (T_R/1000)^{a_{i,7}+a_{i,8}M} \\
C_5 &= a_{i,9} M^{a_{i,10}} (T_R/1000)^{a_{i,11}+a_{i,12}M} \\
KT_R^s M^n &= a_{i,17} T_R^{1.54} M^4 \ .
\end{aligned}
\qquad (4.2.2\text{-}3)
$$

The source location, as determined by the focal point on the 7.5° jet boundary of the SPL contours, is given by:

$$
X_o - r_o \cos\theta_o = a_{i,13} M^{a_{i,14}} (T_R/1000)^{a_{i,15}+a_{i,16}M} \ . \qquad (4.2.2\text{-}4)
$$

where θ_o was taken to be 7.5°.

A field point (r,θ) referenced to the jet exit plane centerline is (see Figure 4.2.2-11)

$$
r = \sqrt{r_o^2 + r_s^2 + 2 r_o r_s \cos(\theta_s - \theta_o) + \frac{1}{4} + r_o \sin\theta_o + r_s \sin\theta}
$$

and

$$
\theta = \tan^{-1}\left[\frac{\frac{1}{2} + r_o \sin\theta_o + r_s \sin\theta_s}{r_o \cos\theta_o + r_s \cos\theta_s} \right] .
$$

The constants $a_{i,j}$ are tabulated in Table 4.2.2-2 for the overall and three octave bands. The frequency limits of the overall band are $300 \leq f \leq 76{,}800$ Hz, for the 3.5" nozzles tested. It would be more convenient to quote frequency in terms of non-dimensional Strouhal frequency, however the test was conducted with fixed frequency band limits and fixed nozzle diameter. Thus each velocity would result in a different Strouhal frequency limit. However, in this case the non-dimensional Helmholtz number, $H_N = fD/a_o$ is $.078125 \leq H_N \leq 20$. The H_N limits of the three frequency bands of noise analyzed and included in the computer program are .15625 - .3125, .3125 - .625, and .625 - 1.25.

Computer Program: The analysis has been completely coded for computation. A Fortran program listing for evaluating the near field noise equation and producing a 7" × 10" plot containing contours of constant SPL is included at the end of this section. The following is a description of the program.

Useage, features and limitations: The program requires two sets of input data. The first set, the $a_{i,j}$ coefficients which are read in at lines 14 and 15, is fixed and is not to be changed. These data are stored in the main program in lines 453 through 465. The fixed data are derived from the jet noise tests and are used to calculate the coefficients required in the prediction formula. The second set of input data consists of three cards and is read at lines 19, 35, and 41. These data are not part of the stored program. The data required and the formats follow.

Col.	1	11	21	31	41	43	51
Format	F10.9	F10.9	F10.9	F10.9	I2		F10.9
Card 1	R1	R2	TH(1)	DTH	N		D
Card 2	XL	XH	YL	YH	IPL		

Col.	1	11	21	23
Format	F10.9	F10.9	I2	I2
Card 3	DM	T	MM	MO

The input variables are defined as:

Card 1

R1 is the smallest value of radius from the source location, r_s, to be used in calculating contours. R1 is not to be less than 1.5 (R1 is normalized to exit diameter).

R2 is the largest value of radius, r_s (R2 is normalized to exit diameter).

TH(1) is the beginning value of angle, θ_s in degrees and is not to be less than 7.5°.

DTH is the increment in angle, θ_s, in degrees.

N is the number of times the increment, DTH, is to be added to TH(1). (The maximum angle is, then, θ_{max} = TH(1) + N·DTH and should be on the order of 180° in order to construct a complete contour plot).

D is the increment between SPL contours in decibels.

Card 2

XL is the smallest value printed out on the horizontal plot axis.

XH is the largest value printed out on the horizontal plot axis.

YL is the smallest value on the vertical plot axis.

YH is the largest value on the vertical plot axis. (In order to have the same scale in both directions, use YH - YL = 0.7 × (XH - XL).)

IPL = 1 uses the input values of XL, XH, YL, and YH to determine the scale of the plot.

= 0 uses the maximum and minimum values of y & x based on R2, TH(1) and θ_{max}, to determine the scale of the plot.

Card 3

DM is the nozzle Mach number

T is the exhaust gas total temperature in °R.

MM = 1 gives a plot for the overall band. The band limits are fD = 1050. to 268,800. Hertz-inches.

= 2, 3, or 4 gives an octave band plot. The band limits are:

MM = 2 fD = 2100. to 4200. Hertz-inches

= 3 fD = 4200. to 8400. Hertz-inches

= 4 fD = 8400. to 16,800. Hertz-inches

to obtain the actual frequency limits of the overall and octave bands, divide the normalized band limits by the nozzle diameter in inches.

MO = 1 gives an abbreviated output and is usually all that is required.

= 0 gives full output.

As many as desired of Card 3 can be put in without including Cards 1 and 2. If DM is set to 0., the program returns to the card 2 READ STATEMENT for a new set of plot limits. If IPL in Card 2 is set to -1, the program returns to Card 1 for a complete new set of input data.

Numerical Example: Typical short-form outputs are included as Figure 4.2.2-12 through 4.2.2-14. Figure 4.2.2-12 is a far-field contour plot for

```
      INPUT DATA
4.        100.      7.5       5.        36        5.
-10.      60.       0.        70.       01
1.        2630.     0101
```

NEAR-FIELD SOUND PRESSURE LEVEL CONTOURS FOR A HEATED JET

MACH NO. IS 1.00 TEMPERATURE IS 2630.
OVERALL BAND, EC = 1050, TU EC = 268,800.

THE FOLLOWING DATA ARE USED IN DETERMINING THE VALUES TO BE ASSIGNED TO THE SPL CONTOURS. THE MAXIMUM ALWAYS OCCURS **CLOSEST TO THE EXHAUST BOUNDARY**

THE INCREMENT BETWEEN CONTOURS IS 5. DECIBELS
THE MAX SPL IS 145. DB LOCATED AT 10.0 DIA. AXIALLY
AND AT 3.0 DIA. LATERALLY
THE MIN SPL IS 110. DB LOCATED AT -9.2 DIA. AXIALLY
AND AT 49.4 DIA. LATERALLY
REFERENCED TO THE SOURCE LOCATION
AT 5.0 DIA. AXIALLY AND AT 1.5 DIA. LATERALLY.

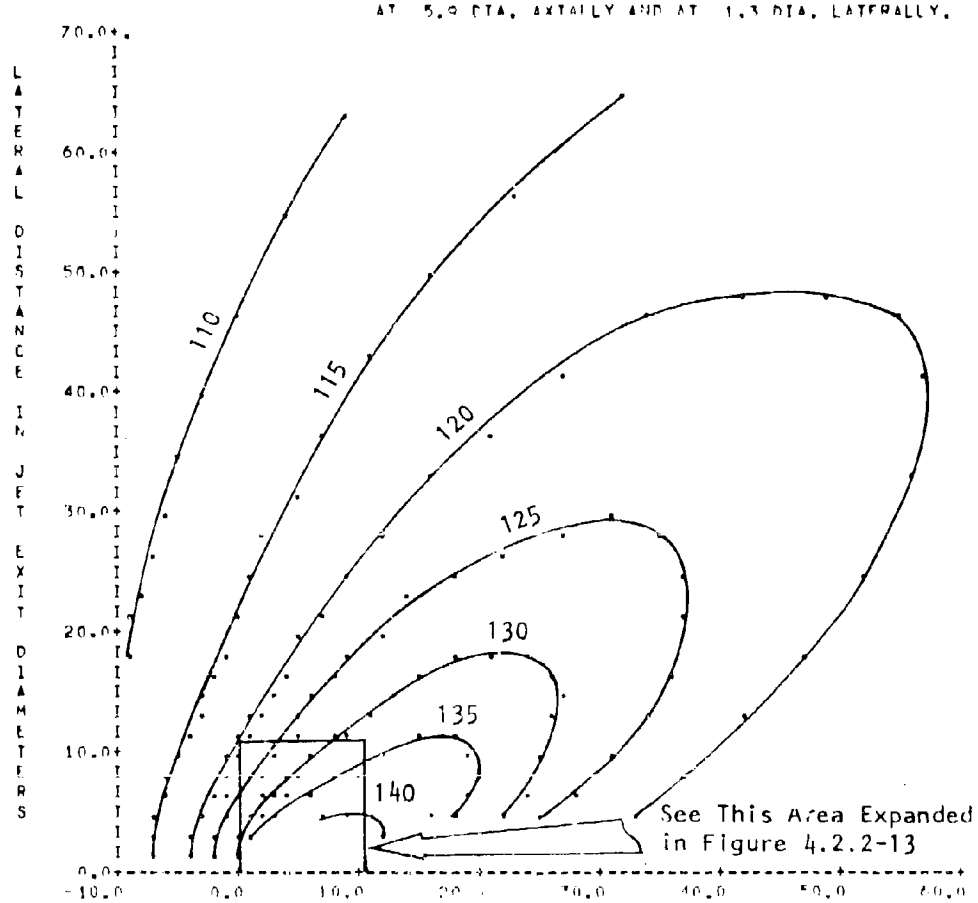

FIGURE 4.2.2-12 ILLUSTRATION OF NEAR-FIELD NOISE CONTOUR CALCULATION

INPUT DATA

1.5	15.	.5	5.	36	5.
-3.	10.5	0.	10.5	01	
1.	2630.	0101			

[illegible] SOUND PRESSURE LEVEL CONTOURS FOR A HEATED JET

MACH NO. IS 1.50 TEMPERATURE IS 2630.
OVERALL RATIO, PO = 1650. TO PO = 2630.

THE FOLLOWING DATA ARE USED IN DETERMINING THE VALUES TO BE
ASSIGNED TO THE SPL CONTOURS. THE MAXIMUM ALWAYS OCCURS
CLOSEST TO THE EXHAUST BOUNDARY
THE INCREMENT BETWEEN CONTOURS IS 2. DECIBELS
THE MAX SPL IS 154. OB LOCATED AT 7.0 DIA. AXIALLY
AND AT 2.3 DIA. LATERALLY
THE MIN SPL IS 126. OB LOCATED AT 0.5 DIA. AXIALLY
AND AT 9.8 DIA. LATERALLY
REFERENCED TO THE SOURCE LOCATION
AT 5.9 DIA. AXIALLY AND AT 1.3 DIA. LATERALLY.

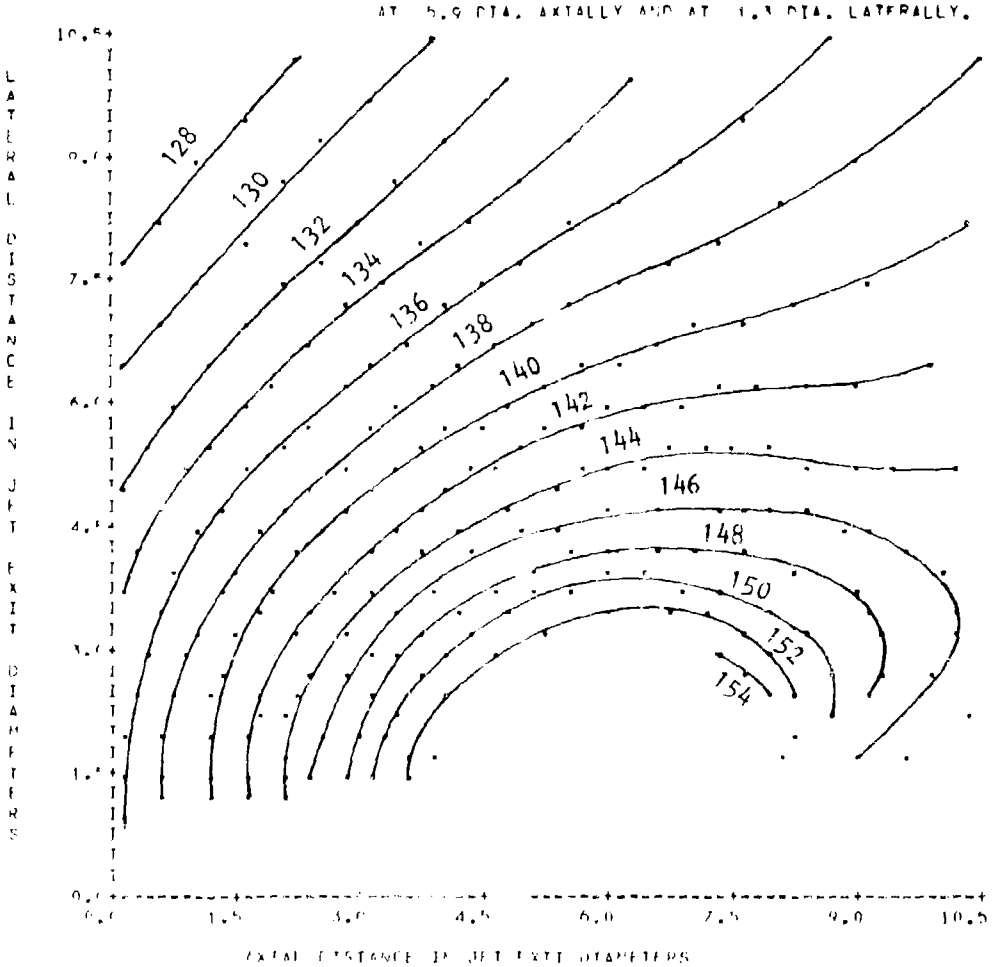

FIGURE 4.2.2-13 EXPANSION OF NEAR-FIELD REGION SHOWN IN FIGURE 4.2.2 12

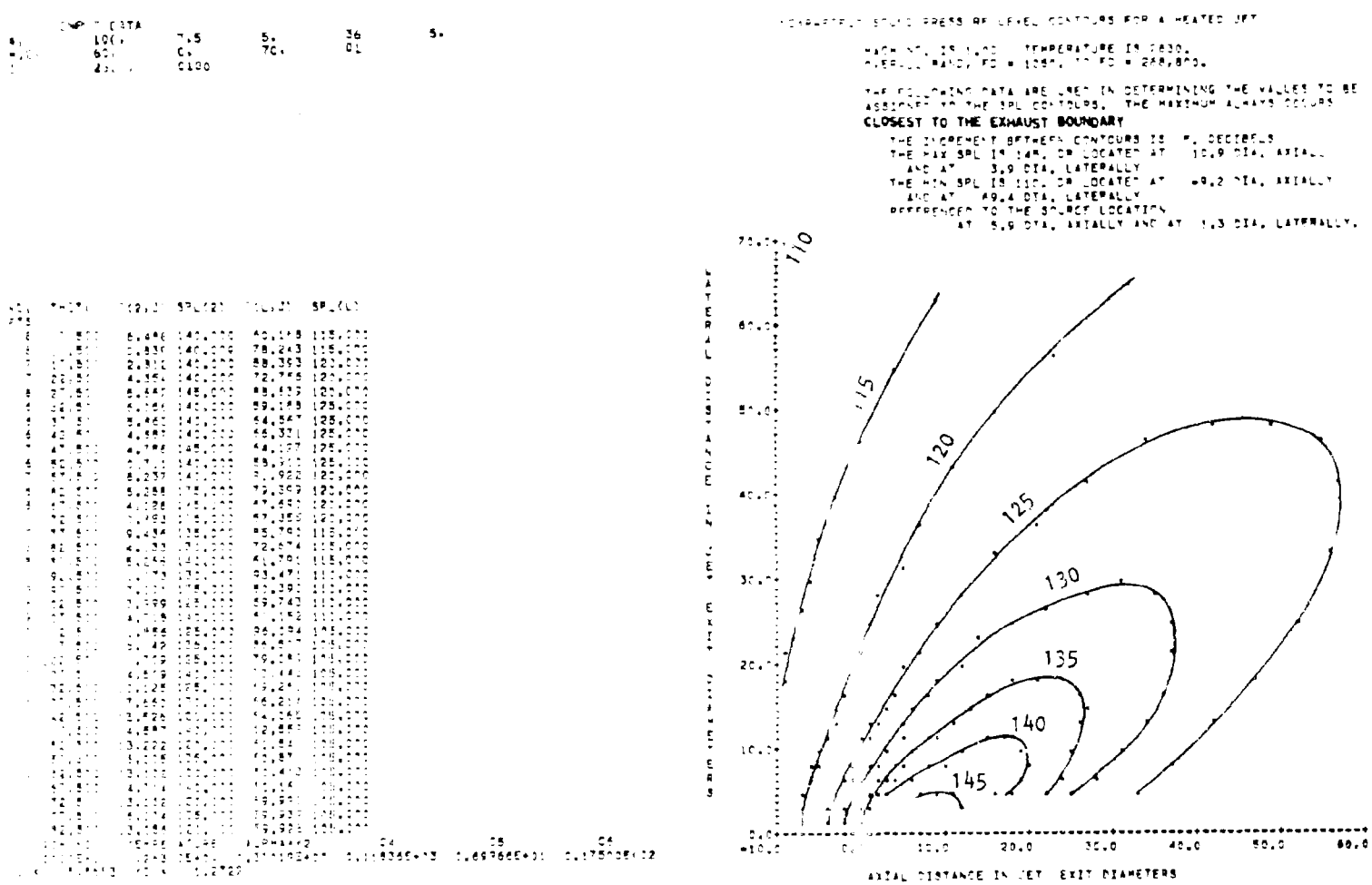

FIGURE 4.2.2-14 ILLUSTRATING LOG FORM OUTPUT

a Mach 1.00 engine operating at 2630 °Rankine total temperature. The SPL plot is for the overall band. The locations of one point on the maximum and minimum SPL contours are given in the heading and the contours must be drawn in by hand. The actual contour shapes are usually apparent at the outer limits of the plot. If these are drawn in first, then the inner contours are more readily detectable. Figure 4.2.2-13 shows an expansion of the small area outlined in Figure 4.2.2-12. Note the variable input data, Cards 1-3, are listed at the top left hand corner.

Figure 4.2.2-14 illustrates the long-form output. The maximum and minimum SPL is given for each radial line, which originates at the source location (also printed). The constants, which are used in evaluation of the Equation 4.2.2-1 are also listed.

The near-field jet noise computer program is listed in Table 4.2.2-3.

NOTE: The term "SP" in subroutine "SØND" is the directivity index in reference to 90°

TABLE 4.2.2-2

COEFFICIENT MATRIX, $a_{i,j}$

	j	i→1	2	3	4
C_2	1	0.8239	0.4176	0.32555	0.74038
	2	-1.24	-1.7269	0.2482	-3.4538
	3	-2.3019	-1.3226	-4.0206	-4.7181
	4	1.4745	1.3507	2.6807	3.2662
C_4	5	45.759	18.932	202.88	331.55
	6	-2.1086	-3.2199	3.8424	0.53294
	7	3.3692	1.3276	10.520	9.5983
	8	-2.3864	-0.1765	-8.0248	-6.829
C_5	9	12.808	8.4045	10.491	10.429
	10	-1.8167	-1.5494	-0.019983	0.36732
	11	-1.7894	-.16571	0.73551	0.89132
	12	1.1641	0.22007	-0.76495	-0.87600
X_o	13	4.912	5.2846	4.5428	2.6963
	14	0.028729	1.3015	0.20763	1.8687
	15	0.789	0.85116	0.27691	3.0174
	16	-0.51772	-0.60053	0.036298	-2.1329
K*	17	4.63×10^{-8}	4.02×10^{-9}	1.23×10^{-8}	9.68×10^{-9}

*A factor of 8.41×10^{-18} to account for the decibel reference pressure exists between the K values, given above, and those given in the computer program. The K values given in Table 4.2.2-2 are for use with Equation (4.2.2-1). (See Equations (2.1.1-2) and (5.2.2-59))

TABLE 4.2.2 3

NEAR FIELD JET NOISE COMPUTER PROGRAM (CONTINUED)

```
/DISPLAY JETNOS
       ACTION IN PROGRESS,
        /JOB GO,NOHAP,TIME=10
             DIMENSION F(16,37),R(16,37),C(17,4),TH(37),IR(37),
            1X(600),Y(600),VT(60),FF(600)
             COMMON IRD,IPR,C,ALP,DM,T,C4,C5,C6,C7,M1,F,R,VT
            1,SHL,SLG,JSH,JSL,D,TH,XO,YO
       C
       C ////////////////////////////////////////////////////////////
             IRD=5
             IPR=6
       C    IRD = SYSTEM INPUT  UNIT DATA SET NUMBER.
       C    IPR = SYSTEM OUTPUT UNIT DATA SET NUMBER.
       C ////////////////////////////////////////////////////////////
       C
             READ(IRD,11)(VT(I),I=1,60)
             READ(IRD,1)((C(I,J),J=1,4),I=1,17)
       C
       C THESE ARE THE COEFFICIENTS FOR THE NEAR-FIELD FUNCTIONS.
       C
          99 READ(IRD,2)R1,R2,TH(1),DTH,N,D
             IF(R1-1.5)90,91,91
          90 WRITE(IPR,12)
             STOP
          91 IF(TH(1)-7.5)92,100,100
          92 WRITE(IPR,13)
             STOP
       C
       C    R1 IS THE SMALLEST VALUE OF RADIUS FOR CALCULATING SPL, AND
       C    R2 IS THE LARGEST VALUE.     R1 IS ALWAYS GREATER THAN 1.50.
       C    TH(1) IS THE SMALLEST VALUE OF THETA FOR CALCULATING SPL.
       C    TH(1) IS ALWAYS GREATER THAN 7.50 DEGREES.    DTH IS THE
       C    INCREMENTAL VALUE OF THETA.    IT WILL BE ADDED N TIMES.
       C    D IS THE INCREMENT FOR SOUND PRESSURE LEVEL CONTOURS.
       C    D IS IN DECIBELS.
       C
         100 READ(IRD,2)XL,XH,YL,YH,IPL
       C
       C SEE PLOTX ROUTINE FOR DEFINITION OF THESE VARIABLES.
       C SET IPL TO -1 IF NEW VALUES FOR R1,R2,TH(1),DTH,N,D, ARE NEEDED.
       C
             IF(IPL)99,130,130
         130 READ(IRD,3)DM,T,M1,M0
       C
       C DM IS THE ENGINE MACH NUMBER.
       C T  IS THE EXHAUST PLANE TEMPERATURE.
       C //////OCTAVE BAND INPUT DESCRIPTION//////
       C      M1 = 1, OVERALL BAND, FO = 1050.0 TO 268800.0.
       C      M1 = 2, FO = 2100.0 TO 4200.0.
       C      M1 = 3, FO = 4200.0 TO 8400.0.
       C      M1 = 4, FO = 8400.0 TO 16800.0.
       C    SET DM = MACH NO. + 0.0 WHEN A NEW PLOT LIMIT FRAME OR
       C    CHANGE IN PLOT CODE IS REQUIRED.
       C   M0 = 0  GIVES FULL PRINTOUT AND PLOT.   TO BE USED WHEN DOUBT
       C                                                    ASSIGNED TO CONTOURS
       C        1  GIVES PLOT AND HEADINGS ONLY
       C
```

TABLE 4.2.2-3 (CONTINUED)

```
      IF(DH)101,100,101
  101 CALL SOUD1
      NB=1
      CALL BLCT(R1,R2,DH,TH(1),0,IR(1))
      DO 200 I=2,N
      IJ=I-(I/4)*4+1
      GOTO(203,201,203,202),IJ
  203 R3=2.5*R1
      GOTO 204
  202 R3=1.5*R1
      GOTO 204
  201 R3=R1
  204 TH(I)=TH(I-1)+DTH
      NB=1
      CALL BLCT(R3,R2,DH,TH(I),0,IR(I))
  200 CONTINUE
      IF(IHO)400,400,402
  400 WRITE(IPR,9)
      WRITE(IPR,7)
  402 NR=0
      K=0
      L=NR
C
C CARTESIAN COORDINATES OF SOUND SOURCE LOCATION.
C
      XO=C(15,I)*DH**C(14,I)*(T*.001)**(C(15,I)+C(16,I)*DH)
      YO=.1516525*XO+.50
      DO 300 J=1,N
      L=IR(J)-1
      IF(IHO)430,430,431
  430 WRITE(IPR,6)IR(J),TH(J),R(2,J),F(2,J),P(L,J),F(L,J)
  431 NR=NR+L
      CT=COS(TH(J)*.0174533)
      ST=SIN(TH(J)*.0174533)
C
C CONVERT FROM POLAR TO CARTESIAN COORDINATES.
C
      DO 300 I=2,L
      K=K+1
      X(K)=CT*R(I,J)+XO
      IF(IPL)301,301,303
C
C IF IPL = 0 DO NOT SUPPRESS POINTS.
C IF IPL IS GREATER THAN ZERO ELIMINATE ALL POINTS OUTSIDE OF
C PICTURE FRAME SPECIFIED BY INPUT DATA XL AND XH.
C
  303 CALL REGION(XL,XH,X(K),IJ)
      GOTO(301,302),IJ
  301 Y(K)=ST*R(I,J)+YO
      YRL=X(K)*.1516525+.50
      CALL REGION(YRL,YH,Y(K),IJ)
      GO TO (360,302),IJ
  360 F(K)=F(I,J)
      GO TO 300
  302 K=K-1
```

TABLE 4.2.2 3 (CONTINUED)

```
  300 CONTINUE
      SML=200.
      SLG=0.
      DO 404 I=1,K
      IF(SML-FF(I))405,405,401
  401 SML=FF(I)
      JSM=I
  405 IF(FF(I)-SLG)404,404,403
  403 SLG=FF(I)
      JSL=I
  404 CONTINUE
      IF(IRD)440,440,441
  440 WRITE(IPR,6)
      WRITE(IPR,5)DM,T,ALP,C4,C5,C6,C7,EM1
      WRITE(IPR,8)XO,YO
  441 CALL PLOTX(X,Y,K,XL,XH,YL,YH,IPL)
      GOTO 180
    1 FORMAT(6F10.5)
    2 FORMAT(4F10.9,I2,3X,F10.9)
    3 FORMAT(2F10.9,2I2)
    4 FORMAT(I4,5F8.5)
    5 FORMAT(7F13.5,I6)
    6 FORMAT(37HO    MACH NO     TEMPERATURE    ALPHA**2,8X,2HC4,11X,
     12HC5,11X,2HC6,11X,2HC7,7X,2HM1)
    7 FORMAT(43H NO.   THETA    R(2,J) SPL(2)  R(L,J)  SPL(L),
     1/,4H PTS)
    8 FORMAT(6HOXO = ,F8.4,7H  YO = ,F8.4)
    9 FORMAT(1H1)
   11 FORMAT(80A1)
   12 FORMAT(43HRT IS LESS THAN 1.5.  YOU DID NOT READ THE ,
     1 15HINSTRUCTIONS.)
   13 FORMAT(33HTH(1) IS LESS THAN 7.5 DEGREES.  ,
     1 34HYOU DID NOT READ THE INSTRUCTIONS.)
      END
      SUBROUTINE PLOTX(X,Y,N,XL,XH,YL,YH,IT)
      DIMENSION A(101),X(1),Y(1),AXIS(5),VT(60),C(17,4),
     1R(16,37),R(16,37),TH(37)
      INTEGER HOLL,BLNK,BIT,ZRO,LMS,A
      COMMON IRD,IPR,C,ALP,DM,T,C4,C5,C6,C7,EM1,L,R,VT
     1,SML,SLG,JSM,JSL,D,TH,XO,YO
      IRD=5
      IPR=6
C
C NOTE     POINTS GIVEN NEED NOT BE IN ORDER - THIS ROUTINE RE-
C      ORDERS THE DATA AS NECESSARY.  THUS, AFTER PLOTTING, THE
C      GIVEN POINTS ARE NOT NECESSARILY IN THE SAME ORDER AS THEY
C      WERE BEFORE THIS ROUTINE WAS CALLED.
C      X    IS THE ARRAY OF X CO-ORDINATES.
C      Y    IS THE ARRAY OF Y CO-ORDINATES.
C      N    IS THE NO. OF (X,Y) POINTS.
C           IF IT = 1 THEN -----
C      XL   IS THE BEGINNING VALUE OF X PRINTED ON THE X AXIS.
C      XH   IS THE LAST VALUE OF X PRINTED ON THE X AXIS.
C      YL   IS THE  BEGINNING VALUE OF Y PRINTED ON THE Y AXIS.
C      YH   IS THE LAST VALUE OF Y PRINTED ON THE Y AXIS.
```

TABLE 4.2.2-3 (CONTINUED)

```
C      IF  =0 WILL CAUSE THE LOWEST AND HIGHEST VALUES IN THE X AND
C          Y ARRAY TO BE USED FOR THE LIMITS OF THE X AND Y AXES OF
C          THE PRINTED GRAPH.
C          =1 WILL CAUSE THE VALUES TO XL,XH,YL, YH, IN
C          THE CALLING SEQUENCE, TO BE USED AS THE LIMITS FOR THE
C          X AND Y AXES.
C
       HOLL =-918536128
       BLNK=1077952576
       BIT=1262501952
       CRO=1512833600
       FMS=1614823488
C
C     ON SYSTEMS WHERE DATA STATEMENTS ARE PERMISSIBLE, DELETE
C     THE 5 CARDS ABOVE AND USE THE DATA STATEMENT WHICH FOLLOWS.
C     OTHERWISE, USE THE CARDS ABOVE WITH THE PROPER DECIMAL
C     EQUIVALENTS.  LITERALLY,  HOLL = 1, BLNK =    , BIT = . ,
C     CRO = + , FMS = -
C
C      DATA HOLL,BLNK,BIT,CRO,FMS/1HH,1H ,1H.,1H+,1H-/
C
       NLY=42
       NLX=100
       NLY1=NLY+1
       NLX1=NLX+1
C
C      NLY IS THE NUMBER OF LINES ON THE VERTICAL AXIS.
C      NLX IS THE NUMBER OF COLUMNS ON THE HORIZONTAL AXIS.
C
       WRITE(IPR,100)
  100  FORMAT(1H1)
       WRITE(IPR,106)
       WRITE(IPR,107)DH,T
       IF(DH-1)31,30,31
    30 WRITE(IPR,108)
       GO TO 32
    31 IH=2**(DH-2)
       FD1=2100.*IH
       FD2=2*FD1
       WRITE(IPR,109)FD1,FD2
    32 WRITE(IPR,110)D
       WRITE(IPR,111)SLG,X(JSL),Y(JSL)
       WRITE(IPR,112)SGL,X(JSH),Y(JSH)
       WRITE(IPR,113)XO,YO
       XSH=X(1)
       XLA=X(1)
       L1=N-1
       DO 2 I=1,L1
       L2=I+1
C
C      ***** THIS SECTION REARRANGES THE GIVEN DATA
C      IN ORDER OF DECREASING Y VALUES, I.E.,
C      YMAX=Y(1) AND YMIN=Y(N).
C
       DO 2 J=L2,N
```

TABLE 4.2.2-3 (CONTINUED)

```
      IF(Y(I)-Y(AJ))1,2,2
    1 DUM=Y(I)
      Y(I)=Y(J)
      Y(J)=DUM
      DUM=X(I)
      X(I)=X(J)
      X(J)=DUM
    2 CONTINUE
C     *****
      IF(II)10,10,11
   11 XSM=XL
      XLA=XH
      YSM=YL
      YLA=YH
      GOTO 12
   10 DO 6 L2=1,N
      IF(XSM-X(L2))4,4,3
    3 XSM=X(L2)
    4 IF(XLA-X(L2))5,6,6
    5 XLA=X(L2)
    6 CONTINUE
      YSM=Y(N)
      YLA=Y(1)
   12 DX=(XLA-XSM)/NLX
      DY=(YLA-YSM)/NLY
      YBASE=NLY+1./6.
      IP=0
      LIN=0
      A(1)=HOLI
   13 LIN=LIN+1
      IM=0
      DO 14 I=2,NLX1
   14 A(I)=BLNK
      IF(LIN-NLY)15,15,23
   15 IP=IP+1
      IF(IP-8)16,16,20
   16 RAT=YBASE-LIN
      IF(Y(IP)-YSM-DY*RAT)20,17,17
   17 DO 19 I=2,NLX1
      RAT=I-0.5
      II=(X(IP)-XSM-DX*RAT)18,18,19
   18 A(I)=BIT
      IM=MAX0(I,IM)
      GOTO 15
   19 CONTINUE
      GOTO 15
   20 IP=IP-1
      IF(LIN-1)21,21,28
   28 IF(MOD((NLY1-LIN),6))22,21,22
   21 RAT=NLY1-LIN
      DUM=YSM+DY*I
      WRITE(IPR,101)VT(LIN),DUM,CRO,(A(I),I=2,IM)
      GOTO 13
   22 WRITE(IPR,102)VT(LIN),(A(I),I=1,IM)
      GOTO 13
```

TABLE 4.2.2-3 (CONTINUED)

```
   23 DO 25 I=1,NLX1
      A(I)=BMS
      IF(MOD(I,10)-1)25,24,25
   24 A(I)=CRO
   25 CONTINUE
      WRITE(IPR,101)VT(LIN),YSM,(A(I),I=1,NLX1)
      IJ=(NLX-1)/10+1
      DO 26 I=1,IJ
      RAT=(I-1)*10
   26 AXIS(I)=XSM+DX*RAT
      WRITE(IPR,103)(AXIS(I),I=1,IJ)
      WRITE(IPR,105)
  101 FORMAT(11X,A1,2X,F4.0,1X,101A1)
  102 FORMAT(11X,A1,7X,101A1)
  103 FORMAT(11X,10F10.0)
  105 FORMAT(/40X,36HAXIAL DISTANCE IN JET EXIT DIAMETERS)
  106 FORMAT(/30X,44HNEAR-FIELD SOUND PRESSURE LEVEL CONTOURS FOR,
     1 11H A HEATED JET)
  107 FORMAT(/40X,12HMACH NO. IS ,F4.2,13H   TEMPERATURE IS ,F5.0)
  108 FORMAT(40X,41HOVERALL BAND, FD = 1050. TO FD = 268,800.)
  109 FORMAT(40X,18HOCTAVE BAND, FD = ,F5.0,9H TO FD = ,F6.0)
  110 FORMAT(/45X,42HTHE FOLLOWING DATA ARE USED IN DETERMINING
     1 18H THE VALUES TO BE ,/
     245X,56HASSIGNED TO THE SPL CONTOURS.  THE MAXIMUM ALWAYS OCCURS,
     3/45X,32HCLOSEST TO THE EXHAUST BOUNDARY.,/
     448X,36HTHE INCREMENT BETWEEN CONTOURS IS ,F4.0,
     5H DECIBELS)
  111 FORMAT(48X,15HTHE MAX SPL IS ,F4.0,15H DB LOCATED AT ,F6.1,
     113H DIA. AXIALLY,/50X,7HAND AT ,F6.1,15H DIA. LATERALLY)
  112 FORMAT(48X,15HTHE MIN SPL IS ,F4.0,15H DB LOCATED AT ,F6.1,
     113H DIA. AXIALLY,/50X,7HAND AT ,F6.1,15H DIA. LATERALLY)
  113 FORMAT(48X,33HREFERENCED TO THE SOURCE LOCATION,/
     1 55X,4H AT ,F4.1,21H DIA. AXIALLY AND AT ,F4.1,
     2 16H DIA. LATERALLY.)
      RETURN
      END
      SUBROUTINE REGI(R1,R2,N,TH,D,IR)
C
C     THIS ROUTINE USES A RECURSIVE INTERPOLATION SCHEME KNOWN AS
C     REGULA FALSI ( FALSE POSITION).  ALTHOUGH CONVERGENCE IS
C     THEORETICALLY GUARANTEED, CERTAIN SPECIAL CASES MAY CONVERGE
C     VERY SLOWLY WHEN DY/DX IS RELATIVELY LARGE.
C
      DIMENSION F(16,37),R(16,37),X(3),Y(3),CC(17,4)
      COMMON IRD,IPR,CC,ALP,DH,I,C4,C5,C6,C7,HH,I,R


      F=.01
      IR=0
      XL=AMIN1(R1,R2)
      XH=AMAX1(R1,R2)
   10 CALL SOND(TH,XL,YL,SP)
      CALL SOND(TH,XH,YH,SP)
      C=ABS(D)
      F(I,N)=YL-AMOD(YL,C)
```

TABLE 4.2.2-3 (CONTINUED)

```
C
C  F(1,N) NOW EQUALS THE LARGEST MULTIPLE OF D WHICH IS
C  LESS THAN YL.
C
      X(3)=1.0
      IF(YH-YL)11,12,12
   11 C=-C
      F(1,N)=F(1,N)-C
      X(3)=-1.0
C
C  COMPUTE ALL INTEGRAL MULTIPLES OF D WHICH LIE BETWEEN YL AND YH.
C
   12 DO 20 I=2,30
      IR=I-1
      F(I,N)=F(IR,N)+C
      IF((F(I,N)-YH)*X(3))20,20,21
   20 CONTINUE
   21 C=X(3)
      IF(IR-15)26,32,27
   27 IR=15
      GO TO 32
   26 IF(IR-1)31,31,32
   32 DO 100 J=2,IR
      X(1)=XL
      X(2)=XH
      Y(1)=YL
      Y(2)=YH
C
C  THE NEXT STATEMENT DETERMINES THE MAXIMUM NO. OF ITERATIONS.
C
      DO 99 KK=1,20
C
C
C
      X(3) = (X(1)+X(2))*.50
      CALL SOND(TH,X(3),Y(3))
      RR=(F(J,N)-Y(3))*C
      IF(ABS(RR)-E)29,29,23
   23 IF(RR)25,29,24
   24 X(1)=X(3)
      Y(1)=Y(3)
      GOTO 99
   25 X(2)=X(3)
      Y(2)=Y(3)
   99 CONTINUE
C
C
C
C
C
C
C
      WRITE(IPR,1)TH,F(J,N),PR
    1 FORMAT(30H DOES NOT CONVERGE AT THETA = ,F6.2,
     112H AND F(J) = ,F10.4,17H WITH RESIDUAL = ,F6.3)
```

TABLE 4.2.2-3 (CONTINUED)

```
      GOTO 100
   29 R(J,N)=X(J)
  100 CONTINUE
   31 IR=IR+1
      F(IR,N)=YH
      R(IR,N)=XH
      F(1,N)=YL
      R(1,N)=XL
      RETURN
      END
      SUBROUTINE SOND(TH,R,SPL,SP)
      DIMENSION C(17,4)
      COMMON IRD,IPR,C,ALP,DM,T,C4,C5,C6,C7,K
C
C THIS SUBROUTINE CALCULATES THE SOUND PRESSURE LEVEL.
C INPUT REQUIRED IS THE ANGLE THETA, AND THE RADIUS R.
C SOND1 CALCULATES ALP,C4,C5,C6, AND C7.
C
      G1=ALP*DM**2
      G2=COS(.01745329*TH)
      RAT=1.0+C6*EXP(-C7*R/4.0)
      G3=1.0+C6*EXP(-C7*R)
      G4=DM*G2
      G5=1.0+C4*EXP(-C5*TH*.01745329)/RAT
      G6=((1.0+G1)/((1.0-G4/G3)**2+G1))**2.5
      G7=(1.0+G2**4)/G5
      SP=10.0*ALOG10(G6*G7)
      G1=DM**2.340/R**2
      G2=10.050*(T/530.0)**.930/R**4
      G3=15.180*DM**.890*(T/530.0)**1.110/R**6
      PL=10.0*ALOG10(G1+G2-G3)
      STH=10.0*ALOG10(C(17,K)*T**1.540*DM**4)
      SPL=SP+PL+STH
      RETURN
      END
      SUBROUTINE SOND1
      DIMENSION C(17,4)
      COMMON IRD,IPR,C,ALP,DM,T,C4,C5,C6,C7,K
C
C     THIS SUBROUTINE COMPUTES VALUES FOR ALP,C4,C5,C6, AND C7
C     FOR USE IN SOND, THE SOUND PRESSURE LEVEL SUBROUTINE.
C     MUST BE GIVEN THE C(I,K) MATRIX, I = 1,17, K = 1,4, AND A
C     VALUE FOR K.  THE VALUES COMPUTED ARE FOR SPECIFIED VALUES
C     OF DM AND T.
C
      W=T*.001
      ALP=C(1,K)*DM**C(2,K)*W**(C(3,K)+C(4,K)*DM)
      C4=C(5,K)*DM**C(6,K)*W**(C(7,K)+C(8,K)*DM)
      C5=C(9,K)*DM**C(10,K)*W**(C(11,K)+C(12,K)*DM)
      C6=17.5*(W/3.0)**(.890*(DM**2-1.0))
      C7=.410*(W/3.60)**(.566*(DM**2-1.0))
      RETURN
      END
      SUBROUTINE REGION(A,B,X,I)
C     THIS SUBROUTINE DETERMINES WHETHER X IS IN THE CLOSED
C     INTERVAL (A,B).
```

TABLE 4.2.2-3 (CONCLUDED)

```
C         IF X IS IN THE INTERVAL, I = 1 IS RETURNED.
C         IF X IS NOT IN THE INTERVAL, I = 2 IS RETURNED.
C
      I=1
      IF(A-X)1,2,3
    1 IF(X-B)2,2,3
    3 I=2
      X=A
    2 RETURN
      END
/DATA
  LATERAL DISTANCE IN JET EXIT DIAMETERS
.82393     .4176      .32555     .74038     -1.24      -1.7269
.2482      -3.4538    -2.3019    -1.3266    -4.0206    -4.7187
1.4745     1.3507     2.6807     3.2662     45.759     18.932
202.88     331.55     -2.1086    -3.2199    3.8424     .53294
3.3692     1.3276     10.52      9.5983     -2.3864    -.1765
-8.0293    -6.829     12.803     8.4045     10.491     10.429
-1.8167    -1.5494    -.019983   .36732     -1.7894    - .16571
.73551     .89132     1.1641     .22007     -.76495    -.876
4.512      5.2846     4.5428     2.6963     -.028729   1.3015
.20763     1.8687     .789       .85116     .27691     3.0174
-.51772    -.60053    .036298    - 2.1329   5.5    E+094.78   E+08
1.46   E+091.15   E+09
ACTION COMPLETE.
BEGIN ACTIVITY.
```

REFERENCES FOR SECTION 4.2.2

1. Thomson, A. G. R., "Acoustic Fatigue Design Data, Part I," AGARDograph No. 162 (AGARD-AG-162, Part I), 1972.

2. Cockburn, J. A. and Jolly, A. C., "Structural-Acoustic Response, Noise Transmission Losses and Interior Noise Levels of an Aircraft Fuselage Excited by Random Pressure Fields," AFFDL-TR-68-2, August 1968.

3. Hermes, P. H., and Smith, D. L., "Measurement and Analysis of the J57-P21 Noise Field," AFFDL-TR-66-147, Wright-Patterson Air Force Base, Ohio, Nov. 1966.

4. Sutherland, L. C. and Brown, D., "Prediction Methods for Near Field Noise Environments of VTOL Aircraft," AFFDL-TR-71-180, Wright-Patterson Air Force Base, Ohio, 1972.

5. Lighthill, M. J., "Sound Generated Aerodynamically," The Bakerian Lecture, 1961, Proceedings of the Royal Society (London)A267, 157-182 (1962).

6. Plumblee, H. E., "Near-Field Noise Prediction Method for Heated Jets," Published in Proceedings of Conf. on Current Development in Sonic Fatigue, Southampton, July 1970.

7. Plumblee, H. E., Ballentine, J. R. and Passinos, B., "Near Field Noise Analyses of Aircraft Propulsion Systems with Emphasis on Prediction Techniques for Jets," AFFDL-TR-67-43, Wright-Patterson Air Force Base, Ohio, 1967.

8. Anon., MIL-8893 (USAF), Military Specification, Airplane Strength and Rigidity, Sonic Fatigue, 31 March 1971.

9. Rogers, O. R., and Cook, R. [illegible]; "Environmental Aspects of Sonic Fatigue," WADC-TN-57-68, Wright-Patterson Air Force Base, Ohio, February 1957.

4.2.3 PROPELLER AND ROTOR NEAR-FIELD NOISE

The following section on propeller (and rotor) noise contains two design methods based on theory, but liberally modified, by experimental observations. Only a brief description of the origins of propeller noise in included. However an excellent review of and bibliography on noise from propellers, rotors and lift fans is given by Marte and Kurtz (1). Also, a very comprehensive study of VTOL effects on propeller and rotor noise is given by Sutherland and Brown (2).

The noise from propellers is generally assumed to have origins from four sources. Three of these are dipole in character. These are torque and thickness, which in an aerodynamic reference result in induced drag and form drag, and result in a lateral dipole acoustic source. Noise from propeller vorticity is broadband in nature and is a longitudinal dipole acoustic source. Propeller thrust generates noise as an acoustic quadrupole. Thrust as well as torque and thickness generate discrete tone sound.

Lowson (3) and Wright (4) have recently developed general theories for propeller noise generation which account for unsteady and unsymmetrical circumferential blade forces. However t ese theories have not been reduced to general design handbook useage. The harmonic content is of great concern and if the accuracy of the prediction methods presented in the following two sections is inadequate, then the Lowson and Wright methods should be incorporated in the user's designprocedures, in the form of computer programs.

In the following sub-sections, two similar propeller noise prediction methods are presented. The first, which has its origins with Metzgar, et al, (5), has been developed for multi-engine conventional propeller driven aircraft. The second prediction method is based on Lowson's (6) work, but relies on empirical relationships derived from published near field propeller noise data. The method is not accurate in the rotor plane, but is satisfactory at angles greater than 15° from the rotor plane. Harmonic roll-off rates and maximum levels at angles away from the propeller plane have been derived from experimental data.

4.2.3.1 Generalized Propeller-Noise Estimating Procedure

A simple generalized method of estimating near- and far-field propeller noise based, in part, upon data in the open literature has been developed by Metzgar, et al. (5) and is also included in the Marte and Kurtz survey report (1). This method is presented here.

The near-field for sound level estimates is defined as locations within one diameter of the propeller tip. The accuracy of the sound level estimates was determined by comparison of predicted and measured sound levels for several propeller configurations during both test stand and flight operations. In general, the accuracy of the predicted near-field overall and fundamental frequency sound levels were found to be within +5 to -9 dB of the measured levels (5). However, for propellers up to

15 ft in diameter, where the tip Mach number to horsepower ratio is less than 0.003 (i.e., $M_t/HP < 0.003$), estimated overall and fundamental frequency noise levels were within ±3 dB of measured levels.

Estimate of Near-Field Propeller Noise: The steps in determining near-field propeller-noise levels on the fuselage (see Figure 4.2.3-1a) during static and dynamic conditions are:

(1) Obtain a reference level L_1 from Figure 4.2.3-2. This gives a partial level based on the power input to the propeller.

(2) Calculate the correction to the partial level for number of blades and propeller diameter; add 20•log 4/B where B is the number of blades; and add 40•log 15.5/D where D is the propeller diameter in feet.

(3) Obtain the correction factor from Figure 4.2.3-3. This accounts for the rotational speed of the propeller (M_t = in-plane tip Mach number) as well as the distance from the point of interest to the propeller disc.

(4) Obtain the correction factor from Figure 4.2.3-4. This corrects for fore and aft (with reference to the plane of propeller rotation) fuselage position.

(5) Obtain the correction factor from Figure 4.2.3-5. This accounts for the effect of a reflecting surface (fuselage) in the sound field.

(6) Sum the data from steps 1 through 5 to estimate the overall sound pressure level at the point of interest.

(7) The harmonic distribution of the noise estimated in steps 1 through 6 is found in Figure 4.2.3-6 (M_h = true tip Mach number, including the forward flight component.)

(8) The harmonic levels of step 7 are combined using the chart in Figure 4.2.3-7 to derive octave band levels. If more than two levels are to be added, add in pairs to increase the accuracy.

Sample Calculation of Near-Field Noise: A sample calculation of near-field noise (see Figure 4.2.3-1b), using the method described in the preceding paragraphs, is presented here.

Aircraft speed (V_1):	125 knots = 210 ft/s
Propeller diameter (D):	9 ft
Power to propeller:	300 hp
Propeller speed (N):	1584 rpm
Number of blades (B):	3

Radial distance (Z) from propeller to interest point: 1.25 ft

Fore/aft distance (X) from propeller to interest point: 0 ft

Speed of sound (a_o): 1125 ft/s

		Partial Noise level, dB
Step 1.	From Fig. 4.2.3-2, L_1	121.0
Step 2.	Add 20•log (4/3)	+2.5
	Add 40•log (15.5/9)	+9.5
Step 3.	Z/D = 1.25/9 = 0.139 $V_t = \pi \cdot D \cdot N/60 = 3.14 \cdot 9 \cdot 1584/60 = 746$ fps $M_t = V_t/a_o = 746/1125 = 0.66$	
	Then, from Figure 4.2.3-3, the correction is:	-1
Step 4.	Z/D = 0.139 X/D = 0 Then, from Figure 4.2.3-4, the correction is	0
Step 5.	X/D = 0 The fuselage has a circular wall, Then from Fig. 4.2.3-5, the correction is	+4
Step 6.	The summation of steps 1 through 5 gives the overall sound pressure level on the fuselage at location Z = 1.25 ft, X = 0 ft.	136.0
Step 7.	Overall sound pressure level = 136.0 The fundamental blade passage frequency - B•N/60 = 79 Hz	

$$M_h = \frac{(V_t^2 + V_f^2)^{1/2}}{a_o} = \frac{(746^2 + 21^2)^{1/2}}{1125} = 0.69$$

1	2	3	4
Harmonic order	Frequency Hz	Harmonic level, dB re overall SPL (from Fig. 4.2.3-6)	Harmonic level, dB
Fundamental	79	-2	134.0
2	158	-9	127.0
3	237	-13	123.0
4	316	-16	120.0
5	395	-18	118.0
6	474	-19	117.0
7	553	-20	116.0
8	632	-20	116.0
9	711	-20	116.0
10	790	-20	116.0

Step 8. The octave band levels are derived by grouping the harmonics (step 7, column 4) of the blade passage frequency within the associated preferred octave bands and combining the levels using Fig. 4.2.3-7.

1	2	3	4
Preferred octave passbands, Hz	Harmonics of blade passage frequency (step 7, column 2)	Harmonic levels, dB (step 7, column 4)	Octave band level, dB
45-90	79	134.0	134.0
90-180	158	127.0	127.0
180-355	237, 316	123.0, 120.0	124.7
355-710	395, 474 553, 632	118.0, 117.0, 116.0, 116.0	123.0
710-1400	711, 790	116.0, 116.0	119.0
1400-2800	-	-	-
2800-3600	-	-	-
5600-11,200	-	-	-
Overall			135.4

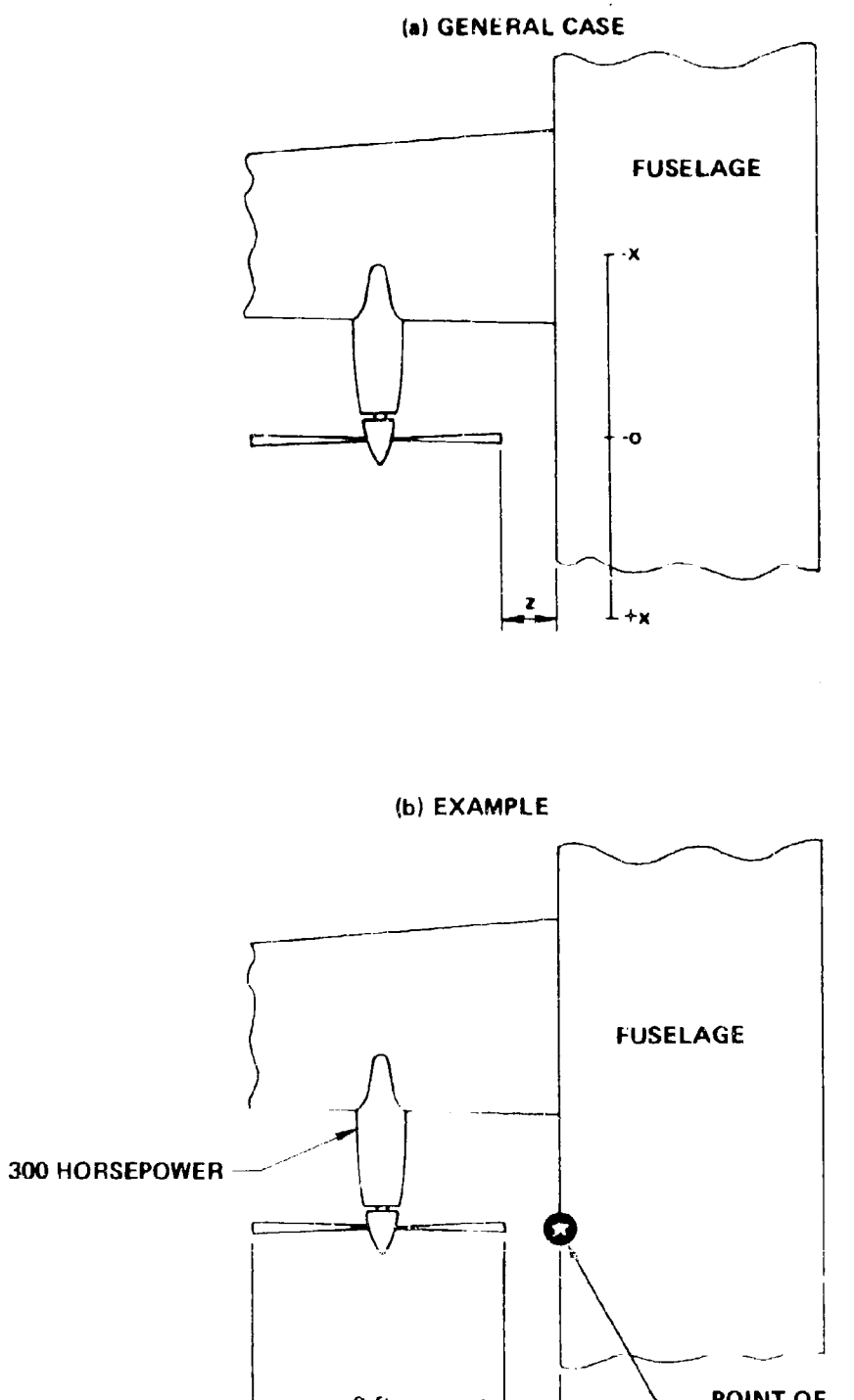

FIGURE 4.2.3-1 FAR-FIELD AXIS SYSTEM FOR PROPELLER SOUND LEVEL ESTIMATES

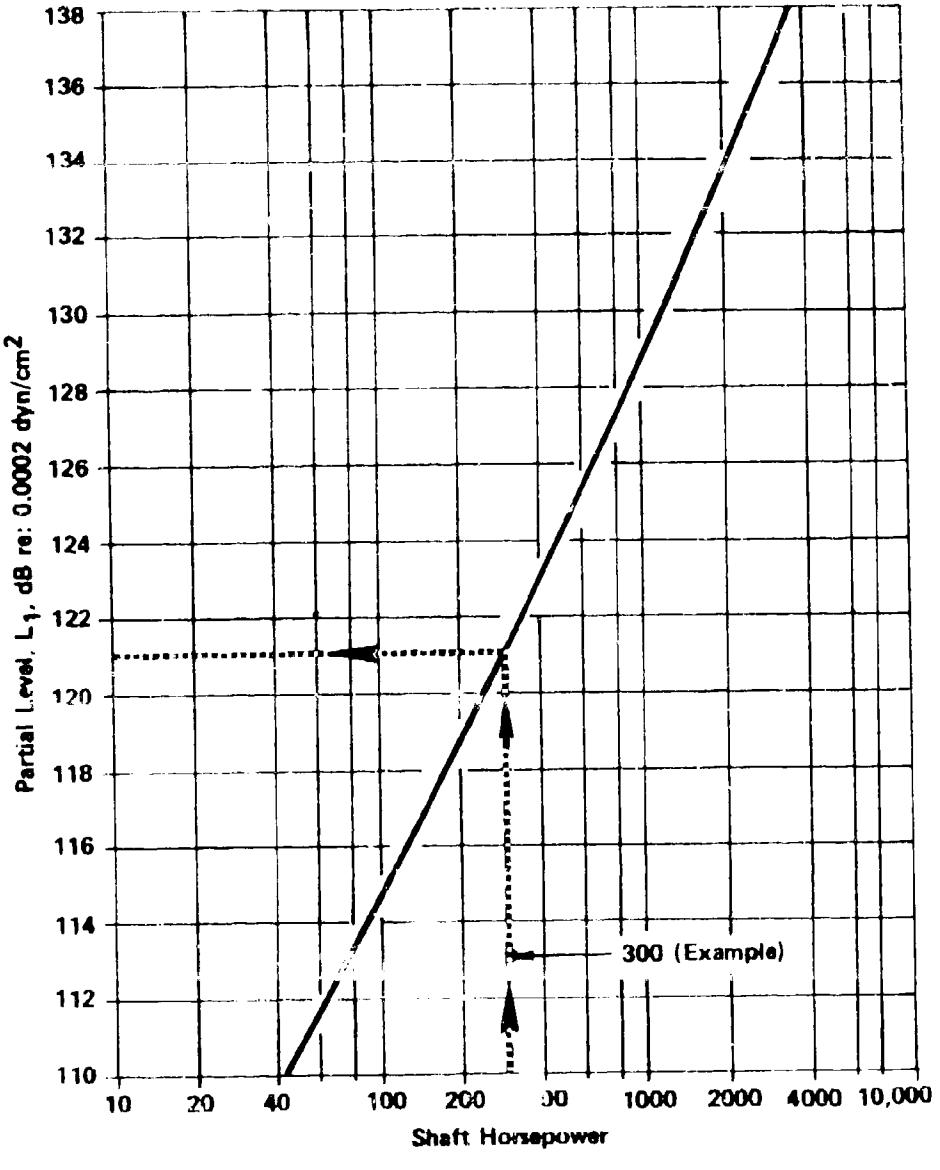

FIGURE 4.2.3-2 PROPELLER NOISE REFERENCE LEVEL SHAFT HORSEPOWER.

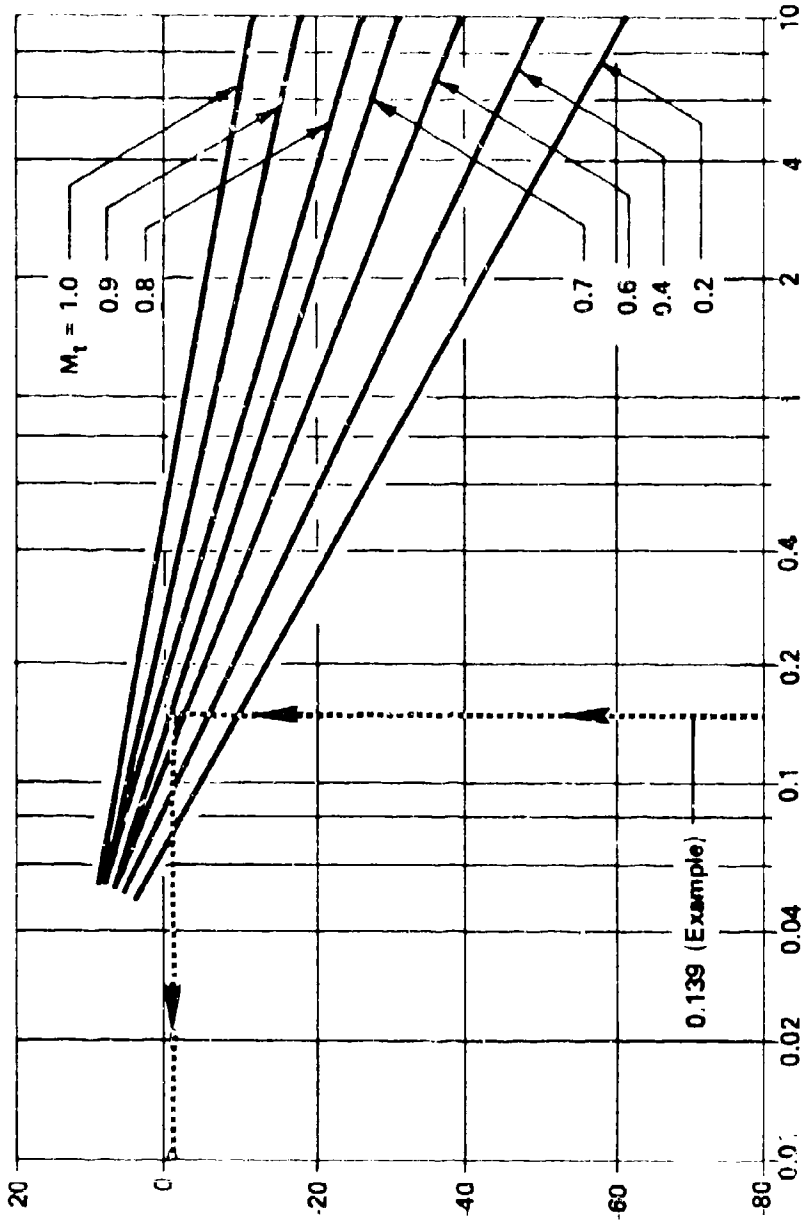

FIGURE 4.2.3-3 CORRECTION FOR SPEED AND RADIAL DISTANCE

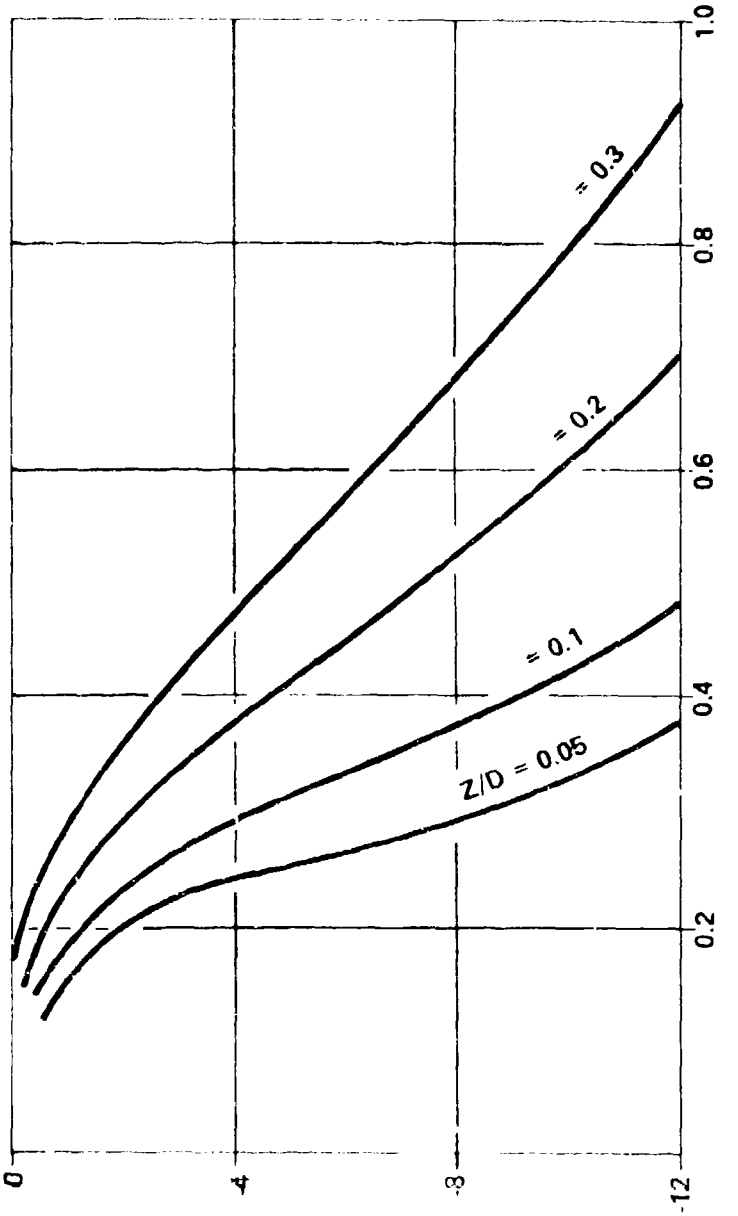

FIGURE 4.2.3-4 VARIATION OF OVERALL, FREE-SPACE PROPELLER NOISE LEVELS WITH AXIAL POSITION, X/D, FORE AND AFT OF PROPELLER PLANE

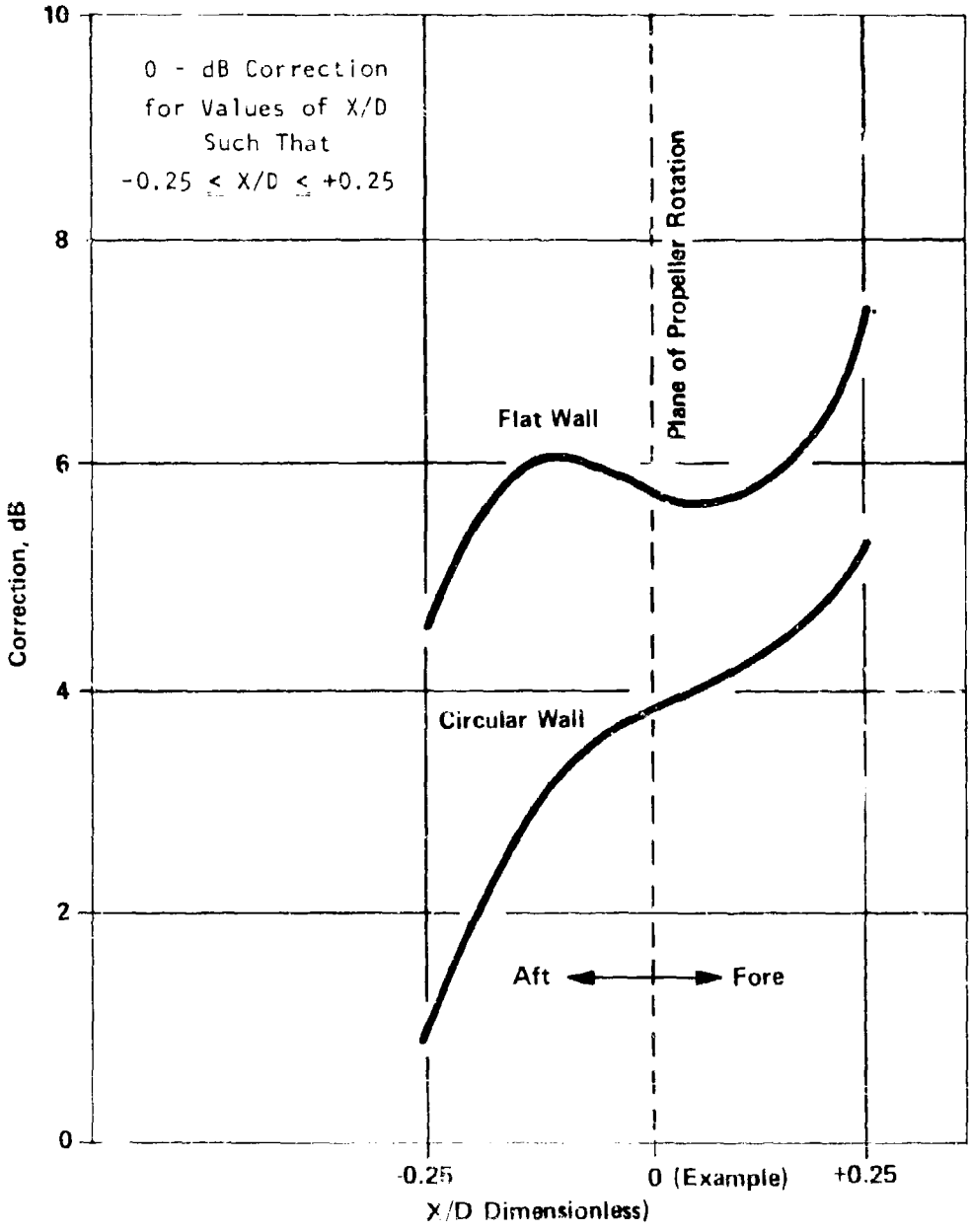

FIGURE 4.2.3-5 EFFECT OF REFLECTIVE SURFACES IN THE PRESSURE FIELD.

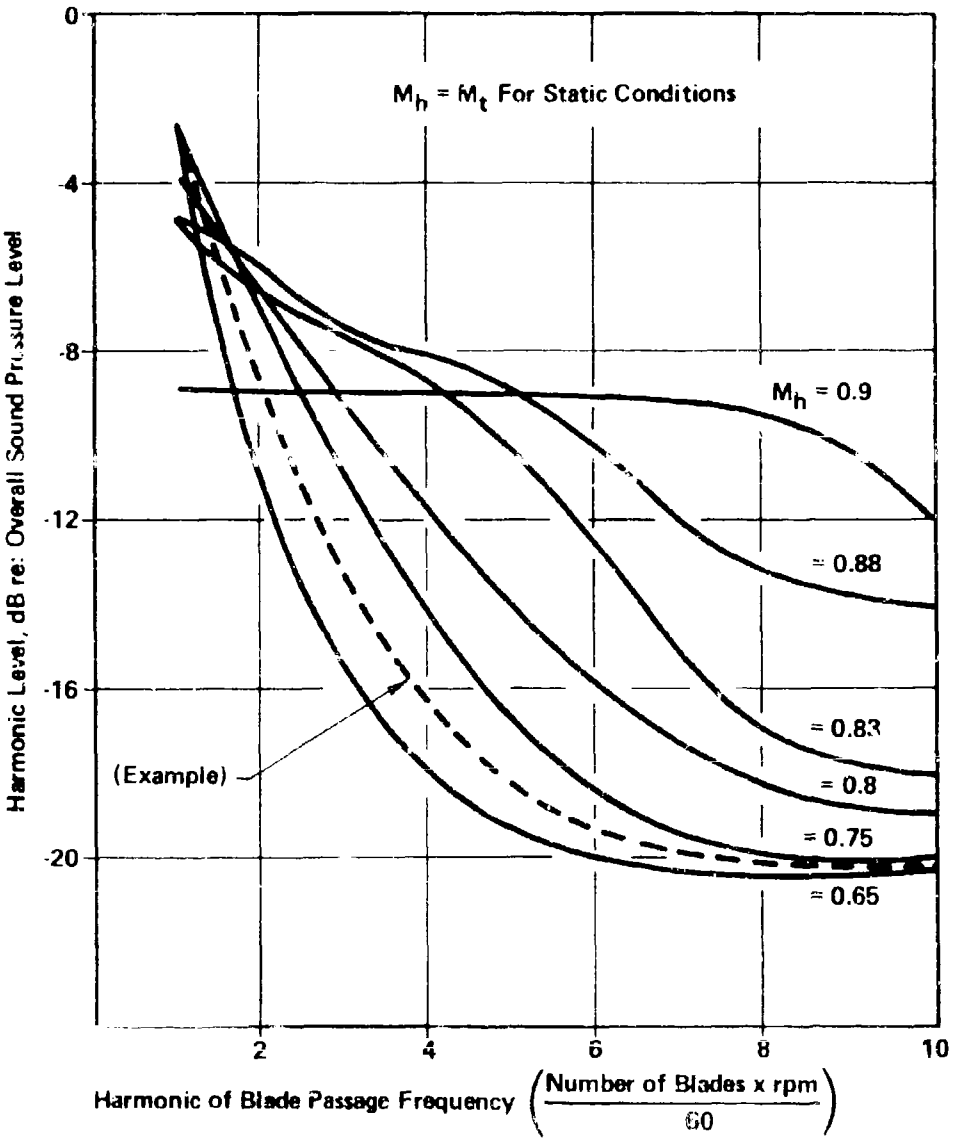

FIGURE 4.2.3-6 HARMONIC DISTRIBUTION OF ROTATIONAL NOISE

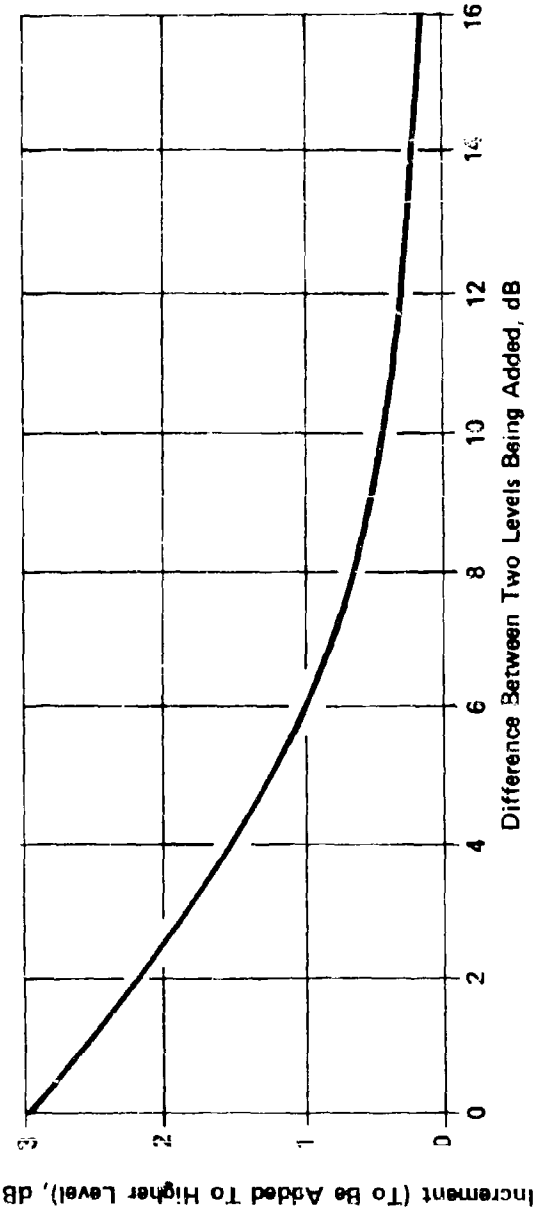

FIGURE 4.2.3-7 CHART FOR COMBINING NOISE LEVELS.

4.2.3.2 Prediction of Propeller/Rotor Near Field Noise Levels

For this section,* the near field of a rotor or propeller is the spatial region within a radius of one rotor-diameter from the center of rotation. In this region, the predominant noise components occur at the blade passage frequency (f_1, Hz) and at multiples thereof (f_2, f_3, etc.). These frequencies are calculated from

$$f_m = \frac{m \times B \times N}{60} \quad \text{Hz} \qquad (4.2.3\text{-}1)$$

where

m = 1, 2, 3, etc.

B = number of blades

N = rotational speed (revolutions per minute)

The noise level prediction method presented requires the first harmonic level (L_1(dB) at f_1(Hz)) to be found by means of Figures 4.2.3-8 and 4.2.3-9 for a position in the plane of the propeller at the desired radius from the propeller center. The level at other azimuthal positions on this radius, and the levels of other harmonics (for m = 2, 3 and 4) at any desired azimuth, will be calculated by the use of corrections (dB) applied to the value of L_1.

Prediction Method:

(1) The required parameters are:

B - the number of blades on each propeller

T - the total thrust developed by each propeller (lb)

N - the rotational speed of the propeller (in rpm)

D - the propeller/rotor diameter (ft)

M_t - the blade tip Mach number

For VTOL aircraft, the maximum thrust is generated at takeoff. In this case, the following approximations can be used to give a preliminary estimate of the thrust and tip Mach no.:

T = Aircraft gross weight/number of propellers

*This method is reproduced from work by Sutherland and Brown (2).

and

$$M_t = \frac{\pi DN}{60 \times 1120} \qquad (4.2.3\text{-}2)$$

(2) Compile or plot a matrix of field points at which sound level estimates are required. For each point, calculate the radius, r (ft) from the center of the propeller, and the azimuthal angle, ψ(degrees) from the disc-plane of the propeller (see Figure 4.2.3-10 for coordinate system definitions). Sound levels will now be estimated for each point at coordinates (r/D, ψ).

(3) From the estimated thrust per blade (T/B) and propeller diameter (D), find level L_1 from Figure 4.2.3-8 or from

$$L_1 = 110 + 20 \cdot \log_{10} (T/B) - 40 \cdot \log D \quad dB \qquad (4.2.3\text{-}3)$$

(4) For the desired field point radius (r/D, $(0.5 \leq r/D \leq 1.0)$, find incremental level $\Delta L^{(1)}$ from Figure 4.2.3-9 or from

$$\Delta L^{(1)} = -40 \cdot \log_{10}[r/D - 0.35] - 6 \quad dB \qquad (4.2.3\text{-}4)$$

(5) For each of the harmonic frequencies $f_m = \frac{m \times B \times N}{60}$ Hz, find the incremental level $\Delta L^{(2)}_m$ from Figure 4.2.3-11 for the appropriate values of M_t and r/D, respectively.

(6) For $\psi = 0$, that is, for levels in the disc-plane, the sound pressure levels, SPL_m(dB re $20\mu N/m^2$) at each frequency f_m(Hz) are given by

$$SPL_m(r/D, \psi) = L_1 + \Delta L^{(1)} + \Delta L^{(2)}_m + \Delta L^{(3)}_{mB,\psi} \quad dB \qquad (4.2.3\text{-}5)$$

where $\Delta L^{(3)}_{mB,\psi}$ is obtained from Figure 4.2.12 for the appropriate values of mB and ψ, respectively.

(7) For structural surface sound pressure levels, add 6 dB to each value if the surface is flat, or 3 to 4 dB for curved surfaces (see also Section 4.2.5).

(8) For field points at $1.0 < r/D < 3.0$ a more elaborate procedure has been developed by Sutherland and Brown (2) which should be referred to if prediction in this region is required. For field points, $r/D > 3$, far-field theories such as those of Lowson (3) and Wright (4) are generally applicable.

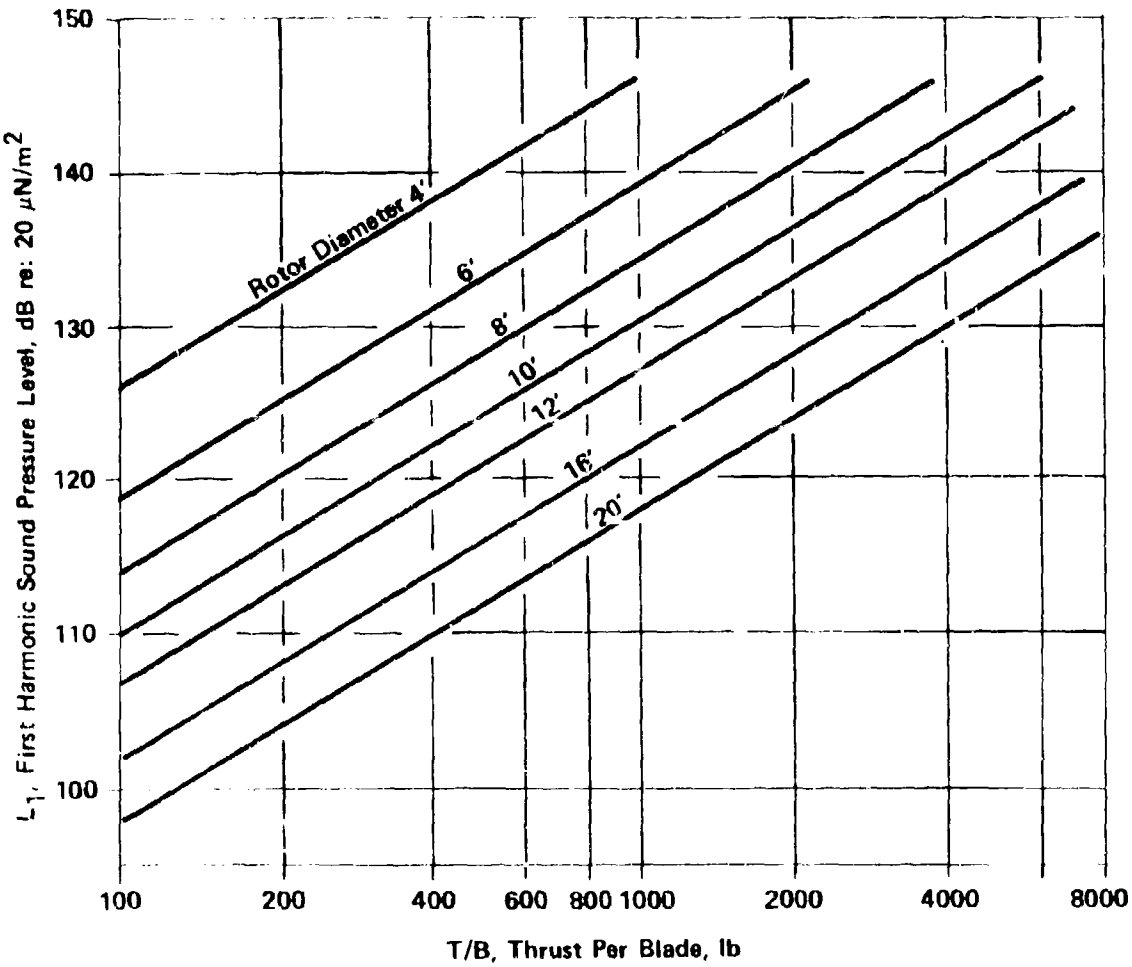

FIGURE 4.2.3-8 PARTIAL SOUND PRESSURE LEVEL, L_1, IN TERMS OF ROTOR DIAMETER AND THRUST PER BLADE

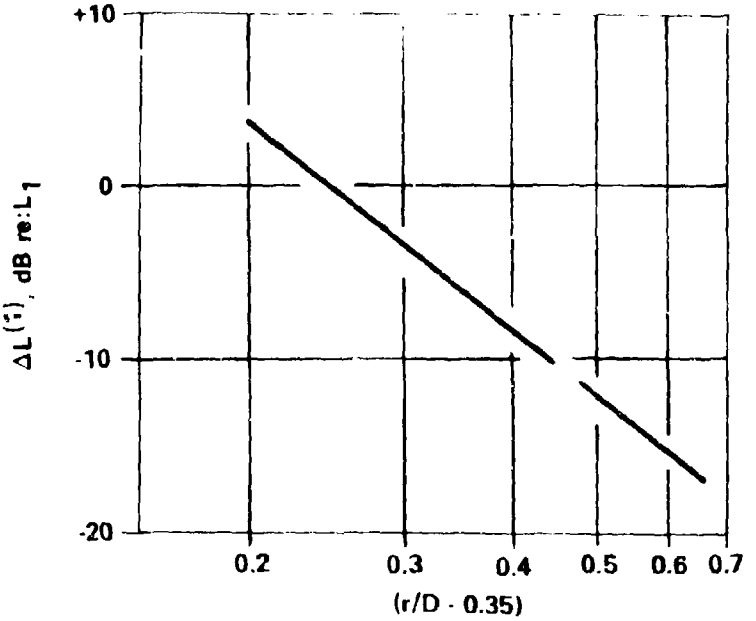

FIGURE 4.2.3-9 SOUND CORRECTION LEVEL, $\Delta L^{(1)}$, FOR REQUIRED OBSERVATION RADIUS FROM ROTOR CENTER, r/D

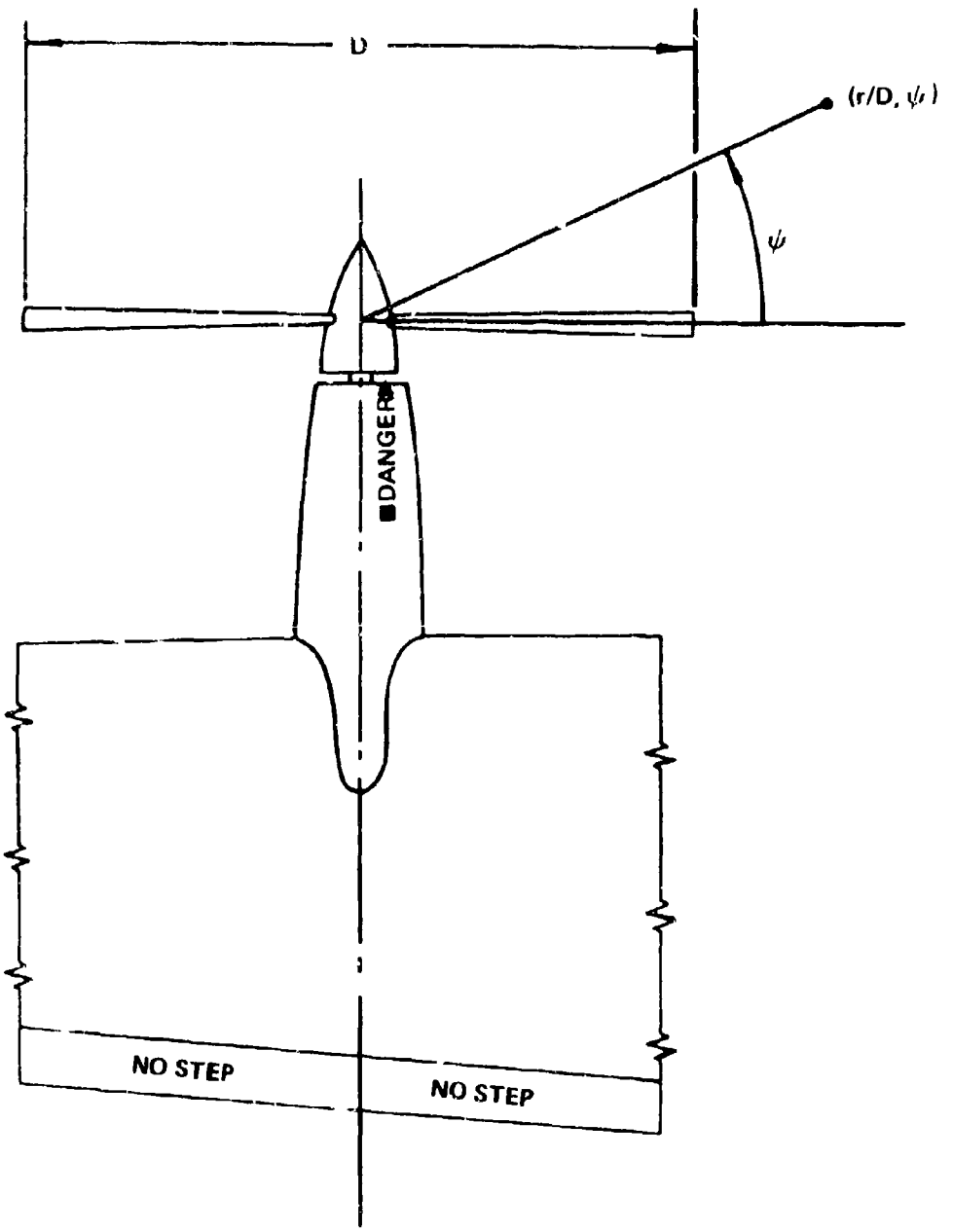

FIGURE 4.2.3-10 PROPELLER COORDINATE SYSTEM FOR NEAR-FIELD NOISE CALCULATIONS

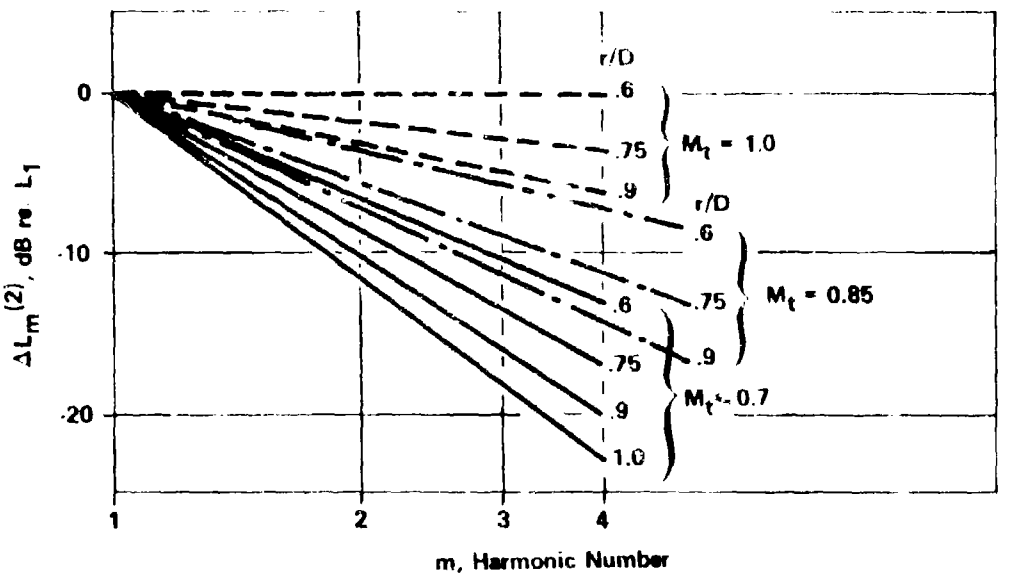

FIGURE 4.2.3-11 SOUND CORRECTION LEVEL, $\Delta L_m^{(2)}$, FOR HARMONIC ORDER, m, IN TERMS OF TIP MACH NUMBER, M_t, AND OBSERVATION RADIUS, r/D

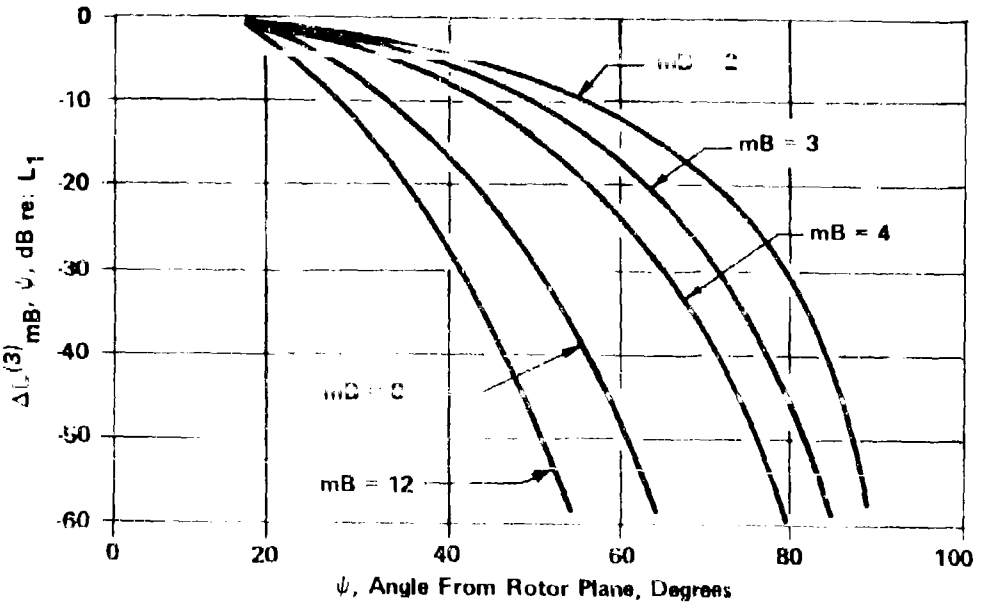

FIGURE 4.2.3-12 SOUND HARMONIC CORRECTION LEVEL, $\Delta L^{(3)}_{mB,\psi}$, FOR AZIMUTHAL ANGLE, ψ (IN DEGREES), FROM ROTOR PLANE

REFERENCES FOR SECTION 4.2.3

1. Marte, J. E. and Kurtz, D. W.; "A Review of Aerodynamic Noise from Propellers, Rotors, and Lift Fans," Jet Propulsion Laboratory. TR-32-1462, January 1970.

2. Sutherland, L. C. and Brown, D.; "Prediction Methods for Near Field Noise Environments of VTOL Aircraft," AFFDL-TR-71-180, Wright-Patterson Air Force Base, Ohio, 1972.

3. Lowson, M. V. and Ollerhead, J. B.; "A Theoretical Study of Helicopter Rotor Noise," Journal of Sound and Vibration, Vol. 9, No. 2, pp. 197-222, March 1969.

4. Wright, S. E.; "Discrete Radiation from Rotating Periodic Sources," Journal of Sound and Vibration, Vol. 17, No. 4, pp. 437-498, 22 August 1971.

5. Metzger, F. B., Magliozzi, B., Towle, G. B., and Gray, L.; "A Study of Propeller Noise Research," Hamilton Standard SP67148, Rev. A, 1961 (revised Nov. 1967).

6. Lowson, M. V.; "The Sound Field for Singularities in Motion," Proceedings of the Royal Society of London, Vol. 286, Series A, pp. 559-572, 1965.

4.2.4 BYPASS FAN ENGINES AND DUCTED PROPELLERS

Although bypass fan engines have been in service for nearly 15 years, no generally applicable methods have been developed for predicting noise within fan ducts. However, it is significant to note that sonic fatigue failures in internal fan duct structure have been noted. Hancock (1) reports the results of noise measurement tests within the TF-34 nacelle and shows an empirical correlation of the data. There is no reason to believe that this correlation is generally applicable to other engines; however, the results are included in this report as being representative of the best available data and may be used as a guide for order of magnitude only. It is strongly recommended that measurements be made in an operational system if fatigue problems are suspected.

A method was developed for estimating near-field noise levels for ducted propellers (outside the duct) by Sutherland and Brown (2). The method, very preliminary in nature, is applicable to VTOL propulsion systems such as ducted propellers, tip-turbine lift fans and other propeller/fan configurations. It includes gross effects of rotor-stator interactions and duct mode characteristics. The method requires the use of the propeller noise calculation procedure of Section 4.2.3.2.

4.2.4.1 Inlet Duct Multiple Pure Tone Noise Level for a High Bypass Ratio Turbofan Engine

The lack of available data and methods for predicting sound levels inside turbojet and turbofan engines has forced engineers and designers to resolve sonic fatigue inlet failures on a case-by-case basis. The description of one such effort is presented by Hancock (1). He presents an experimental program based upon a series of full-scale tests to determine the effect of both engine and aircraft operational parameters on nacelle internal sound levels. An empirical correlation of the data resulted in an order of magnitude estimate for the peak narrow band sound level. This empirical correlation is presented in the form of a design chart.

Derivation: During the development program of an aircraft utilizing a TF-34 turbofan engine, sonic fatigue cracks occurred in the inlet structure and resulted in a design change. The forcing function was in the range of 1 kHz and was assumed to be Multiple Pure Tones (MPT) generated by the supersonic fan blade tips at high power rather than the blade passage at low speeds. These lower frequency tones have been variously called buzz tones, combination tones, and multiple pure tones. They originate as shock waves at the blade leading edges and appear several blade chord lengths forward of the blades at orders of rotational frequency rather than at the blade passage frequency. This phenomenon has been described in the literature (e.g., references 3 and 4).

Hardware Description: A cross section showing relevant engine/inlet conditions is given in Figure 4.2.4-1. The inlet extends forward from the A-4 engine/inlet mating flange shown to approximately 27 inches forward of the TF-34 fan tip. The shroud inner diameter at the fan tip is 43.6 inches. The fan is single stage with 28 blades of 6 1/4 inches chord at the tip and a bypass ratio of 6.23. Other pertinent engine characteristics are summarized in Table 4.2.4-1. This engine has no inlet guide vanes (IGV), and outlet vanes (OGV) are located far enough behind the fan not to affect inlet levels appreciably.

TABLE 4.2.4-1

TURBOFAN CHARACTERISTICS

	TF-34	TF-41-A1
No. of First Stage Fan Blades	28	25
No. of Fan Stages	1	3
Fan Bypass Ratio	6.23:1	0.75:1
RPM at M_V = 1.20 (Std. Day), RPM	6550	7450
Fan Diameter, Inches	43.6	37.8
Fan Mass Flow (Approx.), lb/sec	250	260
Fan Tip Chord, Inches	6.25	6
RPM at Tip Radial M = 1.0, RPM	5760	6650

Acoustic Measurements: Microphone locations are identified in Figure 4.2.3-1 as to three circumferential and five axial stations. The microphones were 0.080 inch in diameter and were installed through the skin to sense surface pressure. Those in the inlet portion of the structure were installed through 1/8 inch diameter flush head rivets and "looked" at the inner surface through 0.040 inch diameter holes approximately 0.030 inch long to prevent slippage into the inlet. This resulted in a cavity resonance of about 7000 Hz, but sharp enough so that data to 5 KHz were not affected. Resolution of higher frequency data would be better done by mounting the diaphram flush.

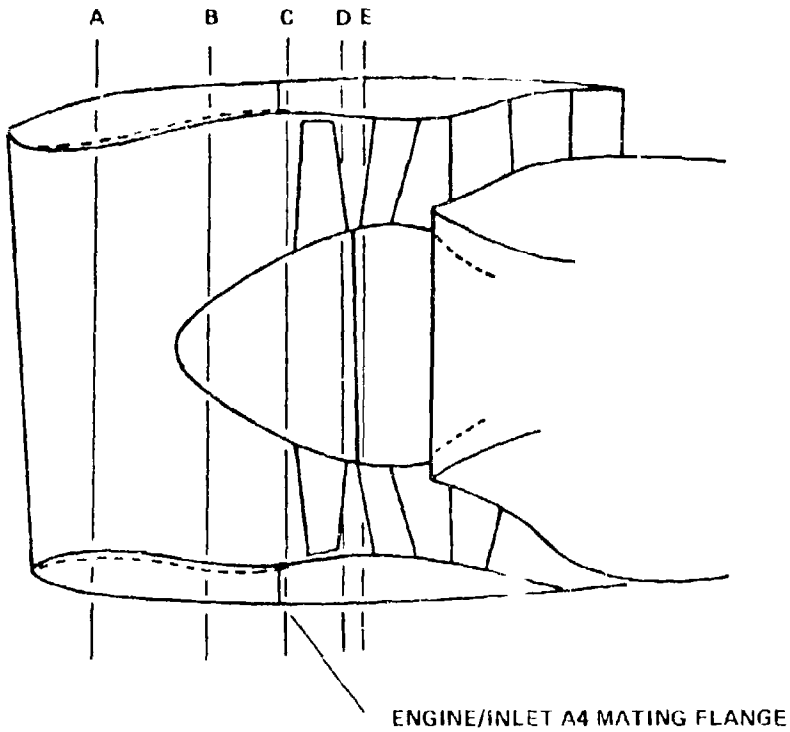

INSTRUMENTATION KEY

MIC NUMBER	1	2	3	4	5	6	7	8	9	10
STATION	A	B	C	D	E	B	B	I	D	D
	54°	54°	45°	45°	45°	215°	300°	50°	225°	315°
DIST FROM FAN TWO TIP (INCHES)	+18.08	+8.31	+.75	-3.44	-4.44	+8.31	+8.31	-3.44	-3.44	-3.44

PLUS INDICATES FORWARD, MINUS INDICATES AFT

FIGURE 4.2.4-1 ENGINE INLET CONFIGURATION AND MICROPHONE LOCATIONS

Structural response was the primary consideration for these measurements, and amplitude definition above 5 KHz was not considered relevant. Pressure measurements were complemented with a number of accelerometers and strain gages located both near and remote from the microphones. Those were important in verifying shaker determined local responses and assessing fatigue life properties under the actual environment, but were not overly important from the standpoint of environment definition. They did, however, allow the early conclusion that failure was caused by local response rather than major hoop or entire panel section response between main frames.

Data were measured on a number of runs with the engine mounted in a test cell to simulate its aircraft mounting. Engine centerline height duplication became a relevant point because of an inlet vortex generated by the presence of the ground plane. Its presence was similar in effect to any other duct obstruction, such as IGV or other protrusion. Inlet levels were increased about 2 dB with the vortex present and varied ±2 dB circumferentially. In general the pressure perturbation area at the base of the vortex covered several square inches with an essentially random characteristic.

This vortex is present during static runs and disappears at a forward aircraft velocity of about 30 Kts. For data recording, fan rpm was slowly varied from idle to maximum power for individual runs. Several cell runs were made, covering an ambient temperature range of 40°F to 95°F. This resulted in maximum attainable fan rpm (N_f) variations from 6400 to 6800 for specific runs.

Figure 4.2.4-2 illustrates narrow band noise spectra obtained at microphone location 2 (8.3 inches forward of the fan) at subsonic and supersonic tip speeds. Blade passage (28 N_f) dominates the subsonic case. With supersonic tips, blade passage has been submerged in the MPT's which now dominate the spectrum. Kester (3) and Philpot (5) have ascribed this phenomenon to non-uniformities between blades and resulting non-uniform sawtooth shock patterns, with non-linear propagation serving to redistribute the energy originally generated with the blade passage.

Various authors (references 5, 6, 7) have proferred methods to calculate overall levels forward of the fan, including MPT contributions. And recently Pickett and Kester (references 8, 9) have shown a general prediction of spectral levels based on a statistical model related to types of blade geometry and manufacturing tolerances. For this design problem, however, it was deemed advisable to empirically define the maximum harmonic levels around 1 KHz, since response in this range had already been determined. Figure 3.2.4-3 shows the relation between overall level, blade passage and the maximum MPT spectral component level occurring between 800 and 2000 Hz as a function of engine rpm. This latter is to be distinguished from blade pass level. To extend the data comparison, available MPT data for the TF-41 engine was utilized. The TF-41 is a three-stage 0.75 bypass ratio fan with 25 first stage blades. Each stage has outlet guide vanes. The variation of overall sound levels with engine RPM is shown for

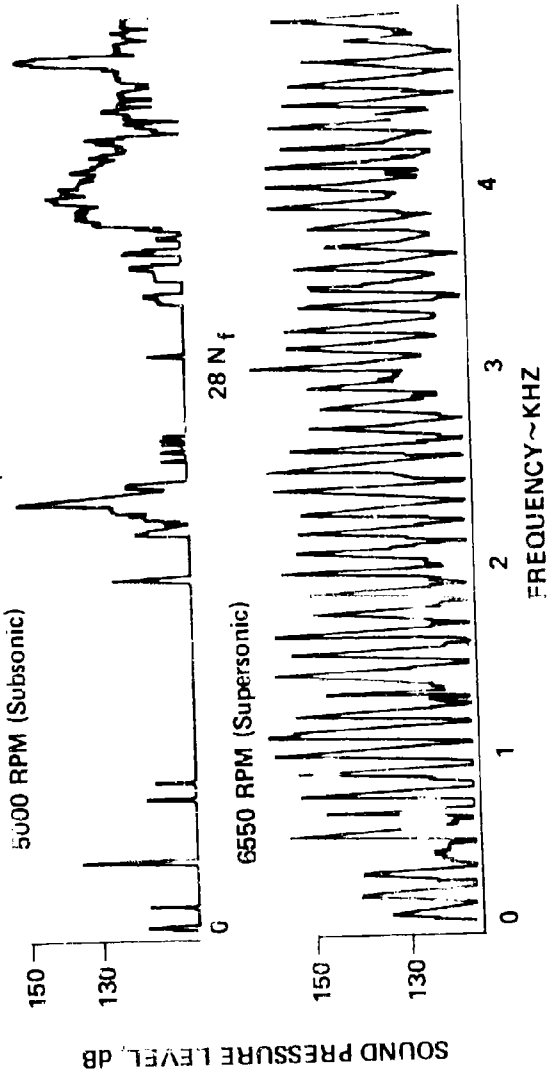

FIGURE 4.2.4-2 10 HERTZ NARROW BAND SPECTRUM AT MICROPHONE LOCATION # 2

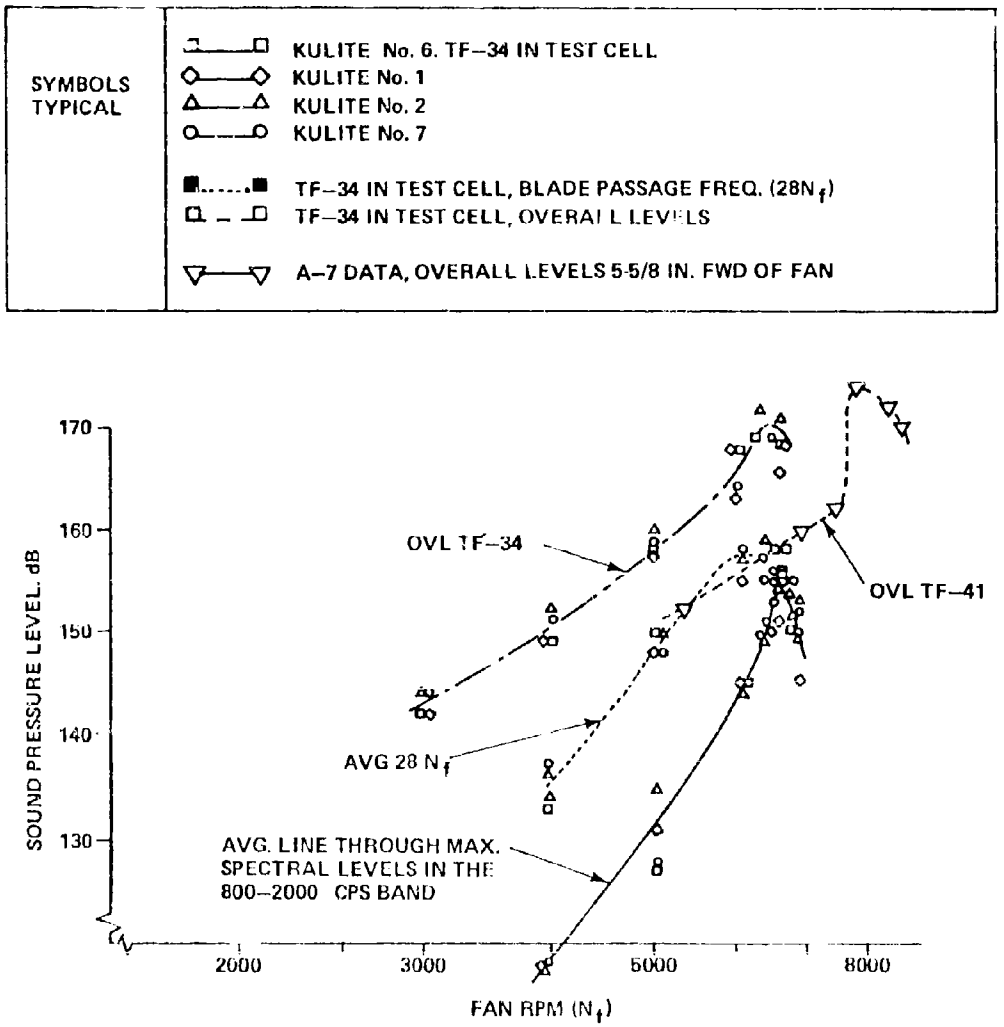

FIGURE 4.2.4-3 INTAKE NOISE LEVEL SUMMARY FROM TEST: ALL MEASUREMENTS

reference. Data in this figure are averaged for the various inlet locations. Overall levels generally follow an $(RPM)^5$ slope. The figure clearly shows that in all cases the inlet levels pass through a peak with increasing rpm. The peak for these data, and that shown in the literature (e.g. reference 3 and 5), occurs at the rpm corresponding to a tip relative Mach number (M_V) of 1.2, i.e., vector sum of axial inflow velocity and tip radial velocity. The axial velocity is a function of inlet airflow characteristics and pressure losses, and requires interpretation in combination with fan performance curves. As shown, the peak for the maximum 800-2000 Hz component is extremely sharp. It was found that with different ambient conditions, causing 1.2 tip M_V to occur at a different rpm, the 1.2 M_V peak also moved along an $(RPM)^6$ slope. This was later confirmed over a wide range of ambient conditions during flight, as was the sharpness of the 800-2000 Hz component peak at 1.2 M_V. Access to a limited number of points in flight and test cell data at different ambient conditions allowed this point to be plotted at engine speeds ranging from 5800 to 6800 rpm. This extremely sharp peak existed in all cases. It was found to vary with an M_V exponent approximating +40 in the range down to 5 dB either side of the peak (M_V = 1.16 - 1.24) and tapered to an exponent of ±24 at 20 dB down. No ready explanation can be offered for this degree of dependence. The TF-41 maximum spectral component in the same frequency range was found to follow a similar trend, although the exponent was not determined. A comparison of spectra at 1.20 M_V is given in Figure 4.2.4-4 for the microphone location just forward of the blade (5.62 in. for the TF-41 and 8.31 for the TF-34). Blade passage tone for the TF-41 remains strong, but the MPT levels are not as high as for the TF-34. Apparently more energy is extracted quicker from the original blade passage tone in the case of the TF-34 than for the TF-41. Reference 9 shows that in certain cases blade suction surface geometry can affect the process - a blade with a larger radius of suction surface curvature (or more nearly flat) will generate a shock pattern extracting more energy. Both fan blades exhibited very nearly flat surfaces to about the three-quarter chord; so obviously this idea did not apply. This is a complex process, and no attempt was made to explain this, beyond a literature review, since TF-41 data were used only in this problem to illuminate the general phenomenon.

Extrapolation to Flight: Once the static test cell noise was defined for a range of operating variables, it remained to extrapolate these or otherwise anticipate the levels during flight to predict life for the new inlet design. Based on available information and a static reference level, a simple empirical relation was developed to describe the maximum MPT spectral level between 800-2000 Hz in terms of flight parameters:

$$\frac{p^2}{} = K M_{ti}^n \rho_a^2 N^6 (BDI)(VP)$$

where K = Reference measured inlet SPL

M_{ti} = Fan Tip Vector Mach No.

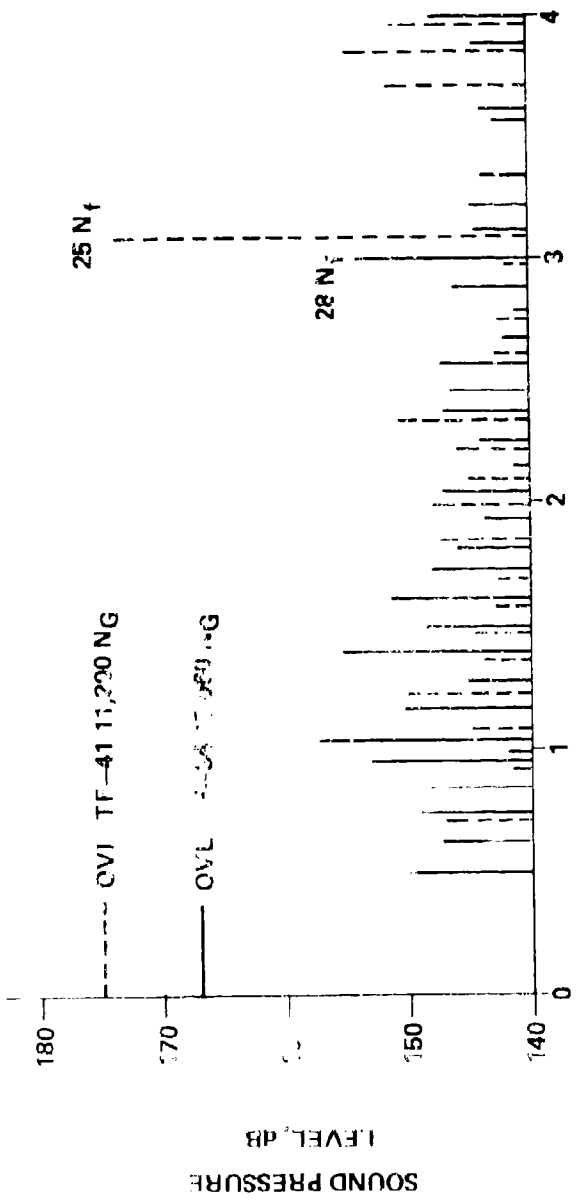

FIGURE 4.2.4-4 COMPARISON OF TF-41 AND TF-34 ENGINE INLET NOISE SPECTRA AT 1.20 FAN TIP RELATIVE MACH NUMBER

n = Experimentally determined exponent varying between 40 at 5 dB down from the peak value at 1.20 M_h and 24 at 20 dB down from the peak.

ρ_a = Local density near the fan tip

N = Fan rotational speed

BDI = Blade Difference Index - a measure of difference between blades of one engine and those of another - assumed ±1 dB averaged over an octave band at high blade loading and ±3 dB at low loading (Reference 8)

VP = Vortex Presence near the ground - disappears at forward speeds near 30 Kts - probably on the order of +2 dB.

These parameters are interrelated to a large extent, and it is probable that a number of other expressions could be developed of equal merit. In any event, these variables have been enumerated for reference and have fit the available data well. In terms of Narrow Band Sound Pressure Level (10 Hz), the above expression is (within 5 dB of the M_V peak):

$$\text{Max SPL(800-2000 Hz)} = K_1 - K_2 \left|\text{Log}\frac{M_h}{1.20}\right| - 20\cdot\log\left(\frac{\rho_o}{\rho_a}\right) - 60\cdot\text{Log}\left(\frac{6650}{N}\right) \pm 3 \text{ db} \qquad (4.2.4\text{-}1)$$

The last term combines the BDI and VP which should average out to about ±3 dB for production engines flown in the nacelle. Recent flight test data have confirmed the expression at altitudes of 10,000, 19,000 and 30,000 ft. within 3 dB. At the two higher altitudes it gave levels 3 dB higher than measured. It was therefore accepted as valid for fatigue life prediction of the inlet. (It is to be emphasized that the 157 dB reference level is a function of engine and nacelle design and if a problem is suspected, then tests should be run on the actual engine).

Design Chart: The chart presented in Figure 4.2.4-5 is a solution to the equation (which gives the SPL in a 10 Hertz bandwidth)

where the constant K_1 should in principal, be determined for each engine, but for present purposes, was determined to be,

$$K_1 = 157 , \qquad (4.2.4\text{-}2)$$

for the TF-34 engine. The constant K_2 was determined to be, $K_2 = 400$, until the term

$$K_2 \left|\log\frac{M_h}{1.20}\right| \geq 20 \qquad (4.2.4\text{-}3)$$

and then the constant K_2 was empirically determined to be $K_2 = 240$.

The other parameters in the equation are defined in the list of symbols above.

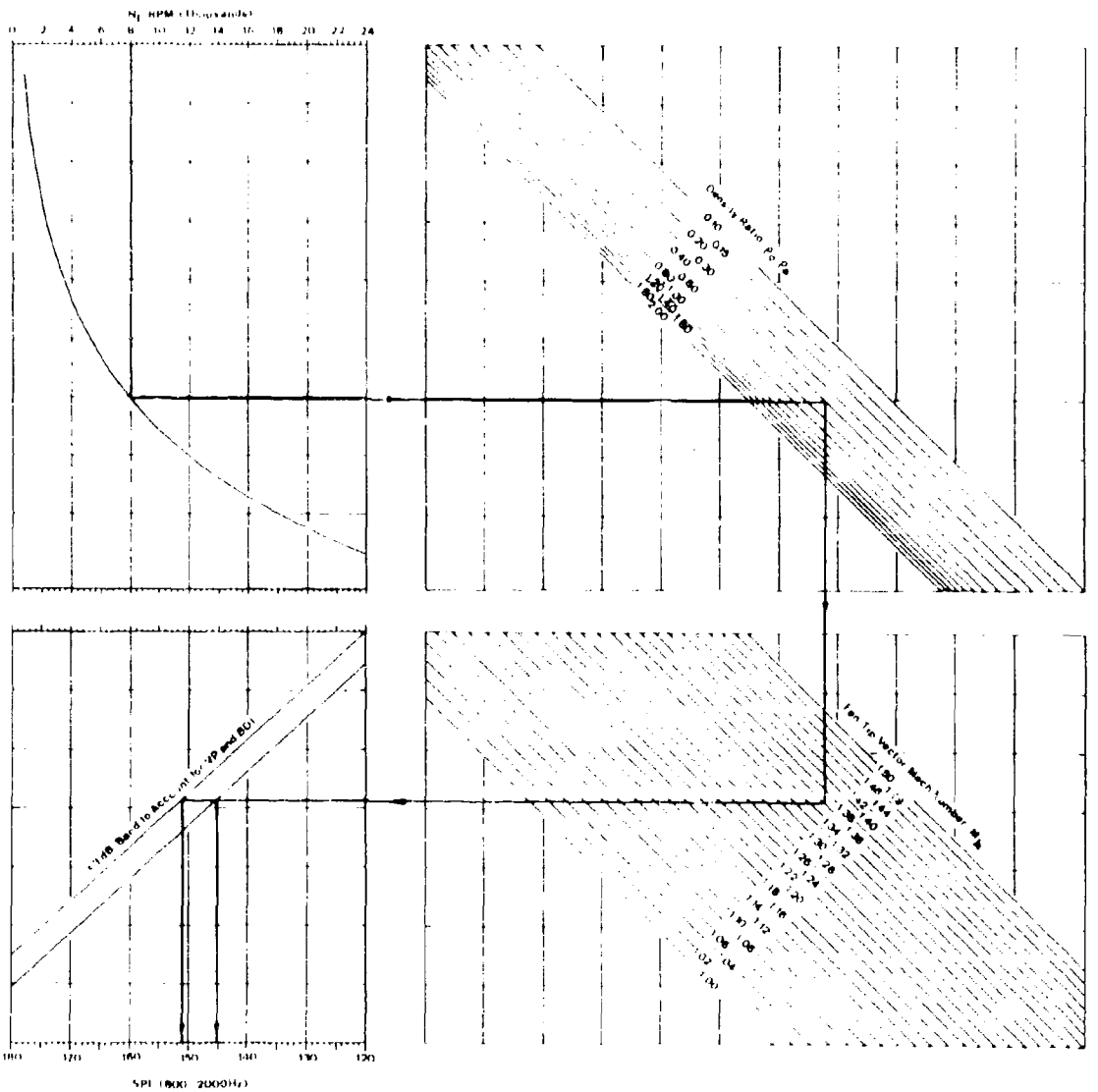

FIGURE 4.2.4-5 DESIGN CHART FOR PREDICTING MAXIMUM SOUND PRESSURE LEVEL (10 Hz. NARROW BAND) IN 800 - 2000 Hz. FREQUENCY BAND FOR BYPASS FAN ENGINE INLETS

4.2.4.2 Noise from Ducted Rotors

In Section 4.2.3.2 a method was presented for determining the near-field noise levels for a free propeller (or rotor). Sutherland and Brown (2) have extended their propeller noise prediction method presented there with some very approximate concepts to permit a gross determination of the effects of a duct on the near-field rotor noise (outside the duct). Rotor-stator interactions are also included in the prediction scheme. This prediction method was compared with limited experimental results by Plumblee, et al., (10) and was found, in that comparison, to be reasonably accurate. However no absolute accuracy or error estimate is possible because of the limited comparisons with experiment.

Prediction Method: The method is designed to be used in conjunction with the free rotor prediction method of Section 4.2.3.2. The following corrections are applied to the free rotor near-field noise levels:

- Duct-Transmission Loss (TL_m)
- Rotor-stator Interaction (Δ_s)
- Directionality Corrections

The additional design parameters required for estimation of these corrections are:

V = the number of stator vanes in close proximity to the rotor disc.

(d/c) = the separation distance between the rotor and stator blades (trailing edge to leading edge) divided by the chord of the downstream blade.

(x/R) = the axial duct-length between the rotor disc and the duct leading-edge, divided by the duct radius (R).

σ = the hub-to-tip radius ratio of the duct.

(1) Calculate the sound harmonic levels for a field point in the disc-plane, at the required r/D, by steps 1 through 6 of Section 4.2.3.2

$$SPL_m(r/D, \psi = 0^0) = L_1 + \Delta L^{(1)} + \Delta L^{(2)}_m \quad dB$$

These levels require the following duct corrections.

(2) Calculate the duct transmission loss, TL_m, as follows:

- If d/c < 2.0, find the lowest value of $\ell = |mB - sV|$, for each harmonic order m.

  s = 0, 1, 2, 3, etc.

If d/c > 2.0, or if no stators are present, $\ell = mB$, for each harmonic order m.

- For each harmonic order (m), find the value of $(k_\ell^{(r)} R)$ from Table 4.2.4-2 for appropriate values of σ and ℓ.

If

$$mBM_t \geq (k_\ell^{(r)} R)$$

then

$$TL_m = 0 \qquad (4.2.4\text{-}4)$$

If

$$mBM_t < (k_\ell^{(r)} R)$$

then

$$TL_m = 8.68\,(x/R)\sqrt{(k_\ell^{(r)} R)^2 - (mBM_t)^2} \quad dB \qquad (4.2.4\text{-}5)$$

TABLE 4.2.4-2

CUT-OFF VALUES OF $(k_\ell^{(r)} \cdot R)$ FOR DUCT SOUND TRANSMISSION

(from Reference 11)

Hub-to-Tip Radius Ratio σ	ℓ = (mB) or $\lvert mB + sV \rvert$						
	2	3	4	8	12	16	32
0	3.06	4.2	5.3	9.7	14.0	18.1	34.6
.25	3.01	4.2	5.3	9.7	14.0	18.1	34.6
.50	2.69	3.9	5.2	9.6	14.0	18.1	34.6
.75	2.30	3.5	4.6	9.5	13.9	17.9	34.6

m = blade passage harmonic order
B = number of blades
V = number of vanes
R = outer (tip) radius
s = any integer (0, 1, 2, 3,...)

(3) Calculate the rotor-stator interaction (Δ_s), as follows:

If

$$d/c \geq 2.0 ,$$

then

$$\Delta_s = 0 \qquad (4.2.4\text{-}6)$$

If

$$d/c < 2.0 ,$$

then

$$\Delta_s = 3 - 20 \log (d/c) \quad dB \qquad (4.2.4\text{-}7)$$

(4) The corrected sound pressure levels in the disc-plane, at the required r/D. are,

$$SPL_m(r/D, \psi = 0^o) = L_1 + \Delta L^{(1)} + \Delta L_m^{(2)} - IL_m + \Delta_s \quad dB \quad (4.2.4\text{-}8)$$

where the first three terms are found from Section 4.3.3.2.

(5) For $\psi \neq 0^o$, that is, for levels outside the disc-plane, the sound pressure levels are corrected to:

$$SPL_m(r/D, \psi) = SPL_m(r/D, 0^o) + \Delta L^{(3)}_{mB,\psi} \quad dB \qquad (4.2.4\text{-}9)$$

where $\Delta L^{(3)}_{mB,\psi}$ is obtained from Figure 4.2.3-12, for the appropriate values of ℓ (instead of mB) found in step 2, and for angle ψ.

(6) For structural surface sound pressure levels, add 6 dB to each value if surface is flat, or 3 dB for curved surfaces (or else refer to Section 4.2.5.2).

REFERENCES FOR SECTION 4.2.4

1. Hancock, R. N.; "Inlet Duct Sonic Fatigue Induced by the Multiple Pure Tones of a High Bypass Ratio Turbofan," Paper presented at the Institute of Environmental Sciences Symposium, Anahelm, California, April 1973.

2. Sutherland, L. C. and Brown, D.; "Prediction Methods for Near Field Noise Environments of VTOL Aircraft," AFFDL-TR-71-160, Wright-Patterson Air Force Base, Ohio, 1972.

3. Kester, J. D.; "Generation and Suppression of Combination Tone Noise from Turbofan Engines," Paper No. 19, Proceedings AGARD Fluid Dynamics Panel, Saint-Louis, France, May 1969.

4. Sofrin, T. G. and Pickett, G. F.; "Multiple Pure Tone Noise Generated by Fans at Supersonic Tip Speeds," International Symposium on the Fluid Mechanics and Design of Turbo-Machinery, Pennsylvania State University, Sept. 1970.

5. Philpot, M. G.; "The Buzz-Saw Noise Generated by a High Duty Transonic Compressor," ASME Paper No. 70-GT-54, May 1970, Published in ASME Transactions, Journal of Engineering for Power, January 1971.

6. Fink, M. R.; "Shock Wave Behavior in Transonic Compressor Noise Generation," ASME Paper No. 71-GT-7, Dec. 1970, Published in ASME Transactions, Journal of Engineering for Industry, October 1971.

7. Mather, J. S. B., Savidge, J. and Fisher, M. J.; "New Observations on Tone Generation in Fans," Journal of Sound and Vibration, Vol. 16, No. 3, pp. 407-418, 8 June 1971.

8. Kester, J. D. and Pickett, G. F.; "Application of Theoretical Acoustics to Jet Engine Noise Reduction," Paper presented at Conference on Reduction of Aircraft Noise at Rolls Royce Ltd., Filton, Bristol, England, January 1971.

9. Pickett, G. F.; "The Prediction of the Spectral Content of Combination Tone Noise," AIAA Paper No. 71-30, AIAA/SAE 7th Propulsion Joint Specialists Conference, Salt Lake City, Utah, June 1971.

10. Plumblee, H. E. Ballentine, J. R. and Passinos, B.; "Near Field Noise Analyses of Aircraft Propulsion Systems with Emphasis on Prediction Techniques for Jets," AFFDL-TR-67-43, Wright-Patterson Air Force Base, 1967.

11. Tyler, J. M. and Sofrin, T. G.; "Axial Flow Compressor Noise Studies," SAE Transactions, pp. 309-322, 1961.

4.2.5 NOISE PREDICTION ON AIRCRAFT SURFACES

Most of the methods presented in the previous sections are based on predicting noise in the free field. In actual situations, there are several effects in the radiation field which alter the free field sound pressure level and distribution. The most critical effects are those due to (1) ground reflection, (2) structural reflections and (3) aircraft forward motion. Therefore, this section will concentrate on a description of simplified prediction methods characterizing these three effects.

4.2.5.1 Ground Reflection Effects for Jets and VTOL Jets

There is no doubt that ground reflections can cause the most drastic modifications of the sound level and spectrum shape at a point of any of the effects discussed. The sound pressure can increase to the point of doubling and at the other extreme can be completely cancelled for a monopole type of source. And, the problem of ground reflection is of even more significance for highly directional sources. For instance, on VTOL aircraft which may have a vertically oriented jet, the ground reflection completely dominates the sound field forward of the jet exhaust.

The problem of ground reflection exists for all types of aircraft noise sources in one of two manners. First, in performing near field noise tests, especially with full-scale hardware, the data to be measured inherently contain ground reflections to some degree. The height above the ground, the distance from the source to the field point and the impedance of the ground surface all have major effects on the reflected contribution. Unless the situation for the near field noise prediction exactly duplicates the test set up, the ground reflection contribution will be erroneous, with a high probability of significant errors in SPL and spectral shape. Second, in the case where the near-field noise prediction method is truly free-field, ground reflections must be evaluated and included if the prediction or the situation warrants it.

The usual method for determining ground reflection effects is to assume an image source which, in effect, presumes a rigid ground plane. This technique has been used for quite some time and was initially proposed as the method to account for jet noise ground reflection by Howes (1). The most recent study of ground reflections was presented by Sutherland and Brown (2). They derived a technique for accounting for source directivity thus providing the most general technique available. Other studies of ground reflection effects are given by Hoch and Thomas (3), Eldred (4), Franken (5) and Morgan, et al. (6).

Derivation: The source, image source and receiver are illustrated in Figure 4.2.5-1. The derivation to follow is after Sutherland and Brown (2). Source directivity is included, however the ground plane is assumed to be rigid, which is not unreasonable for most surfaces over which aircraft operate.

Referring to Figure 4.2.5-1, the mean square sound pressure at a receiver in the sound field of a point source and its image source due to a perfect reflection can be expressed as

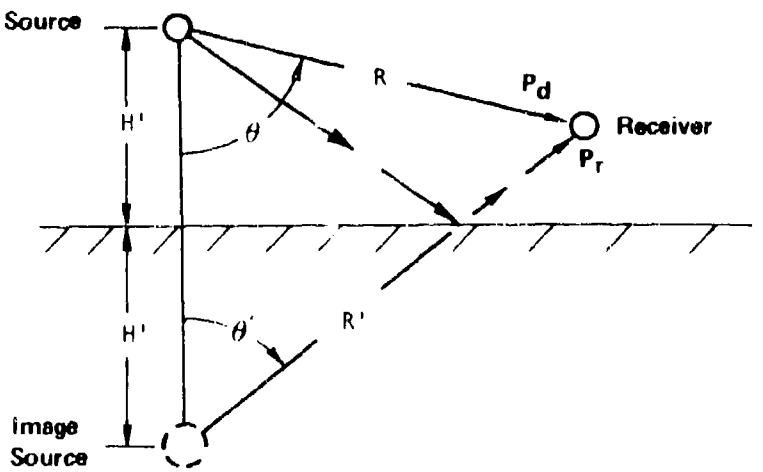

FIGURE 4.2.5-1 NOMENCLATURE AND COORDINATE SYSTEM FOR REFLECTING SOURCE ABOVE INFINITE PLANE

$$\overline{P^2} = \overline{(P_d + P_r)^2} = \overline{P_d^2}[1 + r^2 + 2r\,C] \qquad (4.2.5\text{-}1)$$

where

P_d, P_r = direct and reflected pressures respectively at the receiver

$r^2 = \overline{P_r^2}/\overline{P_d^2}$, ratio of mean square reflected to direct pressures

$C = \overline{P_d P_r} \Big/ \sqrt{\overline{P_d^2}\,\overline{P_r^2}}$, the correlation coefficient between P_d and P_r

and $(\bar{\ })$ signifies a long time average

For a directive point source with a directivity factor $D(\theta)$, the ratio r^2 is given by

$$r^2 = \frac{R^2}{(R')^2} \cdot \frac{D(\theta')}{D(\theta)} \qquad (4.2.5\text{-}2)$$

where

$R' = R\left|1 + 4\left(\frac{H'}{R}\right)^2 - 4\left(\frac{H'}{R}\right)\cos\theta\right|^{1/2}$, the distance from the image source to the receiver

$\theta' = \tan^{-1}\left|\sin\theta \Big/ \left(2\,\frac{H'}{R} - \cos\theta\right)\right|$, the angle between the source-image axis and the radius R'

and

H' = source elevation above the ground plane

If the source consists of an ideal band of white noise, the correlation coefficient C can be shown to be (1,6)

$$C = \frac{\sin[\pi f_c \tau b]}{\pi f_c \tau b} \cos\left|2\pi f_c \tau \sqrt{1 + (b/2)^2}\right| \qquad (4.2.5\text{-}3)$$

where

$\tau = (R' - R)/a_o$, time delay between direct and reflected signals

$b = \Delta f / f_c$

f_c = center frequency of band

Δf = bandwidth of noise (ideal filter)

a_o = ambient speed of sound

For plotting purposes, it is convenient to transform the coordinate system to rectilinear coordinates x, y where x is the vertical distance below the jet exit plane, and y is the lateral distance parallel to the ground plane. Furthermore, by expressing distances in terms of nozzle height and frequencies in terms of the ratio of source height (H') to wavelength $\lambda = a_o/f_c$, then for an <u>octave</u> band of noise, b = 0.707, and one obtains

$$r^2 = \frac{(R/H')^2}{[(R/H')^2 + 4(1 - x/H')]} \frac{D(\theta')}{D(\theta)} \qquad (4.2.5\text{-}4)$$

$$C = \frac{\sin B}{B} \cos 3B$$

where

$$B = \pi G \left| \sqrt{(R/H')^2 + 4(1 - x/H')} - R/H' \right| / \sqrt{2}$$

$G = f \cdot H'/a_o = H'/\lambda$, the ratio of source height to wavelength

$$R/H' = [(x/H')^2 + (y/H')^2]^{1/2}$$

$$\theta = \cos^{-1}\left(\frac{x/H'}{R/H'}\right) \qquad (4.2.5\text{-}5)$$

and

$$\theta' = \tan^{-1}\left(\frac{y/H'}{2 - x/H'}\right)$$

Equations (4.2.5-4) and (4.2.5-5) are used in Equation (4.2.5-1) to determine contours of constant values of the quantity

$$A = 10 \cdot \log[1 + r^2 + 2r\,C] \quad dB \,. \qquad (4.2.5\text{-}6)$$

This is simply the change in sound level in decibels due to introduction of the ground plane. Contours of this reflection correction were computed (2) for three general cases:

(1) A nondirective point source,

(2) A "point source" simulating the far field directivity of an ambient air jet, and

(3) A "point source" simulating a turbojet engine as a heated jet.

For the nondirectional (monopole) source, $D(\theta) = D(0°) = 1$. For an ambient air jet source, the directivity factor can be approximated as

$$D(\theta) = \frac{K(1 + \cos^4 \theta)}{\left[(1 - M \cos \theta)^2 + (\alpha M)^2\right]^{5/2}\left[1 + C_4 e^{-C_5 \theta}\right]} \qquad (4.2.5\text{-}7)$$

where

M is the eddy convection Mach number

$K = 0.56$, an arbitrary constant selected so that $\int D(\theta) \cdot \sin\theta d\theta = 1.0$

$\alpha^2 = 0.3$, a correction factor for finite eddy decay time

$C_4 = 2$, an empirical constant

$C_5 = 12.3$ per radian, an empirical constant

This directivity factor is based on the theoretical model derived by Ribner (7) and modified by an empirical exponential term in the manner proposed by Plumblee (8) to account for the decrease in directivity near the jet axis.

The following constants are used in Equation (4.2.5-7) to simulate the far field directivity of a full scale turbojet engine.

$K = 0.37$
$\alpha^2 = 0.3$
$C_4 = 310$
$C_5 = 9$

} Directivity constants for heated jet .

To give an idea of the effect of source directivity and reflection on the sound field, typical results for a monopole source and a nearly vertically oriented jet are shown in Figure 4.2.5-2 (from Sutherland and Brown (2)). The sound field for the monopole source is, for the case chosen, modified by a maximum of ±4 dB due to the reflection. However for the source with directivity of a vertically oriented jet, an increase of 10 dB is observed, thus illustrating the significance of including ground reflections in a noise estimate procedure.

Tables and Computer Program for Reflection of Octave Bands of White Noise from a Rigid Reflecting Plane: Tables and the computer program utilized for their generation are provided for calculating the change in octave band levels due to ground reflection from a rigid plane for a point source which simulates the directivity of a:

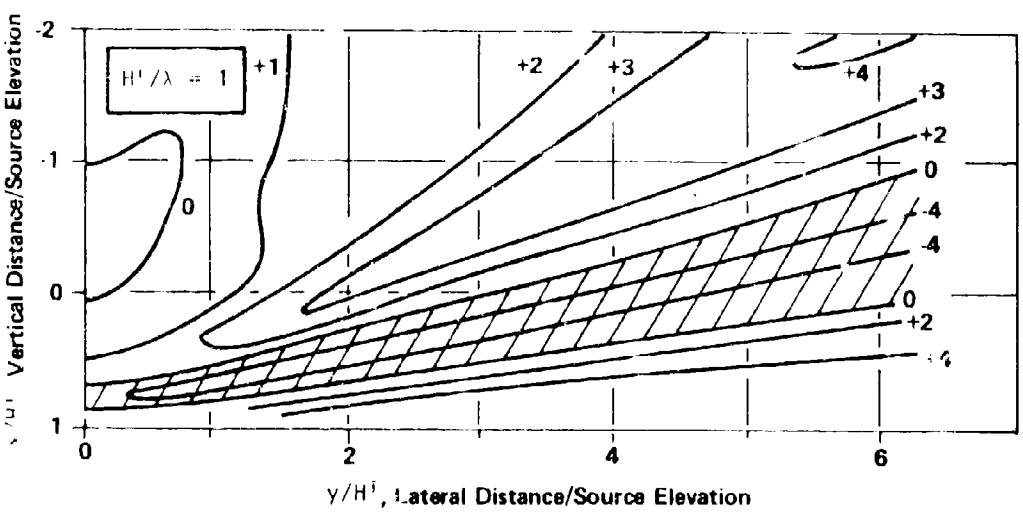

(a) Change in SPL (in decibels) for monopole source above ground plane

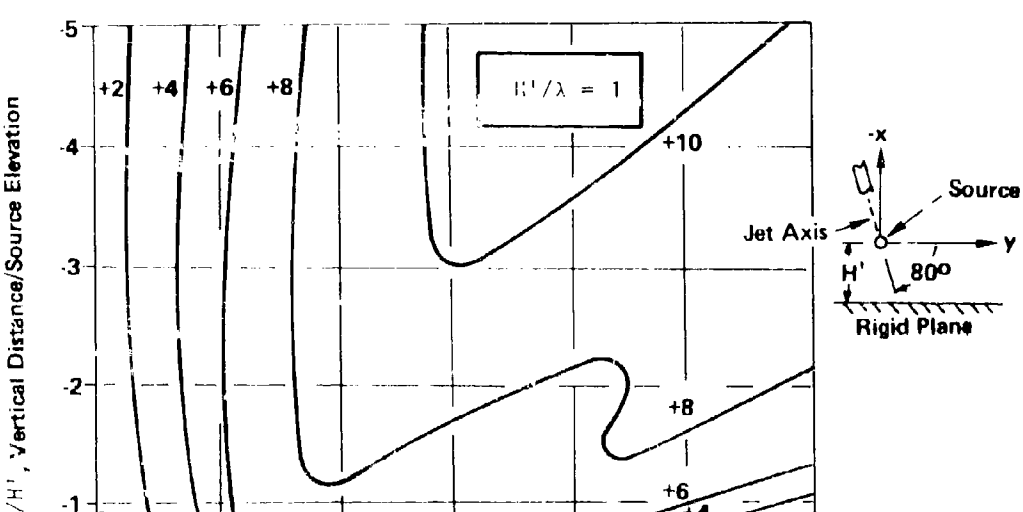

(b) Change in SPL (in decibels) for jet above ground plane

FIGURE 4.2.5-2 EFFECT OF SOURCE DIRECTIVITY ON REFLECTED SOUND FIELD (H'/λ=1).

- Non-directional monopole source

- Jet noise source

The computer program prints tables in a geometrically arranged matrix array of either or both of the following quantities (A & B). The relevant equations are derived in the previous section. The geometry of the problem is illustrated in Figure 4.2.5-3.

$$A = 10 \cdot \log \left[\frac{\text{Mean Square (Direct + Reflected Pressure)}}{\text{Mean Square Direct Pressure}} \right] \quad \text{dB} \qquad (4.2.5\text{-}8)$$

The change in sound level due to introduction of the rigid reflecting plane, and

$$B = L_o - 20 \cdot \log \left(\frac{R}{H} \right) + 10 \cdot \log (D(\theta)) \quad \text{dB} \qquad (4.2.5\text{-}9)$$

the sound level at a position R, θ, in the absence of a reflecting plane, of a point source with a directivity factor $D(\theta)$, and space average sound level L_o at a reference distance H. For printout, the polar coordinates are converted to rectilinear coordinates x and y.

To simulate a jet noise source, the computer program assumes a directivity factor for the point source as given in Equation (4.2.5-7).

Tables: Tables are provided for the case of a monopole source only. Table 4.2.5-1 presents a set of matrix tables of A (Equation 4.2.5-8) for a monopole source for the following range of variables.

- For each table:

  x/H = -2 to +1 in steps of 0.2

  y/H = 0 to 6 in steps of 0.6

- Separate tables are provided for:

  H/λ = 0.25, 0.5, 1, 2, 4, 8 and 100

  The case of H/λ = 100 approximates the condition for which phase effects are negligible in the reflection and the total direct and reflected sound fields are added on an intensity basis.

Table 4.2.5-2 presents a matrix table of A + B for H/λ = 100 with the reference space average sound level of the direct sound field (L_o) arbitrarily set equal to 50 dB.

For convenience, by suitable choice of the intervals for the rectilinear position variables x/H and y/H, the tabular values appear in a geometrically

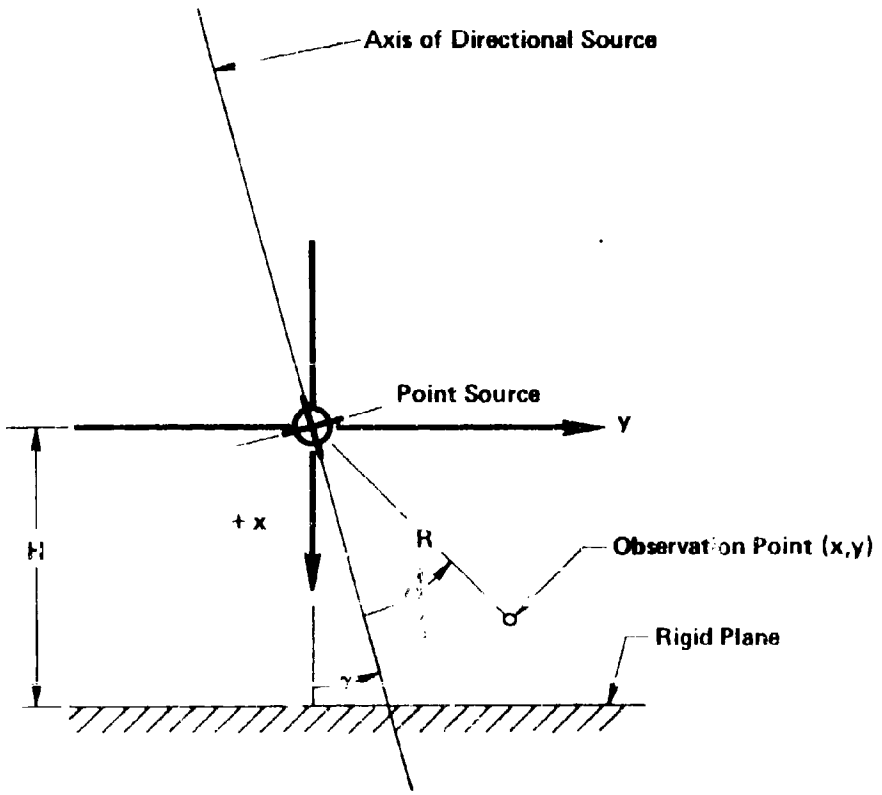

FIGURE 4.2.5-3 GEOMETRY FOR REFLECTION BY RIGID PLANE OF OCTAVE BANDS OF WHITE NOISE FROM A DIRECTIONAL POINT SOURCE.

WAVELENGTH AT CENTER FREQUENCY OF BAND = λ

TABLE 4.2.5-1

CHANGE IN OCTAVE BAND LEVEL DUE TO REFLECTION FROM RIGID PLANE FOR MONOPOLE SOURCE AT ELEVATION H WITH WAVELENGTH λ AT CENTER FREQUENCY OF BAND

(Decibels)

	Vertical Distance X/H	Y/H (Lateral Distance) 0.0	.6	1.2	1.8	2.4	3.0	3.6	4.2	4.8	5.4	6.0
	-2.0	-3.4	-3.7	-4.2	-4.3	-3.4	-2.0	-.6	.6	1.5	2.3	2.8
	-1.8	-3.2	-3.5	-4.1	-4.1	-3.0	-1.5	-.1	1.0	1.9	2.6	3.2
	-1.6	-3.1	-3.4	-4.0	-3.8	-2.5	-.9	.4	1.5	2.3	3.0	3.5
	-1.4	-2.9	-3.2	-3.8	-3.4	-2.0	-.3	1.0	2.0	2.8	3.3	3.8
	-1.2	-2.6	-3.1	-3.7	-3.0	-1.3	.3	1.5	2.5	3.2	3.7	4.1
$\frac{H}{\lambda}$ = 0.25	-1.0	-2.3	-2.9	-3.4	-2.4	-.6	.9	2.1	2.9	3.5	4.0	4.3
	-.8	-2.0	-2.7	-3.1	-1.8	.1	1.6	2.6	3.4	3.9	4.3	4.6
	-.6	-1.6	-2.4	-2.7	-1.0	.9	2.2	3.2	3.8	4.3	4.6	4.8
	-.4	-1.2	-2.2	-2.1	-.1	1.7	2.9	3.7	4.2	4.6	4.9	5.1
	-.2	-.6	-2.0	-1.3	.9	2.5	3.5	4.2	4.6	4.9	5.1	5.3
Source →	-.0	.0	-1.7	-.2	1.9	3.3	4.1	4.6	4.9	5.2	5.3	5.5
	.2	-.8	-1.0	1.2	3.0	4.0	4.6	5.0	5.2	5.4	5.5	5.6
	.4	-.6	.5	2.6	3.9	4.7	5.1	5.3	5.5	5.6	5.7	5.8
	.6	1.4	2.5	4.0	4.8	5.2	5.5	5.6	5.7	5.8	5.8	5.9
	.8	4.0	4.5	5.1	5.5	5.7	5.8	5.9	5.9	5.9	5.9	6.0
Plane →	1.0	6.0	6.0	6.0	6.0	6.0	6.0	6.0	6.0	6.0	6.0	6.0
	-2.0	2.0	2.2	2.5	2.7	2.5	1.6	.3	-1.5	-3.4	-4.8	-5.1
	-1.8	1.9	2.1	2.5	2.6	2.2	1.1	-.5	-2.5	-4.3	-5.1	-4.6
	-1.6	1.7	2.0	2.4	2.5	1.8	.5	-1.5	-3.6	-5.0	-4.8	-3.6
	-1.4	1.6	1.9	2.3	2.2	1.3	.4	-2.7	-4.6	-5.1	-4.0	-2.4
	-1.2	1.2	1.6	2.1	1.5	.6	-1.5	-3.9	-5.1	-4.3	-2.7	-1.2
	-1.0	1.2	1.6	2.1	1.5	-.3	-2.9	-4.9	-4.7	-3.0	-1.3	.0
	-.8	1.0	1.5	1.9	.8	-1.6	-4.3	-5.0	-3.4	-1.5	.0	1.0
	-.6	.8	1.4	1.5	-.2	-3.2	-5.1	-3.8	-1.7	.0	1.2	2.1
$\frac{H}{\lambda}$ = 0.5	-.4	.6	1.3	.9	-1.7	-4.7	-4.3	-1.9	.0	1.4	2.3	3.0
	-.2	.3	1.1	-.2	-3.6	-4.7	-2.2	.0	1.5	2.6	3.3	3.8
Source →	-.0	.0	.7	-2.0	-4.8	-2.5	.1	1.8	2.9	3.6	4.1	4.4
	.2	.3	-.5	-4.1	-2.8	.3	2.1	3.2	3.9	.4	4.7	5.0
	.4	-.8	-3.0	-2.8	.6	2.6	3.7	4.4	4.8	5.1	5.3	5.4
	.6	-2.9	-1.7	1.4	3.3	4.3	4.9	5.2	5.4	5.5	5.6	5.7
	.8	2.4	3.4	4.5	5.1	5.5	5.6	5.8	5.8	5.9	5.9	5.9
Plane →	1.0	6.0	6.0	6.0	6.0	6.0	6.0	6.0	6.0	6.0	6.0	6.0

TABLE 4.2.5-1 (Continued)

(Decibels)

	Vertical Distance X/H	Y/H (Lateral Distance) 0.0	.6	1.2	1.8	2.4	3.0	3.6	4.2	4.8	5.4	6.0
	-2.0	.4	.3	.4	1.2	1.8	1.8	1.7	2.3	3.2	3.8	4.0
	-1.8	.3	.2	.4	1.3	1.8	1.6	1.9	2.7	3.6	4.0	3.9
	-1.6	.2	.1	.5	1.4	1.7	1.6	2.2	3.2	3.8	3.9	3.6
	-1.4	.2	.1	.6	1.5	1.5	1.7	2.7	3.6	3.9	3.7	3.0
	-1.2	.1	-.0	.7	1.5	1.4	2.0	3.2	3.8	3.7	3.1	2.1
	-1.0	.0	-.1	.8	1.4	1.4	2.6	3.6	3.8	3.2	2.1	.6
	-.8	-.0	-.1	1.0	1.2	1.8	3.2	3.7	3.3	2.2	.5	-1.4
	-.6	-.1	-.0	1.0	1.1	2.5	3.5	3.4	2.2	.4	-1.7	-3.8
$\frac{H}{\lambda} = 1$	-.4	-.1	.1	.9	1.5	3.2	3.4	2.3	.3	-2.1	-4.3	-5.0
	-.2	-.1	.3	.7	2.4	3.3	2.3	.1	-2.7	-4.8	-4.7	-3.2
Source →	-.0	.0	.4	1.3	3.1	2.3	-.3	-3.5	-5.1	-3.8	-1.9	.3
	.2	.1	.3	2.5	2.2	-.8	-4.5	-4.5	-2.2	-.3	1.1	2.1
	.4	.2	1.7	1.9	-1.9	-5.1	-2.7	-.1	1.5	2.6	3.3	3.8
	.6	1.6	.6	-4.2	-3.3	.3	2.2	3.4	4.1	4.5	4.8	5.0
	.8	-3.9	-1.7	1.8	3.7	4.6	5.0	5.3	5.5	5.6	5.7	5.8
Plane →	1.0	6.0	6.0	6.0	6.0	6.0	6.0	6.0	6.0	6.0	6.0	6.0
	-2.0	1.0	1.2	1.5	1.0	1.6	1.8	2.2	2.8	2.1	1.4	1.9
	-1.8	.9	1.1	1.4	.9	1.7	1.7	2.5	2.5	1.5	1.6	2.4
	-1.6	.8	1.1	1.2	.9	1.7	1.9	2.7	1.9	1.3	2.1	2.7
	-1.4	.7	1.0	1.0	1.2	1.5	2.3	2.4	1.3	1.8	2.6	2.7
$\frac{H}{\lambda} = 2$	-1.2	.6	.9	.7	1.4	1.5	2.5	1.6	1.4	2.4	2.7	2.4
	-1.0	.5	.9	.5	1.4	2.0	2.1	1.2	2.1	2.6	2.4	2.3
	-.8	.3	.8	.6	1.2	2.3	1.2	1.7	2.6	2.4	2.3	2.9
	-.6	.2	.6	.9	1.5	1.8	1.2	2.4	2.3	2.3	3.0	3.8
	-.4	.1	.3	.9	2.0	.9	2.2	2.3	2.2	3.1	4.0	4.3
	-.2	.0	.1	.9	1.1	1.7	2.2	2.2	.3	4.1	4.2	3.7
Source →	-.0	.0	.4	1.5	1.0	2.1	2.1	3.5	4.2	3.9	2.9	1.5
	.2	-.0	.6	.3	1.9	2.1	3.7	4.0	3.0	1.3	-.9	-3.1
	.4	.6	.1	1.6	2.3	3.9	3.2	1.0	-2.0	-4.5	-4.7	-3.3
	.6	.8	1.0	3.0	3.1	.1	-4.0	-4.6	-2.3	.3	1.1	2.1
	.8	2.7	1.5	-3.9	-3.3	.4	2.4	3.5	4.1	4.6	4.9	5.1
Plane →	1.0	6.0	6.0	6.0	6.0	6.0	6.0	6.0	6.0	6.0	6.0	6.0

TABLE 4.2.5-1 (Continued)

	Vertical Distance Y/H	(Decibels) Y/H (Lateral Distance) 0.0	.6	1.2	1.8	2.4	3.0	3.6	4.2	4.8	5.4	6.0
	-2.0	1.1	1.1	1.1	1.4	1.3	1.8	2.2	2.0	2.2	2.7	2.5
	-1.8	1.0	1.0	1.1	1.6	1.5	1.9	1.8	2.3	2.3	2.7	2.0
	-1.6	.9	.8	1.1	1.5	1.7	2.1	1.8	2.1	2.8	2.1	2.3
	-1.4	.8	.7	1.0	1.1	1.5	1.7	2.1	2.4	2.3	2.1	2.7
	-1.2	.7	.6	.9	1.1	1.8	1.6	2.0	2.6	1.9	2.6	2.4
	-1.0	.6	.4	1.1	1.3	1.7	2.0	2.5	1.8	2.5	2.4	2.9
	-.8	.5	.4	1.0	1.3	1.4	2.0	2.0	2.3	2.4	2.9	3.3
$\frac{H}{X} = 4$	-.6	.3	.4	.7	1.6	1.7	2.3	2.0	2.3	2.9	3.2	2.1
	-.4	.2	.3	.9	1.2	2.1	1.6	2.3	2.8	3.0	1.8	2.0
	-.2	.1	.5	1.2	1.4	1.4	2.2	2.8	2.7	1.6	2.4	3.0
Source →	-.0	✪.0	.3	.9	1.7	2.1	2.8	2.2	1.8	2.8	2.8	2.5
	.2	.1	.6	1.6	1.9	2.8	1.5	2.4	2.8	2.4	2.9	3.8
	.4	.1	.8	1.6	2.6	1.6	2.7	2.4	3.3	4.2	4.4	3.9
	.6	.5	1.1	1.2	2.5	2.4	3.9	4.3	3.3	1.6	-.6	-2.9
	.8	1.7	1.8	3.5	3.6	.4	-3.8	-4.6	-2.3	-.2	1.2	2.2
Plane →	1.0	6.0	6.0	6.0	6.0	6.0	6.0	6.0	6.0	6.0	6.0	6.0
	-2.0	.9	1.0	1.1	1.5	1.7	1.8	2.0	2.1	2.2	2.3	2.5
	-1.8	.8	1.0	1.0	1.2	1.5	2.0	2.0	2.1	2.5	2.4	2.7
	-1.6	.7	.9	1.1	1.3	1.6	1.7	2.1	2.2	2.1	2.4	2.4
	-1.4	.6	.8	1.0	1.3	1.6	1.8	2.1	2.3	2.4	2.6	2.6
	-1.2	.5	.7	1.0	1.3	1.5	1.9	2.2	2.3	2.6	2.4	2.5
	-1.0	.4	.7	.9	1.3	1.7	2.0	1.9	2.4	2.2	2.5	2.7
	-.8	.3	.5	.9	1.4	1.8	2.2	2.1	2.1	2.4	2.7	2.5
$\frac{H}{X} = 8$	-.6	.2	.4	1.0	1.3	1.7	2.0	2.2	2.3	2.6	2.6	2.6
	-.4	.1	.3	.9	1.5	1.7	2.3	2.3	2.4	2.6	2.7	2.9
	-.2	.0	.3	.8	1.5	2.0	2.2	2.3	2.6	3.0	2.3	2.7
Source →	.0	✪.0	.3	.9	1.6	2.1	2.0	2.4	2.8	2.3	2.8	2.8
	.2	.1	.5	1.0	1.8	1.8	2.5	2.0	2.8	2.8	3.5	2.6
	.4	.3	.8	1.5	1.9	2.6	2.6	2.8	3.2	1.8	2.4	3.1
	.6	.8	1.2	1.8	2.3	3.0	2.0	2.5	3.0	2.6	3.0	3.8
	.8	1.3	1.8	1.8	2.8	2.6	4.0	4.4	3.5	1.7	-.5	-2.8
Plane →	1.0	6.0	6.0	6.0	6.0	6.0	6.0	6.0	6.0	6.0	6.0	6.0

TABLE 4.2.5-1 (Concluded)

	Vertical Distance X/H	(Decibels) Y/H (Lateral Distance) 0.0	.6	1.2	1.8	2.4	3.0	3.6	4.2	4.8	5.4	6.0
	-2.0	1.0	1.0	1.2	1.4	1.6	1.8	2.0	2.2	2.3	2.4	2.5
	-1.8	.9	.9	1.1	1.3	1.6	1.8	2.0	2.2	2.3	2.4	2.5
	-1.6	.8	.9	1.1	1.3	1.6	1.8	2.0	2.2	2.3	2.5	2.5
	-1.4	.7	.8	1.0	1.3	1.6	1.9	2.1	2.2	2.3	2.5	2.5
	-1.2	.6	.7	1.0	1.3	1.6	1.9	2.1	2.3	2.4	2.5	2.6
$\frac{H}{\lambda}$ = 100	-1.0	.5	.6	.9	1.3	1.6	1.9	2.1	2.3	2.4	2.5	2.6
	-.8	.3	.5	.9	1.3	1.7	2.0	2.2	2.4	2.5	2.6	2.6
	-.6	.2	.4	.9	1.3	1.7	2.0	2.2	2.4	2.5	2.6	2.7
	-.4	.1	.4	.9	1.4	1.8	2.1	2.3	2.5	2.6	2.6	2.7
	-.2	.0	.3	.9	1.5	1.9	2.2	2.4	2.5	2.7	2.7	2.7
Source →	-.0	.0	.3	1.0	1.6	2.0	2.3	2.5	2.6	2.6	2.7	2.8
	.2	.1	.5	1.2	1.8	2.2	2.4	2.6	2.7	2.8	2.7	2.8
	.4	.3	.7	1.5	2.0	2.3	2.5	2.6	2.7	2.8	2.8	2.9
	.6	.7	1.2	1.9	2.3	2.6	2.7	2.8	2.8	2.9	2.8	2.8
	.8	1.6	1.9	2.4	2.7	2.8	2.8	3.0	3.0	3.0	3.0	3.2
Plane →	1.0	-6.0	-6.0	-6.0	-6.0	-6.0	-6.0	-6.0	-6.0	-6.0	-6.0	-6.0

TABLE 4.2.5-2

OCTAVE BAND LEVEL FOR MONOPOLE SOURCE OF WHITE NOISE AT ELEVATION H ABOVE RIGID PLANE WITH SPACE AVERAGE OCTAVE BAND LEVEL = 50 dB AT RADIUS = H (H/λ = 100)

	Vertical Distance X/H	(Decibels) Y/H (Lateral Distance) 0.0	.6	1.2	1.8	2.4	3.0	3.6	4.2	4.8	5.4	6.0
	-2.0	44.9	44.6	43.8	42.8	41.7	40.7	39.7	38.8	38.0	37.2	36.5
	-1.8	45.8	45.4	44.4	43.2	42.1	40.9	39.9	39.0	38.1	37.3	36.6
	-1.6	46.7	46.2	45.0	43.7	42.4	41.2	40.1	39.1	38.2	37.4	36.7
	-1.4	47.8	47.1	45.7	44.2	42.7	41.5	40.3	39.3	38.4	37.5	36.8
	-1.2	49.0	48.1	46.4	44.6	43.0	41.7	40.5	39.5	38.5	37.7	36.8
	-1.0	50.5	49.3	47.0	45.0	43.3	41.9	40.7	39.6	38.6	37.7	36.9
	-.8	52.3	50.5	47.7	45.4	43.6	42.1	40.9	39.7	38.7	37.8	37.0
	-.6	54.7	51.9	48.3	45.8	43.9	42.3	41.0	39.8	38.8	37.9	37.1
	-.4	58.1	53.2	48.8	46.1	44.1	42.5	41.1	40.0	38.9	38.0	37.2
	-.2	64.0	54.3	49.2	46.3	44.3	42.6	41.2	40.0	39.0	38.0	37.1
Source →	-.0		54.8	49.4	46.5	44.4	42.7	41.4	40.1	39.0	38.0	37.2
	.2	64.0	54.4	49.5	46.6	44.5	42.9	41.5	40.2	39.1	38.1	37.2
	.4	58.2	53.6	49.4	46.7	44.6	42.9	41.5	40.2	39.1	38.1	37.3
	.6	55.2	52.6	49.3	46.7	44.7	43.0	41.5	40.3	39.1	38.1	37.2
	.8	53.5	51.9	49.2	46.8	44.7	43.0	41.6	40.4	39.3	38.2	37.6
Plane →	1.0	-56.0	-54.7	-52.1	-49.7	-47.7	46.0	44.6	43.[illegible]	[illegible]	41.2	40.3

scaled pattern normalized by the source height H. For any table, the positions x and y may be normalized in terms of wavelength by multiplying the x/H and y/H values by H/λ.

Computer Programs: Two computer programs are presented for calculating ground reflection tables such as illustrated in Tables 4.2.5-1 and 4.2.5-2. The first program listed is presented in Table 4.2.5-3 and is coded for operation on a remote computer terminal utilizing a direct input to a time-sharing computer service (2). Table 4.2.5-4 presents a modification of the code listed in Table 4.2.5-3 that is compatible with the computing facility at Wright-Patterson Air Force Base (private communication: R. C. W. van der Heyde, W.P.A.F.B., 1974). This modified code tabulates only the matrix A or B, or A + B as described below.

- Input File Name

  The user types the file name on which is stored the following variables separated by commas (,).

  XL, Lowest Value of x/H

  XH, Highest Value of x/H

  XD, Interval in x/H

  YL, Lowest Value of y/H

  YH, Highest Value of y/H

  YD, Interval in y/H

  MC, Value of M in Equation 4.2.5-7

  AL, Value of α^2 in Equation 4.2.5-7

  C4, Value of C_4 in Equation 4.2.5-7

  C5, Value of C_5 in Equation 4.2.5-7

  K, Value of K in Equation 4.2.5-7

  LO, Value of L_o in Equation 4.2.5-7

  G, Value of γ, incidence angle (in radians) of "jet" axis. (See Figure 4.2.5-3)

  ICODE, An integer from 1 to 7 to define the output form desired as defined below.

  NU, Value of H/λ

TABLE 4.2.5-3

LISTING FOR PROGRAM TO COMPUTE GROUND REFLECTION TABLES
(FOR REMOTE ACCESS TERMINALS)

```
10 DIMENSION X(50),YY(11),A(11,50),B(11,50),AB(11)
15 STRING F(10)
20 REAL K,MC,LO,NU
25 10 WRITE(1,11)
30 11 FORMAT(3/)
35 12 ACCEPT 'INPUT FILE NAME  ',F
40 OPEN(3,F,INPUT,SYMBOLIC,ERR=20)
45 GO TO 30
50 20 DISPLAY 'ERROR IN FILE',F
55 GO TO 12
57 30 READ (3) XL,XH,XD,YL,YH,YD,MC,AL,C4,C5,K,LO,G,ICODE,NU
65 M=(YH-YL)/YD+1
70 N=(XH-XL)/XD+1
75 X(1)=XL
80 PI=3.1415926536
85 DO 40 I=2,N
90 40 X(I)=X(I-1)+XD
95 41 Y=YL-YD
100 DO 1000 I=1,M
105 Y=Y+YD
110 YY(I)=Y
115 DO 100 J=1,N
120 Z=X(J)
125 R=SQRT(Z*Z+Y*Y)
130 IF(R.NE.0.) GO TO 55
135 A(I,J)=-.01
140 B(I,J)=-.01
145 GO TO 100
146 55 ARG=Z/R
147 ARG=ARG*1.E+10
149 ARG=TRUNC(ARG)
149.1 ARG=ARG/(1.E+10)
150 T=(ACOS(ARG)) - G
155 TP=ATAN(Y/(2.-Z))-G
160 CALL DTHETA(K,T,MC,AL,C4,C5,D)
165 IF(D.EQ.0.) D=1.
170 IF(ICODE.EQ.5) GO TO 80
175 CALL DTHETA(K,TP,MC,AL,C4,C5,DP)
180 IF(DP.EQ.0.) DP=1.
185 TM1=SQRT(R*R+4.*(1.-Z))
190 SMALLR=SQRT(DP/D)*(R/TM1)
195 IF(TM1.NE.R) GO TO 60
200 A(I,J)=20.*ALOG10(SMALLR+1.)
205 GO TO 70
210 60 BETA=PI*NU*(TM1-R)/1.4142135624
215 C=SIN(BETA)*COS(3.*BETA)/BETA
```

TABLE 4.2.5-3 (CONTINUED)

```
220 A(I,J)=10.*ALOG10 1.+SMALLR*SMALLR+2.*SMALLR*C)
225 70 IF(ICODE.EQ.1) GO TO 100
230 80 B(I,J)=LO 10.*ALOG10(D/(R*R))
235 100 CONTINUE
240 1000 CONTINUE
245 GO TO (500,500,500,500,550,550,600) ,ICODE
249 500 L=1
250     CALL XHED(MC,AL,C4,C5,K,G,NU,YY,M,L)
255 DO 200 J=1,N
260 200 WRITE(1,210)  X(J),(A(I,J),I=1,M)
265 210 FORMAT(F4.1,11F5.1)
270 GO TO (900,550,600,550) ,ICODE
275 550 CALL XHED(MC,AL,C4,C5,K,G,NU,YY,M,2)
280 DO 300 J=1,N
285 300 WRITE(1,210)  X(J),(B(I,J),I=1,M)
290 IF(ICODE.EQ.2.OR.ICODE.EQ.5) GO TO 900
295 600 CALL XHED(MC,AL,C4,C5,K,G,NU,YY,M,3)
300 DO 420 J=1,N
305 DO 410 I=1,M
310 410 AB(I)=A(I,J)+B(I,J)
315 420 WRITE(1,210)  X(J),(AB(I),I=1,M)
320 900 READ(3,END=950) NU
321 IF(NU.GE.0.) GO TO 41
322 ICODE=-NU
323 READ(3,END=950) NU
325 GO TO 41
330 950 CLOSE(3)
335 GO TO 10
336 336 FORMAT (1F70.64)
340 END
345 SUBROUTINE XHED(MC,AL,C4,C5,K,G,NU,X,N,M)
350 DIMENSION X(11)
351 REAL MC,K,NU
355 STRING F(12)
360 GO TO (1,2,3) ,M
365 1 F='A-MATRIX     '
370 GO TO 4
375 2 F='B-MATRIX     '
380 GO TO 4
385 3 F='A+B - MATRIX'
390 4 WRITE(1,5) F
395 5 FORMAT (3/,T31,A12,2/)
400 WRITE (1,10) MC,AL,C4,C5,K,G,NU
410 10 FORMAT(T6,'MC    ALPHA       C4       C5',7X,'K    GAMMA',
6X,'NU',/,T2,5(F6.2,2X),F6.4,F8.2,2/)
411 WRITE(1,20) (X(I),I=1,N)
415 20 FORMAT(T31,'Y/H',/,T2,'X/H',11F5.1)
420 DISPLAY ' '
425 RETURN
430 END
```

TABLE 4.2.5-3 (CONCLUDED)

```
435  SUBROUTINE DTHETA(A,B,CM,AL,C4,C5,D)
440  C=COS(B)
445  TOP=A*(1.+C**4)
450  BOT=(((1.-CM*C)**2)+AL*CM*CM)**2.5
455  BOT=BOT*(1.+C4*EXP(-C5*B))
460  D=TOP/BOT
465  RETURN
470  END
```

TABLE 4.2.5-4
LISTING FOR PROGRAM TO COMPUTE GROUND REFLECTION TABLES A, B, OR A+B
(CONTINUED)

```
      PROGRAM GRREF(INPUT,OUTPUT,TAPE5=INPUT)
      REAL  K,MC,LO,NU
      DIMENSION X(50), YY(11), A(11,50),B(11,50),AB(11),NFILE(7)
      PI=3.1415926536
      READ1,NFILE
    1 FORMAT(7A10)
      PRINT61,NFILE
   61 FORMAT(1H1,         /A10)
      READ*,XL,XH,XD,YL,YH,YD,MC,AL,C4,C5,K,LO,G,ICODE,NU
      M=(YH-YL)/YD+1
      N=(XH-XL)/XD+1
      X(1)=XL
      DO 110 I=2,N
      X(I)=X(I-1)+XD
  110 CONTINUE
  111 Y=YL-YD
      DO 134 I=1,M
      Y=Y+YD
      YY(I)=Y
      DO 133 J=1,N
      Z=X(J)
      R=SQRT(Z**2+Y**Y)
      IF(R.NE.0.) GO TO 115
      A(I,J) =-.01
      B(I,J)=-.01
      GO TO 133
  115 ARG=Z/R*1.E10
      IA=ARG
      AZ=IA
      ARG=ARG-AZ
      ARG=ARG*1.E-10
      T=(ACOS(ARG))-G
      TP=ATAN(Y/(2.-Z))-G
```

TABLE 4.2.5-4
(CONTINUED)

```
      CALL DTHETA(K,T,MC,AL,C4,C5,D)
      IF(D.EQ.0.)D=1.
      IF(ICODE.EQ.5)GO TO 132
      CALLDTHETA(K,TP,MC,AL,C4,C5,DP)
      IF(DP.EQ.0.)DP=1.
      TM1=SQRT(R*R+4.*(1.-Z))
      SMALLR= SQRT(DP/D)*(R/TM1)
      IF(TM1.NE.R)GO TO 127
      A(I,J)=20.*ALOG10(SMALLR+1.)
      GO TO 131
  127 BETA=PI*NU*(TM1-R)*.7071067814
      C=SIN(BETA)*COS(3.*BETA)/BETA
      A(I,J)=10.*ALOG10(1.+SMALLR*SMALLR+2.*SMALLR*C)
  131 IF(ICODE.EQ.1) GO TO 133
  132 TM1=R*R
      B(I,J)=L0+10.*ALOG10(D/TM1)
  133 CONTINUE
  134 CONTINUE
      GOTO(140,140,140,140,160,160,175), ICODE
  140 L=1
      CALL XHED(MC,AL,C4,C5,K,G,NU,YY,M,L)
      DO 145J=1,N
      PRINT51,X(J),(A(I,J),I=1,M)
  145 CONTINUE
   51 FORMAT(F34.1,11F5.1)
      GO TO(150,160,175,160),ICODE
  150 READ     (5,*)NU
      IF(EOF(5).NE.0)STOP
      IF(NU.GE.0)GOTO111
      STOP
  160 LA=2
      CALLXHED(MC,AL,C4,C5,K,G,NU,YY,M,LA)
      DO170 J=1,N
  170 PRINT51,X(J),(B(I,J),I=1,M)
      IF(ICODE.EQ.2.OR.ICODE.EQ.5)GOTO150
  175 LA=3
      CALL XHED(MC,AL,C4,C5,K,G,NU,YY,M,LA)
      DO 182J=1,N
      DO 181I=1,M
      AB(I)=A(I,J)+B(I,J)
  181 CONTINUE
      PRINT51,X(J),(AB(I),I=1,M)
  182 CONTINUE
      GO TO 150
      END
```

TABLE 4.2.5-4
(CONCLUDED)

```
      SUBROUTINE XHED(MC,AL,C4,C5,K,G,NU,X,N,M)
      DIMENSION X(11)
      REAL MC,K,NU
      PRINT52,MC,AL,C4,C5,K,G,NU
   52 FORMAT(T9,*MC*,T21,*ALPHA*,T33,*C4*,T45,*C5*,T57,*K*,T68,*GAMMA*,
     *T81,*NU*/2X,7F12.4)
      GOTO(101,103,105),M
  101 F="A-MATRIX   ."
      GOTO 106
  103 F="B-MATRIX    "
      GOTO 106
  105 F="A+B-MATRIX
  106 PRINT51,F
   51 FORMAT(//,T31,8A10,//)
      PRINT53,(X(I),I=1,N)
   53 FORMAT(T61,8Y/H*/T32,*X/H*,11F5.1)
      RETURN
      END


      SUBROUTINE DTHETA(A,B,CM,AL,C4,C5,D)
      C=COS(B)
      TOP=A*(1.+C**4)
      BOT=(((1.-CM*C)**2)+AL*CM*CM)**2.5
      BOT=BOT*(1.+C4*EXP(-C5*B))
      D=TOP/BOT
      RETURN
      END
```

The input file may be extended to allow additional cases to be run for different values of H/λ with or without a change in output code in the following manner.

For no change in output code, add additional values of NU (H/λ) after the first value, separating each by a comma (,).

For a subsequent change in output code for any values of NU except the first, add, in the same manner, the following:

-ICODE, the negative of the new desired output code

NU, etc. the new values of NU for new output code

This extension may be continued for as many new values of NU and ICODE as desired for the same values of all other variables. The output code allows the following combinations of output for a given value of NU.

ICODE	Matrix Tables Printed (See Equations 4.2.5-8 and 9)
1	A
2	A and B
3	A and A + B
4	A, B and A + B
5	B
6	B and A + B
7	A + B

Special Instructions

For the case of a monopole, set K and $G(\gamma) = 0$. This sets the directivity index to unity and properly orients the coordinates for a non-directional source.

For a B or A + B output case, the value of LO (L_o) should be less than about 80 to maintain at least one space between rows.

For a geometrically scaled printout on a standard teletype terminal or computer printer, the interval YD ($\Delta y/H$) must be three times XD ($\Delta x/H$).

The program prints out the values of MC through K, G and NU at the top of each table where $A1\ (\alpha^2)$ is identified as ALPHA and $G(\gamma)$ is identified as GAMMA.

The value of K may be selected arbitrarily but, for physically rational results, should be adjusted so that the integral of $D(\theta) \cdot \sin\theta$ from 0 to π is unity. Suitable values of the directivity parameters in Equation 4.2.5-7 which satisfy this constraint are given in the derivation to simulate far field directivity of an ambient air jet and a turbojet engine.

After inputting the first file name, the computer prints the requested tables and then requests a new file name. Any number of additional files may thus be provided for new cases with new directivity constants.

Termination of the program is executed by the normal abort procedure for the remote terminal system.

4.2.5.2 Pressure Level on Fuselage Structures

The noise prediction methods in Sections 4.2.2 through 4.2.4 are, in general, for free-field radiation. In this section, a method will be developed for computing the increase in sound pressure on a circular fuselage for wing or fuselage mounted engines. The order of magnitude of the effect is, of course, to increase the sound pressure level up to a maximum of 6 decibels, so that it is not nearly as severe an effect as the ground reflection from a vertically oriented jet. The details are, however, worth considering in a final design study. Otherwise, an estimated factor varying from 0 - 6 dB should be added to the free field levels. This factor is in addition to the ground reflection factor.

For multi-engines, the sound field from each engine is solved independently and the levels are added, assuming that the sources are uncorrelated (thus equal levels at a point will increase the SPL by 3 dB).

The following derivation was taken from Cockburn and Jolly (9).

Derivation for Wing-Mounted Engines: A typical fuselage and engine configuration for this case is shown in Figure 4.2.5-4. The distance between the center lines of the fuselage and engine is assumed to be at least fifteen jet diameters and the location of a typical source in the exhaust flow is indicated in the figure. The initial problem is to define the sound field for a single source in the jet flow, S, and determine the sound field at a point on the fuselage surface, Q, for a frequency, ω. The coordinate system adopted is shown in Figure 4.2.5-5. The acoustic wave is considered to be a plane wave of strength P_o at the point where it reaches the fuselage, and the pressure fluctuations, without scattering effects are given by;

$$P = P_o e^{ik(x - a_o t)} \qquad (4.2.5\text{-}10)$$

where

k is the wave number of the particular source $= 2\pi/\lambda$

λ is the wavelength $= a_o/f$

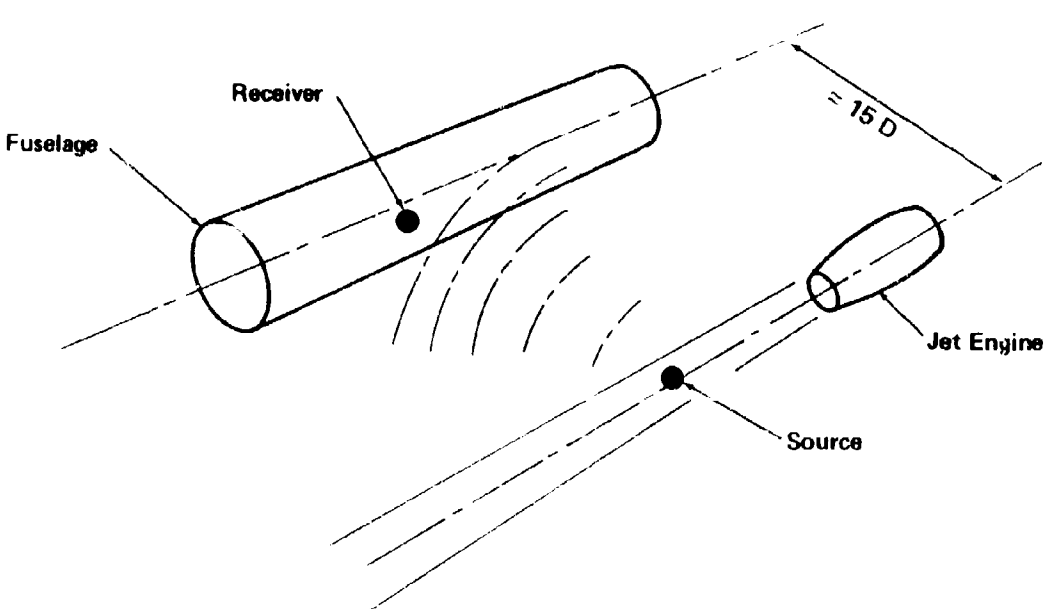

FIGURE 4.2.5-4 RELATIONSHIP BETWEEN FUSELAGE AND JET ENGINE FOR WING-MOUNTED ENGINES

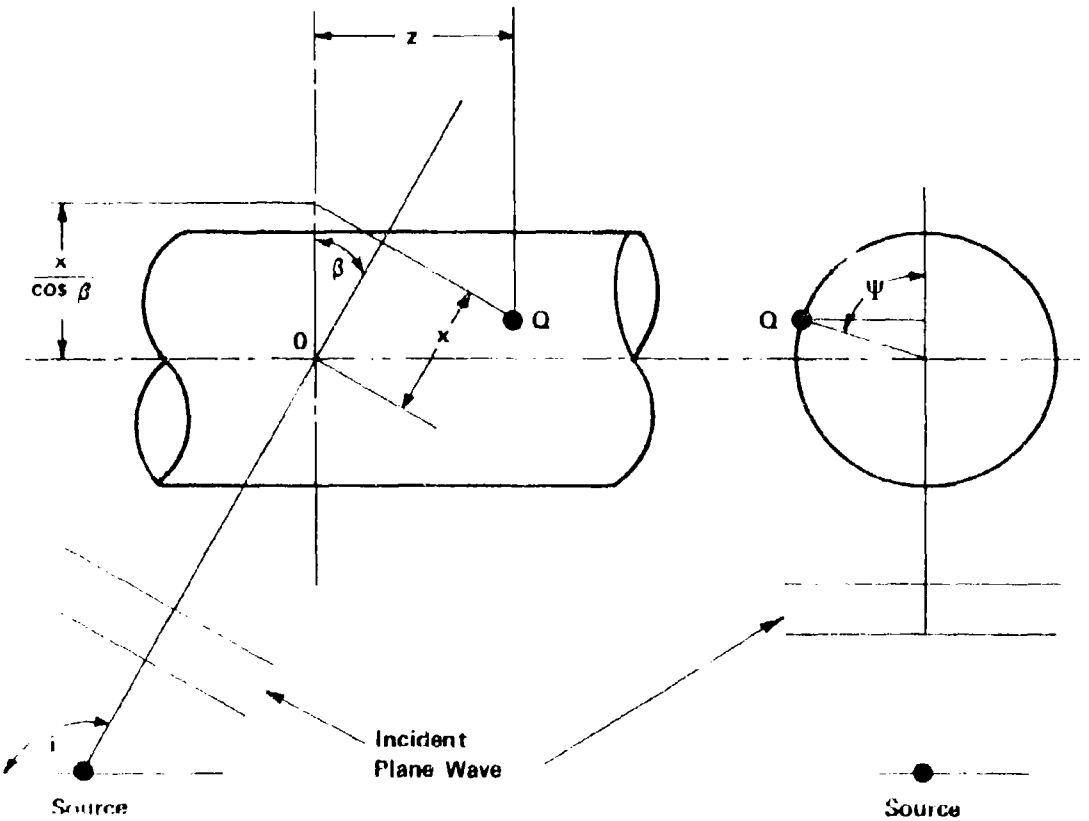

FIGURE 4.2.5-5 COORDINATE SYSTEM FOR WING-MOUNTED ENGINES

a_o is the speed of sound

t is time

and x is the distance in the direction of propagation (see Figure 4.2.5-5)

The wave direction is such that the normal to the wave makes an angle β to the normal to the axis of the fuselage. The point on the surface of the fuselage is given by (a, z, ψ), where a is the radius of the fuselage, z is the dimension along the axis, and ψ is the angle around the fuselage measured from the projection of the line joining the source to the fuselage on the perpendicular cross-section. When the angle ψ is zero, the point is on the far side of the fuselage, completely hidden from the source.

The solution for the scattering case was shown by Potter (10) to be;

$$P = \frac{4P_o}{ka \cos \beta} \sum_{m=0}^{\infty} \frac{\cos m\psi}{C'_m} e^{i\left(-\gamma'_m + \frac{\pi m}{2}\right)} e^{ikz \sin \beta} e^{-2\pi i f t} \qquad (4.2.5\text{-}11)$$

where C'_m and γ'_m are functions of ka cos β,

$$C'_o = 2\left|J_1^2 (ka \cos \beta) + N_1^2 (ka \cos \beta)\right|^{1/2} \qquad (4.2.5\text{-}12)$$

$$C'_m = \frac{1}{2}\left|\left|J_{m+1}(ka \cos \beta) - J_{m-1}(ka \cos \beta)\right|^2 + \left|N_{m-1}(ka \cos \beta) - N_{m+1}(ka \cos \beta)\right|^2\right|^{1/2} \qquad (4.2.5\text{-}13)$$

$$\gamma'_o = \mathrm{Tan}^{-1}\left[\frac{-J_1(ka \cos \beta)}{N_1(ka \cos \beta)}\right] \qquad (4.2.5\text{-}14)$$

$$\gamma'_m = \mathrm{Tan}^{-1}\left[\frac{J_{m+1}(ka \cos \beta) - J_{m-1}(ka \cos \beta)}{N_{m-1}(ka \cos \beta) - N_{m+1}(ka \cos \beta)}\right] \qquad (4.2.5\text{-}15)$$

where

J and N are Bessel functions of the first and second kind.

z is the axial distance along the fuselage

ψ is the angle around the fuselage from the projected direction of propagation of the wave on a circular section (i.e., the wave impinges directly on the cylinder at the angular point $\psi = \pi$ radians).

This result was developed from that given by Morse in Reference 11, for a normally incident plane wave scattered by a cylinder, by Potter in Reference 10, and proved mathematically by Wenzel in Reference 12.

The actual pressure var ation on the fuselage surface is given by the real part of Equation (4.2.5-11). It should be noted that this expression is only applicable to wing-mounted engines where the sound field for a given source can be approximated as a plane wave at the point where it strikes the fuselage. The equation describing the pressure fluctuations is limited to some extent by the fact that the effects of spherical radiation have not been included. Furthermore, the surface of the fuselage was assumed to be perfectly rigid, which is not the case in practice. The complete solution, involving the scattering of an obliquely incident spherical radiation by a finite non-rigid structure will be extremely complicated and is not considered in the present study.

Equation(4.2.5-11)can be reduced to a simpler form for presentation and computation as follows.

The pressure at a point on the fuselage surface, due to an obliquely incident plane wave of frequency f is,

$$P = A \cos (2\pi ft + \Phi) \qquad (4.2.5\text{-}16)$$

where

$$A = (x^2 + y^2)^{1/2}$$

$$\Phi = \mathrm{Tan}^{-1} \left(\frac{y}{x}\right)$$

$$x = D_o(EG - FH)$$

$$y = D_o(FG + EH)$$

$$D_o = \frac{4P_o}{\pi ka \cos \beta} \qquad (4.2.5\text{-}17)$$

$$E = \sum_{m=0}^{\infty} \frac{\cos m\psi}{C'_m} \sin \left(-\gamma'_m + \frac{\pi m}{2}\right)$$

$$F = \sum_{m=0}^{\infty} \frac{\cos m\psi}{C'_m} \cos \left(-\gamma'_m + \frac{\pi m}{2}\right)$$

$$G = \cos (kz \sin \beta)$$

$$H = \sin (kz \sin \beta)$$

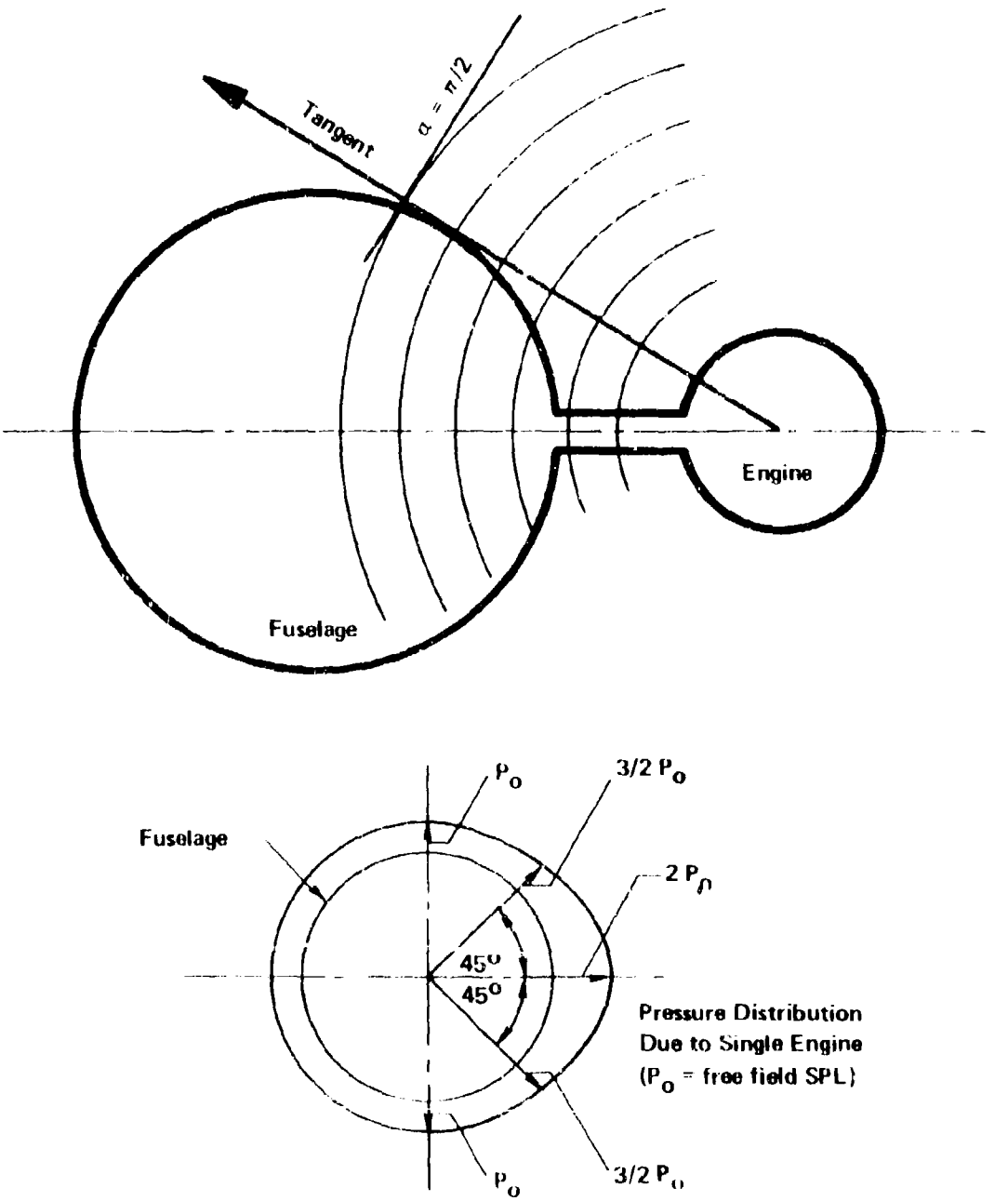

FIGURE 4.2.5-6 GEOMETRY AND PRESSURE DISTRIBUTION FOR FUSELAGE-MOUNTED ENGINES

and P_o = free-field pressure calculated from the source methods of Section 4.2.2 and 4.2.3.

Derivation for Fuselage Mounted Engines : In this case the engines will be so close to the fuselage that the technique of scattering is not suitable. However, since the structure adjacent to the jet is loaded by the sources in the immediate vicinity, the source allocation method can be used for determining the free-field sound pressure level and conversion to fuselage pressure loadings may be achieved by use of a simple equation. For an obliquely incident wave, as shown in Figure 4.2.5-6, the pressure at a point on the fuselage surface may be determined from the equation;

$$P = P_o \left(\frac{\cos 2\alpha + 3}{2}\right) \qquad (4.2.5\text{-}18)$$

where α is the angle between the wavefront and the tangent to the surface, $-\pi/2 \leq \alpha \leq \pi/2$, and P_o is the free-field pressure calculated from the source methods. The resulting pressure loading on the fuselage, obtained from Equation (4.2.5-18) is shown in Figure 4.2.5-6.

4.2.5.3 Effects of Aircraft Forward Motion on Near Field Noise

Although there is a quality of uncertainty surrounding the prediction of near-field acoustic loads for propulsion system noise sources most of the mechanisms controlling both the noise generation and radiation are reasonably well understood. That is to say, the physical mechanisms controlling the noise generation have been postulated and experimentally verified, or else, parametric studies have been conducted in sufficient detail to permit a valid "curve-fitting" exercise over a sufficient range of the control parameters to permit prediction. But, in the case of forward flight effects on aircraft noise, and in particular, near-field noise, this is not the case. Not very much conclusive experimental evidence exists on the effect of flight on propulsion system near-field noise.

A number of observations do exist, however, and they will be mentioned. These observations primarily relate to the subject of far-field noise prediction, however some can be carried over to the near-field region.

There are two categories of acoustic sources, i.e., those attached to the flying vehicle and those convecting away from the vehicle with the jet flow. Most sources, such as propeller noise, fan noise and shock cell noise, are attached to (or dragged along by) the vehicle. However, jet noise sources are convecting away from the vehicle at the jet turbulence convection velocity.

There are also two major effects of forward velocity. These are source alteration due to flight and sound propagation modification.

It has been assumed in the past that the jet noise source strength was modified by a relative velocity factor. In the far-field, where jet noise was approximately proportional to V_j^8, the forward motion effect was taken to be $(V_j - V_f)^8 = V_{rel}^8$. The relative velocity effect as just presented has not

been experimentally verified, even in the far-field. One reason, suggested by Kobrynski (13), is due to the change in jet mixing length with forward motion. After accounting for this, he found that the total sound power from the jet could be expressed as

$$P = \frac{K\rho_j^2 A V_j^8}{\rho_o a_o^5} \left[1 - \left(\frac{V_t}{V_j}\right)\right]^4 ,$$

which results in a dependance considerably less than V_{rel}^8. Kobrynski's paper contains many practical expressions relative to jet noise due to forward motion, however, these will not be dealt with in any more detail here because of the far-field derivation. However, the above expression could be used as a guide in determining the total sound power reduction as a result of vehicle motion.

Forward motion effects on propeller and fan noise source alteration are accounted for by the tip vector velocity, which includes the forward velocity. The relative tip velocity factor seems to be an adequate representation of what actually happens, as opposed to the relative velocity effect for jet noise which is not representative of experimental observations.

The modifications of the noise field resulting from forward flight due to sound propagation effects can be separated into four identifiable quantities, which are:

- The change in distance through which the sound propagates,
- The Doppler frequency shift
- Convective amplification
- Acoustic/mean flow interactions.

The first factor is a simple geometric problem and can be easily accounted for and modifications in SPL can be determined. The Doppler shift factor is also easily determined in terms of frequency shift. However, the latter two factors will not have much meaning relative to near field noise prediction methods, especially the "n" field jet noise methods, since they are purely empirical.

The effect of motion on the change in distance and angle through which the sound propagates for a jet noise source which is convecting away from the moving aircraft is discussed by Franken (14). In his discussion of forward motion effects, referring to Figure 4.2.5-7, assume that the forward motion moves the receiver from its actual position R to an apparent position R' on a line parallel to the direction of motion. This change in position is shown in Figure 4.2.5-7 for the receiver either upstream or downstream of the source. The motion changes the angle θ into the angle Φ.

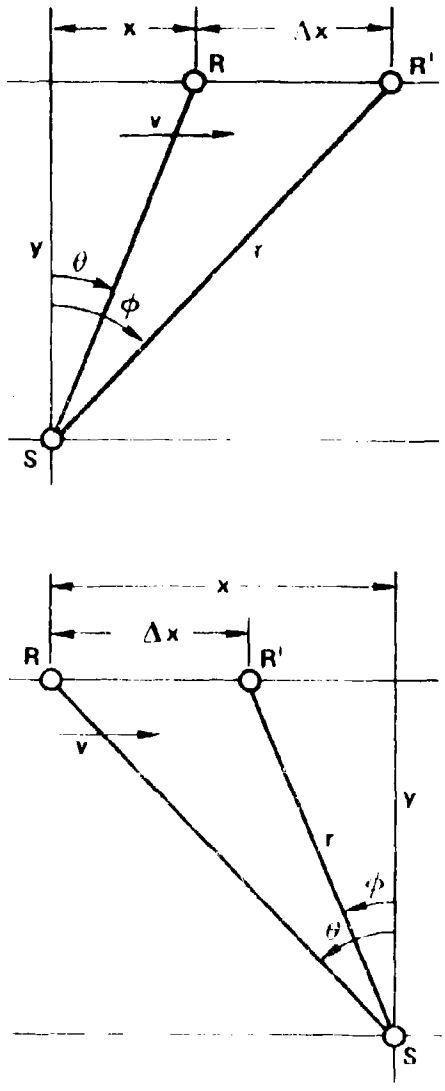

FIGURE 4.2.5-7 EFFECTS OF FORWARD MOTION, SHOWING BOTH SOURCE AND RECEIVER GEOMETRY

Using the geometry of Figure 4.2.5-7, we may determine the relationship between θ and Φ. The sound wave travels distance r at velocity a_o in the same time that the receiver is convected over distance Δx at velocity V, or

$$\frac{r}{a_o} = \frac{\Delta x}{V} \qquad (4.2.5\text{-}19)$$

Also, from the triangle whose hypotenuse is r,

$$r^2 = y^2 + (x + \Delta x)^2 \qquad (4.2.5\text{-}20)$$

Since by definition

$$\tan \theta = \frac{x}{y}, \quad \tan \Phi = \frac{x + \Delta x}{y}, \quad M = \frac{V}{a_o} \qquad (4.2.5\text{-}21)$$

we obtain

$$\tan \Phi = \frac{1}{(1 - M^2)} \left[\tan \theta + M \sqrt{1 - M^2 + (\tan \theta)^2}\right] \qquad (4.2.5\text{-}22)$$

Associated with this motion there occurs a Doppler change in frequency and wavelength perceived by the receiver, so that

$$\lambda/\lambda_o = 1 - M \sin \Phi , \qquad (4.2.5\text{-}23)$$

where λ is the perceived wavelength at vehicle Mach number M, and λ_o is that observed at rest.

Plots of Equations (4.2.5-22) and (4.2.5-23) for several values of M appear in Figure 4.2.5-8. The right hand graph gives the apparent angle Φ in terms of the angle θ and Mach number M; the left-hand graph may then be used to find the change in observed wavelength. It may be seen that at supersonic speeds no jet noise propagates upstream of the noise source (positive values of Φ). (It should be noted that at very high speeds pressure fluctuations other than jet noise (such as boundary layer noise) may become significant.)

As an example, the angular transformation of Figure 4.2.5-8 has been applied to the near-field noise contours of a contemporary turbojet engine for the value of Mach 0.8. Both sets of contours are shown in Figure 4.2.5-9 where the broken lines represent sound pressure levels during static operation and the solid lines the estimated sound pressure level contours for M = 0.8. In making the transformation shown in Figure 4.2.5-9, the simplifying assumption that the sound sources are located near the jet exhaust nozzle has been made. For greater refinement one may transform contours of noise measured in bands of frequency, specifying the corresponding noise source location at some position downstream of the nozzle.

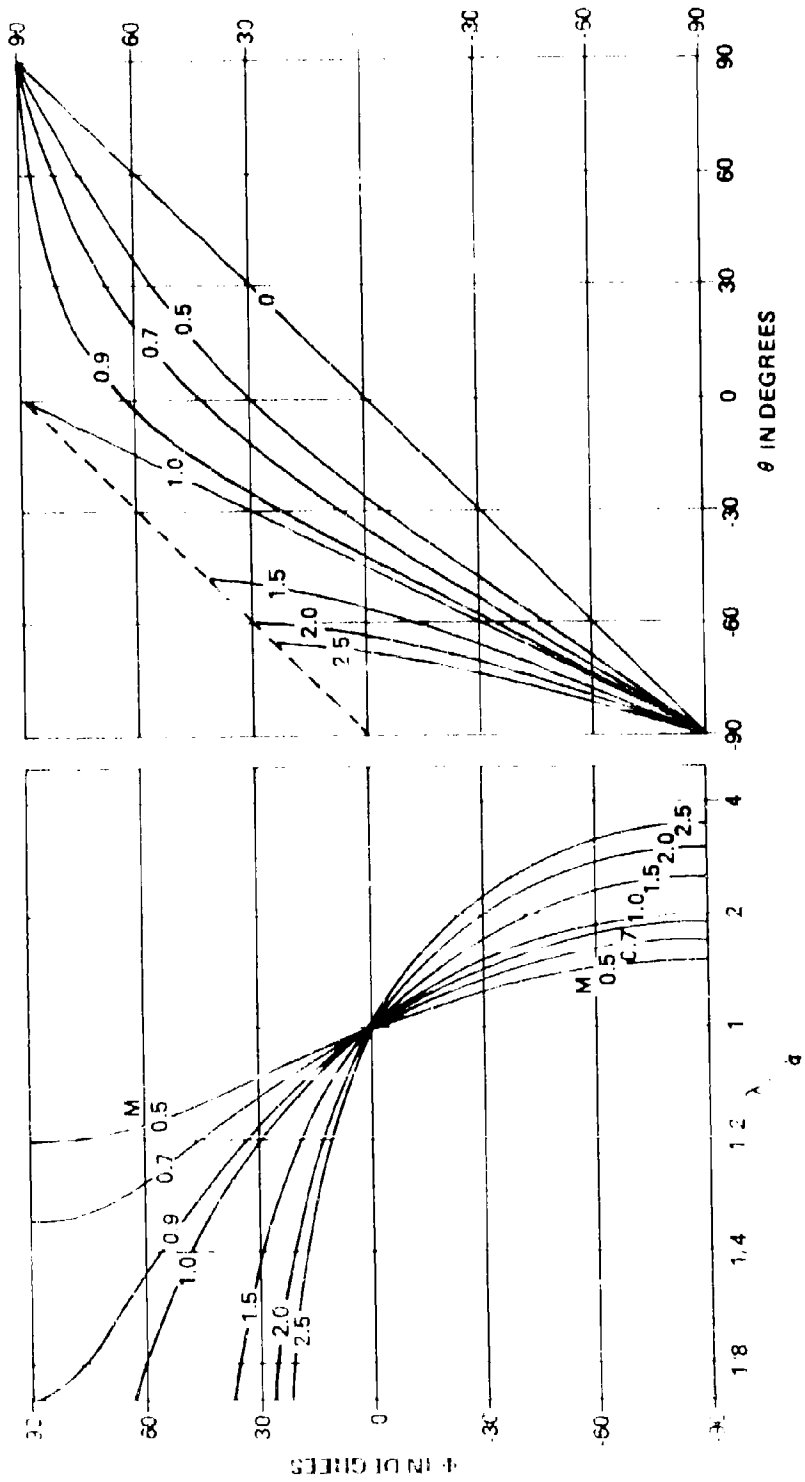

FIGURE 4.2.5-6 EFFECTS OF FORWARD MOTION ON CHANGES IN ANGLE AND OBSERVED WAVELENGTH

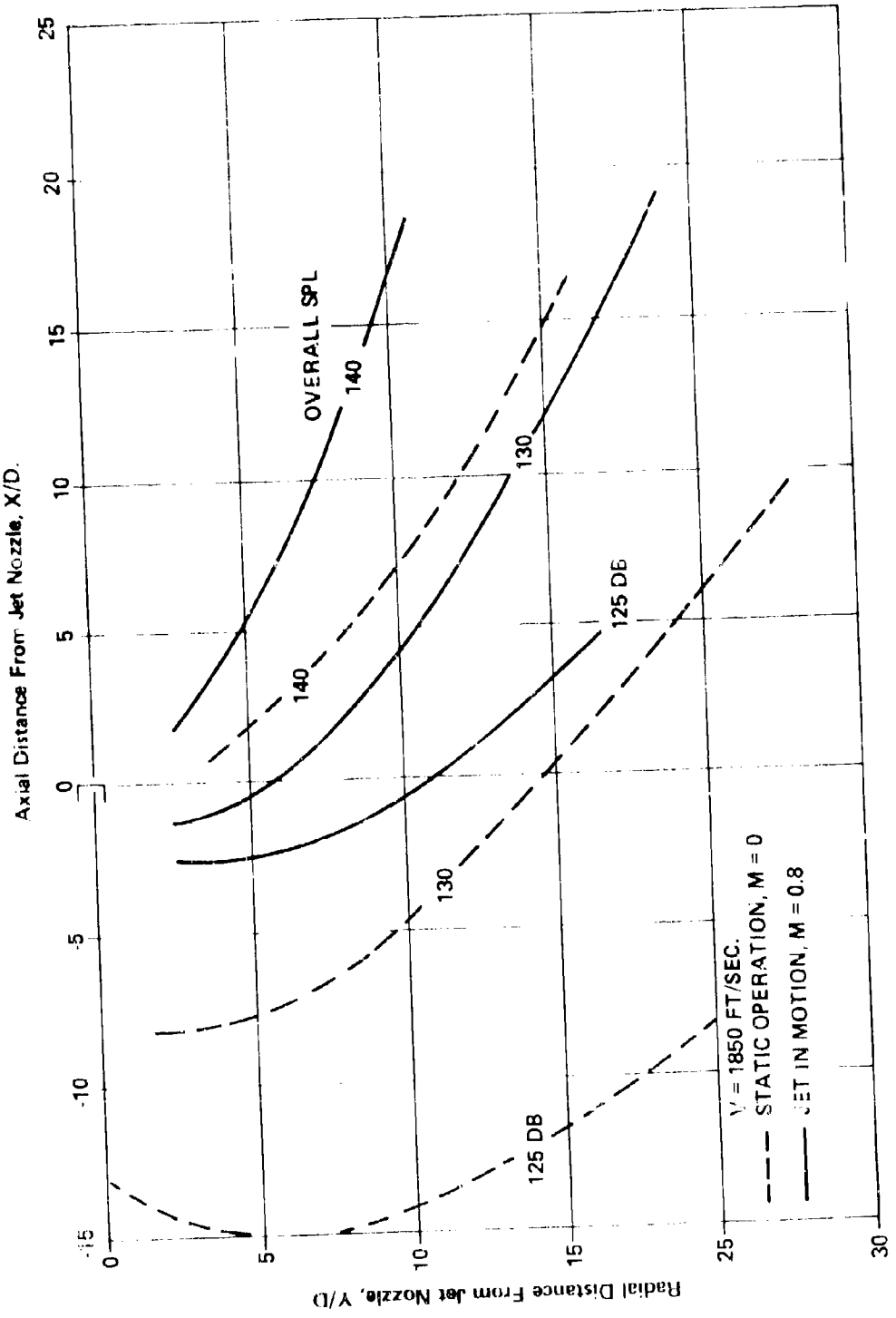

FIGURE 4.2.5-9 EFFECT OF FORWARD MOTION ON NEAR-FIELD JET NOISE

REFERENCES FOR SECTION 4.2.5

1. Howes, W. L.; "Ground Reflection of Jet Noise," NASA TR-R-35, 1959.

2. Sutherland, L. C. and Brown, D.; "Prediction Methods for Near Field Noise Environments of VTOL Aircraft," AFFDL-TR-71-180, Wright-Patterson Air Force Base, Ohio, 1972.

3. Hoch, R. and Thomas P.; "Influence Des Reflexions Sur Les Spectres De Pression Acoustique Des Jets," Paper presented at the Colloque d'Acoustique Aeronautique, Toulouse, France 6-8 March, 1968.

4. Eldred, K. M., White, R. W., Mann, M. A. and Cottis, M. G.; "Suppression of Jet Noise with Emphasis on the Near Field," ASD-TDR-62-578, Wright-Patterson Air Force Base, Feb. 1963.

5. Franken, P. A.; "A Theoretical Analysis of the Field of a Random Noise Source Above an Infinite Plane," NACA-TN-3557, November 1955.

6. Morgan, W. V., Sutherland, L. C., and Young, K. J.; "The Use of Acoustic Scale Models for Investigating Near Field Noise of Jet and Rocket Engines," WADD-TR-61-178, Wright Patterson Air Force Base, April 1961, AD 268 576.

7. Ribner, H. S., "The Generation of Sound by Turbulent Jets," Advances in Applied Mechanics, Vol. 8, pp. 104-178, Academic Press, Inc., N.Y., 1964.

8. Plumblee, H. E., Ballentine, J. R. and Passinos, B.; "Near Field Noise Analyses of Aircraft Propulsion Sy ems with Emphasis on Prediction Techniques for Jets," AFFDL-TR-67- , Wright-Patterson Air Force Base, 1967.

9. Cockburn, J. A. and Jolly, A. C.; "Structural-Acoustic Response, Noise Transmission Losses and Interior Noise Levels of an Aircraft Fuselage Excited by Random Pressure Fields," AFFDL-TR-68-2, Wright-Patterson Air Force Base, August 1968.

10. Potter, R. C., "Correlation Patterns of the Acoustic Pressure Fluctuations on the S-IC Vehicle Due to the Exhaust Noise at the Test and Launch Stand," Wyle Research Staff Report WR66-19, 1966.

11. Morse, P. M.; Vibration and Sound, McGraw-Hill Book Co., 1948.

12. Wenzel, A. R.;"Surface Pressure Correlation Functions for a Cylinder in a Diffuse Reverberant Sound Field," Wyle Laboratories Research Staff Report WR 66-14, 1966.

13. Kobrynski, M.; "On the Calculation of the Maximum Sound Pressure Spectrum from Stationary and Mobile Jets," Journal of Sound and Vibration, Vol. 7, No. 2, pp. 263-286, March 1968.

14. Franken, P. A., "Methods of Space Vehicle Noise Prediction," WADC TR 58-343, Vol. II, Wright-Patterson Air Force Base, Sept. 1960.

4.3 AERODYNAMIC NOISE

Aerodynamic noise, in the context of this report, is the noise generated by the airflow, over structural surfaces, resulting from forward flight. It can be boundary layer noise, oscillating shock noise, cavity noise, noise from separated flows, etc. The near field fluctuating pressure due to turbulent boundary layers (sometimes referred to as pseudo-sound) is probably the most widely studied aerodynamic noise source. Boundary layer noise, oscillating shock and separated flow are not as significant a loading action as propulsion noise.

The potentially most damaging aerodynamic noise source is the resonant acoustic response of cavities with one side exposed to an aerodynamic flow. Cavity noise has been known to cause sonic fatigue failures in several instances. Thus, it seems that from the standpoint of acoustic fatigue considerations, cavity noise ranks as the worst offender.

4.3.1 SYMBOLS AND DEFINITIONS

The notation used in this section is as follows:

a_o	ambient speed of sound
f	frequency in Hertz
f_m	cavity resonant frequency
G_{p^2}	power spectral density of pressure fluctuations
g_n	defined by $g_n = \xi_n + i\eta_n$
k	wavenumber, $2\pi f/a_o$
L	typical dimension
L_x	cavity length
L_y	cavity width
L_z	cavity depth
M	free-stream Mach no.
m	an integer defining the order of the cavity resonance
n_x	length mode number
n_y	width mode number
P_m	m^{th} modal peak sound pressure in cavity
p	rms sound pressure
p_o	reference sound pressure
q	dynamic pressure, $1/2\ \rho U^2$
R	radiation resistance
Re_x	Reynolds no.
St	Strouhal frequency, fL/U
U	free-stream velocity
X	radiation reactance, $\log_e(f\delta_b/U)$ in Section 4.3.3
α_n	constant in Equation (4.3.2-5) relating to mode no.
γ	ratio of specific heats of gas
δ_b	boundary layer thickness
η_n	imaginary solution of boundary function
ν	kinematic viscosity
ξ_n	real solution of boundary function
ρ	density of air at rest
χ	cavity axis in longitudinal direction
ω	radian frequency, $2\pi f$
ω_o	reference frequency

4.3.2 CAVITY NOISE

The noise of cavities located in aerodynamic surfaces has been studied for over 20 years. The noise ranges from the high frequency resonant response, characteristic of small electronic openings, to the very low frequency response, characteristic of bomb bays. Cavity noise can be very intense, leading to crew annoyance and fatigue or even, in several cases, to structural fatigue. Cavity noise, evidenced in both subsonic and supersonic flight, is excited by the unstable boundary layer flowing by the cavity opening.

There have been several research investigations on cavity noise, dating back to Blokhintsev's (1) work in 1945. Krishnamurty (2) conducted an extensive experimental study of the sound radiated from the cavity. He concluded that the phenomenon was associated with the inherent instability of the separated boundary layer. Plumblee, et al. (3) showed by means of a theoretical and experimental wind tunnel study that the acoustic modes of the cavity were acting as selective amplifiers of certain frequencies from the excitation spectrum resulting from the boundary layer instability. Among other things, this study presented methods (which were fairly complex) for computing cavity resonant frequencies for subsonic and supersonic Mach numbers. East (4) later, in another extensive test and data correlation program, verified the frequency formulas developed by Plumblee (3). In a later study, Rossiter (5) developed an empirically based formula which relates the Strouhal frequency, St, to the Mach no. and Mode no. for shallow cavities. Heller, et al. (6) modified the Rossiter formula to account for the stagnation sound speed (i.e., it was hypothesized that the cavity sound speed equals the stagnation sound speed) giving better agreement with experimentally determined resonant frequencies for the first five length modes of the shallow cavity over a Mach number range of $0.5 \leq M \leq 3$. Shaw et al. (7,9) and Smith et al. (8), used the results of Heller (6) and extensive flight data acquired by the AFFDL to develop a cavity noise prediction scheme for determining frequencies and SPL from 0.6 to 1.3 Mach number for cavities with length to depth (L_x/D) ratios in this range of 4 to 7.

This section will present the empirically determined prediction method of Shaw (7,9) which incorporates the results from Heller's study (6). Also, the theoretically based prediction method derived by Plumblee (3) is included to permit parametric studies based on cavity dimensions and Mach no.

4.3.2.1 Cavity Noise Prediction Method - Empirical

Derivation: The prediction procedure given in this section is purely empirical and is based on the wind tunnel test data of Heller, et al. (6) and the flight test results of Shaw, et al. (7,9). When Heller (6) completed his program, it was not established that scaling from models to full size flight vehicles would be successful. Shaw's work, although displaying some differences, especially in the longitudinal sound pressure distribution, generally confirmed the validity of scaling.

Both series of tests were conducted on long shallow cavities with an aspect ratio (length/depth) of 4 to 7. Previous studies indicated that geometric frequency scaling could be achieved through the use of a Strouhal number and that SPL's could be scaled with dynamic pressure. The

comparison presented in Shaw's work confirmed the Strouhal number scaling and added validity to the dynamic pressure scaling hypothesis for certain cavity positions, but in other regions, q scaling was not valid.

The three parameters of interest relative to cavity noise are (1) the resonant frequencies of response, (2) the peak response amplitude and (3) the SPL distribution. The experiments in References (6) through (9) were designed to permit definition of the items listed above. It was determined that the sound pressure spectra was composed of two parts. One was a broad-band random background noise and the other was a set of resonant high energy tones.

Further descriptions of the tests and hardware is included in References (6) through (9). The following is a description of the prediction scheme by Shaw (7,9) and Smith (8).

Prediction Method: The following steps are taken to estimate the acoustic response of a cavity:

(1) Determine the resonant frequencies with the modified Rossiter expression (Reference 6):

$$f_m = \frac{U}{L_x}\left[\frac{(m - 0.25)}{\frac{M}{\left(1+\frac{\gamma-1}{2}M^2\right)^{1/2}} + 1.75}\right], \quad m = 1,2,3 \qquad (4.3.2\text{-}1)$$

where U is the free-stream velocity, L_x is the cavity length and M is the free stream Mach number, or else refer to Figure 4.3.2-1.

(2) Determine the peak one-third octave normalized SPL for f_1, f_2, and f_3 using Figure 4.3.2-2 or the following relationships for $L_x/D = 4.0$ (see Figure 4.3.2-2).

$$20\cdot\log(P_2 \text{ max}/q) = 9.0 - 3.3(L_x/D) + 20\cdot\log(-M^2 + 2M - 0.7) \qquad (4.3.2\text{-}2)$$

$$20\cdot\log(P_1 \text{ max}/q) = 20\cdot\log(P_2 \text{ max}/q) - 2(L_x/D)^2 + 26(L_x/D) - 86 \qquad (4.3.2\text{-}3)$$

$$20\cdot\log(P_3 \text{ max}/q) = \begin{cases} 20\cdot\log(P_2 \text{ max}/q) - 11 & \text{for } L_x/D < 4.5 \\ 20\cdot\log(P_2 \text{ max}/q) & \text{for } L_x/D \geq 4.5 \end{cases} \qquad (4.3.2\text{-}4)$$

where P max are the maximum fluctuating pressures for each mode frequency, f_n, and q is the free-stream dynamic pressure.

(3) Determine the peak one-third octave band amplitude at the desired longitudinal position for each resonant frequency from the following equation or for $L_x/D = 4.0$, Figure 4.3.2-3:

$$20\cdot\log\left(\frac{P_n}{q}\right)_{x/L_x} = 20\cdot\log\left(\frac{P_{n\,max}}{q}\right) - 10[1.0 + (0.33L_x/D - 0.60)(1 - x/L_x) - |\cos(\alpha_n x/L_x)|] \quad n = 1,2,3 \qquad (4.3.2\text{-}5)$$

where $\alpha_1 = 3.5$

$\alpha_2 = 6.3$

$\alpha_3 = 10.0$

(4) Determine the peak normalized one-third octave band level of the broadband spectrum at the location in the cavity from Equation (4.3.2-6) or, for $L_x/D = 4.0$, Figure 4.3.2-4

$$20\cdot\log\left(\frac{P_b}{q}\right)_{x/L_x} = 20\cdot\log\left(\frac{P_{2\,max}}{q}\right) + 3.3(L_x/D) - 28 + 3(1-L_x/D)(1-x/L_x) \qquad (4.3.2\text{-}6)$$

(5) Determine the normalized broadband spectrum from Figure 4.3.2-5.

(6) Determine the absolute levels by adding $20\cdot\log q$ to the levels, where $20\cdot\log q$ is determined from Figure 4.3.2-6 from the appropriate attitude and velocity.

Another significant finding from the flight test was that for certain cavity locations the dynamic pressure (q) scaling did not account for the total variation in the SPL with altitude; however, at two cavity locations scaling with q did account for the complete change in the SPL with a change in the altitude, i.e., the SPL referenced to q was the same for any altitude. Previous investigators have shown that for a fixed Mach number q scaling accounted for any significant change in the SPL for various pressure altitudes. The reason they did not observe this phenomena could be due to the cavity positions analyzed. The position selected could be one at which q scaling accounts for all pressure altitude variations.

The prediction method presented above is based on empirical results which were selected to give the highest sound pressure levels in the cavity. Although scaling with q failed at some points in the cavity, the predicted levels will be conservative at these locations.

Example: For clarity, an example is presented illustrating use of the prediction method and a comparison is made of results of this method to those obtained from Reference 6.

Consider the case of an aircraft flying at Mach 0.9 near sea level with an open nearly rectangular cavity 20 feet long and 5 feet deep ($L_x/D = 4.0$). It is desired to predict the aero-acoustic environment at the center and at the rear of the cavity. The solution is obtained as follows:

From Step (1), Equation(4.3.2-1), or Figure 4.3.2-1 the first 3 mode frequencies are determined to be:

$$f_1 = 15 \text{ Hz}$$
$$f_2 = 34 \text{ Hz}$$
$$f_3 = 54 \text{ Hz}$$

Equations (4.3.2-2), (-3) and (-4) or Figure 4.3.2-2 of Step 2 are used to calculate the maximum normalized amplitude for each mode frequency and results in the following values:

$$20 \cdot \log (P_1 max/q) = -29 \text{ dB}$$
$$20 \cdot \log (P_2 max/q) = -15 \text{ dB}$$
$$20 \cdot \log (P_3 max/q) = -26 \text{ dB}$$

The amplitude of each mode frequency at the center and rear of the cavity is determined from Equation (4.3.2-5). The results, referenced to $20 \mu N/m^2$, are:

for $x/L_x = 0.5$
$SPL_1 = 146$ dB
$SPL_2 = 168$ dB
$SPL_3 = 150$ dB

for $x/L_x = 1.0$
$SPL_1 = 160$ dB
$SPL_2 = 174$ dB
$SPL_3 = 161$ dB

where $20 \cdot \log q$ was determined from Figure 4.2.2-7.

Step 4, Equation (4.3.2-6), is then used to obtain the peak normalized one-third octave band levels of the broadband spectrum at the two locations and are

$$20 \cdot \log \left(\frac{P_b}{q} \right)_{x/L_x = 0.5} = -34$$
$$20 \cdot \log \left(\frac{P_b}{q} \right)_{x/L_x = 1.0} = -30$$

The final step is to determine the broadband spectrum from Figure 4.3.2-5.

The spectra obtained are shown in Figure 4.3.2-7 along with the spectrum one would predict using the scheme offered in Reference 6. The current results show resonant modes 1 and 3 completely attenuated for the center position, this is due to the longitudinal mode shapes. The $x/L_x = 0.5$ position is seen to be a node for the mode 1 and 3 frequencies while an antinode for mode 2. Thus, there is almost 30 dB difference between the two prediction schemes at the center of the cavity for modes 1 and 3. However, it should be noted that the prediction schemes agree fairly well for the maximum level predicted at the rear of the cavity for the mode 2 frequency.

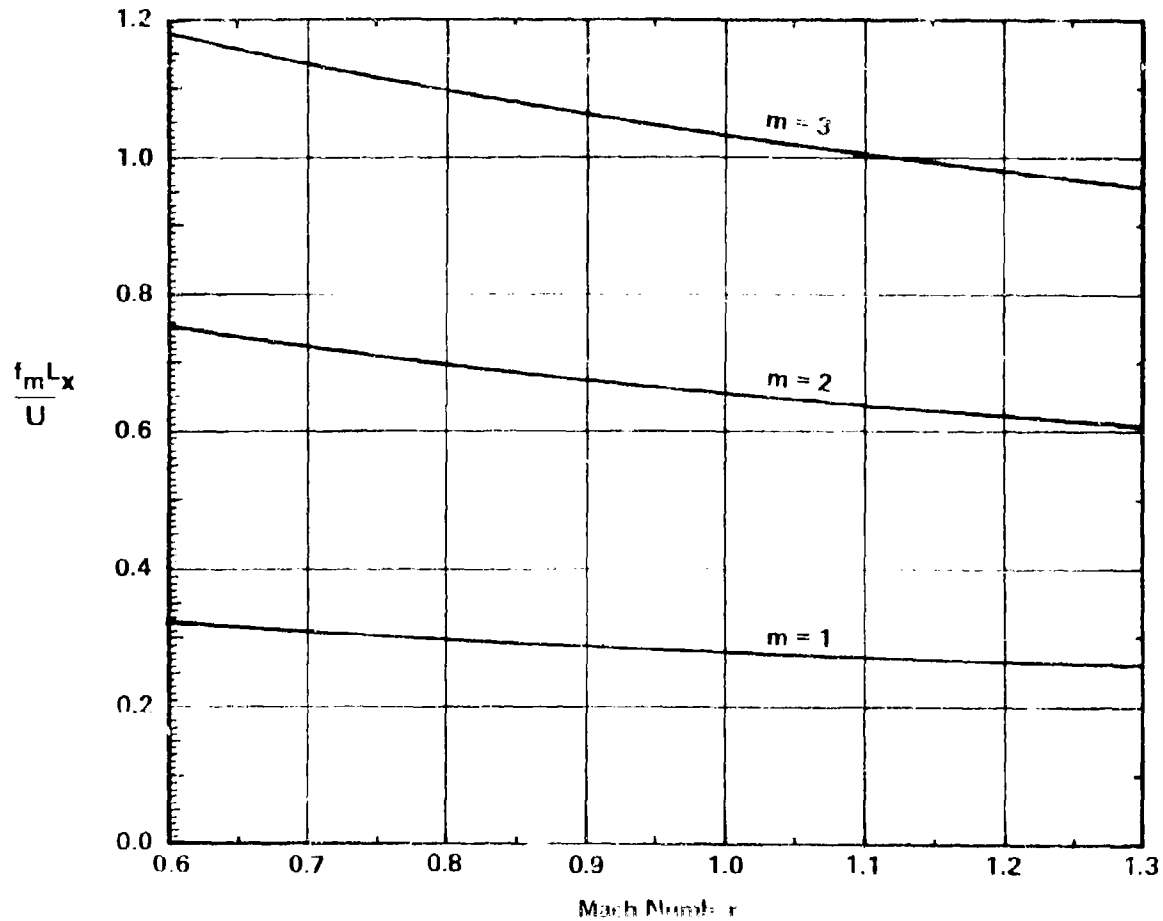

FIGURE 4.3.2-1 VARIATION OF CAVITY RESONANT STROUHAL FREQUENCIES WITH MACH NUMBER FOR FIRST THREE LENGTH MODES

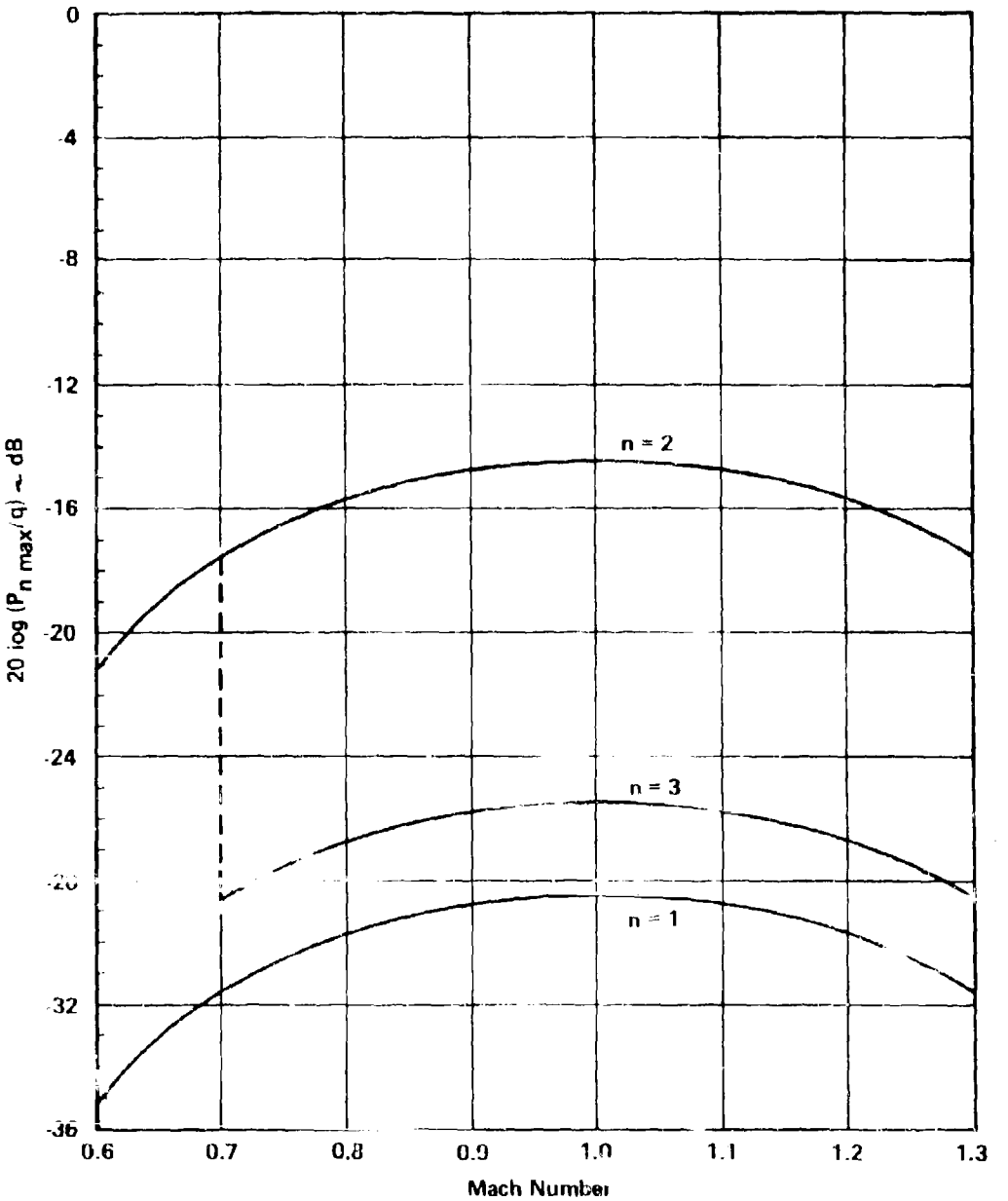

FIGURE 4.3.2-2 VARIATION OF MODAL PEAK AMPLIFICATION WITH MACH NUMBER FOR FIRST THREE MODES (L_x/D = 4.0)

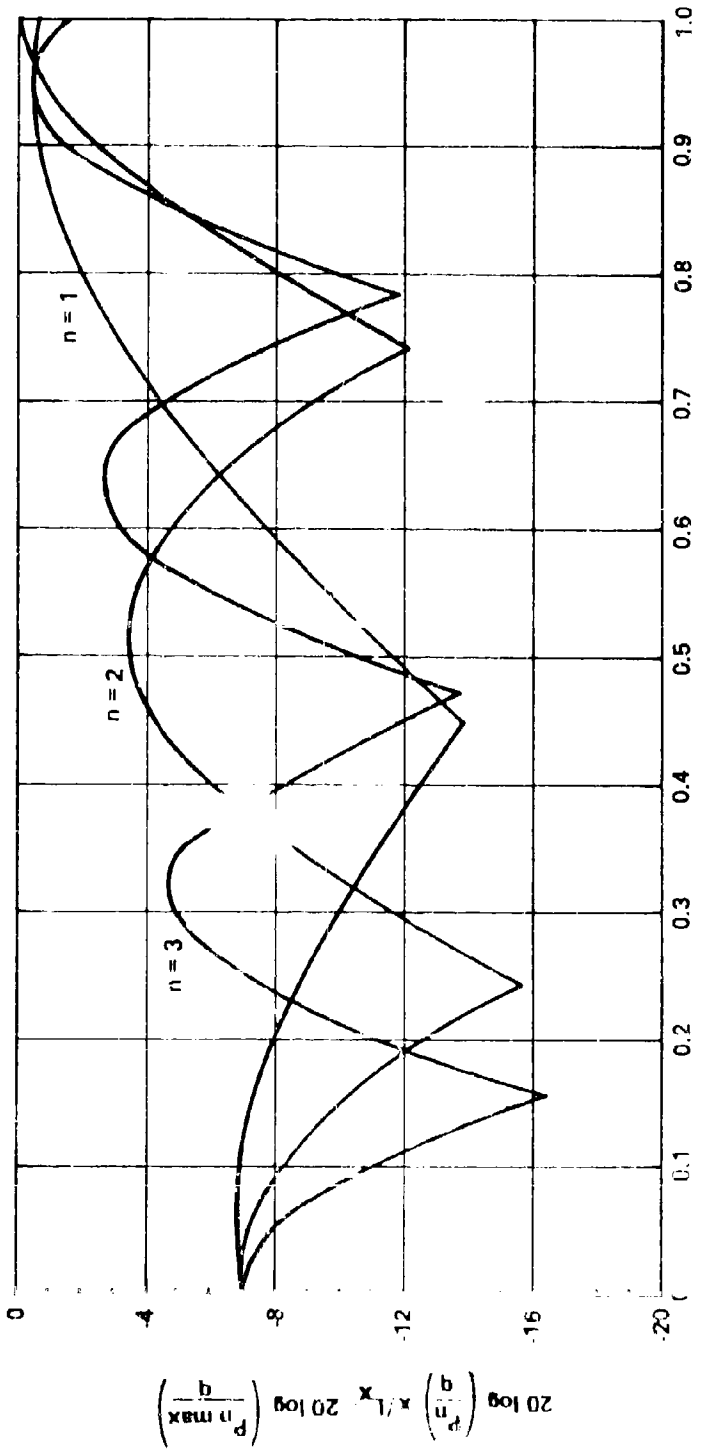

FIGURE 4.3.2-3 MODAL PRESSURE DISTRIBUTION ALONG CAVITY LENGTH ($L_x/D = 4.0$)

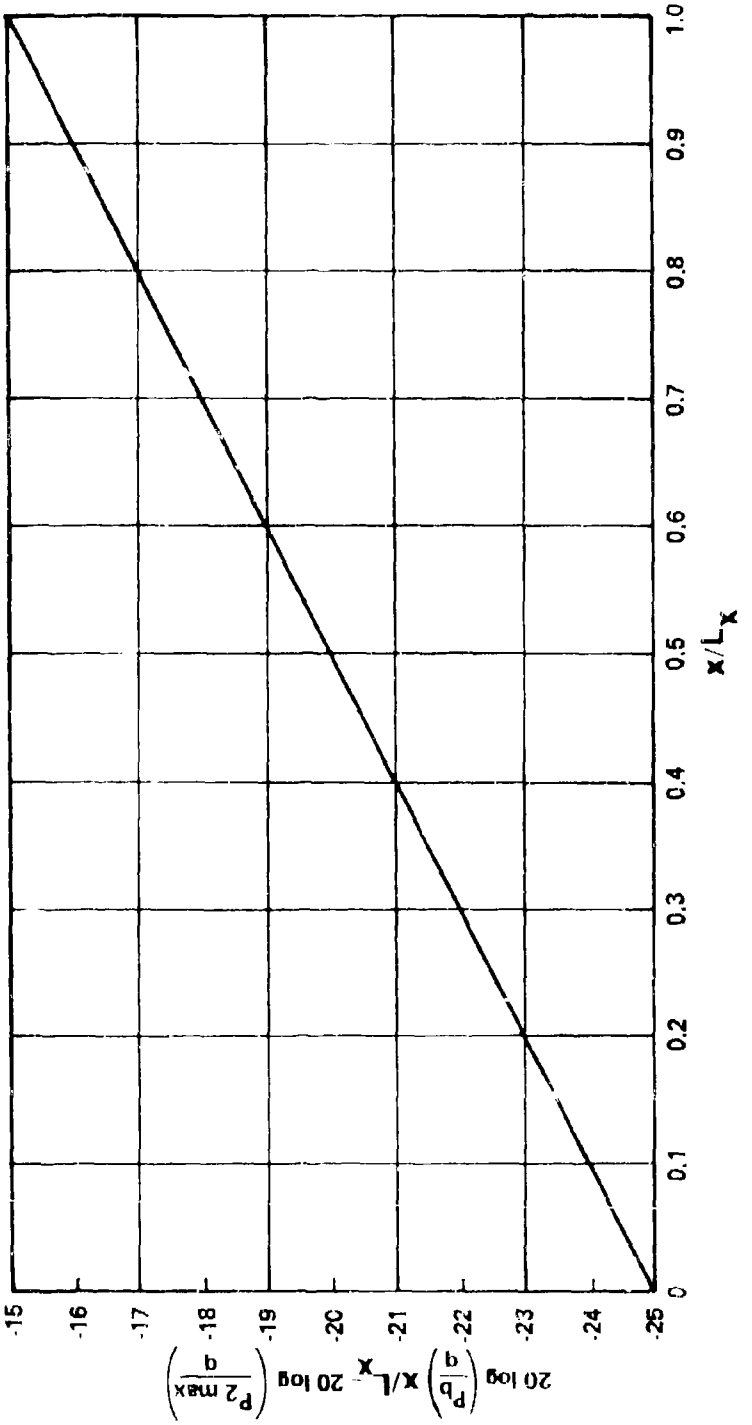

FIGURE 4.3.2-4 VARIATION OF BROADBAND SPECTRUM LEVEL WITH CAVITY POSIT ON

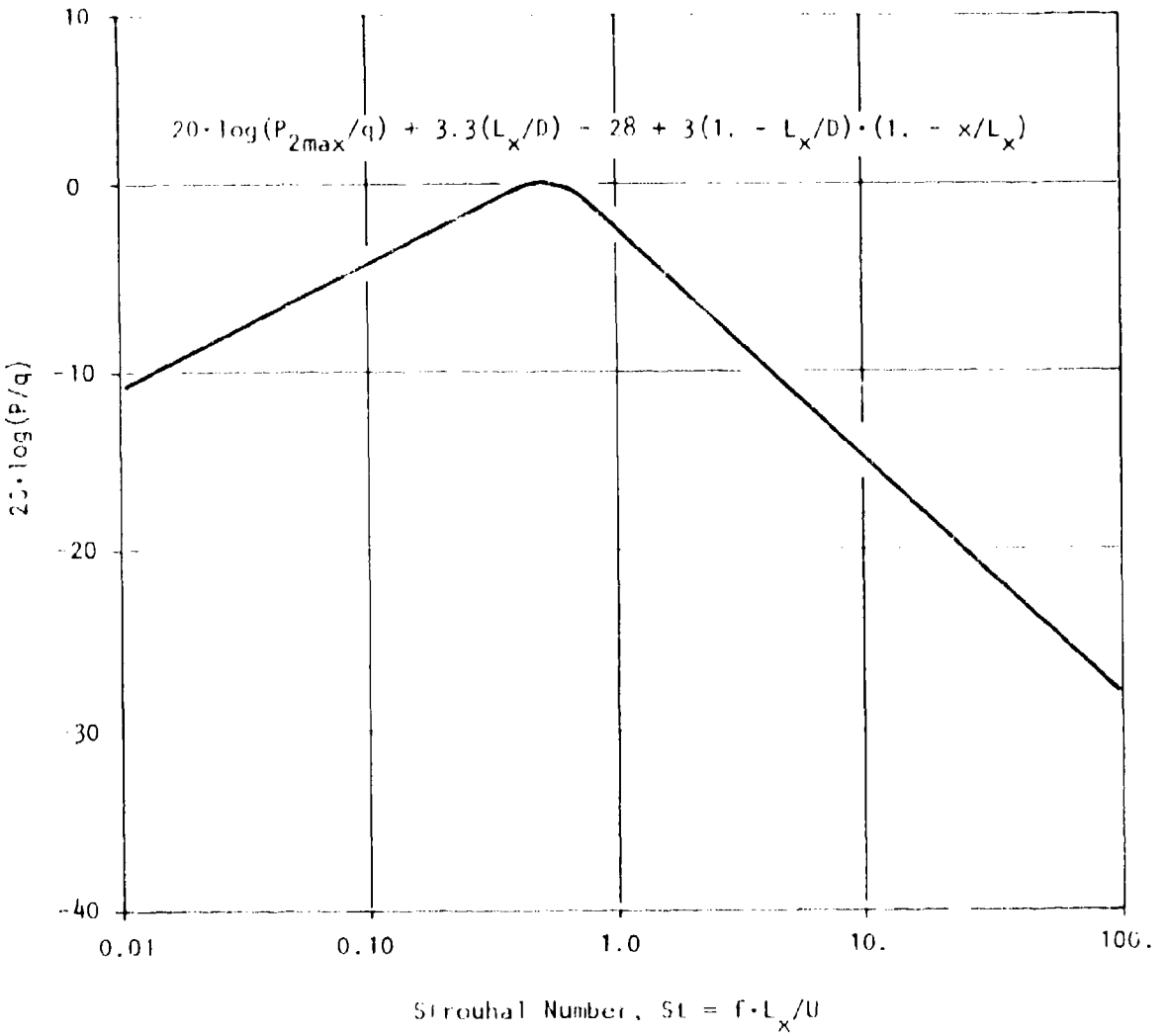

FIGURE 4.3.2-5 BROAD BAND CAVITY NOISE SPECTRUM SHAPE

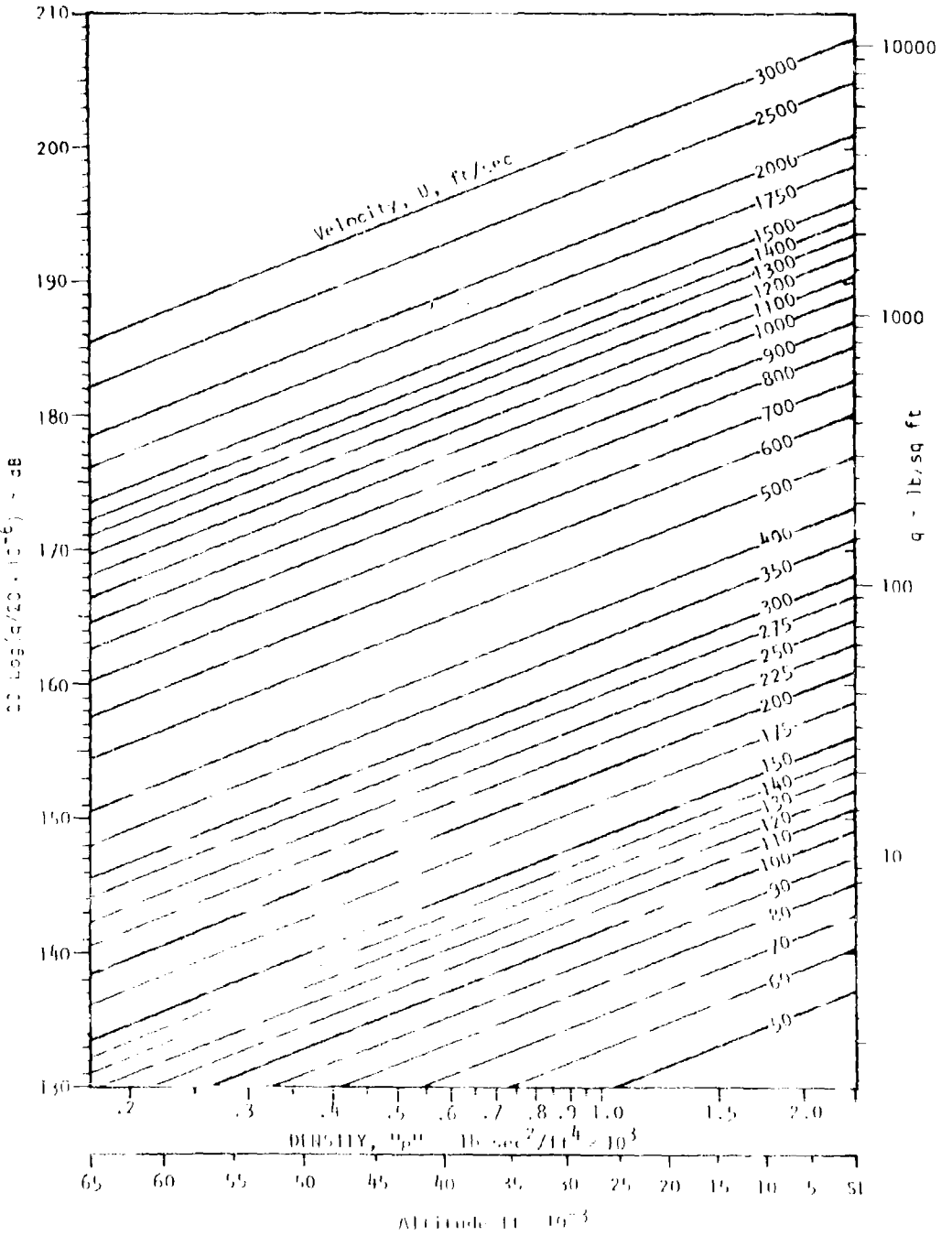

FIGURE 4.3.2-6 DESIGN CHART FOR DETERMINING REFERENCE "q" DECIBEL LEVEL

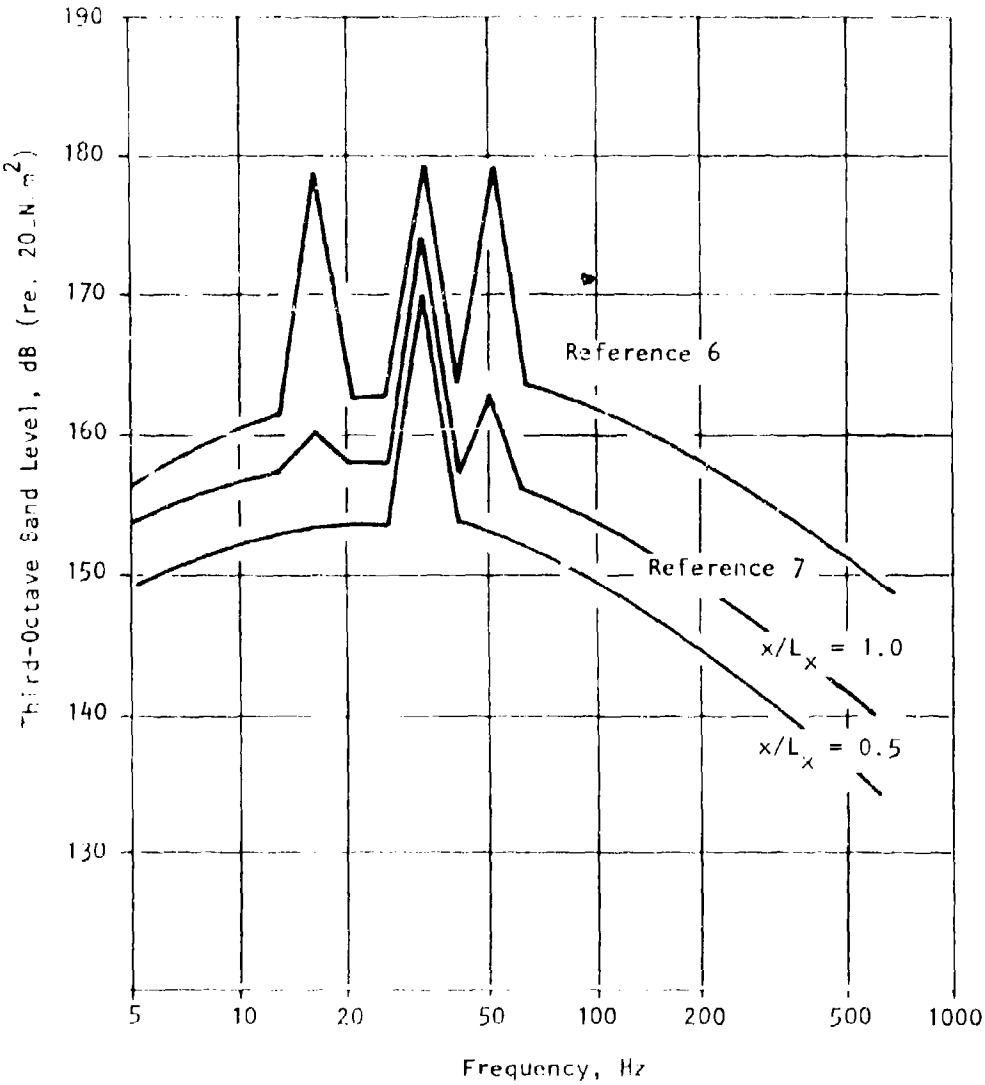

FIGURE 4.3.2-7 EXAMPLE OF COMBINED SPECTRAL CALCULATIONS

4.3.2.2 Cavity Noise Prediction Method-Theoretical

Derivation: In a study aimed at discovering the mechanisms of acoustic amplification within rectangular cavities with the open side exposed to a high velocity airflow, Plumblee, et al. (3) conducted a theoretical and experimental study of the acoustic response of cavities.

The experimental program was focused on tests conducted with a variable dimension cavity on the side of an ogive shaped aerodynamic model installed in the AEDC 40"x40" supersonic wind tunnel. Cavity length was varied from 0.5" to 8" and depth was 1" to 3.5" for cavity widths of 2" and 4". Tunnel speed was varied from Mach 1.75 to Mach 5.0. Smaller scale models were tested with exposure to pipe flow over a Mach number range of 0.2 to 3.0. Sound pressure level was measured within the cavity at several locations and with a flush-mounted microphone in the aerodynamic body of the pipe surface just upstream of the cavity. The reference 3 report details the results of the experiment.

The theoretical study presented a rather idealized viewpoint of the acoustic response of the cavity in an attempt to understand the gross acoustic mechanisms involved.

It was assumed that the cavity could be represented (as is sometimes done in determining the acoustic response of open ended pipes and ducts) by a rectangular rigid walled volume with a rigid vibrating piston mounted in the wall exposed to the air flow. It was assumed that if the radiation impedance of the open side, represented by the rigid piston, were known, then the sound pressure distribution for an assumed (or measured) source distribution within the cavity could be calculated. Thus, the theoretical study was first concerned with determining the radiation impedance of a rigid rectangular piston with one side exposed to a subsonic or supersonic airflow parallel to the piston surface. Next the source response of a rectangular volume with five walls rigid and one wall with finite acoustic impedance was determined. Finally, the source strength spectrum was rather crudely estimated from empirical data.

In order to determine the resonant frequencies and "amplification" of the cavity for design purposes, the impedance for the piston in a parallel flow was plotted as a function of frequency for various piston aspect ratios and flow velocities. Also, the soft-wall response equation in cartesian coordinates was solved and displayed graphically to aid in the response calculation.

Details of the prediction method for determining response of long shallow cavities (length to depth ratio greater than one) and deep cavities (length to depth ratio equal to or less than one) is given in the following section. The method is intended to enable a designer to assess the frequencies and acoustic pressure loading to be expected on the structural surface of a cavity.

a. Cavities with length to depth ratios less than one. It was determined from experiment that in this simple case, the cavity responds primarily in a depth mode. The mode response was shown to be predominant for the fundamental

mode for most configurations tested, with relatively strong response in the second depth mode.

The pressure response amplitude at the bottom of the deep cavity, referenced to the pressure at the cavity opening, is given by the following equation,

$$\frac{p}{p_o} = \left[[R \sin(kL_z)]^2 + [X \sin(kL_z) - \cos(kL_z)]^2 \right]^{-1/2} \qquad (4.3.2\text{-}7)$$

where k, the wavenumber = $2\pi f/a_o$
f is frequency in Hertz
a_o is speed of sound in fps
L_z is cavity depth in ft.
R is the radiation resistance of the cavity opening given in Figures 4.3.2-8 through 4.3.2-12
X is the radiation reactance of the cavity opening given in Figures 4.3.2-8 through 4.3.2-12

To calculate the response amplitudes and frequency perform the following steps:

(1) Evaluate the non-dimensional frequency, $\omega L_x/a_o$, where L_x is cavity length in the flow direction.

(2) Determine the cavity width to length aspect ratio, L_y/L_x.

(3) Select the appropriate radiation impedance curve from Figures 4.3.2-8 through 4.3.2-12 which most closely matches the aspect ratio determined in (2) above. Linear interpolation between impedance curves of different aspect ratio is suggested.

(4) Determine the radiation resistance R and reactance X from the figure selected in (3) above.

(5) Evaluate Eq.(4. 2-7)for a number of frequencies from $.5 \leq kL_z \leq 10$ to determine the peak amplitude at the first two resonant frequencies. Numerical evaluation is the only way to determine the resonant frequencies, since R & X are functions of frequency.

(6) For convenience, convert the amplification factor to decibels by performing the operation

$$20 \cdot \log_{10}\left(p/p_o\right).$$

b. Cavities with length to depth ratio greater than one. In these case the length modes are predominant, and it is necessary to employ the more general theory. Frequencies may be determined from the characteristic frequency equation

$$f_N^2 = \frac{a_o^2}{4}\left[\left(\frac{n_x}{L_x}\right)^2 + \left(\frac{n_y}{L_y}\right)^2 - \left(\frac{g_n}{L_z}\right)^2\right] \qquad (4.3.2\text{-}8)$$

where

$$g_n = \xi_n + i\eta_n$$

On the basis of experimental evidence, the transverse modes are not normally excited, thus the resonant frequencies may be reasonably approximated by

$$f_N^2 = \frac{a_o^2}{4}\left[\left(\frac{n_x}{L_x}\right)^2 - \left(\frac{g_n}{L_z}\right)^2\right] = \frac{a_o^2}{4}\left[\left(\frac{n_x}{L_x}\right)^2 - \left(\frac{\xi_n}{L_z}\right)^2 + \left(\frac{\eta_n}{L_z}\right)^2 - \frac{2i\xi_n\eta_n}{L_z^2}\right] . \qquad (4.3.2\text{-}9)$$

Because of the frequency dependent nature of g_n, determination of f_n becomes an iterative process, as outlined by the following steps.

(1) It may be helpful in initiating this process to take the first approximation of frequency as that for a closed cavity, that is

$$f_N^2 = \frac{a_o^2}{4}\left[\left(\frac{n_x}{L_x}\right)^2 + \left(\frac{n_z}{L_z}\right)^2\right] . \qquad (4.3.2\text{-}10)$$

(2) Enter the impedance curves of Figures 4.3.2-8 through 4.3.2-12 and determine values of R and X at the appropriate non-dimensional frequency, $\omega L_x/a_o$.

(3) Calculate the constants a and b as follows:

$$a = \frac{2f_N L_z X}{a_o(R^2 + X^2)} \qquad b = \frac{2f_N L_z R}{a_o(R^2 + X^2)} \qquad (4.3.2\text{-}11)$$

(4) Take the values of a and b calculated in step 3 and using Figure 4.3.2-13 read the values of ξ_n and η_n for the desired mode. If the value of b is negative, treat it as positive in determining ξ_n and η_n, but record η_n as a negative number. In other words, η_n always carries the sign of b.

(5) With the values of ξ_n and η_n from step 4 a second approximation of natural frequency, f_N can be calculated as follows (neglecting damping):

$$f_N = \frac{a_o}{2}\left[\left(\frac{n_x}{L_x}\right)^2 + \left(\frac{\eta_n}{L_z}\right)^2 - \left(\frac{\xi_n}{L_z}\right)^2\right]^{1/2} \qquad (4.3.2\text{-}12)$$

(6) Examine f_N in comparison with the first approximation of f. If $f_N - f$ is positive, choose a higher value of f and if negative, a lower value of f, and go back to step 2. When a change of sign of $f_N - f$ is obtained,

these points should be plotted as a curve of $f_N - f$ vs. f. This method will give the approximate intercept on the f-axis. More iterations can be made for higher accuracy.

It should be pointed out that in this process, certain values of a and b in an iterative sequence may cause the values of ε_n and η_n to cross a dotted mode line in Figure 4.3.2-13, thus apparently denoting a change of mode. When this occurs, the apparent mode change may be disregarded and continuity of the iteration maintained.

It is also observed that some modes may have a resonant frequency in the vicinity of the crossover point, where radiation resistance changes from negative to positive. In such cases two distinct resonances may be calculated.

(7) The absolute pressure response in the cavity can be calculated, based on the theory in Reference (3). However, the absolute amplitude depends on the definition of "source" strength. In the calculations presented in (3) a source strength and distribution was assumed, based on limited measurements. Rather than try to present that data here, we will instead present a method for calculating the amplification of the cavity at the point P defined by (x,y,z), based on a simple source located at a point S, defined by (x',y',z'). The amplification is based on the ratio of the level in the cavity to the free field level of the simple source defined by $i\omega\rho Q_0/4\pi r$,

where Q_0 is the simple source strength
r is distance from the center of the source to the cavity point
ω is the radian frequency
ρ is density.

The amplification ratio at $\omega = Re(\omega_N)$, is given by (for a single mode, N, defined by $N = (n_x, n_y, q_n)$

$$\left|\frac{P_N}{P_0}\right| = \left|\frac{2\pi r L_z\ \psi_N(P)\psi_N(S)}{L_x L_y \Lambda_N \varepsilon_n \eta_n}\right| \qquad (4.3.2\text{-}13)$$

where

$$\psi_N = \cosh\left(\frac{\pi q_n z}{L_z}\right)\cos\left(\frac{\pi n_y y}{L_y}\right)\cos\left(\frac{\pi n_x x}{L_x}\right) \qquad (4.3.2\text{-}14)$$

$$\Lambda_N = \frac{L_x L_y}{8}\left(\frac{\sinh 2\pi q_n}{2\pi q_n} + \frac{1}{2}\right) \quad \begin{matrix} n=0 & \varepsilon=1 \\ n>0 & \varepsilon=2 \end{matrix} \qquad (4.3.2\text{-}15)$$

$$r = \sqrt{(x-x')^2 + (y-y')^2 + (z-z')^2} \qquad (4.3.2\text{-}16)$$

and ε_n and η_n are defined above. The decibel value of amplification is defined as

$$20 \cdot \log_{10}\left(\frac{P_N}{P_S}\right) .$$

Sample Calculation for Long Cavity:

DATA:

$$n_x = 2,\ n_y = 0,\ n = 0,\ L_x = 8.",\ L_y = 2.",\ L_z = 3.5"$$

$$x = .5",\ x' = 0,\ z = 0,\ z' = 3.5",\ y = 1,\ y' = 1$$

Going through the steps outlined at the beginning of the section, the following results are obtained.

(1) Using Eq. (4.3.2 10), the first approximation to frequency f_N is, $f_{N1} = 2650$ Hz.

(2) Using the above frequency of 2650 Hz, values of impedance from Figure 4.3.2-4 for $L_y/L_x = .25$, are:

$$R = .846 \qquad X = .564$$

(3) Impedance and frequency from steps (1) and (2) yield the constants:

$$a = .73 \qquad b = 1.10$$

(4) From Figure 4.3.2-13 the values of ε_n and η_n for n = 0 are:

$$\varepsilon_o = .14 \qquad \eta_o = .56$$

(5) The second approximation to natural frequency, using the values of step (4), is

$$f_{N2} = 2045 \text{ Hz}$$

(6) Compare f_N of step (5) with f_N of step (1)

$$f_{N2} - f_{N1} = -605 \text{ Hz}$$

The result is negative, therefore choose a lower value of f_N, say $f_{N3} = 2150$ Hz, to insert into step (2).

After calculation of steps (2) – (5), a natural frequency $f_{N4} = 2070$ Hz is found. Comparison with f_{N3} gives a value of -80 Hz so that smaller values of f_N must be chosen. Choosing $f_{N5} = 2000$ Hz yields a value of $f_{N6} = 2070$ Hz.

For the final iteration use a value of f_N in step (2) of 2070 Hz. This results in a value of f_N = 2070 Hz in step (5). Therefore the correct value of f is 2070 Hz. The correct values of ξ_o and η_o are ξ_o = .16, η_o = .59.

(7) Using the input constants and the above values of ξ_n and η_n, the amplification is computed as

$$\psi_N(P) = 0.9239$$

$$\psi_N(S) = -.2909 + .4644\,i$$

$$\Lambda_N = .0558 + .0486\,i$$

$$\left|\frac{P_N}{P_S}\right| = 381.5$$

and

$$20 \cdot \log_{10}\left|\frac{P_N}{P_S}\right| = 51.6 \text{ dB}$$

If the source were taken as the boundary layer spectrum level at this particular frequency of 2070 Hz, then an estimate of the SPL in the cavity is possible.

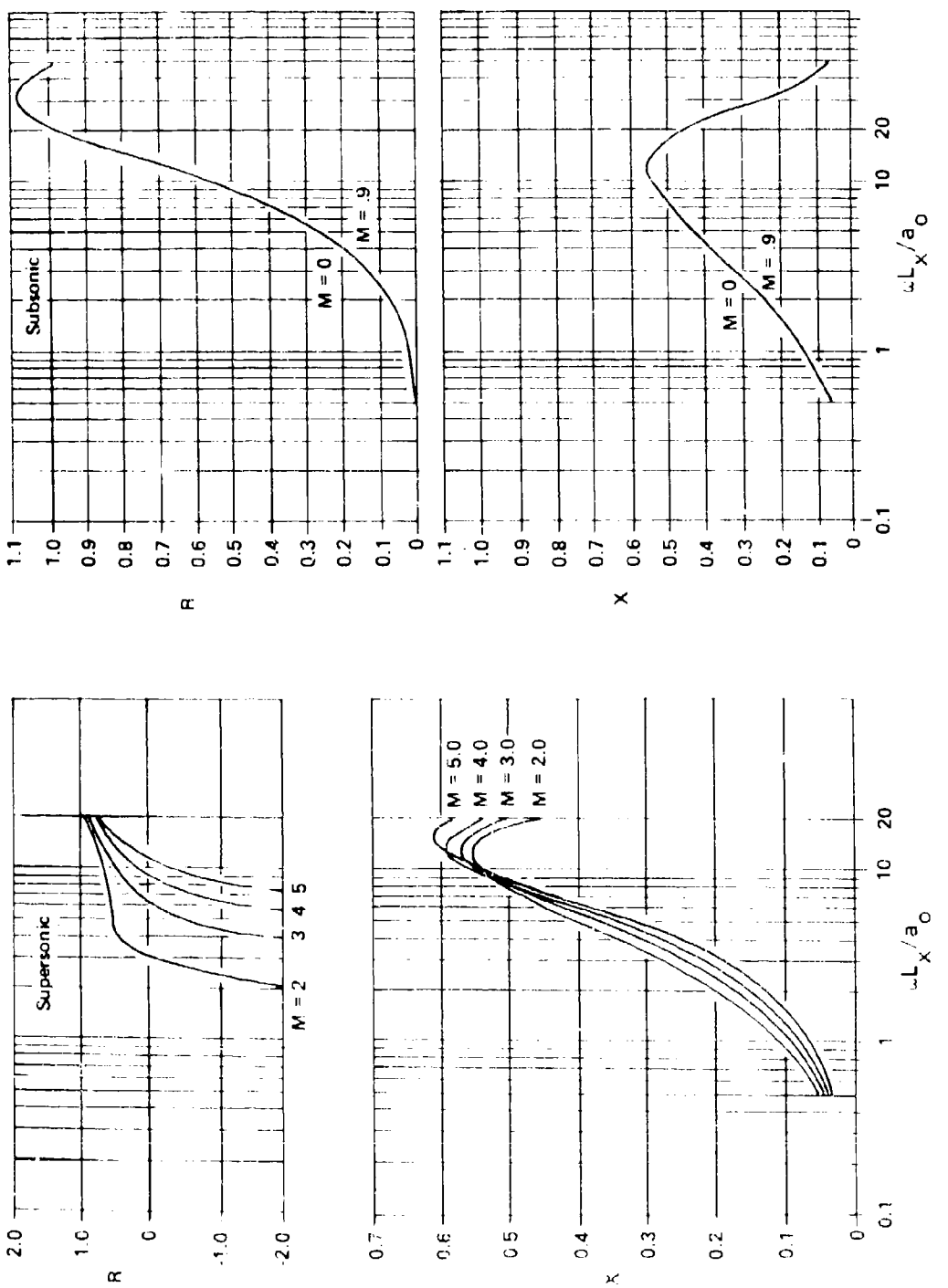

FIGURE 4.3.2-3 RADIATION IMPEDANCE FOR RIGID PISTON WITH GRAZING FLOW, $L_y/L_x = 0.125$

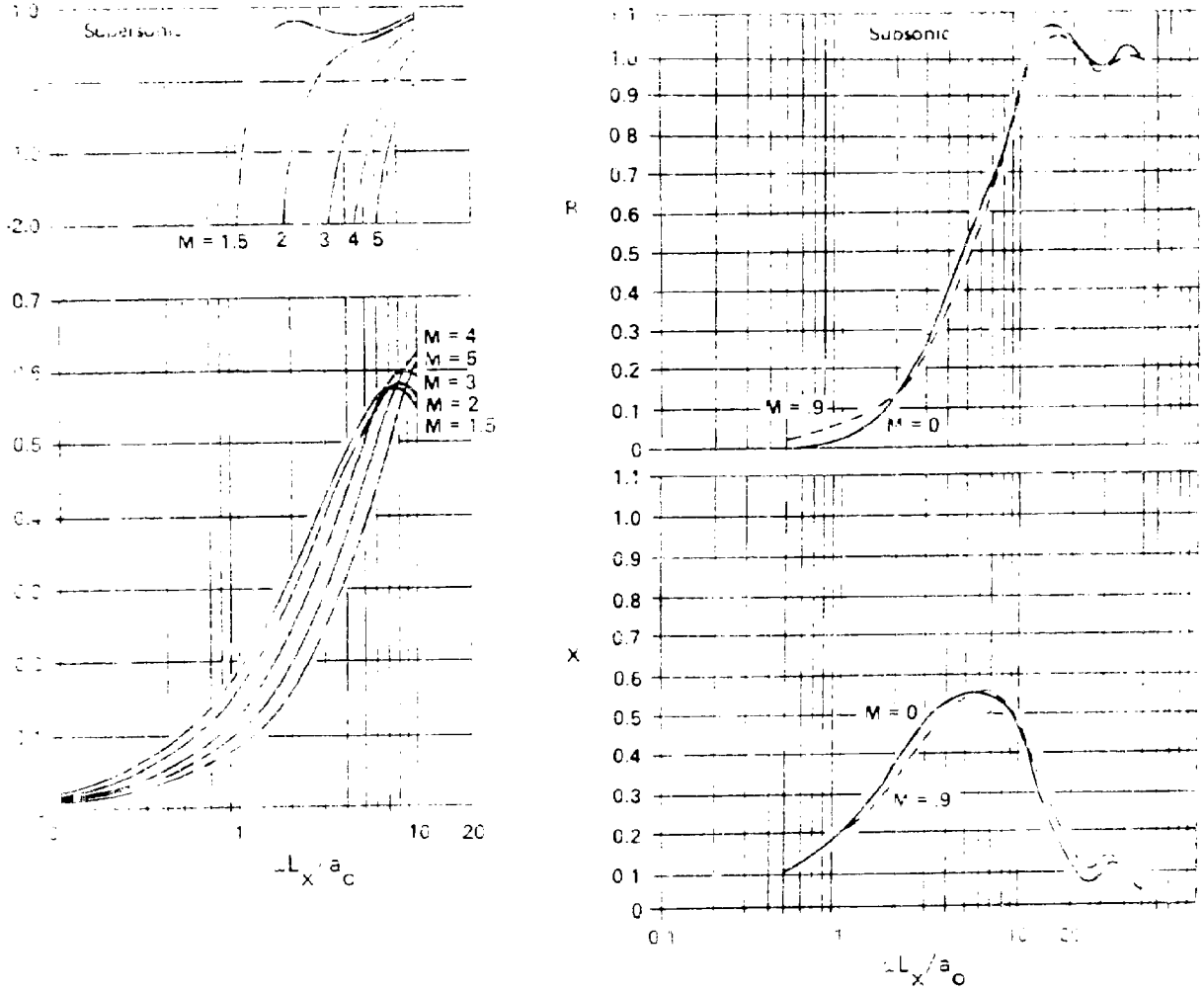

FIGURE 4.3.2-3 RADIATION IMPEDANCE FOR RIGID PISTON WITH GRAZING FLOW, a_c/a_o = 0.850

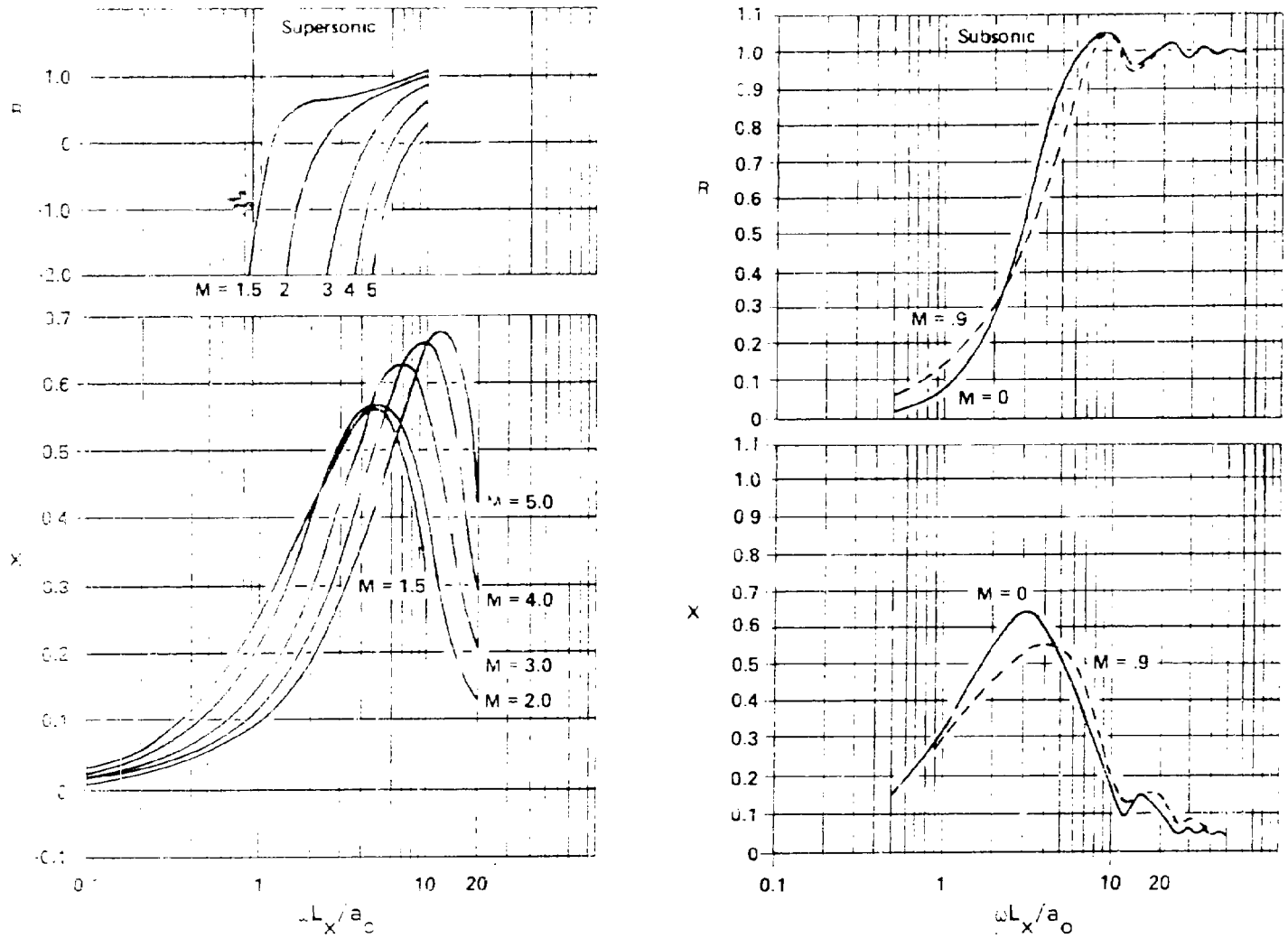

FIGURE 4.3.2-10 RADIATION IMPEDANCE FOR RIGID [illegible]TON WITH GRAZING FLOW, L_y/L_x = 0.500

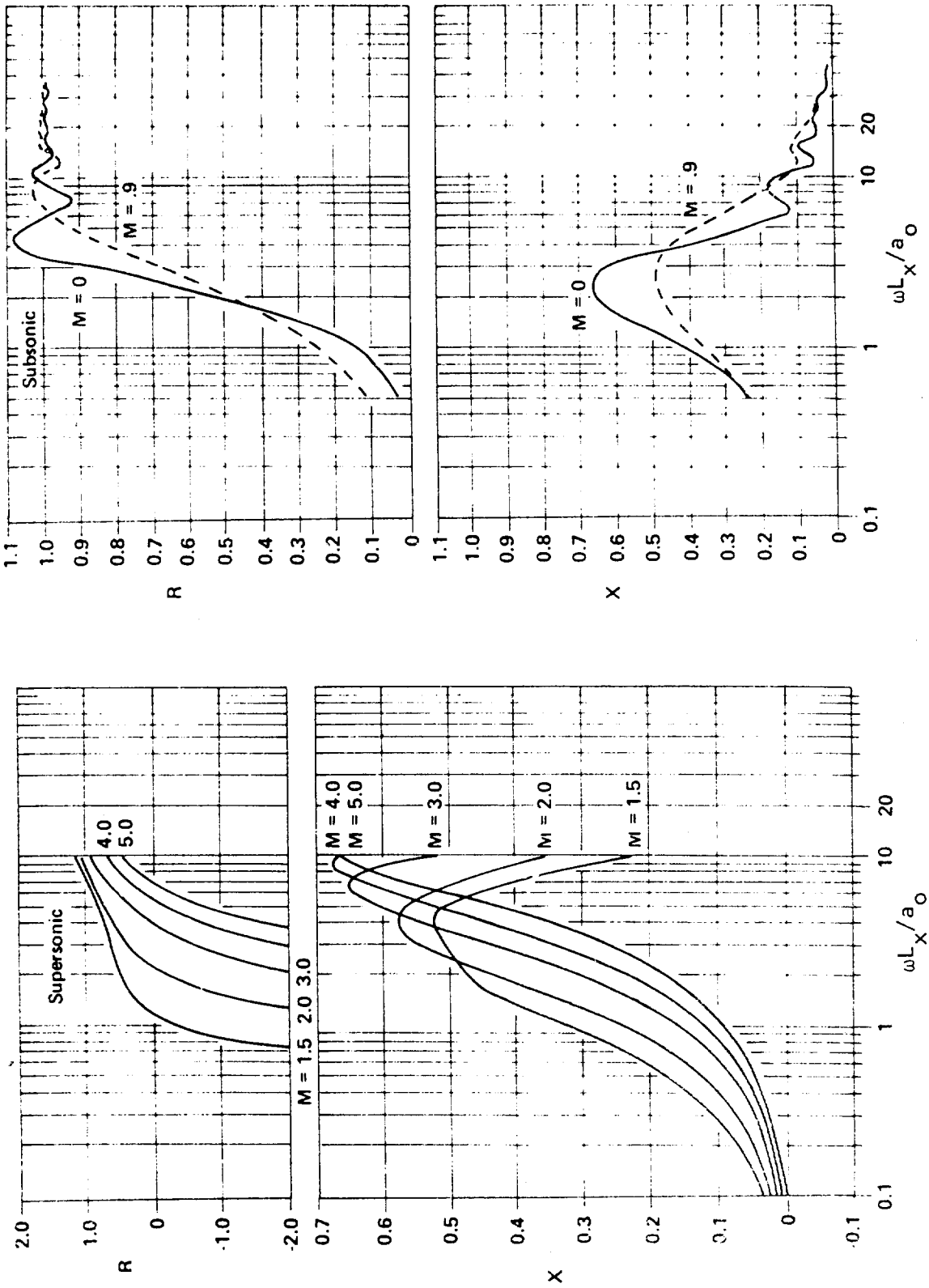

FIGURE 4.3.2-11 RADIATION IMPEDANCE FOR RIGID PISTON WITH GRAZING FLOW, $L_y/L_x = 1.00$

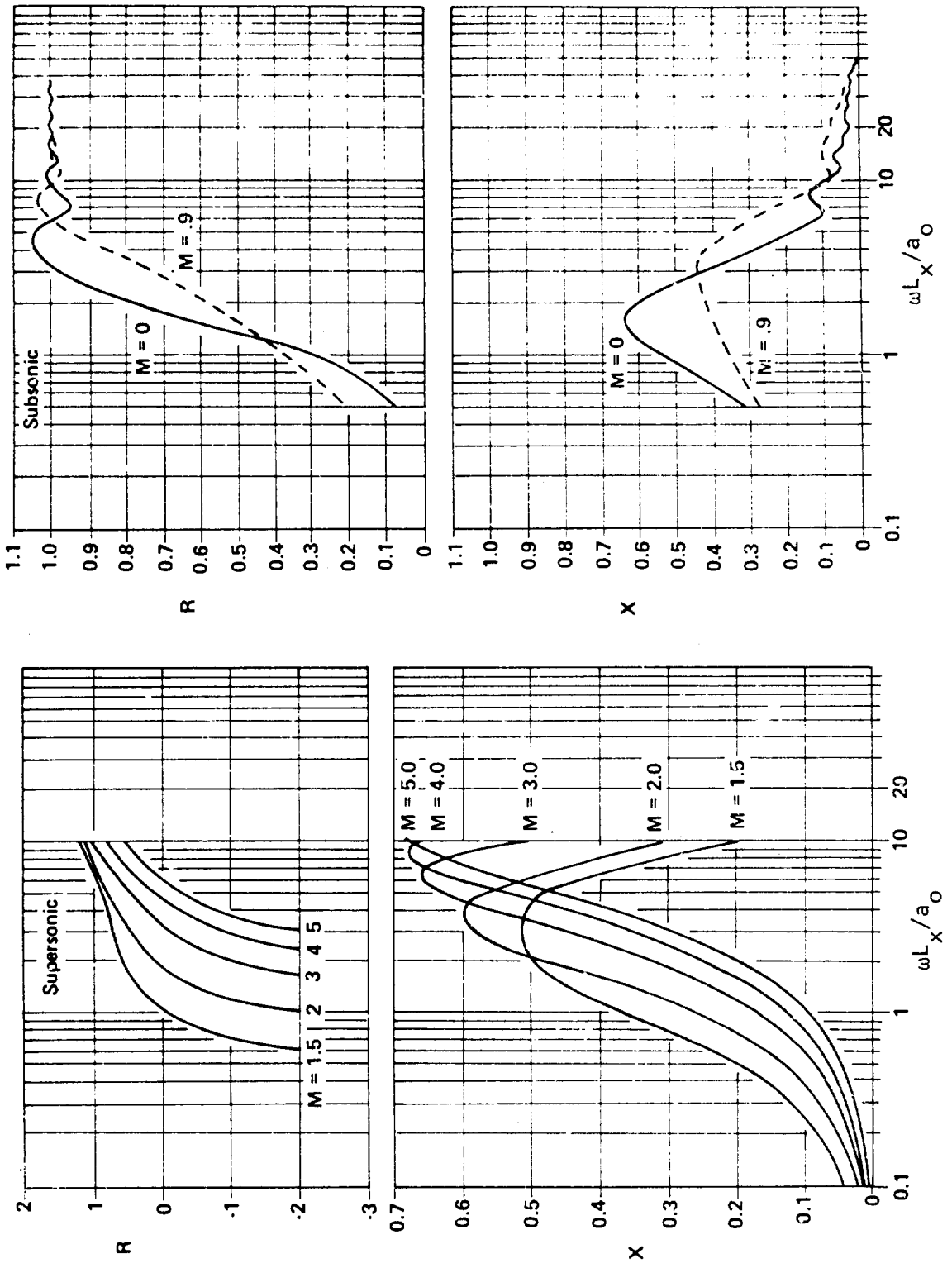

FIGURE 4.3.2-12 RADIATION IMPEDANCE FOR RIGID PISTON WITH GRAZING FLOW, $L_y/L_x = 2.00$

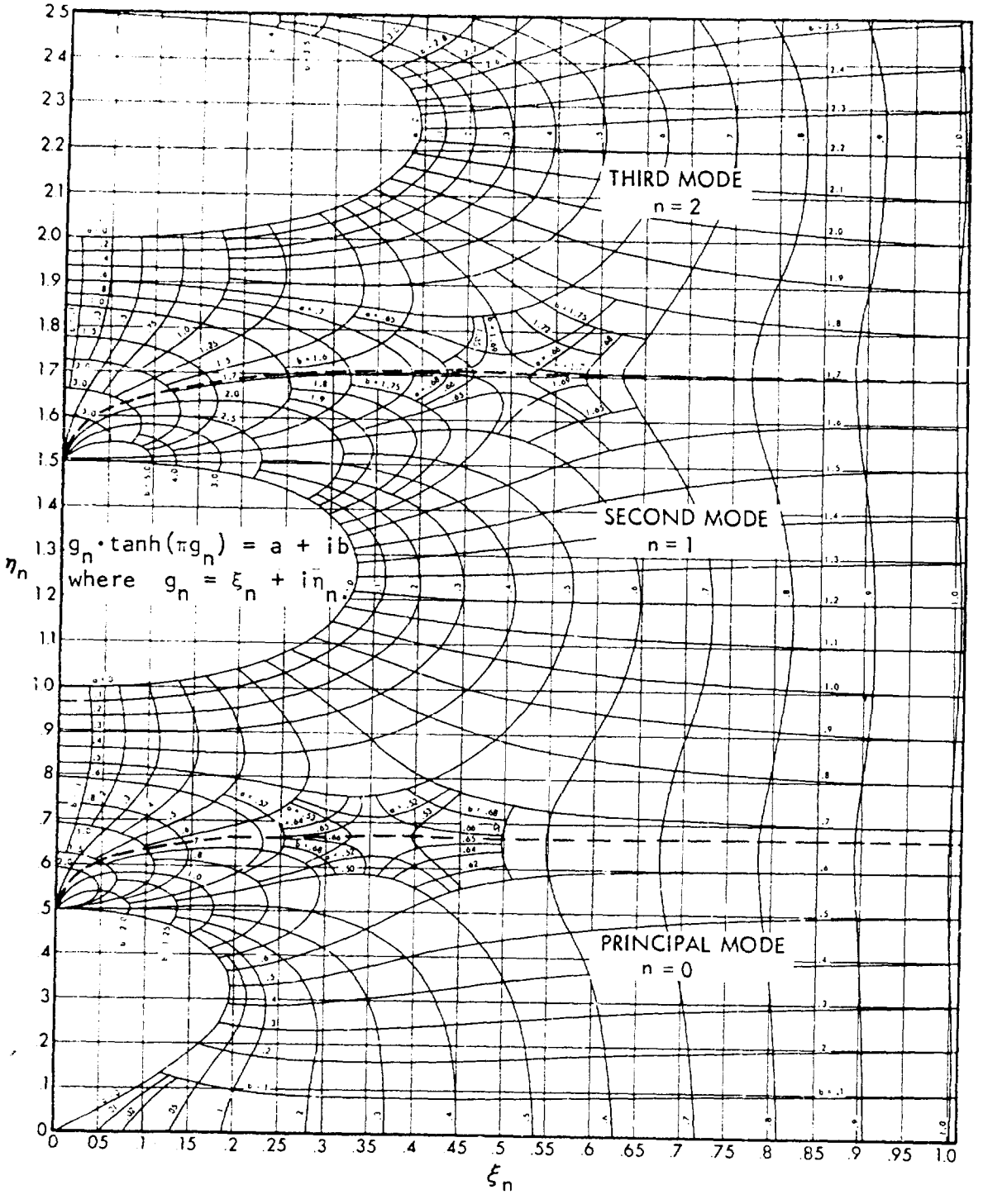

FIGURE 4.3.2-13 SOLUTIONS TO BOUNDARY CONDITION FUNCTION, $g_n \tanh(\pi g_n) = a + ib$

REFERENCES FOR SECTION 4.3.2

1. Blokhintsev, E. I.; "Excitation of Resonance by Air Flow," SLA Translation Pool No. 270 (ONR) from ZhTF, 15, pp. 63-70, 1945.

2. Krishnamurty, K.; "Sound Radiation from Surface Cutouts in High Speed Flow," Ph.D. Thesis, California Institute of Technology, 1956.

3. Plumblee, H. E., Lassiter, L. W., and Gibson, J. S.; "A Theoretical and Experimental Investigation of the Acoustic Response of Cavities in an Aerodynamic Flow," WADC TR 61-75, January 1961.

4. East, L. F.; "Aerodynamically Induced Resonance in Rectangular Cavities," Journal of Sound and Vibration, Vol. 3, No. 3, pp. 277-287, 1966.

5. Rossiter, J. E., "Wind Tunnel Experiments on the Flow over Rectangular Cavities at Subsonic and Transonic Speeds," ARC R & M 3438, 1966.

6. Heller, H. H., Holmes, G., and Covert, E. E.; "Flow-induced Pressure Oscillations in Shallow Cavities," AFFDL-TR-70-104, December 1970.

7. Shaw, L. L., Smith, D. L., Talmadge, R. D., and Seely, D. E.; "Aero Acoustic Environment of a Rectangular Cavity with a Length to Depth Ratio of 4," AFFDL-TM-74-19-FYA, January 1974.

8. Smith, D. L., Shaw, L. L., Talmadge, R. D., and Seely, D. E.; "Aero-Acoustic Environment of Rectangular Cavities with Length to Depth Ratios of Five and Seven," AFFDL-TM-74-79-FYA, April 1974.

9. Shaw, L. L. and Smith, D. L.; "Aero-Acoustic Environment of Rectangular Cavities with Length to Depth Ratios in the Range of Four to Seven," Paper Presented at the 45th Shock and Vibration Symposia, Dayton, Ohio, October 1974.

4.3.3 BOUNDARY LAYER NOISE

Boundary layer noise makes a very significant contribution to the noise in an aircraft interior and in many segments of the flight profile is the major interior noise contribution. Boundary layer noise can also become intense enough to cause sonic fatigue failure. Thus, methods for predicting boundary layer noise are pertinent to this report.

The study of response of structures to boundary layer noise began in earnest in the mid-1950's. Corcos and Liepmann (1) published an analysis of the noise radiation into a fuselage from a turbulent boundary layer. However, they hypothesized the characteristics of the flow field. Since then, there have been numerous experimental and theoretical studies on boundary layer noise. These have been concerned with subsonic, transonic, supersonic and even hypersonic flight. Measurements have been at both model and full scale.

Several papers have been written which summarize particular aspects of boundary layer noise, but no one volume seems to contain a treatise on the subject. One of the more recent papers, that by Coe and Chyu (2) summarizes the results of numerous tests at NASA on the characteristics of boundary layer noise at supersonic speed. They give prediction formulae and methods for determining, among other things, overall level, power spectrum and cross spectra (or cross correlation coefficients) in regions of attached and separated flow. This work, as well as the numerous publications by Maestrello, of which references 3-4 are representative, the work of Lowson (5) and that of Bies (6) are representative of the state-of-the-art. As a result of this extensive work, it has been determined that not only is the level and spectrum of boundary layer noise important, but also that the correlation scale can be important in determining the response of structures. However in this report we will concern ourselves only with the prediction of level and spectrum, since a finite correlation scale is not in context with the structural response methods presented as design charts. Thus it will be assumed that the correlation scale is larger than a structural element in all the response calculations.

In two recent studies, Ungar (7) and Cockburn and Jolly (8) presented design oriented methods for predicting boundary layer noise level and spectra as well as correlation properties, over a wide range of flight Mach no. Results from these two sources of information will be presented in this abbreviated prediction method. If more extensive data are required, refer to the references in this section which will in turn lead to other references on the subject.

Description: The overall level of turbulent boundary layer noise has for many years been accepted as being represented by a ratio with the dynamic pressure, $q = 1/2\,\rho U^2$. It turns out that results from experimental data suggest that

$$p/q = 0.006 \,, \qquad (4.3.3\text{-}1)$$

where p is the rms overall sound pressure.

However, more recent work and data correlations by Lowson (5) show that for attached boundary layers over smooth surfaces,

$$p/q = \frac{0.006}{1 + 0.14\ M^2} \quad . \qquad (4.3.3\text{-}2)$$

Ungar (7) suggests that the constant of 0.006 should be increased to 0.01 for rough surfaces.

The measurements of Coe and Chyu (2) generally confirm this result up to a Mach no. of approximately 2.5, above which p/q seems to remain constant with Mach no.

The relationship of Equation (4.3.3-2) is presented in Figure 4.3.3-1. To determine the overall sound pressure level, based on density and Mach no., Figure 4.3.3-2 should be used.

For attached flows, the spectral distribution is defined adequately in a design chart by Cockburn and Jolly (8). The following discussion is based upon the Cockburn and Jolly work and Coe and Chyu's (2) work.

The frequency spectra of attached turbulent boundary layer pressure fluctuations are found to scale on a Strouhal number basis; that is the frequency is non-dimensionalized by multiplying by a typical length and dividing by a typical velocity. However, the choice of correct typical lengths and velocities is far from easy. Free stream velocity is generally used for the non-dimensionalized velocity, although the use of a typical eddy convection velocity, itself a function of frequency, would correspond more closely with the physical situation. For simplicity, free stream velocity, U, will be used here.

Definition of a typical length is more difficult. Boundary layer thickness δ_b, displacement thickness δ^*, and momentum thickness $\bar{\theta}$ have all been used by various authors. For subsonic boundary layers most results have been taken for equilibrium flows with a similar ratio of these characteristic lengths, so that non-dimensionalization using any of these gives very similar collapse. In supersonic flows the typical lengths do vary widely with Mach number, but no final conclusion can be drawn on the relative merits of the data collapse against any particular length. Perhaps the most generally used typical length is δ^*, the displacement thickness. However, for the handbook the boundary layer thickness δ_b will be used for three reasons; firstly, it is easier to predict, secondly, it is related to a physical characteristic of the flow, the size of the largest eddies; and thirdly, it gives a slightly improved collapse of the only available supersonic data.

The principal problem in predicting subsonic spectra under any scheme is estimation at the low frequencies. Experiment, both in flight and in wind tunnels, shows considerable low frequency scatter from the very low values reported by Hodgson (9) for a glider, to the high values reported by Gibson (10) and Maestrello (11) for full scale aircraft, although Hodgson's results were taken at low Reynolds number on a far from equilibrium boundary layer, and are therefore not considered relevant here. It is extremely difficult to define any single curve from the available data. Bies (6), has published a detailed review of spectral measurements in a wind tunnel and in flight and suggested the curves shown in Figure 4.3.3-3 as mean curves through the data. The scatter about these curves is about ±5 dB. These curves have

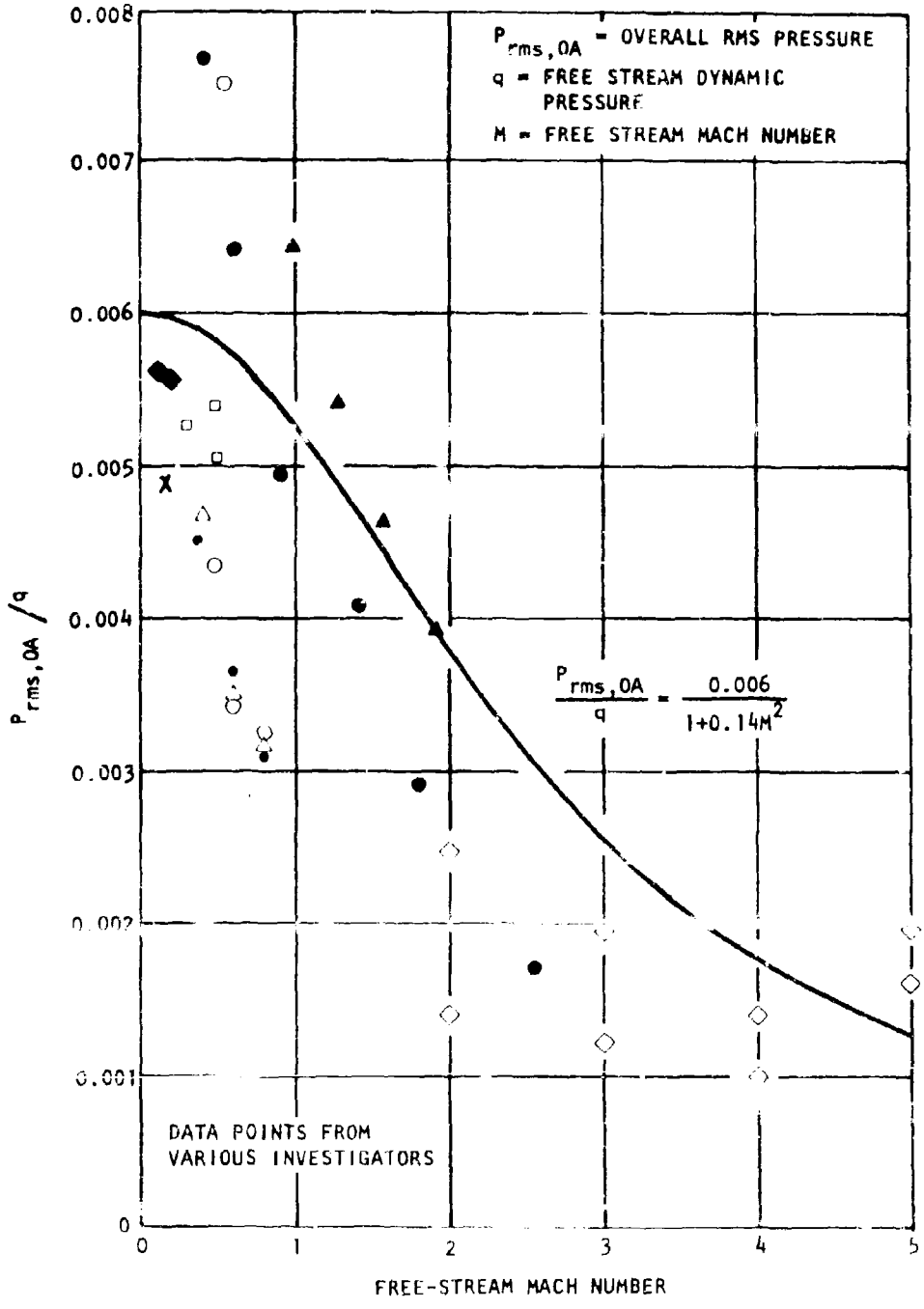

FIGURE 4.2.3-1 MACH NUMBER DEPENDENCE OF NORMALIZED OVERALL RMS PRESSURE FLUCTUATIONS

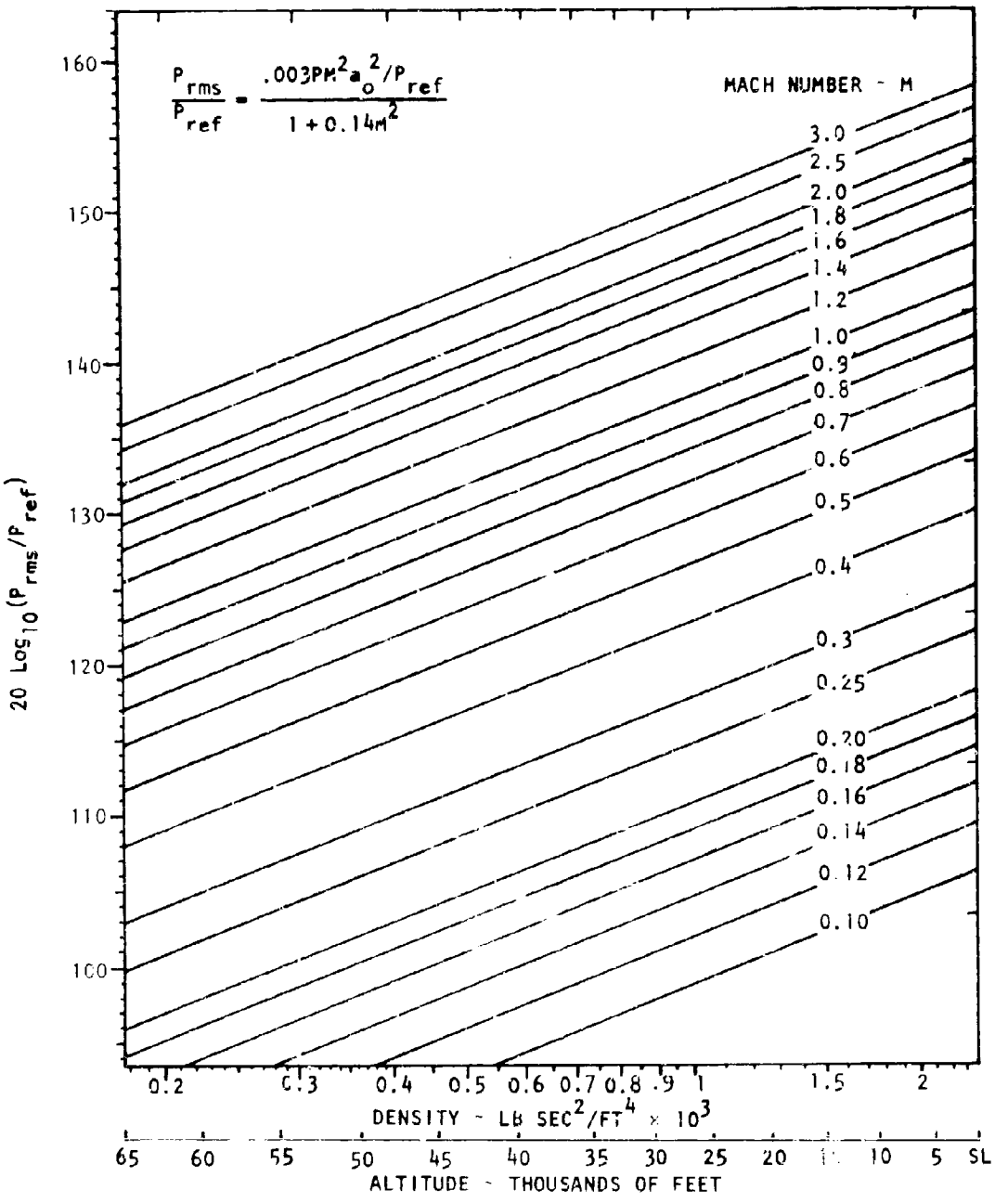

FIGURE 4.3.3-2 VARIATION OF OVERALL BOUNDARY LAYER SPL WITH MACH NUMBER AND DENSITY

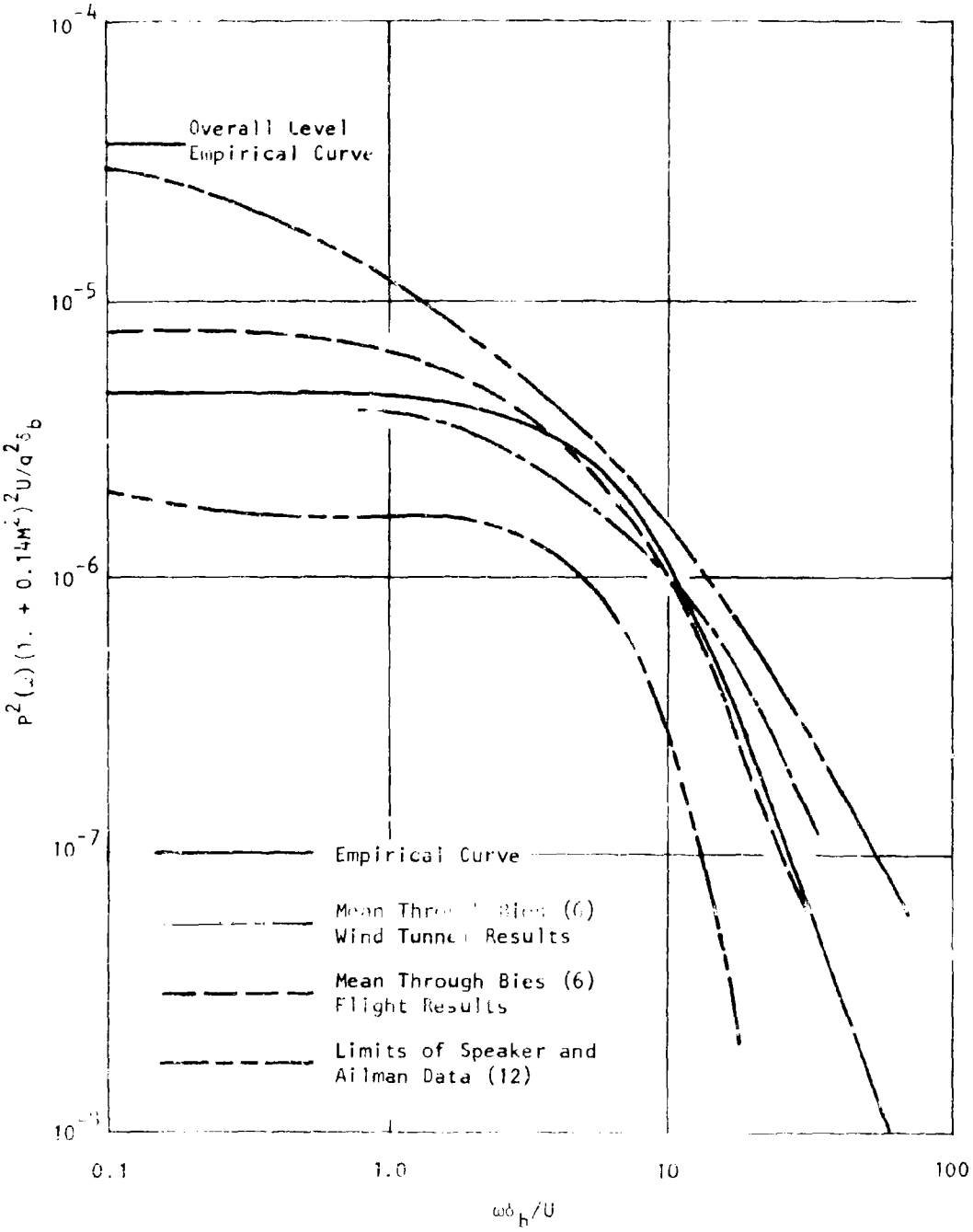

FIGURE 4.3.3-3 COMPARISON OF EMPIRICAL CURVE WITH DATA FROM BIES

been converted to the present basis by assuming that the wind tunnel results were taken at a typical Mach number of 0.5 and a typical Reynolds number of 10^7 while the flight results were typified by the values M = 0.8 and $Re_x = 10^8$. Values of the boundary layer parameters were estimated from the curves given by Bies, using the above values.

Since it is desired to apply the empirical results from the present study to the supersonic case, and there are, at present, no reliable in flight supersonic measurements, the supersonic wind tunnel data of Speaker and Ailman (12) have been reviewed carefully and are shown in Figure 4.3.3-3. An empirical curve fit for the frequency spectrum (which is close to the mean empirical curves derived from Bies) results and is a good representation of the Speaker and Ailman data for the supersonic cases and is given by Lowson (13) as;

$$\frac{p^2(\omega)}{q^2} = \left[\frac{0.006}{1 + 0.14\,M^2}\right] \cdot \frac{1}{\omega_o\left[1 + \left(\frac{\omega}{\omega_o}\right)^2\right]^{3/2}} \qquad (4.3.3\text{-}3)$$

where the typical frequency ω_o has been taken as equal to $8U/\delta_b$. This curve is shown in Figure 4.3.3-3 and has the advantage of being analytical as well as matching the available data. As can be seen, the curve is probably conservative at the high frequencies for the highest Mach numbers.

The data by Coe and Chyu (2) seem to have smaller Mach no. effects (or else less scatter) over the range $1.6 < M < 3.5$ and they also have derived an empirical curve fit to the data. The equations are

$$\frac{G_p U}{q^2 \delta_b} = \exp(-12.470 - 0.639X - 0.269X^2 + 0.015X^3 + 0.017X^4 + 0.002X^5) \qquad (4.3.3\text{-}4)$$

for attached flows

and

$$\frac{G_p U}{q^2 \delta_b} = \exp(-8.094 - 1.239X - 0.259X^2 - 0.090X^3 - 0.014X^4 - 0.001X^5) \qquad (4.3.3\text{-}5)$$

for separated flows

where $X = \log_e(f\delta_b/U)$

f is frequency

U is free-stream velocity

G_p is power spectral density of pressure fluctuations.

A curve of Equations (4.3.3-4) and (4.3.3-5) is given in Figure 4.3.3-4.

Typically, low Mach number wind tunnel spectra decay at 20 dB per decade at high frequencies, while the present high Mach spectra decay at 40 dB per

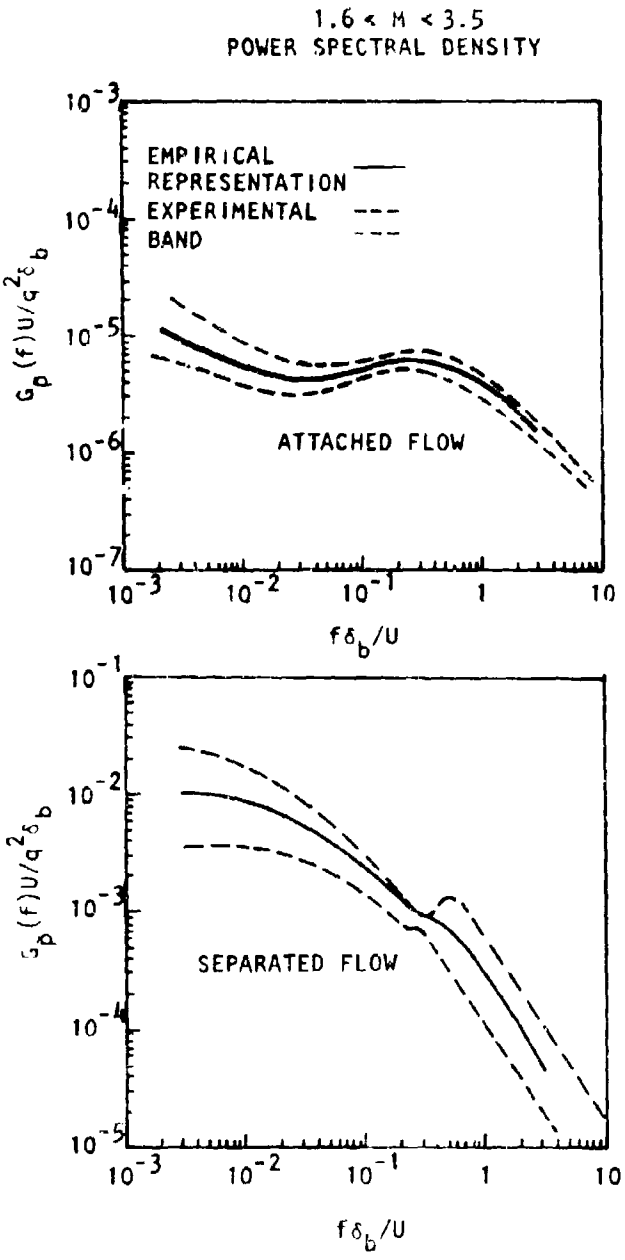

FIGURE 4.3.3-4 EMPIRICAL REPRESENTATION OF SUPERSONIC BOUNDARY LAYER SPECTRA FOR SEPARATED AND ATTACHED FLOW (REFERENCE 2)

decade. Little independent data is available to substantiate this trend, although Maestrello's results (11) taken at $0.63 < M < 0.78$ do show some increase in decay rate. Since the trend to increased rates of decay above a Mach number of about 0.8 cannot be conclusively verified, it seems desirable to exercise some caution in making predictions.

The later data of Coe and Chyu do not, in fact, confirm this trend for high Mach no. It instead reverses the high roll-off rate and approaches something close to 10 dB/decade. Thus, the curve of Figure 4.3.3-4 should be used for the high Mach no. data.

Since the formulae given here requires a knowledge of the boundary layer thickness, δ_b, the empirical equation suggested by Bies (6) is recommended, namely,

$$\frac{\delta_b}{x} = 0.37\ Re_x^{-0.2}\left[1 + \left[\frac{Re_x}{6.9 \times 10^7}\right]^{2}\right]^{0.1} \qquad (4.3.3\text{-}6)$$

where x is the distance from the leading edge of the body, $Re_x = U\,x/\nu$, and ν is the kinematic viscosity. This result is shown in Figure 4.3.3-5.

NOTE: Ground Level Conditions Assumed - Kinematic Viscosity at $15^{\circ}C = 1.59 \cdot 10^{-4}$ ft/sec

Dashed Lines Indicate Calculation of δ_b for a Distance of 1.5 feet and U = 1000 ft/sec.

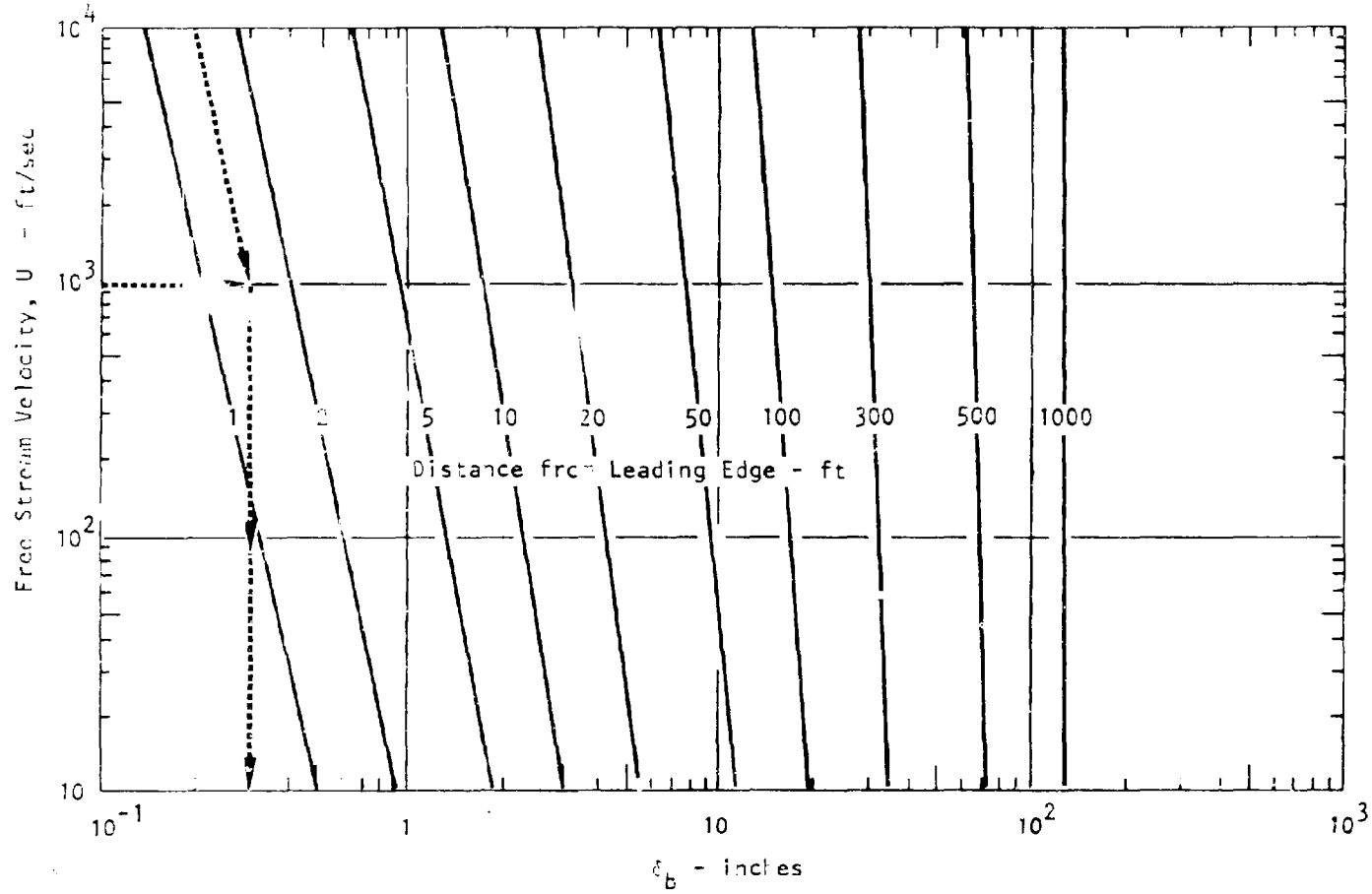

FIGURE 4.3.3-5 BOUNDARY LAYER THICKNESS, δ_b, FROM EQUATION 4.3.3-6

REFERENCES FOR SECTION 4.3.3

1. Corcos, G. M. and Liepmann, H. W.; "On the Contribution of Turbulent Boundary Layers to the Noise Inside a Fuselage," NASA TM 1420, 1956.

2. Coe, C. F. and Chyu, W. J., "Pressure Fluctuation Inputs and Response of Panels Underlying Attached and Separated Supersonic Turbulent Boundary Layers," Paper no. 5, AGARD-CP-113, Advisory Group for Aerospace Research & Development, North Atlantic Treaty Organization, 1972.

3. Maestrello, L.; "Measurement and Analysis of the Response Field of Turbulent Boundary Layer Excited Panels," Journal of Sound and Vibration, Vol. 7, No. 3, pp. 270-292, 1965.

4. Maestrello, L.; "Boundary Layer Pressure Fluctuations on the 707 Prototype," paper presented at the 64th Meeting of the Acoustical Society of America, Seattle, Washington, Nov. 7-10, 1962.

5. Lowson, M. V.; "Prediction of Turbulent Boundary Layer Pressure Fluctuations," AFFDL-TR-67-167, Wright Patterson Air Force Base, October 1967.

6. Bies, D. A.; "A Review of Flight and Wind Tunnel Measurements of Boundary Layer Pressure Fluctuations and Induced Response," NASA CR-626, October 1966.

7. Ungar, E. E., Madden, R., Lyon, R. H., and Bender, E. K.; "A Guide for Predicting the Vibrations of Fighter Aircraft in the Preliminary Design Stages," AFFDL-TR-71-63, Wright-Patterson Air Force Base, April 1973.

8. Cockburn, J. A. and Jolly, A. C.; "Structural-Acoustic Response, Noise Transmission Losses and Interior Noise Levels of an Aircraft Fuselage Excited by Random Pressure Fields," AFFDL-TR-68-2, Wright-Patterson Air Force Base, August 1968.

9. Hodgson, T. H.; "Pressure Fluctuations in Shear Flow Turbulence," Ph.D. Thesis, University of London, 1962.

10. Gibson, J. S.; "Boundary Layer Noise Measurements on a Large Turbofan Aircraft," Paper No. I-10, 70th Meeting of the Acoustical Society of America, Nov. 1965.

11. Maestrello, L.; "Use of a Turbulance Model to Calculate Vibration and Radiation Responses of a Panel with Practical Suggestions for Reducing Sound Level," Journal of Sound and Vibration, Vol. 5, pp. 407-448, 1967.

12. Speaker, W. V. and Aikman, C. M.; "Spectra and Space-Time Correlations of the Fluctuating Pressures at a Wall Beneath a Supersonic Turbulent Boundary Layer Perturbed by Steps and Shocks," NASA CR-486, 1966.

13. Bull, M. K.; "Properties of the Fluctuating Wall Pressure Field of a Turbulent Boundary Layer," AGARD Report 455, April 1963.

SECTION 5

STRUCTURAL CONFIGURATIONS AND RESPONSE

The topic of sonic fatigue is usually related to the consideration of the prediction of fatigue life of aircraft structural components exposed to high intensity acoustic excitation. Section 3 presents a discussion of the significance of aircraft operations on estimating the exposure of structure to high intensity noise. Section 4 presents techniques for estimating the acoustic environment with emphasis placed upon the most common sources of high intensity noise related to military aircraft operation. This section presents a discussion of structural response to acoustic excitation both from the formulation of the theory and the established design techniques and methods that have evolved during the past 20 years.

Section 5 is divided into five subsections. Section 5.1 presents a basic description of the topics of random vibration of mechanical systems and various analytical techniques that can and have been used to approach sonic fatigue design problems. Section 5.2 presents selected analytical results that describe the response characteristics of various idealized structural configurations to acoustic excitation. Section 5.3 presents sonic fatigue design techniques that have been established from laboratory testing of various specific structural configurations. Section 5.4 discusses the various methods used to join structural members as related to aircraft construction and discusses each method in relation to sonic fatigue design requirements. Section 5.5 presents a discussion of stress concentration factors as related to configurations encountered in aircraft construction and their importance to the sonic fatigue design problem.

Undoubtedly, the designer will find the data presented in Section 5.3 to be the most useful of the entire section; however, if the particular structural configuration being considered does not correspond to those listed, then the designer must refer to the other sections and use basic techniques - as described - to establish estimates for the sonic fatigue resistance of his structure.

5.1 BASIC CONSIDERATIONS

To understand the limitations upon which sonic fatigue analyses and design methods have been established, the designer must be aware of the basis upon which particular techniques have been established. Since the variety and combinations of aircraft structural configurations cover such a broad range, the designer will undoubtedly encounter configurations that have not been used previously. This section is included to acquaint the designer with the basic considerations required to understand the scope and limitations of established design methods.

Section 5.1.1 considers the topic of random vibration, and Section 5.1.2 discusses methods of vibration analysis as related to complex aircraft structure. Hopefully, these two sections will either serve as a useful introduction to the designer who is encountering the topic of sonic fatigue for the first time or serve as a refresher to the designer who has been away from the topic. Each section is brief; however, the individual can extend the presentation by going to the references listed at the end of each section.

5.1.1 RANDOM VIBRATIONS

Random vibration has become an important topic in recent years primarily as a result of advances in high speed flight. To design structures and equipment that are capable of withstanding the randomly fluctuating loading resulting from turbulent air and noise resulting from turbulent boundary layers, cavity resonance, and propulsion system noise, designers are finding that they have to understand random vibration and design components that can withstand the random loading. It is beyond the scope of this report to present a complete description of either mechanical vibrations or the statistical tools required for a thorough understanding of random vibrations. However, it is appropriate to present quantitative results to understand the significance of the design data presented in the following sections. First, mechanical vibrations shall be discussed in the context of the frequency response of structure to time varying loading. Next, the statistical tools required to describe the random loading and the resulting random structural response are presented. Finally, a discussion of the various types of methods used to obtain quantitative results are presented.

5.1.1.1 Notation

c	Viscous damping coefficient
f	Frequency, Hz
f_n	Natural frequency, Hz
$G_{\dot{x}}(f)$	Power spectral density function
$H(f)$	Frequency response function
k	Spring constant
m	Mass of system
$p(x)$	Amplitude probability density function
T	Time interval, fatigue life, or kinetic energy
t	Time

5.1.1.2 Frequency Response of Structure

Mechanical vibration analysis is simply a statement of equilibrium between inertia, damping, elastic, and applied forces. All methods rely upon the development of a model of the structure suitable for analysis. For simple structures, such as described in Section 5.2, it may be possible to achieve a high degree of simulation between the real world and the analytical

model. In reality, all structural models are approximations so that the designer must always know the limitations of the approximations. From an analytical standpoint, only one or two degree-of-freedom lumped parameter systems can be easily handled without extensive calculations. The basic considerations for lumped parameter systems and the development of the governing equations can be found in any standard textbook on mechanical vibrations (1), (2).

For a one degree-of-freedom mechanical system the frequency response function and its relation to the input, $X(f)$, and the output, $Y(f)$, is

$$Y(f) = H(f)X(f) \qquad (5.1.1\text{-}1)$$

where

$H(f) = |H(f)|e^{-i\phi(f)}$ is the frequency response function

$|H(f)|$ = Is the absolute value of $H(\omega)$ and is called the system gain factor

$\phi(f)$ = Is the associated phase angle

To define the system frequency response function, $H(f)$, one must define the input or forcing function, $X(f)$, and the desired output function, $Y(f)$. Two important one degree-of-freedom systems are illustrated in Figure 5.1.1-1. The system gain factors, $|H(f)|$, are presented in Table 5.1.1-1 for various combinations of input functions and output functions.

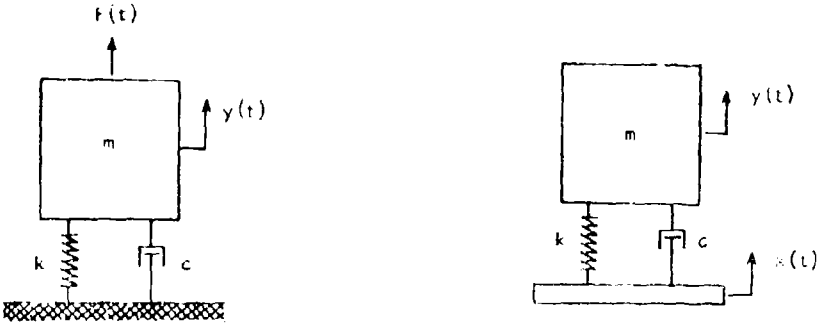

(a) Mechanical System with Force Input (b) Mechanical System with Foundation Motion Input

FIGURE 5.1.1-1 TWO CONFIGURATIONS OF ONE DEGREE-OF-FREEDOM SYSTEMS

TABLE 5.1.1-1

SUMMARY OF FREQUENCY RESPONSE FUNCTIONS
FOR SIMPLE MECHANICAL SYSTEM
(REF. 11)

Values for the Response Function $\lvert H(f) \rvert$ of a Simple Mechanical System as a Function of the Input and Output Parameters		Foundation Motion Input			Force Input
		Displacement $x(t)$ in.	Velocity $\dot{x}(t)$ in./sec.	Acceleration $\ddot{x}(t)$ in./sec.^{2}	Force (in displacement units) $x(t) = F(t)/k$ in.
In terms of displacement output, in.	Absolute displacement $y(t)$	$\frac{D_1}{D_2}$	$\frac{D_1}{2\pi f D_2}$	$\frac{D_1}{4\pi^2 f^2 D_2}$	$\frac{1}{D_2}$
	Relative displacement $z(t) = y(t)-x(t)$	$\frac{f^2}{f_n^2 D_2}$	$\frac{f}{2\pi f_n^2 D_2}$	$\frac{1}{4\pi^2 f_n^2 D_2}$	
In terms of velocity output, in./sec.	Absolute velocity $\dot{y}(t)$	$\frac{2\pi f D_1}{D_2}$	$\frac{D_1}{D_2}$	$\frac{D_1}{2\pi f D_2}$	$\frac{2\pi f}{D_2}$
	Relative velocity $\dot{z}(t) = \dot{y}(t)-\dot{x}(t)$	$\frac{2\pi f^3}{f_n^2 D_2}$	$\frac{f^2}{f_n^2 D_2}$	$\frac{f}{2\pi f_n^2 D_2}$	
In terms of acceleration output, in./sec.^{2}	Absolute acceleration $\ddot{y}(t)$	$\frac{4\pi^2 f^2 D_1}{D_2}$	$\frac{2\pi f D_1}{D_2}$	$\frac{D_1}{D_2}$	$\frac{4\pi^2 f^2}{D_2}$
	Relative acceleration $\ddot{z}(t) = \ddot{y}(t)-\ddot{x}(t)$	$\frac{4\pi^2 f^4}{f_n^2 D_2}$	$\frac{2\pi f^3}{f_n^2 D_2}$	$\frac{f^2}{f_n^2 D_2}$	

$$D_1 = \sqrt{1 + [2\zeta(f/f_n)]^2} \qquad D_2 = \sqrt{[1 - (f/f_n)^2]^2 + [2\zeta(f/f_n)]^2}$$

$$f_n = \frac{1}{2\pi}\sqrt{\frac{k}{m}} \qquad \zeta = \frac{c}{2\sqrt{km}}$$

In studying Table 5.1.1-1, it is noticed that several parameters are required to obtain quantitative results. Namely, the characteristics of the structure such as mass, m; viscous damping, c; and stiffness, k, are required as is the relative quantity f/f_n which describes the effectiveness of the excitation frequency, f, in causing the system to respond at its natural frequency, f_n.

Since all forms of excitation relevant to sonic fatigue exhibit generally broad frequency content - in particular jet noise - it is reasonable to suspect that part of the design problem is to determine the dynamic response of a system in the frequency domain with reasonable accuracy. That is, the designer should be able to predict the response frequencies of the structure with the implication that more than a one degree-of-freedom model may be required for a vibration analysis. If such is the case, then the designer should consult more advanced books on mechanical vibration (3), (4).

For the design methods presented in Sections 5.2 and 5.3, it has been totally assumed that the structure exhibits a single mode of response as characterized by the one degree-of-freedom system. This assumption is usually confirmed by experimental results. Plots of the system gain factors as a function of the frequency ratio f/f_n are presented in Figure 5.1.1-2. Here it is seen that damping, ζ, plays a significant role in determining the structural response of the system. For aircraft structure, Hay (5) has assembled the results of many experimental programs to determine the damping of typical structure. Hay's results are presented in Figure 5.1.1-3 and indicate that for normal configurations, the damping exhibited by aircraft structure is small (on the order of 0.02). Hence, the designer can expect significant structural response as exhibited by a sharp resonance peak unless artificial damping treatments are used. If artificial damping treatments are considered, the designer should recognize that significant increases in modal coupling can occur that negate the single response mode assumption. For a discussion of damping mechanisms and treatments the designer should consult Mead (6), Bert (7), or Henderson (8).

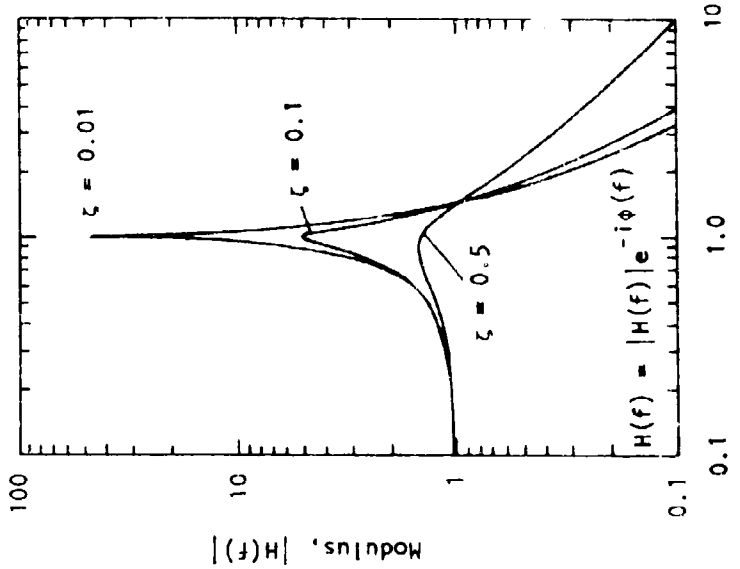

(b) Displacement Response to a Foundation Motion Input

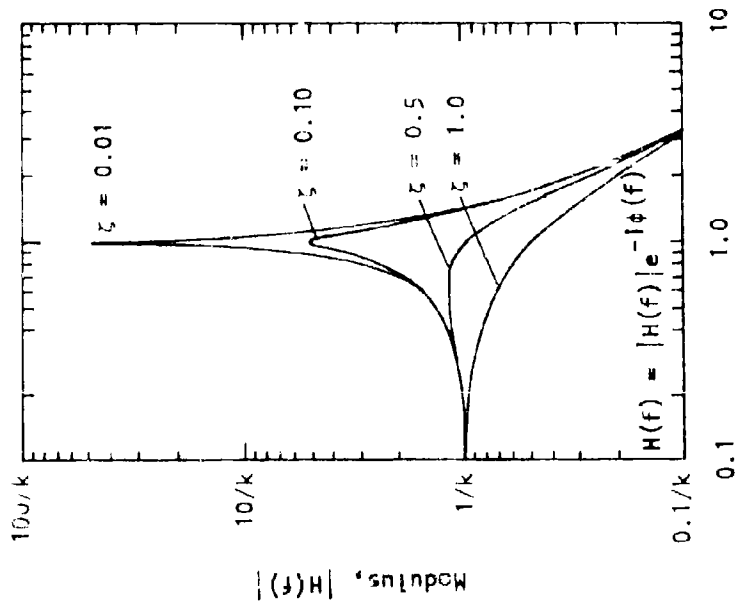

(a) Displacement Response to a Force Input

FIGURE 5.1.1-2 MECHANICAL SYSTEM FREQUENCY RESPONSE AS A FUNCTION OF FREQUENCY RATIO

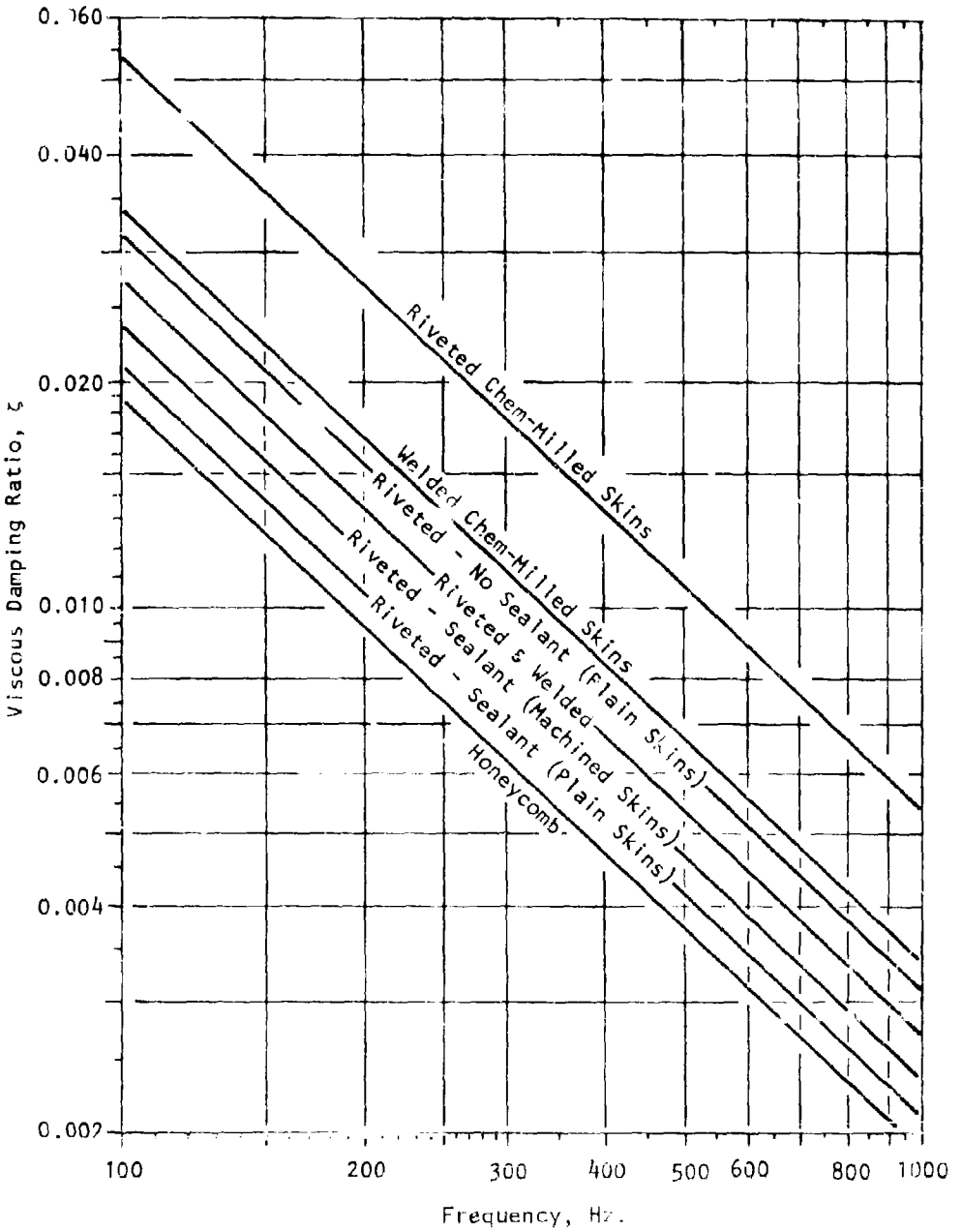

FIGURE 5.1.1-3 DAMPING RATIO VERSUS FREQUENCY FOR TYPICAL STRUCTURE

5.1.1.3 Statistical Tools for Random Vibration

Mechanical vibration problems can involve the response of a system to deterministic or to random time varying forces. Deterministic forces or inputs imply that the magnitude of the input is known instantaneously at all times. Random forces or inputs imply that the magnitude is not known or predictable in advance for any time. The designer may now suspect that even if the structural characteristic were perfectly described by the system frequency response, H(f), it would be impossible to estimate the system response, Y(f), to any degree of accuracy better than one could describe the input or forcing function, X(f). Good basic presentations of random vibration theory are given by Robson (9) and by Crandall and Mark (10).

Typical time histories of random processes are illustrated in Figure 5.1.1-4. Broad-band or wide-band noise is characterized by a random amplitude and no single predominant frequency. Broad-band noise is typical of boundary layer turbulence and jet exhaust pressure fluctuations. If the structure is lightly damped, then the structure will significantly respond only in the frequency range near resonance ($f/f_n = 1$). Any structural response quantity such as acceleration or stress will then exhibit a random amplitude (since the input amplitude is random) but will exhibit a single predominant frequency (the structure acts like a filter in the frequency domain). Hence, structural response quantities can be expected to exhibit narrow-band time histories such as illustrated in Figure 5.1.1-4. It is assumed that any random process is such that its statistical characteristics do not vary with time or, strictly speaking, the random process is assumed to be stationary and ergodic. By stationary, it is meant that the statistical averages do not vary with time when averaged over several sample time histories. By ergodic, it is meant that averages obtained for any one time history are identical to the averages obtained for all other time histories. For a much more complete description of the concepts one should consult the references: (9), (10), (11), (12). Hence, for a stationary and ergodic random process (either forcing function or system response) the designer must be able to describe statistically the amplitude and frequency content of the random process and need consider only one typical time history for each quantity.

5.1.1.3.1 Amplitude Statistics

It is first required to define parameters that describe the amplitude of a random process as follows:

Mean or Average Value: The mean or average value of a time varying quantity can be evaluated by integrating the value over a very long time period, T, and dividing by the time period. Mathematically, the mean value is given by

$$\overline{x(t)} = \lim_{T \to \infty} \frac{1}{T} \int_0^T x(t)\,dt \quad . \qquad (5.1.1\text{-}2)$$

If the mean value is not zero, it is usually convenient to adjust the scale of x(t) so that the mean value is zero.

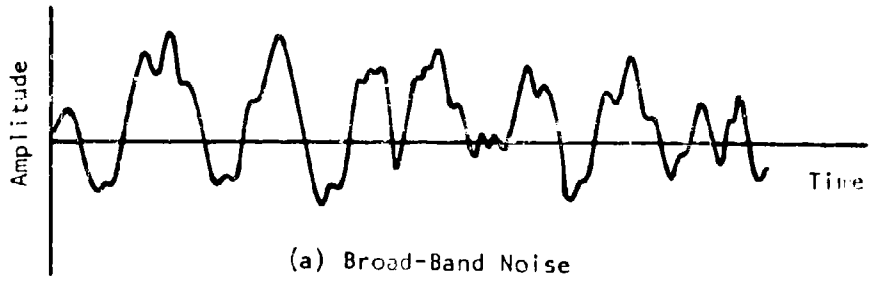

(a) Broad-Band Noise

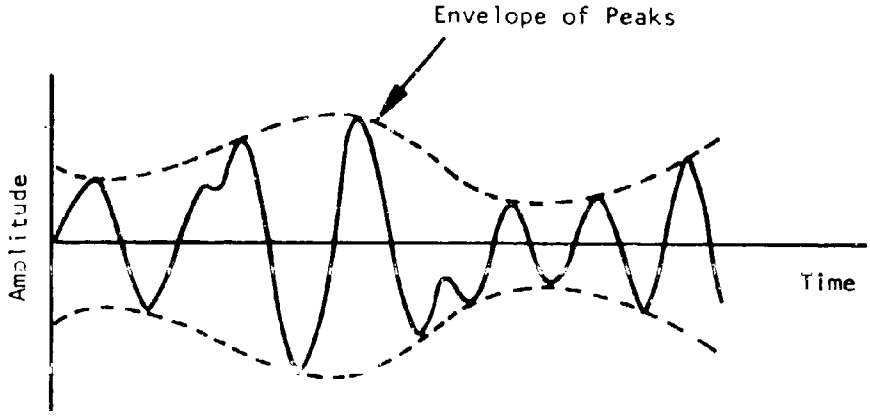

(b) Narrow-Band Noise

FIGURE 5.1.1-4 TWO CLASSIFICATIONS OF RANDOM TIME HISTORIES

Mean Square Value: The mean square value of a time varying quantity is obtained by integrating the square of the value over a very long time period, T, and dividing by the time period. Mathematically, the mean square value is given by

$$\overline{x^2(t)} = \lim_{T \to \infty} \frac{1}{T} \int_0^T x^2(t)dt. \qquad (5.1.1\text{-}3)$$

The root mean square or rms value of the time varying quantity is simply the square root of the mean square value.

Variance: The variance, σ^2, of a time varying quantity is given as the difference between the mean square value and the square of the mean value of the quantity as

$$\sigma^2 = \overline{x^2(t)} - [\overline{x(t)}]^2 \qquad (5.1.1\text{-}4)$$

The standard deviation of the time varying quantity is simply the square root of the variance. If the mean value of the time varying quantity is zero, then from Equations (5.1.1-3) and (5.1.1-4) the standard deviation is equal to the root mean square value of the time varying quantity.

Probability Density Function: The object of analyzing a random process is to determine the likelihood of encountering extreme or maximum values or to determine the percentage of time a random quantity will exceed a given level. Figure 5.1.1-5 illustrates a sample of a random time history taken over a time interval T. The probability that the function x(t) lies in the interval between x and x + Δx is that percentage of time which the function has values in that interval. This probability or percentage of time is expressed mathematically as

$$\text{Prob}[x < x(t) < x + \Delta x] = \sum_i t_i / T \qquad (5.1.1\text{-}5)$$

If the interval, Δx, is small, a probability density function, p(x) is defined as

$$\text{Prob}[x < x(t) < x + \Delta x] = p(x)\Delta x \qquad (5.1.1\text{-}6a)$$

or

$$p(x) = \frac{1}{T} \left(\frac{\sum t_i}{\Delta x}\right) \qquad (5.1.1\text{-}6b)$$

To precisely define p(x), one needs to consider very small intervals, Δx, and very long periods, T, so that mathematically the probability density function is defined as

$$p(x) = \lim_{\Delta x \to 0} \lim_{T \to \infty} \frac{1}{T} \left(\frac{\sum t_i}{\Delta x}\right)$$

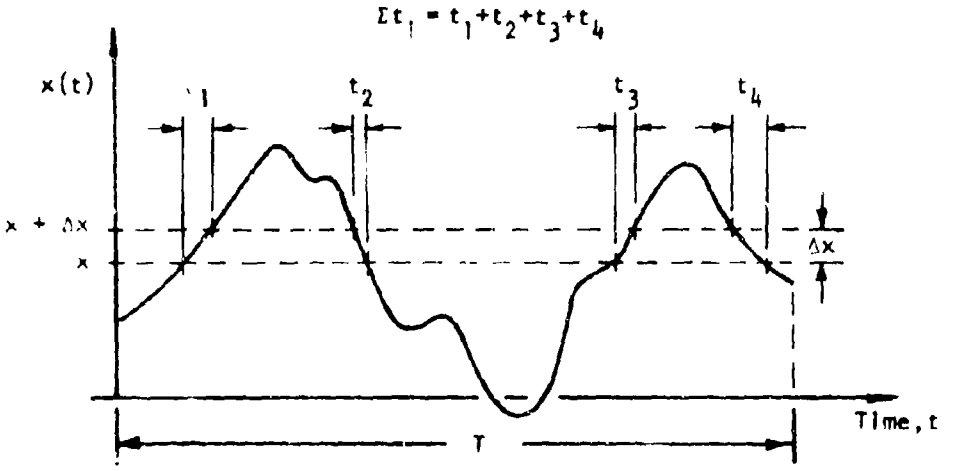

FIGURE 5.1.1-5 ILLUSTRATION OF THE A CUMULATED TIME THAT A SIGNAL SPENDS IN AN AMPLITUDE INTERVAL $x < x(t) < x + \Delta x$

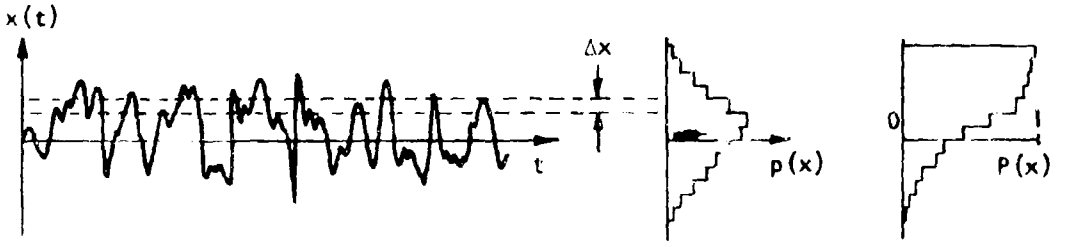

FIGURE 5.1.1-6 ILLUSTRATION OF THE RELATION OF THE AMPLITUDE PROBABILITY DENSITY AND THE CUMULATIVE PROBABILITY FUNCTIONS TO A RANDOM AMPLITUDE TIME HISTORY

Once p(x) has been determined over the range of values of x(t), then the probability or percentage of time that the amplitude x(t) is within the limits $a < x(t) < b$ is obtained from Equation (5.1.1-6a) by summing or integrating so that

$$\text{Prob}[a < x(t) < b] = \int_a^b p(x)dx \qquad (5.1.1\text{-}7a)$$

Since the probability of x(t) being between the limits $-\infty$ and $+\infty$ is 1.0 (an absolutely certain event) it follows that

$$\int_{-\infty}^{\infty} p(x)dx = 1.0 \qquad (5.1.1\text{-}7b)$$

and the probability that x exceeds a given level L is simply

$$\text{Prob}[L \leq x(t)] = 1.0 - \int_{-\infty}^{L} p(x)dx \qquad (5.1.1\text{-}7c)$$

Electronic instrumentation is available to determine either the probability function or the probability density function of actual random amplitude time histories. The process is illustrated conceptually in Figure 5.1.1-6.

Mathematically, several special probability density functions have been defined (13) with two of these functions being especially important in the discussion of random vibrations. The first, and most important, probability density function to be discussed is the Gaussian or normal probability density function is defined as

$$p(x) = \frac{1}{\sigma\sqrt{2\pi}} \exp[-(x - \bar{x})^2/2\sigma^2] \qquad (5.1.1\text{-}8a)$$

where $\bar{x}$ is the mean value and σ is the standard deviation. The second probability density function is called the Rayleigh probability density function and is defined as

$$p(x) = \frac{x}{\sigma^2} \exp[-x^2/2\sigma^2] \quad x \geq 0 \qquad (5.1.1\text{-}8b)$$

Tables for plotting the Gaussian probability density function and probability of exceeding a level, Equation (5.1.1-7c), are presented in almost any text or set of mathematical tables (11), (14). Figure 5.1.1-7 presents a plot of the probability of exceeding the rms level versus the ratio of the instantaneous level to the rms level for a Gaussian random process. Hence, if the instantaneous value of the time varying quantity exhibits a Gaussian probability density or is assumed to exhibit such tendency and if the rms value of the time varying quantity is known then Figure 5.1.1-7 can be used to determine the probability that the instantaneous value will exceed the rms value. Conversely, if the rms value for a set of instantaneous values is known, then one can plot the points on Figure 5.1.1-7 to determine how closely the process is estimated by a Gaussian probability distribution

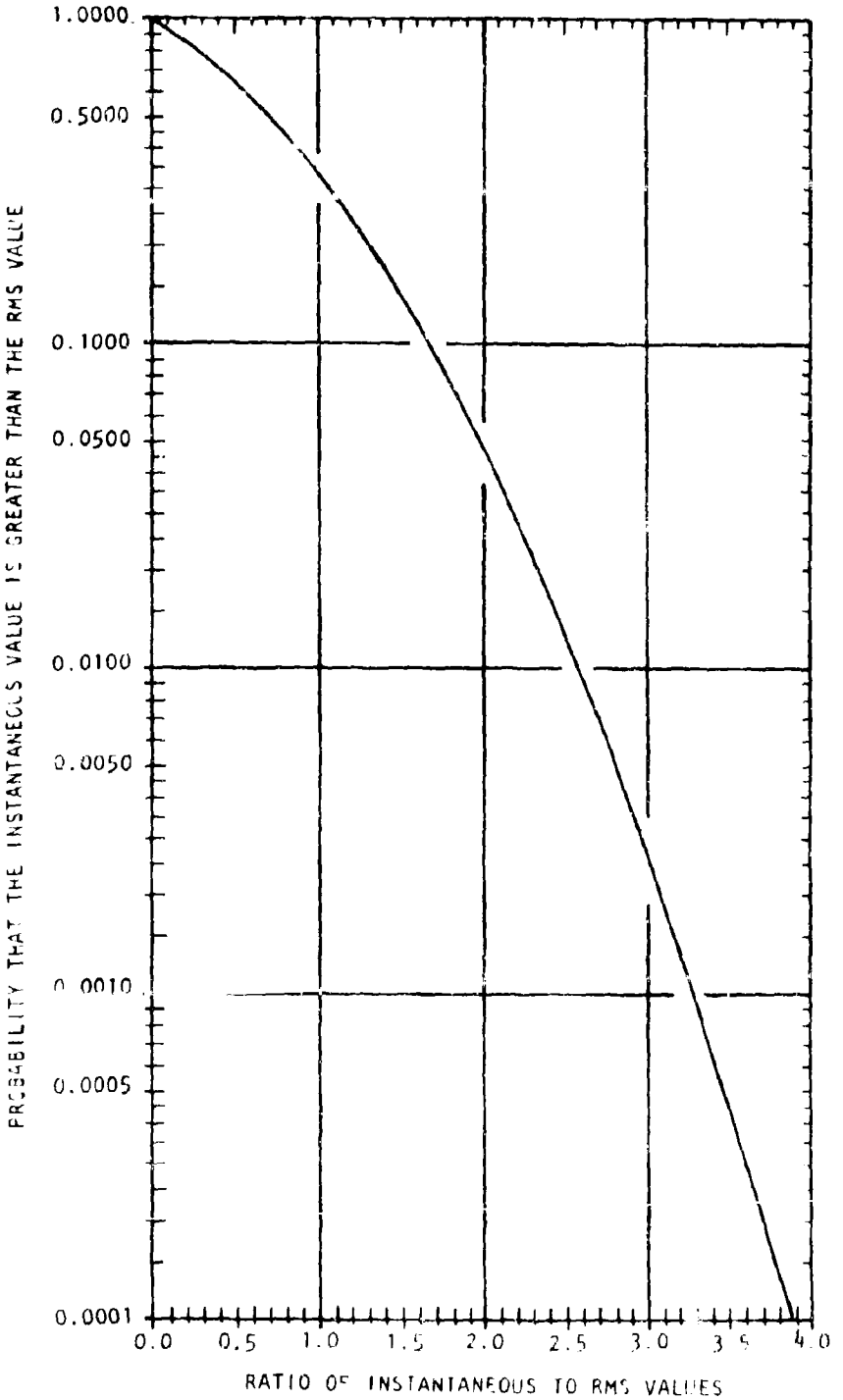

FIGURE 5.1.1-7 GAUSSIAN PROBABILITY DISTRIBUTION

Suppose, for example, that the rms value of a Gaussian time varying displacement record is equal to 1.20 inches. Then, from Figure 5.1.1-7, it is seen that the probability that the displacement exceeds 2.0 inches (in both the positive and negative directions) is equal to 0.10 or 10% ($x/\sigma = 2.0/1.2 = 1.67$).

The Gaussian or normal probability distribution is not a mere mathematical convenience since many random processes occurring in nature exhibit Gaussian probability distributions. The usefulness of the Gaussian distribution function stems from the Central Limit Theorem of statistics (12) which states that sums of independent random variables will exhibit approximately Gaussian distributions regardless of the underlying distributions. Many physically observed phenomena in practice actually represent the net effect of numerous contributing variables so that the Gaussian distribution function constitutes a good approximation to commonly occurring distributions.

The Rayleigh distribution function is important when one considers estimating the probability that either the instantaneous value will lie within the envelope of a narrow-band random process exhibiting a Gaussian probability distribution (see Figure 5.1.1-4) or the distribution of peaks of a narrow-band random process exhibiting a Gaussian probability distribution. The peak distribution problem is useful in design, for example, when it is required to convert sinusoidal fatigue curves for a material to equivalent random fatigue curves when estimating the fatigue life of a structure. This procedure is described in Section 6.5.1. A plot of the Rayleigh probability density function is presented in Figure 5.1.1-8.

5.1.1.3.2 Frequency Content

Since mechanical systems are sensitive to frequency, it is required that the designer knows the frequency content of the random loading to the system or the random response of the system. The frequency interval for which the random process has a value is called the frequency spectrum of the process.

Power Spectral Density (PSD) Function: For design purposes, the designer needs to know the amplitude of the random process at various frequencies. The power spectral density function or simply spectral density function is a measure of the frequency content of a random process. The definition of the spectral density function shall follow a simple path with the more mathematically rigorous course left to the requirements of the reader (see (9), (10), (13)).

If a time varying signal (the noise measured at a point near a jet engine, for example) is sent through a band pass filter, the filter allows only signals that have a frequency of $f_c \pm \Delta f/2$ to pass. The signal that is passed through the filter, $\Delta x(t)$, is measured in terms of its mean square value, $\overline{\Delta x^2(t)}$.

The spectral density function is then defined in terms of the mean square filtered signal as

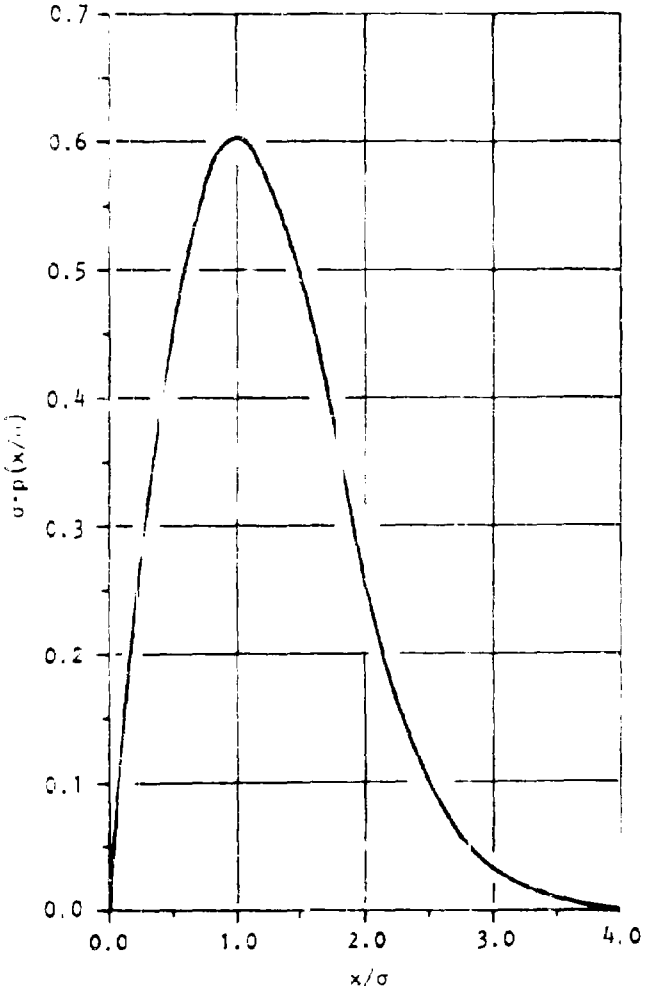

Rayleigh Probability Density Function

$\sigma \cdot p(z) = z \cdot \exp(-z^2/2)$

$z=x/\sigma$	$\sigma \cdot p(z)$	$z=x/\sigma$	$\sigma \cdot p(z)$
0.0	0.0000	2.0	0.2707
0.1	0.0995	2.1	0.2315
0.2	0.1960	2.2	0.1956
0.3	0.2868	2.3	0.1633
0.4	0.3692	2.4	0.1347
0.5	0.4412	2.5	0.1098
0.6	0.5012	2.6	0.0885
0.7	0.5479	2.7	0.0705
0.8	0.5809	2.8	0.0556
0.9	0.6003	2.9	0.0433
1.0	0.6065	3.0	0.0333
1.1	0.6007	3.1	0.0254
1.2	0.5841	3.2	0.0191
1.3	0.5584	3.3	0.0142
1.4	0.5254	3.4	0.0105
1.5	0.4870	3.5	0.0077
1.6	0.4449	3.6	0.0055
1.7	0.4008	3.7	0.0039
1.8	0.3562	3.8	0.0028
1.9	0.3125	3.9	0.0019
2.0	0.2707	4.0	0.0013

FIGURE 5.1.1-8 RAYLEIGH PROBABILITY DENSITY FUNCTION

$$G_x(f) = \Delta\overline{x^2(t)}/\Delta f \qquad (5.1.1\text{-}9)$$

It is important to note that the magnitude of the spectral density function, $G_x(f)$, depends upon the band width of the filter used to determine its value. If the signal represents pressure, then the units of the spectral density function are $(psi)^2/Hz.$, for example. The total spectral density curve is obtained by examining each frequency interval and plotting the spectral density associated with each band center frequency, f_c, over all values of the frequency domain. Typical spectral density function for broad-band noise (i.e., jet pressure excitation), and narrow-band noise, typical of the stress response of the structure, are presented in Figure 5.1.1-9.

The spectral density functions illustrated in Figure 5.1.1-9, are typical results for a continuous representation of the spectral density function when the filter bandwidth, Δf, used to measure the signal becomes very small (mathematically approaches zero). Thus, the definition of the spectral density function becomes

$$G_x(f) = \frac{d}{df}\left(\overline{x^2(t)}\right) \qquad (5.1.1\text{-}10a)$$

or

$$d\overline{x^2(t)} = G_x(f)df \qquad (5.1.1\text{-}10b)$$

Hence, to determine the mean square value of the time varying signal, it is only required to integrate Equation (5.1.1-10b) over the entire frequency spectrum to obtain

$$\overline{x^2(t)} \quad \int_0^\infty G_x(f)df \qquad (5.1.1\text{-}10c)$$

This result should be compared to Equation (5.1.1-3).
Note: When reading the literature on random vibrations it is usually found that analytical results are expressed in radian frequency, ω, with the frequency spectrum defined on the interval $-\infty < \omega < \infty$ so that the mean square value of a quantity is expressed as

$$\overline{x^2(t)} = \int_{-\infty}^{\infty} S_x(\omega)d\omega = 2\int_0^\infty S_x(\omega)d\omega \qquad (5.1.1\text{-}10d)$$

where the symmetry of the spectral density has been used to obtain the second result (i.e., $S_x(-\omega) = S_x(\omega)$). Since $\omega = 2\pi f$, a change of variable in Equation (5.1.1-10d) results in

$$\overline{x^2(t)} = 4\pi\int_0^\infty S_x(f)df \qquad (5.1.1\text{-}10e)$$

Comparing Equations (5.1.1-10c) and (5.1.1-10e), it is seen that

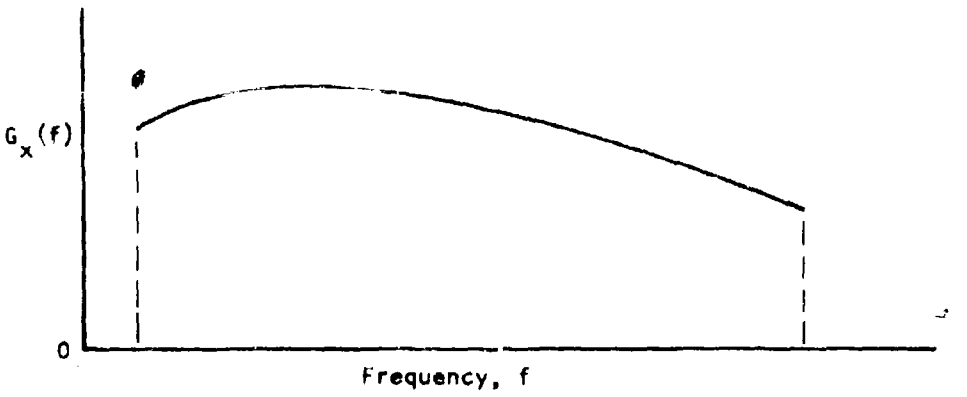

(a) Broad Band Spectral Density Function

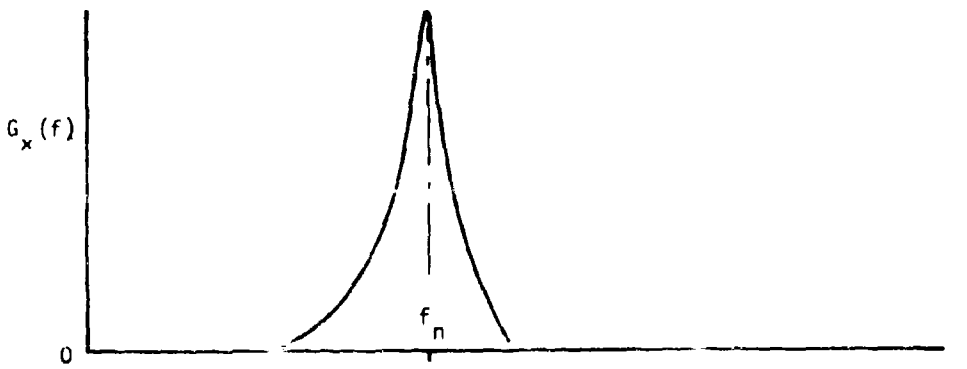

(b) Narrow Band Spectral Density Function

FIGURE 5.1.1-9 TYPICAL SPECTRAL DENSITY FUNCTIONS

$$G_x(f) = 4\pi S_x(f) \qquad (5.1.1\text{-}10f)$$

so that when one is considering spectral density functions the factor of 4π must be considered when changing the limits of integration and converting from radian frequency, ω, to circular frequency, f.

5.1.1.4 Response of a Mechanical System to Random Excitation

Section 5.1.1.2 described the structural response of a mechanical system in terms of the frequency response function, H(f). Section 5.1.1.3 presented definitions and discussion of the statistical tools required to describe random time varying quantities and the frequency resolution of a random time varying quantity. This section shall present a description of how a mechanical system responds to a random forcing input. In particular, it is important to obtain an expression for the mean square value of the system response. The mean square response is important since if the linear mechanical system is forced by a random input that exhibits Gaussian probability characteristics then the system response also exhibits Gaussian probability characteristics and the only quantity required to describe the probability density or the cumulative probability of the response is the mean square value of the response (9), (10).

For the purposes of this discussion, the most direct approach to consider for calculating the mean square response of a mechanical system will be to consider the frequency analysis of the input or forcing function and the frequency response of the system. By using correlation techniques and the impulse response of the system, one could also obtain results by analysis in the time domain (see Robson (9) or Bendat(10)). The frequency description of a random signal is considered by determining the power spectral density of the system response as described in Section 5.1.1.3.2.

The frequency resolution of the response, y(t), of a mechanical system due to a time varying input, x(t), is given by Equation (5.1.1-1). If the time varying input, x(t), and the response, y(t), are both sent through a band pass filter, squared, and averaged then one obtains the result

$$\overline{\Delta y^2(t)} = \overline{Y^2(f)} = |H(f)|^2 \, \overline{X^2(f)} = |H(f)|^2 \overline{\Delta x^2(t)} \qquad (5.1.1\text{-}11)$$

where the Δ symbol before $\overline{y^2(t)}$ and $\overline{x^2(t)}$ implies that the signals have been filtered. Then, one obtains

$$G_y(f) = \frac{\overline{\Delta y^2(t)}}{\Delta f} = |H(f)|^2 \frac{\overline{\Delta x^2(t)}}{\Delta f} = |H(f)|^2 G_x(f) \qquad (5.1.1\text{-}12a)$$

or

$$G_y(f) = |H(f)|^2 G_x(f) \qquad (5.1.1\text{-}12b)$$

The result presented by Equation (5.1.1-12b) is the central result of the random vibration analysis for a one degree-of-freedom system. Mathematically rigorous developments of this result are presented in the References. The implication of this result for design use is extremely significant. Namely, the designer need only be interested in determining the system gain factor, $|H(f)|$, and the input or forcing spectral density function, $G_x(f)$, to determine the response spectral density function, $G_y(f)$. Once the system response spectral density function is determined, then the mean square value of the response is obtained from Equation (5.1.1-10c) as

$$\overline{y^2(t)} = \int_0^\infty G_y(f)df = \int_0^\infty |H(f)|^2 G_x(f)df \ . \qquad (5.1.1\text{-}13)$$

One immediate simplification can be made for the result presented in Equation (5.1.1-13). If the mechanical system is lightly damped (see Figures 5.1.1-2 and 5.1.1-3) and the input forcing exhibits a broad-band frequency spectrum (see Figures 5.1.1-4 and 5.1.1-9) that varies slowly with frequency, then $G_x(f)$ will be essentially constant in the frequency interval about which the mechanical system exhibits significant response ($f \approx f_n$) so that one obtains the approximation

$$\overline{y^2(t)} \approx G_x(f_n)\int_0^\infty |H(f)|^2 df \ . \qquad (5.1.1\text{-}14)$$

This approximation is convenient for design purposes since many forcing functions important to sonic fatigue design exhibit spectral density functions that vary slowly with frequency, and to obtain simple design equations, the integration required by Equation (5.1.1-14) is more easily performed than that required by Equation (5.1.1-13). In addition, if this approximation is valid so that the result of Equation (5.1.1-14) can be used, then the designer can separate the consideration of loading actions as expressed by $G_x(f)$ and the structural characteristics as expressed by $H(f)$. The only interrelationship between the two is that $G_x(f)$ must be evaluated at the response frequency, f_n, so that when the designer alters $H(f)$ to reduce the mean square response he must recognize also that f_n and hence $G_x(f_n)$ may be altered.

For sonic fatigue design, the input force - as described above - results from a random pressure acting over a surface area. The techniques required to determine the appropriate "lumping" of a random pressure acting over a surface area is presented in detail in Section 5.2.2.2.6.

5.1.1.5 Miles' Single Degree-of-Freedom Theory

Miles (15) proposed a single degree-of-freedom model to represent the response of a plate to jet noise excitation and proposed a technique for estimating the fatigue life of the structure based upon the use of Miner's Cumulative Damage Theory (16). The results of Sections 5.1.1.2 through 5.1.1.4 apply - in particular Equation 5.1.1-14 - so that the system response to an excitation spectrum that varies slowly with frequency in the frequency range near the natural frequency is given by

$$\overline{y^2(t)} = \left(\frac{y_o}{F_o}\right)^2 f_n G_x(f_n) \int_o^\infty \frac{dr}{[(1-r^2)^2 + 4\zeta^2 r^2]} \qquad (5.1.1\text{-}15)$$

$r = f/f_n$ $\qquad$ ζ = damping ratio

where y_o is the static displacement response to a static generalized force of magnitude F_o. The evaluation of the integral in Equation (5.1.1-15) is rather complicated (See Crandall (10)) but can be obtained in rather simple form as

$$\int_o^\infty \frac{dr}{[(1-r^2)^2 + 4\zeta^2 r^2]} = \frac{\pi}{4\zeta}, \quad \zeta << 1 \qquad (5.1.1\text{-}16)$$

Then, one obtains the simple result from the mean square displacement response as

$$\overline{y^2(t)} \approx \frac{\pi}{4\zeta} f_n G_x(f_n) \left(\frac{y_o}{F_o}\right)^2 \qquad (5.1.1\text{-}17)$$

Assuming a linear relationship between stress and displacement, the mean square stress response for light damping is simply

$$\overline{\sigma^2(t)} \approx \frac{\pi}{4\zeta} f_n G_x(f_n) \left(\frac{\sigma_o}{F_o}\right)^2 \qquad (5.1.1\text{-}18)$$

where σ_o is the static stress resulting from a static force of magnitude F_o. The results presented in Equations (5.1.1-17) and (5.1.1-18) are the mathematical statement of Miles' Single Degree-of-Freedom Theory. The extension of this theory to multi-degree-of-freedom systems is presented in Section 5.2.2.2.6 and is specialized to the case of random pressure loading of plate-like structure. The implication of Miles' results are significant in that the designer really needs to be concerned only with estimating the natural frequencies of the system (usually the fundamental mode is all that is required) and to determine the static stress response of the system at the points of interest resulting from a unit magnitude force (or pressure) in order to calculate the mean square stress response of the system.

From Section 5.1.1.3, it is seen that once the mean square response is determined then all probability data is established if the response is Gaussian. For the linear mechanical system upon which the results given by Equations (5.1.1-17) and (5.1.1-18) are based, the system response will be Gaussian if the excitation is Gaussian. In particular, for these results the assumed peaked frequency response results in a narrow band Gaussian process for describing the system response.

The mean square stress response, $\overline{\sigma^2(t)}$, given by Equation 5.1.1-18 is now used to estimate the fatigue life of a structure. Miles' presents a closed-form

estimate for fatigue life by assuming that Miner's Cumulative Damage Theory (16) (also proposed by Palmgren (17) and now called the Palmgren-Miner Cumulative Damage Rule) applies and that the S-N characteristics of the material are such that the S-N curve is linear when plotted on log-log paper. Here it is assumed that the stress, s, is a constant amplitude alternating stress with complete stress reversals from -S to +S (i.e., sinusoidal time history). Miles analysis of fatigue life estimates will be presented here to illustrate the relationship to the Cumulative Damage Theory although this approach has been judged to be highly conservative (18). More detail concerning various cumulative damage theories will be presented in Section 6.

Noting that experimentally obtained sinusoidal S-N data usually exhibits wide scatter, Miles assumed that the relationship between the number of cycles-to-failure, N(s), at a stress level s is given by the relationship

$$N(s) = c/s^b \qquad (5.1.1\text{-}19)$$

where the constants c and b are parameters dependent upon the material. Since the random stress will vary in amplitude it is necessary to establish an estimate of the "damage" done to the material by a number of stress reversals, n(s), less than the number of stress reversals, N(s), required to cause failure at the stress level, s. Miner (16) assumed that damage was accumulated linearly so that at a stress level s_i the damage is given by the ratio n_i/N_i ($n_i = n(s_i)$ and $N_i = N(s_i)$) and that the cumulative damage is given by

$$D_M = \sum_i (n_i/N_i) \qquad (5.1.1\text{-}20)$$

with failure occurring when $D_M = 1.0$. As discussed in Section 6, various other more complicated cumulative damage theories are available, but the improvement (if any) in obtaining analytical fatigue life estimates - especially for random stress reversals - is not generally warranted.

Miles, for convenience, introduces a reduced stress, s_r, which produces the same fatigue damage as the spectrum (n_i, s_i) after the same total number of cycles, Σn_i, so that from Equations (5.1.1-19) and (5.1.1-20) one obtains the result

$$s_r = \left[\sum_i n_i s_i^{kb} / \sum_i n_i \right]^{1/kb} \qquad (5.1.1\text{-}21)$$

where k is a factor on the order of 1.0 to 2.0. The results to this point are based upon a sinusoidal constant amplitude time history for the stress.

The extension of these results to obtain an estimate of the equivalent random stress is of a lightly damped structure is now required. The probable number of cycles of random stress having an amplitude in the range (s, s + ds) in a time, T, is

$$n(s) = f_n T p(s) ds \qquad (5.1.1\text{-}22)$$

where p(s) is the probability density of the stress peaks. For a narrow-band Gaussian random process the probability density for peaks is a Rayleigh distribution function as given by Equation (5.1.1-8b) and illustrated in Figure 5.1.1-8.

From Miner's Cumulative Damage Rule, the expected or probable damage resulting from stress peaks in the range (s, s + ds) with a frequency f_n for a time period T is

$$\frac{n(s)}{N(s)} = f_n T \frac{p(s)}{N(s)} ds \qquad (5.1.1\text{-}23a)$$

and the total expected damage $E[D_M]$ for all stress amplitudes is

$$E[D_M(T)] = f_n T \int_0^\infty \frac{p(s)}{N(s)} ds \qquad (5.1.1\text{-}23b)$$

and the time to failure is ($E[D_M(T)] = 1$),

$$T = [f_n \int_0^\infty (p(s)/N(s))ds]^{-1} \text{ sec.} \qquad (5.1.1\text{-}23c)$$

For an assumed Rayleigh probability density function and a constant amplitude S-N curve that is linear on a log-log plot, the integral in Equation (5.1.1-23c) is evaluated as

$$\int_0^\infty \frac{p(s)ds}{N(s)} = 2^{b/2} (\bar{\sigma})^b \cdot \Gamma(1 + b/2)/c \qquad (5.1.1\text{-}23d)$$

where $\bar{\sigma} = \sqrt{\sigma^2(t)}$ is the root mean square stress and $\Gamma(x)$ is the Gamma Function which is tabulated in standard mathematical tables (14). For large positive values of the argument x (not necessarily integer values) the Gamma Function is approximated by the expression

$$\Gamma(x + 1) = \sqrt{2\pi} e^{-x} x^{x+1/2} \quad x > 2 \qquad (5.1.1\text{-}23e)$$

The estimate for fatigue life is then given by

$$T = c[2^{bk} f_n \bar{\sigma}^b \Gamma(1 + b/2)]^{-1} \text{ sec.} \qquad (5.1.1\text{-}23f)$$

As mentioned above, the constants b and c are determined from a log-log plot of constant amplitude S-N data (which is assumed to be linear) and the method has proven in practice to yield conservative fatigue life estimates (10). It

should be noted that the natural frequency, f_n, that is used in Equation (5.1.1-22) and in the subsequent developments is more properly described as an "expected frequency" based upon the rate at which the signal crosses a defined level (usually zero) with a positive slope. The expected frequency, $f_e^+(a)$, is defined in terms of the joint probability of the signal, $y(t)$, and its time derivative, $\dot{y}(t)$, as follows

$$f_e^+(a) = \int_o^\infty \dot{y} p(a,\dot{y}) d\dot{y} \qquad (5.1.1\text{-}24g)$$

where a is the level crossed by $y(t)$ with positive slope. For a Gaussian process with zero mean then

$$f_e^+(a) = \frac{1}{2\pi} \frac{\sigma_{\dot{y}}}{\sigma_y} \exp\ (-a^2/2\sigma_y^2) \qquad (5.1.1\text{-}24h)$$

where σ_y is the rms level of y and $\sigma_{\dot{y}}$ is the rms level of $\dot{y}$. A more complete discussion of this consideration is presented by Robson (9) and Crandall (10)

To overcome the conservative fatigue life estimates, an early technique utilized by designers was to obtain so-called equivalent random fatigue curves from constant amplitude sinusoidal S-N data by assuming that the random stress peaks exhibited a Rayleigh distribution and that Miner's hypothesis of cumulative damage applies. Letting $N(s)$ denote the number of cycles to failure at a constant amplitude stress level s as determined from test data, and letting $N_r(\bar{\sigma})$, be the number of cycles to failure for a random amplitude stress, $\bar{\sigma}$, then the expected damage is (see Equation (5.1.1-23b)

$$E[D_M(s)] = N_r(\bar{\sigma}) \int_o^\infty \frac{p(s)}{N(s)} ds \qquad (5.1.1\text{-}25)$$

At failure $E[D_M(s)] = 1$, so that

$$N_r(\bar{\sigma}) = [\int_o^\infty \frac{p(s)}{N(s)} ds]^{-1} \qquad (5.1.1\text{-}26)$$

Since N(s) is known from experiment, any convenient numerical integration of Equation (5.1.1-25) can be used at each rms stress level, $\bar{\sigma}$. Hence, the constant amplitude S-N data can be converted to equivalent random amplitude fatigue data $\bar{\sigma} - N_r$ on a point by point basis. This technique has been used in the past by McGowan (19) to obtain design results, especially for fatigue curves that are based upon certain values of stress concentration or other complications. It is recommended for design use only if random amplitude fatigue data is not available for the material and the joining method proposed for the specific design. Wang (20) presents techniques for estimating the probability of failure due to combined load spectra (combination of maneuver loads and acoustic loads) and fatigue damage for the case of broad band random amplitude stress is discussed by Bernard and Shipley (21). More practical design methods are presented in Sections 5.3 and 6.0.

5.1.2 METHODS OF VIBRATION ANALYSIS

The formulation and solution of equations of motion for natural vibrations of various structural configurations may be a rather simple task or one involving the use of extensive computation. Since natural vibrations never really occur in physical structures, it may seem to be academic to even discuss the topic. However, since the knowledge of the natural frequencies and normal modes of the structure is required by the designer to estimate the structural response, the designer should be aware of the various methods that have been applied to the solution of the problem of sonic fatigue of aircraft structures and of the degree of approximation that the various methods represent.

The designer must understand the significance of the approximations which result from the use of a particular method for a specific structural configuration. This understanding will often dictate the choice of method. Basic to this understanding is the awareness by the designer that all methods of vibration analysis are approximate in an engineering sense. Factors such as variations in material properties, dimensional tolerances, etc. cause the differences to exist between the physical structure and the idealized structure (mathematical model) used in the analysis. These differences may be a more significant consideration that the smaller differences that would result from using alternate analytical methods. In particular, the design methods presented in this handbook are based upon very simple approximate structural models of highly complicated aircraft structure. This approach has proven to be acceptable in accuracy for the solution of sonic fatigue design problems (22).

5.1.2.1 Classification of Methods

Methods of vibration analysis may be classified under three general categories according to the mathematical form of the governing equations (3),(23). These three general categories are differential equation methods, integral equation methods, and energy methods. The distinction between the three categories is logical on a mathematical basis and, hence, to some extent on the degree of effort required to obtain quantitative results. The most salient distinction between the three categories is the manner in which the boundary conditions are handled. In addition the degree of structural complexity that may be easily included in the model (discontinuities, etc.) is somewhat dependent upon the method. Of the three techniques, energy methods have found the most widespread and common use as an analysis tool for the sonic fatigue problem. A brief discussion of differential equation methods and integral equation methods will be presented with a more detailed consideration of energy methods presented.

5.1.2.2 Differential Equation Methods

The vibration analysis of a structure requires the solution of the governing partial differential equations describing the motion of the system. For natural vibrations, the prescribed boundary conditions must be satisfied explicitly to obtain unique solutions. The frequency or characteristic equation results directly from the mathematical conditions imposed by enforcing the boundary conditions on the general solution. Using this method, it is

impossible to obtain either frequency or mode shape estimates that do not satisfy the boundary conditions. The types of structures for which solutions to the governing equations of motion are possible are strings, bending and twisting of beams, membranes, circular plates and rectangular plates with simply supported edges (4). These structures hardly conform to those types encountered in practice by a designer.

Appendix B.1 presents the vibration analysis of slender straight elementary beams either in bending or torsion. The governing differential equations of motion for coupled bending-torsion motion of thin-walled open section beams are also presented with indications of the complexity of the solution. To indicate the amount of calculation required to investigate the vibration of a beam with elastic rotational constraint the reader should consider Carmichael's analysis (24) presented in Section 5.2.2.2.4. Carmichael's vibration analysis of a plate with elastic rotational edge constraints uses the differential equation solution of a beam problem as the basis for applying an energy method (Rayleigh-Ritz Technique). Indeed, the results for plate and cylindrical shell vibration presented in Section 5.2.2 and 5.2.3 all rely upon energy methods using the differential equation solution of the beam vibration problem as a basis.

5.1.2.3 Integral Equation Methods

Integral equation methods involve the solution of governing integral equations. An integral equation is an equation in which the function to be determined (i.e., the solution) appears under an integral sign. The kernel of these integral equations (25) include influence functions (Green's Functions) that will, by usual methods of derivation, satisfy the boundary conditions of the problem. That is, auxiliary conditions are, in a sense, already written into the equation so that the boundary conditions are implicitly satisfied through the use at appropriate influence functions. This method is used extensively in the solution of acoustics problems (26) but is only rarely used in structural dynamics (23).

5.1.2.4 Energy Methods

Energy methods are based upon the use of one or more of the energy principles of mechanics: conservation of energy, virtual work, Hamilton's principle, Lagrange's equations, etc. Energy methods are the most practical approach for the vibration analysis of complex structure and are the most widely used analysis method for sonic fatigue problems. Langhaar (27) presents a basic discussion of energy methods with the application of these techniques to structural dynamics presented by Hurty and Rubinstein (3) and Bisplinghoff (23). Basically, energy methods - as applied in practice - make use of one or more displacement functions selected somewhat arbitrarily to approximate the natural mode functions. If the natural modes determined by the analysis are to satisfy the prescribed boundary conditions, it is necessary that the approximate or assumed displacement functions satisfy the boundary conditions. The accuracy of the solution, however, depends upon whether or not the boundary conditions are satisfied.

5.1.2.4.1 Rayleigh Method

Rayleigh's method is based upon a principle stated by Lord Rayleigh in his famous work Theory of Sound in 1877 (28). Rayleigh's principle, stated in modern terminology, is as follows (4) : In a natural mode of vibration of a conservative system the frequency of the vibration is a minimum. That is, at any instant the energy of a conservative system in free vibration is partly kinetic and partly potential with the total energy being constant and the time rate of change of the total energy being zero. Denoting the kinetic energy by T(t) and the potential energy by U(t) at an instant of time, t, the principle of conservation of energy is stated as

$$T(t) + U(t) = \text{constant} \qquad (5.1.2\text{-}1a)$$

and the time rate of change of the total energy is

$$\frac{d}{dt}\left(T(t) + U(t)\right) = 0 \ . \qquad (5.1.2\text{-}1b)$$

Both the kinetic and potential energy are proportional to the square of the amplitude of the mode, and the displacements vary harmonically in time with frequency ω. Hence, for a linear system, the amplitude of the mode is arbitrary when using Rayleigh's method to determine the frequency. From the above result, it is evident that the maximum value of the kinetic energy and that the maximum value of the potential energy must be equal. Hence, an alternate form of Equation (5.1.2-1b) is

$$-T_{max} = U_{max} \qquad (5.1.2\text{-}2)$$

Since the motion is harmonic, $T_{max} = -\frac{1}{2}\omega^2 MA^2$ and $U_{max} = \frac{1}{2}KA^2$ where M is called the modal mass (or generalized mass) and K is called the modal stiffness (or generalized stiffness). Hence, Rayleigh's method yields the result for the normal mode response frequency

$$\omega^2 = K/M \quad (\text{rad/sec})^2 \qquad (5.1.2\text{-}3)$$

The application of Rayleigh's method requires that the frequency be a minimum. That is, the first variation of the frequency (26), must minimize Equation (5.1.2-3) so that

$$\delta(\omega^2) = \delta(K/M) = 0 \qquad (5.1.2\text{-}4)$$

Hurty (4) shows that the requirement stated in Equation (5.1.2-4) implies that the assumed mode function used to obtain K and M must satisfy the differential equation governing and the natural boundary conditions of the problem. If the assumed mode does not satisfy these conditions completely,

then the frequency estimate is not a minimum but slightly higher than the exact result.

Rayleigh's method is extremely useful since reasonably accurate frequency estimates can be obtained explicitly for many structural configurations. Other more refined methods using more than a single assumed mode require extensive computation to obtain quantitative results. Additionally, Rayleigh's method is a very versatile and direct method in that one only needs to make a reasonable guess at the mode and to use this result to obtain the expressions for the kinetic and potential energy of the structure. Leissa (29) has shown that in some cases Rayleigh's method provides frequency estimates as accurate as the more refined Rayleigh-Ritz procedure for the vibration analysis of rectangular thin plates.

5.1.2.4.2 Rayleigh-Ritz Method

This method is an extension of the Rayleigh method and is based upon the premise that a number of assumed functions can be linearly superimposed to provide a closer approximation of the exact natural modes than can be had using a single function as in Rayleigh's method. This method was proposed by Ritz (30) and allows not only a better approximation of the fundamental mode frequency and mode shape but also allows the calculation of higher mode frequencies and mode shapes. Using several approximate functions leads to the more accurate results at the expense of increased effort in computation. An example of the application of the Rayleigh-Ritz method is given in Section 5.2.2 for the estimation of the fundamental mode frequency, mode shape, and stress response of a rectangular plate with opposite edges elastically restrained in translation.

The Rayleigh-Ritz procedure assumes that N functions, $\phi_i(x)$, that satisfy at least the geometric boundary conditions are used to approximate the assumed displacement function, w(x), as a series

$$w(x) = \sum_{i=1}^{N} \phi_i(x) W_i \qquad (5.1.2\text{-}5a)$$

The coefficients W_i are determined so that the "best" approximation to the natural modes is obtained by requiring the frequency to be stationary at the natural frequencies, ω_i, as required by the Rayleigh Principle (Equation (5.1.2-4)). By substituting the assumed deflection w(x) given by Equation (5.1.2-5a) into Equation (5.1.2-4) and differentiating the result with respect to each of the coefficients, W_i, a set of N homogeneous equations are obtained in the form

$$\frac{\partial \omega_0^2}{\partial W_i} = 0 \qquad i = 1,\ldots,N \qquad (5.1.2\text{-}5b)$$

These equations contain the undetermined frequency parameter, ω^2, so that the resulting problem is an n dimensional eigenvalue problem (25). The solution of this eigenvalue problem requires a computer for N > 3 so that the technique is not readily applied to problems that do not justify extensive calculation (see Equations 5.2.2-21, 5.2.2.2-22, and 5.2.2-23).

An alternate approach to the Rayleigh-Ritz Method is the use of Lagrange's equations to obtain the equations of motion based upon an assumed series expansion of a deflection shape (3), (4), (23), (25), (26). The results obtained are identical. The utility of using this approach is that the system of governing equations can be developed and estimates made as to the effect of increasing the number of terms in an attempt to improve accuracy. If the effect is small, then it is possible to rationalize an assumed single mode approximation to obtain simple design equations. This technique is used in Section 5.2.3 to develop frequency expressions for open cylindrical shells with the penalty being a restriction on the range of geometrical parameters for which the results are sufficiently accurate.

5.1.2.4.3 Numerical Methods

Methods used to model structural systems can be basically divided into analytical methods and numerical methods. The techniques described previously are classified as analytical methods since they are basically focused at obtaining explicit closed-form quantitative results for simple structural configurations. The analysis techniques discussed here are applicable to the analysis of complex structure such as found in aircraft design. For such complex structure, numerical methods must invariably be employed in order to accurately model the structural configuration. To utilize these methods for sonic fatigue design the designer must consider the cost and time required for coding a digital computer or to implement a general analysis method in order to model the structure under consideration.

Numerical methods can be subdivided into two categories: numerical solutions to differential equations and matrix methods based upon discrete-element idealization. Numerical solutions to differential equations are somewhat restricted so that these techniques can be practically applied only to simple structural configurations. For the sonic fatigue problem, matrix methods have been successfully applied to obtain estimates for natural frequencies, mode shapes, and response to random acoustic excitation.

Matrix methods develop the complete structural theory using matrix algebra through all stages of the analysis. The structure is first idealized into an assembly of discrete structural elements with an assumed form of displacement or stress distribution. The complete solution is obtained by combining these individual approximate displacement or stress distributions in a manner which satisfies, respectively, the force-equilibrium and displacement-compatibility conditions at the junctions of these elements. The formulation of the analysis in matrix algebra is convenient in that one does not have to write out the lengthy equations and the result is in a form ideally suited for solution on a digital computer. Two matrix methods shall be discussed here: transfer matrix methods and finite element methods.

Transfer Matrix Methods: The transfer matrix method is an iterative matrix technique that can be used for structural configurations that are idealized as one dimensional structures. For the sonic fatigue problem, the idealization is usually made for a row of panels transversely supported by flexible stringers (see Figure 5.2.1-12). Whereas the properties of the structure are considered constant in the direction of the width and the boundary conditions along the length taken as either simple supports or clamped supports, the

stiffener spacing and elastic characteristics in the direction of the length of the structure are taken as variables. The technique is capable of predicting natural frequencies, normal mode shapes, normal mode stress resultants, and stress response to forced excitation.

Prentis and Leckie (31) present a basic description of the derivation of the transfer matrix for simple structural configurations and the application of the method to simple lumped parameter mechanical systems. The general analysis techniques to apply the transfer matrix method to structural systems is presented in the textbook by Pestel and Leckie (32). The problem of the forced response to random excitation of multi-spanned beam and panel systems is discussed by Lin (33). A survey article by Lin and Donaldson (34) focusing upon the application of transfer matrix methods to the analysis of aircraft panels will provide the designer with a broad literature source and a discussion of the basic techniques as applied to aircraft structure. The analysis of a row of curved multi-spanned panels is presented by McDaniel (35) and by Henderson (36).

Finite Element Methods: Finite element methods are classified into two basic categories depending upon whether displacements or forces are the unknowns. The structural idealization is based upon dividing the structure into a set of subregions or elements and mathematically assembling the elements to form the structure using either force-equilibrium conditions (displacement method) or displacement-compatibility conditions (force method).

Two basic text books on matrix structural analysis are those by Przemieniecki (37) and by Zienkiewicz (38). The two complementary matrix methods of formulation of any structural problem are the displacement (or stiffness) method where displacements are selected as unknowns and the force (or flexibility) method where forces are unknowns. For structural dynamics problems, the displacement method has been the most extensively used technique applied to aircraft and sonic fatigue analyses. The application of finite element methods for the solution of acoustic fatigue problems requires a complete and thorough understanding of the particular computer code or program utilized and the characteristics of the finite elements used to model the structure. The most thoroughly documented finite-element displacement method generally available to the aircraft industry is the NASTRAN program developed for and maintained by NASA. A summary of this computer code is given by Butler and Michel (39)

The application of finite element methods to the sonic fatigue problem associated with stiffened panel structure is discussed by Lindberg (40). This paper reviews and comments upon the state-of-the art techniques for applying finite element methods. A consistent finite element method for random response problems and consideration of appropriate lumping techniques for modeling the modal force cross spectral matrix of the acoustic excitation is described by Olson (41). Jacobs and Lagerquist present a finite element analysis of panel response to turbulent boundary layers (42) and to complex random loads in general (43).

The use of numerical methods for estimating the response of complex structural configurations to random acoustic excitation is perhaps more of a research

tool than a recommended design technique if cost is considered. As a research tool, however, these methods can be utilized to establish the effect of parameter variations on structural response to acoustic excitation and, hence, develop prediction techniques suitable for design use. For example, the design method developed by Holehouse (44) for assessing the sonic fatigue resistance of diffusion bonded honeycomb panels utilized the finite element method to predict response frequencies and static stress response. Based upon Miles single degree-of-freedom analysis (see Equation (5.1.1-18)), these predicted results were used to correlate experimental data and to develop design charts (see Figures 5.3.4-5 and 5.3.4-6).

REFERENCES FOR SECTION 5.1

1. Thomson, W. T.; Vibration Theory and Applications, Prentice-Hall, Inc. Englewood Cliffs, N. J., 1965.

2. Bishop, R. E. D., and Johnson, D. C.; The Mechanics of Vibration, Cambridge University Press, 1960.

3. Hurty, W. C., and Rubinstein, M. F.; Dynamics of Structures, Prentice-Hall, Inc. Englewood Cliffs, N. J., 1964.

4. Nowacki, W.; Dynamics of Elastic Systems, John Wiley and Sons, Inc., New York, 1963.

5. Hay, J. A.; "Experimentally Determined Damping Factors,: Symposium on Acoustic Fatigue, AGARD-CP-113, Advisory Group for Aerospace Research and Development, North Atlantic Treaty Organization, Sept. 1972.

6. Mead, D. J.; "The Damping of Stiffened Plate Structures," Paper No. 26, Acoustical Fatigue in Aerospace Structures, Proceedings of the Second International Congress, Dayton, Ohio, April 29 - May 1, 1964.

7. Bert, C. W., "Material Damping: An Introductory Review of Mathematical Models, Measures and Experimental Techniques," Journal of Sound and Vibration, Vol. 29, No. 2, 1973, pp. 129-153.

8. Henderson, J. P.; "Vibration Analysis of Curved Skin-Stringer Structures Having Tuned Elastomeric Dampers," AFML-TR-72-240, Air Force Materials Laboratory, Wright-Patterson Air Force Base, Ohio, 1972.

9. Robson, J. D.; An Introduction to Random Vibration, Elsevier Publishing Company, New York, 1964.

10. Crandall, S. H., and Mark, W. D.; Random Vibration in Mechanical Systems, Academic Press, New York, 1963.

11. Bendat, J. S., and Piersol, A. G.; Measurement and Analysis of Random Data, John Wiley & Sons, Inc., New York, 1966.

12. Papoulis, A.; Probability, Random Variables, and Stochastic Processes, McGraw-Hill Book Company, New York, 1965.

13. Lin, Y. K.; Probabilistic Theory of Structural Dynamics, McGraw-Hill Book Co., New York, 1967.

14. Selby, S. M. (Ed.), Standard Mathematical Tables, 14th Edition, The Chemical Rubber Company, Cleveland, Ohio.

15. Miles, John W.; "On Structural Fatigue Under Random Loading," Journal of the Aeronautical Sciences, Vol. 21, No. 11, pp. 753-762, November 1954.

16. Miner, M. A.; "Cumulative Damage in Fatigue," Journal of Applied Mechanics, Vol. 12, No. 3, pp. 159 164, September 1945.

17. Palmgren, A.; "Die Lebensdauer von Kugellagern," Ver. Deut. Ingr., Vol. 68, pp. 339-341, 1924.

18. Belcher, P. M.; Van Dyke, J. D., Jr.; and Eshleman, A. L., Jr.; "Development of Aircraft Structure to Withstand Acoustic Loads," Aero/Space Engineering, pp. 24-30, June 1959.

19. McGowan, P. R.; "Structural Design for Acoustic Fatigue," ASD-TDR-63-820, Air Force Flight Dynamics Laboratory, United States Air Force, Wright-Patterson Air Force Base, Ohio, October 1963.

20. Wang, A. P.; "Random Spectrum and Structural Probability of Failure," Journal of Sound and Vibration, Vol. 17, No. 3, 1971, pp. 357-362.

21. Bernard, M. C., and Shipley, J. W.; "Fatigue Damage under Wide-Band Random Stress," Journal of Acoustical Society of America, Vol. 47, No. 1 (Part 2), 1970.

22. Clarkson, B. L.; "Stresses in Skin Panels Subjected to Random Acoustic Loading," The Aeronautical Journal of the Royal Aeronautical Society, Vol. 72, November 1968, pp. 1000-1010.

23. Bisplinghoff, R. L.; Ashley, H.; and Halfman, R. L.; Aeroelasticity, Addison-Wesley Publishing Company, Inc., 1955.

24. Carmichael, T. E.; "The Vibration of a Rectangular Plate with Edges Elastically Restrained against Rotation," Quarterly Journal of Mechanics and Mathematics, Vol. 12, Pt. 1, 1959. pp. 29-42.

25. Hildebrand, F. B.; Methods of Applied Mathematics, Prentice-Hall, Inc., Englewood Cliffs, N. J., 1960.

26. Morse, P. M., and Feshback, H.; Methods of Theoretical Physics, McGraw-Hill Book Co., 1953.

27. Langhaar, H. L.; Energy Methods in Applied Mechanics, John Wiley and Sons, Inc., 1962.

28. Lord Rayleigh; The Theory of Sound (1st Ed.), 1877, (2nd Ed.), 1894, Republished by Dover Publications, Inc., New York, 1945.

29. Leissa, A. W.; "Free Vibration of Rectangular Plates," Journal of Sound and Vibration, Vol. 31, No. 3, 1973. pp. 257-293.

30. Ritz, W.; Gesammelte Werke, Paris, 1911.

31. Prentis, J. M., and Leckie, F. A.; Mechanical Vibrations: An Introduction to Matrix Methods, Longmans, Green & Co. Ltd., London, 1963.

32. Pestel, E., and Leckie, F.; Matrix Methods in Elastomechanics, McGraw-Hill Publishing Company, New York, 1963.

33. Lin, Y. K.; "Response of Multi-Spanned Beam and Panel Systems under Noise and Excitation," AFML-TR-64-348, Part I, Air Force Materials Laboratory, Wright-Patterson Air Force Base, Ohio, 1965.

34. Lin, Y. K., and Donaldson, B. K.; "A Brief Survey of Transfer Matrix Techniques with Special Reference to the Analysis of Aircraft Panels," Journal of Sound and Vibration, Vol 10, No. 1, pp. 103-143, 1969.

35. McDaniel, T. J.; "Dynamics of Stiffened Cylindrical Shells with Spatially Varying Curvature," AFML-TR-72-134, Air Force Materials Laboratory, Wright-Patterson Air Force Base, Ohio, 1972.

36. Henderson, J. P.; "Vibration Analysis of Curved Skin-Stringer Structures Housing Tuned Elastomeric Dampers," AFML-TR-72-240, Air Force Materials Laboratory, Wright-Patterson Air Force Base, Ohio, 1972.

37. Przemieniecki, J. S.; Theory of Matrix Structural Analysis, McGraw-Hill Book Company, New York, 1968.

38. Zienkiewicz, O. C.; Finite Element Procedures in the Solution of Plate and Shell Problems, John Wiley & Sons, Inc., New York, 1965.

39. Butler, T. G., and Michel, D.; "NASTRAN, Summary of the Functions and Capabilities of the NASA Structural Analysis Computer System," NASA-SP-260, National Aeronautics and Space Administration, Washington, D. C., 1971.

40. Lindberg, G. M.; "Accurate Finite Element Modeling of Flat and Curved Stiffened Panels," Paper No. 6, AGARD-CP-113, Symposium on Acoustic Fatigue, Advisory Group for Aerospace Research and Development, North Atlantic Treaty Organization, Sept. 1972.

41. Olson, M. D.; "A Consistent Finite Element Method for Random Response Problems," Computers & Structures, Vol. 2, Pergamon Press, 1972, pp. 163-180.

42. Jacobs, L. D., and Lagerquist, D. R.; "A Finite Element Analysis of Simple Panel Response to Turbulent Boundary Layers," AFFDL-TR-67-81, Air Force Flight Dynamics Laboratory, Wright-Patterson Air Force Base, Ohio, 1967.

43. Jacobs, L. D., and Lagerquist, D. R.; "Finite Element Analysis of Complex Panel Response to Random Loads," AFFDL-TR-68-44, Air Force Flight Dynamics Laboratory, Wright-Patterson Air Force Base, Ohio, 1968.

44. Holehouse, I.; "Sonic Fatigue of Diffusion-Bonded Titanium Sandwich Structure," Paper 15, AGARD-CP-113, Symposium on Acoustic Fatigue, Advisory Group for Aerospace Research and Development, North Atlantic Treaty Organization, September 1972.

5.2 SIMPLE STRUCTURES

All sonic fatigue design methods are based upon the consideration of the dynamic response characteristics of simple structural elements such as plates and shells. The object of including these topics in this report is to provide a source of useful data to the designer when he is faced with either very preliminary calculations or extrapolation of detail design data that cannot be represented by the structural configurations or environmental factors discussed in Section 5.3.

5.2.1 CLASSIFICATION OF SIMPLE STRUCTURES

Aircraft structure is almost universally modeled as either a plate or a shell with various complicating details defining the specific structural configuration. This section is divided into two subsections. Section 5.2.2 presents a discussion of the vibration and response of plates to acoustic excitation. Complicating effects, as related to plate vibration, are discussed such as inplane loading, elastic edge restraint, etc. Some of these results may be new to the designer and, hopefully, the presentation will allow the designer a broad basis for approaching sonic fatigue design problems.

Section 5.2.3 presents a discussion of the vibration of circular cylindrical shells with emphasis being placed on simplified results. The discussion on moderately deep circular cylindrical shells will hopefully prevent the designer from improperly using the results based upon shallow shell theory. For a more complete discussion of any specific topic, the reader is advised to study the references

When applying the results of Section 5.2, the designer may require data based upon beam theory. Appendix B has been included in the report to fulfill this requirement.

5.2.2 VIBRATION OF PLATES

The topic of plate vibration has received much attention in the literature. Recently, Leissa (1) completed a compendium on the topic of free plate vibration that exceeds the limited scope of this report. Leissa's objectives were to provide a comprehensive set of available results for the frequencies and mode shapes of free vibration of plates for the design or development engineer and to provide a summary of all known results for the researcher in the field of plate vibrations. As a result, Leissa presents a very thorough and well-organized set of useful design oriented results for all shapes of plates with various boundary conditions.

The objective of this section of this report has been to consider only those cases of plate geometry and boundary conditions that are encountered frequently in aircraft design. As a result, most attention is given to rectangular plates. Consideration of plate vibration is important first because available design techniques, such as presented in Section 5.3 for specific structural configurations, may not coincide with the design engineer's specific problem, and secondly, most of the design methods used in practice are developed using results presented in this section. That is, flat stiffened skin structure is usually idealized as an array of individual plates experiencing some (usually unknown) degree of edge restraint. This section presents results suitable for design use rather than lengthy deviations with the final result being techniques for estimating structural response.

Except for the technique for estimating buckled plate response, small deflection plate theory is used. Estimates of the response frequencies are obtained with the Rayleigh method (Leissa (2) presents an excellent discussion of the accuracy of the Rayleigh-Ritz method as applied to frequency estimates). Stress response is obtained using tabulated data presented by Timoshenko (3). The discussion of response of plates to random acoustic excitation follows the work of Clarkson (4).

5.2.2.1 Notation

A	Surface area
$A(\xi)$	Amplitude function, Eqn. (5.2.2-18) and Table 5.3.2-4
A_o	Plate response amplitude due to uniform static pressure
a	Length of plate in x-direction (short dimension)
$B(\xi)$	Amplitude function, Eqn. (5.2.2-18) and Table 5.3.2-4
b	Length of plate in y-direction (long dimension)
C_m, C_n	Constants defined in Table 5.2.2-1
$C_1^*, C_2^*, ..$	Defined by Eqn. (5.2.2-22)

D	$Eh^3/12(1-\nu^2)$, bending rigidity of isotropic plate
$D_1, D_2, \ldots$	Bending rigidities of an orthotropic plate See Fig. 5.2.2-27 and Eqn. (5.2.2-83)
$d(F)$	Narrow band space correlation coefficient, Eqn. (5.2.2-36)
E	Young's modulus for an isotropic material
E_{11}, E_{22}	Young's modulus for an orthotropic material
f_{mn}	Frequency of vibration of $(m,n)^{th}$ mode, Hz.
f_o	Fundamental mode frequency at ambient temperature
G	Shear modulus of an isotropic material
G_{12}	Shear modulus of an orthotropic material
$G_p(f)$	Spectral density function of acoustic excitation
$H(\omega)$	Frequency response function
h	Thickness of plate
I	Second area moment of inertia of a stiffener
J	St. Venant's torsion constant
K, K_o	Factors used in various developments, see specific use in each section
$L(\ )$	Linear stress operation, Eqn. (5.2.2-68)
$M_{11}, M_{12}, \ldots$	Bending moments for orthotropic plates, Eqn. (5.2.2-86)
N_x, N_y	Inplane loading stress resultants for x and y directions, respectively
n	Mode number for y-direction
R	Function definint plate response, see specific use in each section
r	T/T_c
S_{1mn}, S_{2mn}	Defined by Eqn. (5.2.2-72)
T	Uniform temperature rise of plate above ambient

T_c	Critical on buckling temperature of plate
u,v,w	Displacement components of plate in x,y,z directions
$X(x),Y(y)$	Assumed modes for approximate plate vibration analysis
x,y,z	Coordinate directions, Fig. 5.2.2-1
α	Coefficient of linear expansion
α_r	Eigenvalues of the r^{th} beam mode
γ	Weight per unit volume
ζ	Viscous damping ratio
ν	Poisson's ratio for an isotropic material
ν_{12},ν_{21}	Poisson's ratio for an orthotropic material
ξ	Dimensionless parameter describing elastic rotational edge restraint of plate
π	Constant = 3.14159
ρ	Mass per unit volume
σ	Bending or membrane stress (subscripts used to specialize notation)
τ	Shear stress (subscripts used to specialize notation)
$\phi(\zeta)$	Function of elastic rotational edge restraint parameter (See Table 5.2.2-4)
$\Omega_{rs}(\omega)$	Function defining coupling between structural response modes and acoustic excitation
ω	Frequency, radians/sec.

5.2.2.2 Rectangular Isotropic Plates

This section provides design oriented methods for estimating the response of rectangular isotropic plates to random acoustic loading. Section 5.2.2.2.1 provides design equations and nomographs for estimating the natural frequencies of rectangular isotropic plates with either all edges clamped or all edges simply supported. Section 5.1.2.2.2 provides design equations for estimating the effect of inplane loading on the frequency response of a rectangular plate. For the case of plates stressed as a result of a temperature increase, design equations are presented in Section 5.2.2.2.3 for estimating both frequency response and thermal stresses for the buckled plate. Section 5.2.2.2.4 presents design techniques for estimating the fundamental mode response frequency and static stress response of plates subjected to elastic edge restraint. Two cases are considered: either elastic rotational restraint with no translation allowed or elastic translational restraint with no rotation allowed. Section 5.2.2.2.5 presents simple design techniques for estimating static stress response of rectangular plates subjected to a uniform static pressure of unit magnitude. Finally, Section 5.2.2.2.6 presents the derivation of plate response to random acoustic excitation. Particular emphasis is placed upon describing the physical situations for which the general equations can be simplified to obtain design-oriented results. Miles' single degree-of-freedom theory (5) is a special result.

Each section contains example problems illustrating the use of the methods described. Using these results and, in particular, the development presented in Section 5.2.2.2.6, it is possible for the designer to obtain estimates for the stress response of a plate structure that does not conform to the configurations presented in Section 5.3.

5.2.2.2.1 Estimation of Natural Frequencies

This section presents design equations and nomographs for estimating the natural frequencies of initially unstressed rectangular plates of isotropic material such as usually encountered in aircraft practice. The restriction on isotropic material implies that the material elastic characteristics are not dependent upon orientation with respect to the general structural axis system (plate boundary). See Figure 5.2.2.1.

Derivation: The Rayleigh Method for estimating the response frequency of an uncoupled mode of vibration of an isotropic plate is used. Results are presented for plates with all edges either simply supported or clamped. The results for a plate with all edges simply supported is exact and yields a lower bound for the frequency estimate. The result for a plate with all edges clamped is obtained by assuming a panel mode shape in the form of clamped-clamped beam modes and yields an upper bound for the frequency estimate. These analytical results have proven in practice to yield acceptable bounds for the response frequencies of plates encountered in practice. Results for other boundary conditions are presented by Warburton (6).

The results presented here comprise design equations and nomographs. The general design equations are presented. Then, assuming a value of $E^*/\gamma = 11.26 \cdot 10^6, (E^* = E/(1-\nu^2))$ the design equations are specialized and nomographs based upon the specialized design equations are presented. The value for E^*/γ is representative of metallic aircraft materials with the resulting error in the frequency estimate being less than 3%.

Design Equations: The design equations for the $(m,n)^{th}$ mode of vibration of the plate are as follows:

All Edges Simply Supported

$$f_{mn}^2 = \frac{\pi^2 D}{4\rho h}\left[(m/a)^2 + (n/b)^2\right]^2 \quad Hz^2 \qquad (5.2.2\text{-}1)$$

All Edges Clamped

$$f_{mn}^2 = \frac{D}{4\pi^2\rho h}\left[(C_m/a)^4 + (C_n/b)^4 + 2A_{mn}/a^2b^2\right] \quad Hz^2 \qquad (5.2.2\text{-}2)$$

$$A_{mn} = \alpha_m C_m \alpha_n C_n \left(4 - 2\alpha_m C_m - 2\alpha_n C_n + \alpha_m C_m \alpha_n C_n\right)$$

where the constants α_m, C_m, etc. are defined in Table 5.2.2-1.

TABLE 5.2.2-1
VALUES OF α_m AND C_m FOR EQUATION (5.2.2-2)

m	α_m	C_m
1	0.982,502,22	4.730,040,8
2	1.000,777,31	7.853,204,6
3	0.999,966,45	10.995,607,8
4	1.000,001,45	14.137,165,5
5	0.999,999,93	17.278,759,6

Nomographs: The design equations presented above were used to prepare nomographs for the first nine modes of a flat rectangular panel. These nomographs are based upon specializing the design equations for a typical value of material properties such that $E^*/\gamma = 11.26 \cdot 10^6$.

The resulting specialized design equations and nomographs are presented in Figures 5.2.2-2 through -10. Boundary conditions are presented on the panel aspect ratio lines b, indicating clamped edges by a solid line and simply supported edges by a dashed line. Hence, from each nomograph one can determine both the clamped edge and supported edge response frequency for a given panel mode.

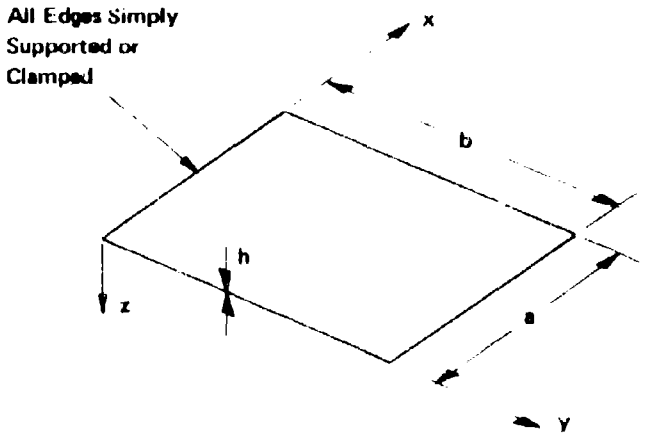

(a) Rectangular Plate Geometry

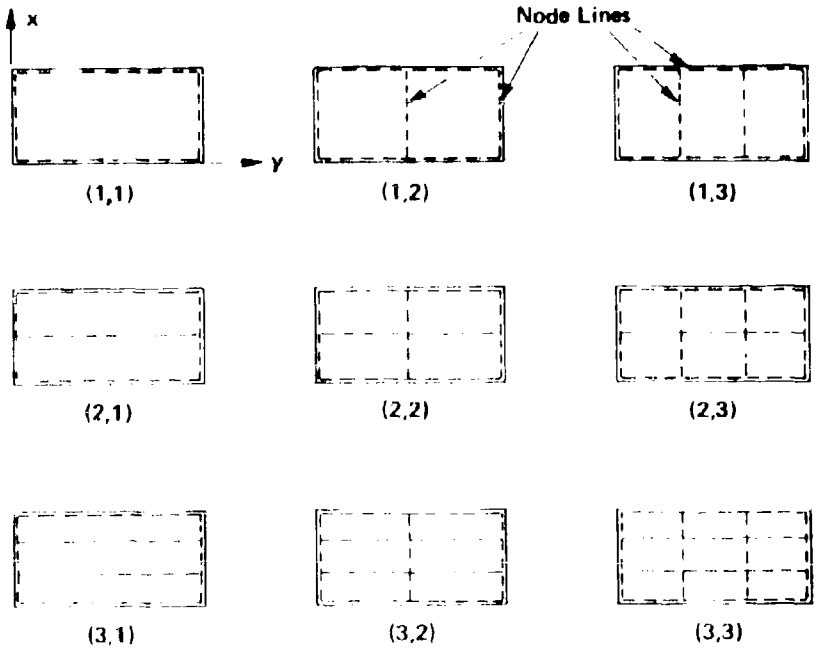

(b) Rectangular Plate Mode Nomenclature (m,n)

FIGURE 5.2.2-1 RECTANGULAR PLATE GEOMETRY AND VIBRATION MODE NOMENCLATURE

Design Equations

Supported Edges $f_{11} = 9.452 \cdot 10^4 h(1/a^2 + 1/b^2)$

Clamped Edges $f_{11} = 1.178 \cdot 10^5 h\sqrt{(3.307/a^4 + 3.307/b^4 + 2/a^2b^2)}$

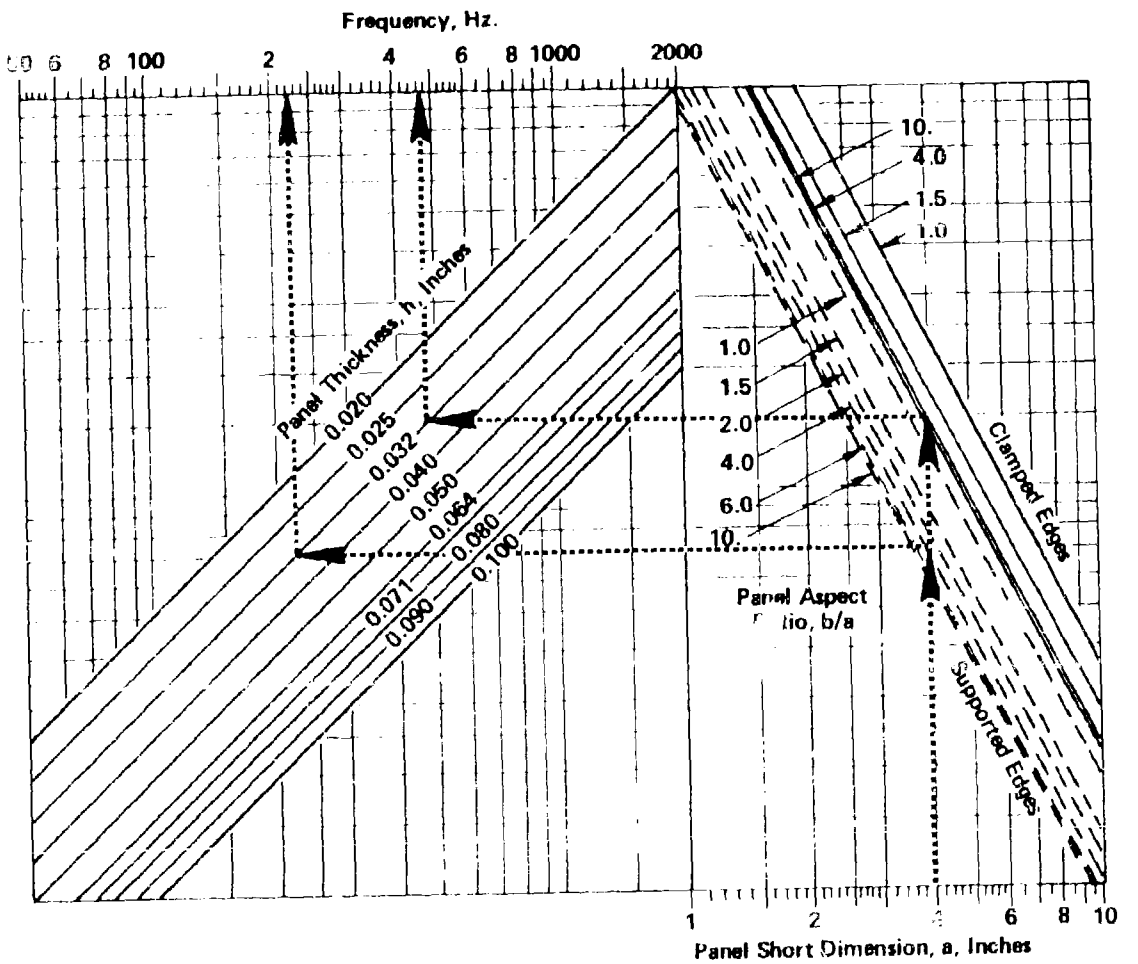

FIGURE 5.2.2-2 NOMOGRAPH FOR CALCULATING FUNDAMENTAL MODE RESPONSE FREQUENCY

Design Equations

Supported Edges $f_{12} = 9.452 \cdot 10^4 h(1/a^2 + 4/b^2)$

Clamped Edges $f_{12} = 2.280 \cdot 10^5 h\sqrt{(0.884/a^4 + 6.714/b^4 + 2/a^2b^2)}$

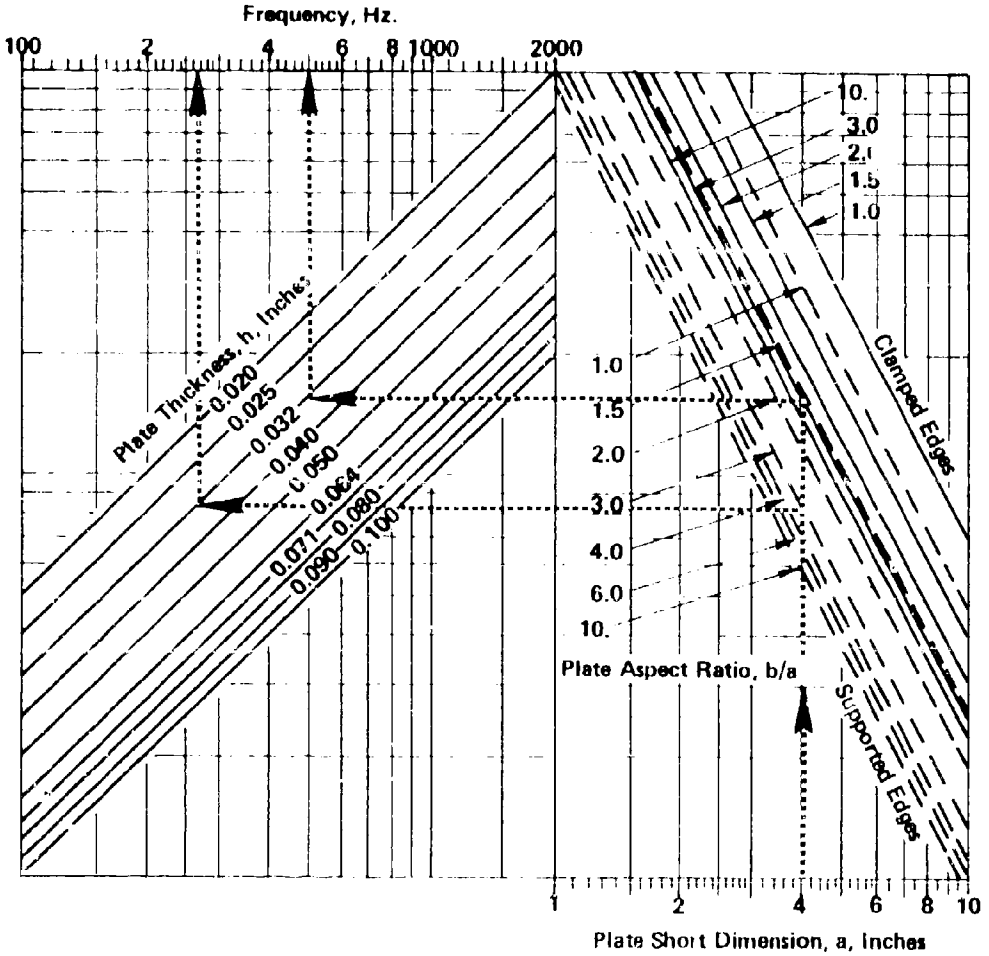

FIGURE 5.2.2-3 NOMOGRAPH FOR CALCULATING (1,2) MODE RESPONSE FREQUENCY

Design Equations

Supported Edges $f_{13} = 9.452 \cdot 10^4 h(1/a^2 + 9/b^2)$

Clamped Edges $f_{13} = 3.341 \cdot 10^5 h\sqrt{(0.411/a^4 + 12.01/b^4 + 2/a^2b^2)}$

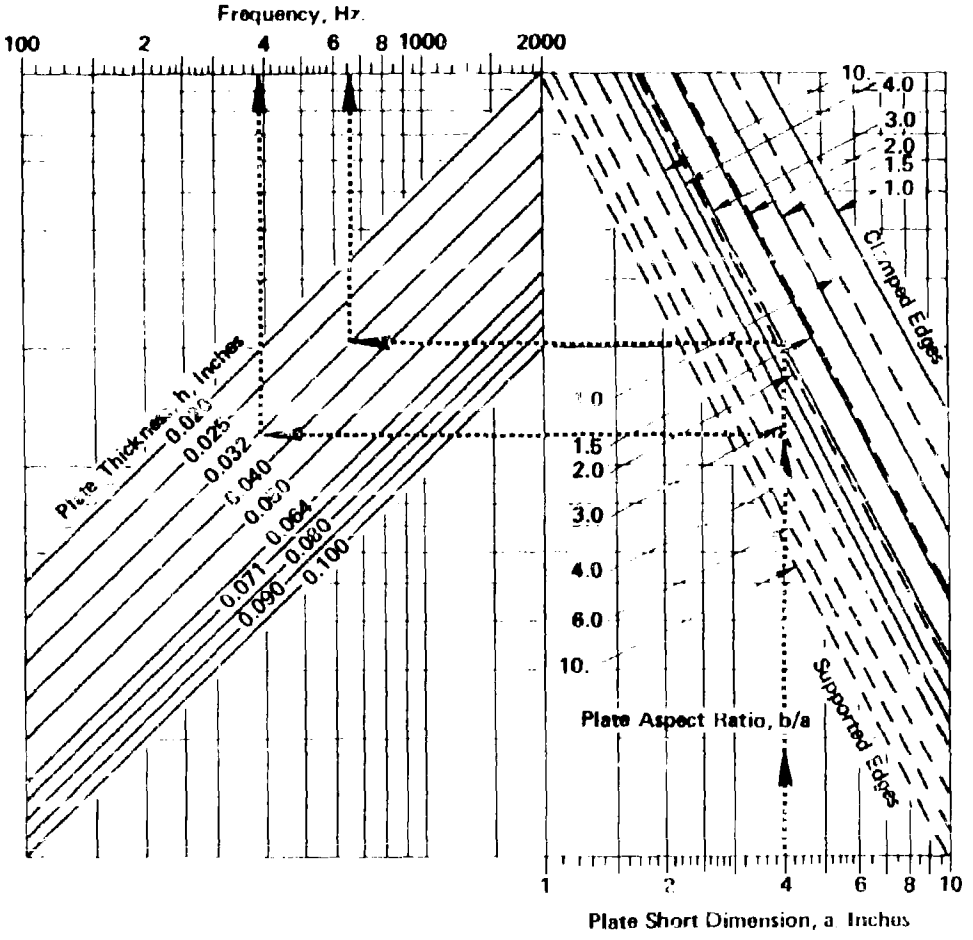

FIGURE 5.2.2-4 NOMOGRAPH FOR CALCULATING (1,3) MODE RESPONSE FREQUENCY

Design Equations

Supported Edges $f_{21} = 9.452 \cdot 10^4 h(4/a^2 + 1/b^2)$

Clamped Edges $f_{21} = 2.280 \cdot 10^5 h\sqrt{(6.714/a^4 + 0.884/b^4 + 2/a^2b^2)}$

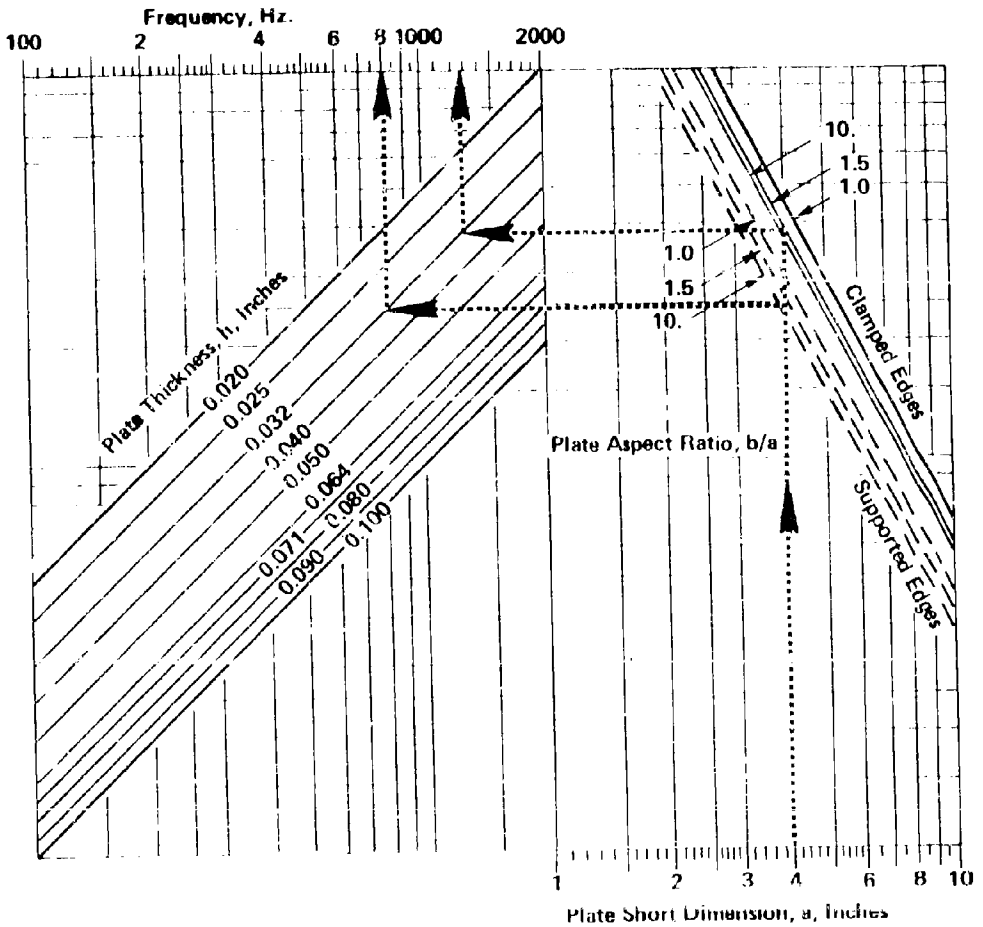

FIGURE 5.2.2-5 NOMOGRAPH FOR CALCULATING (2,1) MODE RESPONSE FREQUENCY

Design Equations

Supported Edges $f_{22} = 9.452 \cdot 10^{4} h(4/a^2 + 4/b^2)$

Clamped Edges $f_{22} = 4.410 \cdot 10^{5} h/(1.794/a^4 + 1.794/b^4 + 2/a^2 b^2)$

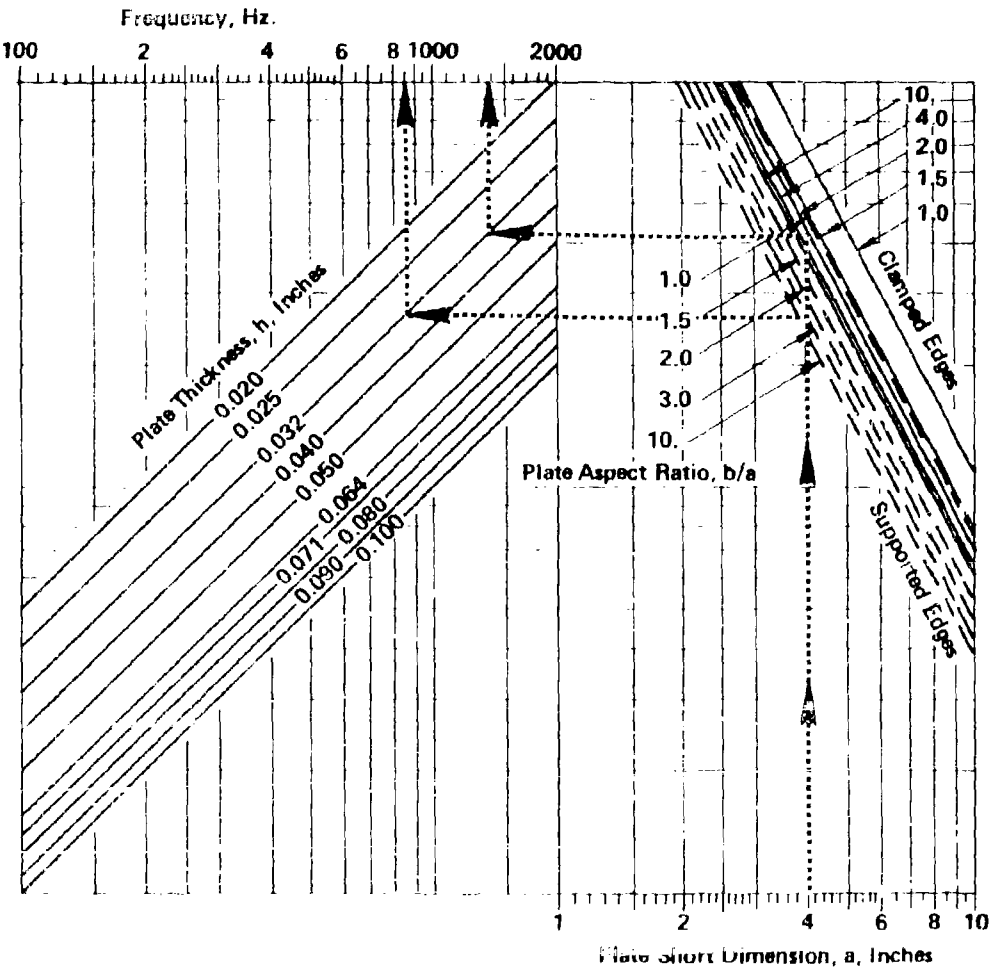

FIGURE 5.2.2-6 NOMOGRAPH FOR CALCULATING (2,2) MODE RESPONSE FREQUENCY

Design Equations

Supported Edges $f_{23} = 9.452 \cdot 10^4 h(4/a^2 + 9/b^2)$

Clamped Edges $f_{23} = 6.463 \cdot 10^5 h\sqrt{(0.835/a^4 + 3.209/b^4 + 2/a^2b^2)}$

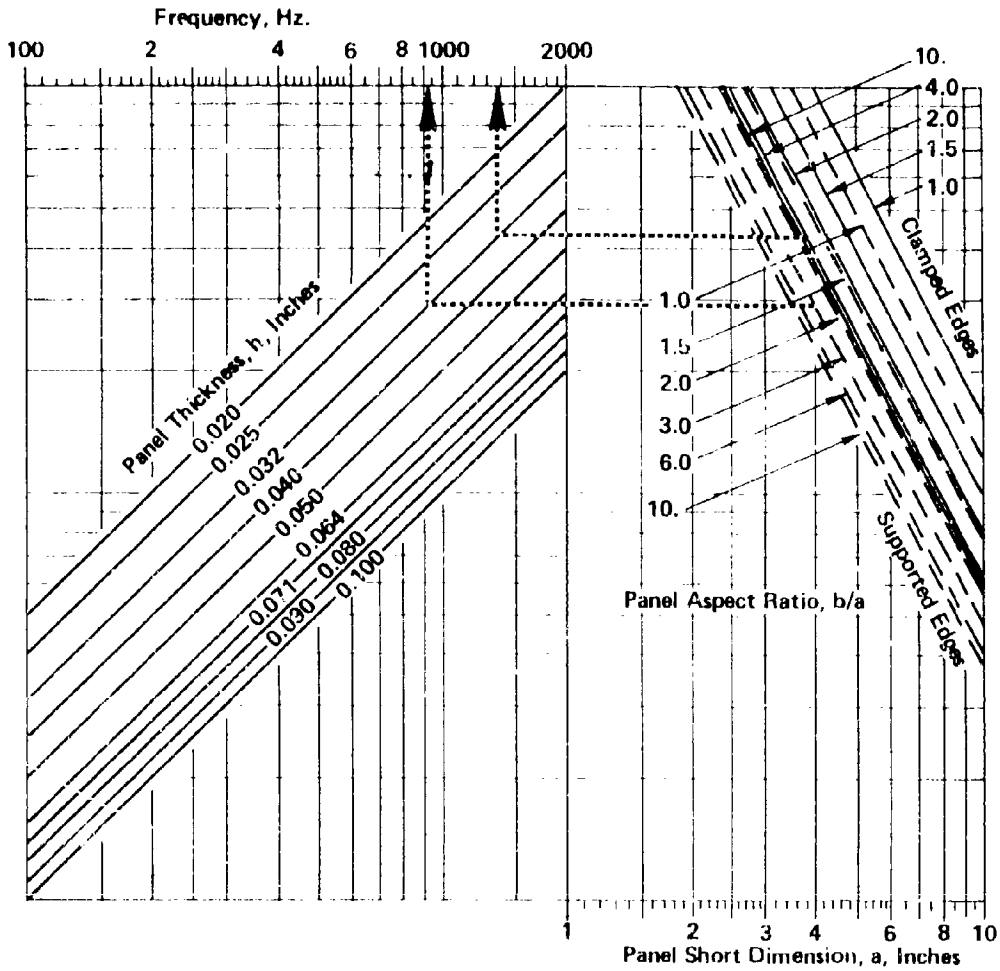

FIGURE 5.2.2-7 NOMOGRAPH FOR CALCULATING (2,3) MODE RESPONSE FREQUENCY

Design Equations

Supported Edges $f_{31} = 9.452 \cdot 10^{4} h(9/a^2 + 1/b^2)$

Clamped Edges $f_{31} = 3.341 \cdot 10^{5} h\sqrt{(1 .01/a^4 + 0.411/b^4 + 2/a^2b^2)}$

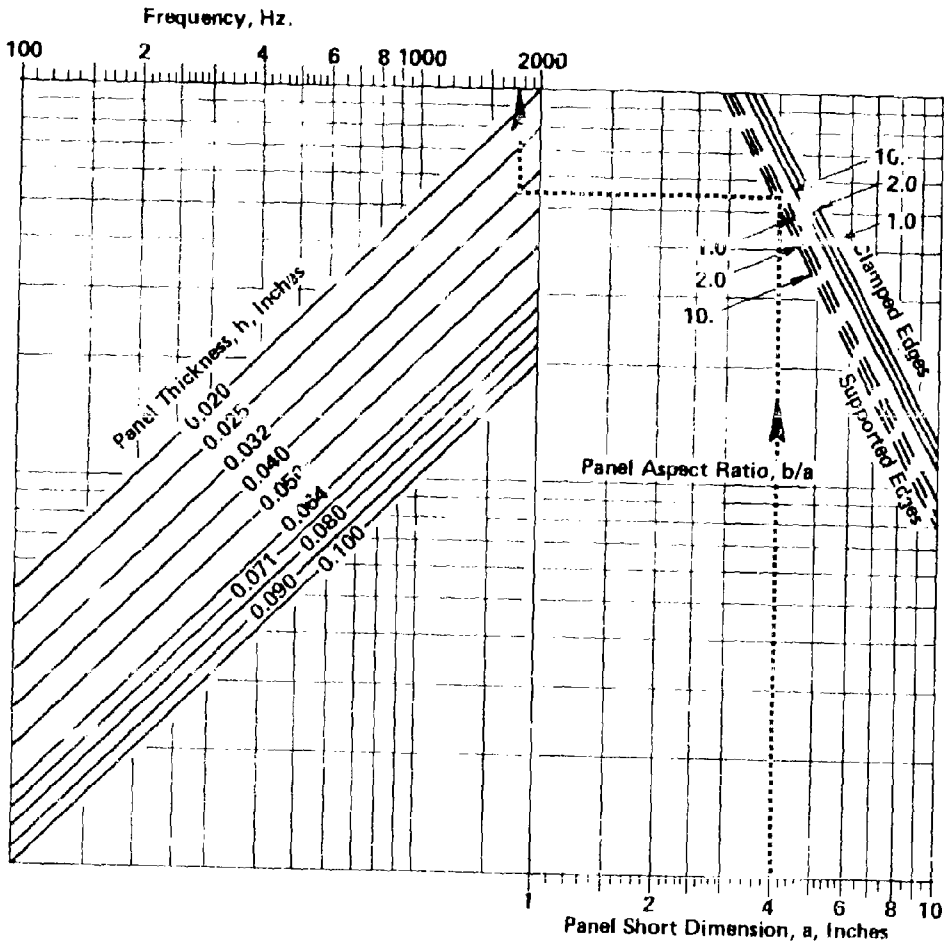

FIGURE 5.2.2-8 NOMOGRAPH FOR CALCULATING (3,1) MODE RESPONSE FREQUENCY

Design Equations

Supported Edges $f_{32} = 9.452 \cdot 10^4 h(9/a^2 + 4/b^2)$

Clamped Edges $f_{32} = 6.463 \cdot 10^5 h\sqrt{(3.209/a^4 + 0.835/b^4 + 2/a^2b^2)}$

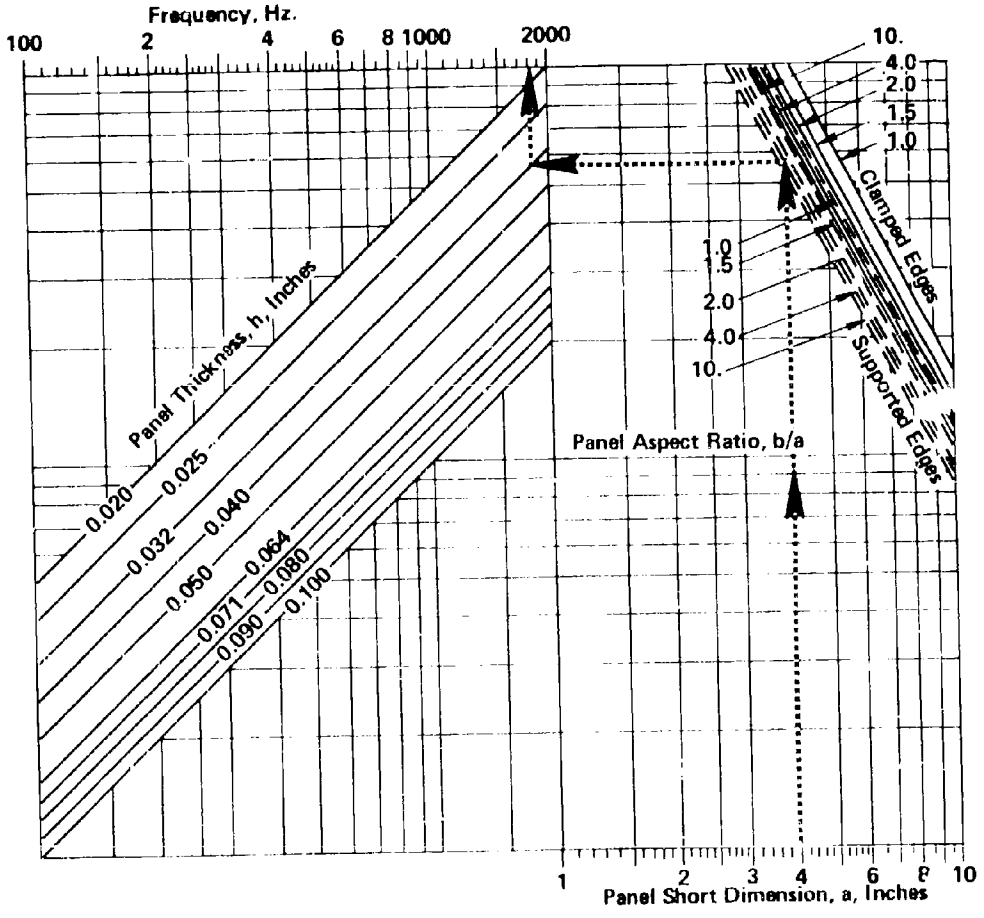

FIGURE 5.2.2-9 NOMOGRAPH FOR CALCULATING (3,2) MODE RESPONSE FREQUENCY

Design Equations

Supported Edges $f_{33} = 9.462 \cdot 10^4 h(9/a^2 + 9/b^2)$

Clamped Edges $f_{33} = 9.472 \cdot 10^5 h\sqrt{(1.494/a^4 + 1.494/b^4 + 2/a^2b^2)}$

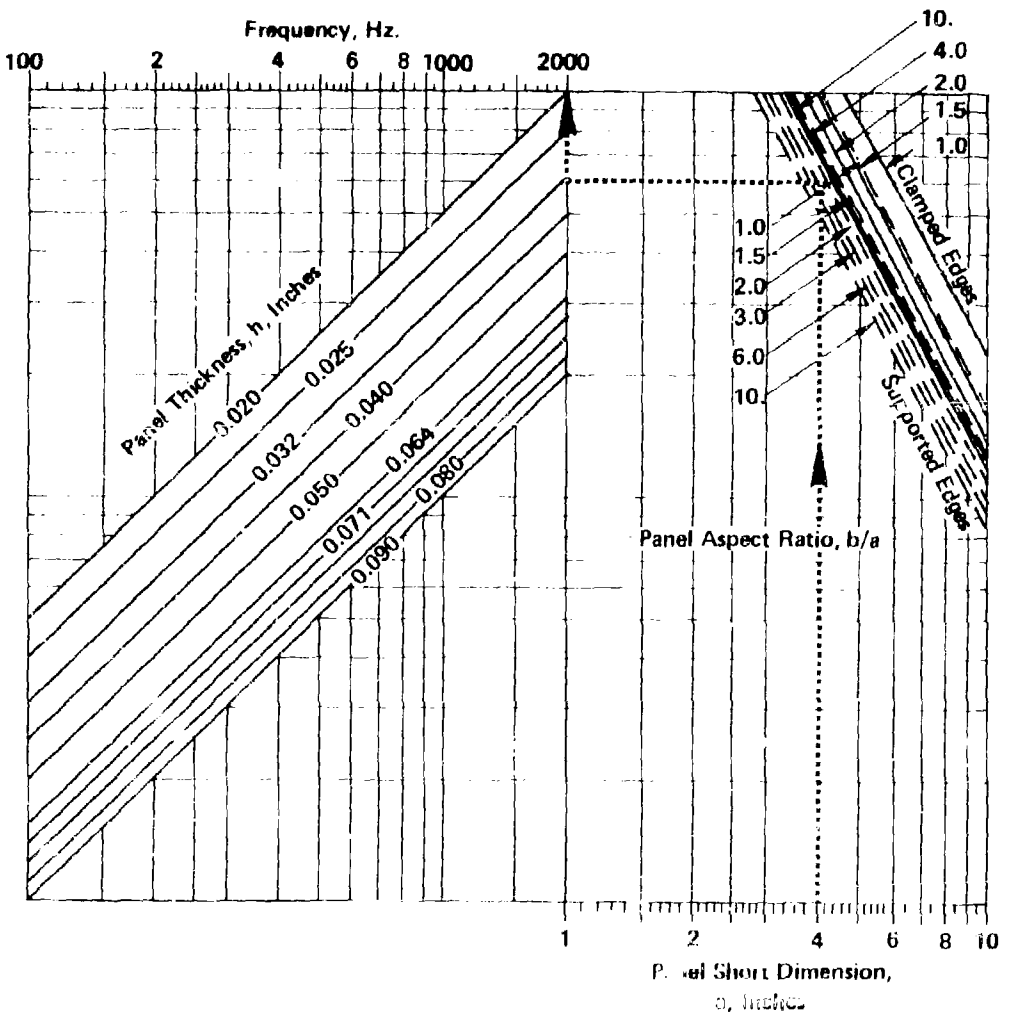

FIGURE 5.2.2-10 NOMOGRAPH FOR CALCULATING (3,3) MODE RESPONSE FREQUENCY

Example: It is anticipated that a panel structure with dimensions a = 4.0 inches, b = 12.0 inches and h = 0.032 inches will experience significant acoustic excitation in the frequency range from 200 Hz to 1000 Hz. Determine the response frequencies of the panel assuming both simply supported and clamped edges using both the design nomographs and the design equations.

From the design nomographs, Figures 5.2.2-2 through 5.2.2-10, the response frequencies are easily determined as follows: beginning at the bottom right hand edge enter the chart for the value of the plate short dimension, a, and proceed vertically until the aspect ratio line, b/a, is encountered for either supported edges and/or clamped edges; proceed horizontally to the left until the plate thickness line is encountered; and then proceed vertically to read the plate response frequency for the mode at the upper left hand edge of the chart.

At the top of each design chart, the design equation upon which the graphical construction is based is presented. Note: It is assumed that $E^*/\gamma = 11.26 \cdot 10^6$ for these charts and equations.

The results for this example are presented below with both the nomograph results and the design equation results indicated.

	Simply Supported Edges		Clamped Edges	
Mode	Design Eqn.	Nomograph	Design Eqn.	Nomograph
(1,1)	210 Hz.	225 Hz.	445 Hz.	465 Hz.
(1,2)	273 Hz.	265 Hz.	497 Hz.	495 Hz.
(1,3)	378 Hz.	385 Hz.	591 Hz.	600 Hz.
(2,1)	777 Hz.	795 Hz.	1221 Hz.	1250 Hz.
(2,2)	840 Hz.	860 Hz.	1259 Hz.	1380 Hz.
(2,3)	945 Hz.	930 Hz.	1354 Hz.	1380 Hz.
(3,1)	1722 Hz.	1760 Hz.	2337 Hz.	-
(3,2)	1785 Hz.	1820 Hz	2398 Hz.	-
(3,3)	1890 Hz.	1940 Hz.	2495 Hz.	-

5.2.2.2.2 Effect of Inplane Loading

This section presents design equations for estimating the effect on response frequencies of rectangular isotropic plates subjected to inplane loading. The literature (1) has presented design oriented results only for the case of simply supported edges and zero inplane shear loading for plates with general aspect ratios. The results presented here apply only to plates subjected to inplane tensile loading in the range of linear material response and to inplane compressive loading below the buckling load for the plate. The plate geometry and inplane loading nomenclature is presented in Figure 5.2.2-11.

Derivation: The Rayleigh method for estimating the response frequency of an uncoupled mode of vibration of an isotropic plate subjected to inplane loading is used as described by Leissa (1, pp. 176-177). The general results of this section are for design guidance only. The effect of including inplane shear loading is discussed by Dickinson (7).

Design Equations: The design equation for the $(m,n)^{th}$ mode of vibration of a rectangular plate with all edges simply supported and subjected to inplane loading as indicated in Figure 5.2.2-11 is expressed

$$f_{mn}^2 = \frac{\pi^2 D}{4\rho h a^2 b^2} \times [(m^2(b/a) + n^2(a/b)]^2 + m^2 N_x/4\rho h a^2 + n^2 N_y/4\rho h b^2 \quad Hz.^2 \qquad (5.2.2\text{-}3)$$

Examination of this result indicates that tensile loading (positive N_x and N_y) increases the response frequency and that compressive inplane loading decreases the frequency. Combinations of compressive loading N_x and N_y that cause the frequency expression to vanish define the buckling configuration of the plate. For compressive loading N_x and N_y, it does not necessarily follow that the lowest frequency mode occurs for the mode numbers $(m,n) = (1,1)$. The result given in Equation (5.2.2-3) applies to plates subjected to tensile loads and plates subjected to compressive loads below the buckling load.

Buckling loads for singly acting loading are as follows:

for $N_y = 0$

$$(N_x)_{cr} = -\frac{\pi^2 D}{m^2 b^2}[m^2(b/a) + n^2(a/b)]^2 \quad lbs/in \qquad (5.2.2\text{-}4)$$

for $N_x = 0$

$$(N_y)_{cr} = -\frac{\pi^2 D}{n^2 a^2}[m^2(b/a) + n^2(a/b)]^2 \quad lbs/in \qquad (5.2.2\text{-}5)$$

Example: For the special case of $N_x = 0$, determine the fundamental mode response frequency of a rectangular simply supported plate as a function of the inplane loading, N_y, and the plate aspect ratio, b/a.

Beginning with Equation (5.2.2-3), setting $N_x = 0$, and nondimensionalizing the frequency by the frequency of a square unloaded simply supported plate, $f_o^2 = \pi^2 D/\rho a^2 b^2$, the result is

$$f_{mn}^2/f_o^2 = \frac{1}{4}\left[m^2(b/a)^2 + n^2(a/b)^2(1 - N_y/(N_{ycr})\right] \qquad (5.2.2\text{-}6)$$

where Equation (5.2.2-5) has been used to simplify the results.

From Equation (5.2.2-6) values of $(f_{mn}/f_o)^2/(1-N_y/(N_{ycr}))$ are calculated. From Equation (5.2.2-5) values of $a^2(N_y)_{cr}/\pi^2 D$ are calculated and normalized to the value of this parameter for b/a = 1.0 and (m,n) = (1,1) (the normalization constant is 4.0). These results are presented in Tables 5.2.2-2 and 5.2.2-3 and are plotted in Figure 5.2.2-12. This figure indicates that near the buckling load for a given plate aspect ratio that the lowest frequency mode is not necessarily the (1,1) mode. This result was originally developed by Herrmann (8).

TABLE 5.2.2-2

VALUES OF $(f_{mn}/f_o)^2/(1-N_y/(N_{ycr}))$

(m,n)	b/a	1.0	2.0	3.0	4.0	5.0
(1,1)		1.00	1.56	2.78	4.52	6.76
(1,2)		6.25	4.00	4.70	6.25	8.41
(1,3)		25.00	10.56	9.00	9.77	11.56
(1,4)		72.25	25.00	17.36	16.00	17.81
(1,5)		169.00	52.56	32.11	26.27	25.00

TABLE 5.2.2-3

NORMALIZED* VALUES OF $a^2(N_y)_{cr}/\pi^2 D$

(m,n)	b/a	1.0	2.0	3.0	4.0	5.0
(1,1)		1.000	1.563	2.778	4.515	6.760
(1,2)		1.563	1.000	1.175	1.563	2.100
(1,3)		2.778	1.175	1.000	1.085	1.285
(1,4)		4.515	1.563	1.085	1.000	1.050
(1,5)		6.760	2.100	1.285	1.050	1.000

*Normalized to $a^2(N_y)_{cr}/\pi^2 D$ for b/a = 1.0 and (m,n) = (1,1)

5.2.2.2.3 Effect of Elevated Temperature

This section presents design equations for estimating the (1,1) mode response frequency and thermal stress distributions for rectangular plates with both simply supported and clamped edges subjected to a uniform temperature increase. The analytical results presented here have provided guidance for developing empirical sonic fatigue design data as described in Section 5.3.1. The basic approach used was originally developed by Shulman (9) with details of this analysis presented by Rudder (10). The plate geometry and thermal (inplane) loading nomenclature is presented in Figure 5.2.2-11.

Derivation: The analysis utilizes the Rayleigh method and small deflection plate theory for the temperature range below the plate buckling temperature, T_c. For the plate buckled vibration response, large deflection von Karman (11) plate theory is utilized with Marguerre's (12) method to estimate the response. All temperature increases are taken relative to a "room temperature" at which the plate is subjected to zero inplane thermal stresses.

Pre-Buckled Response: For small displacement plate theory, the mean stresses are defined in terms of the temperature increase, T, as

$$\bar{\sigma}_x = \bar{\sigma}_y = -E\alpha T/(1-\nu) \qquad (5.2.2-7)$$

For simply supported edges, the frequency of the fundamental mode is for $T \leq T_c$

$$f_{11}^2 = \frac{\pi^2 D}{4\rho h a^2 b^2}(b/a + a/b)^2(1-T/T_c) \quad Hz.^2 \qquad (5.2.2-8a)$$

where
$$T_c = \frac{\pi^2 h^2 (b/a + a/b)}{12\alpha ab(1+\nu)} \quad {}^oF \qquad (5.2.2-8b)$$

For clamped edges, the frequency of the fundamental mode* is for $T \leq T_c$

$$f_{11}^2 = \frac{4\pi^2 D}{9\rho h a^2 b^2}(3(b/a)^2 + 3(a/b)^2 + 2)(1-T/T_c) \quad Hz.^2 \qquad (5.2.2-9a)$$

where
$$T_c = \frac{\pi^2 h^2}{9\alpha ab(1+\nu)(b/a + a/b)}\sqrt{(3(b/a)^2 + 3(a/b)^2 + 2)} \quad {}^oF \qquad (5.2.2-9b)$$

Post-Buckled Response: For the buckled plate response, it is assumed that the total plate amplitude comprises a static buckled amplitude, W_o, and a dynamic amplitude that is small compared to W_o. For the buckled plate, the static inplane loading will not be uniform along the panel edges but will vary with position along the plate edge (see Example 2, this section).

*An assumed mode of the form $\frac{1}{\gamma_i}(1-\cos(\frac{2\pi x}{a}))(1-\cos(\frac{2\pi y}{b}))W$ is used.

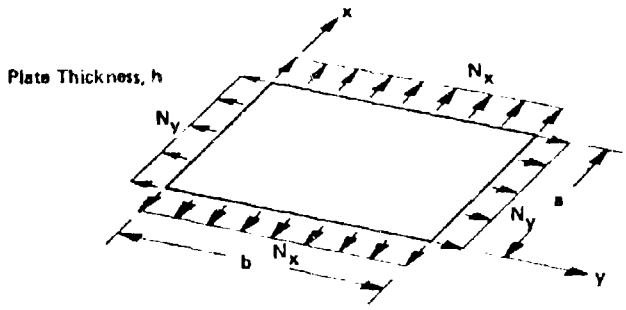

FIGURE 5.2.2-11 RECTANGULAR PLATE GEOMETRY AND INPLANE LOADING NOMENCLATURE

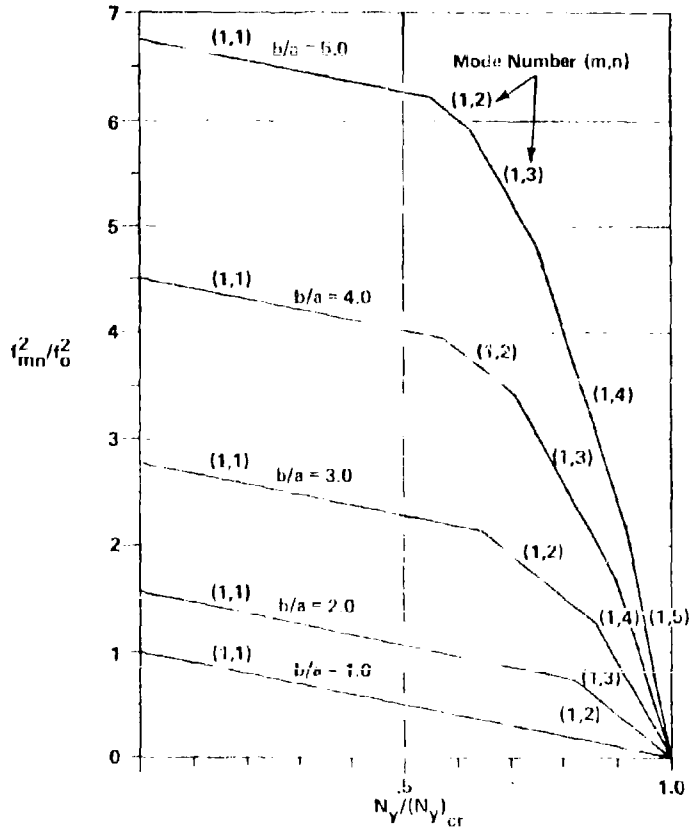

FIGURE 5.2.2-12 VARIATION OF RESPONSE FREQUENCY WITH COMPRESSIVE INPLANE LOADING

for simply supported edges, the membrane stresses are for total inplane edge restraint (inplane displacements vanish) of the plate

$$\sigma_x = \bar{\sigma}_x - \frac{\pi^2 E}{8a^2} \cos\left(\frac{2\pi y}{b}\right) W_o^2 \quad \text{psi} \qquad (5.2.2\text{-}10a)$$

$$\sigma_y = \bar{\sigma}_y - \frac{\pi^2 E}{8b^2} \cos\left(\frac{2\pi x}{a}\right) W_o^2 \quad \text{psi} \qquad (5.2.2\text{-}10b)$$

the mean thermal stresses are

$$\bar{\sigma}_x = -\frac{E\alpha T}{(1-\nu)} + \frac{\pi^2 E}{8ab(1-\nu^2)} (b/a + \nu a/b) W_o^2 \quad \text{psi} \qquad (5.2.2\text{-}10c)$$

$$\bar{\sigma}_y = -\frac{E\alpha T}{(1-\nu)} + \frac{\pi^2 E}{8ab(1-\nu^2)} (\nu b/a + a/b) W_o^2 \quad \text{psi} \qquad (5.2.2\text{-}10d)$$

and the plate buckling amplitude is

$$W_o^2 = 4h^2 (b/a + a/b)^2 (T/T_c - 1)/R \quad \text{in}^2 \qquad (5.2.2\text{-}10e)$$

$$R = 3[(5-\nu^2)(b/a + a/b)^2 - 2(5 + \nu)(1 - \nu)]$$

The response frequency for the buckled <u>simply supported</u> plate is

$$f_{11}^2 = \frac{\pi^2 D}{2\rho h a^2 b^2} (b/a + a/b)^2 (T/T_c - 1) \quad \text{Hz.}^2 \qquad (5.2.2\text{-}11)$$

with T_c given by Equation 5.2.2-8b.

For <u>clamped edges</u>, the thermal mean stresses are

$$\bar{\sigma}_x = -\frac{E\alpha T}{(1-\nu)} + \frac{3\pi^2 E}{32ab(1-\nu^2)} (b/a + \nu a/b) W_o^2 \quad \text{psi} \qquad (5.2.2\text{-}12a)$$

$$\bar{\sigma}_y = -\frac{E\alpha T}{(1-\nu)} + \frac{3\pi^2 E}{32ab(1-\nu^2)} (\nu b/a + a/b) W_o^2 \quad \text{psi} \qquad (5.2.2\text{-}12b)$$

and the plate buckling amplitude is given by

$$W_o^2 = 8h^2((b/a)^2 + (a/b)^2 + 2/3)(T/T_c - 1)/R \quad in^2 \qquad (5.2.2\text{-}12c)$$

$$R = (1-\nu)F^*(b,a) + (9/2)((b/a)^2 + (a/b)^2 + 2\nu)$$

$$F^*(b,a) = (17/8)((b/a)^2 + (a/b)^2) + 4(b/a + a/b)^{-2}$$
$$+ (b/a + 4a/b)^{-2} + (4b/a + a/b)^{-2}$$

The response frequency for the buckled plates with clamped edges is

$$f_{11}^2 = \frac{8\pi^2 D}{9\rho h a^2 b^2}(3(b/a)^2 + 3(a/b)^2 + 2)(T/T_c - 1) \quad Hz^2 \qquad (5.2.2\text{-}13)$$

with T_c given by Equation (5.2.2-9b).

The results of Equations (5.2.2-10e) and (5.2.2-12c) are presented in Figure 5.2.2-13 for an assumed value of $\nu = 0.32$ and represents a design chart for estimating the static buckled plate response, W_o.

Summary of Results: Examining results for estimating the response frequency, it is seen that two simple forms for the response frequency can be obtained in terms of the temperature ratio, $r = T/T_c$, as follows

$$f = f_o\sqrt{(1 - r)} \quad Hz \qquad 0 \leq r \leq 1 \qquad (5.2.2\text{-}14)$$

and

$$f = \sqrt{2}\, f_o\sqrt{(r - 1)} \quad Hz \qquad r \geq 1 \qquad (5.2.2\text{-}15)$$

Equation (5.2.2-14) applied for temperature increases below the buckling temperature, T_c, and (5.2.2-15) applies above the buckling temperature. The parameter f_o is the room temperature response frequency for the particular boundary condition and T_c is the buckling temperature for the boundary condition. These results are plotted in Figure 5.2.2-14.

Example 1: Show that for the case of temperature increase the lowest frequency mode of a simply supported panel is not necessarily the (1,1) mode below the buckling temperature.

From Equation (5.2.2-7), the thermal stresses are

$$\bar{\sigma}_x = \bar{\sigma}_y = -E\alpha T/(1 - \nu)$$

and the in plane loading stress resultants are

$$N_x = N_y = h\bar{\sigma}_x = h\bar{\sigma}_y = -E\alpha Th/(1 - \nu)$$

Using the above expressions for the stress resultants and substituting into Equation (5.2.2-3) one obtains

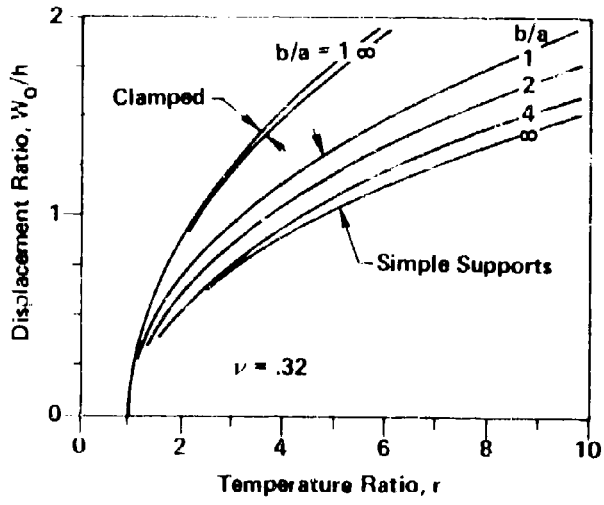

FIGURE 5.2.2-13 VARIATION OF BUCKLING AMPLITUDE WITH TEMPERATURE INCREASE

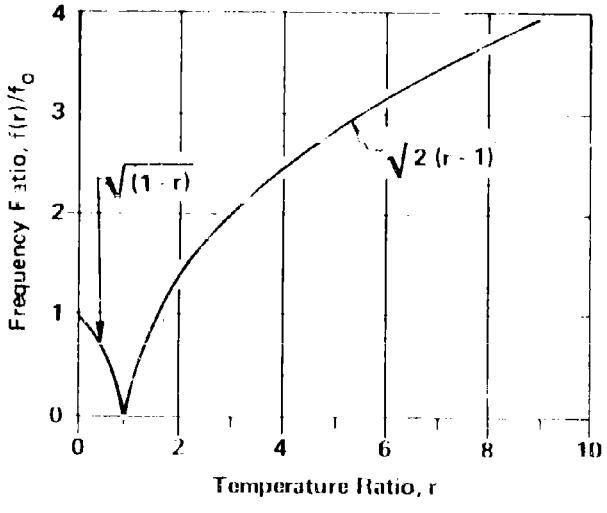

FIGURE 5.2.2-14 VARIATION OF FUNDAMENTAL MODE RESPONSE FREQUENCY WITH TEMPERATURE INCREASE

$$f_{mn}^2 = \frac{\pi^2 D}{4\rho h a^2 b^2}\left[m^2(b/a) + n^2(a/b)\right]^2(1 - T/T_c) \qquad (5.2.2\text{-}16)$$

Comparing this result with Equation (5.2.2-6) it is seen that the results of the Example in Section 5.2.2.2 2 apply (see Figure 5.2.2-12).

Example 2: For a simply supported rectangular panel determine the (1,1) mode response frequency, the thermal stress distribution, and the buckled plate amplitude as a function of temperature increase for the following data:

$a = 6.0$ inches	$b = 12.0$ inches	$h = 0.024$ inches
$\alpha = 5.5 \times 10^{-6}$ in/in/°F	$E = 16.4 \times 10^6$ psi	$\nu = 0.32$
$\gamma = 0.16$ lbs/in^3	$\rho = \gamma/g$	$g = 386.4$ in/sec^2

From Equation (5.2.2-8b) the buckling temperature increase is $T_c = 73^\circ F$.

From Equation (5.2.2-7) the mean thermal stress below the buckling temperature is

$$\bar{\sigma}_x = \bar{\sigma}_y = -\frac{E\alpha T_c}{(1-\nu)}\frac{T}{T_c} = -305.0\, r \quad psi \quad 0 \le r \le 1$$

which is uniformly distributed along the panel.

From Equation (5.2.2-10e) the buckled panel response is

$$W_o^2 = 2.0535 \times 10^{-4}(r-1) \quad in^2 \quad r \ge 1$$

(See Figure 5.2.2-13, for simple supports and $b/a = 2.0$, $h = 0.024$)

From Equations (5.2.2-10c & d) the mean thermal stresses are

$$\bar{\sigma}_x = -135.97 - 169.03r \quad psi \quad r \ge 1$$

$$\bar{\sigma}_y = -73.29 - 231.71r \quad psi \quad r \ge 1$$

From Equations (5.2.2-10a & b)

$$\sigma_x = -(135.97 + 169.03r) - 115.41\cos(0.5236y)(r-1) \quad psi \quad r \ge 1$$

$$\sigma_y = -(73.29 + 231.71r) - 28.85\cos(1.0472x)(r-1) \quad psi \quad r \ge 1$$

This result is plotted in Figure 5.2.2-15 for several values of r to illustrate the thermal stress distribution for the buckled panel.

From Equations (5.2.2-8a &-11) the response frequencies are

$$D = 21.0481 \quad \text{in-lb}$$

$$f_o = 79.4 \quad \text{Hz} \quad \text{(room temperature response frequency)}$$

$$f = 79.4 \sqrt{(1-r)} \quad \text{Hz} \quad r \leq 1$$

$$f = 112.3 \sqrt{(r-1)} \quad \text{Hz} \quad r \geq 1$$

This result is easily achieved by using Figures 5.2.2-2 and 5.2.2-14.

5.2.2.2.4 Effect of Elastic Edge Restraint

This section presents two techniques for estimating the natural frequencies and stress response to a uniform static pressure of unit magnitude of rectangular plates with elastic edge restraint. First, Carmichael's (13) analysis is presented for the case of a plate subjected to elastic rotational edge restraints on all edges. Next, Arcas' (14) analysis is presented for the case of a panel clamped on one pair of opposite edges and elastically restrained in bending on the other two edges. Both techniques are based upon the Rayleigh Method.

Elastic Rotational Edge Restraint

Derivation: Carmichael (13) utilized the Rayleigh-Ritz Method to obtain frequency estimates for rectangular plates with edges elastically restrained against rotation. The basis of this method is the calculation of the mode shapes and frequency parameters associated with a uniform beam whose ends are elastically restrained against rotation. The elastic restraint is assumed to be identical on each end of the beam. Hence, this analysis assumes that the elastic rotational restraint of the plate is comprised of identical frames on opposite edges and identical stringers on opposite edges. The degree of edge restraint is characterized by the parameters ℓ_a and ℓ_b as indicated in Figure 5.2.2-16.

Design Equations: The elastic edge restraint parameters ℓ_a and ℓ_b are such that if they are zero the edge is simply supported and if they are extremely large (greater than 2500) the edge is effectively clamped. To relate these parameters to physical characteristics of beams resisting rotational movement at the panel edges Carmichael's energy expression in terms of ℓ_a and ℓ_b was equated to Langhaar's (11) energy expression for torsional edge restraint. Neglecting stiffener cross-section warping the results are:

$$\ell_a = \frac{(GJ)_x}{Da} \left(\frac{b}{c}\right) \phi(\ell_b) \qquad (5.2.2\text{-}17a)$$

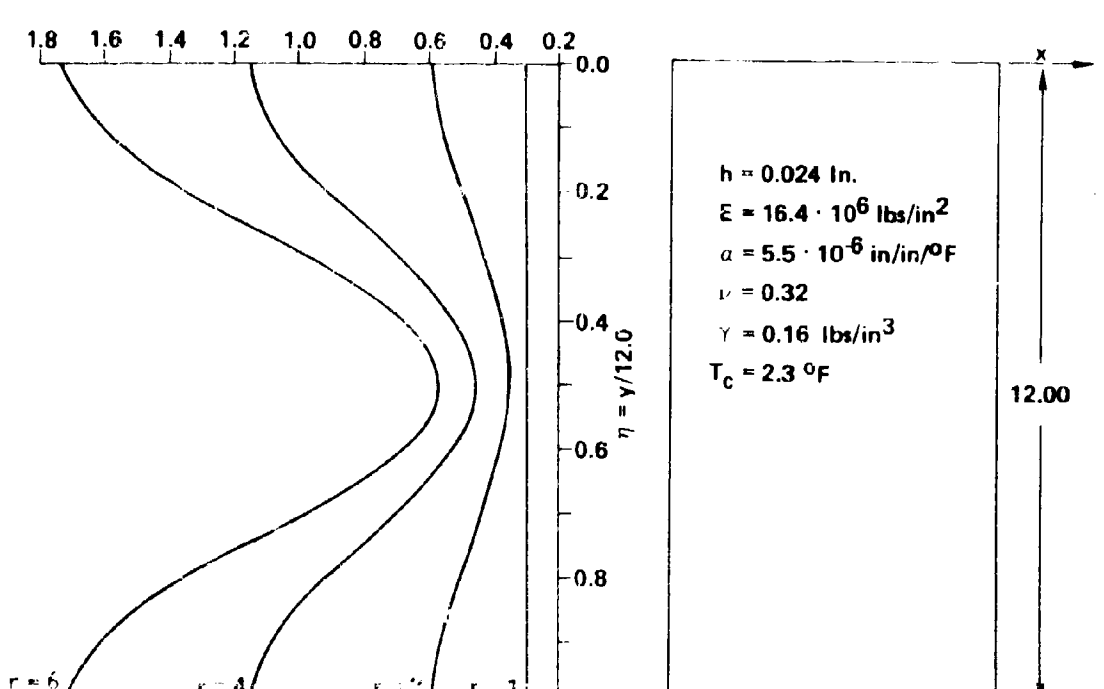

Membrane Stress Distribution For Several Temperature Ratios: $r = T/T_c$

$$\sigma_x = -(136.0 + 169.0\,r) - 115.4\cos(2\pi\eta)\,(r-1)$$

$$\sigma_y = -(73.3 + 231.7\,r) - 28.9\cos(2\pi\xi)\,(r-1)$$

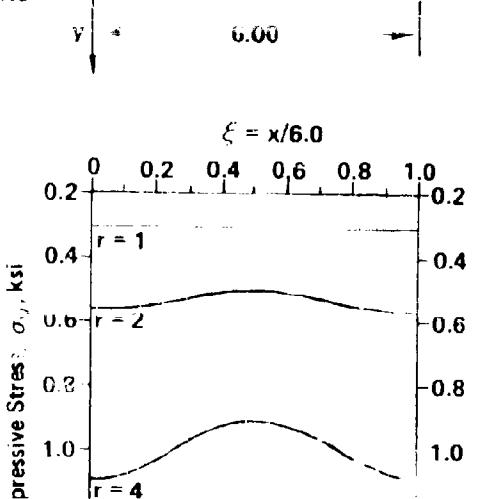

FIGURE 5.2.2-15 VARIATION OF PANEL MEAN STRESS WITH TEMPERATURE INCREASE

$$\xi_a = \frac{(GJ)_x}{Da}\left(\frac{b}{a}\right)\phi(\xi_b)$$

$$\xi_b = \frac{(GJ)_y}{Db}\left(\frac{a}{b}\right)\phi(\xi_a)$$

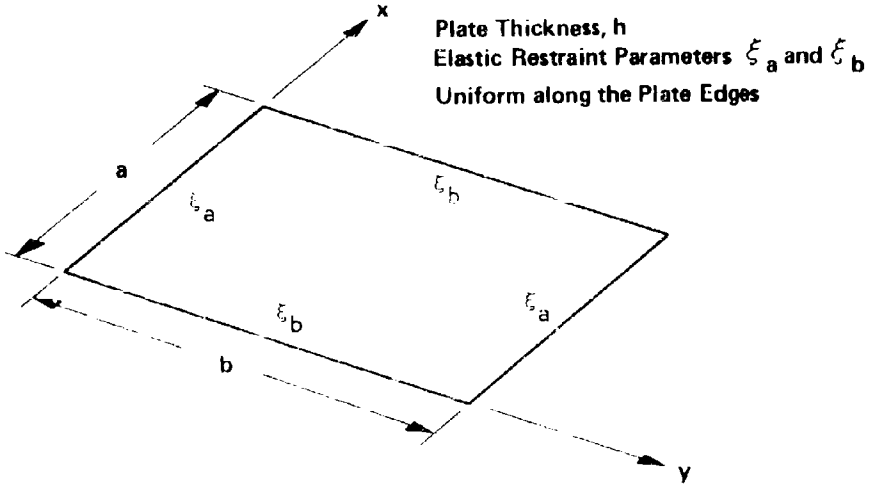

FIGURE 5.2.2-16 PLATE GEOMETRY AND ELASTIC ROTATIONAL EDGE CONSTRAINT NOMENCLATURE

$$\xi_b = -\frac{(GJ)_Y}{Db}\left(\frac{a}{b}\right)\phi(\xi_a) \qquad (5.2.2\text{-}17b)$$

The function $\phi(\xi)$ is tabulated in Table 5.2.2-4. Obviously, an iteration technique is required to determine ξ_a and ξ_b from Equations (5.2.2-17) and Table 5.2.2-4, and a nomograph, Figure 5.2.2-17, has been developed to provide accurate initial guesses.

The expression for the fundamental mode response frequency is, neglecting stringer rotary inertia,

$$f_{11}^2 = \frac{D}{4\pi^2\rho h}\left[\alpha^4(\xi_b)/a^4 + \alpha^4(\xi_a)/b^4 + 2\phi(\xi_a)\phi(\xi_b)/a^2b^2\right] \quad Hz^2 \qquad (5.2.2\text{-}18)$$

To estimate the panel stress response to a uniform static pressure of unit magnitude, it is assumed that only the fundamental mode significantly contributes to the panel deflection. Hence, the assumed fundamental mode is of the form

$$W(x,y) = X_1(x)Y_1(y)A_o \quad \text{in.} \qquad (5.2.2\text{-}19a)$$

where $X_1(x) = (\cosh(\alpha_b x/a) - \cos(\alpha_b x/a))A_b + \sinh(\alpha_b x/a)B_b + \sin(\alpha_b x/a)$

$$Y_1(y) = (\cosh(\alpha_a y/b) - \cos(\alpha_a y/b))A_a + \sinh(\alpha_a y/b)B_b + \sin(\alpha_b y/b)$$

$\alpha_a = \alpha(\xi_a)$, $A_a = A(\xi_a)$, etc. from Table 5.2.2-4.

A_o is the plate amplitude due to a unit magnitude uniform pressure (i.e., 1^opsi) distributed over the plate surface and is obtained by equating the maximum strain energy in bending for the plate to the potential energy of the uniform static pressure. This result is

$$A_o = C_1(\alpha_a)C_1(\alpha_b)a^2b^2/(DF(\alpha_a,\alpha_b,b/a)) \qquad (5.2.2\text{-}19b)$$

where

$$C_1(\alpha_r) = [(\sinh(\alpha_r) - \sin(\alpha_r))A_r + (\cosh(\alpha_r)-1)B_r - \cos(\alpha_r)+1]/\alpha_r$$

$$F(\alpha_a,\alpha_b,b/a) = [C_2(\alpha_b,\alpha_a) + C_4(\alpha_b,\alpha_a)](b/a)^2 + [C_2(\alpha_a,\alpha_b) + C_4(\alpha_a,\alpha_b)](a/b)^2 + C_3(\alpha_a,\alpha_b)$$

$$C_2(\alpha_a,\alpha_b) = \frac{1}{4}[2A_b^2 - B_b^2 + 1 + 2A_b(B_b+1)/\alpha_b][\alpha_a^4(2A_a^2 - B_a^2+1) - 6\alpha_a^3A_a(B_a+1)]$$

TABLE 5.2.2-4

VALUES OF $\alpha(\xi)$, $A(\xi)$, $B(\xi)$, AND $\phi(\xi)$

FOR THE FUNDAMENTAL MODE OF A UNIFORM BEAM WITH

ENDS ELASTICALLY RESTRAINED AGAINST ROTATION (FROM CARMICHAEL, REF. 13)

ξ	$\alpha(\xi)$	$A(\xi)$	$-B(\xi)$	$\phi(\xi)$
0.0	3.1416	0.0	0.0	9.8697
0.25	3.2166	0.0375	0.0346	9.8710
0.5	3.2836	0.0711	0.0668	9.8750
0.75	3.3440	0.1015	0.0946	9.8806
1.	3.3988	0.1293	0.1210	9.8880
1.5	3.4949	0.1785	0.1680	9.9074
2.	3.5768	0.2211	0.2091	9.9320
2.5	3.6477	0.2586	0.2454	9.9604
3.	3.7097	0.2919	0.2780	9.9908
3.5	3.7646	0.3220	0.3074	10.023
4.	3.8135	0.3492	0.3341	10.057
5.	3.8974	0.3970	0.3812	10.126
6.	3.9666	0.4376	0.4214	10.196
7.	4.0250	0.4729	0.4563	10.265
8.	4.0748	0.5037	0.4869	10.332
10.	4.1557	0.5555	0.5383	10.459
12.	4.2185	0.5973	0.5800	10.573
15.	4.2905	0.6472	0.6297	10.726
20.	4.3737	0.7080	0.6904	10.932
25.	4.4304	0.7514	0.7337	11.095
30.	4.4714	0.7840	0.7663	11.223
45.	4.5467	0.8467	0.8289	11.487
60.	4.5880	0.8828	0.8650	11.648
80.	4.6208	0.9124	0.8946	11.785
100.	4.6413	0.9313	0.9135	11.875
150.	4.6697	0.9582	0.9404	12.005
200.	4.6843	0.9723	0.9544	12.074
300.	4.6992	0.9869	0.9691	12.146
500.	4.7114	0.9990	0.9812	12.207
1000.	4.7207	1.0083	0.9905	12.254
∞	4.7300	1.0178	1.0000	12.302

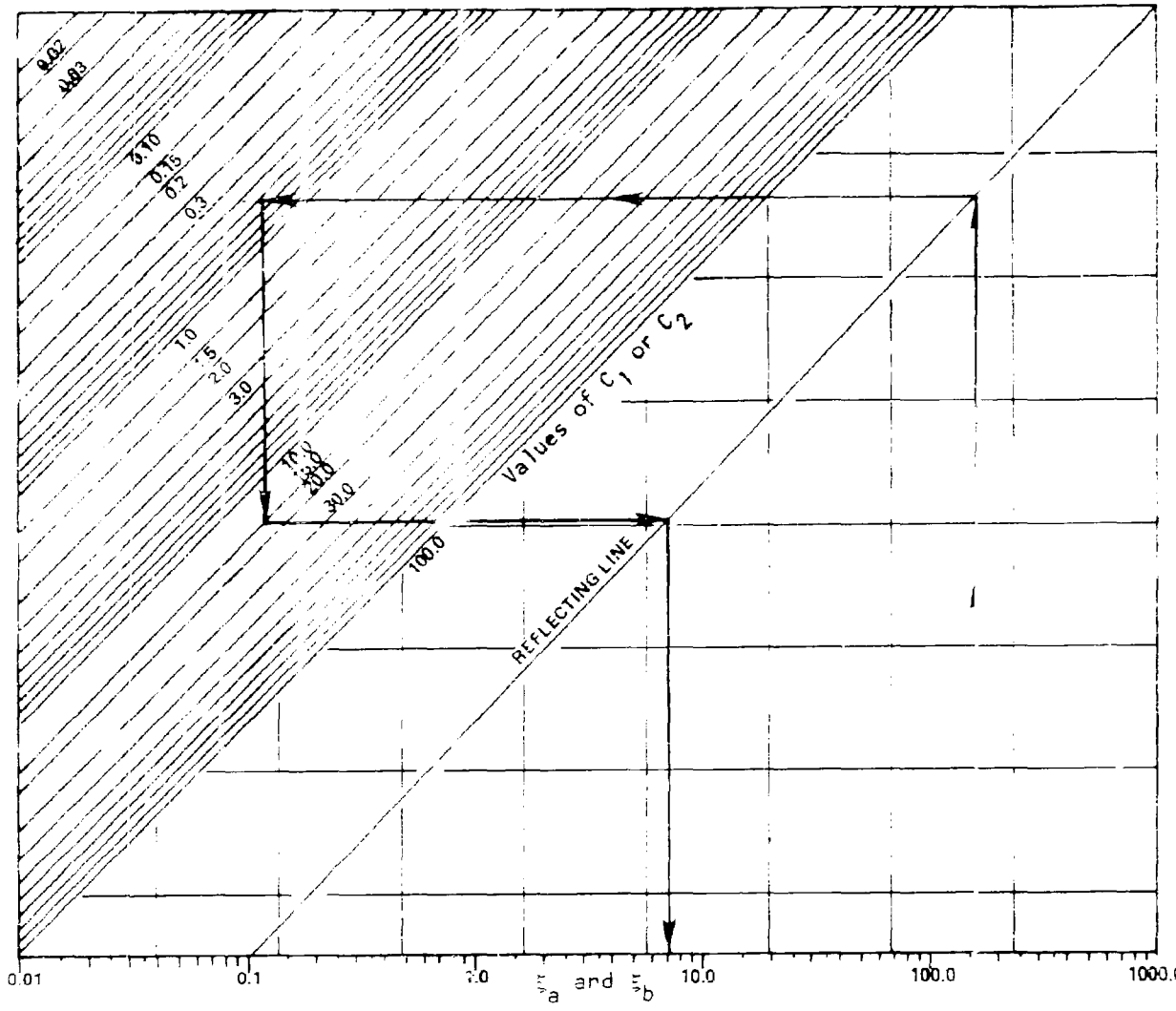

FIGURE 5.2.2-17 NOMOGRAPH FOR SIMULTANEOUS SOLUTION OF $\xi_a = C_1\phi(\xi_b)$ and $\xi_b = C_2\phi(\xi_a)$

$$C_2(\alpha_b,\alpha_a) - \frac{1}{4}[\alpha_b^4(2A_b^2 - B_b^2 + 1) - 6\alpha_b^3 A_b(B_b+1)][2A_a^2 - B_a^2 + 1 + 2A_a(B_a+1)/\alpha_a]$$

$$C_3(\alpha_a,\alpha_b) = \frac{1}{2}\alpha_a\alpha_b[\alpha_a(B_a^2 + 1) + 2A_a(B_a+1)][\alpha_b(B_b^2+1) + 2A_b(B_b+1)]$$

$$C_4(\alpha_a,\alpha_b) = 2\alpha_a^3 A_a(B_a+1)[2A_b^2 + B_b^2 + 1 + 2A_b(B_b + 1)/\alpha_b]$$

$$C_4(\alpha_b,\alpha_a) = 2\alpha_b^3 A_b(B_b+1)[2A_a^2 - B_a^2 + 1 + 2A_a(B_a + 1)/\alpha_a]$$

At the surface of the plate, z = h/2, the plate stress response to a unit magnitude uniform pressure is given by

$$\sigma_x = \frac{Eh}{2(1-\nu^2)}[W_{,xx} + \nu W_{,yy}] = \frac{EhA_o}{2(1-\nu^2)}[X_{1,xx}Y_1 + \nu X_1 Y_{1,yy}] \quad \text{psi} \quad (5.2.2\text{-}20a)$$

$$\sigma_y = \frac{Eh}{2(1-\nu^2)}[\nu W_{,xx} + W_{,yy}] = \frac{EhA_o}{2(1-\nu^2)}[\nu X_{1,xx}Y_1 + X_1 Y_{1,yy}] \quad \text{psi} \quad (5.2.2\text{-}20b)$$

where A_o is given by Equation (5.2.2-19) and $X_1(x)$ and $Y_1(y)$ are given by Equation (5.2.2-18).

Two example problems will illustrate the procedures. The first example will illustrate the combined effect of plate aspect ratio variation and plate width on the response frequency of the fundamental mode. The second example will illustrate the procedure for calculating frequency stress response in a plate configuration for comparison with Arcas' (14) analysis.

Example: For the indicated data calculate the fundamental response frequency of a rectangular plate with elastic rotational edge restraints as a function of plate aspect ratio. The data is as follows:

$a = 6.0$ in $\quad h = 0.032$ in $\quad \gamma = 0.101$ lb/in^3

$E = 10.3\times10^6$ psi $\quad G = 3.9\times10^6$ psi $\quad \nu = 0.32$

$J_x = 7.51\times10^{-4}$ in^4 $\quad$ (0.080"×0.75"×2.90" equal leg channel, Fig. B.1.1-9)

$J_y = 3.00\times10^{-5}$ in^4 $\quad$ (0.032"×0.75"×1.25" equal leg zee, Fig. B.1.1-8)

From Equations 5.2.2-17

$$\ell_a = 2.5965b\phi(\ell_b)$$

$$\ell_b = 22.4034\phi(\ell_a)/b^2$$

For a plate aspect ratio b/a = 1.0, b = 6.0 and

$$\xi_a = 15.5787\ \phi(\xi_b)$$

$$\xi_b = 0.62232\ \phi(\xi_a)$$

The basic iteration procedure is to guess a value for the larger ξ parameter that is ten(10) times the value of the coefficient on ϕ in Equations 5.2.2-17. For this example we guess $\xi_a = 160$. Enter Figure 5.2.2-17 at the lower right hand side at $\xi_a = 160$, proceed vertically to the reflecting line then horizontally until the line for 0.62 (coefficient on $\phi(\xi_a)$) is encountered. Then, proceed down until the line 15.6 (coefficient on $\phi(\xi_b)$) is encountered. Proceed horizontally to the reflecting line and then vertically to read $\xi_b = 7.2$.

Hence, the initial guess for ξ_a and ξ_b and values of $\phi(\xi_a)$ and $\phi(\xi_b)$ interpolated from Table 5.2.2-4 are as follows:

Guess # 1 $\quad \xi_a = 160 \quad \phi(\xi_a) = 12.0188$

$\qquad\qquad \xi_b = 7.0 \quad \phi(\xi_b) = 10.265$

Check # 1 $\quad \xi_a = 15.579\ (10.265) = 159.92$

$\qquad\qquad \xi_b = 0.6223\ (12.0188) = 7.48$

Now, working entirely from Table 5.2.2-4 we proceed with the iteration

Guess # 2 $\quad \xi_a = 162 \quad \phi(\xi_a) = 12.0216$

$\qquad\qquad \xi_b = 7.5 \quad \phi(\xi_b) = 10.299$

Check # 2 $\quad \xi_a = 15.579\ (10.299) = 160.4$

$\qquad\qquad \xi_b = 0.6223\ (12.0216) = 7.48$

Guess # 3 $\quad \xi_a = 160 \quad \phi(\xi_a) = 12.0188$

$\qquad\qquad \xi_b = 7.5 \quad \phi(\xi_b) = 10.299$

Check # 3 $\quad \xi_a = 15.579\ (10.299) = 160.4$

$\qquad\qquad \xi_b = 0.6223\ (12.0188) = 7.48$

The third guess is sufficiently accurate for design purposes and the procedure rarely requires more than three iterations. Hence, for b/a = 1.0 we have

$$\xi_a = 160 \qquad \phi(\xi_a) = 12.019 \qquad \alpha(\xi_a) = 4.673$$

$$\xi_b = 7.5 \qquad \phi(\xi_b) = 10.299 \qquad \alpha(\xi_b) = 4.050$$

Continuing the procedure one obtains the following results

b	b/a	ξ_a	$\phi(\xi_a)$	$\alpha(\xi_a)$	ξ_b	$\phi(\xi_b)$	$\alpha(\xi_b)$
6.0	1.0	160	12.019	4.673	7.5	10.299	4.050
9.0	1.5	233	12.098	4.699	3.3	9.996	3.743
12.0	2.0	309	12.149	4.699	1.9	9.921	3.560
18.0	3.0	462	12.195	4.709	0.84	9.883	3.364
24.0	4.0	615	12.218	4.714	0.50	9.875	3.284
30.0	5.0	769	12.232	4.716	0.30	9.872	3.230

It is interesting to note that as the panel aspect ratio increases the panel boundary conditions approach clamped edges on the short side and simply supported edges on the long side.

The frequency estimates are obtained from the above results and using Equation 5.2.2-18 and are

b =	6.0	9.0	12.0	18.0	24	30
b/a =	1.0	1.5	2.0	3.0	4.0	5.0
f_{11} =	270	171	136	109	99	93
$a^2 f_{11}/h \cdot 10^{-5}$	3.02	1.92	1.53	1.22	1.11	1.05

The values $a^2 f_{11}/h$ are plotted against panel aspect ratio in Figure 5.2.2-18. This figure presents bounds for clamped edges and simply supported edges with "average" experimental frequency data from Ballentine (15). For comparison, the curve for this example problem with a = 4.0 inches is also presented.

Example: For the data given below calculate the frequency of the fundamental mode and the stress response to a unit magnitude uniform pressure at the plate center and the center of each side of the plate assuming that the short side of the plate is clamped and the long side is elastically restrained against rotation by a solid rectangular section stiffener with depth, d, and width, w. See Figure 5.2.2-19.

The data for the problem is as follows:

$$a = 6.0 \text{ in} \qquad b = 12.0 \text{ in} \qquad h = 0.032 \text{ in}$$

$$d = 0.75 \text{ in} \qquad w = 0.10 \text{ in} \qquad \gamma = 0.101 \text{ lbs/in}^3$$

$$E = 10.3 \cdot 10^6 \text{ psi} \qquad G = 3.9 \cdot 10^6 \text{ psi} \qquad \nu = 0.32$$

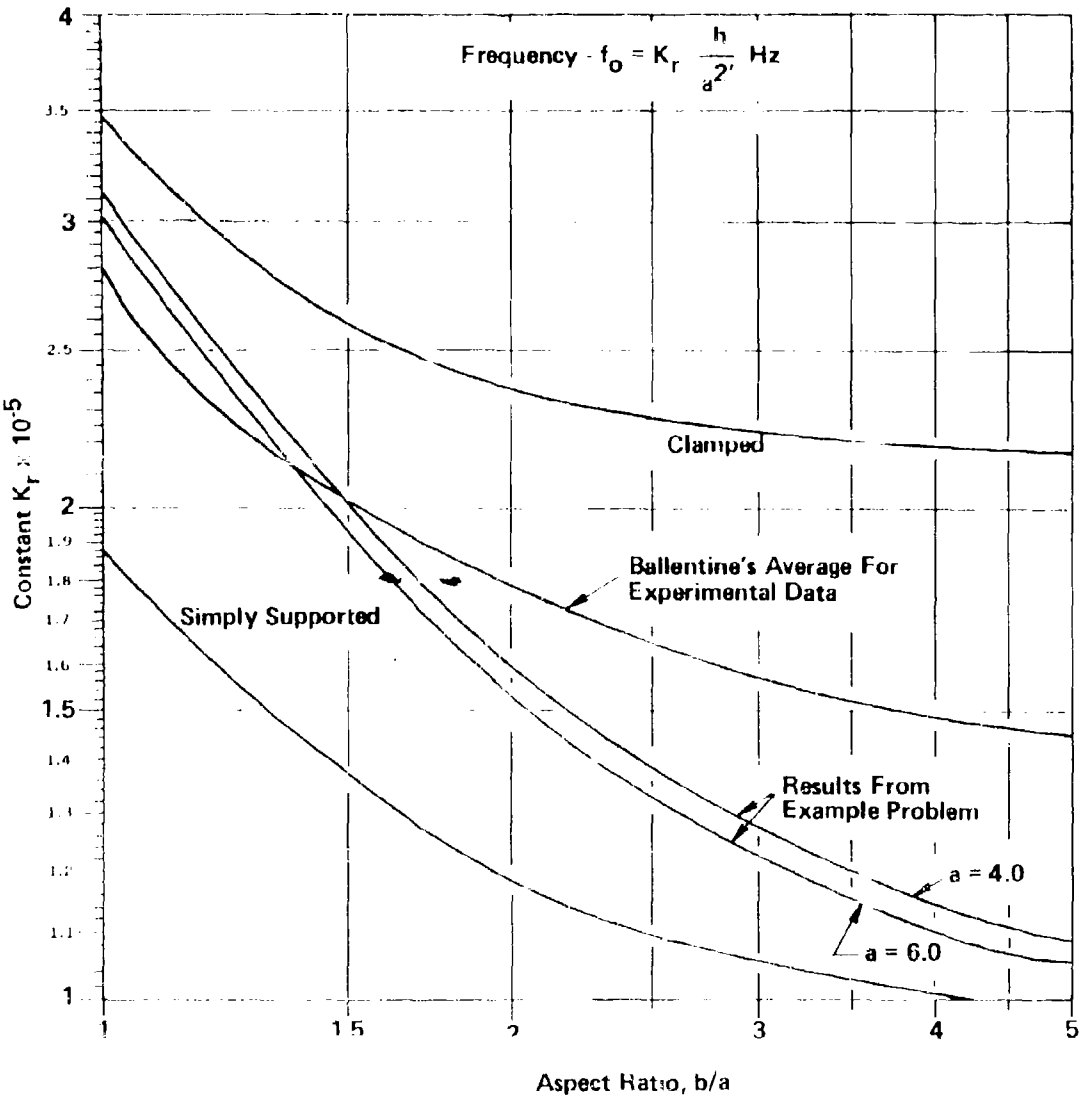

FIGURE 5.2.2-18 PLOT OF FUNDAMENTAL MODE FREQUENCY CONSTANT AND COMPARISON TO ANALYTICAL AND EXPERIMENTAL RESULTS

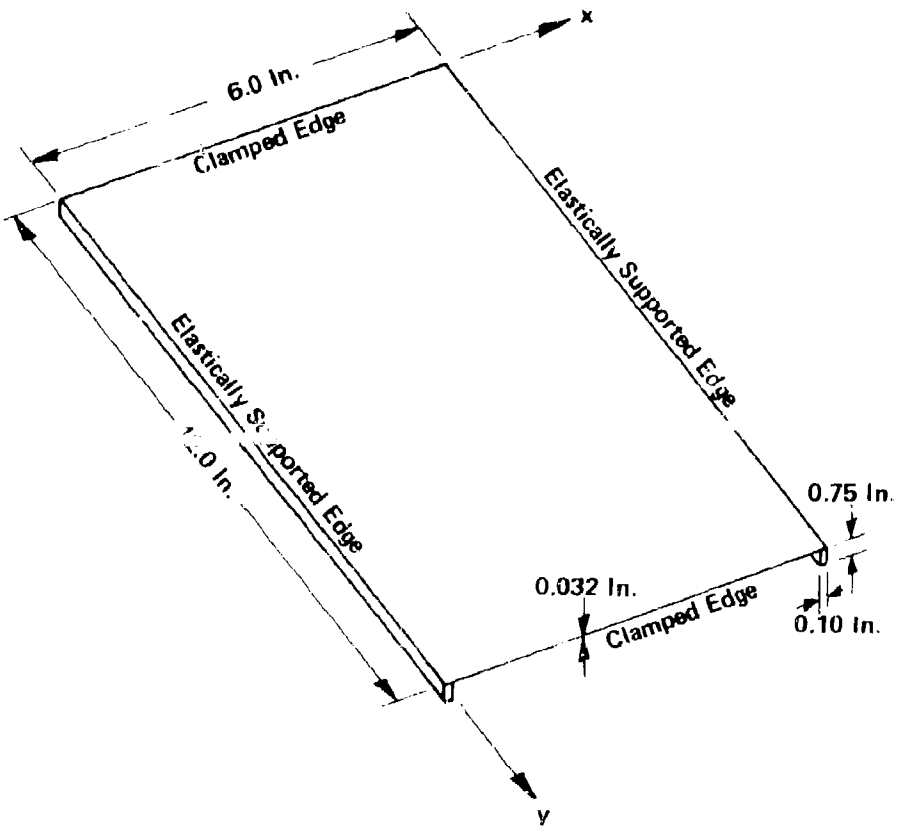

FIGURE 5.2.2-19 PLATE GEOMETRY AND ELASTIC BENDING EDGE CONSTRAINT NOMENCLATURE FOR EXAMPLE PROBLEM

Since the short side of the plate is clamped we set $\xi_a = \infty$ and from Table 5.2.2-4 and Equation (5.2.2-17b) that $\xi_b = 12.302\ (GJ)_y a/Db^2$.

The value of J_y is given by

$$J_y = 16k\ W^3 d = 3.648\times10^{-3}$$

where the value $k = 0.304$ is obtained from Table 8.1.1-1

Then, the value for ξ_b is calculated as

$$\xi_b = 12.302(3.9\times10^6)(3.648\times10^{-3})(6.0)/(31.335)(12)^2 = 232.73$$

From Table 5.2.2-4 one obtains

$\xi_a = \infty$	$\xi_b = 232.73$	$B_a = -1.000$	$B_b = -0.9592$
$\alpha_a = 4.730$	$\alpha_b = 4.704$	$\phi_a = 12.302$	$\phi_b = 12.098$
$A_a = 1.0178$	$A_b = 0.9771$		

From Equation (5.2.2-18) the frequency of the fundamental mode is estimated to be 209 Hz.

To estimate the stress response, one must first calculate A_o from Equations (5.2.2-19). For the above data the results are

$C_1(\alpha_a) = 0.8455$	$C_1(\alpha_b) = 0.8341$
$C_2(\alpha_a,\alpha_b) = 520.165$	$C_2(\alpha_b,\alpha_a) = 491.670$
$C_4(\alpha_a,\alpha_b) = 0.00$	$C_4(\alpha_b,\alpha_a) = 17.195$
$C_3(\alpha_a,\alpha_b) = 958.975$	

Then, one obtains $A_o = 0.0335$ in (i.e., deflection is approximately one plate thickness).

From Equations (5.2.2-19 and -20), one obtains the results

$X_1(a/2) = 1.5842$	$X_{1,xx}(a/2) = -0.7450$
$Y_1(b/2) = 1.6165$	$Y_{1,yy}(b/2) = -0.1922$
$Y_1(0) = 0.0$	$X_{1,xx}(0) = 1.2012$
$Y_1(0) = 0.0$	$Y_{1,yy}(0) = 0.3163$

$$\frac{EhA_o}{2(1-\nu^2)} = 6.8575\times10^3$$

Finally, at the center of the plate

$$\sigma_x(a/2, b/2) = 6.8575 \cdot 10^3[(-.745)(1.6165) + (.32)(1.5842)(-0.1922)]$$

$$\sigma_x(a/2, b/2) = -8927 \text{ psi} = -8.93 \text{ ksi}$$

$$\sigma_y(a/2, b/2) = -4.73 \text{ ksi}$$

and at the edges of the plate

$$\sigma_x(0, b/2) = 13.32 \text{ ksi}$$

$$\sigma_y(a/2, 0) = 3.44 \text{ ksi}$$

Elastic Translational Edge Restraint

Derivation: Arcas (14) has presented a modified form of Clarkson's (4) analysis to estimate the fundamental mode frequency and stress response of a rectangular plate clamped on opposite edges and elastically restrained in translation on the other two edges. The elastic restraint is such that the panel edge does not rotate as it translates. Both techniques assume that the plate fundamental mode is of the form

$$W(x,y) = (KW_1(x,y) + W_2(y))A_o \qquad (5.2.2\text{-}21)$$

where $W_1(x,y) = X_1(x)Y_1(y)$ represents the mode for a panel clamped on all edges and $W_2(y)$ is the deflection function of the edge stiffener.

Clarkson assumed simple trigonometric mode functions for $X_1(x)$, $Y_1(y)$, and $W_2(y)$ whereas Arcas assumed $X_1(x)$ and $Y_1(y)$ were of the form of a clamped-clamped beam fundamental mode and $W_2(y)$ was taken as the deflection shape (polynomial) of a uniformly loaded clamped-clamped beam.

The expressions for the potential and the kinetic energy of the stiffened plate are developed using the mode given in Equation (5.2.2-21), and assuming harmonic motion, the equation for the frequency is obtained (Rayleigh's Method). The frequency expression is then minimized to determine the value of K from a quadratic equation.

Design Equations: Using Arcas' approach, the following results are obtained.

The equation for K is

$$\hat{C}_1 K^2 + \hat{C}_2 K + \hat{C}_3 = 0 \qquad (5.2.2\text{-}22)$$

where

$$\hat{C}_1 = 10.019 \, Dph[3.307(b/a)^2 + \ldots]$$

$$C_2 = 0.4805\,D(\rho h + \rho_B a/a)R - 1.60\rho h(Da + EI)a/b^2$$

$$C_3 = 0.0526\,D\rho_B a/b^2 - 0.0530\rho h\,EIa/b^2 - 0.00036D\rho ha^2/b^2$$

$$R = (3.30/(b/a)^2 + 3.307(a/b)^2 + 2)$$

The equation for the frequency of the fundamental mode is

$$f_{11}^2 = \frac{1}{4\pi^2}\,\frac{(C_1K^2 + C_2K + C_3)}{(C_4K^2 + C_5K + C_6)}\quad Hz^2 \qquad (5.2.2\text{-}23)$$

where

$$C_1 = 151.354D\,[3.307(b/a)^2 + 3.30/(a/b)^2 + 2.0]/ab$$

$$C_2 = 33.136Da/b^3$$

$$C_3 = 0.80(Da + EI)/b^3$$

$$C_4 = \rho hab$$

$$C_5 = 0.0662\rho hab$$

$$C_6 = 0.00159(\rho ha + \rho_B)b$$

The equation for the panel amplitude resulting from a uniform static pressure of unit magnitude is

$$A_o = C_7 a^2 b^2/C_8 \qquad (5.2.2\text{-}24)$$

where

$$C_7 = 20.7K + 1$$

$$C_8 = 30[151.354DRK^2 + 33.136DF(a/b)^2 + 0.8(D + EI/a)(a/b)^2]$$

The equations for the stress response at various points on the panel surface resulting from a uniform static pressure of unit magnitude are

At the panel center

$$\sigma_x(a/2,b/2) = \frac{EhA_o}{2(1-\nu^2)}\,[43.195F/a^2 + \nu(43.195K+1)/b^2]\ psi$$

$$\sigma_y(a/2,b/2) = \frac{EhA_o}{2(1-\nu^2)}\,[43.195\nu K/a^2 + (43.195K+1)/b^2]\ psi \qquad (5.2.2\text{-}25a)$$

At the center of the clamped edges

$$\sigma_y(a/2,0) = \frac{EhA_o}{2(1-\nu^2)b^2}\,[71.064K + 2.0]\ psi \qquad (5.2.2\text{-}25b)$$

At the center of the elastically supported edge

$$\sigma_x(a,b/2) = \frac{EhA_o}{2(1-\nu^2)}\left[71.064K/a^2 - \nu/b^2\right] \quad psi$$

$$\sigma_y(a,b/2) = \frac{EhA_o}{2(1-\nu^2)}\left[71.064\nu K/a^2 - 1/b^2\right] \quad psi \qquad (5.2.2\text{-}25c)$$

At the outside edge of the beam at the beam center

$$\sigma_y(a,b/2) = EdA_o/(2b^2) \quad psi \qquad (5.2.2\text{-}25d)$$

and at the beam end

$$\sigma_y(a,o) = -EdA_o/b^2 \quad psi \qquad (5.2.2\text{-}25e)$$

Example: For the data given below calculate the frequency of the fundamental mode and the stress response to a unit magnitude (1 psi) uniform pressure at the plate center and the center of each side of the plate, assuming that the short side of the plate is clamped and that the long side is elastically restrained against translation (stringer bending) by a solid rectangular section stiffener with depth, d, and width, W. Compare these results with the previous Example.

The data for the example problem is as follows:

$a = 6.0$ in $b = 12.0$ in $h = 0.032$

$d = 0.75$ in $W = 0.20$ in $\gamma = 0.101$ lbs/in^3

$E = 10.3\times10^6$ psi $\nu = 0.32$

Calculate the basic parameters

$D = 31.335$ lb-in $Da = 188.01$ lb-in^2

$I = 7.031\times10^{-3}$ in^4 $EI = 7.242\times10^4$ lb-in^2

$\rho_B = 1.515\times10^{-2}$ lb/in

From Equation (5.2.2-22) one obtains the result

$C_1^* = 15.4514$

$C_2^* = -14.253$

$C_3^* = -0.51585$

and the roots of Equation (5.2.2-22) are

$K_1 = 0.95/32$

$K_2 = -0.034874.$

On physical grounds (see Equation (5.2.2-21)) one realizes that K_1 will yield the minimum frequency as calculated from Equation (5.2.2-23). From Equation (5.2.2-23) one obtains

$C_1 = 1.0575\times10^{3}$ $\quad C_4 = 6.022\times10^{-4}$

$C_2 = 3.6053$ $\quad C_5 = 3.987\times10^{-5}$

$C_3 = 33.615$ $\quad C_6 = 1.7057\times10^{-6}$

The frequency of the fundamental mode response is obtained by substituting the values for C above and K = 0.95732 into Equation (5.2.2-23) to obtain $f_{11} = 208$ Hz. (Using the above values of C and K = -0.034874 one obtains $f_{11} = 917$ Hz.)

For K = 0.95732 one obtains the results $C_7 = 20.8261$ and $C_8 = 2.1736\times10^{6}$, and the panel static amplitude to a uniform unit magnitude pressure of $A_o = 0.0497$ in. from Equation (5.2.2-24).

From Equations (5.2.2-25) one calculates the stress response to unit magnitude uniform static pressure and obtains the results

Panel Center (x,y) = (a/2, b/2)

$\sigma_x(a/2, b/2) = -11,333$ psi = -11.3 ksi

$\sigma_y(a/2, b/2) = -6,034$ psi = -6.0 ksi

Center of Clamped Edge (x,y) = (a/2, 0)

$\sigma_y(a/2,0) = 4,435$ psi = 4.4 ksi

Center of Elastically Restrained Edge (x,y) = (a,b/2)

$\sigma_x(a,b/2) = 17,214$ psi = 17.2 ksi

$\sigma_y(a,b/2) = 5,452$ psi = 5.5 ksi

Outer Edge of Beam (z = d/2)

$\sigma_x(a,b/2) = 1,332$ psi = 1.3 ksi

$\sigma_y(a,0) = -2,665$ psi = -2.7 ksi

Areas presents interesting numerical results illustrating the effect of edge member stiffness. Figure 5.2.2-20 presents a variation of response frequency with plate thickness using the method of this section for a panel with an aspect ratio of 7.0 for three values of edge member moment

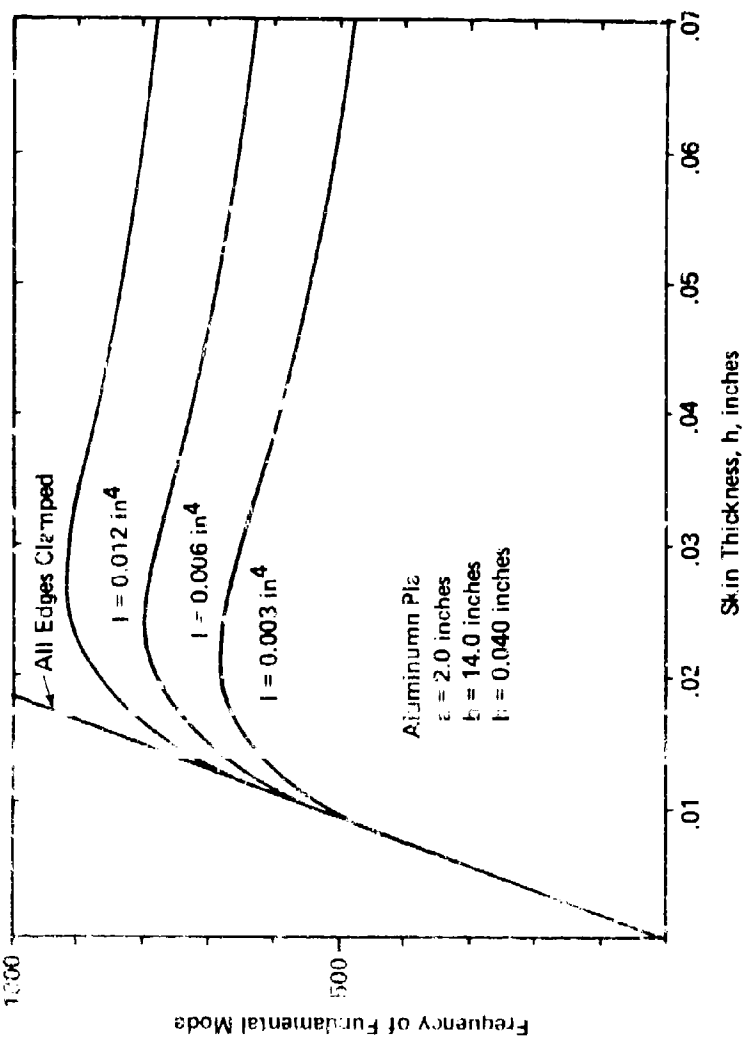

FIGURE 5.2.3-20 VARIATION OF RESPONSE FREQUENCY WITH SKIN THICKNESS AND STIFFENER MOMENT OF INERTIA (REF. 14)

of inertia. Figure 5.2.2-21 illustrates the plate center stress, σ_x, and edge stress σ_x, from Equations (5.2.2-25a and -25c) as a function of edge member moment of inertia for the indicated panel geometry. The corresponding stresses for clamped edges are also presented for comparison. Figure 5.2.2-22 illustrates a comparison between estimated RMS stress and measured RMS stress using Clarkson's (4) method, Arcas' (14) method, and Ballentine's (15) method. Whereas Clarkson and Arcas assume flexible boundaries, and compare results with experimental data for a wide variety of aircraft structural specimens, Ballentine assumed clamped edges and utilized laboratory specimens and a controlled acoustic environment.

5.2.2.2.5 Static Stress Response

This section presents design equations and nomographs for estimating the bending stress response of rectangular isotropic plates subjected to a uniform static pressure of unit magnitude. The boundary conditions considered are all edges clamped and all edges simply supported. For clamped edges stress predictions are obtained at the plate center and at the center of each edge of the plate. For comparison, stress prediction at the center of a simply supported plate is also presented.

Derivation: The results presented here are based upon tabulated values of bending moments for uniformly loaded plates as discussed by Timoshenko (3, pp. 240-245). These tabulations are based upon an assumed value for Poisson's ratio of $\nu = 0.20$. Since most metallic aircraft materials exhibit values of Poisson's ratio closer to 0.3, the techniques presented here result in an error of approximately 7% over panel aspect ratios $1.0 \leq b/a$. This approximation is sufficiently accurate for acoustic fatigue analyses when the static stress estimate is used with Miles' single degree-of-freedom theory (5) to obtain an estimate of the stress response to random acoustic excitation (see Section 5.2.2.2.6).

Design Equation: The stress at a point on the plate surface is given by the expression

$$\sigma_o = 6M_o/h^2 = K_o a^2/h^2 \qquad (5.2.2\text{-}26)$$

where M_o is the bending moment at the point of interest due to a uniform static pressure of unit magnitude and a is the short dimension of the plate.

For $\nu = 0.20$ the values of the parameter K_o are presented in Table 5.2.2-5 for the indicated locations and are plotted in Figure 5.2.2-23. For the plate edge stresses σ_x and σ_y, results of Table 5.2.2-5 and Equation (5.2.2-26) have been used to prepare a nomograph. This edge stress nomograph is presented in Figure 5.2.2-24.

Example: For a rectangular plate with dimensions a = 6.0 inches, b = 9.0 inches and thickness, h = 0.032 inches, calculate the edge and center stresses for clamped edges and the center stresses for supported edges.

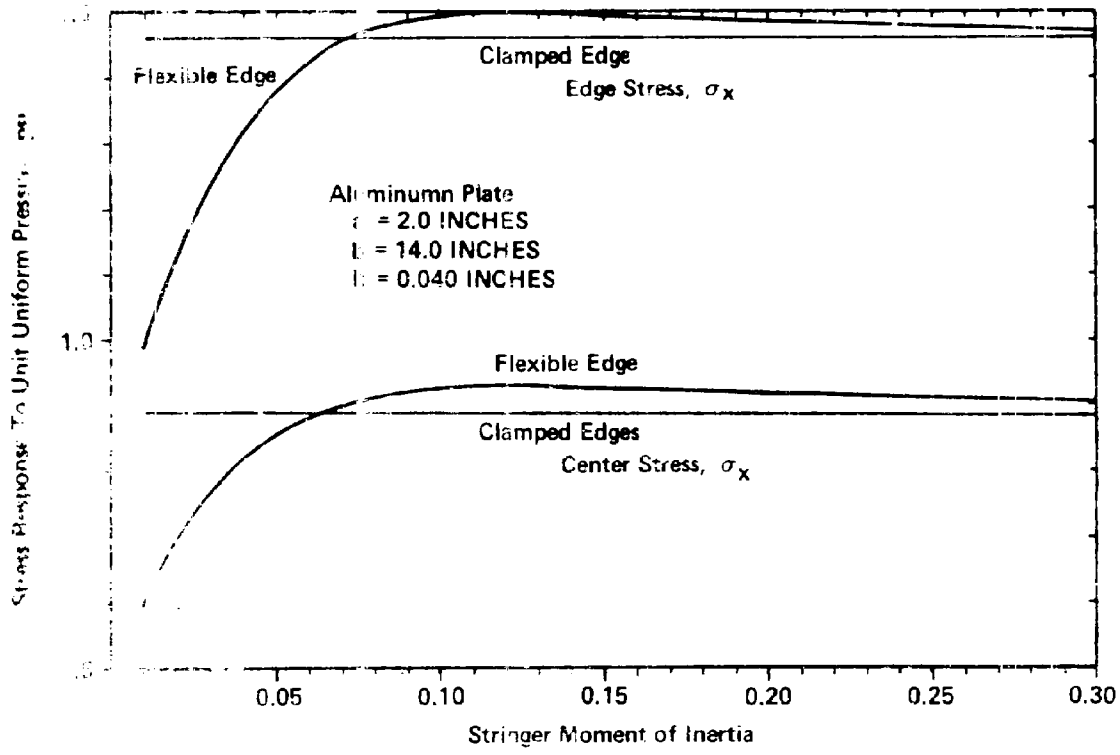

FIGURE 5.2.2-21 VARIATION OF STRESS RESPONSE TO UNIT MAGNITUDE UNIFORM STATIC PRESSURE FOR TYPICAL DATA (REF. 14)

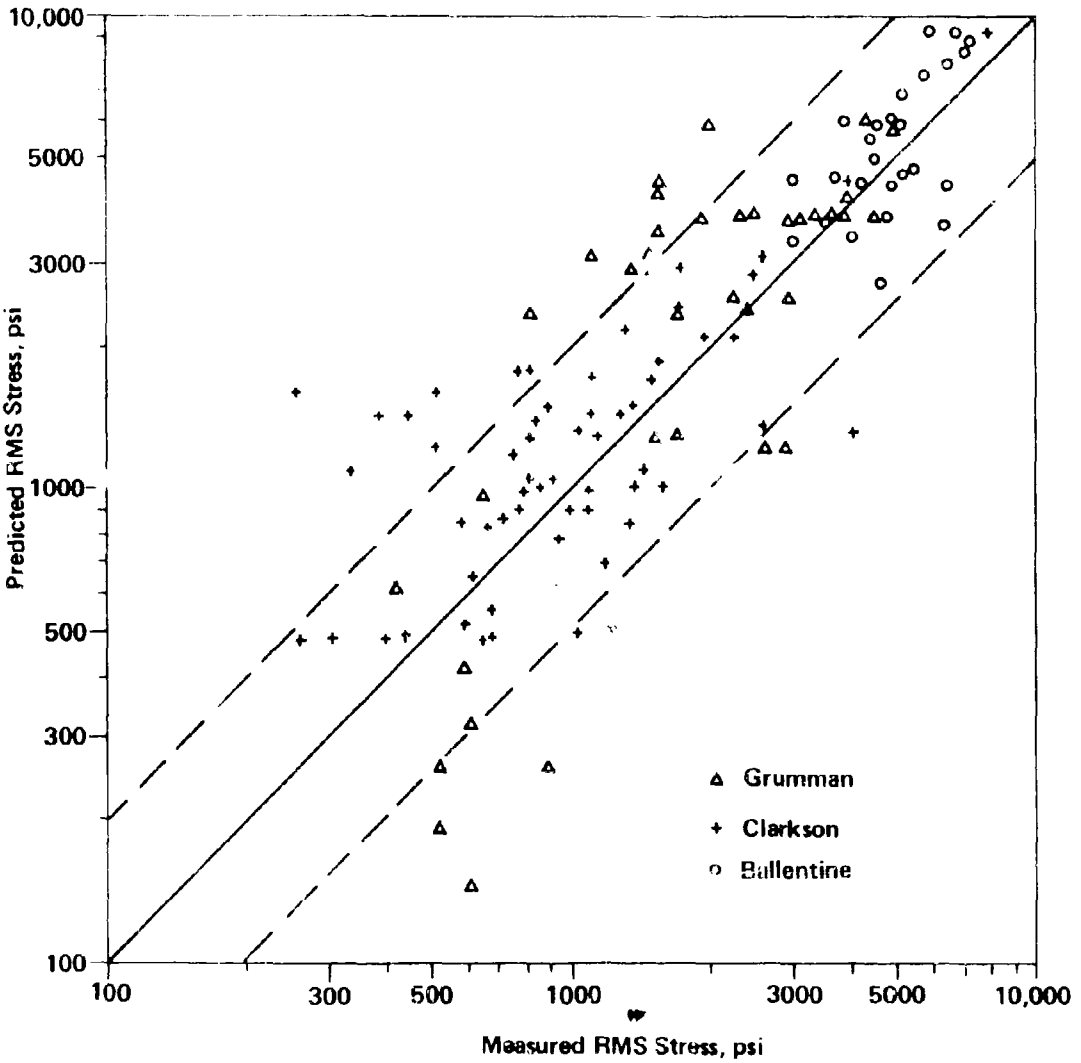

FIGURE 5.2.2-22 COMPARISON OF PREDICTED AND MEASURED RMS PANEL STRESS USING THREE DIFFERENT METHODS (REF. 14)

TABLE 5.2.2-5
STRESS PARAMETER K_o FOR CALCULATING STRESS RESPONSE
OF A PLATE TO UNIFORM STATIC PRESSURE OF UNIT MAGNITUDE

$\nu = 0.20$

Plate Aspect Ratio b/a	Clamped Edges				Supported Edges	
	Plate Edge Stress		Plate Center Stress		Plate Center Stress	
	Center of Long Side	Center of Short Side	Center of Plate		Center of Plate	
	K_o for σ_x	K_o for σ_y	K_o for σ_x	K_o for σ_y	K_o for σ_x	K_o for σ_y
1.0	-0.3078	-0.3078	0.1278	0.1278	0.2652	0.2652
1.1	-0.3486	-0.3228	0.1488	0.1260	0.3102	0.2694
1.2	-0.3834	-0.3324	0.1704	0.1218	0.3552	0.2694
1.3	-0.4122	-0.3378	0.1878	0.1158	0.3960	0.2664
1.4	-0.4356	-0.3408	0.2022	0.1086	0.4308	0.2634
1.5	-0.4542	-0.3420	0.2148	0.1014	0.4704	0.2556
1.6	-0.4680	-0.3426	0.2232	0.0942	0.5016	0.2484
1.7	-0.4794	-0.3426	0.2310	0.0876	0.5310	0.2412
1.8	-0.4872	-0.3426	0.2370	0.0816	0.5562	0.2346
1.9	-0.4932	-0.3426	0.2412	0.0756	0.5796	0.2268
2.0	-0.4974	-0.3426	0.2448	0.0708	0.5994	0.2202
∞	-0.4998	-0.3426	0.2502	0.0498	0.7500	0.1500

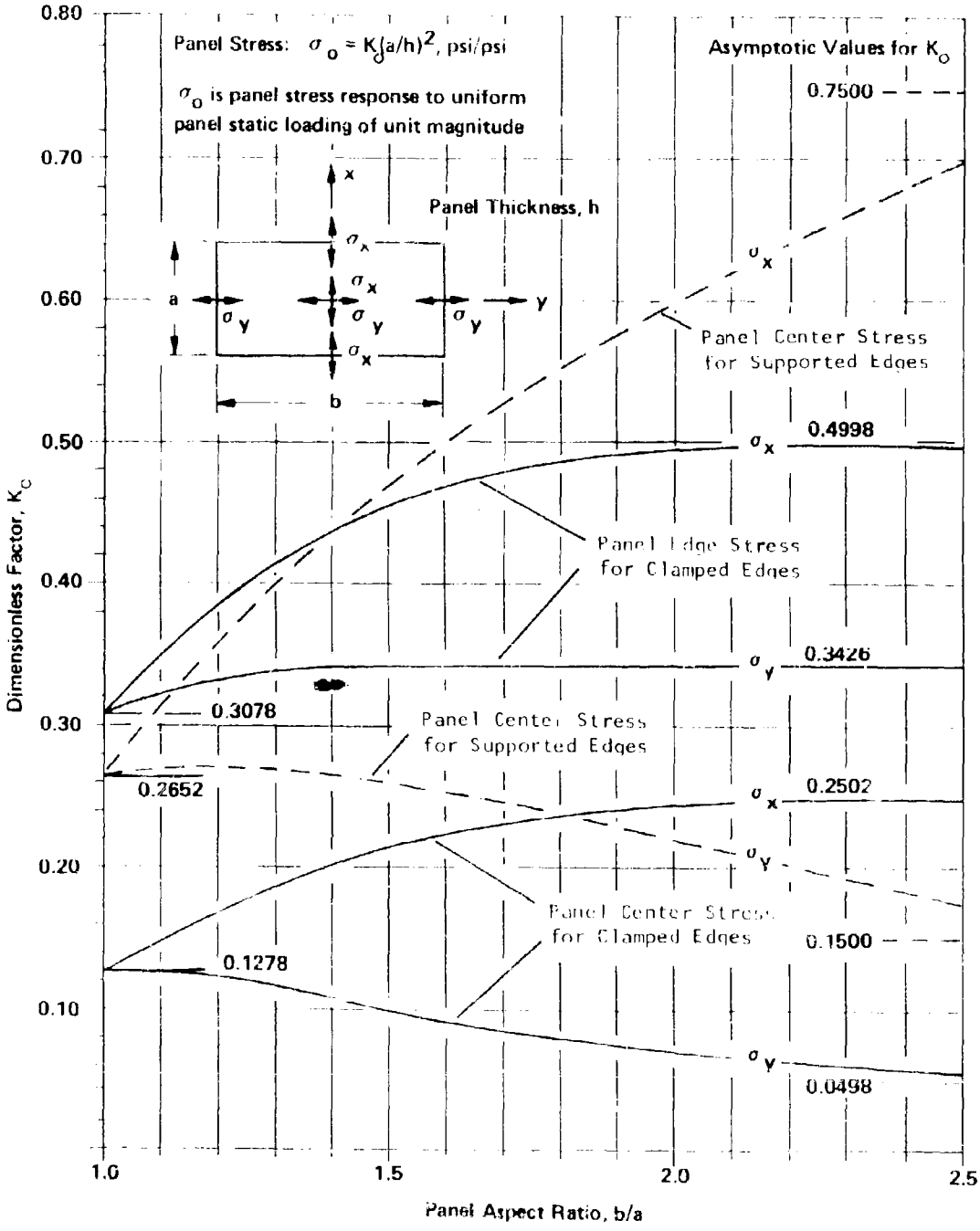

FIGURE 5.2.2-23 NOMOGRAPH FOR CALCULATING DIMENSIONLESS STRESS FACTOR FOR A UNIT MAGNITUDE UNIFORM STATIC PRESSURE ($\nu = 0.2$)

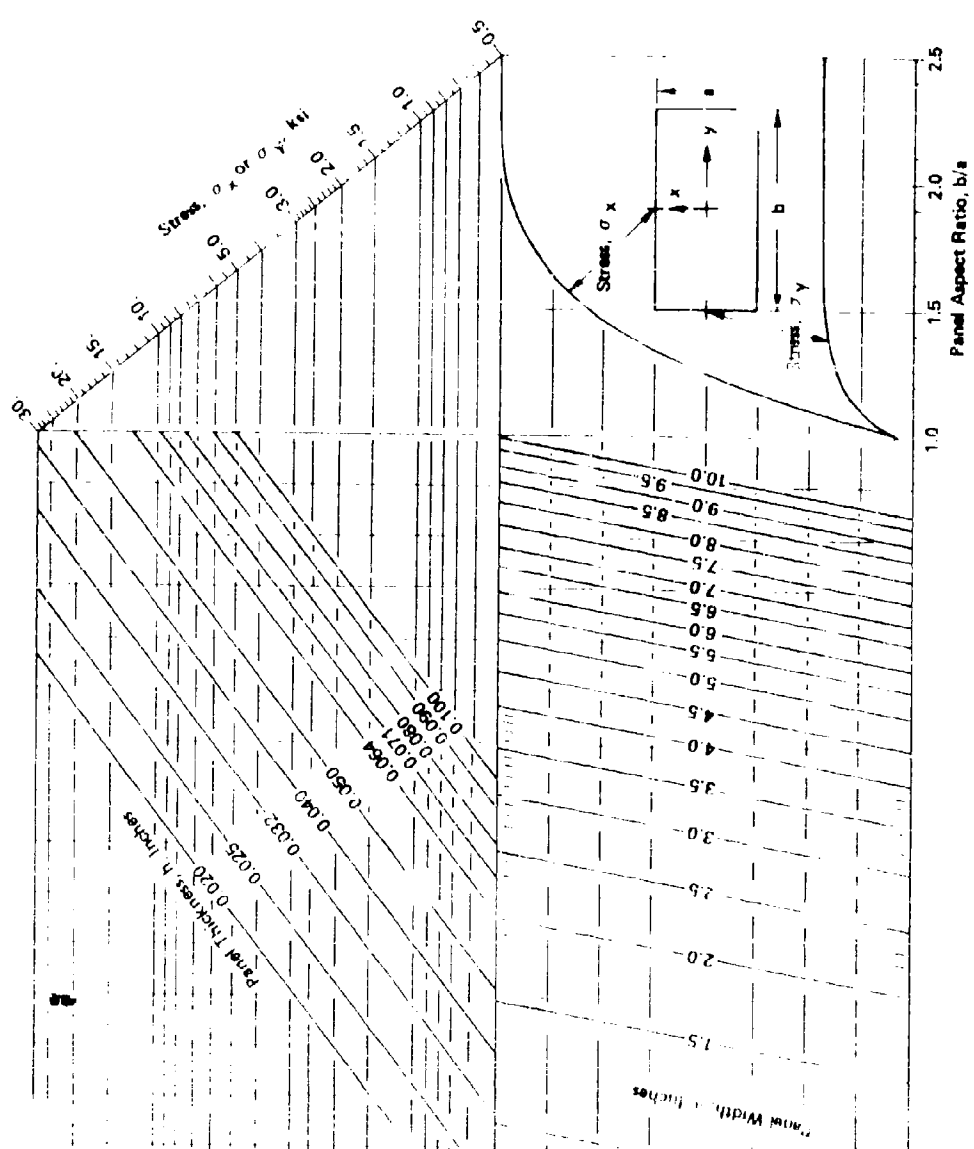

FIGURE 5.2.2-24 NOMOGRAPH FOR CALCULATING STRESS RESPONSE OF PLATE IN KSI DUE TO A UNIFORM STATIC PRESSURE OF UNIT MAGNITUDE IN PSI

For a plate with aspect ratio b/a = 1.5, one can use either Table 5.2.2-5 or Figure 5.2.2-24. For each position the parameter $(a/h)^2 = 3.516 \times 10^4$ is required and one obtains the following result.

At the center of the long side of the plate for clamped edges

$$\sigma_x = 3.516\times10^4(-0.4542) = -1.597\times10^4 \text{ psi} = -15.97 \text{ ksi}$$

(From Figure 5.2.2-24 the value is -15 ksi)

At the center of the short side of the plate for clamped edges

$$\sigma_y = 3.516\times10^4(-0.3420) = -1.202\times10^4 \text{ psi} = -12.02 \text{ ksi}$$

(From Figure 5.2.2-24 the value is -11 ksi).

At the center of the plate for clamped edges

$$\sigma_x = 3.516\times10^4(0.2148) = 7.55\times10^3 \text{ psi} = 7.55 \text{ ksi}$$

$$\sigma_y = 3.516\times10^4(0.1014) = 3.57\times10^3 \text{ psi} = 3.57 \text{ ksi}$$

and for supported edges

$$\sigma_x = 3.516\times10^4(0.4204) = 1.654\times10^4 \text{ psi} = 16.54 \text{ ksi}$$

$$\sigma_y = 3.516\times10^4(0.2556) = 8.987\times10^3 \text{ psi} = 8.99 \text{ ksi}.$$

5.2.2.2.6 Response of Plates to Random Pressure Loading

This section presents the development of the theory required to apply the general analysis of Section 5.3.1 to plate-like structures exposed to pressure loading. The magnitude of the pressure loading is assumed to vary randomly in both time and space (position on the plate). This loading results in stresses the magnitude of which also varies randomly with time. It is assumed that the excitation pressures are a stationary and ergodic random process with a Gaussian (normal) probability distribution. Linear small deflection plate theory is assumed to apply so that the panel stress response exhibits a Gaussian (normal) probability distribution. Hence, the emphasis of this section is to obtain estimates of the mean square values of the various quantities of interest.

Particular emphasis shall be placed upon additional assumptions required during the development of simplified results from general expressions. The significance of modal coupling resulting from either the pressure loading or the damping exhibited by the structure is explained so that the designer will appreciate the importance of the approximations. The results presented in Section 4.0 for loading actions are integrated with the results presented previously for estimating natural frequencies and stress to obtain the random response of the plate.

Derivation: The development presented here is based upon the analysis of Powell (16) and the excellent paper by Clarkson (4) with results quoted from Eringen (17) and Wagner (18). General results are presented first with the expressions then specialized to the case of rectangular plates. The normal mode method is used to emphasize the approximations required to obtain simplified results. Emphasis is placed upon simplified results since most empirical design equations, and the resulting nomographs, are based upon these simplifications. These results allow the designer to apply basic theory of Section 5.2 to his particular situation when the structural configuration differs significantly from the available design techniques presented in Section 5.3.

When a continuous structure, such as an aircraft fuselage or control surface, is excited by broad band random pressures the resulting structural vibration can be treated as the summation of responses in a large number of modes. The resulting structural response will, in general, appear to be broad band. For some structures, however, only a few modes or only a single mode may predominate the response. If the latter case is the situation, then many simplifications are possible and useful approximate results are obtained.

Using the normal mode method, it is assumed that the transverse displacement of the structure surface can be expressed as a summation of the normal modes of vibration of the structure as follows:

$$W(\bar{x},t) = \sum_r W_r(\bar{x})\xi_r(t) \qquad (5.2.2\text{-}27)$$

where $\bar{x}$ is a point on the surface, $W_r(\bar{x})$ is the mode shape of the r^{th} mode, and $\xi_r(t)$ is the generalized coordinate of the r^{th} mode.

Following standard techniques, such as described in Section 5.1.2, the spectral density of the displacement at point $\bar{x}$ on the surface of the structure can be expressed in terms of the assumed normal modes of the structure, the dynamic characteristics of the structure, and the characteristics of the pressure field as:

$$G_W(\bar{x},\omega) = \sum_r \sum_s W_r(\bar{x})W_s(\bar{x})\Omega_{rs}(\omega) \qquad (5.2.2\text{-}28a)$$

where

$$\Omega_{rs}(\omega) = \frac{H_r(\omega)H_s^*(\omega)}{M_r M_s} \int_{A_1}\int_{A_2} W_r(\bar{x}_1)W_s(\bar{x}_2)G_p(\bar{x}_1,\bar{x}_2,\omega)\,dA(\bar{x}_1)\,dA(\bar{x}_2) \qquad (5.2.2\text{-}28b)$$

M_r is the generalized mass of the r^{th} mode

$H_r(\omega) = 1/(\omega_r^2 - \omega^2 + 2i\zeta_r\omega_r\omega)$, for viscous damping

$H_r(\omega) = 1/(\omega_r^2 - \omega^2 + i\eta_r\omega_r^2)$, for hysteretic damping

$H_r^*(\omega)$ = complex conjugate of $H_r(\omega)$

$\omega_r = 2\pi f_r$ is the undamped natural frequency of the r^{th} mode

$G_p(\bar{x}_1, \bar{x}_2, \omega)$ is the cross-spectral density of the excitation pressure of the points $\bar{x}_1$ and $\bar{x}_2$

$i = \sqrt{-1}$.

Similar to Equation (5.2.2-28), the general expression for the spectral density of velocity is

$$G_{\dot{w}}(\bar{x},\omega) = \sum_r \sum_s W_r(\bar{x})W_s(\bar{x})\omega^2\Omega_{rs}(\omega) \quad . \tag{5.2.2-29}$$

The spectral density of acceleration is

$$G_{\ddot{w}}(\bar{x},\omega) = \sum_r \sum_s W_r(\bar{x})W_s(\bar{x})\omega^4\Omega_{rs}(\omega) \quad . \tag{5.2.2-30}$$

and the spectral density of stress is

$$G_\sigma(\bar{x},\omega) = \sum_r \sum_s L(W_r(\bar{x}))\cdot L(W_s(\bar{x}))\Omega_{rs}(\omega) \tag{5.2.2-31}$$

where $\sigma(\bar{x}) = L(W_r(\bar{x}))$ is the stress at $\bar{x}$ and

$L(\ )$ is a linear operator relating stress to displacement.

The mean square spectral density of a quantity is obtained by integrating the spectral density expression over all frequencies. That is, the mean square displacement response is

$$\overline{w^2(\bar{x},t)} = \int_0^\infty G_w(\bar{x},\omega)d\omega = \sum_r \sum_s W_r(\bar{x})W_s(\bar{x})\int_0^\infty \Omega_{rs}(\omega)d\omega \tag{5.2.2-32}$$

and the expressions for the mean square velocity, acceleration, and stress are, respectively

$$\overline{\dot{w}^2(\bar{x},t)} = \sum_r \sum_s W_r(\bar{x})W_s(\bar{x})\int_0^\infty \omega^2\Omega_{rs}(\omega)d\omega \tag{5.2.2-33}$$

$$\overline{\ddot{w}^2(\bar{x},t)} = \sum_r \sum_s W_r(\bar{x})W_s(\bar{x})\int_0^\infty \omega^4\Omega_{rs}(\omega)d\omega \tag{5.2.2-34}$$

$$\overline{w^2(\bar{x},t)} = \sum_r \sum_s L(W_r(\bar{x})) \cdot L(W_s(\bar{x})) \int_0^\infty \Omega_{rs}(\omega) d\omega \qquad (5.2.2\text{-}35)$$

Three difficulties arise in attempting to apply the theory to obtain practical results. First, one must consider the number of terms used to approximate the surface deflection as expressed in Equation (5.2.2-27). In general, many terms must be taken; however, the simplest case of a single term is often a reasonable assumption for approximating experimentally observed response data. It is now logical to describe the various physical situations that will allow one to retain only a few terms or, indeed, a single term for the plate displacement $w(\bar{x},t)$ and, hence, all other response quantities.

From Equation (5.2.2-28), the expression for the displacement spectral density function comprises a product of assumed modes and a modal coupling term $\Omega_{rs}(\omega)$. The term $\Omega_{rs}(\omega)$ is comprised of a product of terms $H_r(\omega)H_s^*(\omega)$ that describe the coupled mechanical frequency response of the system and an integration over the area of the plate that describes the modal coupling resulting from the form of the pressure loading. To determine the significance of the coupling terms, one must now consider the effects of both mechanical coupling, $H_r(\omega)H_s^*(\omega)$, and the structural-pressure coupling (joint acceptance) terms.

Finally, to obtain simplified results, the integrations in the frequency domain, as indicated in Equations (5.2.2-32) through (5.2.2-35), must be obtainable in a reasonably simple form (i.e., numerical integration must be avoided: See Robson (19)).

The first approximation involves the coupling terms $H_r(\omega)H_s^*(\omega)$. It is assumed that the natural frequencies ω_r and ω_s are well separated in frequency and that the modal damping factors ζ_r, ζ_s or η_r, η_s are small enough such that the modes appear uncoupled. Figure 5.2.2-25 illustrates the effect of spacing of natural frequencies and modal damping ($\eta_1 = \eta_2$) on the magnitude of the coupling terms as reported by Robson (19). Figure 5.2.2-25a illustrates the case of equal natural frequencies, $\omega_1 = \omega_2$, and Figure 5.2.2-25b is for $\omega_2 = 1.5\,\omega_1$. It should be noted that typical values for η_1 are more on the order of 0.03 than the values used by Robson so that in practice the response curves are much more sharply peaked at resonance. For widely separated natural frequencies, the coupling terms $H_r(\omega)H_s^*(\omega)$ are small and the direct modal response terms, $H_r(\omega)H_r^*(\omega)$, are all that one need to consider provided that the pressure structural response coupling is also small.

To understand the significance of the pressure-structural coupling it is necessary to know the form of the cross spectral density of the excitation pressure, $G_p(\bar{x}_1, \bar{x}_2, \omega)$. In many cases, it is reasonable to assume

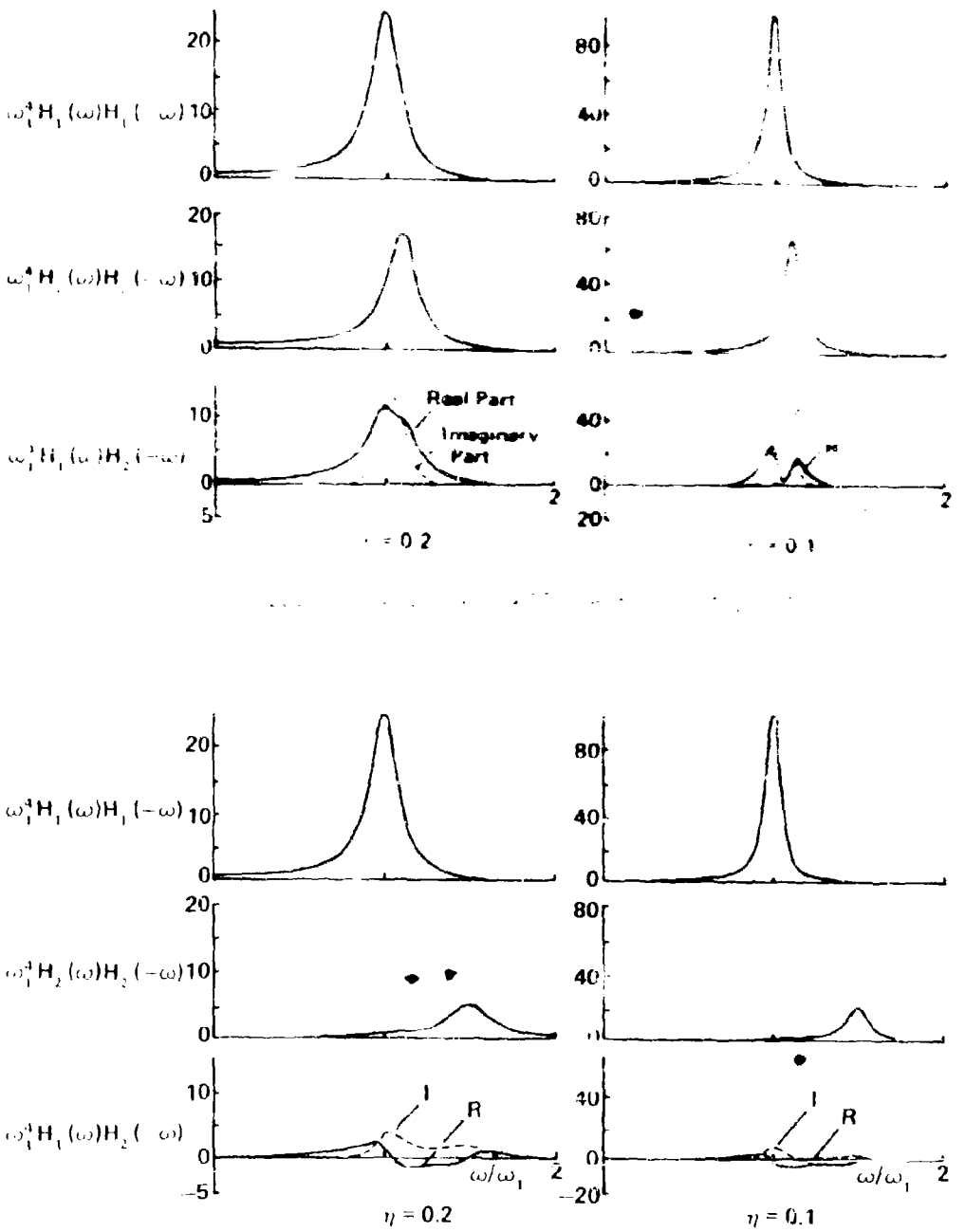

(b) Spectral Response Coefficients ($\omega_2/\omega_1 = 1.5$)

FIGURE 5.2.2 25 PLOTS OF MODAL COUPLING RESPONSE VERSUS FREQUENCY RATIO FOR A TWO DEGREE OF FREEDOM SYSTEM (REF. 19)

that the pressure field is homogeneous. That is, the pressure cross-spectral density is a function only of the separation distance, $\bar{r} = \bar{x}_2 - \bar{x}_1$, between the points $\bar{x}_1$ and $\bar{x}_2$. Further, it is convenient to separate explicitly the space coordinates and the frequency dependence of the pressure cross-spectral density so that for a homogeneous pressure field, one obtains the form

$$G_p(\bar{x}_1, \bar{x}_2, \omega) = G_p(\omega)d(\bar{r}) \qquad (5.2.2\text{-}36)$$

In using Equation (5.2.2-36), it has been assumed that the direct spectral density of the pressure, $G_p(\omega)$, is the same at each point on the surface of the structure and that the narrow (frequency) band space correlation coefficient, $d(\bar{r})$, has been normalized by the spectral density ($d(r)$ will take on values in the range ± 1). The utility of this representation is that the frequency can be explicitly removed from the integration required to obtain $S_{rs}(\omega)$ which yields

$$S_{rs}(\omega) = \frac{H_r(\omega)H_s^*(\omega)G_p(\omega)}{M_r M_s} \int_{A_1}\int_{A_2} W_r(\bar{x}_1)W_s(\bar{x}_2)d(\bar{x}_2-\bar{x}_1)dA(\bar{x}_1)dA(\bar{x}_2) \qquad (5.2.2\text{-}37)$$

The integral appearing in Equation (5.2.2-37) is a modified form of the "crossjoint acceptance" of the pressure-structure coupling as originated by Powell (16).

For most aircraft configurations, the direct spectral density of the excitation pressure, $G_p(\omega)$, varies considerably over the surface of the aircraft as a result of the strong directional characteristics of jet noise (See Figure 4.2.2-6) If one considers a small section of the aircraft surface (typically less than $2.5D^2$, D = diameter of jet exhaust nozzle), such as a single plate or array of plates, it is reasonable to assume that the spectral density of the excitation pressure is constant in magnitude over the surface of the plate.

Considering the narrow band space correlation coefficient, $d(\bar{r})$, one assumption that has found application in theoretical studies of plate response to boundary layer excitation has been to assume that $d(\bar{r})$ is a Dirac delta function in space so that the double area integration indicated in Equation (5.2.2-37) reduces to a single integration of the square of the mode shape (which cancels with a generalized mass term) and the double summation in Equation (5.2.2-28) reduces to a single summation of direct terms (17). More realistically, however, for boundary layer excitation $d(\bar{r})$ is of the form of a damped exponential wave so that the modes are highly coupled. Bozich (20) presents such a result wherein a complicated explicit expression for the "cross joint acceptance" is obtained. Reviewing the results of Section 4.3.3 one sees that boundary layer excitation generally is not amenable to a simplified structural response analysis since the modes are, in general, highly coupled (see for example the paper by Coe and Chyu (21)).

In the case of jet noise, the spatial scale of the correlation coefficient is on the same order as the mode wave length resulting in modal coupling. In practice, however, the structural damping is very small and the resonance effect will dominate the response. Hence, for jet noise the modal coupling terms will be small except for the case of closely spaced natural frequencies. Mercer (22) has investigated the effect of including the coupling terms for the case of a continuous beam on many supports excited by acoustic pressures (the response frequency spectrum is similar to a row of coupled plates). Typically, coupling terms contributed only 5 to 10 percent to the overall rms response level. It is, in general, sufficiently accurate to neglect the cross terms due to the relatively small errors accruing from this approximation. Generally, one must still consider many of the direct terms as being potentially significant since broadband acoustic excitation may excite many modes.

Neglecting the cross terms, one obtains from Equations (5.2.2-28) the simplified expression for the spectral density of displacement, for example, as

$$G_w(\bar{x},\omega) = \sum_r W_r^2(\bar{x})\Omega_{rr}(\omega) \qquad \text{in}^2\text{-sec/radian} \qquad (5.2.2\text{-}38)$$

where

$$\Omega_{rr}(\omega) = \frac{G_p(\omega)}{M_r^2}\,|H_r(\omega)|^2 \int_{A_1}\int_{A_2} W_r(\bar{x}_1)W_r(\bar{x}_2)\,d(\bar{x}_2-\bar{x}_1)\,dA(\bar{x}_1)\,dA(\bar{x}_2)$$

Similarly, the expressions for the mean square response quantities are obtained for displacement as

$$\overline{w^2(x,t)} = \sum_r W_r^2(\bar{x}) \int_0^\infty \Omega_{rr}(\omega)\,d\omega \qquad \text{in}^2 \qquad (5.2.2\text{-}39)$$

for velocity as,

$$\overline{\dot{w}^2(\bar{x},t)} = \sum_r W_r^2(\bar{x}) \int_0^\infty \omega^2\Omega_{rr}(\omega)\,d\omega \qquad (\text{in/sec})^2 \qquad (5.2.2\text{-}40)$$

for acceleration as

$$\overline{\ddot{w}^2(\bar{x},t)} = \sum_r W_r^2(\bar{x}) \int_0^\infty \omega^4\Omega_{rr}(\omega)\,d\omega \qquad (\text{in/sec}^2)^2 \qquad (5.2.2\text{-}40)$$

and for stress as

$$\overline{\sigma^2(\bar{x},t)} = \sum_r L^2(W_r(\bar{x})) \int_0^\infty \Omega_{rr}(\omega)\,d\omega \qquad (\text{psi})^2 \qquad (5.2.2\text{-}41)$$

$$L^2(W_r(\bar{x})) = L(W_r(x)) \cdot L(W_r(\bar{x}))$$

To obtain results one requires integrations of the form $\int_{\omega} F(\omega)d\omega$ or more explicitly

$$\int_0^\infty |H_r(\omega)|^2 G_p(\omega)d\omega \qquad (5.2.2\text{-}42a)$$

$$\int_0^\infty \omega^2 |H_r(\omega)|^2 G_p(\omega)d\omega \qquad (5.2.2\text{-}42b)$$

$$\int_0^\infty \omega^4 |H_r(\omega)|^2 G_p(\omega)d\omega \qquad (5.2.2\text{-}42c)$$

which are all functions of the natural frequency, ω_r, and the modal damping ζ_r or η_r. From Equation (5.2.2-28) one obtains for viscous damping

$$|H_r(\omega)|^2 = H_r(\omega)H_r^*(\omega) = ((\omega_r^2 - \omega^2)^2 + 4\zeta_r^2\omega_r^2\omega^2)^{-1} \qquad (5.2.2\text{-}43a)$$

and for hysteretic damping

$$|H_r(\omega)|^2 = H_r(\omega)H_r^*(\omega) = ((\omega_r^2 - \omega^2)^2 + \eta_r^2\omega_r^4)^{-1}. \qquad (5.2.2\text{-}43b)$$

For small damping in each mode ($\zeta_r \leq 0.05$), the response curves will be highly peaked so that with the assumption of well separated frequencies one can simplify the above integrations if $G_p(\omega)$ can be considered to be constant in the frequency band surrounding each resonance peak. With this approximation, one can obtain explicit integrations as follows

$$\int_0^\infty |H_r(\omega)|^2 G_p(\omega)d\omega = G_p(\omega_r)\int_0^\infty |H_r(\omega)|^2 d\omega = \frac{\pi G_p(\omega_r)}{4\zeta_r\omega_r^3} \qquad (5.2.2\text{-}44a)$$

$$\int_0^\infty \omega^2 |H_r(\omega)|^2 G_p(\omega)d\omega = G_p(\omega_r)\int_0^\infty \omega^2 |H_r(\omega)|^2 d\omega = \frac{\pi G_p(\omega_r)}{4\zeta_r\omega_r} \qquad (5.2.2\text{-}44b)$$

$$\int_0^\infty \omega^4 |H_r(\omega)|^2 G_p(\omega)d\omega = G_p(\omega_r)\int_0^\infty \omega^4 |H_r(\omega)|^2 d\omega = \pi\omega_r(1+4\zeta_r^2)G_p(\omega_r)/4\zeta_r \qquad (5.2.2\text{-}44c)$$

where $|H_r(\omega)|^2$ has the form of Equation (5.2.2-43a). To obtain similar results for light hysteretic damping one can substitute $\zeta_r = \eta_r/2$.

Typically, suitable values for the modal damping ratios are $0.005 \leq \zeta_r \leq 0.05$ so that the above results are valid for all types of aircraft structure (see Section 5.3) with the only restriction being that the natural frequencies be well separated and that the excitation spectral density $G_p(\omega)$ varies slowly with frequency.

More general forms of the integrations given in Equation (5.2.2-42) are presented by James (23), and by Crandall (14, p. 72) for $G_p(\omega)$ can

be expressed as a polynomial in ω. Wagner and Rama Baht (18) presents the results for such integrations for an exponential form of the excitation power spectral density illustrating the complicated form of the response power spectral density when modal coupling is important.

Substituting from Equation (5.2.2-44) into the expression for the mean square displacement response spectral density, Equation (5.2.2-39) one obtains

$$\overline{w^2(\bar{x},t)} = \sum_r \frac{\pi I_{rr} G_p(\omega_r)}{4\zeta_r \omega_r^3 M_r^2} W_r^2(\bar{x}) \quad in^2 \qquad (5.2.2\text{-}45)$$

where $$I_{rr} = \int_{A_1}\int_{A_2} W_r(\bar{x}_1) W_r(\bar{x}_2) d(\bar{x}_2 - \bar{x}_1) dA(\bar{x}_1) dA(\bar{x}_2)$$

Similarly, one obtains the expressions for the mean square values of the velocity, acceleration, and stress mean square spectral density as

$$\overline{\dot{w}^2(\bar{x},t)} = \sum_r \frac{\pi I_{rr} G_p(\omega_r)}{4\zeta_r \omega_r M_r^2} W_r^2(\bar{x}) \quad (in/sec)^2 \qquad (5.2.2\text{-}46)$$

$$\overline{\ddot{w}^2(\bar{x},t)} = \sum_r \frac{\pi \omega_r}{4\zeta_r M_r^2} (1 + 4\zeta_r^2) I_{rr} G_p(\omega_r) W_r^2(\bar{x}) \quad (in/sec^2)^2 \qquad (5.2.2\text{-}47)$$

and

$$\overline{\sigma^2(\bar{x},t)} = \sum_r \frac{\pi I_{rr} G_p(\omega_r)}{4\zeta_r \omega_r^3 M_r^2} L^2(W_r(\bar{x})) \quad (psi)^2 \qquad (5.2.2\text{-}48)$$

The next simplification involves the form of the integral I_{rr}, Equation (5.2.2-45). If the pressures are exactly in phase over the whole plate, then $d(\bar{x}_2 - \bar{x}_1) \equiv 1.0$ and one obtains

$$I_{rr} = \left[\int_{A_1} W_r(\bar{x}_1) dA(\bar{x}_1)\right]^2 \qquad (5.2.2\text{-}49)$$

It can be shown that the displacement response, $w_o(\bar{x})$, of the plate to a uniform static pressure of unit magnitude at a point on the surface, $\bar{x}$, can be written in the form

$$w_o(\bar{x}) = \sum_r W_{or}(\bar{x}) \qquad (5.2.2\text{-}50)$$

where $$W_{or}(\bar{x}) = \frac{1}{\omega_r^2 M_r} \int_{A_1} W_r(\bar{x}_1) dA(\bar{x}_1) W_r(\bar{x}) = \frac{\sqrt{I_{rr}}}{\omega_r^2 M_r} W_r(\bar{x})$$

Physically, $W_{or}(\bar{x})$ is the r^{th} component of the static displacement response.

Then, one can express Equations (5.2.2-45) through (5.2.2-48) formally as

$$\overline{w^2(\bar{x},t)} = \sum_r \frac{\pi\omega_r}{4\zeta_r} G_p(\omega_r) W_{or}^2(\bar{x}) \quad in^2 \qquad (5.2.2\text{-}51a)$$

$$\overline{\dot{w}^2(\bar{x},t)} = \sum_r \frac{\pi\omega_r^3}{4\zeta_r} G_p(\omega_r) W_{or}^2(\bar{x}) \quad (in/sec)^2 \qquad (5.2.2\text{-}51b)$$

$$\overline{\ddot{w}^2(\bar{x},t)} = \sum_r \frac{\pi\omega_r^5(1+4\zeta_r^2)}{4\zeta_r} G_p(\omega_r) W_{or}^2(\bar{x}) \quad (in/sec^2)^2 \qquad (5.2.2\text{-}51c)$$

and

$$\overline{\sigma^2(\bar{x},t)} = \sum_r \frac{\pi\omega_r}{4\zeta_r} G_p(\omega_r) \sigma_{or}^2(\bar{x}) \quad (psi)^2 \qquad (5.2.2\text{-}51d)$$

$$\sigma_{or}^2 = \frac{I_{rr}}{\omega_r^4 M_r^2} L^2(W_r(\bar{x})) = L^2(w_{or}(\bar{x})) \text{ psi/psi} \qquad (5.2.2\text{-}52)$$

The utility of the forms of Equations (5.2.2-51) is that the designer need be concerned only with determining the undamped response frequencies, ω_r, and the static displacements, $W_{or}(\bar{x})$, or the static stresses, $\sigma_{or}(\bar{x})$, at a point, $\bar{x}$, on the surface of the plate resulting from a uniform static pressure of unit magnitude using any convenient technique. Then, knowing the modal damping, ζ_r (0.02 is a good typical value), and the excitation pressure power spectral density, $G_p(\omega)$, for the range of frequencies, ω_r, the various mean square response quantities can be estimated. The only caution that the designer must exercise is that consistent units must be used in applying these results. For the development to this point is has been assumed that $G_p(\omega)$ has the units $(psi)^2$-sec/radian.

The results presented to this point have been obtained in terms of radian frequency, ω. From a practical standpoint, the design engineer requires expressions in circular frequency, f, in Hertz. To convert the previous results one must substitute $\omega_r = 2\pi f$ and $G_p(\omega_r) = G_p(f_r)/2\pi$ into Equations (5.2.2-51) to maintain consistent units. This result stems from the definition of the excitation spectral density function in terms of the mean square pressure level as

$$\overline{p^2(t)} = \int_0^\infty G_p(\omega)d\omega \quad \frac{1}{2\pi}\int_0^\infty G_p(f)df = \int_0^\infty \phi_p(f)df \qquad (5.2.2\text{-}53)$$

The pressure spectral density function $G_p(f)/2\pi$ or $\Phi_p(f)$ then has the units $(psi)^2/Hz$. The designer must always be aware of the definition of the excitation spectral density function to see that it is properly normalized.

Substituting $\omega_r = 2\pi f_r$ and $G_p(\omega_r) = G_p(f_r)/2\pi$ into Equations (5.2.2-51), one obtains for the mean square displacement

$$\overline{w^2(\bar{x},t)} = \sum_r \frac{\pi f_r}{4\zeta_r} G_p(f_r) W_{or}^2(\bar{x}) \quad in^2 \qquad (5.2.2\text{-}53a)$$

or

$$\overline{w^2(\bar{x},t)} = \sum_r \frac{\pi^2 f_r}{2\zeta_r} \Phi_p(f_r) W_{or}^2(\bar{x}) \quad in^2 \qquad (5.2.2\text{-}53a)$$

For the mean square velocity, one obtains

$$\overline{\dot{w}^2(\bar{x},t)} = \sum_r \frac{\pi^3 f_r^3}{\zeta_r} G_p(f_r) W_{or}^2(\bar{x}) \quad (in/sec)^2 \qquad (5.2.2\text{-}54a)$$

or

$$\overline{\dot{w}^2(\bar{x},t)} = \sum_r \frac{2\pi^4 f_r^3}{\zeta_r} \Phi_p(f_r) W_{or}^2(\bar{x}) \quad (in/sec)^2 \qquad (5.2.2\text{-}54b)$$

For the mean square acceleration, one obtains

$$\overline{\ddot{w}^2(\bar{x},t)} = \sum_r \frac{4\pi^5 f_r^5}{\zeta_r} (1 + 4\zeta_r^2) G_p(f_r) W_{or}^2(\bar{x}) \quad (in/sec^2)^2 \qquad (5.2.2\text{-}55a)$$

or

$$\overline{\ddot{w}^2(\bar{x},t)} = \sum_r \frac{8\pi^6 f_r^5}{\zeta_r} (1 + 4\zeta_r^2) \Phi_p(f_r) W_{or}^2(\bar{x}) \quad (in/sec^2)^2 \qquad (5.2.2\text{-}55b)$$

For the mean square stress, one obtains

$$\overline{\sigma^2(\bar{x},t)} = \sum_r \frac{\pi f_r}{4\zeta_r} G_p(f_r) \sigma_o^2(\bar{x}) \quad (psi)^2 \qquad (5.2.2\text{-}56a)$$

or

$$\overline{\sigma^2(\bar{x},t)} = \sum_r \frac{\pi^2 f_r}{2\zeta_r} \Phi_p(f_r) \sigma_o^2(\bar{x}) \quad (psi)^2 \qquad (5.2.2\text{-}56b)$$

where $$\sigma_o^2(\bar{x}) = \frac{I_{rr}}{\omega_r M_r^2} L^2(W_r(\bar{x})) \qquad (5.2.2\text{-}56c)$$

The usual manner in which the results of Equations (5.2.2-53) through (5.2.2-56) have been applied in practice is the form utilizing $G_p(f_r)$ as the excitation power spectral density function. If the estimated sound pressure level is in the form of a filtered band level (octave band, 1/3 octave band, etc.), then the appropriate expression for $G_p(f_r)$ is

$$G_p(f_r) = \overline{P}_{ref}^2 \times 10^{L/10} \qquad (5.2.2\text{-}57)$$

$$L = L_b - 10 \log \Delta f \ ,$$

L_b = band level of the noise with bandwidth Δf in which the resonant frequency, f_r, occurs.

$$P_{ref} = 0.0002 \text{ dynes/cm}^2 = 2.9 \times 10^{-9} \text{ psi}$$

The units of $G_p(f_r)$ are the units of $(P_{ref})^2$/Hz and one obtains

$$G_p(f_r) = 4\times10^{(L/10-8)} \ (\text{dynes/cm}^2)^2/\text{Hz} \qquad (5.2.2\text{-}58)$$

or

$$G_p(f) = 8.41\times10^{(L/10-18)} \ (\text{psi})^2/\text{Hz} \qquad (5.2.2\text{-}59)$$

The final simplification to be realized is that if only a single mode responds significantly then the summations in Equations (5.2.2-53) through (5.2.2-56) reduce to a single term. This approximation was first presented by Miles' (5) and its use has become known as "Miles' single degree-of-freedom" theory. This approximation is commonly used for all sonic fatigue analyses and the results are for the r^{th} mode (usually the fundamental mode)

$$\overline{w^2(\bar{x},t)} = \frac{\pi f_r}{4\zeta_r} G_p(f_r) W_{or}^2(\bar{x}) \qquad \text{in}^2 \qquad (5.2.2\text{-}60a)$$

$$\overline{\dot{w}^2(\bar{x},t)} = \frac{\pi^3 f_r^3}{\zeta_r} G_p(f_r) W_{or}^2(\bar{x}) \qquad (\text{in/sec})^2 \qquad (5.2.2\text{-}60b)$$

$$\overline{\ddot{w}^2(\bar{x},t)} = \frac{4\pi^5 f_r^5}{\zeta_r} (1+4\zeta_r^2) G_p(f_r) W_{or}^2(\bar{x}) \qquad (\text{in/sec}^2)^2 \qquad (5.2.2\text{-}60c)$$

$$\overline{\sigma^2(\bar{x},t)} = \frac{\pi f_r}{4\zeta_r} G_p(f_r)\sigma_o^2(\bar{x}) \quad (psi)^2 \qquad (5.2.2\text{-}60d)$$

$$\sigma_o^2(\bar{x}) = \frac{I_{rr}}{\omega_r^4 M_r^2} L^2(W_r(\bar{x})) \qquad (5.2.2\text{-}61)$$

$$I_{rr} = [\int_{A_1} W_r(\bar{x}_1)dA(\bar{x}_1)]^2$$

It now remains to present the results of Equations (5.2.2-60) in the specific format associated with thin plates. In particular, rectangular thin plates with either all edges clamped or all edges simply supported will be considered. The results can easily be extended to any level of the previous derivation.

For thin rectangular isotropic plates, the assumed panel displacement function Equation (5.2.2-27) has the form

$$w(x,y,t) = \sqrt{ab} \sum_m \sum_n X_m(x)Y_n(y)\xi_{mn}(t) \quad in. \qquad (5.2.2\text{-}62)$$

where $X_m(x) = \sin(m\pi x/a)$ for supported edges

$= \cosh(C_m x/a) - \cos(C_m x/a) - \alpha_m(\sinh(C_m x/a) - \sin(C_m x/a))$ for clamped edges

$Y_n(x) = \sin(n\pi y/b)$ for supported edges

$= \cosh(C_n y/b) - \cos(C_n y/b) - \alpha_n(\sinh(C_n y/b) - \sin(C_n y/b))$ for clamped edges

$\alpha_m, \alpha_n, C_m, C_n$ are constants defined in Table 5.2.2-1.

For clamped edges, $X_m(x)$ and $Y_n(y)$ are taken as the modes of a clamped-clamped beam (6).

From Equation (5.2.2-50), the modal mass is

$$M_{mn} = \rho hab \int_o^a \int_o^b X_m^2(x)Y_n^2(y)dydx \qquad (5.2.2\text{-}63)$$

$= \rho ha^2b^2/4$ for supported edges

$= \rho ha^2b^2$ for clamped edges

The radian frequency, $\omega_{mn} = 2\pi f_{mn}$, is given by Equations (5.2.2-1) and (5.2.2-2) or can be obtained from Figures 5.2.2-7 through -10.

Assuming that the excitation pressures are exactly in phase over the whole plate then fror Equation (5.2.2-49)

$$I_{mn} = ab\left[\int_0^a \int_0^b X_m(x)Y_n(y)dydx\right]^2 \qquad (5.2.2\text{-}64)$$

$$= \frac{a^3b^3}{\pi^4 m^2 n^2}\left[(-1)^m - 1\right]^2\left[(-1)^n - 1\right]^2 \quad \text{for supported edges}$$

$$= \left(\frac{4\alpha_m\alpha_n}{C_m C_n}\right)^2 a^3b^3\left[(-1)^m-1\right]^2\left[(-1)^n-1\right]^2 \quad \text{for clamped edges}$$

Then, from Equation (5.2.2-50) the static displacement response for the (m,n) mode of the plate for a uniform pressure of unit magnitude is

$$W_{omn}(x,y) = \frac{\sqrt{(I_{mn})}}{\omega_{mn}^2 M_{mn}}\sqrt{ab}\,X_m(x)Y_n(y) \qquad (5.2.2\text{-}64a)$$

For supported edges one obtains from Equation (5.2.2-64a)

$$W_{omn}(x,y) = \frac{4a^2b^2\left[(-1)^m-1\right]\left[(-1)^n-1\right]}{\pi^6 D_{mn}\left[m^2(b/a)+n^2(a/b)\right]^2}\sin(m\pi x/a)\sin(n\pi a/b) \qquad (5.2.2\text{-}64b)$$

$$= \frac{16a^2b^2\sin(m\pi x/a)\sin(n\pi y/b)}{\pi^6 D_{mn}\left[m^2(b/a)+n^2(a/b)\right]^2} \quad ; \; m,n = 1,3,5,\ldots \qquad (5.2.2\text{-}64c)$$

$$= 0; \quad m,n = 2,4,6,\ldots$$

For clamped edges one obtains

$$W_{omn}(x,y) = \frac{4\alpha_m\alpha_n a^2b^2\left[(-1)^m-1\right]\left[(-1)^n-1\right]}{\pi^6 D R_{mn} C_m C_n} X_m(x)Y_n(y) \qquad (5.2.2\text{-}64d)$$

$$= \frac{16\alpha_m\alpha_n a^2b^2}{\pi^6 D R_{mn} C_m C_n} X_m(x)Y_n(y); \; m,n = 1,3,\ldots \qquad (5.2.2\text{-}64e)$$

$$= 0; \quad m,n = 2,4,6,\ldots$$

where $R_{mn} = C_m^4(b/a)^2 + C_n^4(a/b)^2 + 2A_{mn}$

$X_m(x)$ and $Y_n(n)$ are defined by Equation (5.2.2-62) for clamped edges

$\alpha_m, \alpha_n, C_m, C_n$ are defined by Table 5.2.2-1

A_{mn} is defined by Equation (5.2.2-[illegible])

From Equations (5.2.2-64) it is seen that for a spatially uniform excitation pressure in phase over the surface of the plate that only the odd mode response, (m,n) = (1,1), (1,3), (3,1), etc., is predicted as being nonzero by the theory.

$$\overline{w^2(x,y,t)} = \frac{32a^3b^3}{10\sqrt{\rho hD^3}} \sum_m \sum_n \frac{G_p(f_{mn})\sin^2(m\pi x/a)\sin^2(n\pi y/b)}{\zeta_{mn} m^2 n^2 [m^2(b/a) + n^2(a/b)]^3} \quad in^2 \qquad (5.2.2\text{-}65a)$$

$$m,n = 1,3,5,\ldots$$

and for clamped edges

$$\overline{w^2(x,y,t)} = \frac{32a^3b^3}{\sqrt{\rho hD^3}} \sum_m \sum_n \frac{G_p(f_{mn})\alpha_m^2\alpha_n^2}{\zeta_{mn} C_m^2 C_n^2 R_{mn}^{3/2}} X_m^2(x) Y_n^2(y) \quad in^2 \qquad (5.2.2\text{-}65b)$$

$$m,n = 1,3,5,\ldots$$

$$R_{mn} = C_m^4(b/a)^2 + C_n^4(a/b)^2 + 2A_{mn}$$

From Equation (5.2.2-54a) and the above results one obtains the expression from the mean square velocity response for simply supported edges as

$$\overline{\dot{w}^2(x,y,t)} = \frac{32ab}{6\sqrt{(\rho h)^3 D}} \sum_m \sum_n \frac{G_p(f_{mn})\sin^2(m\pi x/a)\sin^2(n\pi y/b)}{\zeta_{mn} m^2 n^2 [m^2(b/a) + n^2(a/b)]} \quad (in/sec)^2 \qquad (5.2.2\text{-}66a)$$

$$m,n = 1,3,5,\ldots$$

and for clamped edges

$$\overline{\dot{w}^2(x,y,t)} = \frac{32ab}{\sqrt{(\rho h)^3 D}} \sum_m \sum_n \frac{G_p(f_{mn})\alpha_m^2\alpha_n^2}{\zeta_{mn} C_m^2 C_n^2 R_{mn}^{1/2}} X_m^2(x) Y_n^2(y) \quad (in/sec)^2 \qquad (5.2.2\text{-}66b)$$

$$m,n = 1,3,5,\ldots$$

From Equation (5.2.2-55a) and the above results one obtains the expression for the mean square acceleration response for simply supported edges as

$$\overline{\ddot{w}^2(x,y,t)} = \frac{32\sqrt{D/(\rho h)^5}}{ab^2} \sum_m \sum_n (1+4\zeta_{mn}^2)\frac{G_p(f_{mn})}{\zeta_{mn} m^2 n^2}[m^2(a/b)+n^2(a/b)]\sin^2(m\pi x/a)\cdot$$

$$\sin^2(n\pi y/b) \qquad m,n = 1,3,5... \qquad (5.2.2\text{-}67a)$$

and for clamped edges

$$\overline{\ddot{w}^2(x,y,t)} = \frac{32}{ab}\sqrt{D/(\rho h)^5} \sum_m \sum_n \frac{(1+4\zeta_{mn}^2)\alpha_m^2\alpha_n^2}{\zeta_{mn} C_m^2 C_n^2} G_p(f_{mn}) R_{mn}^{1/2} X_m^2(x) Y_n^2(y) \qquad (5.2.2\text{-}67b)$$

$$m,n = 1,3,5,...$$

To obtain expressions for the mean square stress response, the linear operator appearing in Equation (5.2.2-56c) must be selected depending upon the type of stress of interest to the designer. For small deflection thin plate theory and plates of rectangular shape the linear operators for the direct bending stresses σ_x and σ_y and the shear stress τ_{xy} are, respectively

$$L_x(W_r(\bar{x})) = -\frac{6D}{h^2}[W_{r,xx} + \nu W_{r,yy}] \qquad (5.2.2\text{-}68a)$$

$$L_y(W_r(\bar{x})) = -\frac{6D}{h^2}[\nu W_{r,xx} + W_{r,yy}] \qquad (5.2.2\text{-}68b)$$

$$L_{xy}(W_r(\bar{x})) = -\frac{6D}{h^2}(1-\nu)W_{r,xy} \qquad (5.2.2\text{-}68c)$$

For simply supported edges $W_{mn}(x,y) = \sqrt{ab}\ \sin(m\pi x/a)\sin(n\pi y/b)$ and from Equations (5.2.2-68) one obtains for the $(m,n)^{th}$ mode $(m,n = 1,3,5,...)$

$$L_x(W_{mn}) = \frac{6\pi^2 D}{h^2\sqrt{ab}}[m^2(b/a) + \nu n^2(a/b)]\sin(m\pi x/a)\sin(n\pi y/b) \qquad (5.2.2\text{-}69a)$$

$$L_y(W_{mn}) = \frac{6\pi^2 D}{h^2\sqrt{ab}}[\nu m^2(b/a) + n^2(a/b)]\sin(m\pi x/a)\sin(n\pi y/b) \qquad (5.2.2\text{-}69b)$$

$$L_{xy}(W_{mn}) = -\frac{6\pi^2 D}{h^2\sqrt{ab}}(1-\nu)mn\cos(m\pi x/a)\cos(n\pi y/b) \qquad (5.2.2\text{-}69c)$$

Then, from Equation (5.2.2-56c) and the above results one obtains for the $(m,n)^{th}$ mode $(m,n = 1,3,5,...)$

$$\sigma^2_{ox}(x,y) = \frac{36(16)^2 a^2b^2[m^2(b/a) + \nu n^2(a/b)]^2}{\pi^8 h^4 m^2 n^2 [m^2(b/a) + n^2(a/b)]^4} \sin^2(m\pi x/a)\sin^2(n\pi y/b) \qquad (5.2.2\text{-}70a)$$

$$\sigma^2_{oy}(x,y) = \frac{36(16)^2 a^2b^2[\nu m^2(b/a) + n^2(a/b)]^2}{\pi^8 h^4 m^2 n^2 [m^2(b/a) + n^2(a/b)]^4} \sin^2(m\pi x/a)\sin^2(n\pi y/b) \qquad (5.2.2\text{-}70b)$$

$$\tau^2_{oxy}(x,y) = \frac{36(16)^2 a^2b^2(1-\nu)^2\cos^2(m\pi x/a)\cos^2(n\pi y/b)}{\pi^8 h^4 [m^2(b/a) + n^2(a/b)]^4} \qquad (5.2.2\text{-}70c)$$

Then, from Equation (5.2.2-56a) the expressions for the mean square stress response of a simply supported rectangular plate are

$$\overline{\sigma^2_x(x,y,t)} = \frac{1152ab}{\pi^6 h^4}\sqrt{D/\rho h}\sum_m\sum_n \frac{G_p(f_{mn})[m^2(b/a)+\nu n^2(a/b)]^2}{\zeta_{mn} m^2 n^2 [m^2(b/a)+n^2(a/b)]^3}\sin^2(m\pi x/a)\sin^2(m\pi y/b) \qquad (5.2.2\text{-}71a)$$

$$\overline{\sigma^2_y(x,y,t)} = \frac{1152ab}{\pi^6 h^4}\sqrt{D/\rho h}\sum_m\sum_n \frac{G_p(f_{mn})[\nu m^2(b/a)+n^2(a/b)]^2}{\zeta_{mn} m^2 n^2 [m^2(b/a)+n^2(a/b)]^3}\sin^2(m\pi x/a)\sin^2(n\pi y/b) \qquad (5.2.2\text{-}71b)$$

$$\overline{\tau^2_{xy}(x,y,t)} = \frac{1152ab}{\pi^6 h^4}\sqrt{D/\rho h}\,(1-\nu)^2\sum_m\sum_n \frac{G_p(f_{mn})\cos^2(m\pi x/a)\cos^2(n\pi y/b)}{\zeta_{mn}[m^2(b/a)+n^2(a/b)]^3} \qquad (5.2.2\text{-}71c)$$

with $m,n = 1,3,5,\ldots$

For a plate with clamped edges the mode shape for the $(m,n)^{th}$ mode is $W_{mn}(x,y) = \sqrt{ab}\,X_m(x)Y_n(y)$ where $X_m(x)$ and $Y_n(y)$ are clamped-clamped beam vibration modes defined by Equation (5.2.2-62). From Equations (5.2.2-68) one obtains for the $(m,n)^{th}$ mode

$$L_x(W_{mn}) = -\frac{6D}{h^2\sqrt{ab}} S_{xmn}(x,y) \qquad (5.2.2\text{-}72a)$$

$$L_y(W_{mn}) = -\frac{6D}{h^2\sqrt{ab}} S_{ymn}(x,y) \qquad (5.2.2\text{-}72b)$$

$$L_{xy}(W_{mn}) = -\frac{6D}{h^2\sqrt{ab}}(1-\nu)C_m C_n X'_m(x)Y'_n(y) \qquad (5.2.2\text{-}72c)$$

where $S_{xmn}(x,y) = C_m^2(b/a)X''_m(x)Y_n(y) + \nu C_n^2(a/b)X_m(x)Y''_n(y)$

$$S_{ymn}(x,y) = \nu C_n^2 (b/a) X_m''(x) Y_n(n) + C_n^2 (a/b) X_m(x) Y_n''(n)$$

$X_m'(x)$ denotes differentiation with respect to the argument of the mode function.

Then, from Equation (5.2.2-56c) and the above results one obtains the stress response in the $(m,n)^{th}$ mode due to a uniform static pressure of unit magnitude as

$$\sigma_{ox}^2(x,y) = \frac{36(16)^2 a^2 b^2 \alpha_m^2 \alpha_n^2}{h^4 C_m^2 C_n^2 R_{mn}^2} S_{xmn}^2(x,y) \qquad (5.2.2\text{-}73a)$$

$$\sigma_{oy}^2(x,y) = \frac{36(16)^2 a^2 b^2 \alpha_m^2 \alpha_n^2}{h^4 C_m^2 C_n^2 R_{mn}^2} S_{ymn}^2(x,y) \qquad (5.2.2\text{-}73b)$$

$$\tau_{oxy}^2(x,y) = \frac{36(16)^2 a^2 b^2 (1-\nu)^2 \alpha_m^2 \alpha_n^2}{h^4 R_{mn}^2} \left(X_m'(x) Y_n'(y)\right)^2 \qquad (5.2.2\text{-}73c)$$

From Equation (5.2.2-56c) and using Equations (5.2.2-73) the expressions for the mean square stress response of a rectangular plate with clamped edges are

$$\overline{\sigma_x^2(x,y,t)} = 1152 \frac{ab}{h^4} \sqrt{D/\rho h} \sum_m \sum_n \frac{G_p(f_{mn}) \alpha_m^2 \alpha_n^2}{\zeta_{mn} C_m^2 C_n^2 R_{mn}^{3/2}} S_{xmn}^2(x,y) \qquad (5.2.2\text{-}74a)$$

$$\overline{\sigma_y^2(x,y,t)} = 1152 \frac{ab}{h^4} \sqrt{D/\rho h} \sum_m \sum_n \frac{G_p(f_{mn}) \alpha_m^2 \alpha_n^2}{\zeta_{mn} C_m^2 C_n^2 R_{mn}^{3/2}} S_{ymn}^2(x,y) \qquad (5.2.2\text{-}74b)$$

$$\overline{\tau_{xy}^2(x,y,t)} = 1152 \frac{ab}{h^4} \sqrt{D/\rho h} (1-\nu)^2 \sum_m \sum_n \frac{G_p(f_{mn}) \alpha_m^2 \alpha_n^2}{\zeta_{mn} R_{mn}^{3/2}} \left(X_m'(x) Y_n'(y)\right)^2 \qquad (5.2.2\text{-}74c)$$

The previous results are summarized in Table 5.2.2-6 where the equation number for a mean square quantity are presented. These results assume that only the direct modal contributions to the total response are significant. In particular it has been assumed that the natural frequencies are widely separated, that the damping is light and that the excitation pressure spectral density function varies slowly with frequency about the natural frequencies.

TABLE 5.2.2-6

SUMMARY OF RESULTS FOR RESPONSE CALCULATIONS

TABLE OF EQUATION NUMBERS

Mean Square Quantity	All Edges Supported	All Edges Clamped
$\overline{w^2(x,y,t)}$, in^2	(5.2.2-65a) page 270	(5.2.2-65b) page 270
$\overline{\dot{w}^2(x,y,t)}$, $(in/sec)^2$	(5.2.2-66a) page 270	(5.2.2-66b) page 270
$\overline{\ddot{w}^2(x,y,t)}$, $(in/sec)^2$	(5.2.2-67a) page 271	(5.2.2-67b) page 271
$\overline{\sigma_x^2(x,y,t)}$, $(psi)^2$	(5.2.2-71a) page 272	(5.2.2-74a) page 273
$\overline{\sigma_y^2(x,y,t)}$, $(psi)^2$	(5.2.2-71b) page 272	(5.2.2-74b) page 273
$\overline{\sigma_{xy}^2(x,y,t)}$, $(psi)^2$	(5.2.2-71c) page 272	(5.2.2-74c) page 273

The final result is to assume that only the fundamental mode exhibits significant response. Then, for a simply supported plate one obtains

$$\overline{w^2(x,y,t)} = \frac{32a^3b^3}{\pi^{10}\sqrt{ab^3}} \cdot \frac{G_p(f_{11})\sin^2(\pi x/a)\sin^2(\pi y/b)}{\zeta_{11}[(b/a) + (a/b)]^3} \quad (in)^2 \qquad (5.2.2\text{-}75a)$$

$$\overline{\dot{w}^2(x,y,t)} = \frac{32ab}{\pi^6\sqrt{(ab)^3 D}} \cdot \frac{G_p(f_{11})\sin^2(\pi x/a)\sin^2(\pi y/b)}{\zeta_{11}[(b/a) + (a/b)]} \quad (in/sec)^2 \qquad (5.2.2\text{-}75b)$$

$$\overline{\ddot{w}^2(x,y,t)} = \frac{32\sqrt{b/(ab)^5}}{\pi^2 ab^2 \zeta_{11}}(1+4\zeta_{11}^2)G_p(f_{11})[(b/a)+(a/b)]\sin^2(\pi x/a)\sin^2(\pi y/b)$$

$$(in/sec^2)^2 \qquad (5.2.2\text{-}75c)$$

$$\overline{\sigma_x^2(x,y,t)} = \frac{1152ab}{\pi^6 h^4}\sqrt{D/ab}\cdot\frac{G_p(f_{11})[(b/a)+\nu(a/b)]^2}{\zeta_{11}[(b/a)+(a/b)]^3}\sin^2(\pi x/a)\sin^2(\pi y/b)$$

$$(psi)^2 \qquad (5.2.2\text{-}75d)$$

$$\overline{\sigma_y^2(x,y,t)} = \frac{1152ab}{\pi^6 h^4}\sqrt{D/\rho h}\;\frac{G_p(f_{11})[\nu(b/a)+(a/b)]^2}{\zeta_{11}[(b/a)+(a/b)]^3}\sin^2(\pi x/a)\sin^2(\pi y/b) \quad (psi)^2 \qquad (5.2.2\text{-}75e)$$

$$\overline{\tau_{xy}^2(x,y,t)} = \frac{1152ab}{\pi^6 h^4}\sqrt{D/\rho h}\;(1-\nu)^2\;\frac{G_p(f_{11})\cos^2(\pi x/a)\cos^2(\pi y/b)}{\zeta_{11}[(b/a)+(a/b)]^3} \quad (psi)^2 \qquad (5.2.2\text{-}75f)$$

For a plate with all edges clamped, one obtains from Table 5.2.2-1

$$\alpha_1 = 0.9825 \qquad C_1 = 4.73004$$

$$A_{11} = 151.3524 \qquad R_{11} = 151.3524[3.307(b/a)^2 + 3.307(a/b)^2 + 2.0]$$

and the mean square response quantities assuming only a fundamental mode response are

$$\overline{w^2(x,y,t)} = \frac{3.7892\cdot10^{-5}\,a^3b^3\,G_p(f_{11})X_1^2(x)Y_1^2(y)}{\sqrt{\rho h D^3}\,\zeta_{11}[3.307(b/a)^2 + 3.307(a/b)^2 + 2]^{3/2}} \quad in^2 \qquad (5.2.2\text{-}76a)$$

$$\overline{\dot{w}^2(x,y,t)} = \frac{4.8420\cdot10^{-3}\,ab\,G_p(f_{11})X_1^2(x)Y_1^2(y)}{\sqrt{(\rho h)^3 D}\,\zeta_{11}[3.307(b/a)^2 + 3.307(a/b)^2 + 2]^{1/2}} \quad (in/sec)^2 \qquad (5.2.2\text{-}76b)$$

$$\overline{\ddot{w}^2(x,y,t)} = 0.7329\sqrt{D/(\rho h)^5}\;\frac{(1+4\zeta_{11}^2)}{ab\zeta_{11}}\,G_p(f_{11})[3.307(b/a)^2+3.307(a/b)^2+2]^{1/2} \cdot X_1^2(x)Y_1^2(y) \quad (in/sec^2)^2 \qquad (5.2.2\text{-}76c)$$

$$\overline{\sigma_x^2(x,y,t)} = 1.152\cdot10^{-3}\;\frac{ab\sqrt{D/\rho h}\,G_p(f_{11})S_{x11}^2(x,y)}{h^4\zeta_{11}[3.307(b/a)^2 + 3.307(a/b)^2+2]^{3/2}} \quad (psi)^2 \qquad (5.2.2\text{-}76d)$$

$$\overline{\sigma_y^2(x,y,t)} = 1.152 \cdot 10^{-3} \frac{ab\sqrt{D/\rho h}\, G_p(f_{11}) S_{y11}^2(x,y)}{h^4 c_{11}[3.307(b/a)^2 + 3.307(a/b)^2 + 2]^{3/2}} \quad (psi)^2 \tag{5.2.2-76e}$$

$$\overline{\tau_{xy}^2(x,y,t)} = 0.57650 \frac{ab\sqrt{D/\rho h}(1-\nu)^2 G_p(f_{11})(X_1'(x)Y_1'(y))^2}{h^4 c_{11}[3.307(b/a)^2 + 3.307(a/b)^2 + 2]^{3/2}} \quad (psi)^2 \tag{5.2.2-76f}$$

In utilizing the results of Equations (5.2.2-76) the following quantities are presented for specific points on the surface of the plate (see Table B.1.1-5, page 551).

Center of Plate:

$$X_1^2(a/2)Y_1^2(b/2) = 6.36160 \tag{5.2.2-77a}$$

$$S_{x11}^2(a/2, b/2) = 1865.8[(b/a) + \nu(a/b)]^2 \tag{5.2.2-77b}$$

$$S_{y11}^2(a/2, b/2) = 1865.8[\nu(b/a) + (a/b)]^2 \tag{5.2.2-77c}$$

Approximate Location of Maximum Shear

$$(X_1'(0.22a)Y_1'(0.22b))^2 = 1.14389 \tag{5.2.2-77d}$$

Edge of Plate:

$$S_{x11}^2(0,b/2) = 5050.1(b/a)^2 \tag{5.2.2-77e}$$

$$S_{y11}^2(a/2,0) = 5050.1(a/b)^2 \tag{5.2.2-77f}$$

The previous results have been based upon the assumption that the excitation power spectral density function, $G_p(f)$, is constant or varies slowly with frequency in the vicinity of the resonant peak. From a practical standpoint, the excitation density are typically smoothed into spectra that appear as a series of straight lines on log-log plots. The slopes in regions of varying spectral density are generally given in terms of decibels per octave. Mathematically, the straight line log-log plots are governed by an equation of the form

$$\log G_p(\Omega) = \log G_p(1) + B \log \Omega \qquad (5.2.2\text{-}78a)$$

where $\Omega = f/f_r$, f_r is the resonant frequency of the r^{th} mode.

The above relationship can alternately be expressed as

$$G_p(\Omega) = G_p(1)\Omega^B \qquad (5.2.2\text{-}78b)$$

The exponent B is related to the dB/octave variation in level using the following procedure. If two frequencies Ω_1 and Ω_2 are n octaves apart then

$$\Omega_2/\Omega_1 = 2^n \qquad (5.2.2\text{-}79a)$$

or
$$n = \log(\Omega_2/\Omega_1)/\log 2 = 3.322 \log(\Omega_2/\Omega_1) \qquad (5.2.2\text{-}79b)$$

The decibel difference between the spectral densities at the two frequencies is

$$dB = 10 \log (G_p(\Omega_2)/G_p(\Omega_1)) \qquad (5.2.2\text{-}80a)$$

or
$$dB = 10\ B \log (\Omega_2/\Omega_1) \qquad (5.2.2\text{-}80b)$$

The dB/octave variation, N, is obtained from Equations (5.2.2-79b) and (5.2.2-80b) as

$$N = dB/n = 3.010B \simeq 3B \qquad (5.2.2\text{-}8\ )$$

Assuming resonant response of a system whose resonant bandwidth lies within the frequency band of excitation, the resonant bandwidth is taken as the effective random bandwidth, $\zeta_r/2$. Figure 5.2.2-26 presents a plot of normalized resonant response as a function of B for various values of the modal damping, ζ_r. That is, if the excitation spectrum as plotted on log-log paper, slopes in the vicinity of a resonant peak with a slope of N dB/octave, then the values for $G_p(f_r)$ appearing in Equations (5.2.2-53) through (5.2.2-75) must be multiplied by the factor indicated by Figure 5.2.2-26. To use this figure one determines N in the vicinity of the resonant response frequency, f_r, moves vertically to the value for modal damping, ζ_r, and proceeds to the left to determine the correction factor. It is noted that for light damping, $\zeta_r \leq 0.05$, less than a 10% error in estimating the resonant response will occur by assuming a constant spectrum level, $G_p(f_r)$.

The above results are from a paper by Pulgrano and Ablowitz (25). They present much more detailed calculation procedures for correcting "white noise" response calculations to account for irregular spectrum shape. In particular, they show how nonresonant response can become significant.

Note: 1. Resonant response is assumed to be the response within an effective bandwidth $\pi\zeta$ wide centered on the resonant frequency

2. N, dB/Octave = 3B

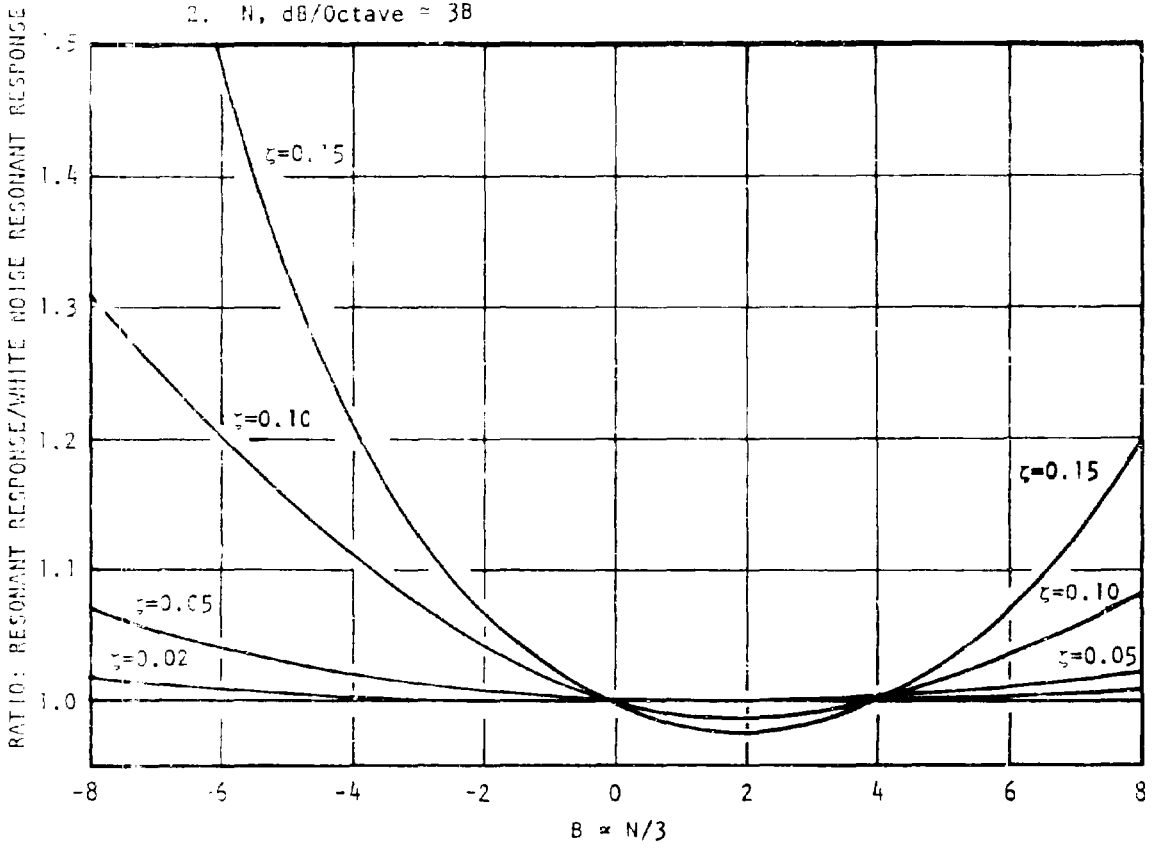

FIGURE 5.2.2-26 VARIATION IN RESONANT RESPONSE WITH ACOUSTIC EXCITATION SPECTRUM LEVEL SLOPING AT N dB/OCTAVE

Example: Using the results of Section 5.2.2.2.6 compute the mean square displacement, velocity, acceleration, and stress response of a rectangular plate exposed to jet noise excitation assuming both simply supported and clamped edge conditions. The data for the plate is as follows: $a = 6.0$ inches, $b = 12.0$ inches, $h = 0.032$ inch, $E = 10.3 \cdot 10^6$ psi, $\nu = 0.32$, and $\gamma = 0.101$ lbs/in^3. The jet noise excitation is assumed to result from a J57-P21 turbojet engine with afterburner operating with the plate located 4 nozzle diameters downstream and 3 nozzle diameters away from the jet axis (see Hermes and Smith (31), p. 76). Assume panel damping is $\zeta = 0.02$ for all modes.

From Section 5.2.2.2.1 the response frequencies for the plate are determined to be as follows

Mode No.	Supported Edges	Clamped Edges
(1,1)	$f_{11} = 105$ Hz.	$f_{11} = 222$ Hz.
(1,3)	$f_{13} = 273$ Hz.	$f_{13} = 437$ Hz.
(3,1)	$f_{31} = 777$ Hz.	$f_{31} = 1072$ Hz.
(3,3)	$f_{33} = 945$ Hz.	$f_{33} = 1354$ Hz.

For a panel with simply supported edges the mean square displacement response is obtained from Equation (5.2.2-65a), assuming for the moment that all odd-odd modes up to the (3,3) mode respond, as

$$\overline{w^2(x,y,t)} = 2.514 \cdot 10^2 [3.2000 G_p(f_{11}) \sin^2(\pi x/a) \sin^2(\pi y/b) + 0.0202 G_p(f_{13}) \sin^2(\pi x/a) \sin^2(3\pi y/b) + 0.00088 G_p(f_{31}) \sin^2(3\pi x/a) \sin^2(\pi y/b) + 0.000054 G_p(f_{33}) \sin^2(3\pi x/a) \sin^2(3\pi y/b)] \text{ (in)}^2$$

From Hermes and Smith (31), p. 76, the third octave band sound levels for frequency bands containing the response frequencies are presented below with the third octave band levels being converted to pressure spectrum levels using Equation (5.2.2-59) as follows

1/3 O.B. Center Frequency, Hz	1/3 O.B. Sound Level, dB	1/3 Octave* Bandwidth, Hz	$G_p(f)$ $(psi)^2/Hz$.
100	127	22.9	$1.841 \cdot 10^{-6}$
200	133	46.0	$3.648 \cdot 10^{-6}$
250	134	58.0	$3.642 \cdot 10^{-6}$
400	137	92.0	$4.582 \cdot 10^{-6}$
800	137	183.0	$2.303 \cdot 10^{-6}$
1000	136	231.0	$1.449 \cdot 10^{-6}$
1250	134	291.0	$7.259 \cdot 10^{-7}$

For simply supported edges

$$G_p(f_{11}) = G_p(105) = 1.841 \cdot 10^{-6}$$
$$G_p(f_{13}) = G_p(273) = 3.642 \cdot 10^{-6}$$
$$G_p(f_{31}) = G_p(777) = 2.303 \cdot 10^{-6}$$
$$G_p(f_{33}) = G_p(945) = 1.449 \cdot 10^{-6}$$

Then, the expression for the mean square displacement response is

$$\overline{w^2(x,y,t)} = 1.481 \cdot 10^{-3} [1.0000 \sin^2(\pi x/a)\sin^2(\pi y/b) + 0.0125 \sin^2(\pi x/a)\sin^2(3\pi y/b) + 0.00034 \sin^2(3\pi x/a)\sin^2(\pi y/b) + 0.00001 \sin^2(3\pi x/a)\sin^2(3\pi y/b)] \quad (in)^2$$

It is seen, for example, that at the center of the plate the fundamental mode contributes 98.7% to the total displacement response. Hence, the assumption of considering only the fundamental mode is appropriate.

From Equation (5.2.2-75b) the mean square velocity response, assuming only the fundamental mode responds, is

$$\overline{\dot{w}^2(x,y,t)} = 651.6 \sin^2(\pi x/a)\sin^2(\pi y/b) \quad (in/sec)^2$$

and the mean square acceleration response is obtained from Equation (5.2.2-75c) as

$$\overline{\ddot{w}^2(x,y,t)} = 2.871 \cdot 10^8 \sin^2(\pi x/a)\sin^2(\pi y/b) \quad (in/sec^2)^2$$
$$= 1.923 \cdot 10^3 \sin^2(\pi x/a)\sin^2(\pi y/b) \quad g^2$$

* See Table 2.1.1-1.

For simply supported edges, the mean square stress response is obtained from Equation (5.2.2-75d, -75e, and -75f) as

$$\overline{\sigma_x^2(x,y,t)} = 4.377\cdot 10^6 \sin^2(\pi x/a)\sin^2(\pi y/b) \quad (psi)^2$$

$$\overline{\sigma_y^2(x,y,t)} = 1.219\cdot 10^6 \sin^2(\pi x/a)\sin^2(\pi y/b) \quad (psi)^2$$

$$\overline{\tau_{xy}^2(x,y,t)} = 4.338\cdot 10^5 \cos^2(\pi x/a)\cos^2(\pi y/b) \quad (psi)^2$$

Assuming a fundamental mode response, for clamped edges the mean square response quantities are obtained from Equation (5.2.2-76) with the results being

$$\overline{w^2(x,y,t)} = 3.3683\cdot 10^{-5}\, X_1^2(x)Y_1^2(y)$$

$$\overline{\dot{w}^2(x,y,t)} = 59.145 X_1^2(x)Y_1^2(y)$$

$$\overline{\ddot{w}^2(x,y,t)} = 1.0403\cdot 10^8\, X_1^2(x)Y_1^2(y)$$

$$\overline{\sigma_x^2(x,y,t)} = 219.08\, S_{x11}^2(x,y)$$

$$\overline{\sigma_y^2(x,y,t)} = 219.08\, S_{y11}^2(x,y)$$

$$\overline{\tau_{xy}^2(x,y,t)} = 1.9103\cdot 10^5 (X_1'(x)Y_1'(y))^2$$

At the center of the plate, one obtains from Table B.1.1-5, page 551.

$$X_1^2(a/2)Y_1^2(b/2) = 6.3616$$

$$S_{x11}^2(a/2,\ b/2) = 8.705\cdot 10^3$$

$$S_{y11}^2(a/2,\ b/2) = 2.425\cdot 10^3$$

Then, at the center of the plate

$$\overline{w^2(a/2,\ b/2,\ t)} = 2.143\cdot 10^{-4} \quad (in)^2$$

$$\overline{\dot{w}^2(a/2,\ b/2,\ t)} = 376.3 \quad (in/sec)^2$$

$$\overline{\ddot{w}^2(a/2,\ b/2,\ t)} = 6.618 \cdot 10^8 \qquad (in/sec^2)^2$$

$$\overline{\sigma_x^2(a/2,\ b/2,\ t)} = 1.907 \cdot 10^6 \qquad (psi)^2$$

$$\overline{\sigma_y^2(a/2,\ b/2,\ t)} = 5.313 \cdot 10^5 \qquad (psi)^2$$

At the edge of the plate

$$S_{x11}^2(0,b/2) = 2.020 \cdot 10^4$$

$$S_{y11}^2(a/2,0) = 1.263 \cdot 10^3$$

and

$$\overline{\sigma_x^2(0,b/2,t)} = 4.425 \cdot 10^6 \qquad (psi)^2$$

$$\overline{\sigma_y^2(a/2,0,t)} = 2.766 \cdot 10^5 \qquad (psi)^2$$

5.2.2.3 Rectangular Specially Orthotropic Plates

This section provides design oriented methods for estimating the response of rectangular specially orthotropic plates to random acoustic loading. By the term "specially orthotropic" it is assumed that the plate material possesses three mutually perpendicular axes of elastic symmetry. Two of the axes are in the plane of the plate parallel to the respective sides of the plate. The third symmetry axis is normal to the other two and hence perpendicular to the plane of the plate. The plate thickness and its transverse displacement are taken to be small so that small deflection theory can be used.

Section 5.2.2.3.1 provides design equations for estimating the response frequencies of specially orthotropic rectangular plates with either all edges clamped or all edges simply supported. Section 5.2.2.3.2 provides design equations for estimating the displacement response and stress response for a plate to a uniform static pressure of unit magnitude assuming a fundamental mode response. Section 5.2.2.3.3 uses the results of the previous section and Equations 5.2.2-60 to estimate the response of the plate to random acoustic excitation.

General references for this section are Timoshenko (3), Ambartsumyan (26), and Ashton (27,28). For plates made of a material whose principal elastic axes are skewed with respect to the plate geometric axes one must resort to numerical techniques as described by Ashton (28) or Mohan and Kingsbury (29).

5.2.2.3.1 Estimation of Natural Frequencies

This section presents design equations for estimating the natural frequencies of rectangular specially orthotropic plates with all edges clamped or all edges simply supported.

Derivation: The Rayleigh Method for estimating the response frequency of an uncoupled mode of vibration was used by Hearmon (30) to extend Warburton's analysis for rectangular isotropic plates (see Section 5.2.2.2.1). The results for a plate with all edges simply supported is exact and yields a lower bound for the frequency estimate for the actual panel installation. The results for a plate with all edges clamped is obtained by assuming a plate mode shape in the form of clamped-clamped beam modes and yields an upper bound for the frequency estimate for the actual panel installation. Hearmon (30) presents results for all six possible combinations of clamped and supported edges. The plate geometry and material axis nomenclature are presented in Figure 5.2.2-27.

Design Equations: The design equations for the frequency of the $(m,n)^{th}$ mode of vibration of the plate are as follows:

All Edges Simply Supported

$$f_{mn}^2 = \frac{\pi^2}{4\rho h}\left[m^4 D_1/a^4 + n^4 D_2/b^4 + 2D_3 m^2 n^2/a^2 b^2\right] \quad Hz^2 \qquad (5.2.2\text{-}82)$$

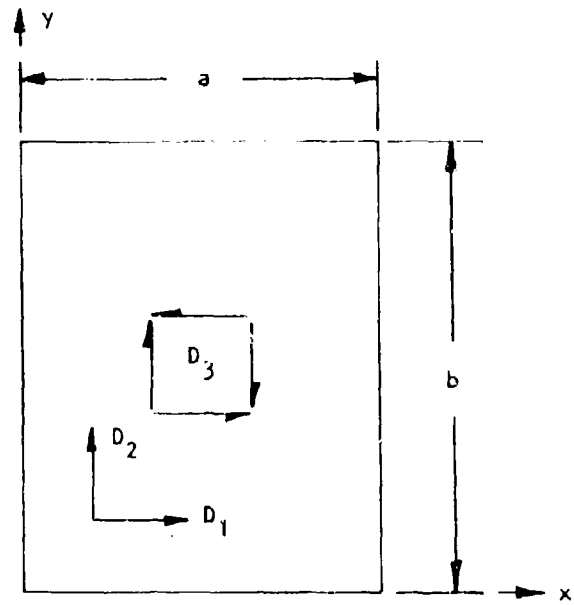

$$D_1 = \frac{E_{11}h^3}{12(1-\nu_{12}\nu_{21})} \qquad D_2 = \frac{E_{22}h^3}{12(1-\nu_{12}\nu_{21})}$$

$$D_3 = D_4 + 2D_{12} \qquad \nu_{21}E_{11} = \nu_{12}E_{22}$$

$$D_4 = \frac{\nu_{21}E_{11}h^3}{12(1-\nu_{12}\nu_{21})} \qquad D_{12} = \frac{G_{12}h^3}{12}$$

FIGURE 5.2.2-27 PLATE GEOMETRY, ELASTIC AXIS, AND BENDING STIFFNESS NOMENCLATURE FOR RECTANGULAR SPECIALLY ORTHOTROPIC PLATES

All Edges Clamped

$$f_{mn}^2 = \frac{1}{4\pi^2\rho h}\left[C_m^4 D_1/a^4 + C_n^4 D_2/b^4 + 2A_{mn}D_3/a^2b^2\right] \quad Hz^2 \qquad (5.2.2\text{-}83)$$

where $D_1 = \dfrac{E_{11}h^3}{12(1-\nu_{12}\nu_{21})}$ $\qquad D_2 = \dfrac{E_{22}h^3}{12(1-\nu_{12}\nu_{21})}$

$$D_3 = \frac{\nu_{21}E_{11}h^3}{12(1-\nu_{12}\nu_{21})} + \frac{1}{6}G_{12}h^3 = \frac{\nu_{12}E_{22}h^3}{12(1-\nu_{12}\nu_{21})} + \frac{1}{6}G_{12}h^3 = D_4 + 2D_{12}$$

and C_m, C_n and A_{mn} are defined in Table 5.2.2-7 for modes up through the (3,3) mode (compare with Table 5.2.2-1).

The mode number nomenclature is as shown in Figure 5.2.2-1.

TABLE 5.2.2-7
VALUES OF C_m, C_n, AND A_{mn} FOR EQUATION (5.2.2-83)

(m,n)	C_m	C_n	A_{mn}
(1,1)	4.730	4.730	151.3
(1,2)	4.730	7.853	565.5
(1,3)	4.730	10.996	1216.7
(2,1)	7.853	4.730	565.5
(2,2)	7.853	7.853	2102.6
(2,3)	7.853	10.996	4548.1
(3,1)	10.996	4.730	1216.7
(3,2)	10.996	7.853	4548.1
(3,3)	10.996	10.996	9785.2

For the fundamental mode Equations (5.2.2-82) and (5.2.2-83) are, respectively

$$f_{11}^2 = \frac{\pi^2}{4\rho h}\left[D_1/a^4 + D_2/b^4 + 2D_3/a^2b^2\right] \quad Hz^2 \qquad (5.2.2\text{-}84a)$$

for simply supported edges and for clamped edges

$$f_{11}^2 = \frac{3.8325}{\rho h}\left[3.307D_1/a^4 + 3.307D_2/b^4 + 2D_3/a^2b^2\right] \quad Hz^2 \qquad (5.2.2\text{-}84b)$$

Example: Compute the fundamental mode response frequency of a rectangular plate with dimensions a = 6.0 inches, b = 12.0 inches, h = 0.032 inches for the following orthotropic material properties (boron epoxy material, 50% resin by volume)

$$E_{11} = 30 \times 10^6 \text{ psi} \qquad \nu_{12} = 0.38$$

$$E_{22} = 3 \times 10^6 \text{ psi} \qquad \nu_{21} = \nu_{12}E_{22}/E_{11} = 0.038$$

$$G_{12} = 1.1 \times 10^6 \text{ psi} \qquad \gamma = 0.0922 \text{ lbs/in}^3$$

The plate bending rigidities are

$$D_1 = \frac{E_{11}h^3}{12(1-\nu_{12}\nu_{21})} = 83.1203 \qquad D_3 = 9.16604$$

$$D_2 = \frac{E_{22}h^3}{12(1-\nu_{12}\nu_{21})} = 8.3120$$

Then, from Equation (5.2.2-84a), the fundamental mode response frequency for simply supported edges is

$$f_{11}^2 = (3.2314 \times 10^5)[83.1203/6^4 + 8.312/12^4 + 2(9.16604)/6^2 \times 12^2] \text{ Hz}^2$$

$$f_{11}^2 = 2.1997 \times 10^4 \text{ Hz}^2$$

$$f_{11} = 148 \text{ Hz} .$$

From Equation (5.2.2-84b), the fundamental mode response frequency for clamped edges is

$$f_{11}^2 = (5.01924 \times 10^5)[274.879/6^4 + 27.4878/12^4 + 18.3321/6^2 \times 12^2] \text{ Hz}^2$$

$$f_{11}^2 = 1.08897 \times 10^5 \text{ Hz}^2$$

$$f_{11} = 330 \text{ Hz} .$$

For the material reoriented 90° so that the elastic properties are

$$E_{11} = 3 \times 10^6 \text{ psi} \qquad \nu_{12} = 0.038$$

$$E_{22} = 30 \times 10^6 \text{ psi} \qquad \nu_{21} = 0.38$$

$$G_{12} = 1.1 \times 10^6 \text{ psi}$$

the above results are, for simply supported edges $f_{11} = 67$ Hz and for clamped edges $f_{11} = 138$ Hz.

5.2.2.3.2 Response of Specially Orthotropic Plates to Uniform Static Pressure

The analysis of Section 5.2.2.2.6 indicates that the response of the plate to a uniform static pressure of unit magnitude is required to estimate the mean square displacement and stress response. This section presents design equations for estimating the static displacement and static stress response of a specially orthotropic plate due to a uniform pressure of unit magnitude. It is assumed that the natural frequencies are well separated so that each response mode can be considered as an uncoupled single degree-of-freedom response. Results for the $(m,n)^{th}$ mode of vibration are presented for specially orthotropic plates with both clamped edges and simply supported edges.

For a specially orthotropic rectangular plate using small deflection theory, the stress-strain relationships are

$$\sigma_1 = \frac{E_{11}\epsilon_1}{(1-\nu_{12}\nu_{21})} + \frac{\nu_{12}E_{22}\epsilon_2}{(1-\nu_{12}\nu_{21})} \qquad (5.2.2\text{-}85a)$$

$$\sigma_2 = \frac{\nu_{21}E_{11}\epsilon_1}{(1-\nu_{12}\nu_{21})} + \frac{E_{22}\epsilon_2}{(1-\nu_{12}\nu_{21})} \qquad (5.2.2\text{-}85b)$$

$$\tau_{12} = G_{12}\gamma_{12} \qquad (5.2.2\text{-}85c)$$

where the orientation of the three mutually orthogonal elastic axes with respect to the plate axes are given in Figure 5.2.2-27.

The strain-displacement relationships for the specially orthotropic material are

$$\epsilon_1 = -zw_{,xx} \qquad \epsilon_2 = -zw_{,yy} \qquad \gamma_{12} = -2zw_{,xy} \qquad (5.2.2\text{-}85d)$$

which relate the material axis system denoted by the subscripts (1,2) to the plate (x,y) axis system.

The stress resultants for the specially orthotropic plate are

$$M_{11} = \int_{-h/2}^{h/2} z\sigma_1 dz = -[D_1 w_{,xx} + D_4 w_{,yy}] \qquad (5.2.2\text{-}86a)$$

$$M_{22} = \int_{-h/2}^{h/2} z\sigma_2 dz = -[D_4 w_{,xx} + D_2 w_{,yy}] \qquad (5.2.2\text{-}86b)$$

$$M_{12} = -\int_{-h/2}^{h/2} z\tau_{12}dz = 2D_{12}w_{,xy} \qquad (5.2.2\text{-}86c)$$

where Equations (5.2.2-85) have been used in Equations (5.2.2-84).

For a point on the surface of the plate, the stresses are given by

$$\sigma_1 = -\frac{6M_{11}}{h^2} \qquad \sigma_2 = \frac{6M_{22}}{h^2} \qquad \tau_{12} = -\frac{6M_{12}}{h^2} \qquad (5.2.2\text{-}87)$$

Assuming an uncoupled response mode of the form $w(x,y) = W_o X_m(x) Y_n(y)$ one obtains the static response amplitude, W_o, of the $(m,n)^{th}$ mode by equating the maximum strain energy to the maximum potential energy of the plate when uniformly loaded by a unit magnitude uniform static pressure.

For simply supported edges the mode shape assumed for the uncoupled $(m,n)^{th}$ mode is of the form

$$w(x,y) = W_o \sin(m\pi x/a)\sin(n\pi y/b) \qquad (5.2.2\text{-}88)$$

and for a specially orthotropic plate with all edges clamped the assumed form of the $(m,n)^{th}$ mode is

$$w(x,y) = W_o X_m(x) Y_n(y) \qquad (5.2.2\text{-}89)$$

where $X_m(x)$ and $Y_n(y)$ are vibration modes for a straight slender beam with both ends clamped.

The displacement response amplitude for the $(m,n)^{th}$ mode for simply supported edge conditions is

$$W_o = \frac{4a^2b^2[(-1)^m-1][(-1)^n-1]}{\pi^6 mn[D_1 m^4 (b/a)^2 + D_2 n^4 (a/b)^2 + 2D_3 m^2 n^2]} \qquad (5.2.2\text{-}90a)$$

and for clamped edge conditions

$$W_o = \frac{4a^2b^2\alpha_m\alpha_n[(-1)^m-1][(-1)^n-1]}{[D_1 C_m^4 (b/a)^2 + D_2 C_n^4 (a/b)^2 + 2D_3 A_{mn}]C_m C_n} \qquad (5.2.2\text{-}90b)$$

where $A_{mn} = \alpha_m C_m \alpha_n C_n (\alpha_m C_m - 2)(\alpha_n C_n - 2)$

and α_m, C_m, etc. are given tables 5.2.2-I and 5.2.2 /

Denoting by a subscript "o" quantities referenced to a unit magnitude uniform static pressure, the stress response for simply supported edges is obtained by using Equations (5.2.2-88) and (5.2.2-90a) in Equations (5.2.2-87) to obtain

$$\sigma_{o1} = \frac{24ab[(-1)^m-1][(-1)^n-1][D_1m^2(b/a) + D_4n^2(a/b)]}{\pi^4h^2mn[D_1m^4(b/a)^2 + D_2n^4(a/b)^2 + 2D_3m^2n^2]} \sin(m\pi x/a)\sin(n\pi y/b) \qquad (5.2.2\text{-}91a)$$

$$\sigma_{o2} = \frac{24ab[(-1)^m-1][(-1)^n-1][D_4m^2(b/a) + D_2n^2(a/b)]}{\pi^4h^2mn[D_1m^4(b/a)^2 + D_2n^4(a/b)^2 + 2D_3m^2n^2]} \sin(m\pi x/a)\sin(n\pi y/b) \qquad (5.2.2\text{-}91b)$$

$$\tau_{o12} = \frac{48abD_{12}[(-1)^m-1][(-1)^n-1]\cos(m\pi x/a)\cos(n\pi y/b)}{\pi^4h^2[D_1m^4(b/a)^2 + D_2n^4(a/b)^2 + 2D_3m^2n^2]} \qquad (5.2.2\text{-}91c)$$

For the fundamental mode, (m,n) = (1,1), the above results for simply supported edges are

$$\sigma_{o1} = \frac{96ab[D_1(b/a) + D_4(a/b)]}{\pi^4h^2[D_1(b/a)^2 + D_2(a/b)^2 + 2D_3]} \sin(\pi x/a)\sin(\pi y/b) \qquad (5.2.2\text{-}92a)$$

$$\sigma_{o2} = \frac{96ab[D_4(b/a) + D_2(a/b)]}{\pi^4h^2[D_1(b/a)^2 + D_2(a/b)^2 + 2D_3]} \sin(\pi x/a)\sin(\pi y/b) \qquad (5.2.2\text{-}92b)$$

$$\tau_{o12} = \frac{192abD_{12}\cos(\pi x/a)\cos(\pi y/b)}{\pi^4h^2[D_1(b/a)^2 + D_2(a/b)^2 + 2D_3]} \qquad (5.2.2\text{-}92c)$$

For a specially orthotropic plate with all edges clamped, the stress response for the uncoupled $(m,n)^{th}$ mode due to a unit magnitude uniform static pressure is obtained by using substituting Equations (5.2.2-89) and (5.2.2-90b) into Equations (5.2.2-87) to obtain

$$\sigma_{o1} = \frac{24\,ab\,\alpha_m\alpha_n[(-1)^m-1][(-1)^n-1]S_{1mn}(x,y)}{h^2[D_1C_m^4(b/a)^2 + D_2C_n^4(a/b)^2 + 2D_3A_{mn}]C_mC_n} \qquad (5.2.2\text{-}93a)$$

$$\sigma_{o2} = \frac{24\,ab\,\alpha_m\alpha_n[(-1)^m-1][(-1)^n-1]S_{2mn}(x,y)}{h^2[D_1C_m^4(b/a)^2 + D_2C_n^4(a/b)^2 + 2D_3A_{mn}]C_mC_n} \qquad (5.2.2\text{-}93b)$$

$$\tau_{o12} = -\frac{48D_{12}ab\alpha_m\alpha_n[(-1)^m - 1][(-1)^n - 1]X_m'(x)Y_n'(y)}{h^2[D_1C_m^4(b/a)^2 + D_2C_n^4(a/b)^2 + 2D_3A_{mn}]} \qquad (5.2.2\text{-}93c)$$

$$S_{1mn}(x,y) = -[C_m^2D_1(b/a)X_m''(x)Y_n(y) + C_n^2D_4(a/b)X_m(x)Y_n''(y)] \qquad (5.2.2\text{-}93d)$$

$$S_{2mn}(x,y) = -[C_m^2D_4(b/a)X_m''(x)Y_n(y) + C_n^2D_2(a/b)X_m(x)Y_n''(y)] \qquad (5.2.2\text{-}93e)$$

For the fundamental mode, (m,n) = (1,1), the above results for clamped edges are

$$\sigma_{o1} = \frac{0.02738\,ab\ S_{111}(x,y)}{h^2[3.307D_1(b/a)^2 + 3.307D_2(a/b)^2 + 2D_3]} \qquad (5.2.2\text{-}94a)$$

$$\sigma_{o2} = \frac{0.02738\,ab\,S_{211}(x,y)}{h^2[3.307D_1(b/a)^2 + 3.307D_2(a/b)^2 + 2D_3]} \qquad (5.2.2\text{-}94b)$$

$$\tau_{o12} = -\frac{1.225\,D_{12}ab\,X_1'(x)Y_1'(y)}{h^2[3.307D_1(b/a)^2 + 3.307D_2(a/b)^2 + 2D_3]} \qquad (5.2.2\text{-}94c)$$

$$S_{111}(x,y) = -22.373[D_1(b/a)X_1''(x)Y_1(y) + D_4(a/b)X_1(x)Y_1''(y)] \qquad (5.2.2\text{-}94d)$$

$$S_{211}(x,y) = -22.373[D_4(b/a)X_1''(x)Y_1(y) + D_2(a/b)X_1(x)Y_1''(y)] \qquad (5.2.2\text{-}94e)$$

Similar to Equations (5.2.2-76) one obtains the following results for specific points on the surface of the plate (see Table B.1.1-5) for the fundamental mode

Center of Plate

$$\left.\begin{aligned} X_1(a/2)Y_1(b/2) &= 2.5222 \\ S_{111}(a/2,\ b/2) &= 43.195[D_1(b/a) + D_4(a/b)] \\ S_{211}(a/2,\ b/2) &= 43.195[D_4(b/a) + D_2(a/b)] \end{aligned}\right\} \qquad (5.2.2\text{-}95a)$$

Edge of Plate

$$\left.\begin{aligned} S_{111}(0,\ b/2) &= -71.063D_1(b/a) \\ S_{211}(a/2,\ 0) &= -71.063D_2(a/b) \end{aligned}\right\} \qquad (5.2.2\text{-}95b)$$

Approximate Location of Maximum Shear:

$$X_1'(0.22a)Y_1'(0.22b) = 1.06953 \qquad (5.2.2\text{-}95c)$$

5.2.2 3.3 Response of Specially Orthotropic Plates to Random Acoustic Excitation

This section combines the results of Sections 5.2.2.3.1 and 5.2.2.3.2 to obtain design equations for estimating the mean square stress response of specially orthotropic rectangular plates excited by random acoustic pressures. It is assumed that only the fundamental mode responds significantly and that the excitation spectral density varies slowly with frequency about the fundamental mode resonant frequency.

The basic relationship for estimating the mean square stress assuming a single mode stress response is given by Equation (5.2.2-60d) for the r^{th} mode as

$$\overline{\sigma^2(x,y,t)} = \frac{\pi f_r}{4\zeta_r} G_p(f_r)\sigma_o^2(x,y) \qquad (5.2.2\text{-}96)$$

Assuming a fundamental mode response and all edges of the plate to be simply supported, one combines Equations (5.2.2-84a) and (5.2.2-92) to obtain the mean square stress response as

$$\overline{\sigma_1^2(x,y,t)} = \frac{1152ab\, G_p(f_{11})[D_1(b/a) + D_4(a/b)]^2}{\pi^6\sqrt{\rho h}\, h^4\zeta_{11}[D_1(b/a)^2 + D_2(a/b)^2 + 2D_3]^{3/2}} \sin^2(\pi x/a)\sin^2(\pi y/b) \qquad (5.2.2\text{-}97a)$$

$$\overline{\sigma_2^2(x,y,t)} = \frac{1152\, ab\, G_p(f_{11})[D_4(b/a) + D_2(a/b)]^2}{\pi^6\sqrt{\rho h}\, h^4\zeta_{11}[D_1(b/a)^2 + D_2(a/b)^2 + 2D_3]^{3/2}} \sin^2(\pi x/a)\sin^2(\pi y/b) \qquad (5.2.2\text{-}97b)$$

$$\overline{\tau_{12}^2(x,y,t)} = \frac{4608\, ab\, D_{12}^2 G_p(f_{11})\cos^2(\pi x/a)\cos^2(\pi y/b)}{\pi^6\sqrt{\rho h}\, h^4\zeta_{11}[D_1(b/a)^2 + D_2(a/b)^2 + 2D_3]^{3/2}} \qquad (5.2.2\text{-}97c)$$

Assuming a fundamental mode response and all edges of the plate to be clamped, one combines Equations (5.2.2-84b) and (5.2.2-94) to obtain

$$\overline{\sigma_1^2(x,y,t)} = \frac{1.153\cdot10^{-3}\, ab\, G_p(f_{11})S_{111}^2(x,y)}{\sqrt{\rho h}\, h^4\zeta_{11}[3.307D_1(b/a)^2 + 3.307D_2(a/b)^2 + 2D_3]^{3/2}} \qquad (5.2.2\text{-}98a)$$

$$\overline{\sigma_2^2(x,y,t)} = \frac{1.153\cdot10^{-3}\,ab\,G_p(f_{11})S_{211}^2(x,y)}{\sqrt{\rho h}\,h^4\zeta_{11}[3.307D_1(b/a)^2 + 3.307D_2(a/b)^2 + 2D_3]^{3/2}} \qquad (5.2.2\text{-}98b)$$

$$\overline{\tau_{12}^2(x,y,t)} = \frac{2.3072\,ab\,D_{12}^2G_p(f_{11})[X_1'(x)Y_1'(y)]^2}{\sqrt{\rho h}\,h^4\zeta_{11}[3.307D_1(b/a)^2 + 3.307D_2(a/b)^2 + 2D_3]^{3/2}} \qquad (5.2.2\text{-}98c)$$

$$S_{111}^2(x,y) = 500.6[D_1(b/a)X_1''(x)Y_1(y) + D_4(a/b)X_1(x)Y_1''(y)]^2 \qquad (5.2.2\text{-}98d)$$

$$S_{211}^2(x,y) = 500.6[D_4(b/a)X_1''(x)Y_1(y) + D_2(a/b)X_1(x)Y_1''(y)]^2 \qquad (5.2.2\text{-}98e)$$

The relationships given by Equations (5.2.2-95) are useful in evaluating the quantities $X_1'(x)Y_1'(y)$, $X_1''(x)Y_1(y)$ and $X_1(x)Y_1''(y)$ at specific points on the plate (see Table B.1.1-5).

Example : Compute the mean square stress response of a rectangular specially orthotropic plate with dimensions a = 6.0 inches, b = 12.0 inches, h = 0.032 inches for the following orthotropic material properties (boron epoxy material, 50% resin by volume):

E_{11} = 30 × 10^6 psi ν_{12} = 0.38

E_{22} = 3 × 10^6 psi $\nu_{21} = \nu_{12}E_{22}/E_{11}$ = 0.038

G = 1.1 × 10^6 psi γ_1 = 0.0922 lbs/in^3

Assume a sound pressure spectrum level of 130 dB at the fundamental mode resonance and ζ_{11} = 0.02.

From the example problem of Section 5.2.2.3.1 one obtains

D_1 = 83.120 in.lb. D_3 = 9.166 in.lb. D_{12} = 3.004 in.lb.

D_2 = 8.312 in.lb. D_4 = 3.159 in.lb.

The fundamental mode resonant frequencies are f_{11} = 148 Hz. for all edges simply supported and f_{11} = 330 Hz for all edges clamped.

From Equation (5.2.2-59) the acoustic pressure spectral density function is

$$G_p(f_{11}) = 8.41 \times 10^{(130/10-18)} = 8.41\times10^{-5}\ (\text{psi})^2/\text{Hz}.$$

For all edges simply supported one obtains from Equations (5.2.2-97)

$$\overline{\sigma_1^2(x,y,t)} = 5.3194 \times 10^8 \sin^2(\pi x/a)\sin^2(\pi y/b) \quad (psi)^2$$

$$\overline{\sigma_2^2(x,y,t)} = 2.0721 \times 10^6 \sin^2(\pi x/a)\sin^2(\pi a/b) \quad (psi)^2$$

$$\overline{\tau_{12}^2(x,y,t)} = 6.8178 \times 10^5 \cos^2(\pi x/a)\cos^2(\pi y/b) \quad (psi)^2$$

For all edges clamped one obtains from Equations (5.2.2-98)

$$\overline{\sigma_1^2(x,y,t)} = 3.1941 S_{111}^2(x,y) \quad (psi)^2$$

$$\overline{\sigma_2^2(x,y,t)} = 3.1941 S_{211}^2(x,y) \quad (psi)^2$$

$$\overline{\tau_{12}^2(x,y,t)} = 5.768\times10^4 (X_1'(x)Y_1'(y))^2 \quad (psi)^2$$

$$S_{111}^2(x,y) = 500.6[166.2X_1''(x)Y_1(y) + 1.58X_1(x)Y_1''(y)]^2$$

$$S_{211}^2(x,y) = 500.6[6.138X_1''(x)Y_1(y) + 4.16X_1(x)Y_1''(y)]^2$$

At the center and the edges of the clamped plate one obtains

$$\overline{\sigma_1^2(a/2,b/2,t)} = 1.679\times10^8 \quad (psi)^2$$

$$\overline{\sigma_2^2(a/2,b/2,t)} = 6.538\times10^5 \quad (psi)^2$$

$$\overline{\sigma_1^2(0,\ b/2,\ t)} = 4.458\times10^8 \quad (psi)^2$$

$$\overline{\sigma_2^2(a/2,\ 0,\ t)} = 2.786\times10^5 \quad (psi)^2$$

REFERENCES FOR SECTION 5.2.2

1. Leissa, A. W.; Vibration of Plates, NASA SP-160, National Aeronautics and Space Administration, Washington, D. C., 1969.

2. Leissa, A. W.; "Free Vibration of Rectangular Plates," Journal of Sound and Vibration, Vol. 31, No. 3, 1973, pp. 257-293.

3. Timoshenko, S., and Woinowsky-Kraeger, S.; Theory of Plates and Shells, Second Ed., McGraw-Hill Book Company, New York, 1959.

4. Clarkson, B. L.; "Stresses In Skin Panels Subjected to Random Acoustic Loading," The Aeronautical Journal of the Royal Aeronautical Society, Vol. 72, Nov. 1968, pp. 1000-1010.

5. Miles, J. W.; "On Structural Fatigue Under Random Loading," Journal of the Aeronautical Sciences, Vol. 21, Nov. 1954.

6. Warburton, G. B.; "The Vibration of Rectangular Plates," Proceedings of the Institute of Mechanical Engineers," Serial A, Vol. 168, No. 12, 1954, pp. 371-384.

7. Dickinson, S. M.; "Lateral Vibration of Rectangular Plates Subject to In-Plane Forces," Journal of Sound and Vibration, Vol. 16, No. 4, 1971, pp. 465-472.

8. Herrmann, G.; "The Influence of Initial Stress on the Dynamic Behavior of Elastic and Viscoelastic Plates," Pub. Int. Ass. for Bridge and Struct. Eng., Vol. 16, 1956, pp. 275-294.

9. Shulman, Y.;"On the Vibration of Thermally Stressed Plates In the Pre-Buckling and Post-Buckling States," MIT TR 25-25, Jan. 1958.

10. Schneider, C. W. and Rudder, F. F.; "Acoustic Fatigue Resistance of Aircraft Structure at Elevated Temperatures," paper (73-944) AIAA Aero-Acoustics Conference, Seattle, Washington, Oct. 15-17, 1973.

11. Langhaar, H. L.; Energy Methods In Applied Mechanics, John Wiley and Sons, Inc. 1962, pp. 159-164.

12. Bleich, F., Buckling Strength of Metal Structures, McGraw-Hill Book Company, 1952, pp. 467-478.

13. Carmichael, T. E. "The Vibration of a Rectangular Plate with Edges Elastically Restrained Against Rotation," Quarterly Journal of Mechanics and Mathematics, Vol. 12, pt. 1, 1959, pp. 29-42.

14. Arcas, N. R.; "Prediction of Stress and Fatigue Life of Acoustically-Excited Aircraft Structure," 39th Shock and Vibration Bulletin, Part 3, Shock and Vibration Information Center, Naval Research Laboratory, Washington, D. C., January 1969.

REFERENCES FOR SECTION 5.2.2 (CONTINUED)

15. Ballentine, J. R., et al.; "Refinement of Sonic Fatigue Structural Design Criteria," AFFDL-TR-67-156, Air Force Flight Dynamics Laboratory, Wright-Patterson Air Force Base, Ohio, Jan. 1968.

16. Powell, Alan; "On the Fatigue Failure of Structures due to Vibrations Excited by Random Pressure Fields," Journal of the Acoustical Society of America, Vol. 30, No. 12, Dec. 1958, pp. 1130-1135 (also pp. 1136-1139).

17. Eringen, A. C.; "Response of Beams and Plates to Random Loads," Journal of Applied Mechanics; Vol. 24, pp. 46-52, 1957.

18. Wagner, Hans, and Rama Bhat, B.; "Linear Response of an Elastic Plate to Actual Random Load," Ingenieur-Archiv, Vol. 39, pp. 149-158, 1970.

19. Robson, J. D.;"The Random Vibration Response of a System Having Many Degrees of Freedom," The Aeronautical Quarterly, pp. 21-30, February 1966.

20. Bozich, D. J.; "Spatial Correlation in Acoustic-Structural Coupling," Journal of the Acoustical Society of America," Vol. 36, No. 1, Jan. 1964.

21. Coe, C. F. and Chyu, W. J.; "Pressure Fluctuation Inputs and Response of Panels Underlying Attached and Separated Supersonic Turbulent Boundary Layers," Paper No. 5, AGARD-CP-113 Symposium on Acoustic Fatigue, 26-27 September 1972.

22. Mercer, C. A.; "Response of a Multi-supported Beam to a Random Pressure Field," Journal of Sound and Vibration, Vol. 2, pp. 293-306. 1965.

23. James, H. M., et al.; Theory of Servomechanisms, MIT Radiation Laboratory Series, Vol. 25, McGraw-Hill Book Company, pp. 333-339 & 369-370, 1947.

24. Crandall, S. H. and Mark, W. D.; Random Vibration in Mechanical Systems, Academic Press, 1963.

25. Pulgrano, L. J., and Ablowitz, M.; "The Response of Mechanical Systems to Bands of Random Excitation," 39th Shock and Vibration Bulletin, Part 3, Shock and Vibration Information Center, Naval Research Laboratory, Washington, D. C., January 1969.

26. Ambartsumyan, S. A.; Theory of Anisotropic Plates, Progress in Materials Science Series, Vol. II, Technomic Publishing Company, Stamford, Conn., 1970.

27. Ashton, J. E., and Whitney, J. M.; Theory of Laminated Plates, Progress in Materials Science Series, Vol. IV, Technomic Publishing Company, Stamford, Conn., 1970.

28. Ashton, J. E., Halpin, J. C., and Petit, P. H.; Primer on Composite Materials: Analysis, Progress in Materials Science Series, Vol. III, Technomic Publishing Co., Stamford, Conn. 1969.

29. Mohan, D., and Kingsbury, H. B.; "Free Vibrations of Generally Orthotropic Plates," Journal of the Acoustical Society of America, Vol. 50, No. 1 (Part 2), 1971.

30. Hearmon, R. F. S.; "The Frequency of Flexural Vibration of Rectangular Orthotropic Plates with Clamped or Supported Edges," Trans. of the ASME, Journal of Applied Mechanics, Dec. 1959.

31. Hermes, P. H., and Smith, D. L.; "Measurement and Analysis of the J57-P21 Noise Field," AFFDL-TR-66-147, Wright-Patterson Air Force Base, Ohio, Nov. 1966.

5.2.3 VIBRATION OF OPEN CIRCULAR CYLINDRICAL SHELLS

The topic of shell vibration has received as much attention in the literature as has the topic of plate vibration (see Section 5.2.2). Following his compendium on plate vibration Leissa (1) has completed an extensive compilation of the literature on shell vibration. As pointed out by Leissa (1) two factors complicate the topic of shell vibration: first, there is no one accepted theory used to obtain the equations of motion; secondly, the choice of boundary conditions is much greater than that for flat plates. For example, there are 21 distinct combinations of clamped, simply-supported, or free edges for a flat rectangular plate (two combinations are presented in Section 5.2.2); however, there are 136 combinations of simple boundary conditions for closed shells and 18496 combinations for open shells. For most practical situations, one only need to consider the cases of all edges simply supported or all edges clamped to obtain a bound on frequency estimates. Since Leissa (1) presents such a complete development of shell theory and a compilation of results with numerical studies comparing the various theories, one interested in the detailed analysis should refer to this publication as a primary reference.

The explicit results presented here are based upon the work of Sewall (2) and Plumblee (3) for shallow shells and the work of Gontkevich (4) and (5), as reported by Leissa (1), for open circular cylindrical shells that need not be shallow. The panel geometry and nomenclature are illustrated in Figure 5.2.3-1.

5.2.3.1 Shallow Open Circular Cylindrical Shells

This section provides design equations for estimating the natural frequencies of shallow open circular cylindrical shells. The definition of a shallow shell is based upon the ratio of the rise of the shell, h^*, to the smallest side of the shell measured in the plane of its supports. This condition for open circular cylindrical shells is, according to Vlasov (6),

$$h^*/a \quad \text{or} \quad h^*/\ell \leq 0.20 \ . \tag{5.2.3-1a}$$

Referring to Figure 5.2.3-1 one obtains

$$[1 - \cos(\Phi/2)]R/a \leq 0.20 \tag{5.2.3-2a}$$

if a is the shorter dimension and

$$[1 - \cos(\Phi/2)]/\sin(\Phi/2) \leq 0.40 \tag{5.2.3-2b}$$

if $\ell = 2R \sin(\Phi/2)$ is the shorter dimension.

All results in this section require that Equations (5.2.3-2) are satisfied for the theory to be valid.

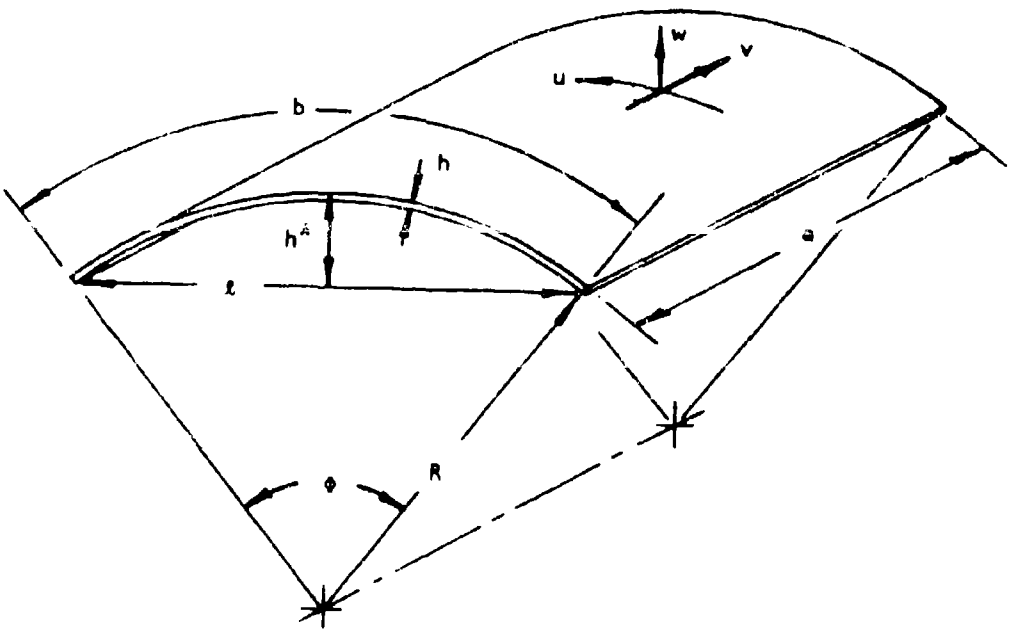

ARC LENGTH: $b = R\phi$

SPAN: $\ell = 2R \sin(\phi/2)$

RISE: $h^* = R[1-\cos(\phi/2)]$

m = number of half waves in generator direction

n = number of half waves in circumferential direction

FIGURE 5.2.3-1 OPEN CIRCULAR CYLINDRICAL SHELL GEOMETRY AND NOMENCLATURE

Sewell (2) used an assumed mode approach and used Donnell-Mushtari theory (1) to obtain a general frequency expression for shallow open cylindrical shells neglecting tangential inertia effects. The results are for the $(m,n)^{th}$ mode

$$\omega_{mn}^2 = \frac{C}{\rho h}\,(\Delta_I + \Delta_E) \qquad (5.2.3\text{-}3)$$

where $\Delta_I = \dfrac{D}{CM_{mn}}\,[I_2 + I_3 + 2\nu I_6 + 2(1-\nu)I_1]$

$$\Delta_E = \frac{1}{R^2}\,[1 - F_1/F_2]$$

$$F_1 = I_5^2\left(I_2 + \frac{1-\nu}{2}\,I_1\right) - 2\nu I_4 I_5\left(\nu I_6 + \frac{1-\nu}{2}\,I_1\right) + \nu^2 I_4^2\left(I_3 + \frac{1-\nu}{2}\,I_1\right)$$

$$F_2 = M_{mn}\left[\left(I_2 + \frac{1-\nu}{2}\,I_1\right)\left(I_3 + \frac{1-\nu}{2}\,I_1\right) - \left(\nu I_6 + \frac{1-\nu}{2}\,I_1\right)^2\right]$$

$$D = \frac{Eh^3}{12(1-\nu^2)} \qquad C = \frac{Eh}{(1-\nu^2)}\,.$$

The quantities M_{mn}, I_1, I_2,...,I_6 are presented in Table 5.3.2-1 for the shells with all edges simply-supported and all edges clamped. The form of Equation (5.2.3-3) depends upon the edge conditions, the form of the assumed modes, and the assumption that the modes are uncoupled.

Using the results from Table 5.2.3-1 in Equation (5.2.3-3) the expression for the response frequency of the $(m,n)^{th}$ mode of a shallow open cylindrical shell with all edges simply supported is (see Equations (5.2.3-2))

$$f_{mn}^2 = \frac{\pi^2 h}{4\rho h a^2 b^2}\,[m^2(b/a) + n^2(a/b)]^2 + \frac{Em^4}{4\pi^2\rho h a^2[m^2 + n^2(a/b)^2]^2} \quad Hz^2 \qquad (5.2.3\text{-}4)$$

Comparing this result with the flat panel frequency expression, Equation (5.2.2-1), one sees that the first term is exactly the result for a flat rectangular panel with simply supported edges and that the second term is the curvature effect.

Using the results from Table 5.2.3-1 in Equation (5.2.3-3) the expression for the fundamental mode response frequency of a shallow open cylindrical shell with all edges clamped and an assumed value of Poisson's ratio $\nu = 0.32$ is (see Equations (5.2.3-2)).

TABLE 5.2.3-1

MODAL FUNCTIONS IN THE FREQUENCY EQUATION (5.2.3-3)
FOR AN OPEN CIRCULAR CYLINDRICAL SHELL
(See Tables 5.2.2-1, B.1.1-5 and Figure 5.2.3-1)

Integral	Simply Supported Edges	Clamped Edges
$M_{mn} = \int_0^b \int_0^a X_m^2 Y_n^2 dx ds$	$\frac{ab}{4}$	ab
$I_1 = \int_0^b \int_0^a (X_m' Y_n')^2 dx ds$	$\frac{\pi^4 m^2 n^2}{4ab}$	$\frac{\alpha_m \alpha_n}{ab} C_m C_n (\alpha_m C_m - 2)(\alpha_n C_n - 2)$
$I_2 = \int_0^b \int_0^a (X_m'' Y_n)^2 dx ds$	$\frac{\pi^4 m^4 b}{4a^3}$	$\frac{b}{a^3} C_m^4$
$I_3 = \int_0^b \int_0^a (X_m Y_n'')^2 dx ds$	$\frac{\pi^4 n^4 a}{4b^3}$	$\frac{a}{b^3} C_n^4$
$I_4 = \int_0^b \int_0^a X_m X_m'' Y_n^2 dx ds$	$-\frac{\pi^2 m^2 b}{4a}$	$-\frac{b}{a} \alpha_m C_m (\alpha_m C_m - 2)$
$I_5 = \int_0^b \int_0^a X_m^2 X_m'' Y_n Y_n'' dx ds$	$-\frac{\pi^2 n^2 a}{4b}$	$-\frac{a}{b} \alpha_n C_n (\alpha_n C_n - 2)$
$I_6 = \int_0^b \int_0^a X_m X_m'' Y_n Y_n'' dx ds$	I_5	I_1

$$f_{11}^2 = \frac{14.051\ Eh^2}{4\pi^2\rho a^2 b^2}\left[3.307(b/a)^2 + 3.307(a/b)^2 + 2\right]$$

$$+ \frac{E}{4\pi^2\rho R^2}\left\{\frac{1.0685(b/a)^2 + 0.6692(a/b)^2 + 7.3243}{(b/a)^2 + (a/b)^2 + 9.4419}\right\} \quad Hz^2 \qquad (5.2.3\text{-}5)$$

The second term in brackets varies from 0.678 to 1.043 as b/a varies from 0.1 to 10.0.

Again, the form of Equation (5.2.3-5) is the first term being the expression for the flat panel fundamental mode frequency and the second term is the curvature effect for the fundamental mode.

Plumblee (3) developed an expression for the fundamental mode frequency of a shallow open cylindrical shell with all edges clamped using an approach similar to Sewall (2). Both Plumblee and Sewall noted that experimental results for the lower order modes -- especially the fundamental mode frequency -- fell between the cases of all edges simply supported and all edges clamped. Plumblee empirically determined constants for the fundamental mode frequency expression to obtain for $\nu = 0.32$.

$$f_{11}^2 = \frac{14.051\ Eh^2}{4\pi^2\rho a^2 b^2}\left[3.307(b/a)^2 + 3.307(a/b)^2 + 2.0\right] + \frac{0.2788\ E}{4\pi^2\rho R^2} \quad Hz^2 \qquad (5.2.3\text{-}6)$$

Plumblee (3) also presents the derivation of an expression for the ratio of the root mean square stress response at the center of the straight edge of the shell in the circumferential direction to obtain

$$\frac{(\sigma_y)_{curved}}{(\sigma_y)_{flat}} = \left[1 + \frac{0.006a^2b^2}{h^2R^2\left[\left(\frac{b}{a}\right)^2 + \left(\frac{a}{b}\right)^2 + 0.604\right]}\right]^{-3/4} \times \left[1 + \frac{0.453b^2}{Rh}\left(\frac{\left(\frac{b}{a}\right)^2 + 0.034}{\left(\frac{b}{a}\right)^4 + 9.62\left(\frac{b}{a}\right)^2 + 1}\right)\right] \qquad (5.2.3\text{-}7)$$

The stress $(\sigma_y)_{flat}$ is obtained from Section 5.2.2.2.6 using Equations (5.2.2-76e) and (5.2.2-77f) to obtain

$$(\sigma_y)_{flat}^2 = \frac{1.7726a^3\sqrt{E/\rho}\ G_p(f_{11})}{bh^3\zeta_{11}\left[3.307(b/a)^2 + 3.307(a/b)^2 + 2\right]^{3/2}} \quad (psi)^2 \qquad (5.2.3\text{-}8)$$

In using the results of Equations (5.2.3-7) and (5.2.3-8) it has been assumed that the acoustic pressure spectrum level is constant for the frequency range including the flat panel and the curved panel response frequency. In addition it has been assumed that $\nu = 0.32$.

A nomograph giving both the curved to flat plate frequency ratio and the curved to flat plate stress ratio was developed by Plumblee and is presented in Figure 5.2.3-2.

Example: Compute the fundamental mode response frequency of an open cylindrically curved shell for both all edges simply supported and all edges clamped. Compare Sewall's analytical results, Equation (5.2.3-4) and (5.2.3-5), to Plumblee's analytical-empirical relationship, Equation (5.2.3-6). The data for the problem is as follows: $a = 11.25$ inches, $b = 9.0$ inches, $h = 0.032$ inches, $R = 72$ inches, $E = 10.3 \cdot 10^6$ psi, $\nu = 0.32$, and $\gamma = 0.101$ lbs/in^3.

First, one must check to see that the shell geometry is such that shallow shell theory applies. Since the shorter panel dimension is the straight edge ($a = 9.0$ inches) the shallow shell criterion is given by Equation (5.2.3-2a) with the result

$$\Phi = 9/72 = 0.125$$

$$[1 - \cos(\Phi/2)]R/a = 0.0125 \leq 0.20 \ .$$

Hence, shallow shell theory applies so that the results of Section 5.2.3.1 apply.

For the fundamental mode, $(m,n) = (1,1)$, the frequency expression for the shell with all edges simply supported is given by Equation (5.2.3-4) which yields

$$f_{11}^2 = 3.789 \cdot 10^3 + 29.323 \cdot 10^3 = 33.112 \cdot 10^3 \quad Hz^2$$

$$f_{11} = 182 \quad Hz.$$

For the fundamental mode the frequency expression for the shell with all edges clamped is given by Equation (5.2.3-5) which yields

$$f_{11}^2 = 1.3006 \cdot 10^4 + 1.49706 \cdot 10^5 = 1.62712 \cdot 10^5 \quad Hz^2$$

$$f_{11} = 403 \ Hz.$$

Plumblee's analytical-empirical expression for the fundamental mode response frequency, Equation (5.2.3-6) for an open circular cylindrical shell has the constant 0.2788 appearing in the curvature term determined from experimental laboratory data for shells with all edges clamped. Substituting the above data into Equation (5.2.3-6) one obtains

$$f_{11}^2 = 1.3006 \cdot 10^4 + 5.3681 \cdot 10^4 = 6.66857 \cdot 10^4 \quad Hz^2$$

$$f_{11} = 258 \ Hz.$$

It should be noted that the first term in both Equation (5.2.3-5) and Equation (5.2.3-6) represents the fundamental mode response frequency of a flat rectangular plate with dimensions $a \times b$ and thickness h.

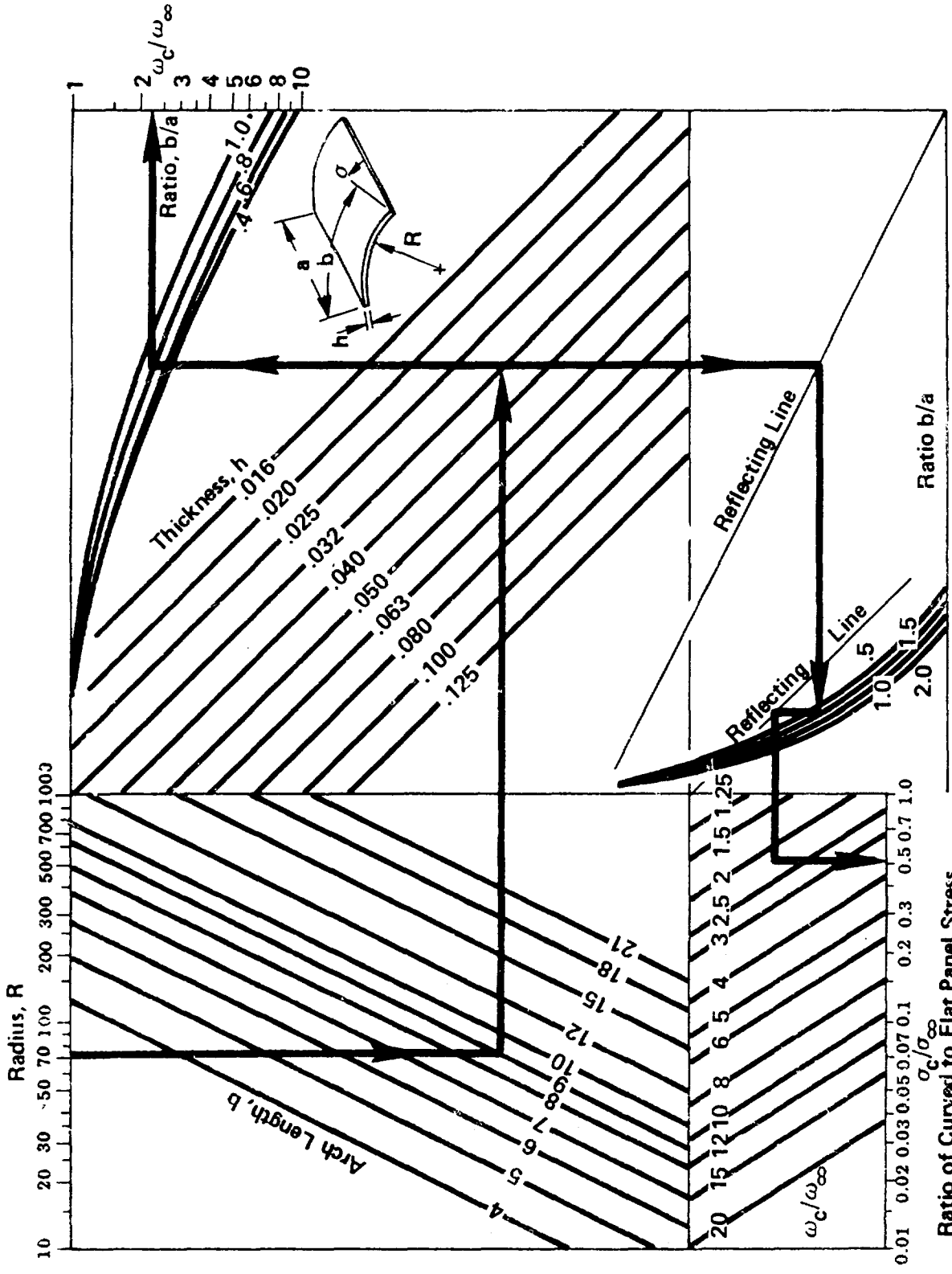

FIGURE 5.2.3-2 NOMOGRAPH FOR CALCULATING FREQUENCY AND STRESS RATIOS FOR SHALLOW OPEN CIRCULAR CYLINDRICAL SHELLS (REF. 3)

Using the results of Equation (5.2.3-7), one obtains the root mean square stress response of the shell at the middle of the straight edge in terms of the flat plate stress response as

$$(\sigma_y)_{curved} = 0.71(\sigma_y)_{flat}$$

Assuming that the curved shell is exposed to a random acoustic excitation pressure with a spectrum level of 135 dB that is constant over the frequency range 100 Hz to 300 Hz (this is required so that the excitation pressure at 114 Hz (flat panel fundamental mode response frequency) and at 258 Hz is constant).

Then, from Equation (5.2.2-59)

$$G_p(f_{11}) = 2.65948 \cdot 10^{-4} \text{ (psi)}^2/\text{Hz}.$$

and assuming a damping ratio of $\zeta_{11} = 0.02$ one substitutes the curved panel data of this example into Equation (5.2.3-8) to obtain

$$(\sigma_y)^2_{flat} = 7.986 \cdot 10^{8} \text{ (psi)}^2$$

$$(\sigma_y)_{flat} = 2.826 \cdot 10^{4} \text{ psi} = 28.3 \text{ ksi}$$

Then, from the above results the root mean square stress response for the open circular cylindrical shell is

$$(\sigma_y)_{curved} = 0.71(\sigma_y)_{flat} = 0.71(28.3) = 20.1 \text{ ksi}$$

Note: The nomograph presented as Figure 5.3.2-2 was apparently developed as a result of Plumblee's earlier work (7) and calculates the stress response to sinusoidal excitation rather than random excitation.

5.2.3.2 Moderately Deep Open Circular Cylindrical Shells

Very often designers are faced with the task of predicting the response frequencies of open circular cylindrical shells the geometry of which exceeds the limitations of Equations (5.2.3-2). For lack of a better method, very often in these cases shallow shell theory is misused by designers. The problem of applying the appropriate theory is compounded in that coupling effects between the inplane displacements and the transverse displacement of the shell must be considered and that accurate mode shapes must be considered when applying approximate techniques such as the Rayleigh-Ritz Method.

To consider the coupling effects, even if one were to retain only a single term in the displacement functions, frequencies can only be obtained by solving at least a 3×3 eigenvalue problem. This is a trivial problem for a computer; however, it is not very convenient for occasional quick design

estimates. The second aspect of the problem of estimating response frequencies using an assumed mode method is that the straight beam eigenfunctions even though convenient do not represent accurately the expected transverse displacement of a cylindrical shell. Thompson (8) illustrates the effect of curvature on mode shape using the results of a finite element analysis.

Both Sewall and Plumblee used assumed mode shapes in the form of products of straight beam functions to obtain results for shallow shells. Leissa (1), pp. 165-170, reports the work of Gontkevich who developed a method of analysis of open circular cylindrical shells using straight beam functions for the generator direction and circular arch vibration modes for the circumferential direction. (See Lang (9) and Archer (10)). Gontkevich's method requires the solution of a 3×3 linear algebra eigenvalue problem. However, if one can consider moderately deep open circular cylindrical shells, then it is appropriate to neglect the coupling between the inplane and transverse displacements.

For moderately deep open circular cylindrical shells - neglecting coupling effects between the transverse displacement and the inplane displacements - the frequency expression for the shell has the form

$$f_{mn}^2 = \frac{E^*/\rho}{4\pi^2 R^2} + \frac{(E^*/\rho)h}{48\pi^2 a^2 b^2}\left\{\alpha_m^4\left(\frac{b}{a}\right)^2 + \frac{\alpha_n^4 \eta_n}{\theta_n}\left(\frac{a}{b}\right)^2 + 2\alpha_m^2 \delta_m \frac{\alpha_n^2}{\theta_n}\left[\delta_n - \nu(\gamma_n + \delta_n)\right]\right\} \quad Hz^2 \tag{5.2.3-9}$$

where $E^* = E/(1-\nu^2)$, m is the number of half-waves in the direction of the generator (straight edge), and n is the number of half-waves in the circumferential direction.

For the fundamental mode of a moderately deep open circular cylindrical shell with all edges clamped the expression for the frequency is

$$f_{11}^2 = \frac{E^*/\rho}{4\pi^2 R^2} + \frac{(E^*/\rho)h}{48\pi^2 a^2 b^2}\left\{500.6\left(\frac{b}{a}\right)^2 + \frac{\alpha_1^4 \eta_1}{\theta_1}\left(\frac{a}{b}\right)^2 + 24.605\,\frac{\alpha_1^2}{\theta_1}\left[\delta_1 - \nu(\gamma_1 + \delta_1)\right]\right\} \quad Hz^2 \tag{5.2.3-10}$$

where the quantities α_1, γ_1, δ_1, η_1, θ_1 are functions of the included angle of the cylindrical shell (see Figure 5.2.3-1) and are presented in Figure 5.2.3-3. Leissa (1) presents more general results considering both higher order modes and other boundary conditions. If the assumption of uncoupled inplane and transverse vibrations cannot be made, then the reader is advised to refer to Leissa (1) or Gontkevich (4) and (5) and to check the analysis closely since typographical errors apparently originated in the original work.

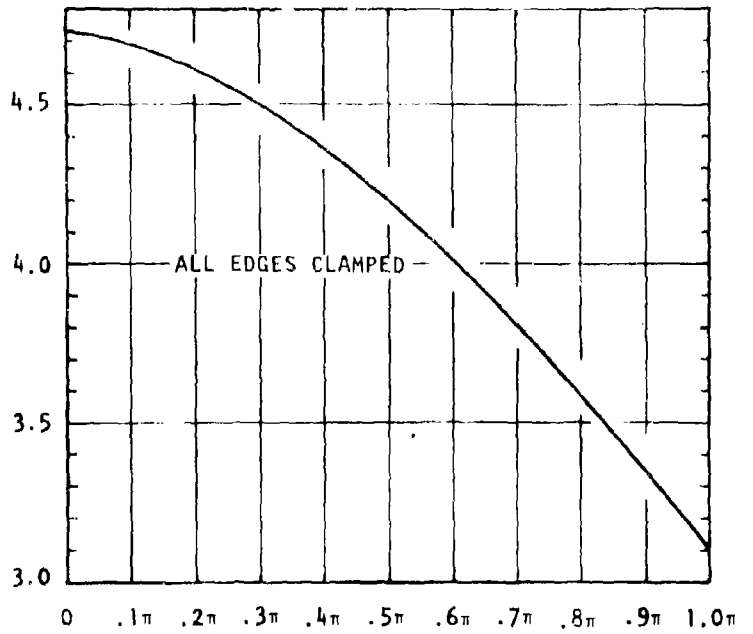

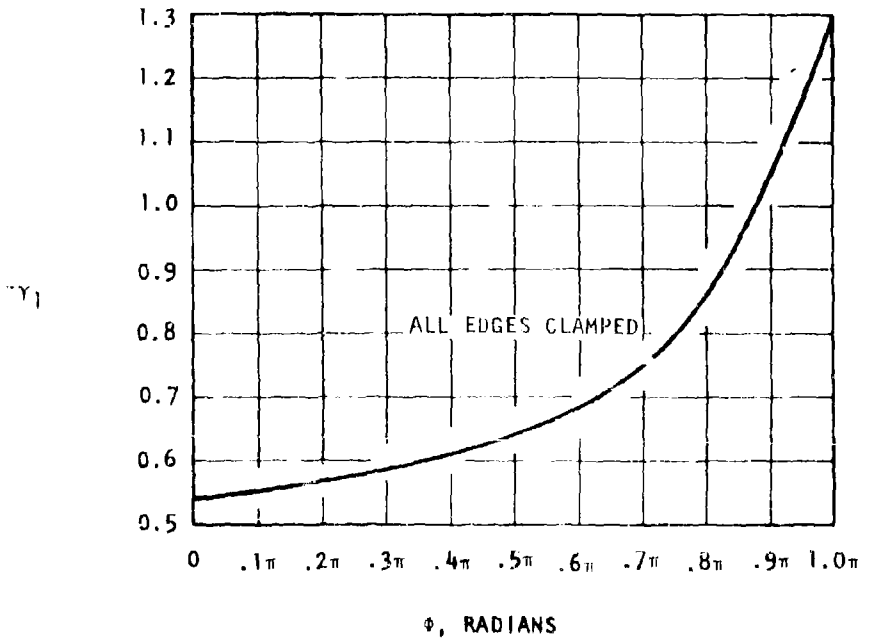

FIGURE 5.2.3-3 PLOT OF α_1, γ_1, δ_1, η_1, AND θ_1 FOR MODERATELY DEEP OPEN CIRCULAR CYLINDRICAL SHELLS (REF. 1) CONTINUED

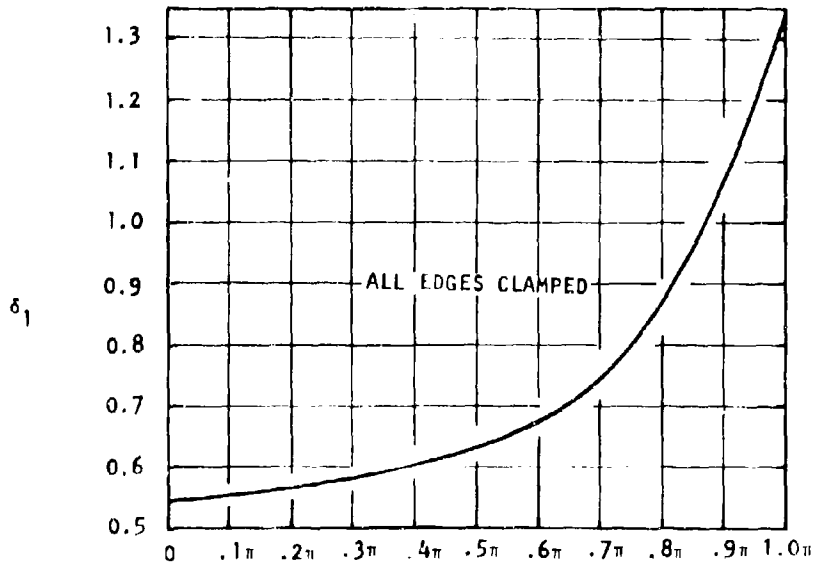

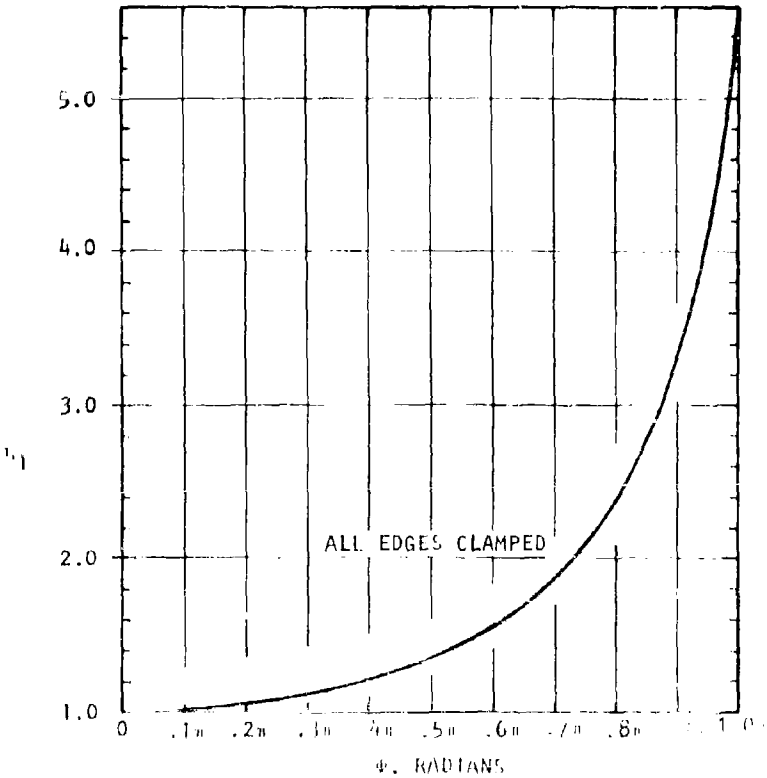

FIGURE 5.2.3) CONTINUED

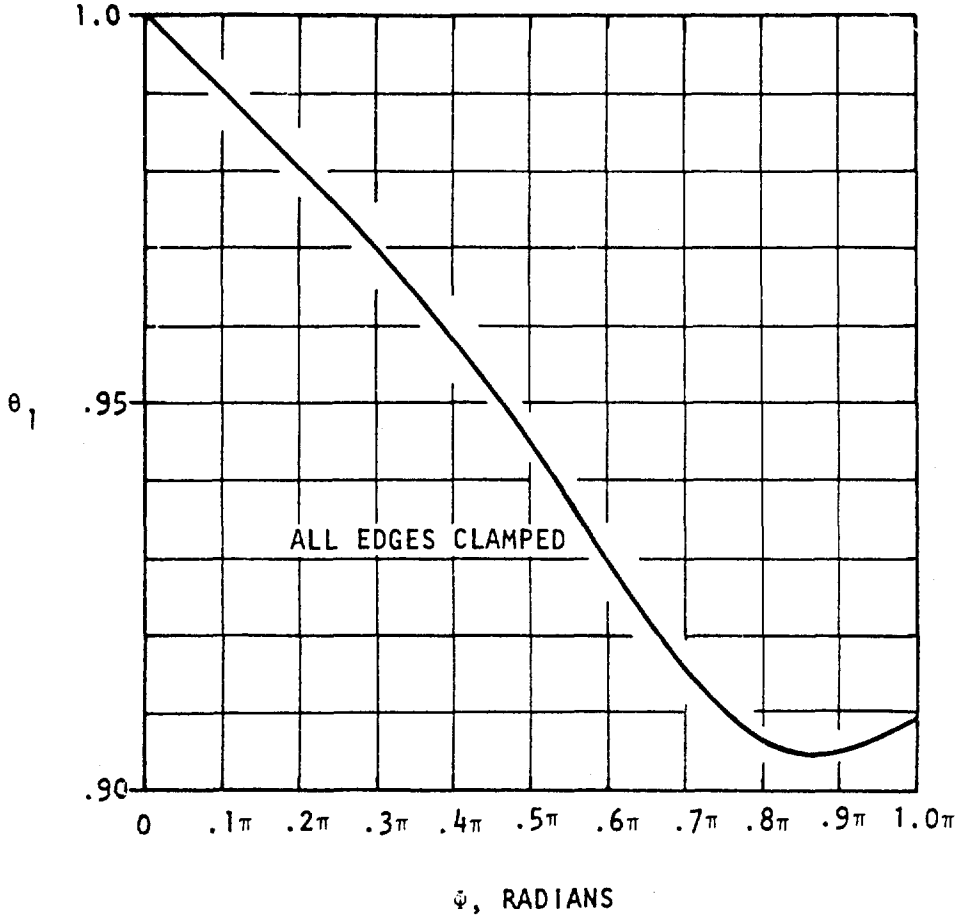

FIGURE 5.2.3-3 CONCLUDED

Example: Compute the fundamental mode response frequency of an open circular cylindrical shell with all edges clamped for the following data: $a = 10.0$ inches, $b = 75.4$ inches ($\Phi = 60^{o} = 0.33\pi$ rad), $h = 0.032$ inches, $R = 72$ inches, $E = 10.3 \cdot 10^{6}$ psi, $\nu = 0.32$, and $\gamma = 0.101$ lbs/in^3.

First from Equation (5.2.3-2a) one checks to see if shallow shell theory applies

$$[1 - \cos(\Phi/2)]R/a = 0.965 \geq 0.20$$

and, obviously, it does not apply.

From Figure 5.2.3-3, one obtains the following data for $\Phi = 0.33\pi$ radians

$$\alpha_1 = 4.46 \qquad \delta_1 = 0.590 \qquad \theta_1 = 0.9665$$

$$\gamma_1 = -0.593 \qquad \eta_1 = 1.160$$

Then, for the above data one obtains from Equation (5.2.3-10)

$$f_{11}^2 = 2.145 \cdot 10^5 + 5.216(2.846 \cdot 10^4 + 8.353 + 2.983 \cdot 10^2) \quad Hz^2$$

$$f_{11}^2 = 2.145 \cdot 10^5 + 1.501 \cdot 10^5 = 3.646 \cdot 10^5 \quad Hz^2$$

$$f_{11} = 604 \quad Hz.$$

REFERENCES FOR SECTION 5.2.3

1. Leissa, A. W.; Vibration of Shells, NASA SP-288, National Aeronautics and Space Administration, Scientific and Technical Office, Washington, D. C., 1973.

2. Sewall, J. L.; "Vibration of Cylindrically Curved Panels with Simply Supported on Clamped Edges and Comparison with Some Experiments," NASA TN D-3791, National Aeronautics and Space Administration, January, 1967.

3. Plumblee, H. E., et al.; "Refinement of Sonic Fatigue Structural Design Criteria," AFFDL-TR-67-156, Air Force Flight Dynamics Laboratory, Air Force Systems Command, Wright-Patterson Air Force Base, Ohio; January, 1968.

4. Gontkevich, V. S.; "Natural Vibrations of Plates and Snells," A. P. Filipov, Ed., Nauk Dumka (Kiev), 1964 (Translated by Lockheed Missiles and Space Company).

5. Gontkevich, V. S.; "Natural Vibrations of Rising Cylindrical Shells," Trans. Akad. Nauk USSR (Kiev), Laboratoriya Hidraulichnykh Mashyn. Sbornik Trudov, No. 10, 1962, pp. 27-37.

6. Vlasov, V. Z.; "General Theory of Shells and Its Applications in Engineering," NASA TT F-99, National Aeronautics and Space Administration, 1964.

7. Ballentine, J. R.; Plumblee, H. E., and Schneider, C. W.; "Sonic Fatigue in Combined Environment," AFFDL-TR-66-7, Air Force Flight Dynamics Laboratory, Wright-Patterson Air Force Base, Ohio, May 1966.

8. Thompson, A. R. G.; "Acoustic Fatigue Design Data - Part I," AGARDograph No. 162 (AGARD-AG-162 - Part I), Advisory Group for Aerospace Research and Development, North Atlantic Treaty Organization, May 1972.

9. Lang, T. E.; "Vibration of Thin Circular Rings, Part I. Solutions for Modal Characteristics and Forced Excitation and Part II. Modal Functions and Eigenvalues of Constrained Semicircular Rings," Technical Report No. 32-261, Jet Propulsion Laboratory California Institute of Technology, 1962.

10. Archer, R. R.; "Small Vibrations of Thin Incomplete Circular Rings," International Journal of Mechanical Sciences, Vol. 1, p. 45, 1960.

5.3 BUILT-UP STRUCTURES

The designer will find the data presented in this section to be the most specific and reliable techniques for estimating the sonic fatigue resistance of various structural configurations. These results are, generally, the easiest methods to use since many of the design methods are presented in the form of design charts or nomographs. Most of these results have been established by extensive sonic fatigue tests of the specific structural configurations. The designer is cautioned; however, to always read the text preceding the specific design method to establish the basis (and hence the limitations) of each technique.

This section is divided into eight subsections with each subsection devoted to a specific structural configuration. Each subsection is further subdivided by topic depending upon the amount of data reported in the literature. The structural configurations presented here are skin-stringer panels, box structure, wedge structure, honeycomb sandwich panels, chem-milled panels, corrugated panels, bonded-beaded panels, and laminated plates.

For quick reference to data contained in this section, the subdivision of topics is presented as follows:

5.3.1 STIFFENED-SKIN PANELS

The structural configuration for stiffened-skin panels as considered here is a flat sheet of material stiffened by frames and stringers intersecting at right angles. The earliest sonic fatigue analysis for this type of structure was performed by McGowan (1). Later, Ballentine (2) refined McGowan's work to obtain an improved design method for sizing the skin thickness. Subsequently, Rudder (3) refined McGowan's method for sizing the stiffeners, and Schneider (4) developed techniques to account for elevated temperatures.

Ballentine's design technique has been compared to various other techniques and available experimental data by Arcas (5) and Phillips (6) and has proven to be as accurate as any other method for selecting skin thickness for sonic fatigue resistant structure. A typical test specimen, as used by Ballentine (2), Rudder (3), and Schneider (4), is illustrated in Figure 5.3.1-1.

5.3.1.1 Notation

The following notation is used in this section. Other parameters are defined as they are introduced.

a	Panel bay short dimension, inches
b	Panel bay long dimension, inches
d	Depth of stringer, inches
E	Young's modulus at ambient temperature, psi
E_e	Young's modulus at elevated temperature, psi
f_o	Fundamental mode response frequency at ambient temperature, Hz.
$f(r)$	Fundamental mode response frequency at elevated temperature, Hz.
f_{11}	Frequency of the fundamental mode, Hz.
h	Skin thickness, inches
N	Fatigue life, cycles to failure
r	Temperature ratio, T/T_c
$S_p(f_{11})$	Excitation power spectral density at fundamental frequency, $(psi)/\sqrt{Hz}$.
T	Temperature increase above ambient temperature of panel (assumed to be uniform), ^oF.
T_c	Temperature increase above ambient temperature required to cause panel to buckle, ^oF.
$\overline{W}$	Mean square displacement response of panel, inches
W_o	Buckling amplitude of panel, inches

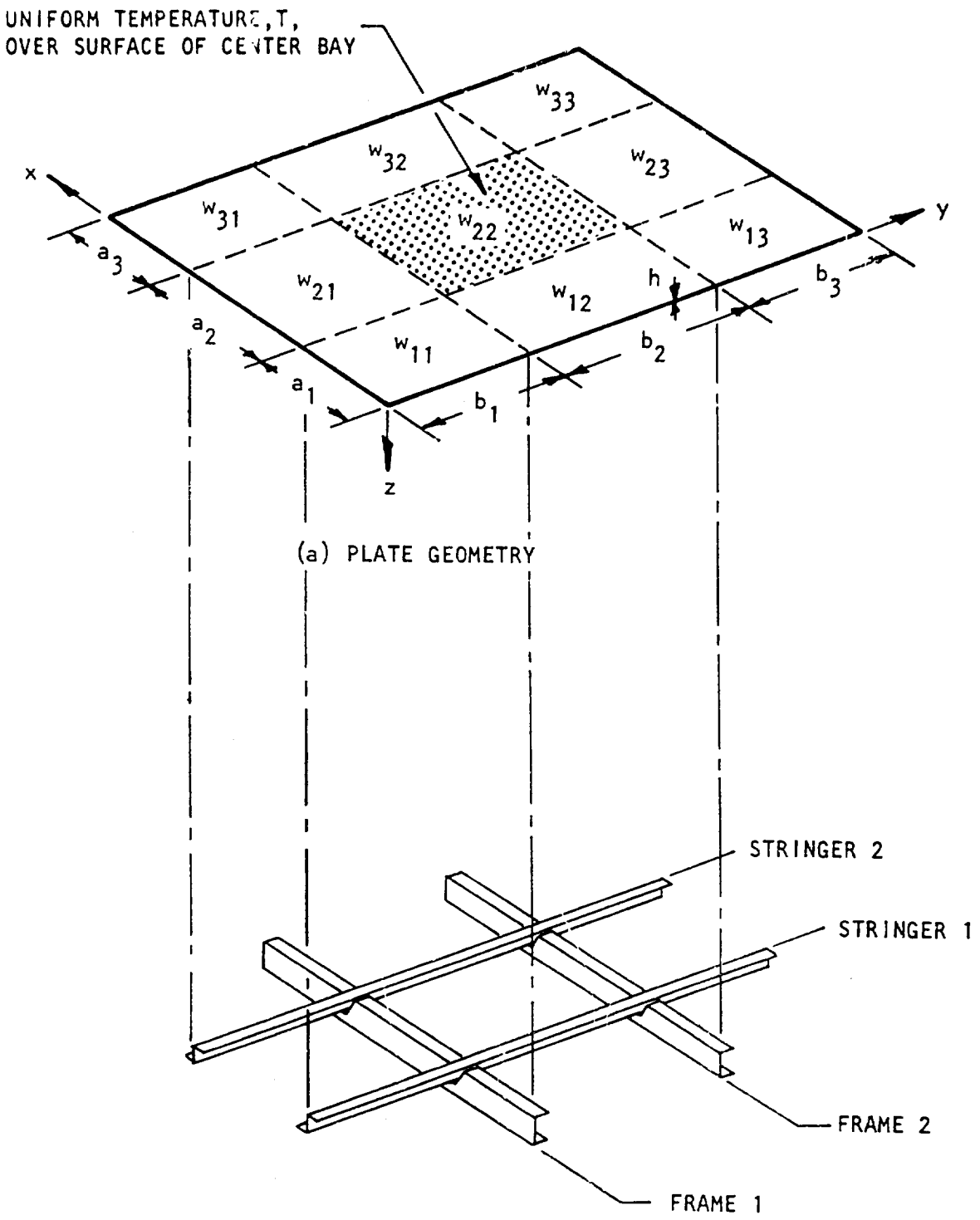

FIGURE 5.3.1-1 MULTIBAY FLAT STIFFENED PANEL CONFIGURATION

α	Coefficient of Linear Expansion for skin material, in/in/^{o}F.
ζ, ζ_{11}	Fundamental mode damping ratio
ν	Poisson's ratio
ρ	Mass density of panel
$\overline{\sigma}_f$	Root mean square flange stress, ksi
$\overline{\sigma}_s$	Root mean square skin dynamic stress, ksi
σ_T	Panel thermal stress, psi or ksi, as noted
σ_x, σ_y	Panel mean stress, psi or ksi, as noted
$\sigma_{x_b}, \sigma_{y_b}$	Panel buckling stress, psi or ksi, as noted

5.3.1.2 Skin Design Criteria for Ambient Temperatures

This section presents a design equation and a nomograph for estimating the stress response and fatigue life of flat stiffened aluminum alloy panels at ambient temperature (i.e., no thermal mean stress) when exposed to broad band random acoustic excitation. The skin design criteria for sonic fatigue resistance was developed by Ballentine (2). This technique presents a stress estimation and fatigue life prediction based upon correlating simple analytical results (such as presented in Section 5.2.2) with laboratory experimental data. Details of the structural configuration, test techniques, and response data can be obtained from the original report.

Derivation: The basis for the skin design criterion is as follows: a) the fundamental mode of a single flat rectangular plate forming an array of plates is the predominant mode; b) stiffeners forming the edge support of the plate are typical in size to that encountered in aircraft structure; c) a regression analysis of strain and failure data obtained in laboratory sonic fatigue tests of nine-bay structural specimens; d) specimens manufactured from 7075-T6 aluminum alloy structure.

The design criterion is expressed in terms of the root mean square stress response at the center of the long side (rivet line) of the plate. The stress estimates are valid for aluminum alloys in general.

The stress response prediction method and the design nomograph presented in this section were derived from laboratory sonic fatigue tests of 30 stiffened-skin panel designs with 2 specimens of each design tested simultaneously to check repeatability. Broadband random acoustic excitation was used to simulate the service loading. The range of design parameters for

the stiffened-skin specimens were

skin thickness	0.020 inch	to	0.100 inch
rib thickness	0.027 inch	to	0.125 inch
rib spacing	3.00 inches	to	10.00 inches
aspect ratio	1.50	to	3.00

Design Equation: The design equation for estimating the dynamic stress at the center of the long side of a flat rectangular plate at ambient temperature with edge restraints typical of aircraft construction is given as

$$\bar{\sigma}_s = 1.62 \times 10^{-4} (E/\rho)^{1/4} \frac{a^{1.25} S_p(f_{11}) (b/a)^{1.75}}{h^{1.75} \zeta^{0.56} [3(b/a)^2 + 3(a/b)^2 + 2]^{0.84}} \quad \text{ksi} \qquad (5.3.1\text{-}1)$$

$$S_p(f_{11}) = \sqrt{G_p(f_{11})}$$

Nomograph: The design equation given above was used to prepare a nomograph for its solution. The stress values obtained from this nomograph were related to the random fatigue failures experienced during Ballentine's test program to obtain an estimate of fatigue life. In using Equation (5.3.1-1), one must first obtain an estimate of the fundamental mode response frequency from Figure 5.2.2-2 for clamped edges for the values of a,b, and h and use the value of $G_p(f_{11})$ corresponding to this response frequency. To develop the design nomograph it was assumed that $(E/\rho)^{1/4} \approx 443$ to obtain

$$\bar{\sigma}_s = \frac{0.072\, a^{1.25} S_p(f_{11}) (b/a)^{1.75}}{h^{1.75} \zeta^{0.56} [3(b/a)^2 + 2(a/b)^2 + 2]^{0.84}} \quad \text{ksi} \qquad (5.3.1\text{-}2)$$

$$S_p(f_{11}) = \sqrt{G_p(f_{11})}$$

The design nomograph based upon Equation (5.3.1-2) is presented in Figure 5.3.1-2.

Example: A flat aluminum-alloy, skin stringer structure is required to withstand an estimated service noise spectrum level of 120 dB. The design life is 5×10^8, the damping ratio is assumed to be 0.012, the assumed stringer spacing is a = 4.75 inches, and the aspect ratio is assumed to be 1.5. Following through the nomograph, Figure 5.3.1-2, as indicated by the arrows to obtain the skin thickness of h = 0.032 inches. From Figure 5.2.2-2 the fundamental mode response frequency is determined to be 370 Hz. At this frequency, the service noise spectrum level is checked with the noise spectrum level used above. If necessary, an iteration is made to obtain agreement.

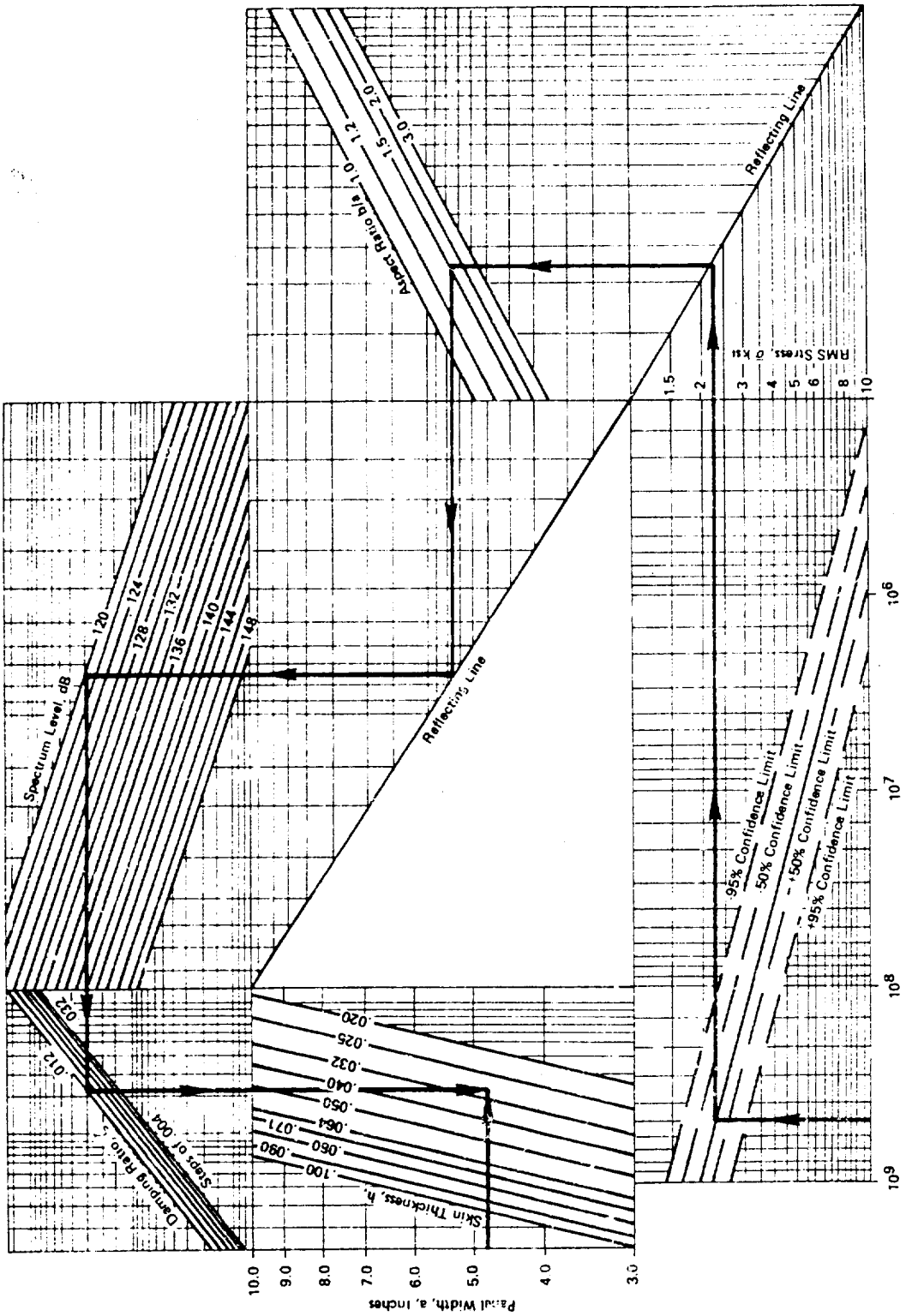

FIGURE 5.3.1-2 NOMOGRAPH FOR STRESS AND FATIGUE LIFE FOR STIFFENED PANEL SKIN AT AMBIENT TEMPERATURES - EQUATION (5.3.1-2) - (REF. 2)

To establish stringer geometry to provide a sonic fatigue life consistent with the skin design established by the methods of this section proceed to the next section

5.3.1.3 Stiffener Design Criteria for Ambient Temperatures

For stiffened-skin structure, such as illustrated in Figure 5.3.1-2, the skin and the stiffeners represent a coupled system so that the design life of each element must be considered together to establish an optimum design. Ballentine (2) used McGowan's (1) rib-flange design criteria to design the substructure for the stiffened-skin panel specimens described in Section 5.3.1.2. Ballentine observed no rib failures during the conduct of his experimental program. Rudder (3) refined McGowan's rib-flange design criteria by conducting acoustic fatigue tests under laboratory conditions using broadband random acoustic excitation.

This section presents a design equation and nomograph for estimating the stress response and fatigue life of stiffeners of flat stiffened aluminum alloy panels at ambient temperature (i.e., no mean thermal stress). It is possibly significant that Ballentine's specimens utilized extruded aluminum stiffeners with no failures observed and that Rudder's specimens utilized stiffeners brake-formed from flat sheet metal stock using standard aircraft manufacturing processes. Details of the rib configurations, test techniques, and response data can be obtained from the original reports.

Derivation: The stiffener design criteria are based upon an assumed fundamental mode response of a single bay of a multibay array of rectangular flat panels. The acoustic loading on the surface of the stiffened panel is transferred to the stiffeners predominately by a transverse shear loading, causing the stiffeners to bend and twist (see Appendix B.1.1). It is assumed that the stiffener is clamped at its end so that the loading is reacted at the clip attachment to the frame.

The flange stress design criterion is based upon specimens manufactured from 7075-T6 aluminum alloy material and may be used for aluminum alloys in general with design judgement. The criterion is based upon laboratory sonic fatigue tests of 12 stiffened panel designs with two specimens of each design tested simultaneously. The skin failures observed by Rudder were consistent with Ballentine's prediction method presented in Section 5.3.1.2. The range of design parameters covered in Rudder's experimental program were

skin thickness	0.032 inch	to	0.050 inch
stiffener thickness	0.025 inch	to	0.040 inch
stiffener spacing	6.0 inches	to	9.0 inches
stiffener shape	zee, channel, and hat cross section		
panel aspect ratio	2.0	to	3.0

Design Equation: The design equation for estimating the dynamic stress at the end of a stiffener at the clip attachment to the frame of a flat rectangular stiffened panel at ambient temperatures is given as

$$\bar{\sigma}_f = 0.372 \left[\frac{b^3 d\, S_p(f_{11}) \sqrt{f_{11}/\zeta_{11}}}{I^*[(b/a) + (a/b)]} \right]^{1/5} \quad \text{ksi} \qquad (5.3.1\text{-}3)$$

$$S_p(f_{11}) = \sqrt{G_p(f_{11})}$$

$$I^* = (I_{xx} I_{zz} - I_{zz}^2)/I_{zz}$$

Nomograph: The design equation given above was used to prepare a nomograph for its solution. The stress values obtained from this nomograph were related to the random fatigue failures experienced during Rudder's test program to obtain an estimate of fatigue life. In using Equation (5.3.1-3), one must first obtain an estimate of the fundamental mode response frequency from Figure 5.2.2-2 for clamped edges for the values of a, b, and h and use the value of $G_p(f_{11})$ corresponding to this response frequency. The stiffener thickness and shape are considered in the value of I^*. Expressions for the stiffener cross section parameters I_{xx}, I_{zz}, and I_{xz} are presented in Figures B.1.1-8 through -10. It will be necessary to iterate on the stiffener geometry (I^* and d) checking panel response frequency and excitation spectrum level at each step. It is suggested that the panel dimensions a, b, and h be selected first using the results of Section 5.3.1.2. It is also suggested that the design life for the stiffener be selected to be greater than that for the skin especially if the substructure is in a location that cannot be easily inspected. In this respect, the designer's judgement is very important. The design nomograph is presented in Figure 5.3.1-3.

Example: It is required to estimate the sonic fatigue life of an equal leg zee section aluminum stiffener with height d = 1.25 inches, thickness h_f = 0.040 inches, and flange width of 0.75 inch (I^* = 0.01255 inches^4, from Figure B.1.1-8) with the stiffener used with an aluminum panel with dimensions a = 9.0 inches, b = 18.0 inches and skin thickness h = 0.040 inches. Assume a spectrum level of 132 dB and damping ζ_{11} = 0.015.

From Figure 5.2.2-2 the fundamental mode response frequency is estimated to be 148 Hz. From Figure 5.3.1-2 or Equation (5.3.1-2) the estimated root mean square skin stress is 15.2 ksi with an estimated fatigue life of 1.5×10^5 cycles. From Figure 5.3.1-3 or Equation (5.3.1-3) one obtains an estimated root mean square flange stress of 4.27 ksi with an estimated fatigue life of 1.5×10^6 cycles.

For a response frequency of 148 Hz, the minimum cyclic life for the stringer is

$$\text{Life} = \frac{N}{3600\, f} = \frac{1.5 \times 10^6}{3600 \times 148} = 2.8 \text{ hrs.}$$

and for the skin

$$\text{Life} = \frac{1.5 \times 10^5}{3600 \times 148} = 0.282 \text{ hrs}$$

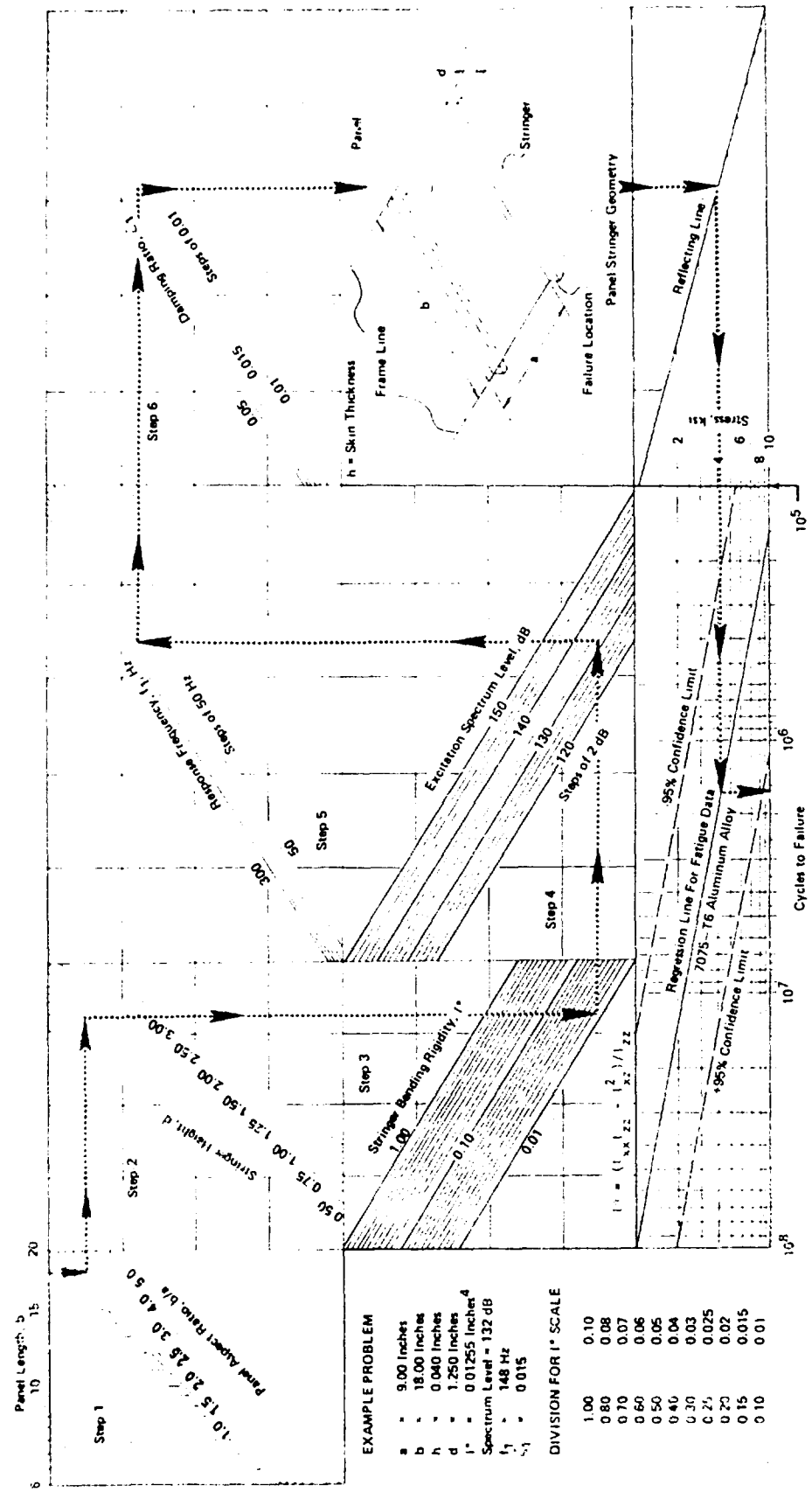

FIGURE 5.3.1-3 NOMOGRAPH FOR STRESS AND FATIGUE LIFE FOR STIFFENED PANEL STRINGER AT AMBIENT TEMPERATURES - EQUATION (5.3.1-3) - (REF. 3)

for a service spectrum level of 132 dB.

5.3.1.4 Skin Design Criteria for Elevated Temperatures

The response of stiffened-skin structure to a combined random acoustic and thermal environment was first considered by Ballentine (7). Recently, Schneider (4) and Jacobson (8) have conducted research programs to establish design criteria for structure at elevated temperatures. The analytical basis for the empirically determined design equations and nomographs presented in this section are discussed in Sections 5.2.2.2 and 5.2.2.3.

The basic effect of elevated temperatures is to induce inplane loading into the heated skin causing the skin to buckle between rivet lines. Once the panel buckles, the mean stress distribution varies along the edges of the panel being a minimum at the center of the panel edge (see Figure 5.2.2-15). If the buckled panel is exposed to random acoustic excitation, the panel may "oil can" or exhibit "snap-through" buckling causing large nonlinear strains and a very early fatigue failure. If the panel does not exhibit the "oil caning" effect, the fact that the panel has buckled will cause both the response frequency to increase and the mean stress distribution to vary significantly along the panel edge. The criterion for predicting an "oil can" effect developed by Jacobson (8) is presented for guidance. The criterion and design procedure developed by Schneider (4) is presented for panels that do not exhibit significant oil canning.

5.3.1.4.1 Skin Oil Canning Criterion

The prediction of oil canning of a thin-skin multibay panel is based upon the assumptions that each bay is represented as a simply supported plate with the geometry taken as the nominal dimensions of the bay. An iterative prediction technique is utilized to determine the panel dynamic amplitude resulting from the acoustic excitation. Then, the panel buckling amplitude due to the temperature rise above the ambient temperature is calculated.

Assuming that the panel responds in the fundamental mode and that the panel edges are completely restrained from movement in the plane of the panel, the criterion for predicting the presence of oil canning is that the following two inequalities are satisfied

$$1.5 < W_o/\overline{W} < 6.0 \qquad (5.3.1\text{-}4)$$

$$\overline{W}/h > 0.3$$

The constants appearing in Equation (5.3.1-4) were determined by thermal-acoustic response tests of three bay panel structure. The physical reasoning for the constants is as follows: If $W_o/\overline{W} > 1.5$, then it is implied that there is no stable curved configuration in the thermal-acoustic environment since the instantaneous dynamic deflections occur repeatedly whose amplitudes are greater than that corresponding to thermal buckling; $W_o/\overline{W} > 6.0$ implies that the dynamic deflection during acoustic response is less than the thermal buckling and the peaks of the acoustic excitation

and acoustic response will not cause the panel curvature to change from concave to convex or vice versa; if $\overline{W}/h < 0.3$ the panel dynamic displacement is small compared to the panel thickness with the resulting stresses being so small that sonic fatigue failure is not likely to occur.

To utilize the criterion, it is necessary to calculate the parameters W_o and $\overline{W}$. Assuming that the thermal buckling amplitude is small relative to the panel width and the panel is heated uniformly by a temperature rise, T, above ambient, from shallow strip theory one obtains

$$W_o = 0.707\, a \sqrt{\alpha T} \qquad \text{inches} \qquad (5.3.1\text{-}5)$$

where α is the coefficient of linear expansion for the material.

To determine the root mean square displacement response, $\overline{W}$, an iterative solution is required since the panel stiffness and hence response depends upon the panel response.

The expression for the fundamental mode response frequency is

$$f_{11} = \frac{1}{2\pi} \sqrt{K/M}\ , \quad \text{Hz} \qquad (5.3.1\text{-}6a)$$

where $K = \pi^4 D[1/a^2 + 1/b^2]^2 + \frac{\pi^4}{4} Eh[1/a^4 + 1/b^4]\overline{W}^2$

$$M = \rho h = \gamma h/386.4$$

The expression for the root mean square displacement response is - assuming a fundamental mode response and a constant acoustic pressure spectrum level in the frequency range of interest

$$\overline{W} = \frac{0.657}{K}\left[\frac{\pi f_{11} G_p(f_{11})}{4\zeta_{11}}\right]^{1/2} \qquad \text{inches} \qquad (5.3.1\text{-}6b)$$

An example will illustrate the iterative procedure for determining $\overline{W}$ and hence evaluating the oil canning criterion of Equation (5.3.1-4).

Example: A rectangular aluminum panel is to be exposed to random acoustic excitation with an average spectrum level of 116 dB while the panel is heated from 80°F to 100°F. The physical parameters for the problem are: $a = 8.0$ inches, $b = 16.0$ inches, $h = 0.040$ inches, $\gamma = 0.10$ lbs/in^3, $\zeta = 0.03$, $\alpha = 12.7 \times 10^{-6}$ in/in/°F, $E = 10.5 \times 10^6$ psi, and $\nu = 0.33$

The following parameters are independent of the panel dynamic response and are calculated first

$$D = Eh^3/12(1-\nu^2) = 62.84 \quad \text{in.lb.}$$

$$M = (0.10)(0.04)/386.4 = 1.035 \times 10^{-5} \ \text{lb.sec}^2/\text{in}^3$$

$$G_p(f_{11}) = 3.35 \times 10^{-6} \ (\text{psi})^2/\text{Hz.}$$

Then, from Equation (5.3.1-6a)

$$K/M = 2.256 \times 10^5 + 2.653 \times 10^3 \overline{W}^2 \qquad (a)$$

and from Equation (5.3.1-6b)

$$\overline{W} = 6.151 \times 10^{-3} \sqrt{f_{11}}/K \qquad (b)$$

The iteration procedure is to guess a value for $\overline{W}$, calculate the frequency from Equation (5.3.1-6a) using (a) above, and to use Equation (b) above to calculate $\overline{W}$. The procedure is repeated until the calculated value for $\overline{W}$ agrees with the guessed value.

Initially, one assumes $\overline{W}$ = 0.020 inches ($\overline{W}$ is one half the plate thickness) then from (a)

$$K_1/M = 2.256 \times 10^5$$

$$K_1 = 2.335 \ \text{lb/in}^3$$

$$f_1 = 75.6 \ \text{Hz.}$$

From (b), $\overline{W}_1 = 0.0229$ inches

Since the initial guess was low, guess $\overline{W}_2 = 0.023$ inch. Then, from (a)

$$K_2/M = 2.256 \times 10^5$$

$$K_2 = 2.335$$

$$f_2 = 75.6 \ \text{Hz.}$$

and from (b), $\overline{W}_2 = 0.0229$ inch.

Hence, the iteration is complete since the assumed value for $\overline{W}$ is essentially equal to the calculated value for $\overline{W}$.

For the temperature rise T = 100°F - 80°F = 20°F, one obtains from Equation (5.3.1-5), $W_o = 0.0902$ inch.

Then, $W_o/\overline{W} = 0.0902/0.023 = 3.92$

$$\overline{W}/h = 0.023/0.040 = 0.58$$

hence, from the criterion of Equation (5.3.1-4) it is expected that oil canning will occur (Jacobsen reports that a specimen tested under the conditions of this example did experience oil canning).

5.3.1.4.2 Skin Design Criteria

Stiffened panel structure exposed to a uniform temperature rise above the ambient temperature and not experiencing oil canning can be assessed as to the sonic fatigue life using the design procedure developed by Schneider (4). The procedure requires the calculation of several parameters using either design equations or nomographs.

Derivation: The skin design criteria for elevated temperatures is based upon an empirical correlation of experimental data of the analysis presented in Section 5.2.2.2.3. Certain of the assumptions used in the analytical development were negated by the empirical data correlation. The criteria are based upon laboratory sonic fatigue tests of 23 panel designs with two specimens of each design tested simultaneously. Thirteen of the panel designs were manufactured from 7075-T6 aluminum alloy material and ten of the panel designs were manufactured from 6AL-4V annealed titanium alloy. The range of physical parameters for the specimen designs were

skin thickness	0.024 inch to 0.063 inch
rib thickness	0.036 inch to 0.071 inch
rib spacing	5.0 inches to 9.0 inches
aspect ratio	1.5 to 3.0

The range of environmental parameters was based upon design limitations of the alloys considered as

7075-T6 aluminum	300°F maximum
6AL-4V annealed titanium	600°F maximum

Schneider (4) suggests that extension of the design procedure beyond the above limitations - especially material/temperature limits - should be taken with caution.

Design Equations: The design equations for estimating the thermal-acoustic response for flat stiffened-skin structure at elevated temperatures are presented below. An example will illustrate their use.

(a) Skin Buckling Temperature: The buckling temperature of a single panel of a multibay panel array as illustrated in Figure 5.3.1-1 is defined as the temperature rise above ambient temperature that will cause the skin to buckle and is given by

$$T_c = \frac{5.25h^2[b/a + a/b]}{\alpha ab(1 + \nu)} \quad {}^{o}F \text{ above ambient} \qquad (5.3.1\text{-}7)$$

The temperature ratio is defined as $r = T/T_c$ where T is the temperature rise of the structure above ambient.

(b) Skin Buckling Amplitude: The maximum buckling amplitude at the center of the panel is given by

$$W_o = 0 \quad \text{for} \quad r < 1 \tag{5.3.1-8a}$$

$$W_o = 2.50h\sqrt{(r-1)/R}\,[b/a + a/b]^{1.75} \quad \text{inches} \tag{5.3.1-8b}$$

$$\text{for} \quad r > 1$$

where $$R = 3[(5 - \nu^2)(b/a + a/b)^2 - 2(5 + \nu)(1 - \nu)]$$

(c) Mean Stress: The thermal stress, σ_T, due to the temperature rise of the constrained panel, and the skin buckling stresses, σ_{x_b} and σ_{y_b}, result in the following equations for the mean stress at the center of each side of the panel:

Center of the panel long side ($y = b/2$)

$$\sigma_x = [\sigma_T + \sigma_{x_b}] \times 10^{-3} \quad \text{ksi} \tag{5.3.1-9a}$$

Center of the panel short side ($x = a/2$)

$$\sigma_y = [\sigma_T + \sigma_{y_b}] \times 10^{-3} \quad \text{ksi} \tag{5.3.1-9b}$$

where $$\sigma_T = -E_e \alpha T/(1 - \nu)$$

$$\sigma_{x_b} = \frac{0.82\, E_e W_o^2}{ab(1 - \nu^2)}\,[(2 - \nu^2)b/a + \nu a/b]$$

$$\sigma_{y_b} = \frac{1.66\, E_e W_o^2}{ab(1 - \nu^2)}\,[\nu\, b/a + (2-\nu^2)a/b]$$

It is required to evaluate the mean stresses at both sides of the panel since the mean stress at the center of the short side is generally greater than the mean stress at the center of the long side. The fatigue life is estimated from random S-N curves for various mean stress levels so that the combination of dynamic and mean stress is important in determining the location of potential failure. This is in contrast to the ambient temperature situation where one can assume that failure will occur at the center of the long side of the panel.

(d) Elevated Temperature Response Frequency: The fundamental mode frequency for a temperature increase, T, is given by the following equations

$$f(r) = f_o[0.60 + 0.40\sqrt{1-r}] \quad \text{Hz} \quad 0 \leq r \leq 1 \tag{5.3.1-10a}$$

$$f(r) = f_o[0.60 + 0.44\sqrt{r-1}] \quad \text{Hz} \quad r \geq 1 \tag{5.3.1-10b}$$

$$f_o = 0.79\sqrt{E^*/\rho}\; h[1/a^2 + 1/b^2] \quad \text{Hz} \quad r = 0 \tag{5.3.1-10c}$$

$$E^* = E/(1-\nu^2)$$

(e) Dynamic Stress: The dynamic stresses at any temperature can be computed by the following equations

Center of the panel long side (y = b/2)

$$\bar{\sigma}_x = 3.60 \times 10^{-4} \frac{(b/h)^2 \sqrt{f(r)/\zeta}\, S_p(f(r))}{[3(b/a)^2 + 3(a/b)^2 + 2]} \quad \text{ksi} \qquad (5.3.1\text{-}11a)$$

Center of the panel short side (x = a/2)

$$\bar{\sigma}_y = 13.0 \times 10^{-4} \frac{(a/h)^2 \sqrt{f(r)/\zeta}\, S_p(f(r))}{[3(b/a)^2 + 3(a/b)^2 + 2]} \quad \text{ksi} \qquad (5.3.1\text{-}11b)$$

The elevated temperature panel response frequency, f(r), must be used for these calculations. The dynamic stresses at both locations must be calculated for elevated temperature applications because of the interaction of the mean stresses and the dynamic stresses.

Note: The expression for $\bar{\sigma}_x$, Equation (5.3.1-11a), evaluated at ambient conditions is slightly greater than Ballentine's criteria given by Equation (5.3.1-1). The expression for the ambient temperature fundamental mode response frequency, f_o, given by Equation (5.3.1-10c) yields estimates that are approximately 10% less than that given by Figure 5.2.2-2 for clamped edges.

Example: A flat stiffened panel structure is to be designed for a service life of 100 hours at a sound pressure spectrum level of 140 dB and a service temperature of 500°F. Stainless steel PH15-7 M_o is selected as the alloy to be used for this structure. The physical dimensions of the panel are a = 6.0 inches, b = 18.0 inches, h = 0.050 inch, ζ = 0.016 with the ambient temperature taken as 80°F.

From MIL-HDBK-5B(9), the material properties are $\gamma = 0.277$ lb/in^3, $\alpha = 6.1 \times 10^{-6}$ in/in/°F, $E = 29.0 \times 10^6$ psi at 80°F and $E_e = 26.98 \times 10^6$ psi at 500°F.

A fatigue curve for the alloy at the design temperature was obtained by Schneider (4) from MIL-HDBK-5B, with the compressive mean stresses extrapolated, to estimate the mean stress on fatigue life. This axial loading, constant amplitude, fatigue curve was converted to an equivalent random amplitude fatigue curve using the method of Section 6.5.1. This equivalent random amplitude fatigue curve is presented in Figure 5.3.1-4.

From Equation (5.3.1-7) the temperature rise required to cause the skin to buckle is

$$T_c = \frac{5.25(.050)^2(3.33)}{(6.1 \times 10^{-6})(6)(18)(1.32)} = 50.3°\text{F} \text{ above ambient}$$

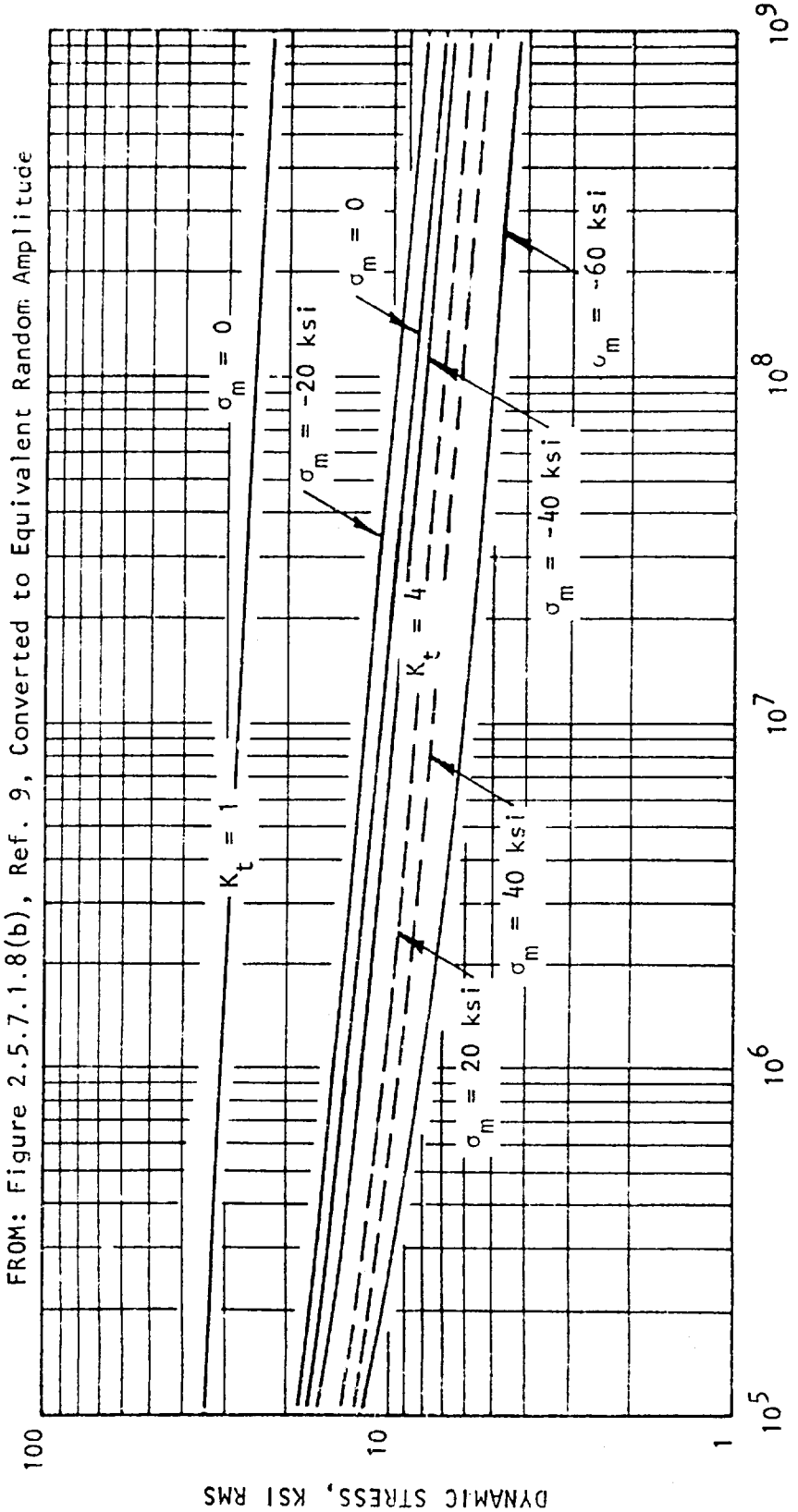

FIGURE 5.3.1-4 RANDOM LOADING FATIGUE CURVE FOR PH15-7Mo STAINLESS STEEL AT 500°F

The temperature ratio is r = (500-80)/50.3 = 8.35.

From Equation (5.3.1-8b) the buckling amplitude is

$$R = 3[(4.8976)(3.33)^2 - 2(5.32)(0.68)] = 141.2$$

$$W_o = 2.50(0.50)(7.35/141.2)^{1/2}(3.33)^{1.75} = 0.234 \text{ inch}$$

From Equations (5.3.1-9) the mean stresses are determined (using the value of E at the service temperature) to be

$$\sigma_T = -(26.97 \times 10^6)(6.1 \times 10^{-6})(420)/0.68 = -101.6 \text{ ksi}$$

$$\sigma_{x_b} = \frac{(0.82)(26.97 \times 10^6)(.234)^2}{(6)(18)(0.8976)}((1.8976)(3.0) + 0.32/3.0)$$

$$\sigma_{x_b} = 72.4 \text{ ksi}$$

$$\sigma_{y_b} = \frac{(1.66)(26.97 \times 10^6)(.234)^2}{(6)(18)(0.8976)}(0.32(3.0) + (1.8976)/3.0)$$

$$\sigma_{y_b} = 40.3 \text{ ksi}$$

and the mean stresses at the center of each side of the panel are

$$\sigma_x = -101.6 + 72.4 = -29.2 \text{ ksi}$$

$$\sigma_y = -101.6 + 40.3 = -61.3 \text{ ksi}$$

From Equation (5.3.1-10c) the ambient temperature fundamental mode response frequency is

$$f_o = (0.79)(3.231 \times 10^7 \times 386.4/0.277)^{1/2}(0.050)(3.086 \quad 10^{-2})$$

$$f_o = 259 \quad \text{Hz.}$$

The response frequency at the service temperature of 500°F is calculated from Equation (5.3.1-10b) as

$$f(r) = f_o[0.60 + 0.44(7.35)^{1/2}] = 1.793\ f_o = 464 \text{ Hz.}$$

The acoustic pressure spectral density corresponding to a spectrum level of 140 dB is

$$S_p(r(r)) = \sqrt{G_p(f(r))} = 2.9 \times 10^{(140/20-9)} = 2.9 \times 10^{-2} \quad psi/\sqrt{Hz}$$

From Equations (5.3.1-11) the dynamic stress response is calculated to be

$$\bar{\sigma}_x = 3.6 \quad 10^{-4}(18/0.05)^2(464/0.016)^{1/2}(2.9 \quad 10^{-2})/29.33$$

$$\sigma_x = 7.85 \text{ ksi}$$

$$\bar{\sigma}_y = 13.0 \quad 10^{-4}(6/0.05)^2(464/0.016)^{1/2}(2.9 \quad 10^{-2})/29.33$$

$$\bar{\sigma}_y = 3.15 \text{ ksi}$$

From Figure 5.3.1-4 and a stress concentration factor $K_T = 4$ with the dynamic stress $\bar{\sigma}_x = 7.85$ ksi and a mean stress of -29.2 ksi, one determines the fatigue life to be 4.5×10^8 cycles. For $\bar{\sigma}_y = 3.15$ ksi and a mean stress of -61.3 ksi one determines a fatigue life greater than 10^{10} cycles.

At the elevated temperature response frequency of 464 Hz, the minimum cyclic life of the structure is

$$\text{Life} = \frac{N}{3600f(r)} = \frac{4.5 \times 10^8}{(3600)\ (464)} = 269 \text{ Hours.}$$

Since the calculated Life is greater than the design service life of 100 hours the design should be optimized by reducing the skin thickness so that the estimated fatigue life is equal to or greater than the 100 hour requirement.

Nomographs: The design equations given above (Equations (5.3.1-7) through (5.3.1-11)) were used to prepare nomographs for their solution. The strain values and random fatigue failures experienced during Schneider's (4) test program were used to modify Ballentine's ambient temperature skin design nomograph, Figure 5.3.1-2, to account for effects of temperature increase. Schneider's modification of Ballentine's nomograph is presented in Figure 5.3.1-5 with the random fatigue curves for 7075-T6 aluminum alloy and 6A1-4V titanium alloy for the ambient and elevated temperatures indicated. The use of Figure 5.3.1-5 is identical to that described for the ambient temperature skin design nomograph given in Figure 5.3.1-2 except that the panel response frequency must now be determined from Equations 5.3.1-10 or using the following nomographs.

(a) Skin Buckling Temperature Nomograph: The solution for the skin buckling temperature (temperature rise required to cause the skin to buckle) as given by Equation (5.3.1-7) is presented in nomograph form in Figure 5.3.1-6.

(b) Skin Buckling Amplitude Nomograph: The solution for the skin buckling amplitude as given by Equation (5.3.1-8b) is presented in Figure 5.3.1-7 as a nomograph. The temperature ratio $r=T/T_c$ is required with T_c from Figure 5.3.1-6.

(c) Thermal Stress and Buckling Stress Nomographs: The compressive mean stress experienced by a heated panel in the prebuckled configuration is given by $\sigma_T = -E\alpha T/(1-\nu)$. A nomograph for calculating σ_T is presented in Figure 5.3.1-8. The compressive mean stress experienced by a heated panel in the buckled configuration is given as the sum of two terms $\sigma_T + \sigma_b$. The buckling stress, σ_b, must be evaluated both for the long side of the panel, σ_{x_b}, and the short side of the panel, σ_{y_b}. Figure 5.3.1-9 presents a nomograph for calculating σ_{x_b} and Figure 5.3.1-10 is a nomograph for calculating σ_{y_b}. The valves for σ_T, σ_{x_b} and σ_{y_b} as determined from Figures 5.3.1-8 through 5.3.1-10 are combined as follows:

$$\sigma_x = \sigma_T + \sigma_{x_b} \quad \text{ksi}$$

$$\sigma_y = \sigma_T + \sigma_{y_b} \quad \text{ksi}$$

The difference in this result and Equations (5.3.1-9) is that the nomographs calculate σ_T, σ_{x_b} and σ_{y_b} in ksi directly. Figures 5.3.1-9 and 5.3.1-10 require the value for the buckling amplitude, W_o, and the buckling temperature, T_c, from Figures 5.3.1-7 and 5.3.1-6, respectively.

In using Figures 5.3.1-9 and 5.3.1-10, use the value for Young's modulus corresponding to the service temperature.

(d) Elevated Temperature Response Frequency: The elevated temperature response frequency, as calculated from Equations (5.3.1-10), is also estimated using the nomographs presented in Figures 5.3.1-11 and 5.3.1-12. The ambient temperature fundamental mode response frequency is obtained from Figure 5.3.1-11 with Figure 5.3.1-12 being used to obtain the elevated temperature response frequency.

Computer Programs: A digital computer program developed by Rudder and Schneider (4) is presented here for calculating the dynamic response and life of a multi-bay, flat stiffened-skin structure exposed to simultaneous acoustic and thermal environments. Five sub-programs are required for the dynamic analysis program. These programs were developed for the Univac 1106 computer using Fortran V; however, the programs can readily be adapted to any digital computer.

Analysis Program: The input data format for the analysis program is shown in Table 5.3.1-1 and the input parameters are defined in Table 5.3.1-2. The computer program is listed in Table 5.3.1-3 while Table 5.3.1-4 contains a sample of the output format.

Sub-programs Required: The following sub-programs are required for this analysis program :

ETEMP (T, IFF) - Table 5.3.1-5

ALPHA (T, IFF) - Table 5.3.1-6

SN(SDYN, STEMP, TEMP, CTF, IFF) - Table 5.3.1-7

CTEMP (TCALP, TC, IFF) - Table 5.3.1-8

PROP (OPT, B, H, T, A, RJ, GAMAT, XIP) - Table 5.3.1-9

The input and output parameters for each sub-program are given in the following subsections. A listing of each of the sub-programs is contained in Tables 5.3.1-6 through 5.3.1-8. Since these sub-programs are either functions or subroutines, the input and output are controlled by the calling program.

(a) Sub-programs ETEMP and ALPHA: These functions compute modulus of elasticity and coefficient of thermal expansion, respectively, for aluminum and titanium alloys as a function of temperature. The basic alloy properties are from MIL-HDBK-5B. The input parameters are:

T - Input Temperature at which elastic modulus or coefficient of thermal expansion desired - ^{o}F

IFF - Alloy Code,

= 1 Titanium Alloy (6A1-4V annealed)

= 2 Aluminum Alloy (7075-T6)

(b) Sub-program SN: This subroutine computes the fatigue life of aluminum and titanium alloys as a function of dynamic and thermal mean stresses. The input parameters are:

SDYN - Dynamic Stress - ksi rms

STEMP - Thermal (or Mean) Stress - ksi

TEMP - Temperature - ^{o}F

IFF - Alloy Code,

= 1 Titanium Alloy (6A1-4V annealed)

= 2 Aluminum Alloy (7075-T6)

The output to the calling program is CTF - Life in cycles to failure.

(c) Sub-program CTEMP: This subroutine computes the skin critical buckling temperature for aluminum or titanium structures. The input parameters are:

TCALP - Product of critical buckling temperature and coefficient of thermal expansion; computed using Equation (5.3.1-7)

IFF - Alloy code,

= 1 Titanium Alloy (6A1-4V Annealed)

= 2 Aluminum Alloy (7075-T6)

The single output parameter to the calling program is:

TC - Critical buckling temperature - ^{o}F above ambient.

(d) Sub-program PROP: This program computes stiffening member properties such as area and moment of inertia. The basic relations are given in Figure B.1.1-8 through B.1.1-10. Three different sectional shapes are available, a zee, a channel, or a hat section with the parameters described in Figures B.1.1-8 through B.1.1-10.

The input parameters are

OPT - Option code to select sectional shape,

= 0 zee-section

= 1 channel section

B - Flange width of stiffening member - inch

H - Height of stiffening member - inch

T - Thickness of stiffening member - inch

The output parameters to the calling program are:

A - Cross-sectional area - in^2

RJ - St. Venant's Torsion Constant - in^4

GAMAT - Warping constant for thin-walled open-section beam, with the pole taken at the shear center - in^6

XIP - Polar moment of inertia, referenced to rotation about the attachment point - in^4

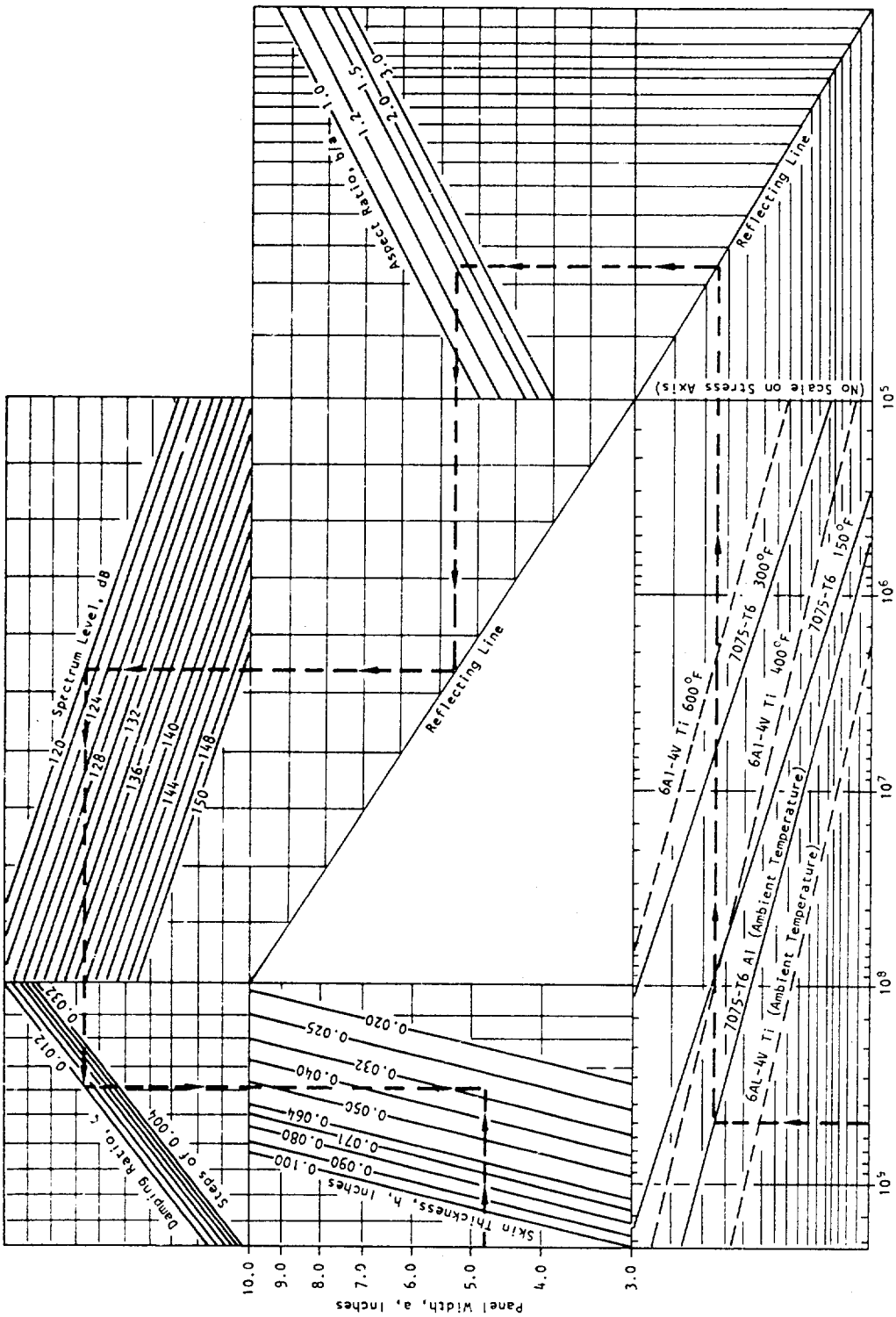

FIGURE 5.3.1-5 NOMOGRAPH FOR FATIGUE LIFE OF STIFFENED PANEL SKIN AT AMBIENT AND ELEVATED TEMPERATURES (REF. 4)

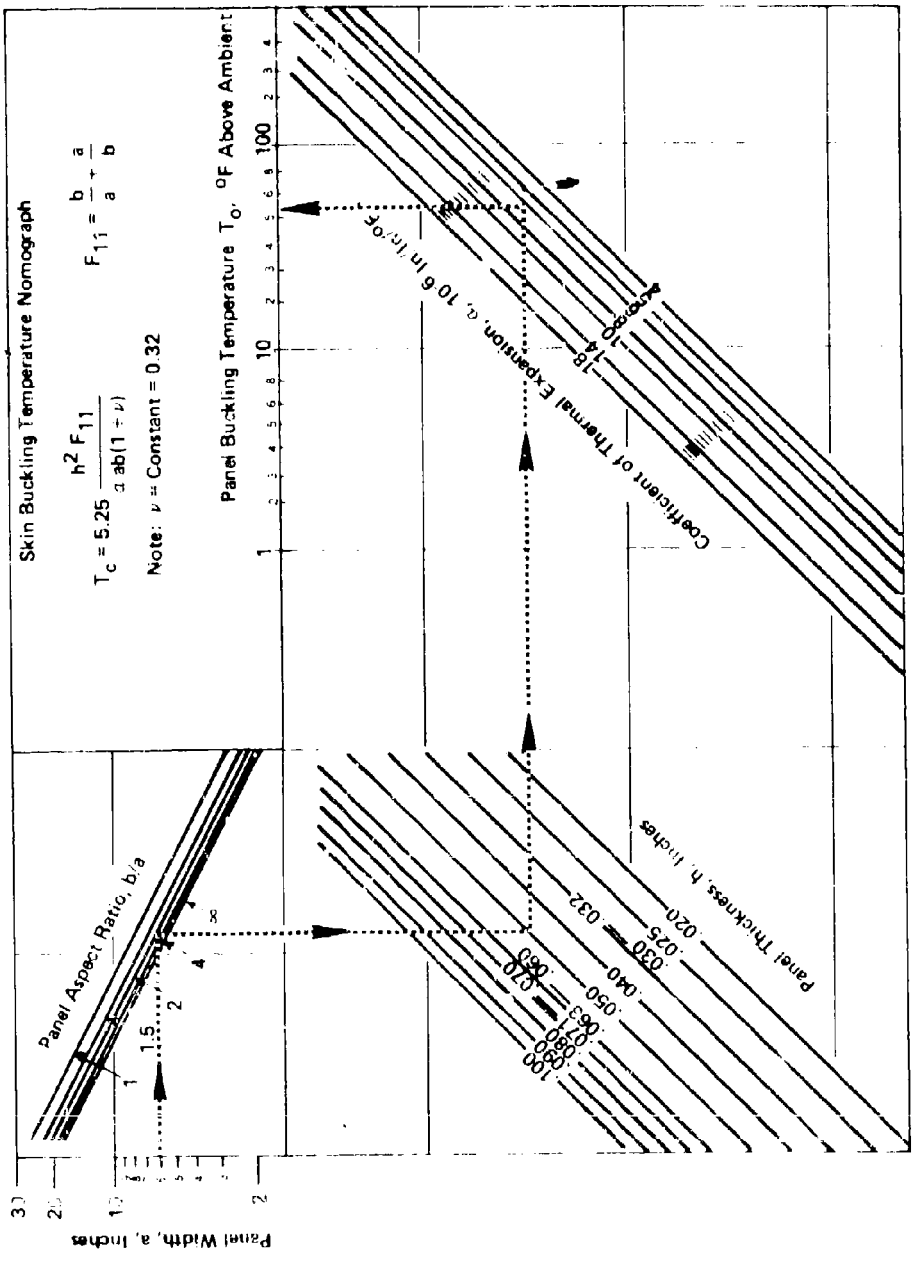

FIGURE 5.3.1-6 SKIN BUCKLING TEMPERATURE NOMOGRAPH (REF. 4)

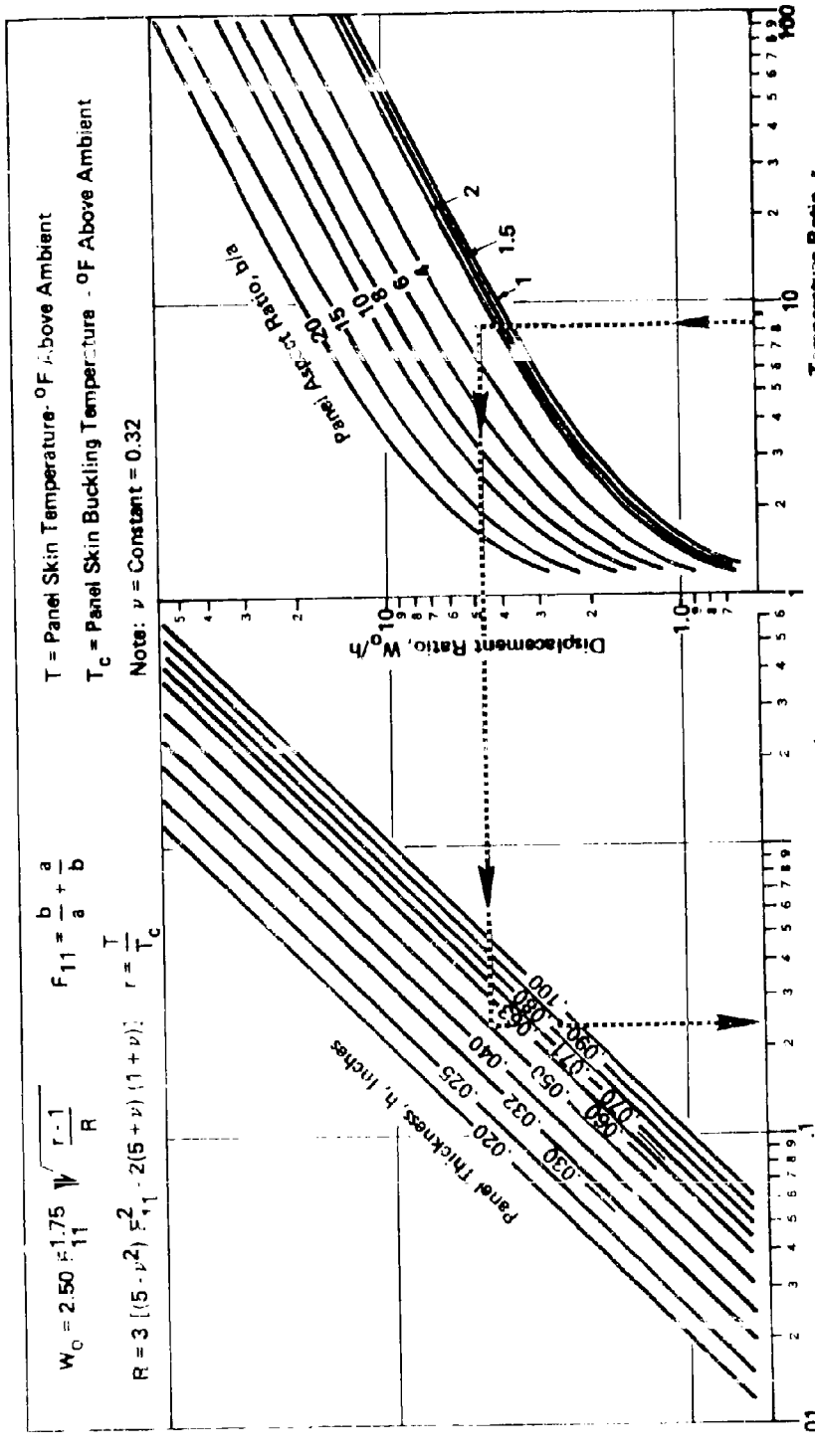

FIGURE 5.3.1-7 SKIN BUCKLING AMPLITUDE NOMOGRAPH (REF. 4)

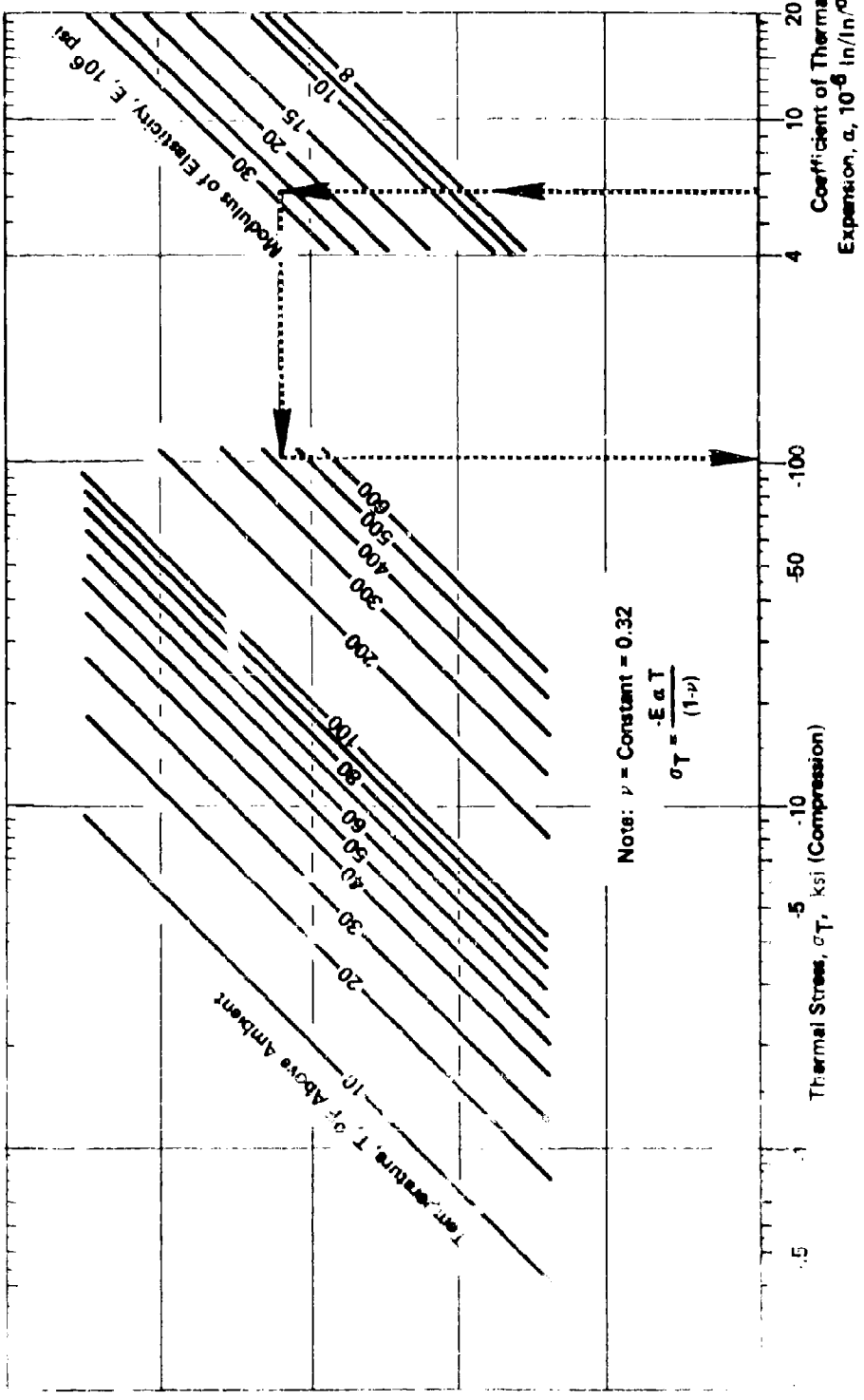

FIGURE 5.3.1-8 THERMAL STRESS NOMOGRAPH (REF. 4)

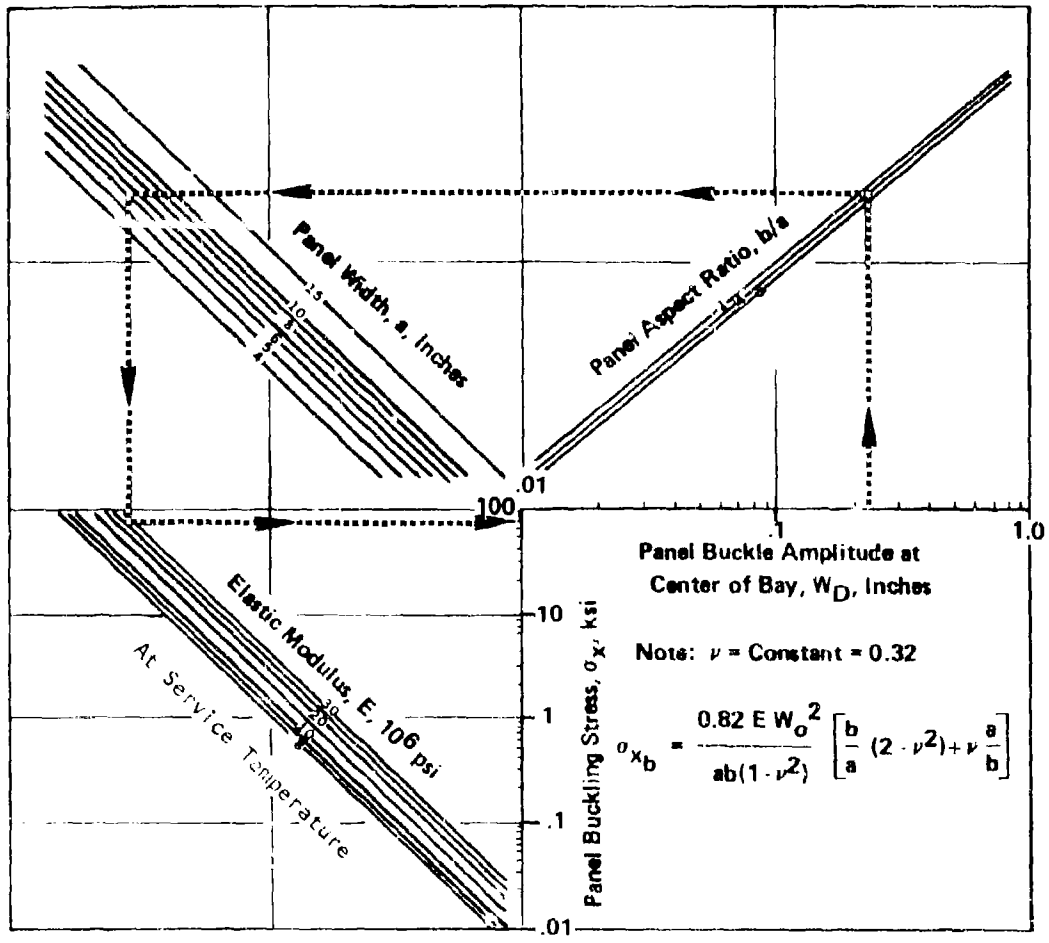

FIGURE 5.3.1-9 BUCKLING STRESS NOMOGRAPH : X-DIRECTION STRESS (REF. 4)

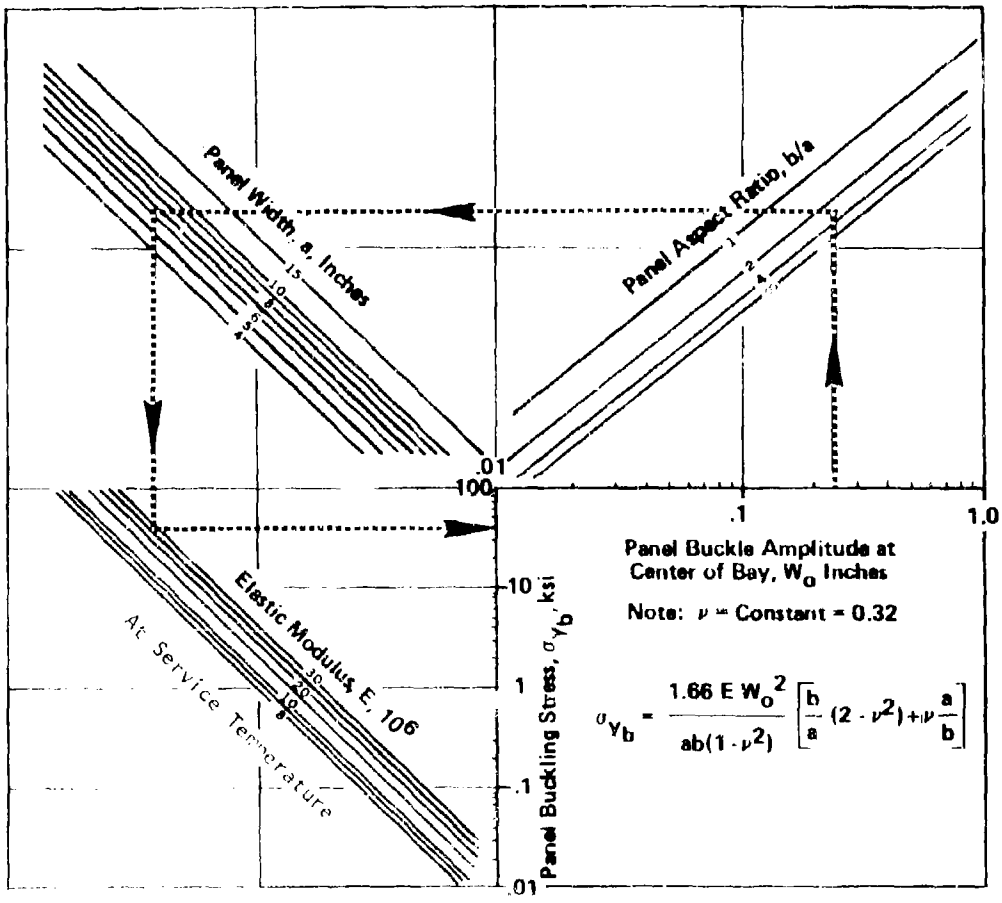

FIGURE 5.3.1-10 BUCKLING STRESS NOMOGRAPH: Y DIRECTION STRESS (REF. 4)

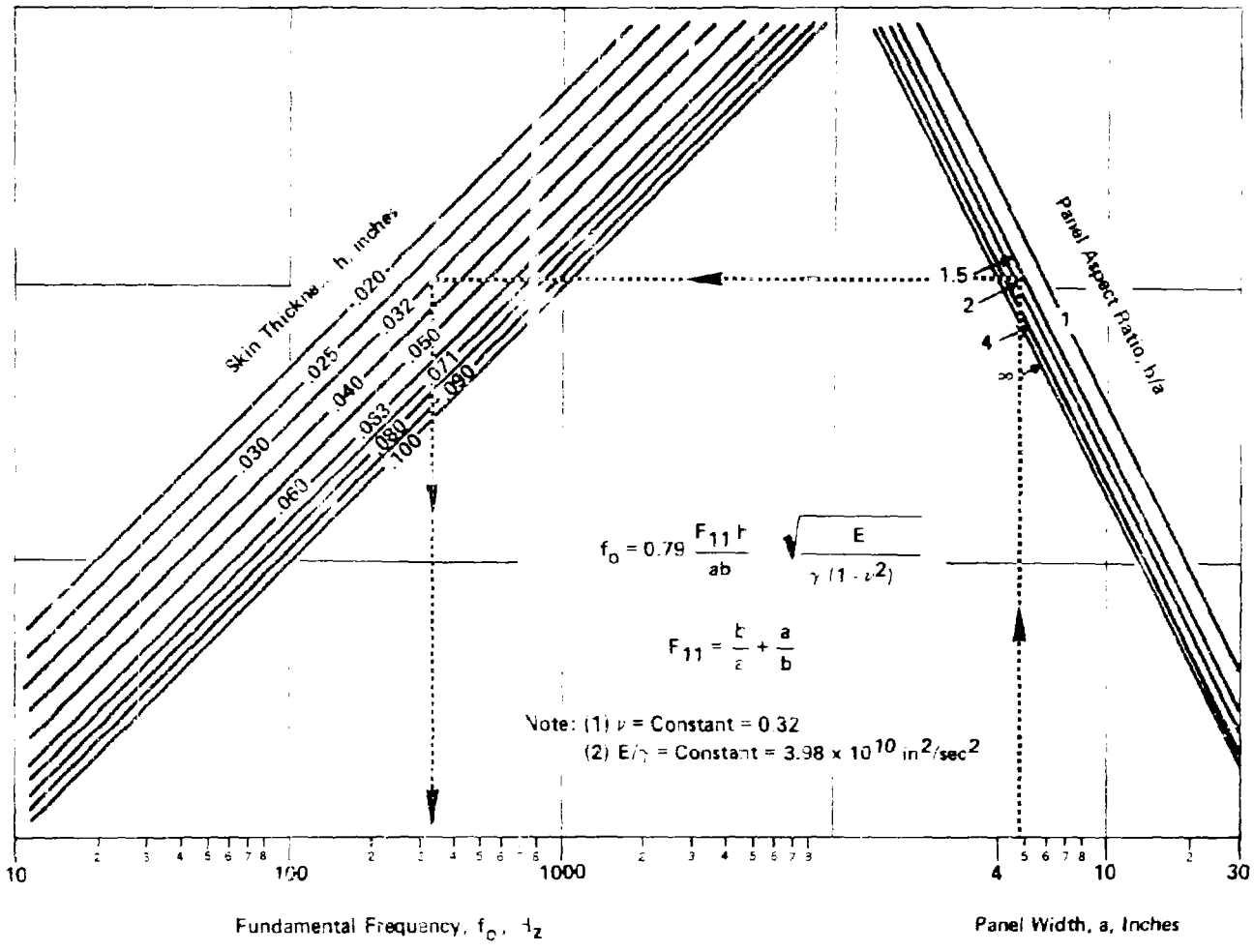

FIGURE 5.3.1-11 AMBIENT TEMPERATURE FUNDAMENTAL FREQUENCY NOMOGRAPH (REF. 4)

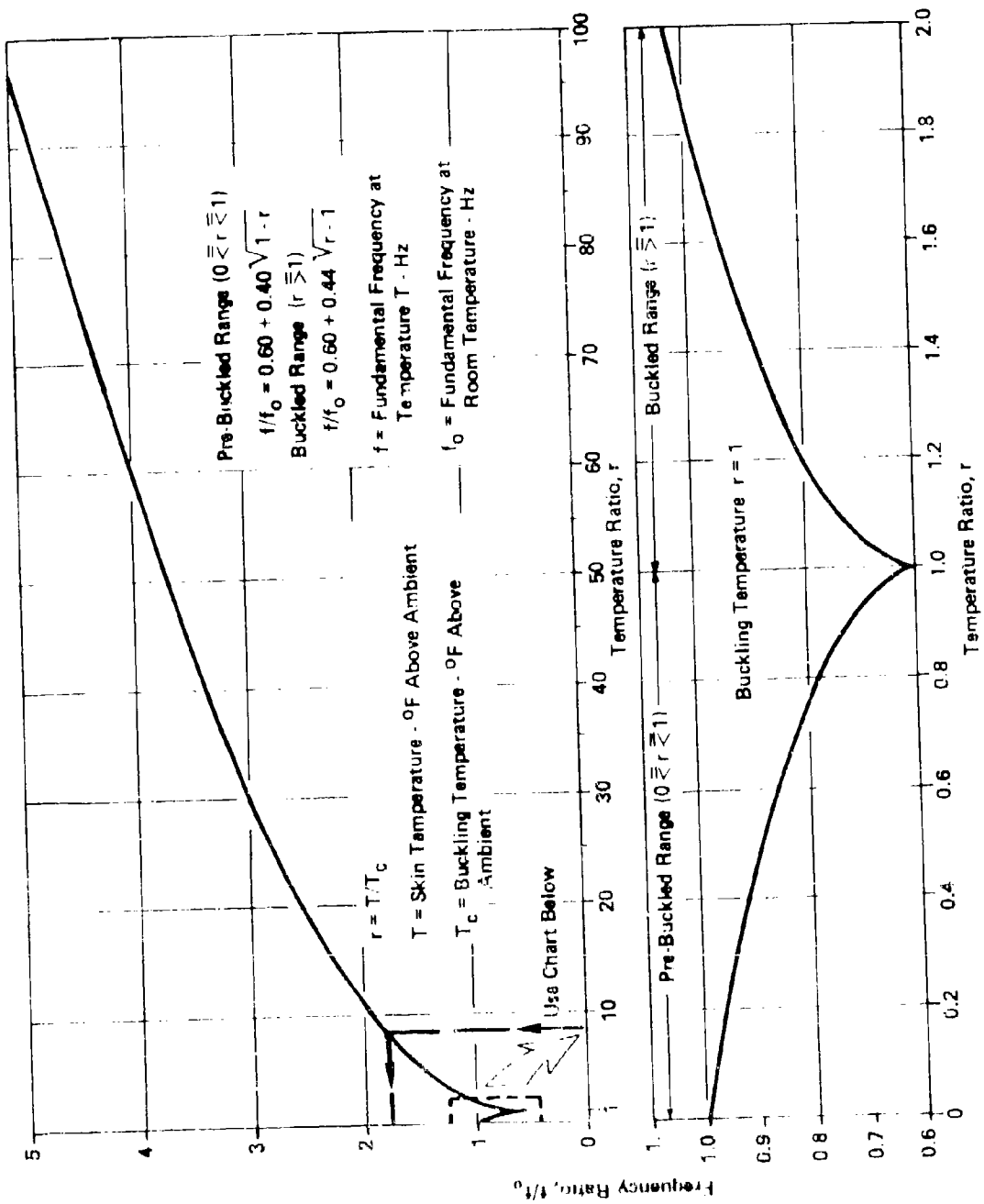

FIGURE 5.3.1-12 ELEVATED TEMPERATURE FUNDAMENTAL FREQUENCY NOMOGRAPH (REF. 4)

TABLE 5.3.1-1

DYNAMIC ANALYSIS COMPUTER PROGRAM INPUT FORMAT

CARD 1

NAME	NCASE	IFF
COL (FORMAT)	1 (12)	3 (12)

CARD 2

NAME	OPTX	BX	HX	TX
COL (FORMAT)	1 (12)	3 (F8.4)	11 (F8.4)	19 (F8.4)

CARD 3

NAME	OPTY	BY	HY	TY
COL (FORMAT)	1 (12)	3 (F8.4)	11 (F8.4)	19 (F8.4)

CARD 4

NAME	A1	A2	B2	B1
COL (FORMAT)	1 (F8.4)	9 F8.4)	17 (F8.4)	25 (F8.4)

CARD 5

NAME	TS	RHO	RNU	DAMP
COL (FORMAT)	1 (F8.4)	9 (F8.4)	17 (F8.4)	25 (F8.4)

CARD 6

NAME	PSL	T
COL (FORMAT)	1 (F8.4)	9 (F8.4)

TABLE 5.3.1-2

DYNAMIC ANALYSIS COMPUTER PROGRAM

INPUT PARAMETER DEFINITION

NCASE	Two-digit identification number
IFF	Alloy identification code, =1 Titanium Alloy (6Al-4V Annealed) =2 Aluminum Alloy (7075-T6)
OPTX BX HX TX	Input parameters defining stiffening member parallel to x-direction - see Sub-program PROP for definition
OPTY BY HY TY	Input parameters defining stiffening member parallel to y-direction - see Sub-program PROP for definition
A1 A2 B1 B2	Panel bay dimensions - See Figure 5.3.1-1
TS	Skin thickness - inch
RHO	Weight density of skin and stiffening member alloy - lb/in^3
RNU	Poisson's ratio for structure alloy
DAMP	Damping ratio for structure
PSL	Sound pressure spectrum level - dB
T	Structure temperature rise - ^oF above ambient

TABLE 5.3.1-3
COMPUTER PROGRAM LISTING
NINE BAY FLAT STIFFENED PANEL
(CONTINUED)

```
C         THIS PROGRAM CALCULATES THE DYNAMIC RESPONSE OF
C         A NINE-BAY FLAT STIFFENED PANEL EXPOSED TO A
C         UNIFORM ACOUSTIC PRESSURE AND A UNIFORM TEMP-
C         ERATURE RISE. ROOM TEMPERATURE IS 80 DEGREES F.
C
C         T IS A TEMPERATURE RISE, ABOVE ROOM TEMPERATURE
C
C         SUBPROGRAMS REQUIRED: ALPHA(T,IFF), ETEMP(T,IFF),
C           SN(SDYN,STEMP,T,CTF,IFF), CTEMP(TCALP,TC,IFF),
C           AND PROP(OPT,B,H,T,A,ZJ,WC,PIP)
C
C         FUNCTION DEFINATION
C
      F(B,A)=B/A+A/B
      R(B,A,PR)=3.*((5.-PR**2)*(B/A+A/B)**2-2.*(5.+PR)
     1           *(1.-PR))
  200 READ(5,301)NCASE,IFF
      READ(5,302)OPTX,BX,HX,TX
      READ(5,302)OPTY,BY,HY,TY
      READ(5,301)KK
      READ(5,303)A1,A2,B2,B1
      READ(5,303)TS,RHO,RNU,DAMP
      READ(5,303)PSL,T
C     INPUT DATA FORMAT STATEMENTS
  301 FORMAT(2I2)
  302 FORMAT(I2,3F8.4)
  303 FORMAT(4F8.4)
C        CALCULATE SUBSTRUCTURE PROPERTIES
      CALL PROP(OPTX,BX,HX,TX,AX,XJ,WCX,XI)
      CALL PROP(OPTY,BY,HY,TY,AY,YJ,WCY,YI)
      H=TS
      GM=RHO
      PR=RNU
C     CALCULATE STIFFENER STIFFNESS AND MASS
      RX1=0.05066*A1*A1*XJ/(WCX*(1.+PR))
      RX2=0.05066*A2*A2*XJ/(WCX*(1.+PR))
      RY1=0.05066*B1*B1*YJ/(WCY*(1.+PR))
      RY2=0.05066*B2*B2*YJ/(WCY*(1.+PR))
      SKX=WCX*(1.+RX2+2.*(A2/A1)*(1.+RX1))/A2
      SKY=WCY*(1.+RY2+2.*(B2/B1)*(1.+RY1))/B2
      H3=H*H*H
      STR=473.7408*(1.-PR*PR)*(SKX+SKY)/(H3*A2*B2)
      STR=STR/400.0
      A3=(A1/A2)**3
      B3=(B1/B2)**3
```

TABLE 5.3.1-3
(CONTINUED)

```
      GM=GM/386.
      SKM=0.25*GM*H*A2*B2*(1.+2.*A3+2.*B3+4.*A3*B3)
     1     +9.8696*GM*(XI*A2*(1.+2.*A3)/(B2*B2)
     2     +YI*B2*(1.+2.*B3)/(A2*A2))
C       CALCULATE COVER SHEET STIFFNESS AND MASS
      F22=F(B2,A2)
      F21=F(B2,A1)
      F12=F(B1,A2)
      F11=F(B1,A1)
      F1S=F22*F22+2.*(A1/A2)*F21*F21
     1     +2.*(B1/B2)*F12*F12+4.*(A1/A2)*(B1/B2)*F11*F11
C       ROOM TEMP STIFFNESS
      SK0=2.02937*ETEMP(80.,IFF)*H3*(F1S+STR)/((1.-PR*PR)
     1     *A2*B2)
C       ROOM TEMP FREQUENCY
      F0=0.164*SQRT(SK0/SKM)
C       CALCULATE ROOM TEMP MEAN SQUARE STRESS RESPONSE
      AR=3.*(B2/A2)**2+3.*(A2/B2)**2+2.
C       CONVERT DB TO PSI
      SPL=2.91*10.**(PSL/20.-9.)
C       CALCULATE ROOM TEMP DYNAMIC STRESS AT X=0,Y=B2/2
      SX0=1.36*B2*B2*SQRT(F0/DAMP)*SPL/(H*H*AR)
C       CALCULATE ROOM TEMP DYNAMIC STRESS AT X=A2/2,Y=0
      SY0=1.36*A2*A2*SQRT(F0/DAMP)*SPL/(H*H*AR)
C       CONVERT STRESS FROM PSI TO KSI
      SX0=SX0/1000.
      SY0=SY0/1000.
C       CALCULATE ROOM TEMPERATURE LIFE
      CALL SN(SX0,0.1,80.1,CTF1,IFF)
      CALL SN(SY0,0.0,80.1,CTF2,IFF)
      X1=A2/2.
      Y1=0.0
      X2=0.0
      Y2=B2/2.
      STEMP=0.0
C       PRINT ROOM TEMPERATURE RESPONSE
      WRITE(6,400)
      GO TO(201,202),IFF
  201 WRITE(6,405) NCASE
      GO TO 203
  202 WRITE(6,406) NCASE
  203 WRITE(6,410) PSL,T
      WRITE(6,415)
      WRITE(6,416) F0
```

TABLE 5.3.1-3
(CONTINUED)

```
      WRITE(6,420)
      WRITE(6,425)
      WRITE(6,430)  X2,Y2,SX0,STEMP,CTF1
      WRITE(6,430)  X1,Y1,SY0,STEMP,CTF2
C
C        THERMAL STRESS EFFECTS
C
      R22=R(B2,A2,PR)
      R21=R(B2,A1,PR)
      R12=R(B1,A2,PR)
      R11=R(B1,A1,PR)
      F2S=F22*(F22+2.*(A1/A2)**2*F21+2.*(B1/B2)**2*F12
     1    +4.*(A1/A2)**2*(B1/B2)**2*F11)
      RST=R22+2.*A3*R12+2.*B3*R21+4.*A3*B3*R11
      R0=(F1S+STR)/F2S
C        CALCULATE CRITICAL TEMPERATURE RISE, TCR
      TCALP=5.25*H*H*F22/(A2*B2*(1.+PR))
      CALL CTEMP(TCALP,TCR,IFF)
C        **NOTE** TCA AND RS ARE BUCKLING TEMPERATURE
C                 AND TEMPERATURE RATIO FOR AN EQUAL
C                 SIZE SIMPLE PANEL. R9 IS TEMP RATIO
C                 FOR NINE-BAY PANEL
      TCA=TCR/R0
      RS=T/TCA
      R9=T/TCR
      TACT=T+80.0
C        CALCULATE MATERIAL PROPERTIES AT TEMPERATURE
      ES=ETEMP(TACT,IFF)
      ALP=ALPHA(TACT,IFF)
      D=0.0833*ES*H3/(1.-PR*PR)
C        CALCULATE RESPONSE FREQUENCY AT TEMPERATURE,T
      SKT=D*F2S*R0/(A2*B2)
      FQT=0.809*SQRT(SKT/SKM)
C        **NOTE** FQT=F0, ROOM TEMP FREQUENCY
      STLIN=-ES*ALP*T/(1.-PR)/1000.0
      IF(RS-R0)205,205,210
C        PRE-BUCKLED RESPONSE
  205 FTEMP=FQT*(0.60+0.40*SQRT(1.-R9))
      SXT=STLIN
      SYT=STLIN
      W0=0.0
      GO TO 215
C        POST-BUCKLED RESPONSE
  210 FTEMP=FQT*(0.60+0.44*SQRT(R9-1.))
C        CALCULATE PLATE BUCKLING AMPLITUDE, W0
      W0=(3.37-0.20*R0)*H*SQRT(F2S*R0*(R9-1.)/RST)
```

TABLE 5.3.1-3
(CONCLUDED)

```
C          CALCULATE THERMAL STRESSES
       C1=1./(A2*B2*(1.-PR*PR))
       SXT=STLIN+0.81*ES*C1*((2.-PR*PR)*B2/A2+A2*PR/B2)
      1     *W0*W0/100.0
       SYT=STLIN+1.36*ES*C1*(PR*B2/A2+(2.-PR*PR)*A2/B2)
      1     *W0*W0/100.0
C        CALCULATE DYNAMIC STRESS
  215  CONTINUE
       C2=SQRT(FTEMP/F0)
       SX0=C2*SX0
       SY0=C2*SY0
C          CALCULATE ELEVATED TEMPERATURE LIFE
       CALL SN(SX0,SXT,TACT,CTF1,IFF)
       CALL SN(SY0,SYT,TACT,CTF2,IFF)
C          PRINT ELEVATED TEMPERATURE RESPONSE
       WRITE(6,435)
       TA=TCR+80.0
       WRITE(6,440) TCR
       WRITE(6,445) W0
       WRITE(6,416) FTEMP
       WRITE(6,420)
       WRITE(6,425)
       WRITE(6,430) X2,Y2,SX0,SXT,CTF1
       WRITE(6,430) X1,Y1,SY0,SYT,CTF2
       GO TO 200
C          FORMAT STATEMENTS FOR OUTPUT DATA
  400  FORMAT('1',25X,'DYNAMIC RESPONSE OF A',/,19X,
      1'NINE-BAY STIFFENED PANEL EXPOSED TO',/,21X,
      2'ACOUSTIC EXCITATION AND HEATING',/)
  405  FORMAT(29X,'DATA CASE',I4,//,27X,'MATERIAL : TITANIUM')
  406  FORMAT(29X,'DATA CASE',I4,//,27X,'MATERIAL : ALUMINUM')
  410  FORMAT(5X,'EXCITATION SPECTRUM LEVEL = ',F4.0,1X,'DB',
      13X,'TEMPERATURE INCREASE = ',F4.0,1X,'DEG. F',//)
  415  FORMAT(24X,'ROOM TEMPERATURE RESPONSE',/)
  416  FORMAT(20X,'FUNDAMENTAL FREQUENCY =',F7.1,' HZ',/)
  420  FORMAT(5X,'STRESS AT POINT',3X,'DYNAMIC STRESS',3X,
      1'THERMAL STRESS ',3X,'CYCLES TO FAILURE')
  425  FORMAT(8X,'X',7X,'Y',11X,'KSI',14X,'KSI',/)
  430  FORMAT(6X,F5.2,3X,F5.2,5X,F8.3,9X,F8.3,10X,1PE9.2,/)
  435  FORMAT(////,22X,'ELEVATED TEMPERATURE RESPONSE',/)
  440  FORMAT(10X,'BUCKLING TEMPERATURE =',F8.2,' DEG. F'
      1,' ABOVE ROOM TEMPERATURE',/)
  445  FORMAT(18X,'BUCKLING AMPLITUDE =',F8.4,
      1'  INCHES',/)
       END
```

TABLE 5.3.1-4

OUTPUT FORMAT FOR DYNAMIC ANALYSIS COMPUTER PROGRAM

DYNAMIC RESPONSE OF A
NINE-BAY STIFFENED PANEL EXPOSED TO
ACOUSTIC EXCITATION AND HEATING

DATA CASE 4

MATERIAL : ALUMINUM
EXCITATION SPECTRUM LEVEL = 135. DB TEMPERATURE INCREASE = 220. DEG. F

ROOM TEMPERATURE RESPONSE

FUNDAMENTAL FREQUENCY = 175.5 HZ

STRESS AT POINT X	Y	DYNAMIC STRESS KSI	THERMAL STRESS KSI	CYCLES TO FAILURE
.00	6.00	6.076	.000	6.43+06
3.00	.00	5.485	.000	1.03+07

ELEVATED TEMPERATURE RESPONSE

BUCKLING TEMPERATURE = 11.00 DEG. F ABOVE ROOM TEMPERATURE

BUCKLING AMPLITUDE = .2252 INCHES

FUNDAMENTAL FREQUENCY = 417.5 HZ

STRESS AT POINT X	Y	DYNAMIC STRESS KSI	THERMAL STRESS KSI	CYCLES TO FAILURE
.00	6.00	9.371	-16.838	1.32+05
3.00	.00	8.460	-24.342	1.40+05

TABLE 5.3.1-5
SUBPROGRAM LISTING: FUNCTION ETEMP

```
      FUNCTION ETEMP(T,IFF)
C
C        THIS FUNCTION COMPUTES ELASTIC MODULUS FOR
C        ALUMINUM OR TITANIUM ALLOY AS A FUNCTION OF
C        TEMPERATURE
C
C          T - INPUT TEMPERATURE - DEG. F
C          IFF - ALLOY CODE
C              = 1 TITANIUM
C              = 2 ALUMINUM
C
      GO TO (100,200),IFF
C  ***********************************************************
C     MATERIAL 6AL-4V TITANIUM ANNEALED SHEET
C     REFERENCE MIL-HDBK-5B
C     TEMPERATURE LIMITATION 800 DEGREES F
C          RT<T<800 F
 100  IF(800-T)180,150,150
 150  ETEMP=(1.030-0.000375*T)*16.6E+06
      RETURN
C             T>800 F
 180  ETEMP=12.1E+06
      WRITE(6,333)
      RETURN
C  ***********************************************************
C     MATERIAL 7075-T6 SHEET
C     REFERENCE MIL-HDBK-5B
C     TEMPERATURE LIMITATION 600 DEGREES F
C          RT<T<200 F
 200  IF(200-T)220,210,210
 210  ETEMP=(1.020-0.00030*T)*10.3E+06
      RETURN
C          200<T<400 F
 220  IF(400-T)240,230,230
 230  ETEMP=(0.96-0.00070*(T-200))*10.3E+06
      RETURN
C          400<T<600 F
 240  IF(600-T)260,250,250
 250  ETEMP=(0.82-0.0016*(T-400))*10.3E+06
      RETURN
C             T>600 F
 260  ETEMP=0.50*10.3E+06
      WRITE(6,333)
 333  FORMAT(/,5X,'UPPER TEMP LIMIT ON ELAST MODULUS',
     1' EXCEEDED',/)
      RETURN
      END
```

TABLE 5.3.1-6

SUBPROGRAM LISTING: FUNCTION ALPHA

```
      FUNCTION ALPHA(T,IFF)
C
C        THIS FUNCTION COMPUTES COEFFICIENT OF THERMAL
C        EXPANSION FOR ALUMINUM OR TITANIUM ALLOY AS A
C        FUNCTION OF TEMPERATURE
C
C          T - INPUT TEMPERATURE - DEG. F
C          IFF - ALLOY CODE
C              =1  TITANIUM
C              =2  ALUMINUM
C
      GO TO (100,200),IFF
C  ***********************************************
C     MATERIAL 6AL-4V TITANIUM SHEET
C     ANNEALED
C     REFERENCE MIL-HDBK-5B
C     TEMPERATURE LIMITATION 1000 DEGREES F
C          RT<T<200 F
  100 IF(200-T)180,150,150
  150 ALPHA=(4.45+0.00425*T)*1.0E-06
      RETURN
C          200<T<400 F
  180 IF(400-T)185,190,190
  190 ALPHA=(4.80+0.0025*T)*1.0E-06
      RETURN
C          400<T<1000 F
  185 IF(1000-T)195,198,198
  195 WRITE(6,500)
  500 FORMAT(/,5X,'UPPER TEMP LIMIT ON COEFF OF EXPAN ',
     1'EXCEEDED',/)
  198 ALPHA=5.8E-06
      RETURN
C  ***********************************************
C     MATERIAL 7075-T6 SHEET
C     REFERENCE MIL-HDBK-5B
C     TEMPERATURE LIMITATION 600 DEGREES F
C          RT<T<100 F
  200 IF(100-T)220,210,210
  210 ALPHA=(12.4+0.0050*T)*1.0E-06
      RETURN
C          100<T<300 F
  220 IF(300-T)240,230,230
  230 ALPHA=(12.9+0.00275*(T-100))*1.0E-06
      RETURN
C          300<T<400 F
  240 IF(400-T)260,250,250
  250 ALPHA=(13.45+0.00150*(T-300))*1.0E-06
      RETURN
C            T>400 F
  260 ALPHA=13.6E-06
      IF(600-T)280,270,270
  280 WRITE(6,500)
  270 RETURN
      END
```

TABLE 5.3.1-7

SUBPROGRAM LISTING: SUBROUTINE SN

```
      SUBROUTINE SN(SDYN,STEMP,TEMP,CTF,IFF)
C
C         THIS SUBROUTINE CALCULATES FATIGUE LIFE FOR
C         ALUMINUM OR TITANIUM ALLOY AS A FUNCTION OF
C         TEMPERATURE AND MEAN STRESS.  THIS SUBROUTINE
C         IS BASED ON COUPON FATIGUE TEST DATA AT ROOM
C         AND ELEVATED TEMPERATURE.
C
C         ROOM TEMPERATURE IS 80 DEG. F
C
C           SDYN - DYNAMIC STRESS - KSI (RMS)
C           STEMP - THERMAL (OR MEAN) STRESS - KSI
C           TEMP - TEMPERATURE - DEG. F
C           CTF - LIFE IN CYCLES TO FAILURE
C           IFF - ALLOY CODE
C               = 1 TITANIUM
C               = 2 ALUMINUM
C
      GO TO(100,200),IFF
C  ***********************************************************
C         MATERIAL 6AL-4V TITANIUM SHEET ANNEALED
C         TEMPERATURE LIMITATION 600 DEG. F
C
 100  C1=12.58-0.00376*TEMP
      C2=-5.40+0.00176*TEMP
      ARF=C1+C2*ALOG10(SDYN-0.1*STEMP)
      CTF=10.**ARF
      RETURN
C  ***********************************************************
C         MATERIAL 7075-T6 ALUMINUM SHEET
C         TEMPERATURE LIMITATION 300 DEG. F
C
 200  C1=10.89-0.00584*TEMP
      C2=-4.89+0.00347*TEMP
      ARF=C1+C2*ALOG10(SDYN-0.1*STEMP)
      CTF=10.**ARF
      RETURN
      END
```

TABLE 5.3.1-8

SUBPROGRAM LISTING: SUBROUTINE CTEMP

```
      SUBROUTINE CTEMP(TCALP,TC,IFF)
C         THIS SUBROUTINE CALCULATES SKIN BUCKLING
C         TEMPERATURE FOR ALUMINUM OR TITANIUM ALLOY
C         STRUCTURAL PANELS.
C
C           TCALP - PRODUCT OF BUCKLING TEMPERATURE
C                   AND ALPHA FROM CALLING PROGRAM
C           TC - BUCKLING TEMPERATURE - DEG F ABOVE
C                ROOM TEMPERATURE
C           IFF - ALLOY CODE
C               = 1 TITANIUM
C               = 2 ALUMINUM
C
      TC=0.0
      GO TO (100,200),IFF
C  ***** ***********************************************
C         MATERIAL 6AL-4V TITANIUM ANNEALED
C         TEMPERATURE LIMITATION 1000 DEG. F
C
  100 C1=4.45E-06
      C2=4.23E-09
      I=1
    1 C3=80.*C2+C1
      TC=.5*SQRT((C3/C2)**2+4.*TCALP/C2)-.5*C3/C2
      T=TC+80.
      IF(T-260.) 50,50,2
    2 IF(T-360.) 3,3,5
    3 C1=4.9E-06
      C2=2.5E-09
      I=I+1
      IF(I-2) 1,1,50
    5 C1=5.80E-06
      TC=TCALP/C1
   50 TC=TC
      RETURN
```

TABLE 5.3.1-8
(CONCLUDED)

```
C   ********************************************************************
C          MATERIAL 7075-T6 ALUMINUM ALLOY
C          TEMPERATURE LIMITATION 600 DEG. F
C
 200   F1=12.4E-06
       F2=5.0E-09
       II=1
 201   F3=80.*F2+F1
       TC=0.50*SQRT((F3/F2)**2+4.0*TCALP/F2)-0.50*F3/F2
       T=TC+80.
       IF(T-100.)500,500,202
 202   IF(T-300.)203,203,204
 203   F1=12.625E-06
       F2=2.75E-09
       II=II+1
       IF(II-2)201,201,500
 204   IF(T-400.)205,205,206
 205   F1=13.0E-06
       F2=1.5E-09
       II=II+1
       IF(II-2)201,201,500
 206   F1=13.6E-06
       TC=TCALP/F1
 500   TC=TC
       RETURN
       END
```

TABLE 5.3.1-9

SUBPROGRAM LISTING: SUBROUTINE PROP

```
      SUBROUTINE PROP(OPT,B,H,T,A,RJ,GAMAT,XIP)
C
C         SECTION PROPERTIES
C           IF OPT = 0  ZEE SECTION
C           IF OPT = 1  CHANNEL SECTION
C           H= STRINGER HEIGHT, CL TO CL
C           B= FLANGE WIDTH
C           T= STRINGER THICKNESS
C         REFERENCE: AFFDL-TR-71-107
C        WC - WARPING CONSTANT ABOUT SHEAR CENTER
C        GAMAT - WARPING CONSTANT ABOUT ATTACH POINT
C        A - CROSS SECTIONAL AREA
C        RJ- ST. VENANTS TORSION CONSTANT - J
C        XIP - POLAR MOMENT OF INERTIA ABOUT ATTACH POINT
      IF(OPT) 1,1,2
C
C        OPT = 0  ZEE STIFFENER
C
    1 A=T*(H+2.*B)
      D=H**2*(6.*B+H)
      D1=T**2*(3.*H+2.*B)
      XXI=(T*(D+D1))/12.
      D2=2.*B+T
      D3=2.*B-T
      XZI=-(T*H*D2*D3)/8.
      ZZI=(T/12.)*(8.*B**3+H*T**2)
      RJ=(T**3/3.)*(2.*B+H)
      WC=T*B**3*H**2*(B+2.*H)/(12.*(2.*B+H))
      SX=B/2.
      SZ=-H/2.
      D4=SX**2+SZ**2
      D5=D4*A
      XIP=(XXI+ZZI+D5)
      GAMAT=WC+(SZ**2)*ZZI-2.*SX*SZ*XZI+(SX**2)*XXI
      RETURN
C      CHANNEL SECTION
    2 F=2.*B+H
      XBAR=B**2/F
      F1=6.*B+H
      E=3.*B**2/F1
      CX=E+XBAR
      SX=E+(B/2.)
      SZ=-H/2.
      EX=CX-SX
      A=T*(H+2.*B)
      F2=3.*H+2.*B
      XXI=T*(H**2*F1+T**2*F2)/12.
      F3=12.*H*XBAR**2+8.*B**3
      F4=B-XBAR
      F5=B-2.*XBAR
      ZZI=T*(F3-24.*XBAR*B*F4+12.*B*F5*T+6.*F4*T**2+T**3)/12.
      RJ=T**3*F/3.
      F6=3.*B+2.*H
      WC=T*B**3*H**2*F6/(12.*F1)
      GAMAT=WC+(SZ**2)*ZZI+(SX**2)*XXI
      F7=(EX**2+SZ**2)*A
      XIP=(XXI+ZZI+F7)
      RETURN
      END
```

REFERENCES FOR SECTION 5.3.1

1. McGowan, P. R., et. al.; "Structural Design for Acoustic Fatigue," ASD-TDR-63-820, Air Force Flight Dynamics Laboratory, Wright-Patterson Air Force Base, Ohio, October 1963.

2. Ballentine, J. R., et. al.; "Refinement of Sonic Fatigue Structural Design Criteria," AFFDL-TR-67-156, Air Force Flight Dynamics Laboratory, Wright-Patterson Air Force Base, Ohio, January 1968.

3. Rudder, F. F.; "Acoustic Fatigue Resistance of Aircraft Structural Component Assemblies," AFFDL-TR-71-107, Air Force Flight Dynamics Laboratory, Wright-Patterson Air Force Base, Ohio, September 1971.

4. Schneider, C. W.; "Acoustic Fatigue of Aircraft Structures at Elevated Temperatures," AFFDL-TR-73-155, Part I and Part II, Air Force Flight Dynamics Laboratory, Wright-Patterson Air Force Base, Ohio, December 1973.

5. Arcas, N. R.; "Prediction of Stress and Fatigue Life of Acoustically-Excited Aircraft Structure," 39th Shock and Vibration Bulletin, Part 3, Shock and Vibration Information Center, Naval Research Laboratory, Washington, D. C.; January, 1969.

6. Phillips, E. J.; "Assessment of Siren Testing Techniques", Symposium on Acoustic Fatigue, AGARD-CP-113, Advisory Group for Aerospace Research and Development, NATO, September 1972.

7. Ballentine, J. R., et. al.; "Sonic Fatigue in Combined Environment," AFFDL-TR-66-7, Air Force Flight Dynamics Laboratory, Wright-Patterson Air Force Base, Ohio, May 1966.

8. Jacobson, M. J. and Finwall, P. E.; "Effects of Structural Heating on the Sonic Fatigue of Aerospace Vehicle Structures," AFFDL-TR-73-56, Air Force Flight Dynamics Laboratory Wright-Patterson Air Force Base, Ohio, January, 1974.

9. Anon., "Metallic Materials and Elements for Aerospace Vehicle Structures," MIL-HDBK-5B, September, 1971.

5.3.2 BOX STRUCTURE

The broad definition of a box type structure is taken to be two parallel plates stiffened by deep shear webs. Such a structure can be taken as a model for flap, fin, or pylon type structure encountered on modern aircraft. The box structure is classified by the number of cells formed by the intersecting cover sheets and ribs. An illustration of a two-dimensional nine cell box structure is presented in Figure 5.3.2-1.

An analysis of a three cell box structure was first considered by Clarkson and Abrahamson (1) using an assumed mode method. Mead and Sen Gupta (2) and Sen Gupta (3) present an analysis of a three cell box structure using wave propagation methods. Rudder (4) conducted an analytical-experimental program to establish sonic fatigue resistance criteria for nine cell box structure as illustrated in Figure 5.3.2-1. Subsequently, Clarkson and Ashie (5) presented a comparison of analytical results obtained using the NASTRAN finite element displacement method with high intensity acoustic response data for a seven cell box structure. Abrahamson (6) presents a graphical solution to the differential equations of motion for a one cell box structure with an indicated extension for multicell box structure. Thompson and Lambert (7) present design equations, nomographs, and a computer program for estimating the frequency and stress response of nine cell box structure.

5.3.2.1 Notation

a_1, a_2	Length of cover sheet bays in x-direction, Fig. 5.3.2-1
b_1, b_2	Length of cover sheet bays in y-direction, Fig. 5.3.2-1
${}_1D_s$	Cover sheet bending rigidity, Eqn. (5.3.2-2a)
d	Depth of box structure, Fig. 5.3.2-1 Lightening Hole depth, Figs. 5.3.2-11 and -12
E_1	Young's modulus of the cover sheet and rib material
e	Lightening hole bend radius
$F_{mn}(b,a)$	Defined by Equation (5.3.2-3b)
f_{mnq}	Natural Frequency of $(m,n,q)^{th}$ mode, Eqn. (5.3.2-1)
${}_1h_s, {}_2h_s$	Skin thickness, Fig. 5.3.2-1
${}_1h_r, {}_2h_r$	Rib thickness, Fig. 5.3.2-1
K_{mnq}	Modal stiffness of $(m,n,q)^{th}$ mode
K_r, K_s	Defined by Eqn. (5.3.2-2a)

ℓ	General length, see Figs. 5.3.2-4, -5, and -6
M_{mnq}	Modal mass of $(m,n,q)^{th}$ mode
M_r, M_s	Defined by Eqn. (5.3.2-2b)
$\overline{M}_x, \overline{M}_y$	Bending moments, see Figs. 5.3.2-4, -5, and -6
m	Mode number for x-direction
N	Constant in Eqn. (5.3.2-4a); cycles to failure
n	Mode number for y-direction
q	Mode number for z-direction
q_o	Spatially uniform static pressure
R	Radius of lightening hole
S	Rib spacing (general parameter), Figs. 5.3.2-9, -10, and -11
$S_p(f_1)$	Spectral density of acoustic pressure, $(psi)^2/Hz$.
γ	Weight per unit volume
γ_5, γ_6	Bending moment factors, Figs. 5.3.2-4, -5, and -6
$\delta_2, \ldots, \delta_6$	Bending moment factors, Figs. 5.3.2-4, -5, and -6
$\overline{\sigma}_{c_i}$	Stress defined by Eqn. (5.3.2-7)
$\overline{\sigma}_{e_i}$	Stress defined by Eqn. (5.3.2-8), ksi
$\overline{\sigma}_{o_i}$	Stress defined by Eqn. (5.3.2-5), dimensionless

5.3.2.2 Frequency Analysis of a Nine Cell Box Structure

The configuration of the nine cell box structure is illustrated in Figure 5.3.2-1. This configuration was adopted for Rudder's experimental program. The displacement components for each panel (either cover sheet or rib) are taken in terms of a product of sine waves in the directions of the plane of the panel. By emposing a zero shear condition at each intersection of a rib and cover sheet and assuming that all exterior edges of the structure are simply supported, one can obtain a mode shape description of the structure using three mode numbers (m,n,q). The mode number m denotes the number of half sine waves in the x-direction for each panel in the x-y plane; n denotes the number of half sine waves in the y-direction for each panel in the x-y plane; and q denotes the numoer of half sine waves in the z direction. Hence, the panels forming the cover sheets have mode numbers (m,n), the ribs parallel to the x-axis have mode numbers (m,q) and the ribs parallel to the y-axis have mode numbers (n,q). Typical mode shapes in the x-z plane for the middle row of cells of a nine cell box structure with geometry $a_1 = a_2 = a$ and $b_1 = b_2 = b$ are presented in Figure 5.3.2-2. This figure illustrates the important observation that for a fundamental mode in the cover sheet all rib depth modes can be excited.

Derivation: Using assumed modes as described above, Rudder (4) used the Rayleigh method to estimate the response frequency for the (m,n,q)th mode. Assuming that the material properties of all components are identical and that the thickness of the components are as illustrated in Figure 5.3.2-1, then the expression for the response frequency of the (m,n,q) mode is

$$f^2_{mnq} = \frac{K_{mnq}}{4\pi^2 M_{mnq}} \quad \text{Hz.}^2 \qquad (5.3.2\text{-}1)$$

The expression for the modal stiffness, K_{mnq}, is

$$K_{mnq} = \frac{\pi^4 {}_1D_s}{4a_2b_2} m^2n^2 \{[1 + (\frac{2h_s}{1h_s})^3]K_s + 2(\frac{1h_r}{1h_s})^3 K_r\} \qquad (5.3.2\text{-}2a)$$

where $${}_1D_s = E\,{}_1h_s^3/12(1-\nu^2)$$

$$K_s = F_{mn}(b_2, a_2) + 2[(a_1/a_2)F_{mn}(b_2,a_1) + (b_1/b_2)F_{mn}(b_1,a_2) + 2(a_1/a_2)(b_1/b_2)F_{mn}(b_1,a_1)]$$

$$K_r = (d/b_2)[F_{mq}(d,a_2) + 2(a_1/a_2)F_{mq}(d,a_1)] + (d/a_2)({}_2h_r/{}_1h_r)^3[F_{nq}(d,b_2) + 2(b_1/b_2)F_{nq}(d,b_1)]$$

$$F_{mn}(b,a) = [(\frac{m}{n})(\frac{b}{a}) + (\frac{n}{m})(\frac{a}{b})]^2$$

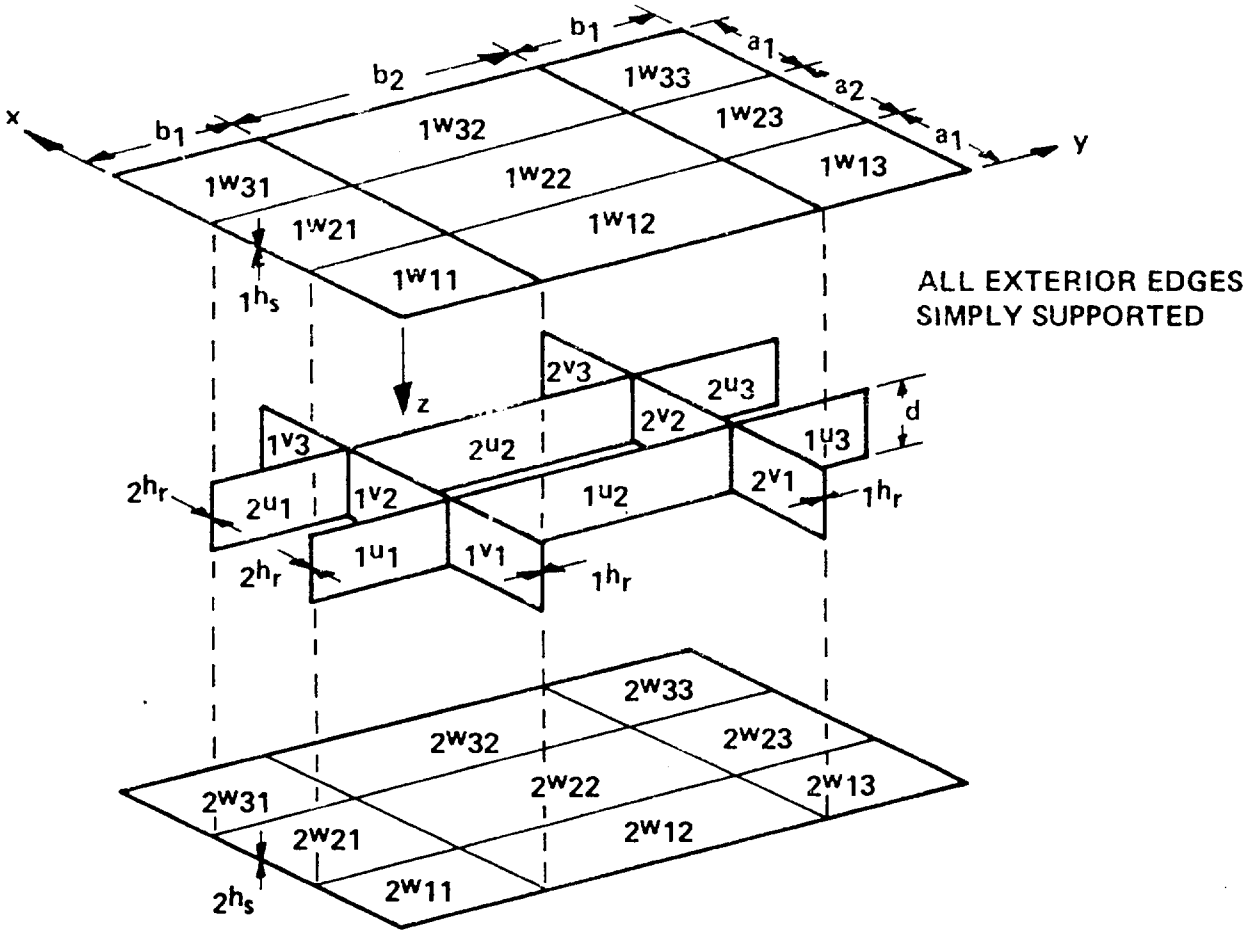

NINE CELL CONFIGURATION (EXPLODED)

FIGURE 5.3.2-1 NINE CELL BOX STRUCTURE CONFIGURATION (REF. 4)

A = d/b

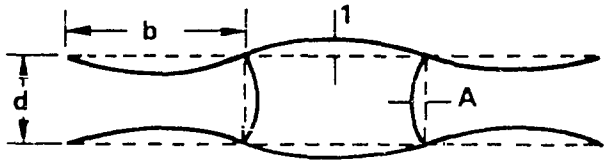

MODE (1,1,1)

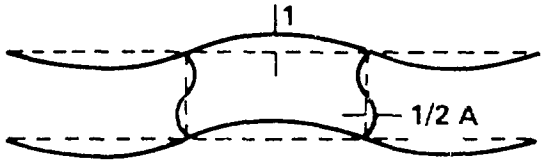

MODE (1,1,2)

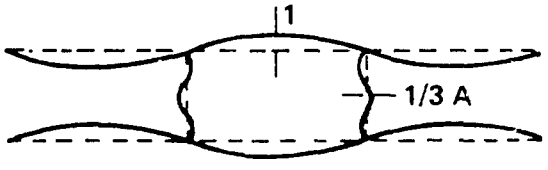

MODE (1,1,3)

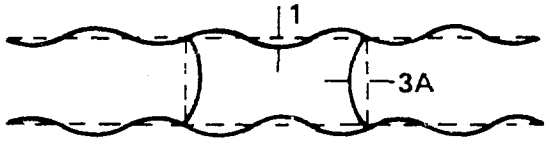

MODE (1,3,1)

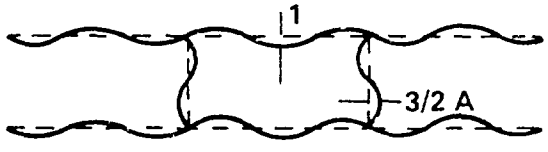

MODE (1,3,2)

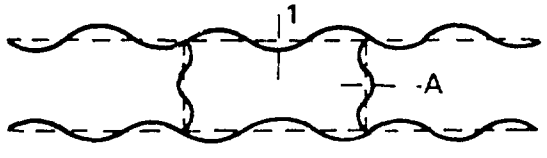

MODE (1,3,3)

(a/2,y,z) PLANE

FIGURE 5.3.2-2 MODE SHAPES FOR BOX STRUCTURE (REF. 4)

The expression for the modal mass, M_{mnq}, is

$$M_{mnq} = \frac{1}{4} \rho_s a_2 b_2 \{(1 + {}_2h_s/{}_1h_s)M_s + 2(\frac{{}_1h_r}{{}_1h_s})(\frac{d}{b_2})^3 (\frac{n}{q})^2 M_r\} \qquad (5.3.2\text{-}2b)$$

where ${}_1\rho_s = \rho\, {}_1h_s$ (ρ is the mass per unit volume)

$$M_s = 1 + 2(a_1/a_2)^3 + 2(b_1/b_2)^3 + 4(a_1/a_2)^3(b_1/b_2)^3$$

$$M_r = 1 + 2(a_1/a_2)^3 + (\frac{{}_2h_r}{{}_1h_r})(\frac{b_2}{a_2})^3 (\frac{m}{n})^2 [1 + 2(b_1/b_2)^3]$$

Equations (5.3.2-2) can be greatly simplified if one considers the special geometry: $a_1 = a_2 = a$, $b_1 = b_2 = b$, ${}_1h_s = {}_2h_s = h_s$, and ${}_1h_r = {}_2h_r = h_r$. Then, the expression for the modal stiffness for the (m,n,q)th mode is

$$K_{mnq} = \frac{3\pi^2 D_s}{2ab} m^2 n^2 \{3F_{mn}(b,a) + (\frac{h_r}{h_s})^3 [(\frac{d}{b})F_{nq}(d,a) + (\frac{d}{a})F_{nq}(d,b)]\} \qquad (5.3.2\text{-}3a)$$

and the expression for the modal mass is

$$M_{mnq} = \frac{3}{2} \rho h_s ab[3 + [1 + (\frac{b}{a})^3 (\frac{m}{n})^2](\frac{h_r}{h_s})(\frac{d}{b})^3 (\frac{n}{q})^2] \qquad (5.3.2\text{-}3b)$$

where $D_s = Eh_s^3/12(1-\nu^2)$

$$F_{mn}(b,a) = [(\frac{m}{n})(\frac{b}{a}) + (\frac{n}{m})(\frac{a}{b})]^2$$

5.3.2.3 Stress Response of a Nine Cell Box Structure

As indicated by Equation (5.2.2-60d), the stress response of the skin and ribs for box structure due to a uniform static pressure of unit magnitude is required to estimate the mean square or rms stress response of the structure. The approach taken here is dependent upon the flexibility of box-type structure as described by Clarkson (8) and is essentially different from the approach taken by Ballentine (see Section 5.3.1.2). The approximate method for computing stresses in continuous slabs as described by Timoshenko (9, pp. 236-245) is presented here -- modified to account for the rib supporting the cover sheet. This modification was first described by Clarkson (8).

Derivation: Timoshenko's approximate method relies upon the synthesis of elementary solutions for uniformly loaded thin rectangular plates to obtain estimates of stresses in continuous slabs. The basic procedure is to divide

the bays of the structure into components such that boundaries between adjacent bays are considered to be clamped. Considering the plan-form of the cover sheet for nine-cell box structure as illustrated in Figure 5.3.2-1 the bays of structure are taken with the boundary conditions as illustrated in Figure 5.3.2-3. Timoshenko presents tabulated data for estimating the bending moments at the panel center and the center of a clamped edge for uniformly loaded plates with various boundary conditions. At a point on the boundary between two plates, the resultant bending moment is approximated by the average value of the component bending moments. As illustrated in Figure 5.3.2-3, four different sets of boundary conditions are to be considered. Case 1 represents a rectangular plate with three edges supported and one edge clamped. Case 2 represents a rectangular plate with two opposite edges supported and two opposite edges clamped. Case 3 represents a rectangular plate with one edge supported and three edges clamped. Finally, Case 4 represents a rectangular plate with all edges clamped. The bending moments at the center of a clamped edge for a rectangular plate with dimensions a × b uniformly loaded by a pressure of magnitude q_o is given by Timoshenko as:

Case 1	$\bar{M}_y = \delta_2 q_o \ell^2$	at $(x,y)^* = (a/2,0)$
Case 2	$\bar{M}_y = \delta_3 q_o \ell^2$	at $(x,y) = (a/2,0)$ & $(a/2,b)$
Case 3	$\bar{M}_x = \gamma_5 q_o \ell^2$	at $(x,y) = (0,b/2)$ & $(a,b/2)$
	$\bar{M}_y = \delta_5 q_o \ell^2$	at $(x,y) = (a/2,0)$
Case 4	$\bar{M}_x = \gamma_6 q_o \ell^2$	at $(x,y) = (0,b/2)$ & $(a,b/2)$
	$\bar{M}_y = \delta_6 q_o \ell^2$	at $(x,y) = (a/2,0)$ & $(a/2,b)$

where ℓ is the smaller of the dimensions a and b and the subscripts on the γ's and δ's (the bending moment factors) follow Timoshenko's notation. Plotted values of the bending moment factors versus panel aspect ratio b/a are present in Figures 5.3.2-4 through 5.3.2-6. For more accurate values of the bending moment factor, the referenced tabulated values can be used. The asymptotic values for the bending moment factors are listed in Table 5.3.2-1.

TABLE 5.3.2-1

ASYMPTOTIC VALUES OF THE BENDING MOMENT FACTORS

b/a	δ_2	δ_3	γ_5	δ_5	γ_6	δ_6
0.0	.1250	.0833	-	-	.0571	.0833
∞	.1250	.1250	.0833	.0566	.0833	.0571

Note: All values for the bending moment factors as presented here are positive instead of negative as presented by Timoshenko.

*(x,y) taken as local coordinates in each bay.

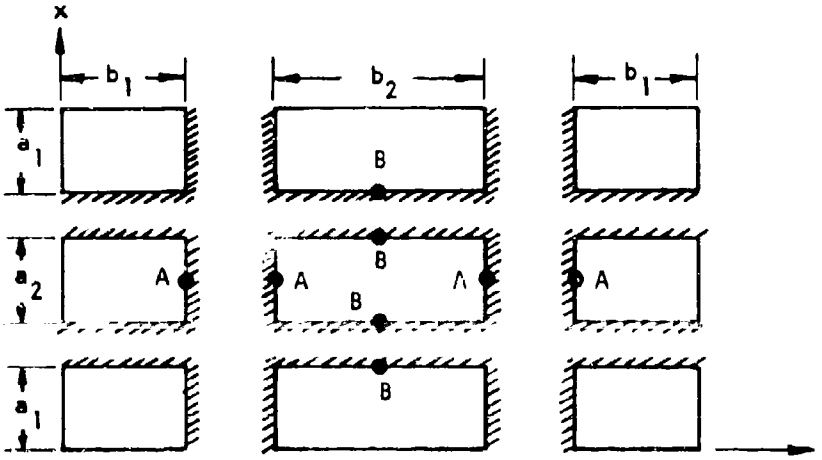

FIGURE 5.3.2-3 COMPONENT BOUNDARY CONDITIONS FOR BOX STRUCTURE STRESS CALCULATION (REF 4)

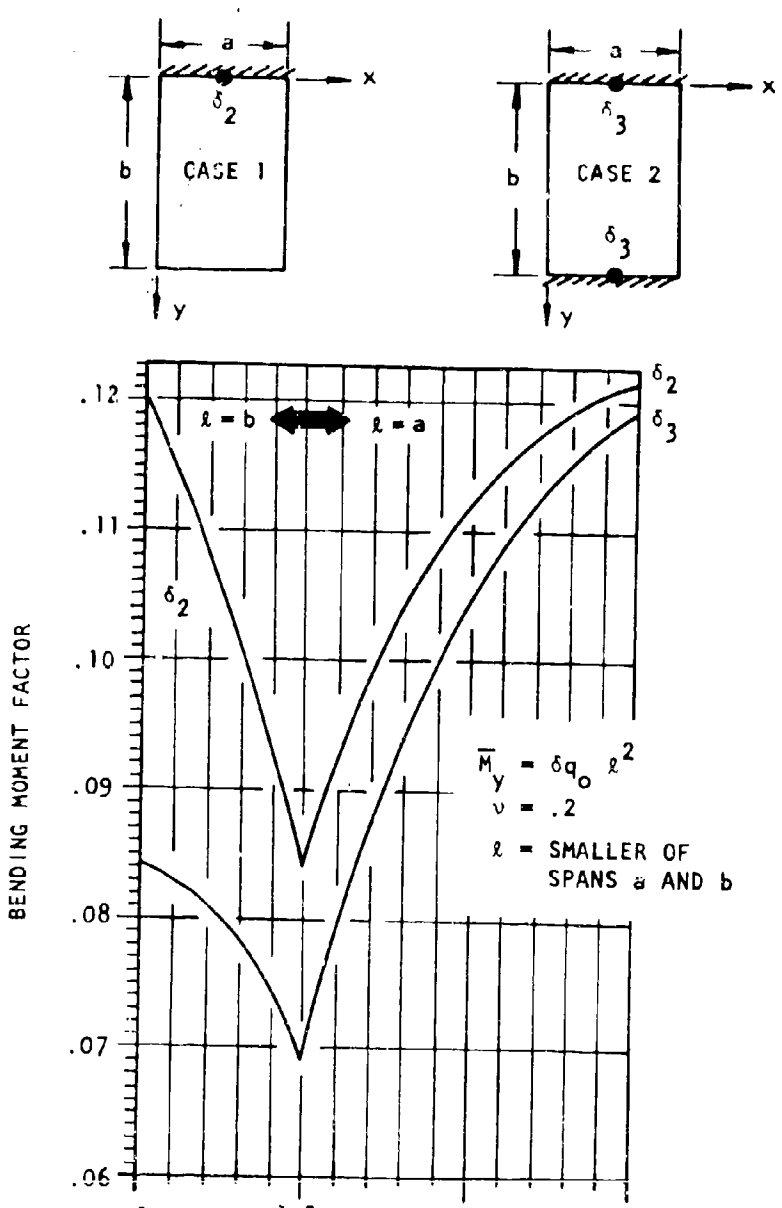

FIGURE 5.3.2-4 BENDING MOMENT FACTOR CASES 1 AND 2 (REF. 4)

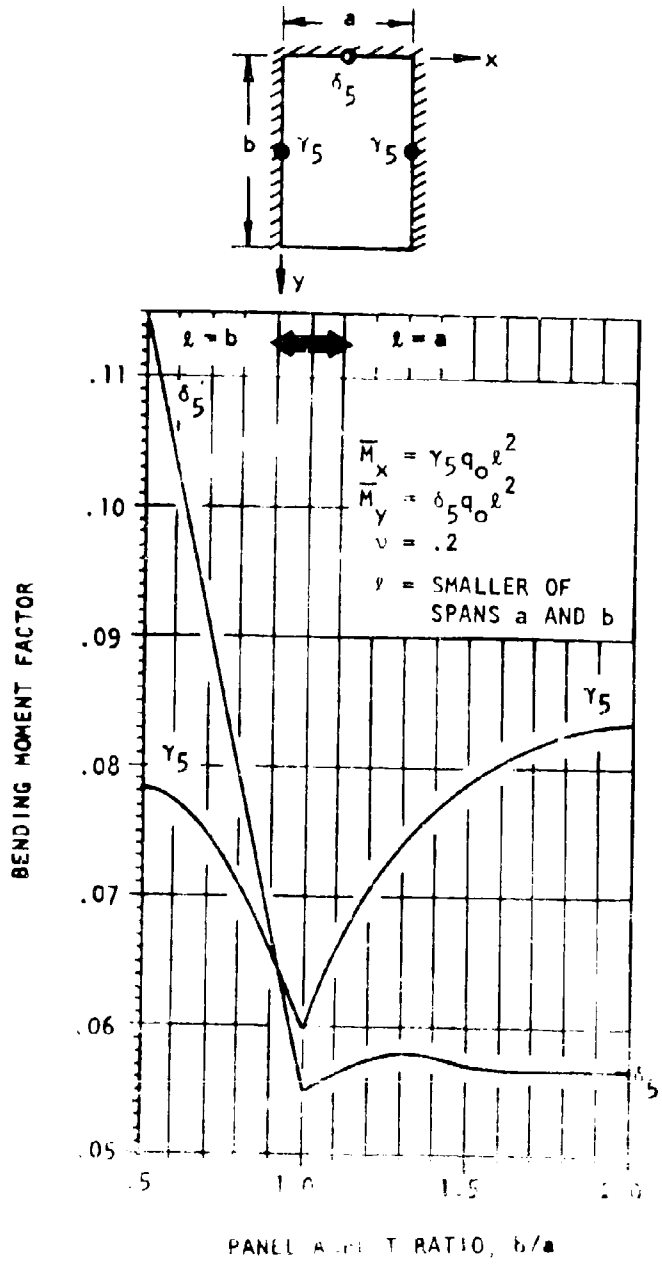

FIGURE 5.3.2-5 BENDING MOMENT [illegible] FOR [illegible] (2-1/4)

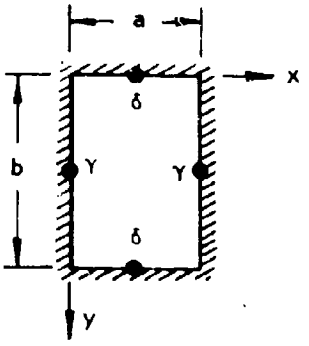

$\bar{M}_x = \gamma_6 q_o \ell^2$ $\bar{M}_y = \delta_6 q_o \ell^2$

$\nu = .2$ ℓ = SMALLER OF SPANS a AND b

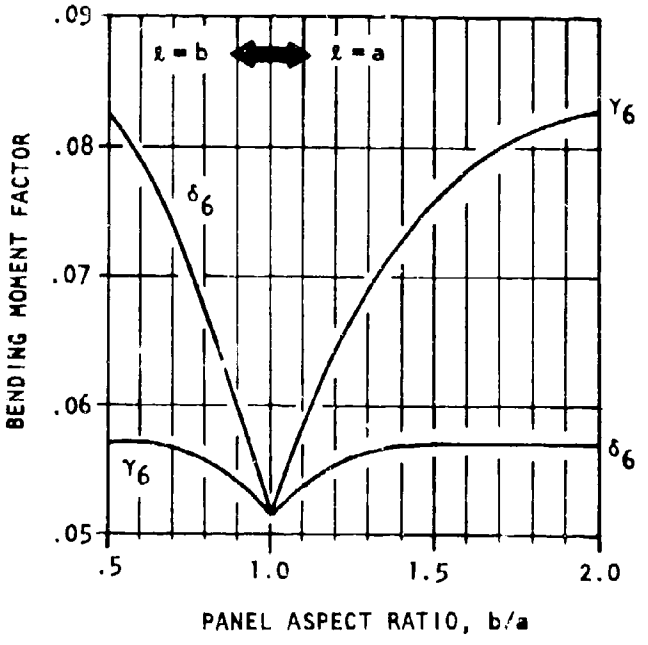

FIGURE 5.3.2-6 BENDING MOMEN: FACTOR CASE 4 (REF. 4)

The use of the plotted or referenced tabulated data for computing bending moments in the cover sheet or rib of the panel arrays shown in Figure 5.3.2-3 is best illustrated by an example.

Example: Considering the panel array illustrated in Figure 5.3.2-1, the value of δ_5 is obtained for the two panels with dimensions $a_2 \times b_1$ and $a_1 \times b_2$ and the values of γ_6 and δ_6 are obtained for the center bay so that for point A

$$\bar{M}_y = (\delta_5 \ell_1^2 + \delta_6 \ell_2^2) q_o / N \qquad (5.3.2\text{-}4a)$$

and for point B

$$\bar{M}_x = (\delta_5 \ell_3^2 + \gamma_6 \ell_2^2) q_o / N \qquad (5.3.2\text{-}4b)$$

where ℓ_1 is the smaller of the two dimensions a_2 and b_1

ℓ_2 is the smaller of the two dimensions a_2 and b_2

ℓ_3 is the smaller of the two dimensions a_1 and b_2

$N = 2$ for very stiff ribs, $h_r >> h_s$

$N = 3$ for very flexible ribs, $h_r \approx h_s$

Stress is obtained from Equations 5.3.2-4 by use of the simple expression

$$\bar{\sigma}_o = 6\bar{M}/h^2 \qquad (5.3.2\text{-}5)$$

where h is the thickness of the cover sheet or rib.

For $a_1 = a_2 = a = 6.0$ and $b_1 = b_2 = b = 18.0$, then from Equations (5.3.2-4a) and (5.3.2-5) (using Figures 5.3.2-5 and 5.3.2-6 or Table 5.3.2-1) the cover sheet static stress at the center of the short side of the center bay is for N = 3

$$\sigma_{oy} = 2[0.0566(6.0)^2 + 0.0571(6.0)^2] q_o / h_s^2$$

$$\sigma_{oy} = 8.1 \; q_o / h_s^2$$

The cover sheet static stress at the center of the long side of the center bay from Equations (5.3.2-4b) and (5.3.2-5) is

$$\sigma_{ox} = 2[(0.0566)(6.0)^2 + (0.0855)(6.0)^2] q_o / h_s^2$$

$$\sigma_{oy} = 10.07 \; q_o / h_s^2$$

where q_o is the magnitude of the uniform static pressure applied to the surface of the box structure.

Design Procedure: Rudder (4) empirically established a design procedure for estimating the root mean square stress response for ribs used in box structure configurations. Rudder recommended that Ballentine's skin design procedure (Section 5.3.1.2) be used to establish the skin thickness requirements if the rib thickness was equal to or greater than the skin thickness.

Rudder's box structure specimens were tested under laboratory conditions using broadband random acoustic excitation. The specimens represented six box structure designs with two specimens of each design to check repeatability. The specimens were manufactured from 7075-T6 aluminum alloy with the following range of design parameters used

skin thickness	0.040 inch	to	0.063 inch
rib thickness	0.020 inch	to	0.063 inch
rib spacing	7.0 inches	to	10.0 inches
height	7.0 inches	to	10.0 inches
panel aspect ratio	2.0	to	4.0

The design procedure is as follows:

(1) For the box structure geometry and material properties estimate the fundamental mode response frequency, f_1, $(m,n,q) = (1,1,1)$ using Equations (5.3.2-1) and (5.3.2-2).

(2) Calculate the root mean square spectral density of the acoustic excitation for the frequency of the fundamental mode using

$$S_p(f_1) = 2.9 \times 10^{(L/20-9)} \qquad (5.3.2\text{-}6)$$

where L is the spectrum level of the acoustic excitation

(3) Calculate the stress response of the structure due to a uniform static pressure of unit magnitude, $q_o = 1$, at the points of interest, $\overline{\sigma}_{oi}$, using the method of this section (see Equations (5.3.2-4) and (5.3.2-5)).

(4) Calculate the root mean square stress response assuming only a fundamental mode response using

$$\overline{\sigma}_{ci} = \sqrt{f_1/\zeta_1}\, S_p(f_1)\overline{\sigma}_{oi} \quad \text{psi} \qquad (5.3.2\text{-}7)$$

where ζ_1 is the damping for the fundamental mode.

Note: If the box structure is exposed to significant acoustic excitation on both sides then Equation (5.3.2-7) must be multiplied by 1.413 (increased by 3dB).

(5) Finally, the stress is obtained from the empirical relationship

$$\bar{\sigma}_{ei} = 0.245(\bar{\sigma}_{ci})^{0.411} \quad \text{ksi} \qquad (5.3.2\text{-}8)$$

Note: In Equation (5.3.2-8) $\bar{\sigma}_{ci}$ is in psi and the result $\bar{\sigma}_{ei}$ is in ksi.

(6) Finally, the fatigue life of the cover sheets is obtained using Ballentine's (10) fatigue curve, Figure 5.3.2-7, and the fatigue life of the ribs is obtained using Rudder's (4) and fatigue curve for rib failures, Figure 5.3.2-8.

The procedure is best illustrated with an example.

Example: Consider a nine cell box structure with the following configuration (see Figure 5.3.2-1)

$a_1 = 11.0$ inch, $b_1 = 12.0$ inches, $a_2 = 10.0$ inches, $b_2 = 20.0$ inches, $d = 10.0$ inches

${}_1h_s = {}_2h_s = 0.063$ inch ${}_1h_r = 0.080$ inch ${}_2h_r = 0.063$ inch

Assume that the material properties are $E = 10.3 \times 10^6$ psi, $\gamma = 0.101$ lbs/in^3, and $\nu = 0.32$.

From Equation (5.3.2-1) and (5.3.2-2) the response frequency for the fundamental mode is 79 Hz. (Box structure typically exhibits low fundamental frequencies compared to stiffened plates.)

From Equations (5.3.2-4) the bending moment at the center of the short side of the center bay for a uniform pressure of unit magnitude is given by

$$\bar{M}_y = [(0.0575)(10)^2 + (0.0575)(10)^2]/3 = 3.84$$

To obtain the static stress resulting from the unit magnitude static pressure one uses Equation (5.3.2-5). For the skin at the middle of the short side (frame line) of the center bay the static skin stress response is

$$\bar{\sigma}_{o1} = (6.0)(3.84)/(0.063)^2 = 5805 \text{ psi}$$

and the frame flange stress response is

$$\bar{\sigma}_{o2} = (6.0)(3.84)/(0.080)^2 = 3600 \text{ psi}$$

For the skin at the middle of the long side (rib line) of the center bay the skin stress response is

$$\bar{\sigma}_{o3} = (6.0)(5.35)/(0.063)^2 = 8088 \text{ psi}$$

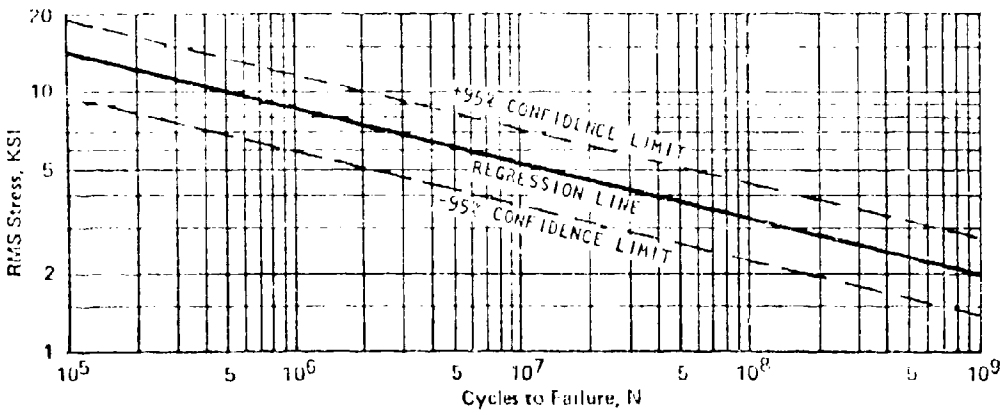

FIGURE 5.3.2-7 RANDOM S-N CURVE FOR BOX STRUCTURE SKIN (REF. 4)

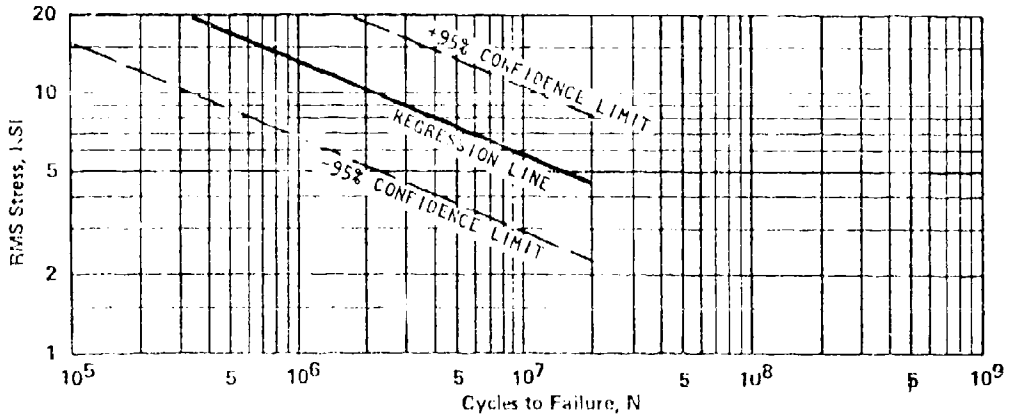

FIGURE 5.3.2-8 RANDOM S-N CURVE FOR BOX STRUCTURE RIBS (REF. 4)

and the rib flange stress response is

$$\bar{\sigma}_{o4} = (6.0)(5.35)/(0.063)^2 = 8088 \text{ psi}$$

For an assumed damping ratio of $\zeta = 0.02$ an assumed sound pressure spectrum level of 124 dB, the theoretical rms stress response is calculated from Equations (5.3.2-6) and (5.3.2-7) as

$$\bar{\sigma}_{ci} = \sqrt{79/0.02} \times 2.9 \times 10^{(124/20-9)} \bar{\sigma}_{oi} \quad \text{psi}$$

$$\bar{\sigma}_{ci} = 0.2889 \ \bar{\sigma}_{oi} \quad \text{psi}$$

Then, substituting for $\bar{\sigma}_{oi}$ into the above equation

$$\bar{\sigma}_{c1} = (0.2889)(5805) = 1677 \text{ psi}$$

$$\bar{\sigma}_{c2} = (0.2889)(3600) = 1040 \text{ psi}$$

$$\bar{\sigma}_{c3} = (0.2889)(8088) = 2336 \text{ psi}$$

$$\bar{\sigma}_{c4} = (0.2889)(8088) = 2336 \text{ psi}$$

From Equation (5.3.2-8) the estimated rms stress response based upon empirical data correlation is

$$\bar{\sigma}_{e1} = 0.245(1677)^{.411} = 5.18 \quad \text{ksi}$$

$$\bar{\sigma}_{e2} = 0.245(1040)^{.411} = 4.26 \quad \text{ksi}$$

$$\bar{\sigma}_{e3} = 0.245(2336)^{.411} = 5.94 \quad \text{ksi}$$

$$\bar{\sigma}_{e4} = 0.245(2336)^{.411} = 5.94 \quad \text{ksi}$$

For the skin stresses $\bar{\sigma}_{e1}$ and $\bar{\sigma}_{e3}$ the number of cycles to failure are estimated from Figure 5.3.2-7 to be approximately 1.1×10^7 and 5.0×10^6 cycles, respectively. For the frame and rib stresses, $\bar{\sigma}_{e2}$ and $\bar{\sigma}_{e4}$ the number of cycles to failure are estimated from Figure 5.3.2-8 to be 1.7×10^7 and $9.4 \ 10^6$ cycles, respectively. At a resonant frequency of 79 Hz. The minimum fatigue life is estimated to be 17 hours for the failure at the center of the skin rib line with the rib failure estimated at 33 hours. The skin-rib thickness combination can be optimized by iteration.

Detail Design Considerations: For the detail design of the attachment of ribs and frames to the skin for box structure configurations the designer is faced with the consideration of certain details in order to optimize the design. The structural configuration is critical at either the bend radius of the rib flange, in the skin at the rivet row on the side next to the heel of the rib, or the failure of the skin-rib attachments.

The rib-skin configuration used by Rudder to develop the design procedure described above is illustrated in Figure 5.3.2-9a. If the design procedure leads to excessive rib thickness, rib cap designs, such as illustrated in Figure 5.3.2-9b, can be selected; however, the designer is cautioned that experimental design criteria for these configurations is limited.

McGowan (10) developed the first series of design criteria for sonic fatigue. His experimental program was based upon sonic fatigue tests using a discrete frequency siren as the noise source rather than broadband random noise as is usually encountered in practice. McGowan's methods have proven to be somewhat conservative; however, two of his detail design considerations have not been refined to this date. To consider the effect of a doubler bonded to the skin, as shown in Figure 5.3.2-9(c), it is suggested that skin thickness may be reduced one gage thickness below that predicted by Rudder's method. This observation is for design guidance only since the designer must apply judgement to the particular configuration.

Additional design guidance, as developed by McGowan, is presented in Figure 5.3.1 10 for sizing the attachment diameter and spacing for skin-rib construction and Figure 5.3.2-11 and 5.3.2-12 present the configuration of a lightening hole in the rib and a design nomograph for estimating the fatigue life. The material used to develop the nomograph in Figure 5.3.2-12 was 2024-T3 aluminum alloy with the equivalent random fatigue curve derived as discussed in Section 6. The fatigue characteristics of 7075-T6 material are similar to that of 2024-T3 so that Figure 5.3.2-12 can be used, with engineering judgement, for aluminum alloy materials in general.

Computer Program: The following computer program, as presented by Rudder (4), can be used to compute the natural frequencies and modal amplitudes for the skin, rib, and frame of a nine cell box structure as illustrated in Figure 5.3.2-1. The program is listed in Table 5.3.2-2 with typical output format listed in Table 5.3.2-3. The alternate to using the computer program is to use Equation 5.3.2-1.

Nine Cell Box Structure Vibration Analysis (BOXVIB)

Subprograms Required: STIFF(SK,I,J,K), MASS(SM,I,J,K), F(N,I,J), SGN(K).

Input Data Format (BOXVIB): Five Cards per Data Case

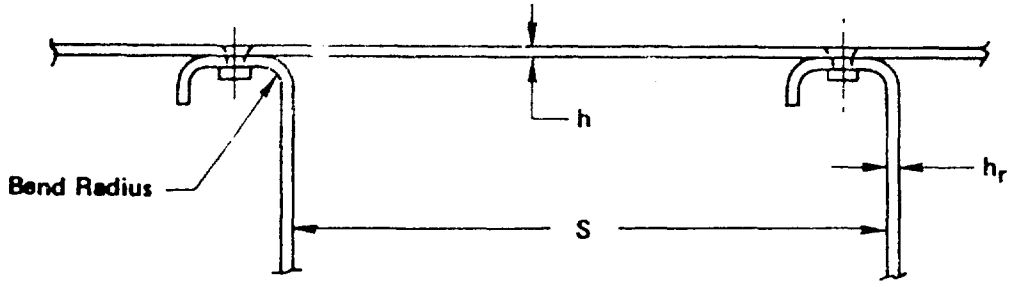

(a) Conventional Skin-Rib Configuration

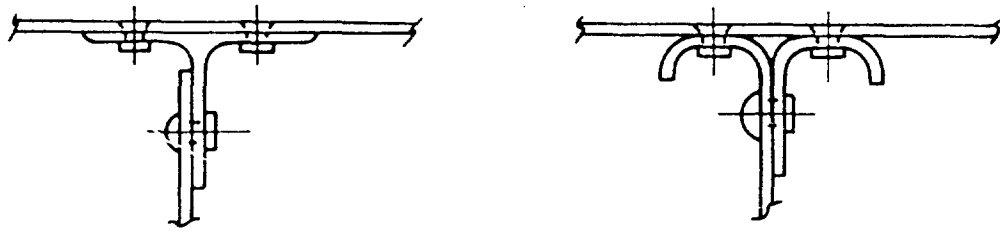

(b) Skin-Rib Configurations for Improved Acoustic Fatigue Resistance

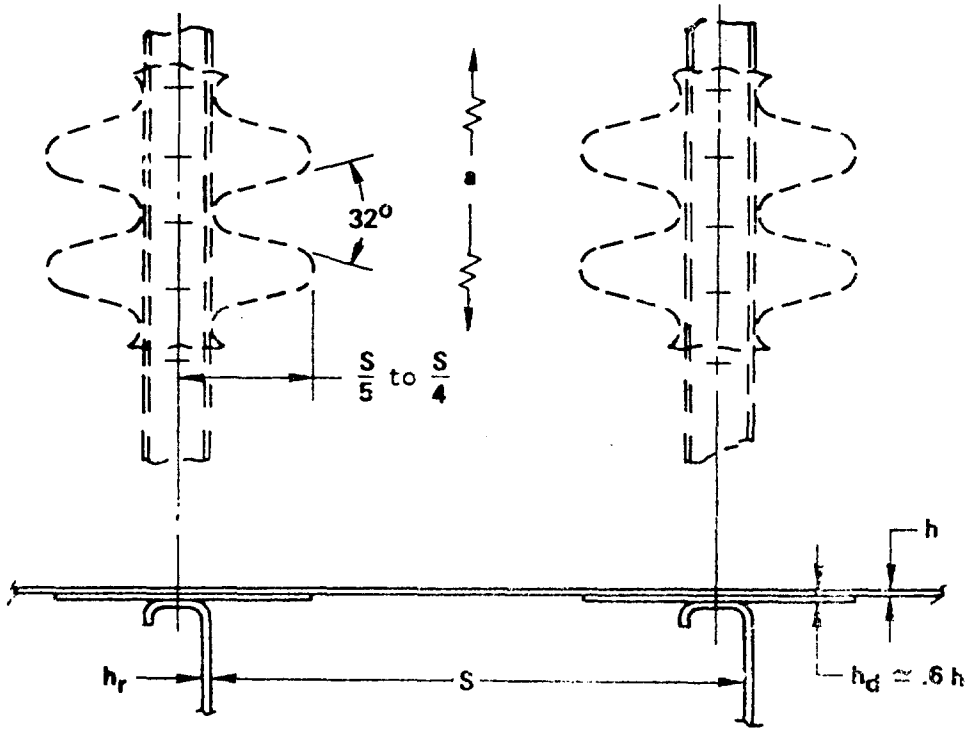

(c) Bonded Doubler Configuration

FIGURE 5.3.2-9 SKIN-RIB ATTACHMENT CONFIGURATIONS (SHEET 11)

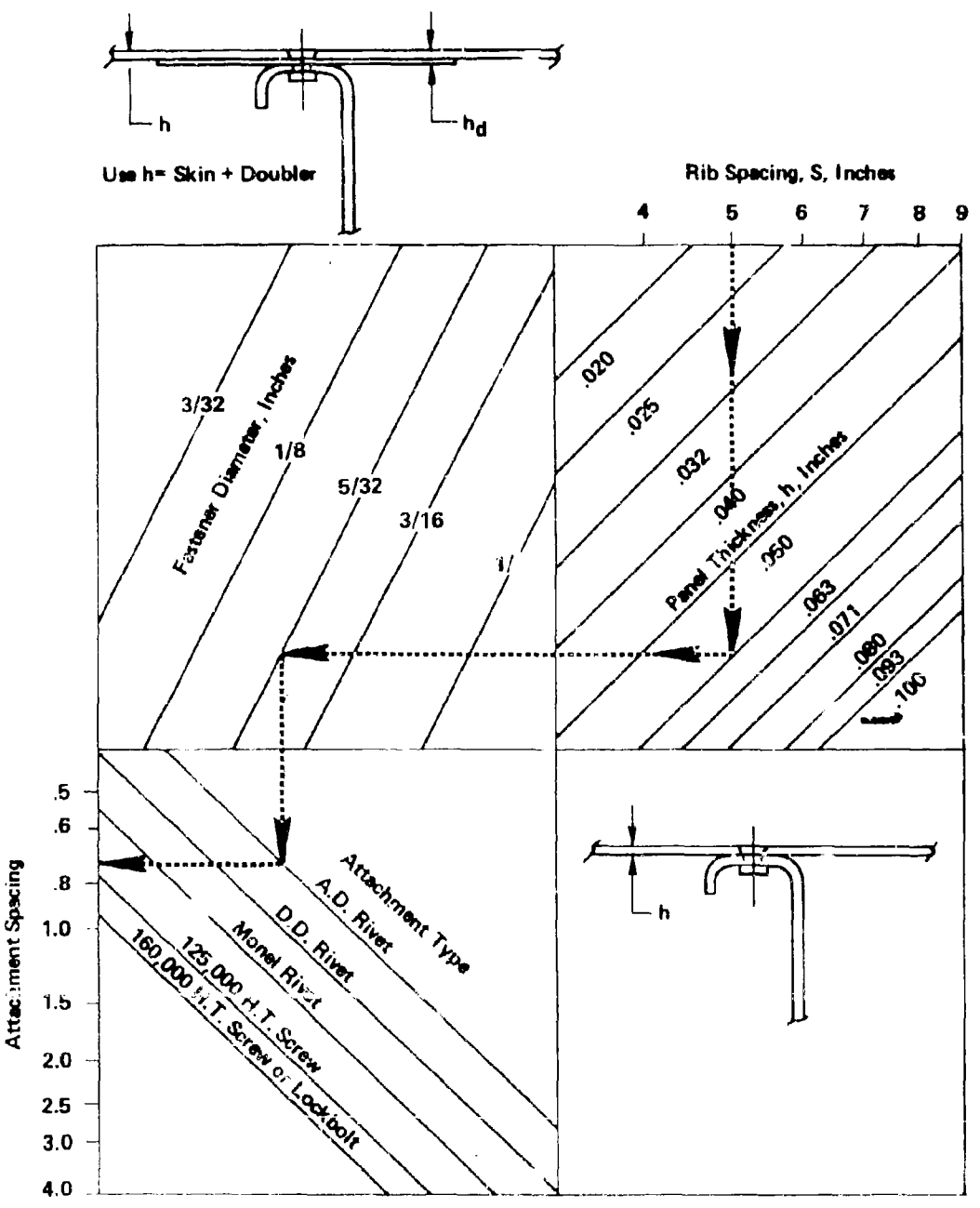

FIGURE 5.3.2-10 NOMOGRAPH FOR DETERMINING ATTACHMENT DIAMETER AND PITCH FOR SKIN RIB CONSTRUCTION (REF. 11)

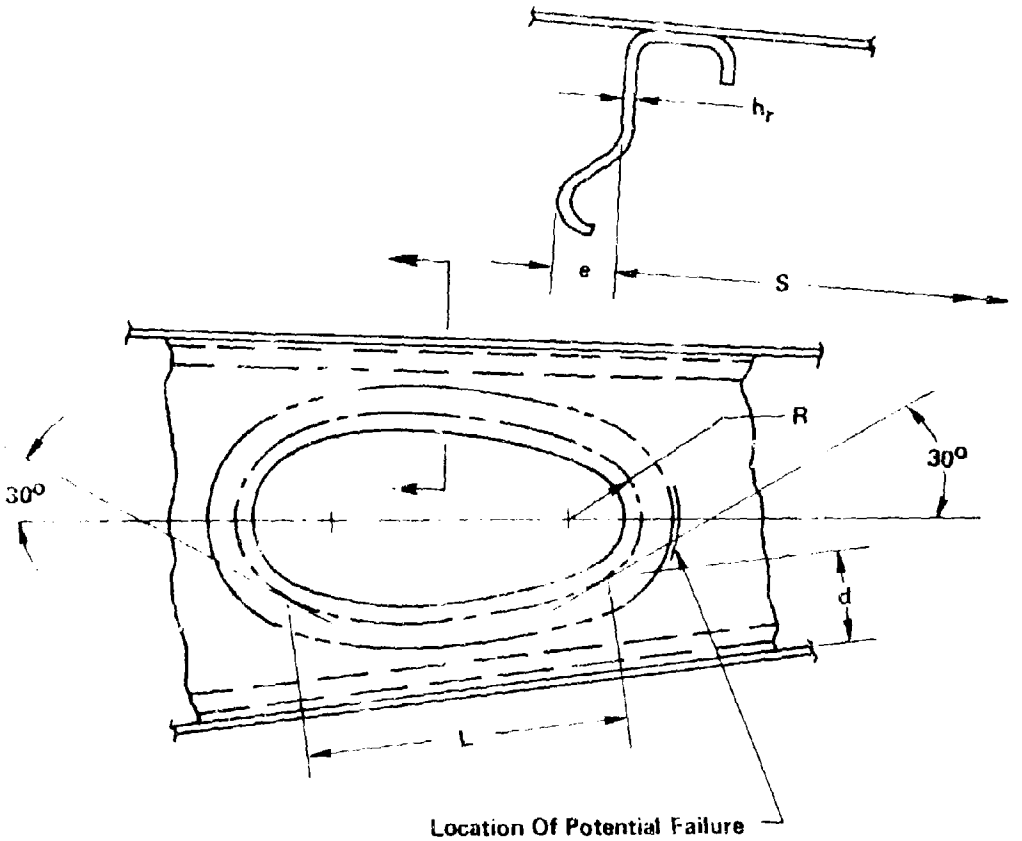

FIGURE 5.3.2-11 GEOMETRY AND NOMENCLATURE FOR R:B LIGHTENING HOLE (REF. 11)

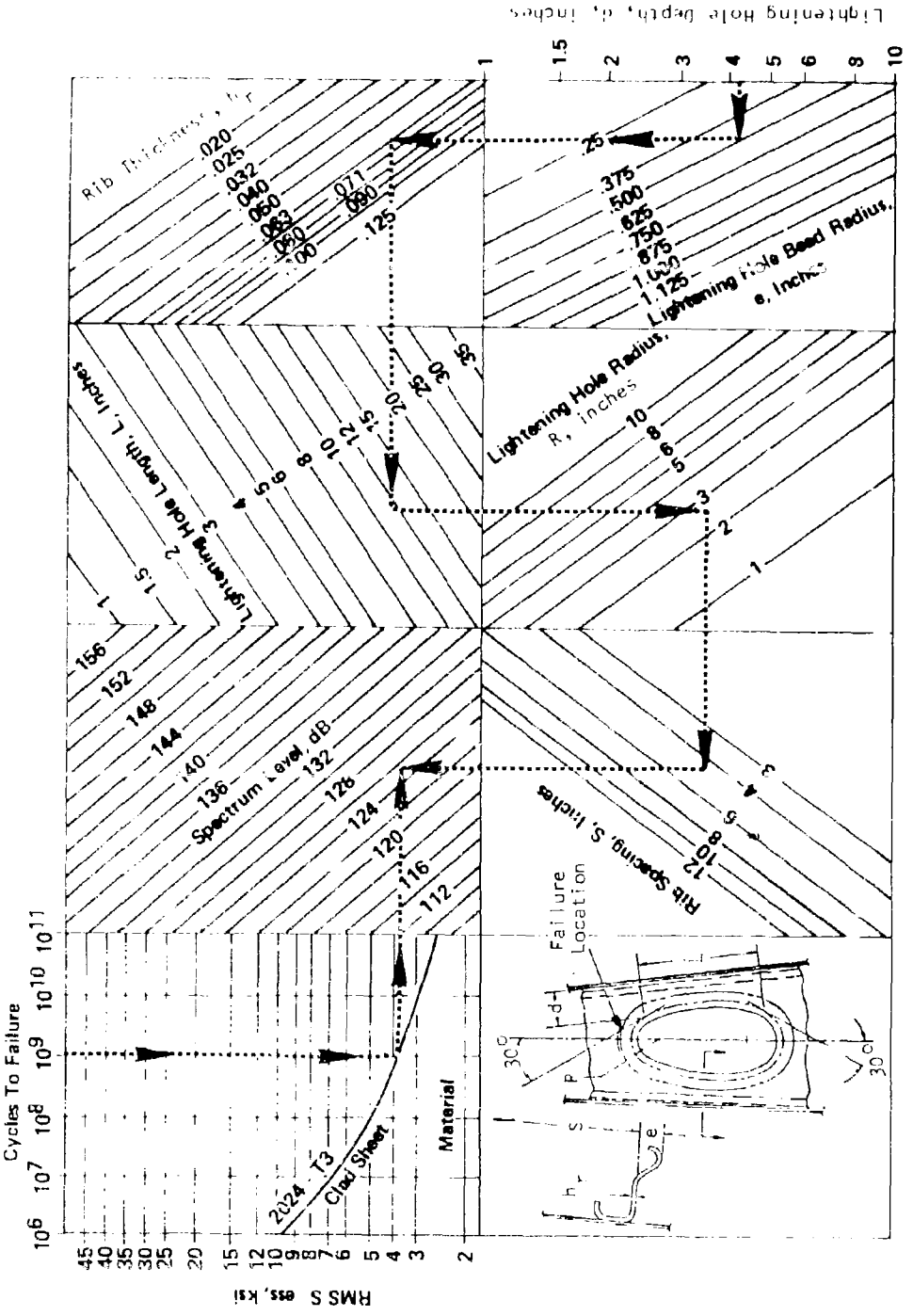

FIGURE 5.3.2-12 LIGHTENING HOLE DESIGN NOMOGRAPH (REF. 11)

TABLE 5.3.2-2

INPUT ATA FORMAT AND COMPUTER PROGRAM LISTING
FREQUENCY ANALYSIS OF A NINE CELL BOX STRUCTURE
(CONTINUED)

CARD 1

COL (FORMAT)	1(I4)	5(I2)
NAME	NDATA	IOUT

CARD 2

COL (FORMAT)	1(I2)	3(I2)	5(I2)	6(I2)	7(I2)	11(I2)
NAME	MS	MF	NS	NF	QS	QF

CARD 3

COL (FORMAT)	1(E11.4)	12(E11.4)	23(E11.4)	34(E11.4)	45(E11.4
NAME	A1	A2	B1	B2	H

CARD 4

COL (FORMAT)	1(E11.4)	12(E11.4)	23(E11.4)	34(E11.4)	45(E11.4)
NAME	T1S	T2S	GMS	ES	PRS

CARD 5

COL (FORMAT)	1(E11.4)	12(E11.4)	23(E11.4)	34(E11.4)	45(E11.4)
NAME	T1R	T2R	GMR	ER	PRR

NDATA	four digit data identification number
IOUT	output option: = 0, frequencies are printed for each mode = 1, frequencies and modal amplitudes are printed for each mode
MS,MF	initial and final values for mode number m
NS,NF	initial and final values for mode number n
QS,QF	initial and final values for mode number q
A1,A2	length of panel bays parallel to x-axis (see Figure 5.3.2-1)
B1,B2	length of panel bays parallel to y-axis (see Figure 5.3.2-1)
H	height of box
T1S/T2S	upper/lower skin thickness (see Figure 5.3.2-1)
GMS	weight density of skin material
ES	Young's modulus for skin material
PRS	Poisson's ratio for skin material
T1R/T2R	rib/frame thickness (see Figure 5.3.2-1)
GMR	weight density of rib and frame material
ER	Young's modulus of rib and frame material
PRR	Poisson's ratio for rib and frame material

TABLE 5.3.2-2

(CONTINUED)

```
      DIMENSION W1(3,3),W2(3,3),U(2,3),V(2,3)
      COMMON A(16),B(7)
      INTEGER QS,Q
      IN=1
      IO=2
100   READ(IN,105) NDATA,IOUT
      READ(IN,115) MS,M,NS,N,QS,Q
      READ(IN,110) A1,A2,B1,B2,H
      READ(IN,110) T1S,T2S,GMS,ES,PRS
      READ(IN,110) T1R,T2R,GMR,ER,PRR
105   FORMAT(I4,T2)
110   FORMAT(5E11.4)
115   FORMAT(6I2)
1     A(1)= A1/A2
      A(2)= H/A1
      A(3)= H/A2
      A(4)= B1/A1
      A(5)= B1/A2
      A(6)= S1/B2
      A(7)= H/B1
      A(8)= B2/A1
      A(9)= B2/A2
      A(10)=H/B2
      A(11)=T2S/T1S
      A(12)=T2P/T1R
      A(13)=T1R/T1S
      A(14)=GMP/GMS
      A(15)=ER/ES
      A(16)=(1.0-PRS*PRS)/(1.0-PRR*PRR)
      CM=GMS*T1S*A2*B2/1544.0
      CK=2.029356*ES*T1S**3/(A2*B2*(1.0-PRS*PRS))
      CF=0.15915493*SQRT(CK/CM)
      C1=A(1)**3
      C2=A(6)**3
      C3=2.0*A(10)**3
      C4=A(9)**3
      C5=A(11)**3
      C6=A(13)**3
      B(1)=(1.0+A(11))*(1.0+2.0*C1+2.0*C2+4.0*C1*C2)
      B(2)=C3*A(14)*A(13)
      B(3)=1.0+2.0*A(1)**3
      B(4)=C4*(1.0+2.0*A(6)**3)*A(12)
      B(5)=1.0+C5
      B(6)=2.0*C6*A(15)*A(16)
      DO 210 K=QS,Q
      WRITE(IO,215)
      WRITE(IO,220) NDATA
```

TABLE 5.3.2-2

(CONTINUED)

```
      IF(ICOUT) 116,116,117
116   WRITE(IO,260)
117   SNQ=SGN(K)
      FQ=FLOAT(K)
      DO 205 I=MS,M
      SNM=SGN(I)
      FM=FLOAT(I)
      DO 205 J=NS,N
      SNN=SGN(J)
      FN=FLOAT(J)
      CALL STIFF(SK,I,J,K)
      CALL MASS(SM,I,J,K)
      FREQ=CF*SQRT(SK/SM)
      SMM=CM*SM
      SKM=CK*SK
      IF(ICOUT) 201,201,120
120   W1(1,1)=SNM*SNN*A(1)*A(6)
      W1(1,2)= SNM*A(1)
      W1(1,3)= W1(1,1)
      W1(2,1)= SNN*A(6)
      W1(2,2)= 1.00000
      W1(2,3)= W1(2,1)
      W1(3,1)= W1(1,1)
      W1(3,2)= W1(1,2)
      W1(3,3)= W1(1,1)
      U(1,2)=-FM*A(3)/FQ
      U(1,1)= SNN*A(6)*U(1,2)
      U(1,3)= U(1,1)
      U(2,1)= SNM*U(1,1)
      U(2,2)= SNM*U(1,2)
      U(2,3)= SNM*U(1,1)
      V(1,2)=-FN*A(10)/FQ
      V(1,1)= SNM*A(1)*V(1,2)
      V(1,3)= V(1,1)
      V(2,1)= SNN*V(1,1)
      V(2,2)= SNN*V(1,2)
      V(2,3)= SNN*V(1,1)
      DO 200 I1=1,3
      DO 200 J1=1,3
      W2(I1,J1)=SNQ*W1(I1,J1)
200   CONTINUE
      GO TO 202
201   WRITE(IO,265) I,J,K,SKM,SMM,FREQ
      GO TO 205
202   WRITE(IO,225) I,J,K,FREQ
      WRITE(IO,230) SMM,SKM
      WRITE(IO,235)
```

TABLE 5.3.2-2
(CONTINUED)

```
      WRITE(IO,240) ((W1(I1,J1),J1=1,3),I1=1,3)
      WRITE(IO,245)
      WRITE(IO,240) ((U(I1,J1),J1=1,3),I1=1,2)
      WRITE(IO,250)
      WRITE(IO,240) ((V(I1,J1),J1=1,3),I1=1,2)
      WRITE(IO,255)
      WRITE(IO,240) ((W2(I1,J1),J1=1,3),I1=1,3)
205   CONTINUE
210   CONTINUE
215   FORMAT(1H1,7X,45HDYNAMIC ANALYSIS OF A NINE CELL-BOX STRUCTURE)
220   FORMAT(/,21X,9HDATA CASE,I5)
225   FORMAT(/,3X,13HMODE NUMBER (,I2,1H,,I2,1H,,I2,1H),7X,
     110HFREQUENCY=,E12.5,3HHZ.)
230   FORMAT(/,3X,11HMODAL MASS=,E12.5,3X,16HMODAL STIFFNESS=,E12.5)
235   FORMAT(//,22X,16HMODAL AMPLITUDES,/,16X,19HUPPER COVER SHEET -,
     17HW1(I,J))
240   FORMAT(10X,E12.5,2X,F12.5,2X,E12.5)
245   FORMAT(/,23X,13HRIBS - U(I,J))
250   FORMAT(/,23X,13HRIBS - V(1,J))
255   FORMAT(/,17X,27HLOWER COVER SHEET - W2(I,J))
260   FORMAT(/,6X,7H(M,N,O),3X,12HMODAL STIFF.,2X,
     111HMODAL  MASS,2Y,14HFREQUENCY, HZ.,/)
265   FORMAT(6X,1H(,I1,1H,,I1,1H,,I1,1H),2X,E12.5,2X,E12.5,2X,F12.5)
      GO TO 100
      END




      SUBROUTINE STIFF(SK,I,J,K)
      COMMON A(16),B(7)
      IJ=I*I*J*J
      CIJ=FLOAT(IJ)
      F22=F(9,I,J)
      SKF=2.0*(A(1)*F(8,I,J)+A(6)*F(5,I,J)+2.0*A(1)*A(6)*F(4,I,J))/F22
      SKF=1.0+SKF
      RKF=(F(3,I,K)+2.0*A(1)*F(2,I,K))*A(10)+
     1(F(10,J,K)+2.0*A(6)*F(7,J,K))*A(3)*A(12)**3
      SK=CIJ*(B(5)*F22*SKF+B(6)*RKF)
      RETURN
      END


      FUNCTION F(N,I,J)
      COMMON A(16),B(7)
      R1=(FLOAT(I)/FLOAT(J))*A(N)
      R=R1+1.0/R1
      F=R*R
      RETURN
      END
```

TABLE 5.3.2-2
(CONCLUDED)

```
      SUBROUTINE MASS(SM,I,J,K)
      COMMON A(16),B(7)
      C1=FLOAT(I)/FLOAT(J)
      C2=FLOAT(J)/FLOAT(K)
      RM=B(3)+B(4)*C1*C1
      SM=B(1)+B(2)*RM*C2*C2
      RETURN
      END



      FUNCTION SGN(K)
      C=1.0
      DO 5 I=1,K
      C=-C
    5 CONTINUE
      SGN=C
      RETURN
      END
```

REFERENCES FOR SECTION 5.3.2

1. Clarkson, B. L. and Abrahamson, A. L.; "The Response of Skin/Rib Structure to Jet Noise," Proc. of a conference on Current Developments in Sonic Fatigue, Institute of Sound and Vibration Research, University of Southampton, England, 6-9 July, 1970, Paper N.1.

2. Mead, D. J. and Sen Gupta, G.; "Propagation of Flexural Waves in Infinite, Damped Rib-Skin Structures," AFML-TR-70-13, Air Force Materials Laboratory, Wright-Patterson Air Force Base, Ohio, 1970.

3. Sen Gupta, G., "Dynamics of Periodically Stiffened Structures Using a Wave Approach," AFML-TR-71-93, Air Force Materials Laboratory, Wright-Patterson Air Force Base, Ohio, May 1971.

4. Rudder, F. F., "Acoustic Fatigue of Aircraft Structural Assemblies", AFFDL-TR-71-107, Air Force Flight Dynamics Laboratory, Wright-Patterson Air Force Base, Ohio, February, 1972.

5. Clarkson, B. L., and Ashie, J.; "Computer Based Analyses of the Response of Box Type Structures to Random Pressures," International Journal of Computers and Structures, Vol. 3, pp 899-912, 1973.

6. Abrahamson, A. L., "Natural Frequencies and Normal Modes of a Four Plate Structure," Journal of Sound and Vibration, Vol. 28, N.2, 1973, pp 259-275.

7. Thomson, A. G. R., and Lambert, R. F., "Acoustic Fatigue Design Data, Part IV", AGARD-AG-162-Part IV, Advising Group for Aerospace Research and Development, North Atlantic Treaty Organization, 1974.

8. Clarkson, B. L.; "Stresses in Skin Panels Subjected to Random Acoustic Loading," The Aeronautical Journal of the Royal Aeronautical Society Vol. 72, Nov. 1968, pp 1000-1010.

9. Timoshenko, S., and Woinowsky-Krieger, S.; Theory of Plates and Shells, Second Edition, McGraw-Hill Book Company, Inc., 1959.

10. Ballentine, J. R., et. al., "Refinement of Sonic Fatigue Structural Design Criteria," AFFDL-TR-67-156, Air Force Flight Dynamics Laboratory, Wright Patterson Air Force Base, Ohio, 1968.

11. McGowan, P. R., et. al., "Structural Design for Acoustic Fatigue", ASD-TDR-63-820, Air Force Flight Dynamics Laboratory, Wright-Patterson Air Force Base, Ohio, 1963.

5.3.3 WEDGE STRUCTURE

Wedge structure is typical of aircraft control surfaces, such as ailerons, trailing edge of flaps, elevators, and rudders. The presentation here is a very simplified approach to a complicated structural dynamics problem as described by Rudder (1). The result is a simple design equation for estimating the natural frequencies of such structure. Clarkson (2) indicates that wedge structure exhibits stress response similar to that exhibited by box structure so that until reliable experimental data are available the methods of Section 5.3.2 can be used as a tentative design procedure for estimating stress response with frequency estimates obtained using the results of this section

5.3.3.1 Notation

The notation used in this section is as follows:

a	Radius of sector-shaped rib (Figure 5.3.3-1b), inches
b	Rib spacing (Figure 5.3.3-1a), inches
E	Young's modulus of cover sheets and ribs, psi
f_{mnq}	Natural frequency of (m,n,q)th mode, Hz
h_{s1}, h_{s2}	Thickness of wedge structure cover sheets (Figure 5.3.3-1a)
h_r	Rib thickness, inches
I_m	Integral evaluated in Table 5.3.3-1
K_{mnq}	Modal stiffness of (m,n,q)th mode (Equation 5.3.3-2)
M_{mnq}	Modal mass of (m,n,q)th mode (Equation 5.3.3-3)
m	Mode number for x_1, x_2, and r directions (Figure 5.3.3-1)
n	Mode number for y direction
q	Mode number for θ direction
r	Radial distance, inches
S	$2\alpha a$, inches
α	Half angle of sector rib, radians
ρ	Weight density of structure material

5.3.3.2 Estimation of Natural Frequencies

The configuration of a three cell wedge structure is illustrated in Figure 5.3.3-1a, with the geometry and nomenclature for a rib illustrated in Figure 5.3.3-1b.

Derivation: The modes of the cover sheets are described in terms of the number of half sine waves of the mode in the plane of the cover sheet using the mode numbers (m,n). The modes of the rib are described in terms of the number of node lines in the circumferential direction by the mode number, n, and by the number of node lines in the radial direction by the mode number, q. Typical rib mode shapes are illustrated in Figure 5.3.3-2.

For structural modes symmetric about the x-y plane (see Figure 5.3.3-1) and imposing a zero shear condition at the intersection of the cover sheets and ribs (i.e., the rib-skin intersection is assumed to remain perpendicular during deformation), the frequency of the (m,n,q)th mode is given by the expression

$$f^2_{mnq} = \frac{K_{mnq}}{4\pi^2 M_{mnq}} \quad q = 1,3,5\ldots \quad Hz^2 \qquad (5.3.3\text{-}1)$$

Assuming that the cover sheets and ribs are manufactured from the same material and that the ribs all have the same thickness and are equally spaced, the expression for the modal stiffness is

$$K_{mnq} = \frac{\pi^4 D_s}{4ab_2} m^2 n^2 \left\{ 3\left[1 + \left(\frac{2h_s}{1h_s}\right)^3\right] F_{mn}(b_2,a) \right. \qquad (5.3.3\text{-}2)$$

$$\left. + \left(\frac{h_r}{1h_s}\right)^3 \left(\frac{2\alpha}{q\pi}\right)^2 \left(\frac{S}{b_2}\right) \left[(\pi m)^2 + 15 + 8\nu + 4\left(\frac{q\pi}{2\alpha}\right)^2 + 4\left[\left(\frac{q\pi}{2\alpha}\right)^2 - 1\right]^2 I_m \right\}$$

and the expression for the modal mass is

$$M_{mnq} = \frac{1}{4} \rho_1 ab_2 \left\{ 3\left(1 + \frac{2h_s}{1h_s}\right) + \frac{h_r}{1h_s}\left(\frac{n}{q}\right)^2 \left(\frac{S}{b_2}\right)^3 \left[1 - \frac{3}{(m\pi)^2}\right] \right\} \qquad (5.3.3\text{-}3)$$

where $1D_s = E\,1h_s^3/12(1-\nu^2)$

$S = 2\alpha a$

$\rho_1 = \gamma\,1h_s/g$

Tabulated values of the integral

$$I_m = \frac{2}{(\pi m)^2} \int_0^{\pi} \frac{1}{t} \sin^2\left(\frac{m\pi r}{a}\right) dr$$

required to evaluate K_{mnq} are presented in Table 5.3.3-1

TABLE 5.3.3-1

VALUES OF THE INTEGRAL I_m

m =	1	2	3	4	5
I_m =	0.24699	0.07888	0.03958	0.02408	0.01632

Example : Calculate the first few natural frequencies of a three cell wedge structure for the following data

$$_1h_s = {}_2h_s = h_r = 0.050 \text{ inches}$$

$$a = b = 10.0 \text{ inches}$$

$$\alpha = 11.46 \text{ degrees } (0.2 \text{ radian})$$

$$\gamma = 0.101 \text{ lbs/in}^3 \quad E = 10.3 \times 10^6 \text{ psi} \quad \nu = 0.302$$

Then, using the computer program following this example or using Equations (5.3.3-2) and (5.3.3-3) the first few response frequencies are

mode number (m,n,q)	f_{mnq}, Hz	mode number (m,n,q)	f_{mnq}, Hz
(1,1,1)	134	(1,3,1)	530
(1,1,3)	298	(1,3,3)	964
(1,2,1)	298	(2,1,1)	261
(1,2,3)	611		

Computer Program: The computer program for calculating the natural frequencies and modal amplitudes for the ribs and skin of a three-cell wedge structure is presented below. The computer program is listed in Table 5.3.3-2 and typical output is listed in Table 5.3.3-3.

REFERENCES FOR SECTION 5.3.3

1. Rudder, F. F.; "Acoustic Fatigue Resistance of Aircraft Structural Component Assemblies," AFFDL-TR-71-107, Air Force Flight Dynamics Laboratory Wright-Patterson Air Force Base, Ohio, 1971.

2. Clarkson, B. L.; "Stresses in Skin Panels Subjected to Random Acoustic Loading," AFML-TR-67-199, Air Force Materials Laboratory, Wright-Patterson Air Force Base, Ohio, June 1967.

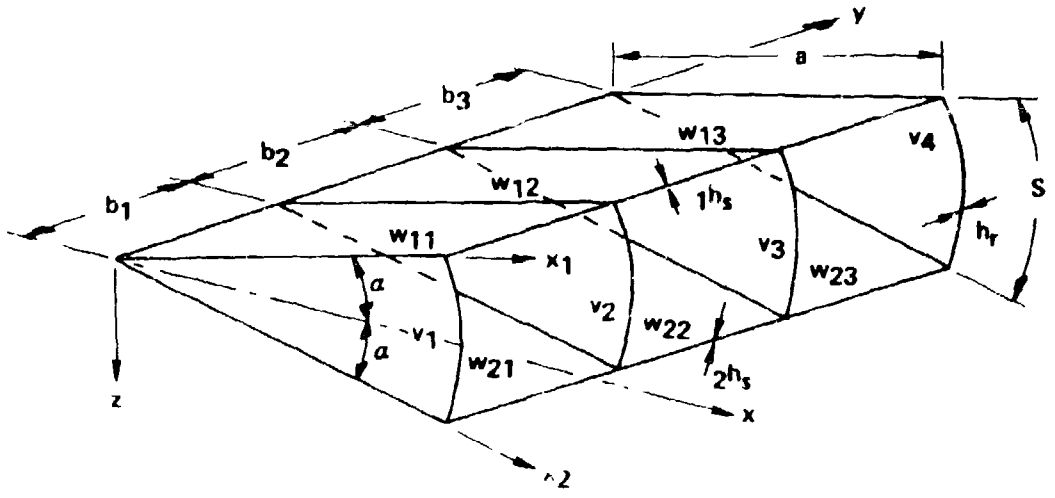

(a) Three Cell Wedge Structure

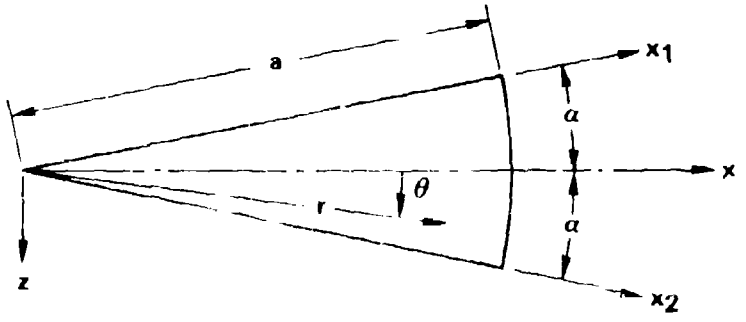

(b) Sector Plate Coordinate System

FIGURE 5.3.3-1 THREE CELL WEDGE STRUCTURE GEOMETRY AND NOMENCLATURE (REF. 1)

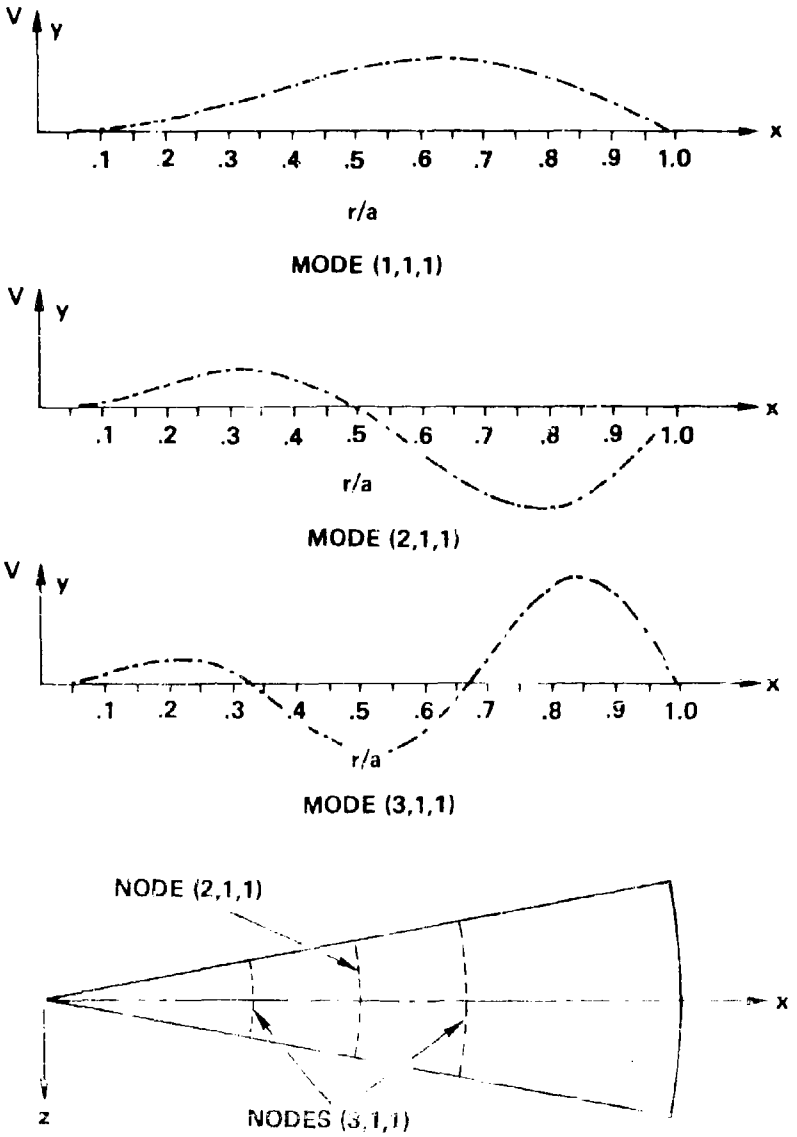

FIGURE 5.3.3-2 TYPICAL RIB MODE SHAPES FOR A WEDGE STRUCTURE (REF. 1)

TABLE 5.3.3-2
INPUT DATA FORMAT AND COMPUTER PROGRAM LISTING
FREQUENCY ANALYSIS OF A THREE CELL WEDGE STRUCTURE
Subprograms Required: SGN(K) (CONTINUED)

Input Data Format (WDGVIB): 5 Cards per Data Case

CARD 1

COL(FORMAT)	1(I4)	5(I2)	7(I2)	9(I2)	11(I2)	13(I2)	15(I2)
NAME	NDATA	MS	MF	NS	NF	QS	QF

CARD 2

COL(FORMAT)	1(E10.4)	11(3I0.4)	21(E10.4)	31(E10.4)
NAME	A1	B1	B2	ALPHA

CARD 3/4

COL(FORMAT)	1(E10.4)	11(E10.4)	21(E10.4)	31(E10.4)
NAME	T1S/T2S	GM1S/GM2S	E1S/E2S	PR1S/PR2S

CARD 5

COL(FORMAT)	1(E10.4)	11(E10.4)	21(E10.4)	31(E10.4)
NAME	T1R	GMR	ER	PRR

NDATA	four digit data identification number
MS,MF	Initial and final values for mode number m
NS,NF	Initial and final values for mode number n
QS,QF	Initial and final values for mode number q
	NOTE: only odd values of q are considered. QF $\leq$ 5.
A1	radius of rib
B1/B2	rib spacing (B3 = B1: see Figure 5.3.3-1b)
ALPHA	TOTAL wedge angle in DEGREES
T1S/T2S	thickness of upper/lower cover sheet (see Figure 5.3.3-1b)
GM1S/GM2S	weight density of upper/lower cover sheet material
E1S/E2S	Young's modulus of upper/lower cover sheet material
PR1S/PR2S	Poisson's ratio of upper/lower cover sheet material
T1R	thickness of rib
GMR	weight density of rib material
ER	Young's modulus of rib material
PRR	Poisson's ratio of rib material

TABLE 5.3.3-2
(CONTINUED)

```
C       THIS PROGRAM EVALUATES THE MODAL MASS AND STIFFNESS,
C       FREQUENCY AND MODE SHAPES OF A WEDGE STRUCTURE
        DIMENSION A(22),E(6),W(2,3),V(20,4)
        REAL IM(10)
        INTEGER Q,QS,QF,QM1D2
        IN=1
        IO=2
        IM(1)=.24699
        IM(2)=.07888
        IM(3)=.03958
        IM(4)=.02408
        IM(5)=.01632
  200   READ(IN,100)MDATA,MS,NF,NS,NF,QS,QF
        READ(IN,101)A1,B1,B2,ALPHA
        ALPHA=.0087266*ALPHA
        READ(IN,101)T1S,GM1S,E1S,PP1S
        READ(IN,101)T2S,GM2S,E2S,PP2S
        READ(IN,101)T1R,GMR,ER,PPR
        A(1)=2.*ALPHA*A1/B2
        A(2)=B1/B2
        A(3)=A1/B2
        A(4)=A1*B2
        A(5)=A1/B1
        A(6)=A(1)**3
        A(7)=E1S*T1S**3/(1.-PR1S*PR1S)/12.
        A(8)=E2S*T2S**3/(1.-PR2S*PP2S)/12.
        A(9)=ER*T1R**3/(1.-PRR*PPR)/12.
        A(10)=GM1S*T1S
        A(11)=A(10)*A(4)/1544.
        A(12)=1.+GM2S*T2S/A(10)
        A(13)=A(12)*(2.*A(2)+1.)*A(11)
        A(14)=GRR*T1R/A(10)*A(6)*A(11)
        A(15)=24.35227*A(7)/A(4)
        A(16)=(1.+A(8)/A(7))*A(15)
        A(17)=(ALPHA/1.570795)**2
        A(18)=A(9)/A(7)*A(1)*A(17)*A(15)
        A(19)=2.*A(16)/A(2)
        A(20)=2./A(17)
        A(21)=(15.+8.*PRR)
        A(22)=2.*A(20)
        DO 3[illegible]
        [illegible](E)
```

TABLE 5.3.3-2
(CONTINUED)

```
      FM=FLOAT(M)
      FM2=FM*FM
      PIMDA=3.14159*FM
      DO 202 N=NS,NF
      SNN=SGN(N)
      FN=FLOAT(N)
      FN2=FN*FN
      FMOFN=FM/FN
      F(1)=((FMOFN/A(5)+A(5)/FMOFN)**2)*A(19)
      F(2)=((FMOFN/A(3)+A(3)/FMOFN)**2)*A(16)
      F(3)=F(1)+F(2)
      DO 201 Q=QS,QF,2
      QM1D2=(Q-1)/2
      SNQ=SGN(Q)
      SNQM1=SGN(QM1D2)
      FQ=FLOAT(Q)
      FQ2=FQ*FQ
      F(4)=((A(20)*FQ2-2.)**2)*IM(M)
      F(5)=9.86959*FM2+A(21)+A(22)*FQ2
      F(6)=A(18)*(F(4)+F(5))/FQ2
      SKM=FM2*FN2*(F(3)+F(6))
      SMM=(1.-.303964/FM2)*A(14)*FN2/FQ2+A(13)
      FREQ=SQRT(SKM/SMM)/6.28318
      W(1,1)=SNN*A(2)
      W(1,2)=1.
      W(1,3)=W(1,1)
      W(2,1)=-W(1,1)
      W(2,2)=-1.
      W(2,3)=W(2,1)
      DO 204 IR=1,20
      R=FLOAT(IR)
      R=.05*R
      CON=A(4)*ALPHA*SNQM1*FN/FQ*R*A(3)
      SMPRA=1.-SIN(PIMDA*R)
      V(IR,1)=CON*SMPRA
      V(IR,2)=CON*SMPRA
      W(1,4)=V(IR,1)
204   W(2,4)=V(IR,2)
      REWIND(10,215)
      WRITE(10,220)NDATA
      WRITE(10,225)M,N,Q,FREQ
      WRITE(10,230)SMM,SKM
```

TABLE 5.3.3-2
(CONCLUDED)

```
      WRITE(IO,235)
      WRITE(IO,240)(W(1,J),J=1,3)
      WRITE(IO,245)
      WRITE(IO,240)(W(2,J),J=1,3)
      WRITE(IO,250)
      DO 205 I=1,20
      P=FLOAT(I)
      P=.05*P
  205 WRITE(IO,241)(P,(V(I,J),J=1,4))
  201 CONTINUE
  202 CONTINUE
  203 CONTINUE
      GO TO 200
  100 FORMAT(I4,6I2)
  101 FORMAT(4E10.4)
  215 FORMAT(1H1,11X,37HDYNAMIC ANALYSIS OF A WEDGE STRUCTURE)
  220 FORMAT(//22X,9HDATA CASE,I5)
  225 FORMAT(/3X,13HMODE NUMBER (,I2,1H,,I2,1H,,I2,1H),5X,10HFREQUENCY=,
     1E12.5,4H,HZ.)
  230 FORMAT(/3X,11HMODAL MASS=,E12.5,2X,16HMODAL STIFFNESS=,E12.5)
  235 FORMAT(//20X,16HMODAL AMPLITUDES,//16X,26HUPPER COVER SHEET - W(1,
     1J),/)
  240 FORMAT(10X,E12.5,2X,E12.5,2X,E12.5)
  241 FORMAT(F5.2,3X,4E12.5)
  245 FORMAT(//16X,26HLOWER COVER SHEET - W(2,J),/)
  250 FORMAT(//17X,22HSECTOR PLATES - V(I,J),/11X,6HSECTOR,6X,6HSECTOR,6
     1X,6HSECTOR,6X,6HSECTOR,/3X,3HR/A,5X,8HPLATE NO,4X,8HPLATE NO,4X,8H
     2PLATE NO,4X,8HPLATE NO,/13X,1H1,11X,1H2,11X,1H3,11X,1H4,//)
      END


      FUNCTION SGN(K)
      C=1.0
      DO 5 I=1,K
      C=-C
    5 CONTINUE
      SGN=C
      RETURN
      END
```

TABLE 5.3.3-3
FREQUENCY ANALYSIS PROGRAM OUTPUT

DYNAMIC ANALYSIS OF A WEDGE STRUCTURE

DATA CASE 2000

MODE NUMBER (2, 1, 1) FREQUENCY= 0.2,011E+03,HZ.

MODAL MASS= 0.19622E-02 MODAL STIFFNESS= 0.52410E+04

MODAL AMPLITUDES

UPPER COVER SHEET - W(1,J)

-0.10000E+01 0.10000E+01 -0.10000E+01

LOWER COVER SHEET - W(2,J)

0.10000E+01 -0.10000E+01 0.10000E+01

SECTOR PLATES - V(I,J)

R/A	SECTOR PLATE NO 1	SECTOR PLATE NO 2	SECTOR PLATE NO 3	SECTOR PLATE NO 4
0.05	0.61808E-02	-0.61808E-02	0.61808E-02	-0.61808E-02
0.10	0.23513E-01	-0.23513E-01	0.23513E-01	-0.23513E-01
0.15	0.48544E-01	-0.48544E-01	0.48544E-01	-0.48544E-01
0.20	0.76090E-01	-0.76090E-01	0.76090E-01	-0.76090E-01
0.25	0.10001E+00	-0.10001E+00	0.10001E+00	-0.10001E+00
0.30	0.11413E+00	-0.11413E+00	0.11413E+00	-0.11413E+00
0.35	0.11327E+00	-0.11327E+00	0.11327E+00	-0.11327E+00
0.40	0.94052E-01	-0.94052E-01	0.94052E-01	-0.94052E-01
0.45	0.55627E-01	-0.55627E-01	0.55627E-01	-0.55627E-01
0.50	0.53703E-06	-0.53703E-06	0.53703E-06	-0.53703E-06
0.55	-0.67988E-01	0.67988E-01	-0.67988E-01	0.67988E-01
0.60	-0.14108E+00	0.14108E+00	-0.14108E+00	0.14108E+00
0.65	-0.21036E+00	0.21036E+00	-0.21036E+00	0.21036E+00
0.70	-0.26631E+00	0.26631E+00	-0.26631E+00	0.26631E+00
0.75	-0.30002E+00	0.30002E+00	-0.30002E+00	0.30002E+00
0.80	-0.30436E+00	0.30436E+00	-0.30436E+00	0.30436E+00
0.85	-0.27509E+00	0.27509E+00	-0.27509E+00	0.27509E+00
0.90	-0.21162E+00	0.21162E+00	-0.21162E+00	0.21162E+00
0.95	-0.11744E+00	0.11744E+00	-0.11744E+00	0.11744E+00
1.00	-0.21481E-05	0.21481E-05	-0.21481E-05	0.21481E-05

5.3.4 HONEYCOMB SANDWICH PANELS

Sonic fatigue design criteria for honeycomb panels was first established by McGowan (1) and later refined by Ballentine (2) for conventional bonded aluminum honeycomb core and facing sheet configurations. Recently, Holehouse (3) has presented sonic fatigue design criteria for diffusion-bonded titanium structure. The results in this section are concerned with flat panels with the effect of curvature discussed.

For honeycomb panels, the fundamental mode response of the panel is the lowest frequency mode. Ballentine (2) reported that certain of his panel designs exhibited two (1,1) type modes the lower frequency mode having mode lines very close to the fastener row and the higher frequency node having node lines formed near the shoulder of the bevel where the tapered edge begins.

For honeycomb panels, three types of sonic fatigue failure can be expected. The most common type of failure is at the edge of the panel at the center of the long side with cracks forming around the fastener holes. Facing sheet failures are also experienced with the failures occurring at the mid span of the long side of the panel. Finally, core shear failure can occur near the edge of the panel at a location of 20% to 30% of the panel short dimension.

5.3.4.1 Notation

a	Short dimension of panel, inches
b	Long dimension of panel, inches
E	Young's modulus of facing sheet material, psi
f_{11}	Fundamental mode frequency of honeycomb panel, Hz.
g	386.4 in/sec^2
h	Facing sheet thickness, inches
h_c	Core thickness, inches
h_d	Edge doubler thickness, inches
h_e, h_e'	Total edge thickness (see note on Figure 5.3.4-1), inch
K	Frequency parameter for Honeycomb panels (see Figure 5.3.4-2)
L_d, L_{d_1}, L_{d_2}	Edge doubler width parameters (see Figure 5.3.4-1), inches
S	Edge attachment spacing (approximately 20 h_c)
$S_p(f_{11})$	Spectral density of acoustic pressure (psi)/$\sqrt{\text{Hz}}$.
γ	Weight density of facing sheet material, lbs/in^3
ζ	Fundamental mode damping ratio
ν	Poisson's ratio
ρ_c	Core density, lbs/ft^3
$\bar{\sigma}$	Rms stress, ksi
σ_o	Stress due to a uniform static pressure of unit magnitude

5.3.4.2 Design Criteria for Flat Aluminum Honeycomb Panels

This section presents design equations and nomographs for estimating the fundamental mode frequency, stress response and fatigue life of flat honeycomb panels with aluminum core and facing sheets. Details of the structural configurations, test techniques and response data can be obtained from Ballentine's original report (2).

The methods presented here were developed by Ballentine from laboratory sonic fatigue tests of 30 honeycomb sandwich panel designs with two specimens of each design tested simultaneously to check repeatibility. The range of honeycomb panel design parameters considered in this experimental program were as follows:

facing sheet thickness	0.008 inch to 0.040 inch
doubler thickness	0.015 inch to 0.090 inch
core thickness	0.25 inch to 0.82 inch
edge thickness	0.025 inch to 0.115 inch
overall specimen size	21 × 21 inches to 37 × 61 inches
aspect ratio	1.0 to 1.7

For the sonic fatigue tests broadband random noise was used to simulate the service loading.

Ballentine (2) also considered aluminum alloy closure pans, tapered doublers and crushed cone edges with no significant change in response frequency, stress response, or fatigue life observed as compared to the basic design using constant thickness doublers, machined core edges, and fiberglass edge closure. The honeycomb panel geometry and nomenclature are presented in Figure 5.3.4-1.

5.3.4.2.1 Estimation of Natural Frequencies

By correlating experimentally determined fundamental mode response frequencies with a simple Rayleigh frequency analysis for a honeycomb panel, Ballentine (2) presents a simple design equation for determining the fundamental mode response frequency of a honeycomb panel with tapered edges as

$$f_{11} = K(h + h_c)/a^2 \quad \text{Hz} \qquad (5.3.4\text{-}1)$$

where K is a function of panel aspect ratio and is presented in Figure (5.3.4-2).

This analysis assumes that the panel response is linear and that the flexural rigidity of the panel results totally from the facing sheets. The core density is assumed to be equal to or greater than 2.0 lbs/ft^3.

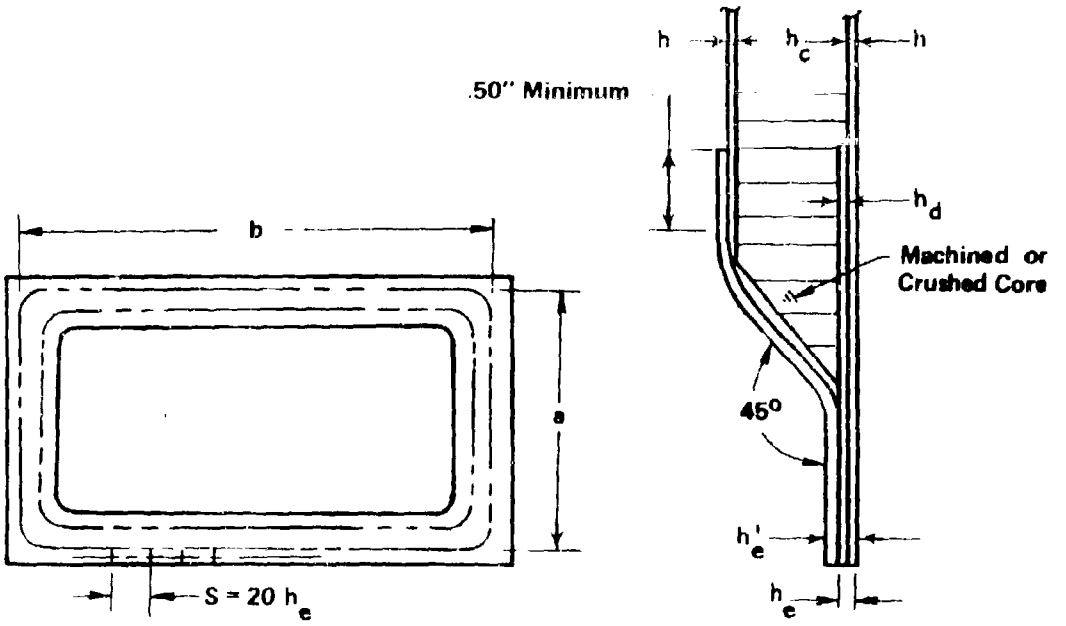

Note: h'_e is edge thickness with metal pan only

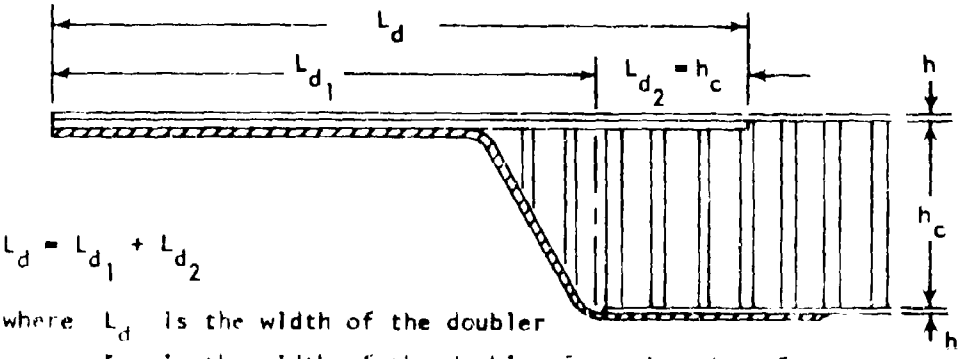

$L_d = L_{d_1} + L_{d_2}$

where L_d is the width of the doubler

L_{d_1} is the width of the doubler from the edge of the panel to the beginning of the full core depth

L_{d_2} is the additional width required and is equal to the core thickness

FIGURE 5.3.4-1 FLAT RECTANGULAR HONEYCOMB SANDWICH PANEL GEOMETRY AND TAPERED EDGE NOMENCLATURE (REF. 2)

FREQUENCY = $f_{11} = K(h + h_c)/a^2$, Hz.

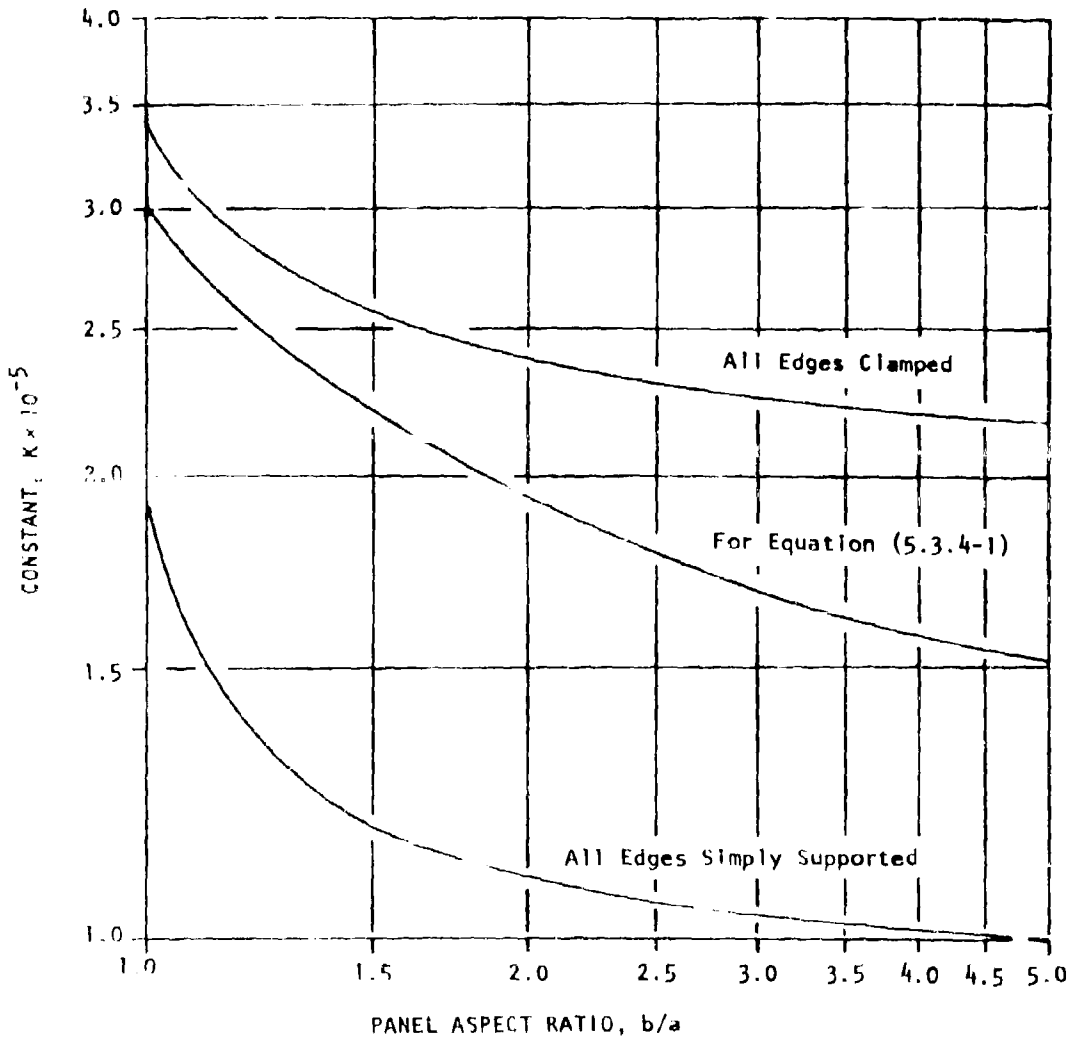

FIGURE 5.3.4-2 NOMOGRAPH FOR FUNDAMENTAL MODE RESPONSE FREQUENCY OF A FLAT RECTANGULAR HONEYCOMB SANDWICH PANEL (REF. 2)

Example: For an aluminum honeycomb panel with the following dimensions calculate the fundamental mode response frequency.

a = 21.0 inches, b = 21.0 inches,
core thickness = 0.25 inch
facing sheet thickness = 0.025 inch
Assume that the core density is greater than 2.0 lbs/ft^3.

From Figure 5.3.4-2 the value of K for b/a = 1.0 is 3×10^5. Then, from Equation (5.3.4-1) the fundamental mode response frequency is estimated to be

$$f_{11} = (3.0 \times 10^5)(0.025 + 0.250)/(21)^2 \quad Hz$$

$$f_{11} = 187 \text{ Hz}$$

5.3.4.2.2 Edge Stress Criteria

The most common type of sonic fatigue failure for honeycomb panels is failure at the center of the edge of the long side of the panel at the attachment line. By correlating sonic fatigue strain data Ballentine developed an empirical design equation for estimating the root mean square edge stress. This design equation is

$$\bar{\sigma} = 1.46 \times 10^{-3} \left(\frac{Eg}{\gamma}\right)^{1/4} \frac{a^{0.51} h_c^{0.5} (b/a)^{1.01} S_p(f_{11})}{h_e^{1.51} \zeta^{0.38} [3(b/a)^2 + 3(a/b)^2 + 2]^{0.57}} \quad ksi \qquad (5.3.4\text{-}2)$$

For aluminum alloys Ballentine assumed $(Eg/\gamma)^{1/4} \approx 445$ so that the above design equation becomes

$$\bar{\sigma} = 0.65 \frac{a^{0.51} h_c^{0.5} (b/a)^{1.01} S_p(f_{11})}{h_e^{1.51} \zeta^{0.38} [3(b/a)^2 + 3(a/b)^2 + 2]^{0.57}} \quad ksi \qquad (5.3.4\text{-}3)$$

Equation (5.3.4-3) was used to develop a design nomograph for estimating the magnitude of panel edge stresses. The failure data observed by Ballentine are also included so that estimates of the panel fatigue life can also be accomplished. This honeycomb panel edge stress design nomograph is presented in Figure 5.3.4-3.

5.3.4.2.3 Facing Sheet Criteria

In addition to establishing the edge thickness for the honeycomb panel, it is also required to establish the facing sheet thickness so that the entire panel design meets the desired fatigue life. Ballentine developed an empirical design equation for estimating the root mean square facing sheet stress response. This design equation is

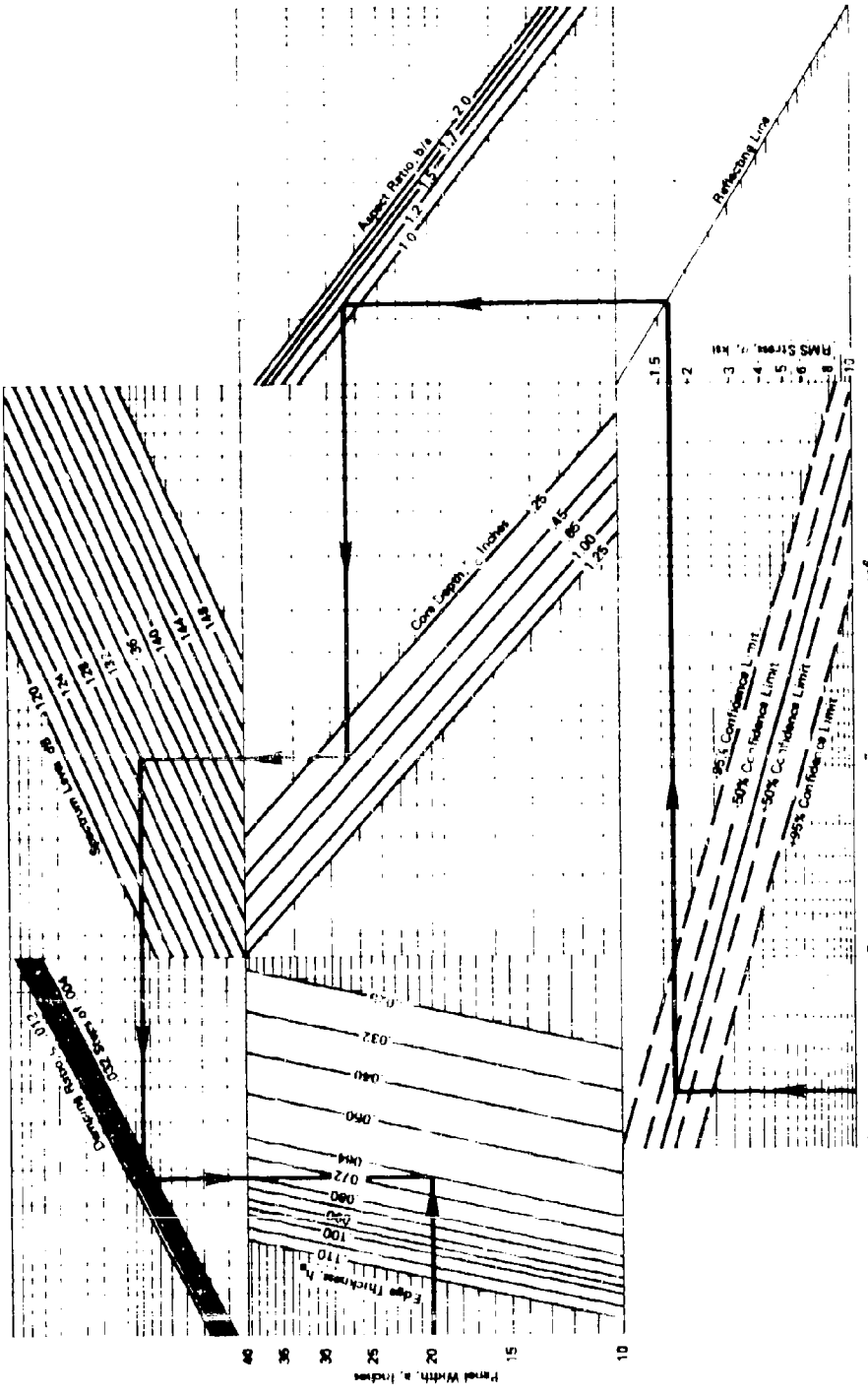

FIGURE 5.3.4-3 NOMOGRAPH FOR ESTIMATING EDGE STRESS RESPONSE AND FATIGUE LIFE OF FLAT RECTANGULAR HONEYCOMB SANDWICH PANELS (REFERENCE 2)

$$\bar{\sigma} = 1.8 \times 10^{-3} (Eg/\gamma)^{1/4} \frac{a^{0.46}[F(b/a)]^{0.73}}{h^{0.73} h_c^{0.23} \zeta^{0.36}} S_p(f_{11}) \quad \text{ksi} \qquad (5.3.4\text{-}4)$$

$$F(b/a) = (b/a)[(b/a)^2 + \nu]/[(b/a) + 1]^{3/2}$$

For aluminum alloys Ballentine assumed $(Eg/\gamma)^{1/4} \approx 445$ so that the above design equation becomes

$$\bar{\sigma} = 0.80 \frac{a^{0.46}[F(b/a)]^{0.73}}{h^{0.73} h_c^{0.23} \zeta^{0.36}} S_p(f_{11}) \quad \text{ksi} \qquad (5.3.4\text{-}5)$$

Equation (5.3.4-5) was used to develop a design nomograph for estimating the magnitude of panel facing sheet stress. The facing sheet failure data observed by Ballentine are also included so that estimates of the panel fatigue life can also be accomplished. The honeycomb panel facing sheet design nomograph is presented in Figure 5.3.4-4.

The edge stress criteria, the facing sheet criteria, and the response frequency criteria must be used together to establish an optimum panel design. An example will illustrate the design procedure.

Example: A flat aluminum alloy honeycomb sandwich structure is required to withstand an estimated service environment noise spectrum level of 130 dB. The design life is 5×10^8 cycles, the damping is assumed to be 0.019, the panel width is 20.0 inches with an aspect ratio of 1.2. The honeycomb core depth is 0.45 inches. Determine the panel edge thickness and facing sheet thickness for this design life.

Using Figure 5.3.4-3, one begins with the service life of 5×10^8 cycles and proceeds through the nomograph as indicated by the path to determine an edge thickness of 0.064 inches. Using Figure 5.3.4-4, as indicated by the path on the figure, the facing sheet thickness is determined to be 0.015 inches.

Using Equation (5.3.4-1) and Figure 5.3.4-2, the fundamental mode response frequency is determined to be

$$f_{11} = 2.5 \times 10^5 \ (0.015 + 0.45)/(20)^2 = 290 \text{ Hz.}$$

The spectrum level of 130 dB is checked to see if it corresponds to the response frequency of 290 Hz. It may be required to iterate the solution to optimize the design.

From this example, it is indicated that the required edge thickness is 0.064 inch and that the required facing sheet thickness is 0.015 inch. The edge thickness is the sum of the facing sheet thickness, the edge doubler thickness, and if a metal closure pan is used, the pan thickness. Assuming that the panel in this example used fiberglass edge closure the doubler thickness is

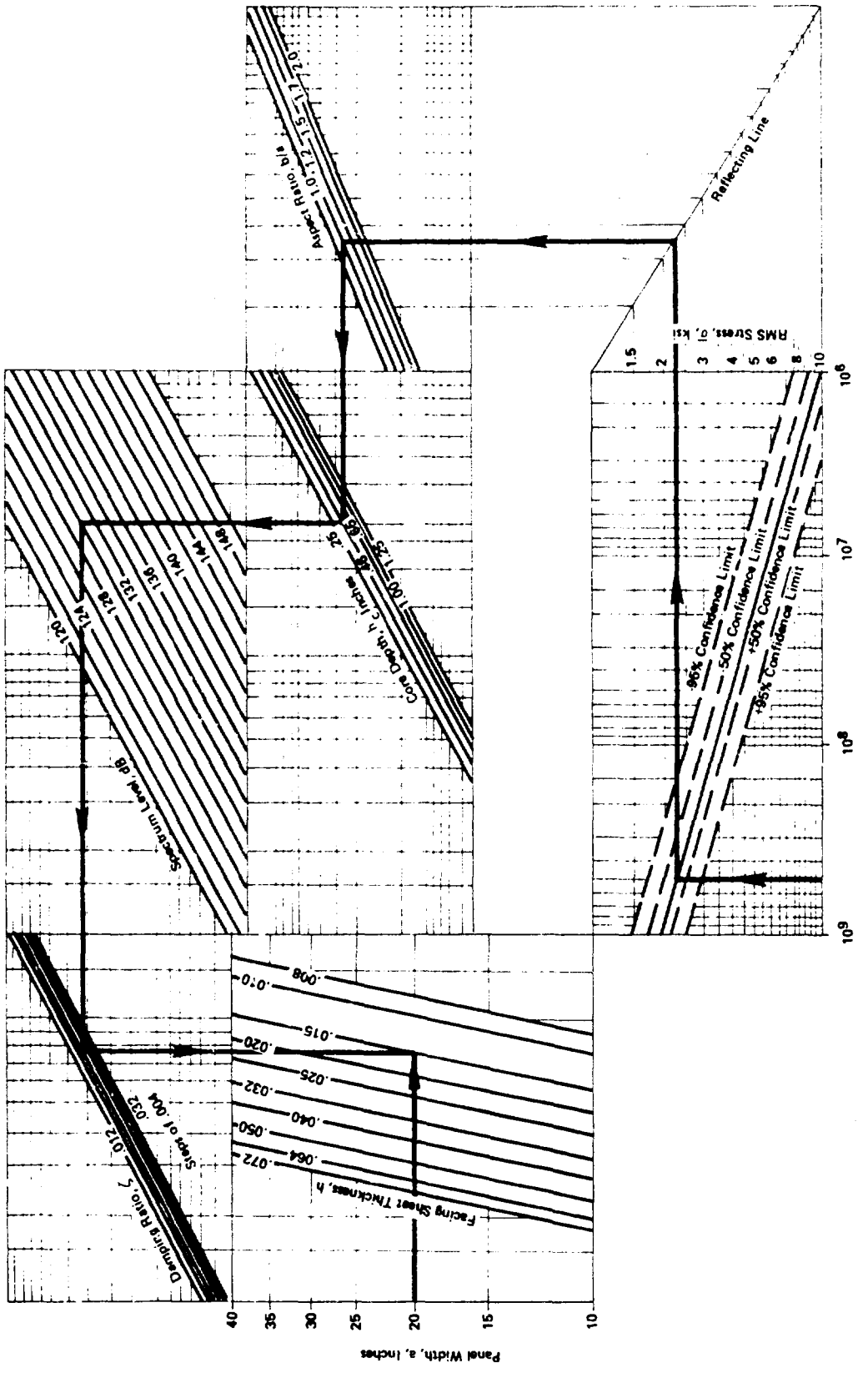

FIGURE 5.3.4-4 NOMOGRAPH FOR ESTIMATING FACING SHEET STRESS RESPONSE AND FATIGUE LIFE OF FLAT RECTANGULAR HONEYCOMB SANDWICH PANELS (REFERENCE 2)

$$h_d = h_e - h_f = 0.064 - 0.015 = 0.049 \text{ inch.}$$

To obtain an optimum length for the doubler one uses the criteria indicated in Figure 5.3.4-1.

5.3.4.3 Design Criteria for Diffusion Bonded Titanium Honeycomb Panels

This section presents equations and nomographs for estimating the fundamental mode frequency and edge stress response and fatigue life of flat honeycomb panels with titanium core and facing sheet material. The joining system considered is a "Liquid Interface Diffusion" (LID) bonding process.

The methods presented in this section were developed by Holehouse (3) from laboratory sonic fatigue tests of ten panel designs. The range of honeycomb panel design parameters considered in this experimental program were as follows:

facing sheet thickness	0.005 inch to 0.020 inch
doubler thickness	0.012 inch to 0.020 inch
core thickness	0.125 inch to 0.50 inch
edge thickness	0.022 inch to 0.060 inch
overall specimen size	18.5 × 25.25 inches
aspect ratio	1.36
panel area density	0.25 to 1.25 lb/ft^2

For the sonic fatigue tests, broadband random noise was used to simulate the service loading. The honeycomb panel geometry and nomenclature are presented in Figure 5.3.4-1. Details of the structural configurations, test techniques, and response data can be obtained from Holehouse's original report (3).

5.3.4.3.1 Estimation of Natural Frequencies

By correlating experimentally determined fundamental mode response frequencies with the results of a finite element frequency analysis of the structural design, Holehouse (3) obtained a simple design equation for the fundamental response frequency of a flat titanium honeycomb panel as

$$f_{11} = 2.88 \, K \, h^{0.194} h_c^{0.913} / a^2 \qquad (5.3.4\text{-}6)$$

where K is a function of panel aspect ratio determined from Figure 5.3.4-2 using the curves labeled "clamped" and "simply supported." The above result for the fundamental mode frequency was incorporated into the first part of a design nomograph for estimating facing sheet stress. This nomograph is presented as Figure 5.3.4-6.

5.3.4.3.2 Estimation of Static Stress Response

The final result of Holehouse's analysis is to develop a prediction of panel edge stress at the center of the long side of the panel resulting from a

random acoustic excitation. Using a single degree-of-freedom analysis (see Equations (5.2.2-60d) and (5.2.2-61)), the static stress response at this point resulting from a uniform static pressure of unit magnitude is required. Holehouse correlated basic panel parameters against analytical results obtained from a NASTRAN finite element analysis to obtain an expression for the maximum edge stress in a clamped panel without an edge doubler. The following expression for the static stress response resulting from a uniform pressure of unit magnitude is

$$\sigma_o = 3.30 \times 10^{-} \; a^2 (b/a)^{0.752} / (hh_c) \qquad (5.3.4\text{-}7)$$

Equation (5.3.4-7) was used to develop the static stress nomograph presented in Figure 5.3.4-5.

5.3.4.3.3 Response to Random Acoustic Excitation

Using a single degree-of-freedom analysis, Holehouse correlated the basic panel parameters and acoustic pressure spectrum levels to obtain an empirical design equation for estimating the root mean square stress response at the center of the long side of the panel. This design equation has the form

$$\bar{\sigma} = \frac{24.71 \; S_p(f_{11}) \sigma_o}{f_{11} \; [1.0034 \quad 1.095^{\beta_c}]} \quad \text{ksi} \qquad (5.3.4\text{-}8)$$

The relationship given in Equation (5.3.4-8) was used to develop a dynamic stress design nomograph. Whereas Holehouse used three nomographs, the development here combined the frequency nomograph with the dynamic stress nomograph. The result is presented in Figure 5.3.4-6. Holehouse included the results of his sonic fatigue failure data so that fatigue life can also be estimated using Figure 5.3.4-6.

Estimates for core shear modulus and core density in terms of the core foil thickness and cell size are obtained from Figure 5.3.4-7. Holehouse (3) states that the stress estimates obtained using Equation (5.3.4-8) will be applicable to joining systems other than LID, but he cautions the designer about using fatigue life estimates from Figure 5.3.4-6 for other joining systems.

Use of the design nomographs are indicated in the figures. Note: The validity of statistically correlating dimensional parameters, as apparently done by Holehouse, is questionable.

5.3.4.4 Curvature Effects

The consideration of sonic fatigue design criteria for honeycomb sandwich panels with curvature is documented in the literature from the analytical standpoint; however, very little experimental data is available to obtain reliable design results. The basic configuration considered is a

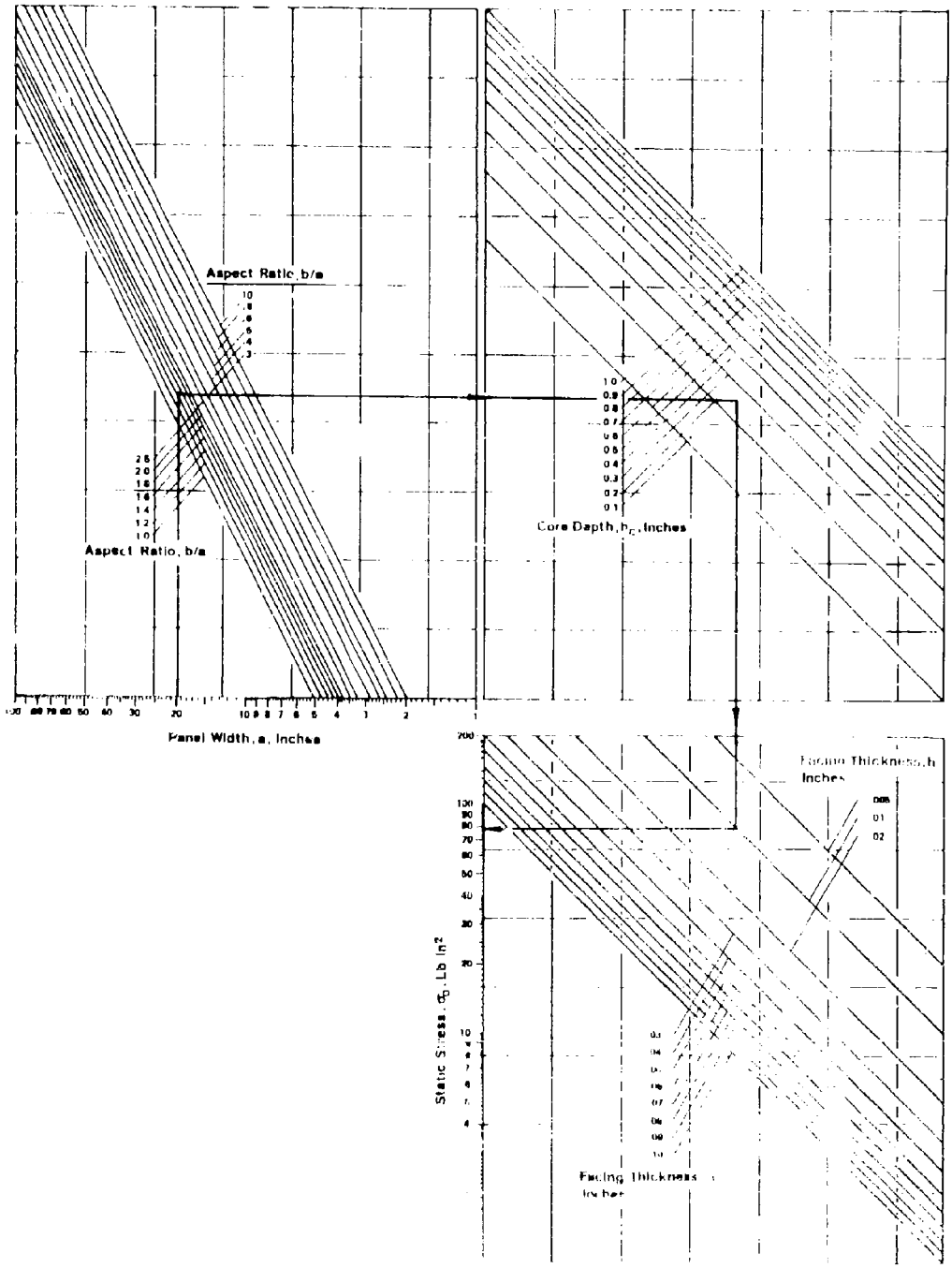

FIG. 3.4-5 STATIC EDGE STRESS RESPONSE DUE TO UNIFORM UNIFORM STATIC PRESSURE FOR DIFFUSION BONDED TITANIUM HONEYCOMB PANELS (REF. 3)

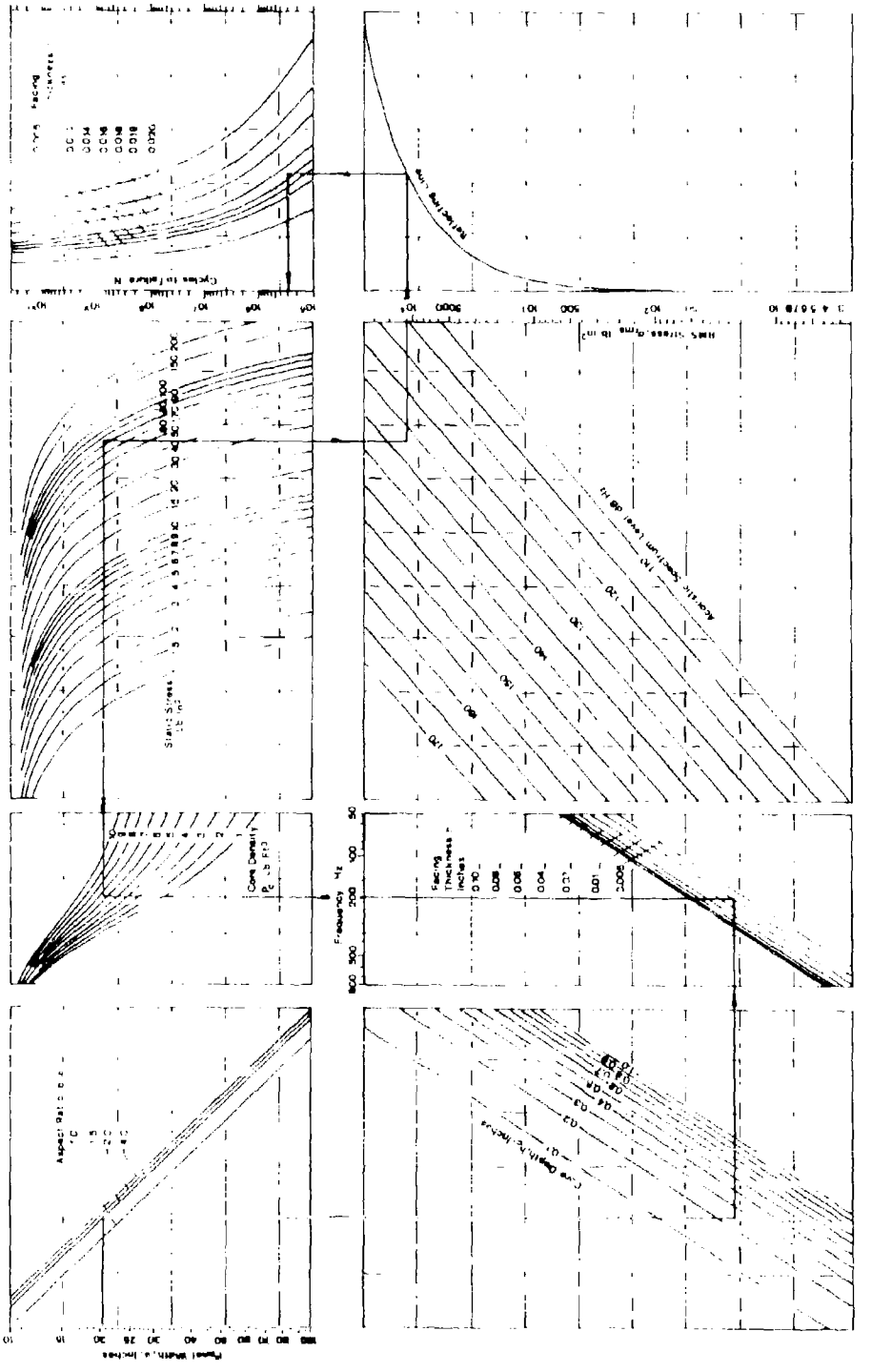

FIGURE 5.3.4-6 NOMOGRAPH FOR ESTIMATING FUNDAMENTAL MODE FREQUENCY, PANEL EDGE STRESS RESPONSE, AND FATIGUE LIFE FOR DIFFUSION BONDED TITANIUM HONEYCOMB PANELS (REF. 3)

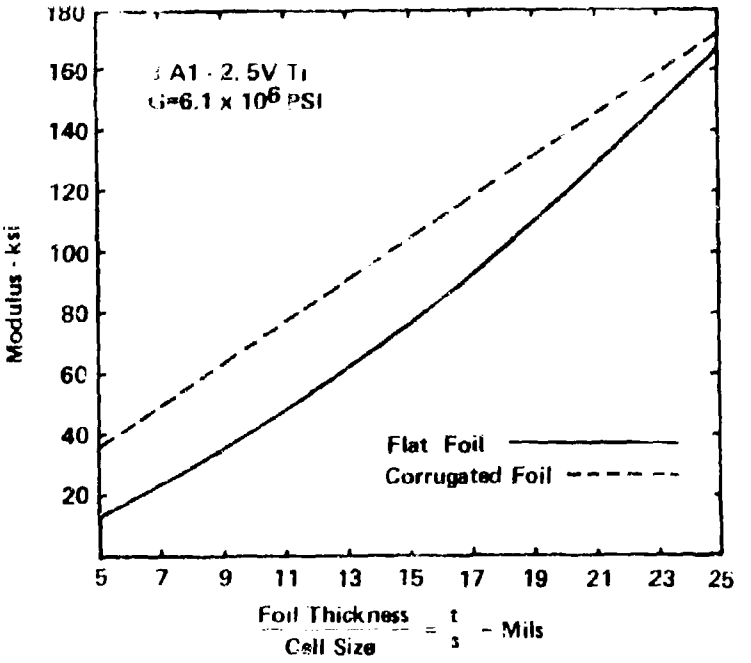

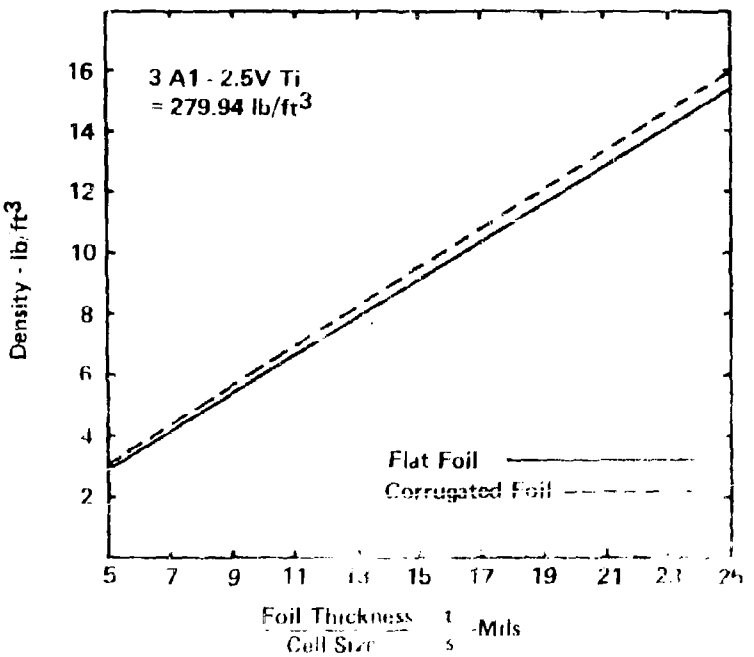

FIGURE 5.3.4-7 CORE SHEAR MODULUS AND DENSITY FOR [illegible] BONDED TITANIUM HONEYCOMB SANDWICH PANELS (REF. [illegible])

circular cylindrical panel. Plumblee (4) presents an analysis of cylindrically curved honeycomb panels using a Rayleigh-Ritz method. His results, although based upon simplifications, require a computer solution. Jacobson (5) also presents an analysis of circular cylindrical honeycomb panels. Thompson and Lambert (6) have developed design equations, a sequence of nomographs, and a computer program for estimating response frequency and stress for circular cylindrical honeycomb panels.

REFERENCES FOR SECTION 5.3.4

1. McGowan, P. R., et al.; "Structural Design for Acoustic Fatigue," ASD-TDR-63-820, Air Force Flight Dynamics Laboratory, Wright-Patterson Air Force Base, Ohio, 1963.

2. Ballentine, J. R., et al.; "Refinement of Sonic Fatigue Structural Design Criteria," AFFDL-TR-67-156, Air Force Flight Dynamics Laboratory, Wright-Patterson Air Force Base, Ohio, 1968.

3. Holehouse, I.; "Sonic Fatigue of Diffusion-Bonded Titanium Sandwich Structure," Paper No. 15, AGARD-CP-113, Advisory Group for Aerospace Research and Development, North Atlantic Treaty Organization, 1972.

4. Ballentine, J. R., et al.; "Sonic Fatigue in Combined Environment," AFFDL-TR-66-7, Air Force Flight Dynamics Laboratory, Wright-Patterson Air Force Base, Ohio, 1966.

5. Jacobson, M. J.; "Stress and Deflection of Honeycomb Panels Loaded by Spatially Uniform White Noise," AIAA Journal, Vol. 6, No. 8, August, 1968.

6. Thompson, A. G. R. and Lambert, R. F.; "Acoustic Fatigue Design Data, Part II," AGARD-AG-162, Part II, Advisory Group for Aerospace Research and Development, North Atlantic Treaty Organization, November, 1972.

5.3.5 CHEM-MILLED PANELS

No data is presently available in the literature to provide design criteria in the form of design equations and nomographs for chem-milled panel structure. Sonic fatigue failure of chem-milled aircraft structure has been reported in the literature by Hancock (1) and van der Heyde (2) has conducted a series of laboratory sonic fatigue tests on chem-milled panel structure. The data reported by van der Heyde is presented here for design guidance. For more detail of the test data and test techniques the original report should be consulted. Other references to chem-milled sonic fatigue data are van der Heyde and Kolb (3) and Berens and West (4).

5.3.5.1 Description of Test Specimens

The chem-milled test specimens used in van der Heyde's sonic fatigue tests were manufactured from 0.175 inch thick 7075-T6 aluminum alloy material. Squares of the material (1.94 inch by 1.94 inch) were removed from the sheet by a chem-milling process leaving a skin of 0.030 inch and stiffeners of 0.18 inch wide by 0.145 inch high. Figure 5.3.5-1 shows the details of the specimen construction. The panels were manufactured according to normal aircraft specifications.

5.3.5.2 Results of the Sonic Fatigue Tests

The sonic fatigue tests were conducted in the wide band sonic fatigue facility of the Air Force Flight Dynamics Laboratory, WPAFB. The fundamental mode response frequencies of the panel were determined using a loud speaker excitation source with the node lines being parallel to the panel edges. Static load and dynamic load test were performed to determine the panel response to increasing static loads and sound pressure levels. The twenty test specimens were divided into four groups with five specimens in each group. Each group was tested at a different sound pressure level. The damping ratios for the panel specimens varied from 0.004 to 0.050 at resonance. The results of the acoustic fatigue tests are presented in Table 5.3.5-1. The failure data for the specimens is presented in Figure 5.3.5-2 and Figure 5.3.5-3 compares the fatigue life of chem-milled structure to that exhibited by skin-stringer and bonded beaded structure.

REFERENCES FOR SECTION 5.3.5

1. Hancock, R. N., "Inlet Duct Sonic Fatigue Induced by Multiple Pure Tones of a High Bypass Ratio Turbofan," Paper presented at the Institute of Environmental Sciences Symposium Anaheim, California, April 1973.

2. van der Heyde, R. C. W., et. al., "Results of Acoustic Fatigue Tests on a Series of Chem-Milled Panels," TM-73-151-FYA, Air Force Flight Dynamics Laboratory, Wright-Patterson Air Force Base, Ohio, December 1973.

3. van der Heyde, R. C. W.; and Kolb, A. W., "Sonic Fatigue of Light-weight Aircraft Structure," Paper No. 20, AGARD-CP-113, Advisory Group for Aerospace Research and Development, North Atlantic Treaty Organization, 1972.

4. Berens, A. P. and West, B. S.; "Experimental Methods in Acoustic Fatigue", AFFDL-TR-71-113, Air Force Flight Dynamics Laboratory, Wright Patterson Air Force Base, Ohio, 1971.

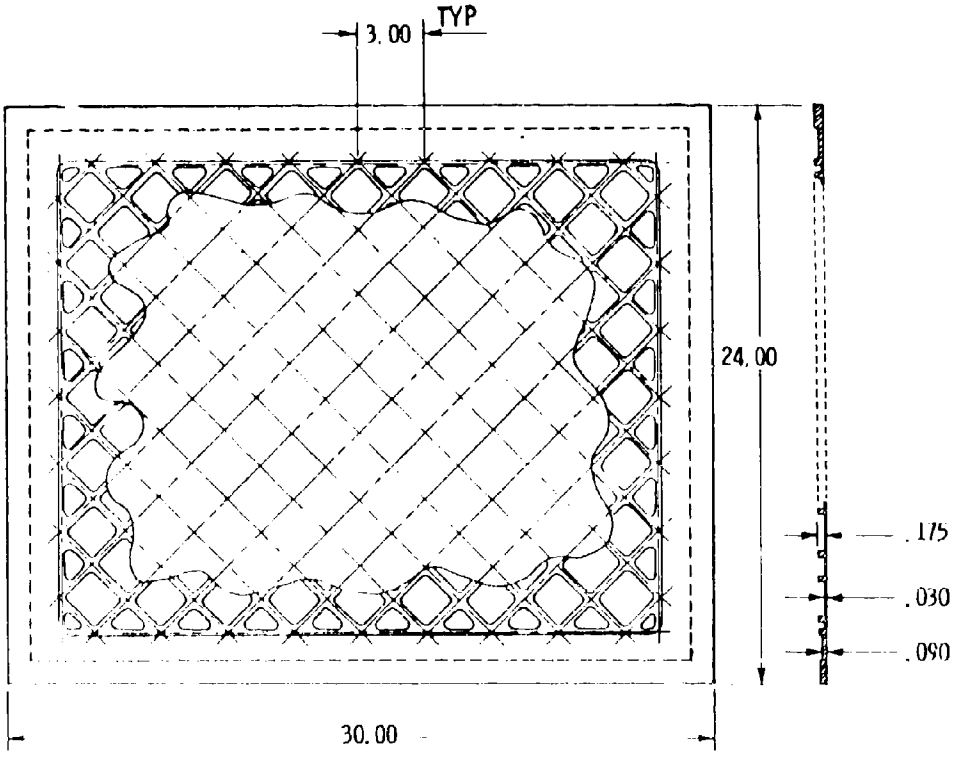

FIGURE 5.3.5-1 CHEM-MILLED PANEL DESIGN (REF. 2)

TABLE 5.3.5-1 STRESS RESPONSE AND FATIGUE DATA FOR CHEM-MILLED PANELS

PANEL NR	NOISE SOURCE*	OVERALL SPL dB	SPECTRUM LEVEL dB	PRINCIPAL STRESS PSI	STRESS LOC 4 PSI	ZERO CROSSINGS SEC^{-1}	LIFE 10^6 CYCLES	FAILURE LOCATION
A-1	M	154.0	134.0	4017.3	2113.5	67	.53	Center
B-1	M	155.5	134.0	4301.1	1830.2	70	2.23	Center
C-1	M	154.5	134.5	4709.5	1778.3	76	1.32	Center
D-1	M	154.5	137.5	6746.7	2985.4	71	.57	Center
E-1	M	155.5	136.5	3410.9	3162.3	79	.63	Center
A-2	M	151.0	132.0	3336.9	1631.2	68	3.55	Center
B-2	M	151.0	131.5	3613.0	1631.2	71	4.47	Center
C-2	M	151.0	132.0	4267.5	1453.8	74	4.66	Center
D-2	M	151.5	134.5	4576.4	2304.1	70	1.26	Center
E-2	M	153.5	135.5	4784.4	2585.2	78	.98	Center
A-3	M	141.5	124.0	2162.8	1059.3	68	49.	
B-3	M	141.5	122.5	1174.6	520.9	67	49.	
C-3	M	143.0	125.5	2636.5	917.3	75	54.	
D-3	M	143.0	127.0	2661.6	1000.0	69	9.65	Edge
E-3	M	144.0	126.5	2056.0	917.3	74	19.11	Edge
A-4	S	154.5	120.5	2053.4	298.5	66	6.89	Edge
B-4	S	155.0	122.0	1830.5	298.5	72	7.52	Edge
C-4	S	154.0	121.5	1429.1	325.5	75	7.56	Edge
D-4	S	154.0	123.0	2428.6	290.1	78	10.90	Edge
E-4	S	154.0	123.0	1931.1	118.8	77	11.64	Edge

*S - is wide band siren source: M - is air modulating system source

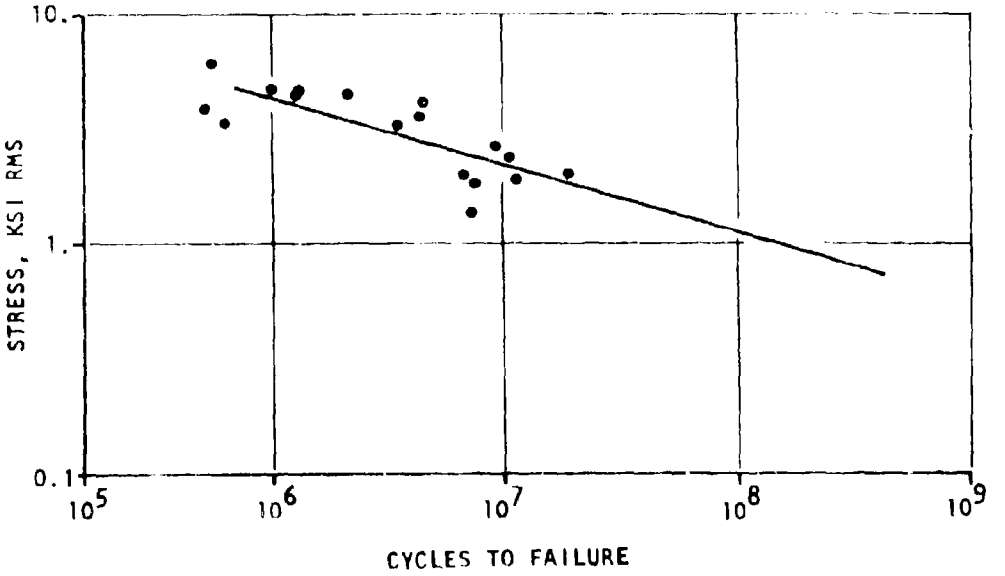

FIGURE 5.3.5-2 RMS STRESS IN KSI VERSUS CYCLES TO FAILURE: CHEM-MILLED STRUCTURE (REF. 2)

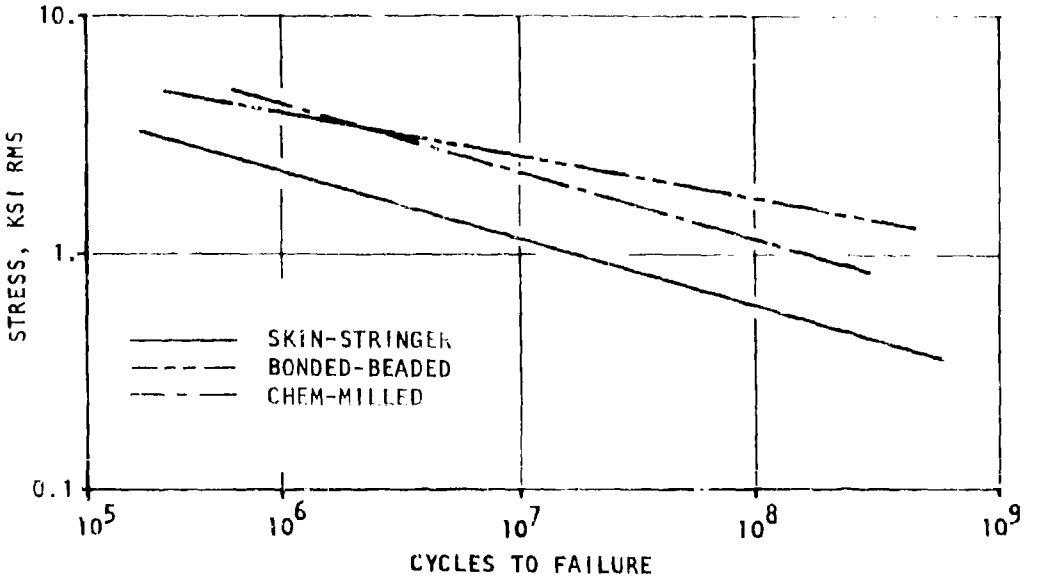

FIGURE 5.3.5-3 RMS STRESS IN KSI VERSUS CYCLES TO FAILURE FOR CHEM-MILLED, BONDED BEADED, AND SKIN-STRINGER STRUCTURE (REF. 2)

5.3.6 CORRUGATED PANELS

Corrugation stiffened panels are typical of supersonic aircraft and have been proposed for use on the NASA Space Shuttle Orbiter. The latter program has recently caused a renewed interest in the sonic fatigue design criteria for corrugated panel structure. McGowan's design criteria (1) for corrugated panels remains as the only existing design criteria. Recent results of sonic fatigue tests have been reported by Baird (2) and by Rucker (3,4) that can provide design guidance.

A limited amount of analytical work is available for obtaining estimates of the response frequencies. Using an orthotropic plate analogy, Stroud (5) has developed general expressions for smeared orthotropic plate constants suitable for use in the methods described in Section 5.2.2.3 for predicting response frequencies of such structure. Fung (6) has criticized this approach on an analytical basis and has formulated a theory of vibration of corrugated panels using divided difference equations or assumed mode methods. Golden (7) has also presented a lumped parameter method for estimating response frequencies of corrugated panels with tapered edges. All of the above references should be consulted prior to using the design criteria presented in this section.

The configuration and nomenclature of the corrugated panel is illustrated in Figure 5.3.6-1.

5.3.6.1 Notation

a	Length of panel transverse to corrugations, inches
b	Length of panel parallel to corrugations, inches
D	$Eh^3/12(1 - \nu^2)$ in.lb.
D_1	Bending rigidity of a single corrugation transverse to its length (see Stroud (5))
E	Young's modulus of material, lbs/in^2
f_{mn}	Natural frequency of (m,n)th mode, Hz.
G	Shear modulus of material, lbs/in^2
h	Thickness of panel skin, inches
h_c	Thickness of corrugation, inches
I	Second area moment of inertia of a single skin-corrugation about the centroid in the plane of the cross section
J	Brendt torsion constant, $1/\int (q^2/h)ds$, for a closed cell
ℓ	Width of corrugation at skin attachment
m	Number of half sine waves in direction transverse to corrugations

N	cycles to failure
n	Number of half sine waves in the direction parallel to corrugations
q	shear flow in skin-corrugation section
ρ	Mass per unit volume of material
ν	Poisson's ratio for the material

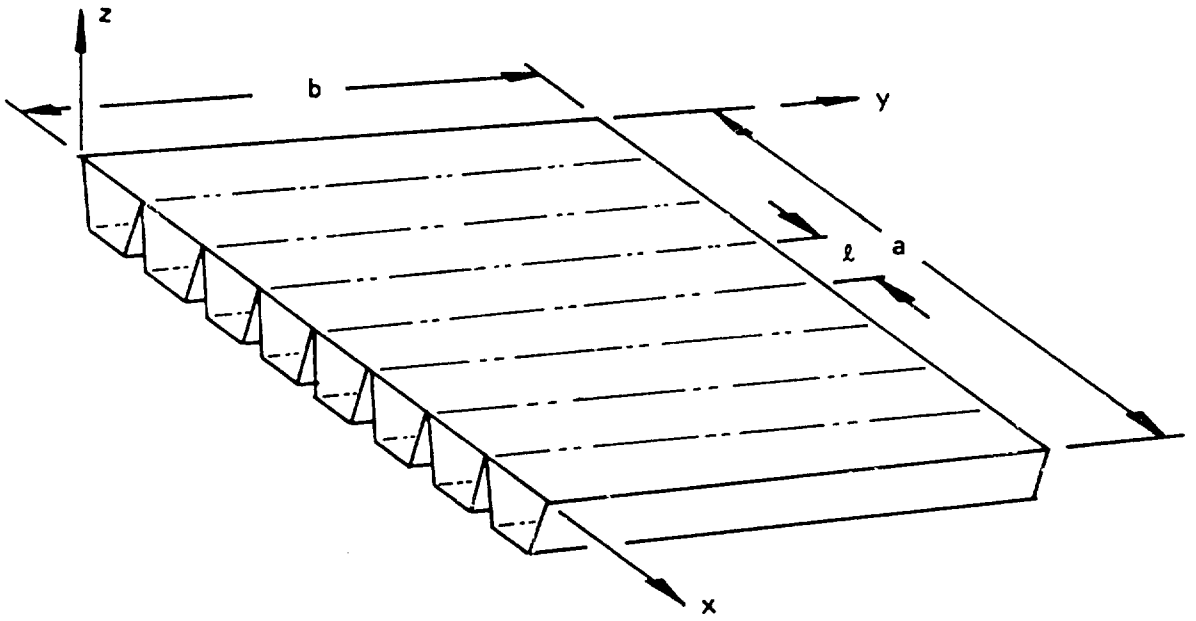

Skin Thickness = h, inches

Corrugation Thickness = h_c, inches

FIGURE 5.3.6-1 CORRUGATED PANEL GEOMETRY AND NOMENCLATURE

5.3.6.2 Estimation of Natural Frequencies

As stated above, the estimation of response frequencies of corrugated panels is still open as to the most appropriate model for the structure. Stroud (5) presents general expressions for the equivalent orthotropic plate constants of a corrugated panel with a single cover sheet. Using Stroud's work, one can calculate the constants D_1, D_2, and D_3 appearing in Equations (5.2.2-82) and (5.2.2-83) to obtain frequency estimates. Fung (6) and Golden (7) present a different approach by considering each corrugation as a torque tube. Using Fung's approach, the expression for the response frequencies of a corrugated panel with all exterior edges simply supported and neglecting rotary inertia terms is

$$f_{mn}^2 = \frac{\pi^2 m^2 n^2}{4\rho h}\left[\left(\frac{m}{n}\right)^2 D_1/a^4 + \left(\frac{n}{m}\right)^2 (EI/\ell)/b^4 + (GJ/\ell + (1-\nu)D)/a^2b^2\right] \quad Hz^2 \qquad (5.3.6\text{-}1)$$

Golden (7) presents data illustrating the importance of considering the effect of tapered edges.

5.3.6.3 Skin and Corrugation Design Criteria

The configuration of the corrugated panel specimens used by McGowan are illustrated in Figure 5.3.6-2. Welded tee sections were used to simulate rib caps parallel to the corrugation and are clipped to the spar cap to form three bays. Formed angles in each bay are spot welded against the crest and transverse to the corrugations to attach each end to the spar cap. The skin-corrugation, skin-spar cap, and rib clip-spar cap attachments are spot welded. The ribs are attached to the skin and corrugation using A286 rivets 5/32 inch in diameter.

The dimensions of the four specimens tested are ℓ_c = 0.75 inch and combinations of skin thickness, h, and corrugation thickness, h_c, as follows:

h, inches	0.020	0.020	0.025	0.025
h_c, inches	0.016	0.020	0.016	0.020

The specimens were manufactured from 6AL-4V annealed titanium alloy.

McGowan's design chart for selecting the skin thickness of a corrugated panel is based upon edge stress criteria and is presented in Figure 5.3.6-3. The nomograph for selecting corrugation thickness is presented in Figure 5.3.6-4. The design procedure is to determine the skin thickness, h, first using Figure 5.3.6-3 and then determine the corrugation thickness from Figure 5.3.6-4 as indicated by the path in the figures. These nomographs must be used with design judgement since the fatigue life determination relies upon an equivalent random fatigue curve and was established using only four specimens. For additional guidance the designer should consult the references of Baird and Rucker.

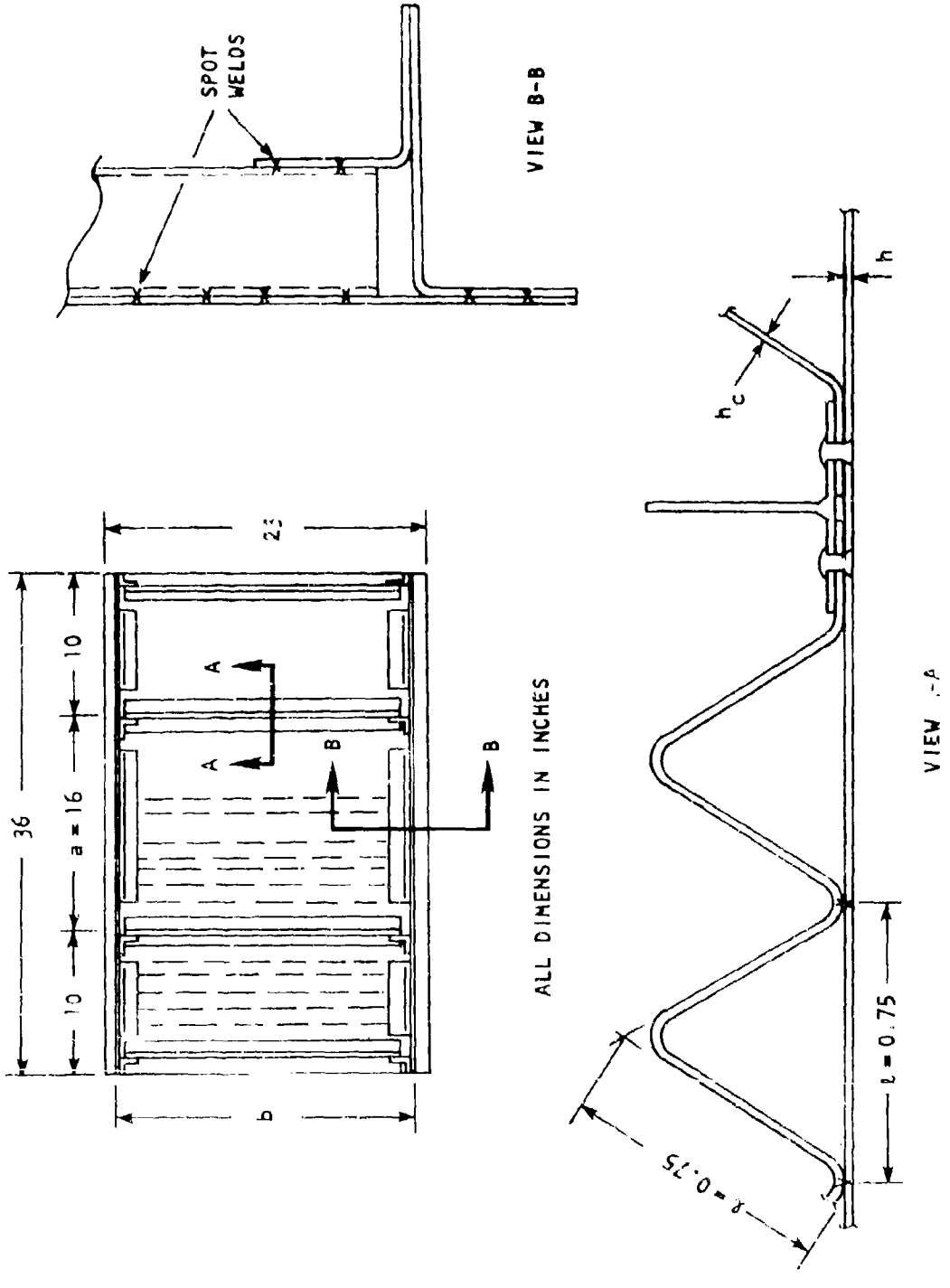

FIGURE 5.3.6-2 CORRUGATED PANEL SONIC FATIGUE TEST SPECIMENS (REF. 1)

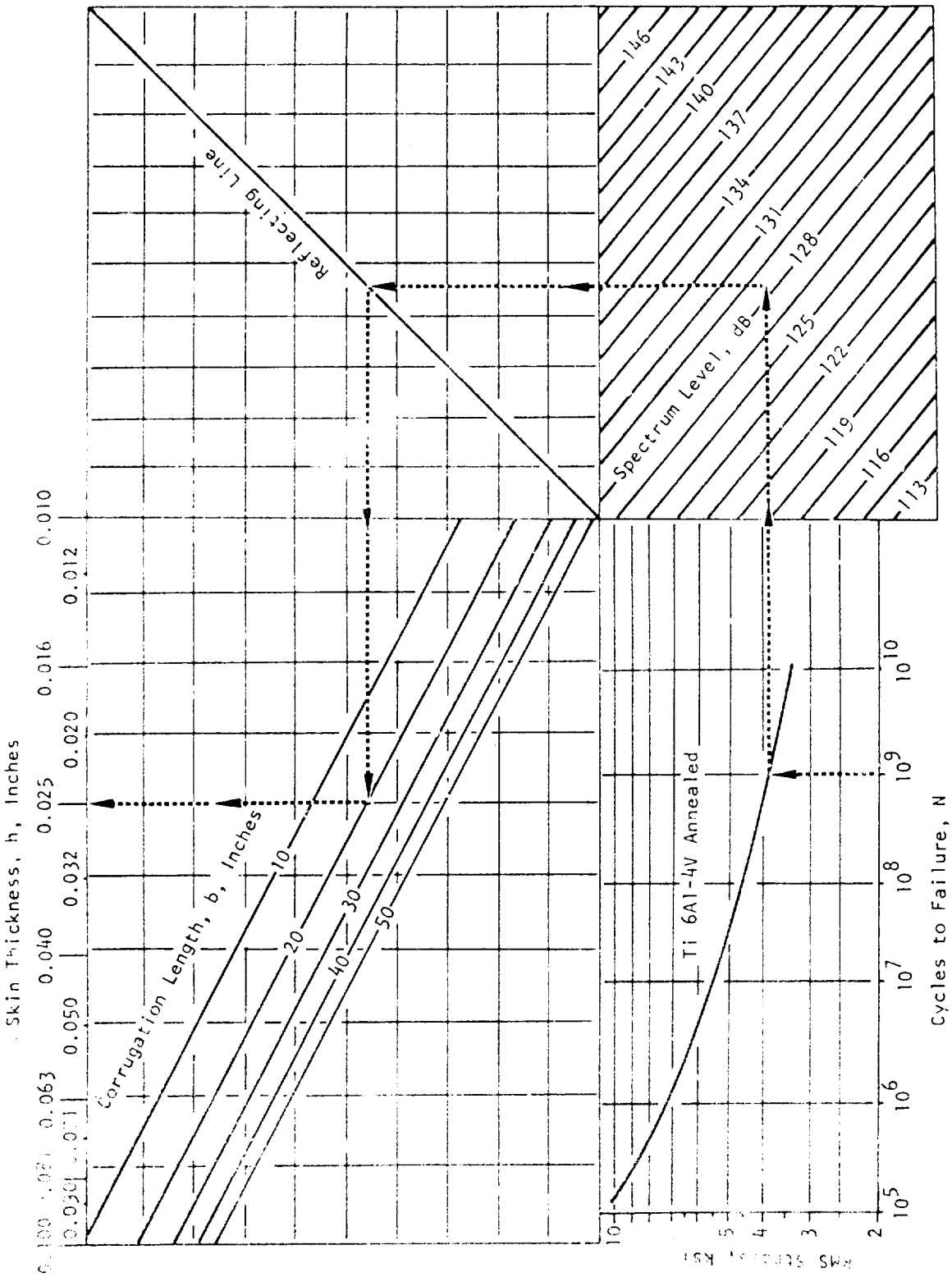

FIGURE 5.3.6-3 NOMOGRAPH FOR CORRUGATED PANEL SKIN THICKNESS BASED ON EDGE STRESS CRITERIA (REF. 1)

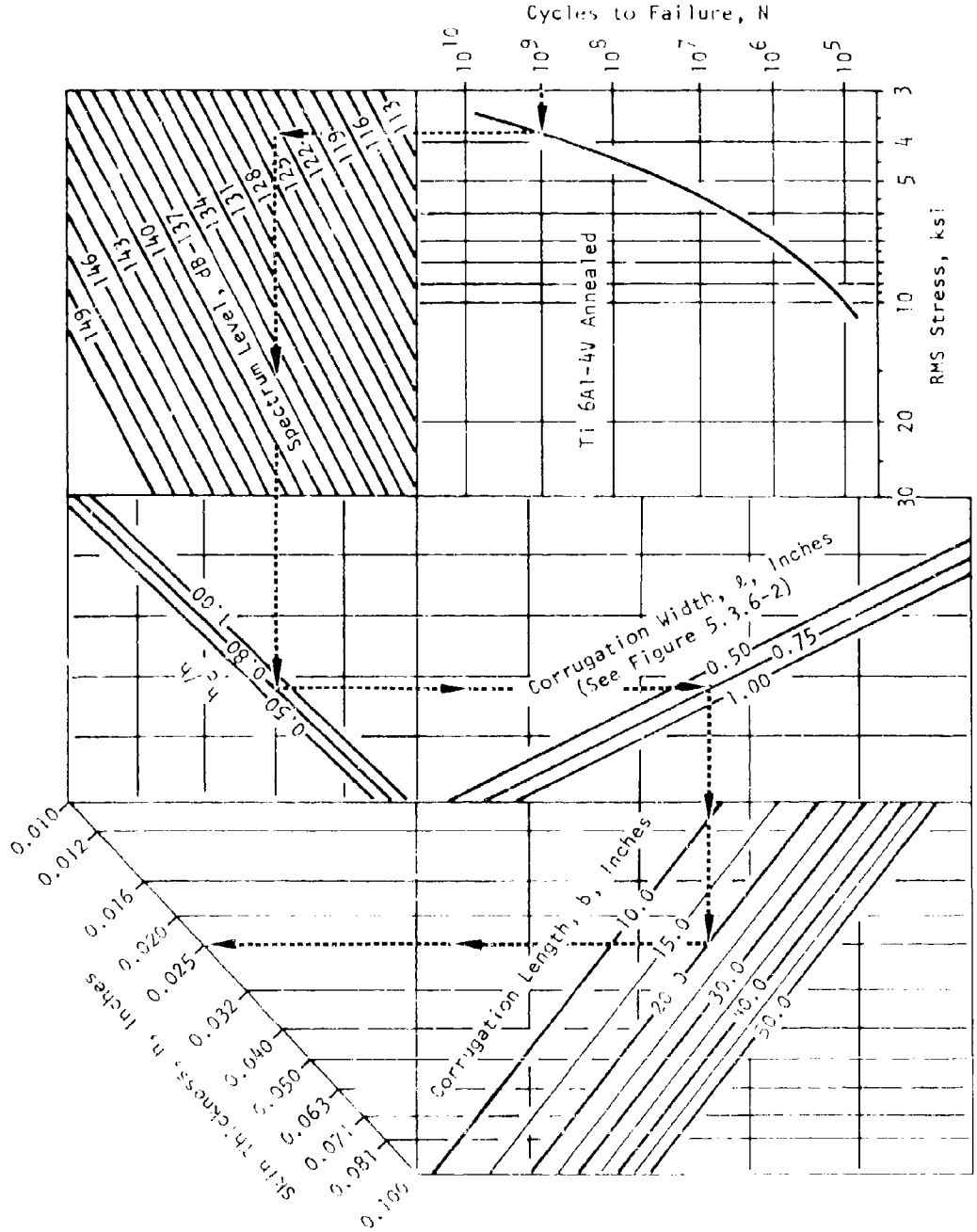

FIGURE 5.3.6-4 NOMOGRAPH FOR CORRUGATED PANEL CORRUGATION THICKNESS (REF. 1)

REFERENCES FOR SECTION 5.3.6

1. McGowan, P. R. et al.; "Structural Design for Acoustic Fatigue," ASD-TDR-63-820, Air Force Flight Dynamics Laboratory, Wright-Patterson Air Force Base, Ohio 1963

2. Baird, E. F., et al.; "Sonic Fatigue Failure Mechanisms in Potential Space Shuttle Orbiter Designs," AIAA Paper No. 74-348, AIAA/ASME/SAE 15th Structures, Structural Dynamics and Materials Conference, Las Vegas, Nevada, April 17-19, 1974.

3. Rucker, C. E., and Grandle, R. E.; "Testing of Space Shuttle Thermal Protection System Panels Under Simulated Reentry Thermoacoustic Conditions," Paper presented at the AIAA/NASA/ASTM/IES Seventh Space Simulation Conference, Los Angeles, Calif., November 12-14, 1973.

4. Rucker, C. E., and Grandle, R. E.; "Thermoacoustic Fatigue Testing Facility for Space Shuttle Thermal Protection System Panels," Presented at 1972 Symposium on Fatigue at Elevated Temperatures, Storrs, Conn., June 18-23, 1972, STP [illegible].

5. Stroud, W. J.; "Elastic Constants for Bending and Twisting of Corrugation-Stiffened Panels," NASA TNR-166, National Aeronautics and Space Administration, Washington, D. C., 1962.

6. Fung, Y. C., "On Corrugation-Stiffened Panels," SM62-33 (AFOSR-3122), Graduate Aeronautical Laboratories, California Institute of Technology, June 1962.

7. Golden, C. T.; "Analytical Method for Determining the Natural Frequencies and Mode Shapes of Orthotropic Plates," M. S. Thesis, Department of Aeronautical Engineering, University of Washington, November 1960.

5.3.7 BONDED BEADED PANELS

McGowan (1) published the first sonic fatigue design criteria for bonded beaded structure. Recently, van der Heyde and Kolb (2) have published the results of sonic fatigue tests of 60 bonded beaded panels. Both references indicate that the critical area for sonic fatigue is the bead edge where the bead tapers into the panel. Van der Heyde and Kolb also observed skin failures along the bead-skin bond line that are apparently dependent upon the ratio of skin thickness to bead thickness and concluded that McGowan's criteria is acceptable for stress prediction but is lacking in fatigue life estimation and requires modification to improve the accuracy.

Golden (3) presents a lumped parameter method for frequency estimates for corrugated or bonded beaded panels. By using a lumped parameter model for a beam with tapered edges to simulate the bending rigidity of the bead, Golden's method predicts a severe curvature change (high bending stress) at the bead edge for the fundamental mode. Golden's method will not assist in the prediction of skin failures along the bead bond line as observed by van der Heyde and Kolb. At this point it is difficult to assess the modifications to McGowan's criteria required to improve the accuracy of the fatigue life estimation. Fortunately, van der Heyde and Kolb's paper present sufficient guidance to aid the designer.

5.3.7.1 Notation

b Bead height, inches
h Skin thickness, inches
h_b Bead thickness, inches
h_d Edge doubler thickness, inches
h_e Total edge thickness of panel, inches
L Length of bead, inches
R Radius of bead (See Figure 5.3.7-2), inches
W Width of bead

5.3.7.2 Data Reported in the Literature

The 60 bonded beaded panel specimens tested by van der Heyde and Kolb comprised 20 specimens each of three designs. These designs are called Type I, II, and III specimens and are illustrated in Figure 5.3.7-1. Types I and II had the beads oriented parallel to the specimen width and Type III had the beads oriented parallel to the specimen length. All specimens were manufactured from 7075-T6 aluminum alloy material. The particular data for each type of specimen is as follows:

Specimen Type	Skin Thickness h, inches	Bead Thickness h_b, inches	Bead Length L, inches
I	0.032	0.032	21.0
II	0.020	0.045	21.0
III	0.032	0.032	27.0

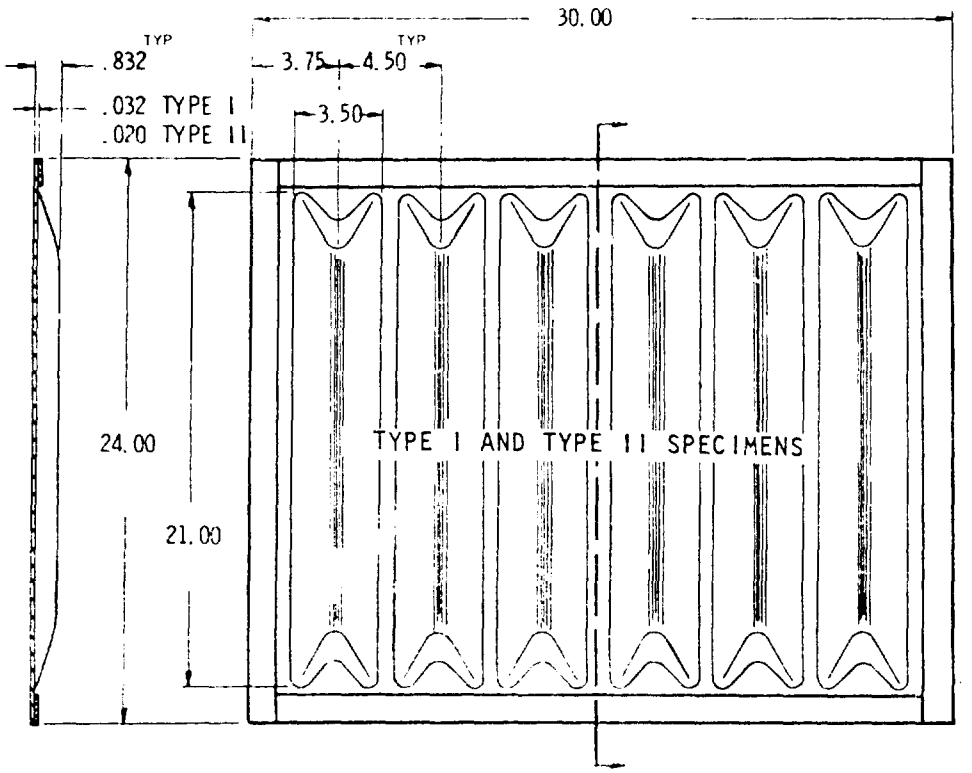

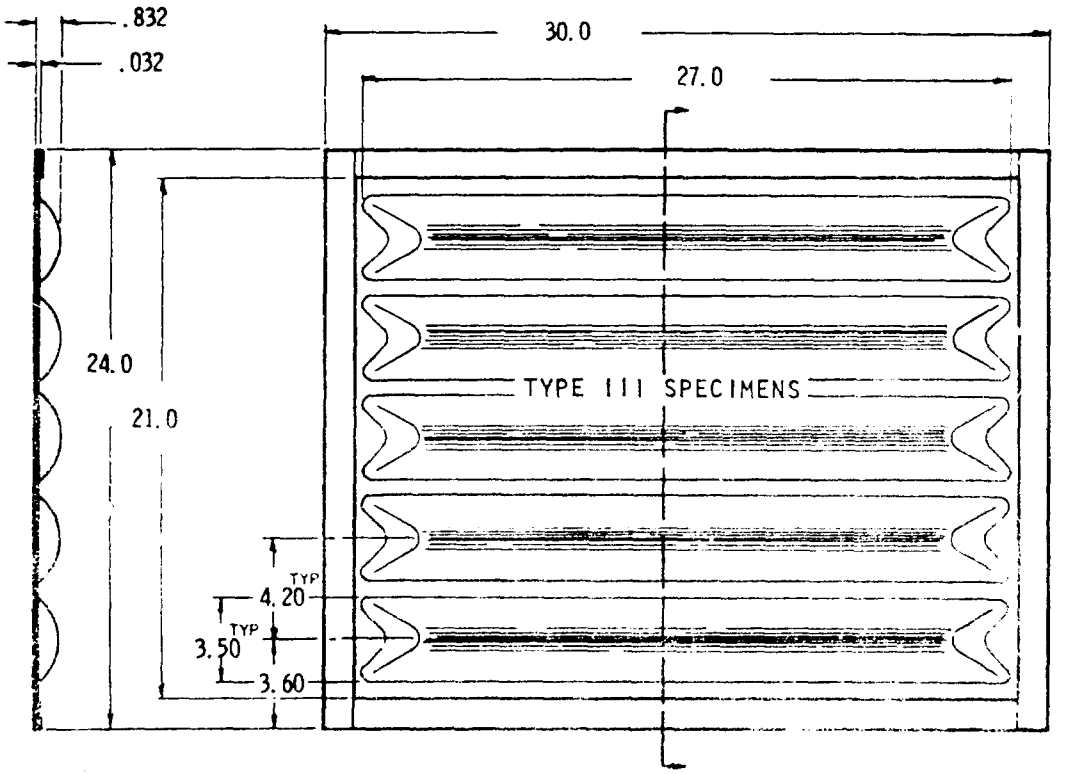

FIGURE 5.3.7-1 BONDED BEADED SPECIMEN DESIGNS (RE[illegible]) (CONTINUED)

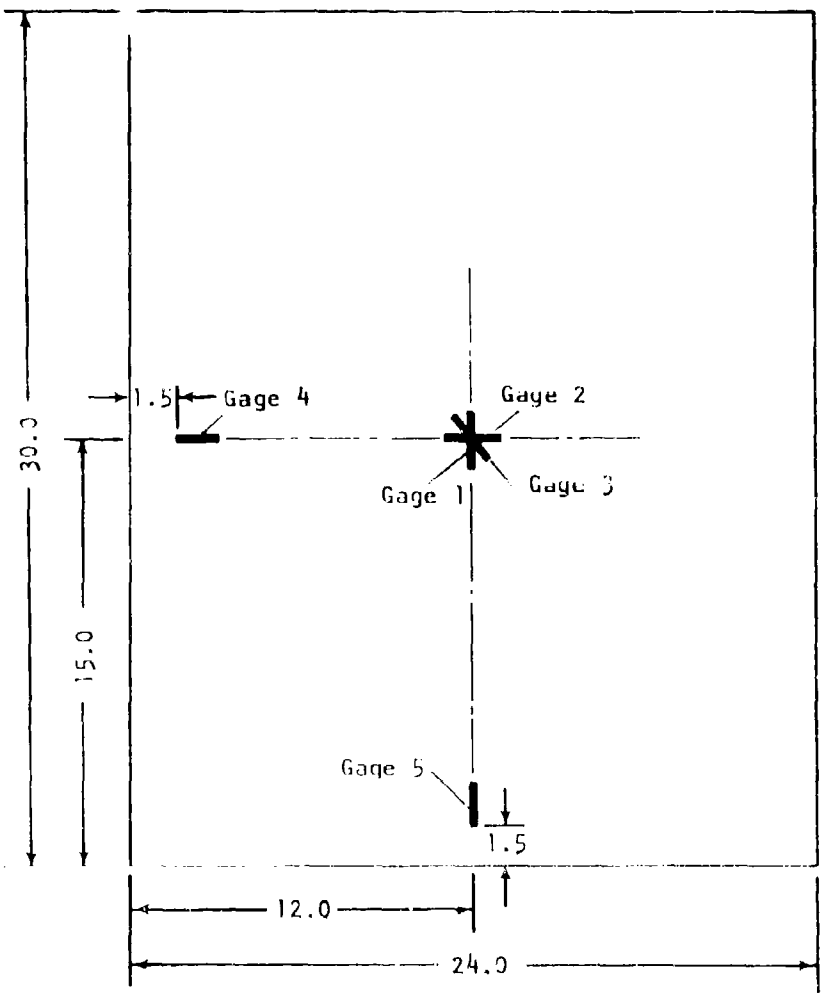

Skin Surface Strain Gage Locations

FIGURE 5.3.7-1 (CONCLUDED)

The strain gage locations for the sonic fatigue tests are also illustrated in Figure 5.3.7-1. The fundamental mode for such structure is similar to that for an isotropic panel with the node lines parallel and near the panel edges. The individual skin bay response between bead lines is the form of a fundamental mode for each bay (high aspect ratio panel) and occurs at a higher frequency than the structure fundamental mode. The sonic fatigue test data is summarized in Tables 5.3.7-1, -2, and -3 for the Type I, II, and III specimens, respectively. This data should be used for guidance when using the design criteria presented in the following section.

5.3.7.3 Design Criteria for Bonded Beaded Panels

As discussed above, McGowan's (1) design criteria yield representative stress estimates but predict fatigue life longer than that observed by van der Heyde and Kolb (2). McGowan's criteria, never the less, is the only technique presently available and is suggested for use if the designer takes the data presented in Section 5.3.7.2 for proper judgement.

McGowan's criteria is based upon a bead end design which presumably provides equal sonic fatigue resistance for the panel edge and bead end. This bead design and nomenclature are presented in Figure 5.3.7-2. The particular data for the specimens tested were as follows: bead thickness, 0.020 inch; bead width, 5.125 inches. The specimen material was 7075-T6 aluminum alloy.

The design nomograph developed by McGowan is used to obtain the bead geometry: h_b, L, and d for the desired fatigue life (Caution: consider the data in Section 5.3.7.2 before selecting fatigue life from this nomograph) and is presented in Figure 5.3.7-3. The bead length L, the bead width, W, and the panel edge thickness, h_e are also determined from Figure 5.3.7-3. Presumably, the skin thickness should equal the bead thickness $\pm$ one gage for an optimum design since McGowan's report is not explicitly clear on this point (See the data in Section 5.3.7.2). The difference between the edge thickness and the bead thickness is the required doubler thickness, h_d. The details of the bead end closure are presented in Figure 5.3.7-2.

For frequency estimates for bonded beaded structure, to check the assumed acoustic excitation spectrum level, Golden's (3) numerical technique seems to be the only reliable method; however, the designer may obtain guidance from van der Heyde and Kolb's test data (2).

REFERENCES FOR SECTION 5.3.7

1. McGowan, P. R.; "Structural Design for Acoustic Fatigue", ASD-TDR-63-820, Air Force Flight Dynamics Laboratory, Wright-Patterson Air Force Base, Ohio, 1963.

2. van der Heyde, R. C. W., and Kolb, A. W.; "Sonic Fatigue Resistance of Light Weight Aircraft Structure," Paper No. 20, AGARD-CP-113, Symposium on Acoustic Fatigue, Advisory Group for Aerospace Research and Development, North Atlantic Treaty Organization, Sept. 1972.

3. Golden, C. T.; "Analytical Method for Determining the Natural Frequencies and Mode Shapes of Orthotropic Plates," M. S. Thesis, Department of Aeronautical Engineering, University of Washington, November 1960.

TABLE 5.3.7-1 STRESS RESPONSE AND FATIGUE DATA FOR

BONDED-BEADED PANELS TYPE I (FIGURE 5.3.7-1)

BEAD LENGTH 21.0 IN, PANEL SKIN .032 IN,

BEAD SKIN .032 IN THICK

STRAIN-GAGE LOCATIONS GIVEN IN FIGURE 5.3.7-1

PANEL NR	SPECTRUM LEVEL	STRESS LOC.1 dB	STRESS LOC.2 PSI	MAXIMUM STRESS PSI	STRESS LOC.4 PSI	STRESS LOC.5 PSI	ZERO CROSSINGS SEC^{-1}	LIFE 10^6 CYCLES	FAILURE LOCATION
A-1	131.4	1482	1189	1657	1778		210	5.670	Bead Edge
B-1	130.5	1462	1353	1866	2661		196	5.292	Bead Edge
C-1	132.2	1412	1064	1660	1259		183	4.612	Bead Edge
D-1	128.0	1982	1384	2418	1155		148	3.730	Bead Edge
E-1	127.9	2178	972	2554	2052		156	3.931	Bead Edge
A-2	129.4	863	728	936	1540		177	9.500	Bead Edge/Edge
B-2	128.4	829	583	941	3003	891	200	18.360	Edge
C-2	130.1	923	669	977	1412		147	16.250	Edge
D-2	125.9	1116	395	1170	1496		168	10.030	Bead Edge/Edge
E-2	125.9	945	707	983	1454		155	10.040	Bead Edge/Edge
A-3	128.4	835	763	954	1496		185	19.810	Edge
B-3	128.6	728	637	812	1208	729	175	66.460	Edge
C-3	128.6	804	510	836	865		166	14.460	Edge
D-3	124.1	889	628	912	1188		150	19.440	Edge
E-3	125.4	859	827	950	2441		155	6.510	Bead Edge
A-4	125.4	794	546	898	1496		176	109.246	Edge
B-4	124.6	841	688	902	1295	917	198	125.	No Failure
C-4	125.6	688	386	746	1372		168	33.809	Edge
D-4	129.9				972		195	42.120	Edge
E-4	121.9	789	553	937	917		160	72.864	Edge

TABLE 5.3.7-2 STRESS RESPONSE AND FATIGUE DATA FOR

BONDED-BEADED PANELS TYPE II (FIGURE 5.3.7-1)

BEAD LENGTH 21.0 IN, PANEL SKIN .020 IN,

BEAD SKIN .045 IN THICK

STRAIN-GAGE LOCATIONS GIVEN IN FIGURE 5.3.7-1

PANEL NR	SPECTRUM LEVEL dB	STRESS LOC.1 PSI	STRESS LOC.2 PSI	MAXIMUM STRESS PSI	STRESS LOC.4 PSI	STRESS LOC.5 PSI	ZERO CROSSINGS SEC^{-1}	LIFE 10^6 CYCLES	FAILURE LOCATION
A-1	131.4	1748	889	2268	1090		213	3.067	Panel Skin
B-1	130.2	1423	760	1771	1372		246	1.771	Panel Skin
C-1	132.4	1603	799	1769	1250		212	2.671	Panel Skin
D-1	128.3	1546	792	1754			233	3.355	Panel Skin
E-1	128.8	1413	963	1614	1059		187	2.693	Panel Skin
A-2	129.4	1243	567	1578	917		259	22.610	Panel Skin
B-2	128.9	1120	655	1322	1258		310	21.204	Panel Skin
C-2	130.1	1190	578	1302	1000		256	17,510	Panel Skin
D-2	126.9	1410	687	1583	613		193	13.201	Panel Skin
E-2	127.9	1040	702	1208	771		265	18.126	Panel Skin
A-3	128.1	1090	692	1291	1259	1122	211	12.154	Edge/Bead Edge
B-3	128.9	1040	641	1331	944	944	258	18.576	Panel Skin
C-3	129.4	1010	649	1248	335	613	210	34.020	Edge
D-3	126.0	1075	576	1238		410	247	64.467	Edge
E-3	127.9	926	673	1194	866	570	315	40.824	Panel Skin
A-4	126.4	895	440	1241	817		121	119.975	Edge
B-4	125.1	841	533	994	794		221	140.	No Failure
C-4	125.9	882	438	1003	398		199	108.355	Bead Edge
D-4	129.9	894	531	1033	771		216	140.	No Failure
E-4	124.9	796	513	904	562		194	116.679	Edge

TABLE 5.3.7-3 STRESS RESPONSE AND FATIGUE DATA FOR

BONDED-BEADED PANELS TYPE III (FIGURE 5.3.7-1)

BEAD LENGTH 27.0 IN, PANEL SKIN .032 IN,

BEAD SKIN .032 IN THICK

STRAIN-GAGE LOCATIONS GIVEN IN FIGURE 5.3.7-1

PANEL NR	SPECTRUM LEVEL dB	STRESS LOC.1 PSI	STRESS LOC.2 PSI	MAXIMUM STRESS PSI	STRESS LOC.4 PSI	STRESS LOC.5 PSI	ZERO CROSSINGS SEC^{-1}	LIFE 10^6 CYCLES	FAILURE LOCATION
A-1	135.6	2289	2318	4167		4467	133	.954	Bead Edge
B-1	132.4	2372	1603	3806		4340	344	1.193	Bead Edge
C-1	136.9	2454	1973	4164		1995	229	1.076	Bead Edge
D-1	133.4	1929	2511	4201		3072	182	.642	Bead Edge
E-1	N/A	2919	2289	4864		N/A	N/A	N/A	Bead Edge
A-2	128.1	2985	1778	4386		3350	336	3.024	Bead Edge
B-2	129.6	2511	1188	3298		3652	307	1.382	Bead Edge
C-2	128.9	2441	1334	3330		2371	330	8.118	Bead Edge
D-2	128.1	2371	1778	3840		3072	341	1.637	Bead Edge
E-2	125.6	2239	1679	3517		3548	434	4.088	Bead Edge
A-3	122.9	1939	1180	3087		3073	234	5.476	Bead Edge
B-3	125.4	1508	686	2203		1333	340	110.	No Failure
C-3	124.4	1372	1290	2502		2175	253	34.064	Edge/Bead Edge
D-3	124.1	1350	1259	2059		1778	253	45.540	Edge/Bead Edge
E-3	122.1	1708	1429	3177		1778	265	34.344	Edge
A-4	124.6	1334	1000	2039		1454	143	5.663	Edge
B-4	126.9	708	178	1213	972	596	163	34.328	Edge
C-4	124.9	772	631	1294		771	160	112.704	Edge
D-4	123.6	1000	818	1876		841	130	58.500	Bonding Failure
E-4	121.9	1841	501	1432		1155	250	76.875	Edge

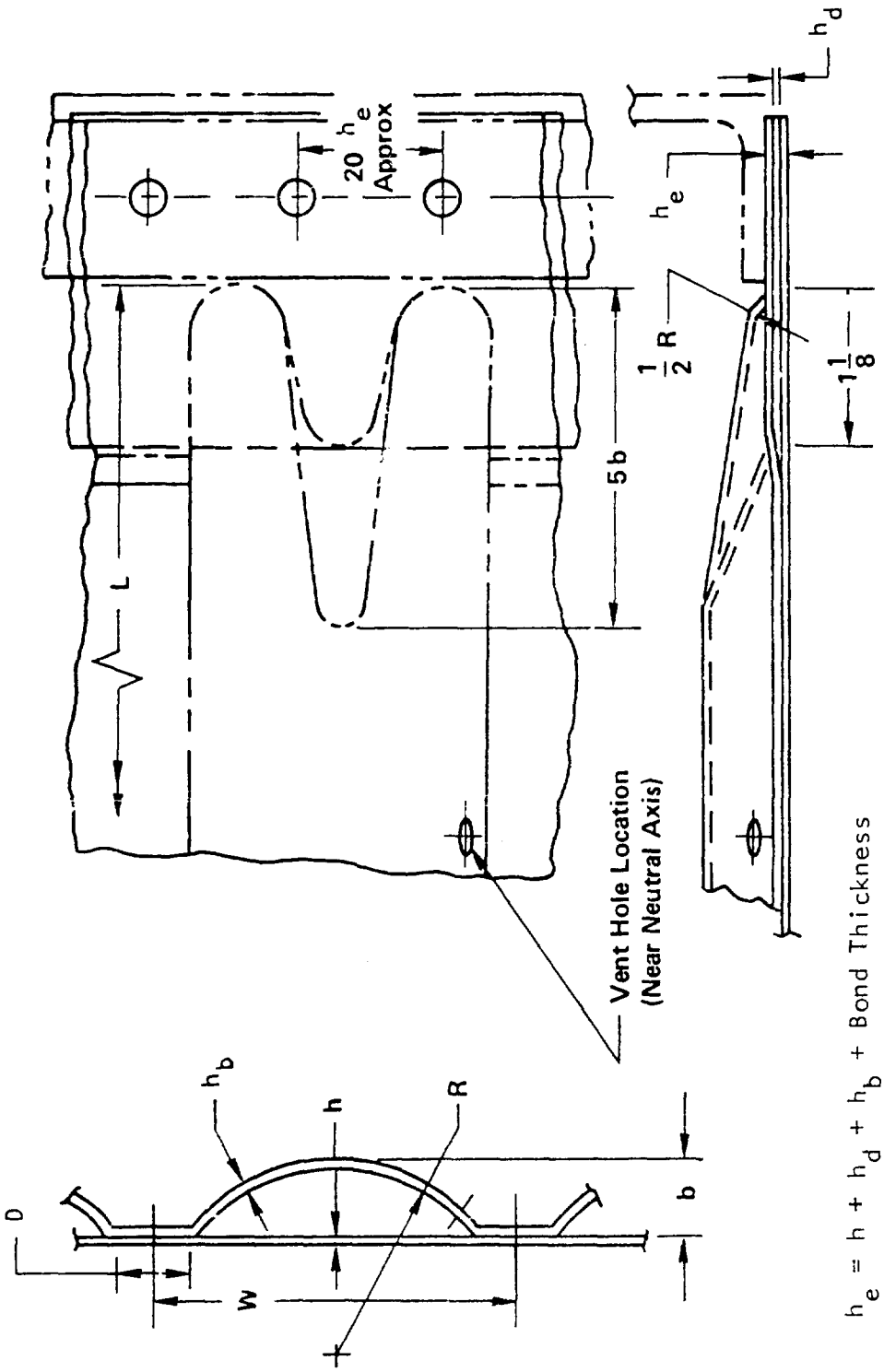

FIGURE 5.3.7-2 BEAD NOMENCLATURE FOR BONDED BEADED PANEL (REF. 1)

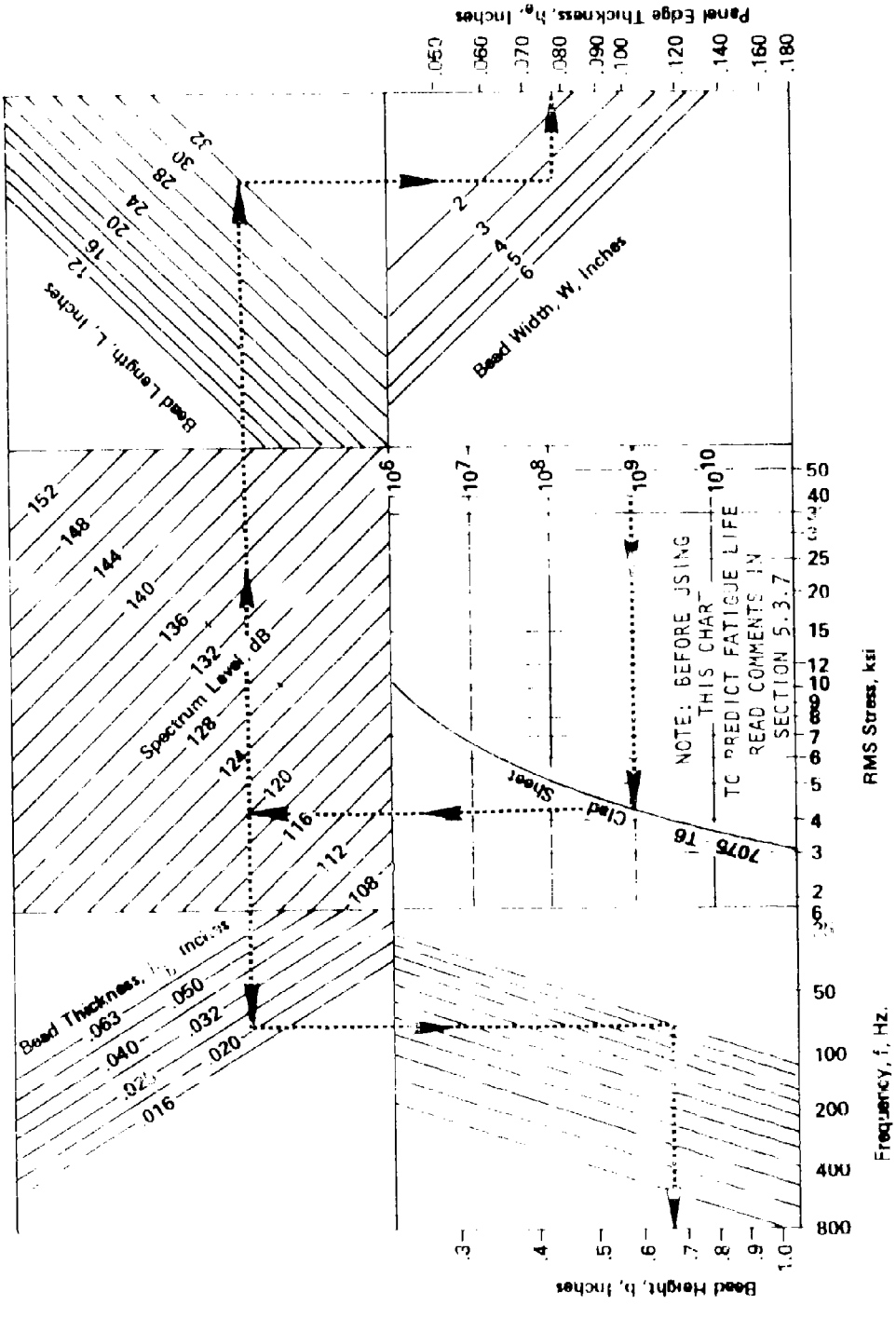

FIGURE 5.3.7-3 NOMOGRAPH FOR BONDED BEADED PANEL SKIN AND BEAD THICKNESS (REF. 1)

5.3.8 ANISOTROPIC P NELS

Anisotropic panels are a separate class of structures that has become important in aircraft design since the introduction of composite materials for aircraft construction in the mid 1960's. The general analysis of anisotropic plates is presented by Ambartsumyan (1) for both static and dynamic response. To obtain numerical results extensive calculations are required for the case of general anisotropy. Fortunately, a practical structure is manufactured in such a way that the plate material can be considered to be orthotropic so that the material elastic properties possess three mutually orthogonal principal axes. If the plate material is homogeneous, the plate is considered to be specially orthotropic and the methods of Section 5.2.2.3 may apply.

For aircraft constructions, the designer is often faced with the consideration of laminated plates with the lamina being orthotropic and possessing different material characteristics, material axis orientation, or thickness. The general analysis of laminated plates is presented by Ashton and Whitney (2). As is the case with general anisotropic plates, to obtain numerical results extensive calculations are required; however, for particular lamina configurations simplified design results are possible.

5.3.8.1 Laminated Plates

The theory of laminated plates is simplified by considering the material properties of the lamina (2). By considering the material properties, the coupling between the membrane strains and the panel curvatures is zero if the lamina are symmetric with respect to the plate midplane. This symmetry requires that both the lamina material axis orientation and the thickness be identical for laminae above and below the plate midplane. Such structure is termed a midplane symmetric laminated plate.

Since the governing equations for laminated plates are too complicated to obtain analytical solutions, approximate techniques are utilized (in particular, energy methods) to obtain numerical results. For midplane symmetric rectangular laminated plates subjected to inplane and transverse loading, the theorem of stationary potential energy has the form

$$\frac{1}{2}\int_o^a\int_o^b \left[D_{11}w_{,xx}^2 + 2D_{12}w_{,xx}w_{,yy} + D_{22}w_{,yy}^2 + 4D_{66}w_{,xy}^2 + 4D_{16}w_{,xx}w_{,xy} + 4D_{26}w_{,yy}w_{,xy} + N_x w_{,x}^2 + N_y w_{,y}^2 + 2N_{xy}w_{,x}w_{,y} - 2qw\right] dydx = \text{stationary value} \qquad (5.3.8\text{-}1)$$

where w is the transverse displacement; N_x, N_y, and N_{xy} are the inplane edge loads (see Figure 5.2.2-11) and q is the transverse loading. The bending rigidities, D_{ij}, are defined in terms of the elastic characteristics of the lamina, Q_{ij}^k, and the thickness of the laminae, h_k, as follows

$$D_{ij} = \frac{1}{3}\sum_{k=1}^{n} Q_{ij}^{k}[h_k^3 - h_{k-1}^3] \qquad (5.3.8\text{-}2)$$

where the summation is over the number of lamina. The distance, h_k, is measured from the plate midplane.

The elastic constants, Q_{ij}^{k}, depend upon the lamina material and the orientation of the lamina principal elastic axes (x^*, y^*) with respect to the geometric (x,y) axis system of the plate. The relationship between the stresses in the k^{th} layer and the panel strains are

$$\begin{bmatrix} \sigma_x^k \\ \sigma_y^k \\ \sigma_{xy}^k \end{bmatrix} = \begin{bmatrix} Q_{11}^k & Q_{12}^k & Q_{16}^k \\ Q_{12}^k & Q_{22}^k & Q_{26}^k \\ Q_{16}^k & Q_{26}^k & Q_{66}^k \end{bmatrix} \begin{bmatrix} \varepsilon_x \\ \varepsilon_y \\ \varepsilon_{xy} \end{bmatrix} \qquad (5.3.8\text{-}3)$$

with the bending strains given by the relationships:

$$\varepsilon_x = -zw_{,xx}; \quad \varepsilon_y = -zw_{,yy} \quad \varepsilon_{xy} = -2w_{,xy} \qquad (5.3.8\text{-}4)$$

The generalized Hooke's law for the lamina material is

$$\{\sigma_i\} = [c_{ij}]\{\varepsilon_j\} \qquad (5.3.8\text{-}5)$$

with the elastic constants, c_{ij}, in terms of the lamina material axis orientation given by

$$c_{11} = c_{11}^* m^4 + 2m^2n^2(c_{16}^* + 2c_{66}^*) + 4mn(c_{16}^* m^2 + c_{26}^* n^2) + c_{22}^* n^4$$

$$c_{12} = m^2n^2(c_{11}^* + c_{22}^* - 4c_{66}^*) - 2mn(c_{16}^* - c_{26}^*)(m^2 - n^2) + c_{12}^*(m^4 + n^4)$$

$$c_{13} = c_{13}^* m^2 + c_{23}^* n^2 + 2c_{36}^* mn$$

$$c_{16} = c_{16}^* m^2(m^2 - 3n^2) - mn[c_{11}^* m^2 - c_{22}^* n^2 - (c_{12}^* + 2c_{66}^*)(m^2 - n^2)] + c_{26}^* n^2(3m^2 - n^2)$$

$$c_{22} = c_{11}^* n^4 + 2m^2n^2(c_{12}^* + 2c_{66}^*) - 4mn(c_{26}^* m^2 + c_{16}^* n^2) + c_{22}^* m^4$$

$$c_{23} = c_{23}^* m^2 + c_{13}^* n^2 - 2c_{36}^* mn$$

$$c_{26} = c_{26}^* m^2(m^2 - 3n^2) - mn[c_{11}^* n^2 - c_{22}^* m^2 + (c_{12}^* + 2c_{66}^*)(m^2 - n^2)]$$
$$+ c_{16}^* n^2(3m^2 - n^2)$$

$$c_{33} = c_{33}^*$$

$$c_{36} = c_{36}^*(m^2 - n^2) + mn(c_{23}^* - c_{13}^*)$$

$$c_{66} = (c_{11}^* + c_{22}^* - 2c_{12}^*)m^2n^2 + 2(c_{26}^* - c_{16}^*)(m^2 - n^2)mn$$
$$+ c_{66}^*(m^2 - n^2)^2$$

The plate and material axis geometry is illustrated in Figure 5.3.8-1 and $m = \cos\theta$, $n = \sin\theta$. The elastic constants, c_{ij}^*, of a unidirectional fiber reinforced composite can be estimated as a function of the constituent material properties and the volume constant of the reinforcement (3).

The reduced stiffness terms, Q_{ij}^k, are related to the elastic constants, c_{ij}^k, for the k^{th} lamina as follows

$$Q_{ij}^k = c_{ij}^k - c_{i3}^k c_{j3}^k / c_{33}^k \qquad (5.3.8\text{-}5)$$

Equations (5.3.8-2) through (5.3.8-5) are the mathematical expression of the "stacking sequence" of laminated plates.

To obtain estimates of the natural frequencies of laminated plates, one substitutes $-\omega^2 \rho h w^2$ for $-2qw$ in Equation (5.3.8-1). The problem of obtaining design oriented results from the above analysis is that one must approximate solutions for the transverse displacement, $w(x,y)$, usually by assuming a series type solution (see Equation (5.2.2-27)). The form of the governing equation (Equation 5.3.8-1) is such that the bending-twist coupling terms, D_{16} and D_{26}, result in a set of coupled equations that require numerical solution rather than a simple uncoupled mode analysis. Rather than being a result of analysis, numerical studies have indicated that neglect of these terms result in high frequency estimates and low displacement response estimates (2). Neglecting the bending-twist couping terms (i.e., $D_{16} = D_{26} = 0$), results in the case of specially orthotropic plates discussed in Section 5.2.2.3.

Wolf and Jacobson (4) present a summary of two research programs concerned with the design and acoustic testing of composite material components. For the analytical approach, they used a simplified theory assuming that the plate specimens were specially orthotropic ($D_{16} = D_{26} = 0$) and they also used a

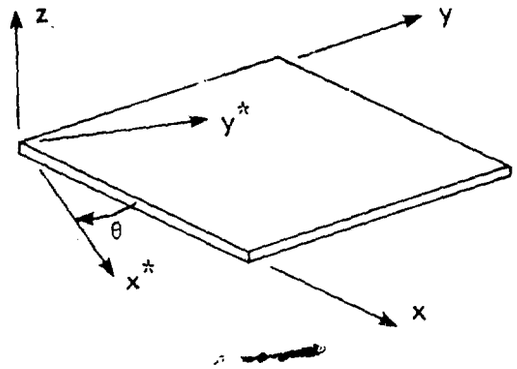

(a) Material Axis Orientation within Lamina

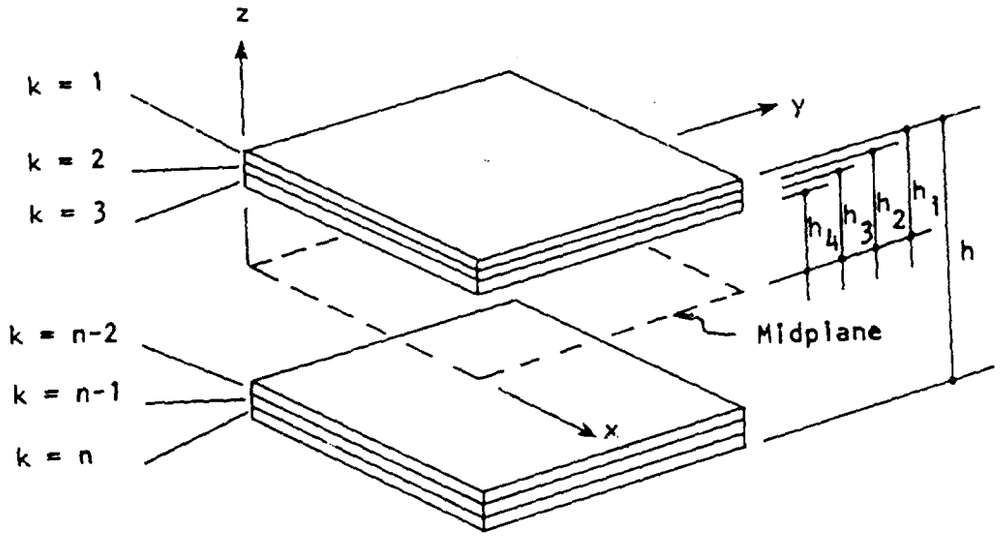

(b) Lamina Coordinates within a Laminate

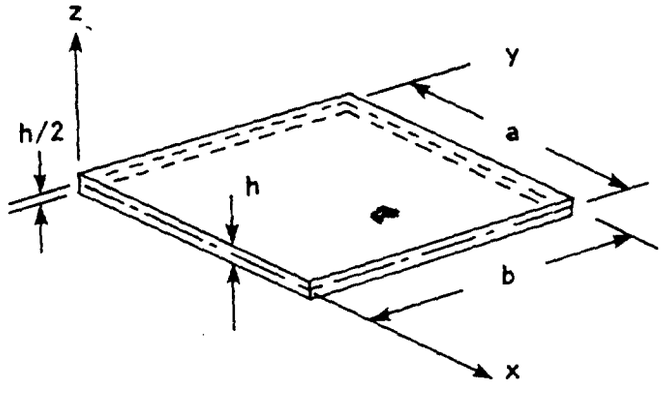

(c) Laminated Plate Geometry

FIGURE 5.3.8-1 LAMINATED PLATE GEOMETRY WITH LAMINA GEOMETRY AND NOMENCLATURE

finite element method to obtain estimates of the plate and stiffener interaction. They describe sonic fatigue test results on simple 8-ply boron-epoxy and 6-ply nine bay cross-stiffened graphite-epoxy panels. Also, the results of fatigue failure data using shaker excitation of 72 beam specimens to develop S-N data for simulated joint configurations are described. The beams consisted of a graphite-epoxy or boron-epoxy material bonded or riveted to a graphite-epoxy or titanium alloy stiffeners.

For the simple plate analysis, the results of Section 5.2.2.3 apply with the bending rigidities D_1, D_2, and D_3 being related to the laminated plate bending rigidities given above as follows:

Section 5.2.2.3	Laminated Plate
D_1	D_{11}
D_2	D_{22}
D_3	$D_{12} + 2D_{66}$

For the simple rectangular plate specimens, the failure mode of these panels typically appeared as a crack in the outer ply immediately adjacent and parallel to the clamped boundary. Generally, the failure would progress through the remaining plys and, if undetected, often resulted in the complete disintegration of a small concentrated area near the plate boundary. This failure was sometimes accompanied by severe delamination of the outer ply.

The simple test specimen panel design were as follows:

Total thickness	0.040 inch
Overall nominal dimensions	12.0 inches × 14.0 inches
Test overall dimensions*	9.0 inches × 11.0 inches

The laminated plates comprised 8 plys of orthotropic boron-epoxy material in a 0° - 90° layup symmetric about the midplane. The outer plys had a fiber orientation of 0°. The matrix material was Narmco 5505 and the boron content was 50% by volume.

The panel damping, determined using the logarithmic decrement method, varied from 0.003 to 0.004 for panels tested in the free-free condition and for panels mounted in the test fixture the damping was typically 0.028.

A comparison between 0.050 inch thick aluminum alloy panels (assumed $K_t = 2.0$) and the boron-epoxy composite panel endurance tests are presented in Figure 5.3.8-2 in terms of sound pressure level versus life in cycles.

The beam specimen shaker tests were conducted to establish S-N data for various material configurations and to establish that such data could be

---

*due to edge mounting in a picture frame test fixture

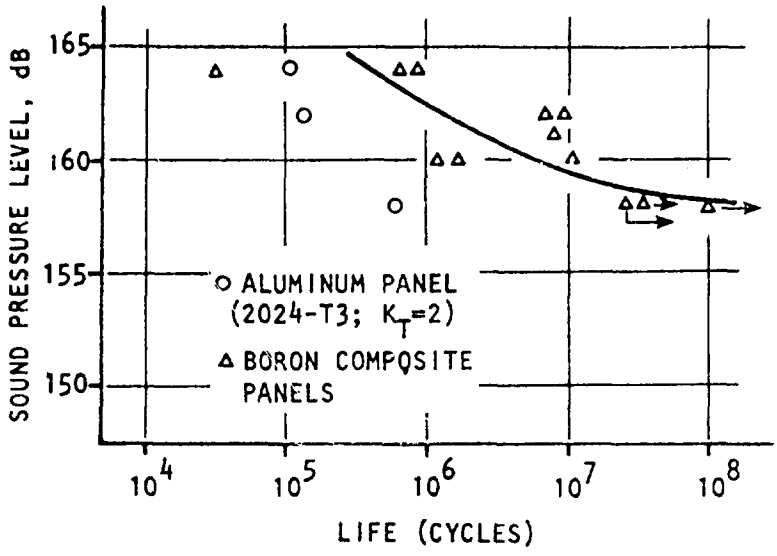

FIGURE 5.3.8-2 BORON-EPOXY AND ALUMINUM PANEL FATIGUE DATA

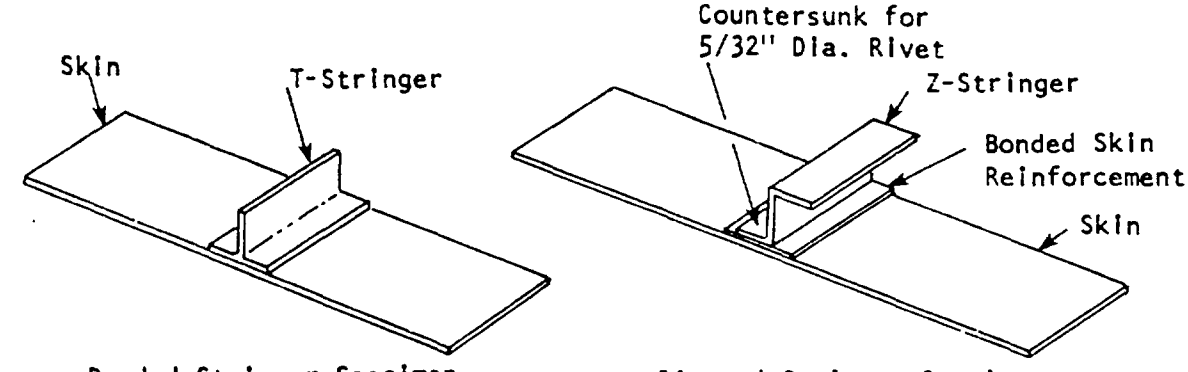

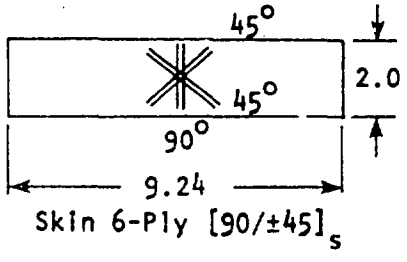

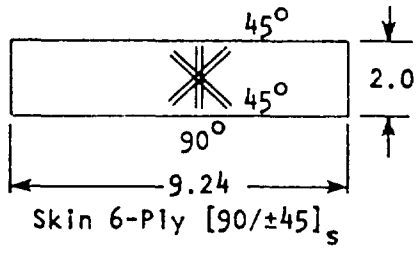

Material	
Skin	Stringer
Graphite-Epoxy	Graphite-Epoxy
Graphite-Epoxy	Titanium Alloy
Boron-Epoxy	Titanium Alloy

Material	
Skin	Stringer
Graphite-Epoxy	Graphite-Epoxy
Graphite-Epoxy	Titanium Alloy
Boron-Epoxy	Titanium Alloy

FIGURE 5.3.8-3 BEAM SPECIMENS FOR SHAKER TESTS

applied to the design of joints of fiber reinforced composite panels in acoustic environments without resorting to sonic tests of complex panel specimens. By carefully designing the beam specimens, Wolf and Jacobson concluded that considerable sonic fatigue design information can be obtained by conducting shaker tests to supplement data generated by sonic fatigue testing of complex panel specimens. The beam test specimen details are presented in Figure 5.3.8-3.

The fatigue failure of all beam specimens initiated in the skin. For the bonded specimens the failure location was at the ends of the bonded joint connecting the skins to the T-section simulated stiffener (see Figure 5.3.8-3). For the riveted specimens, the failure location was at the end of the bond attachment connecting the skin to the back up detail that had been bonded to the skin prior to the riveting.

The S-N curves obtained from the shaker tests of the beam specimens is presented in Figure 5.3.8-4. The original report presents the failure data points. Although enough specimens were not available to establish confidence limits for the shaker S-N data, Wolf and Jacobson (4) concluded that apparently the rms fatigue strain at 10^8 cycles under narrow band random loading of the six-ply $(90/\pm45)_S$ graphite-epoxy and boron-epoxy laminates is at least ten percent of the static, ultimate tensile strain of the six-ply laminates.

Wolf's and Jacobson's test program also included sonic fatigue testing of three nine-bay test panels using six-ply $(0/\pm45)_S$ graphite-epoxy skin and six-ply $(\pm45/0)_S$ graphite-epoxy I-beams and T section stiffeners. Although no failure data was obtained from these tests (the panels exceeded 100 hours of exposure to broad-band high intensity noise with an overall sound pressure level of 166 dB), comparison of the panel response data to the various analytical methods indicates that assuming specially orthotropic analysis and using a single mode approximation as indicated in Section 5.2.2.3 is as accurate as that obtained using finite element methods.

Complete description of the test specimens, test procedure, etc. can be obtained from the paper by Wolf and Jacobson (4). This paper summarizes the results of the combined work of Rupert (5) and Jacobson (6). Jacobson also presents results of sonic fatigue tests of glass fiber reinforced panels in Reference (7).

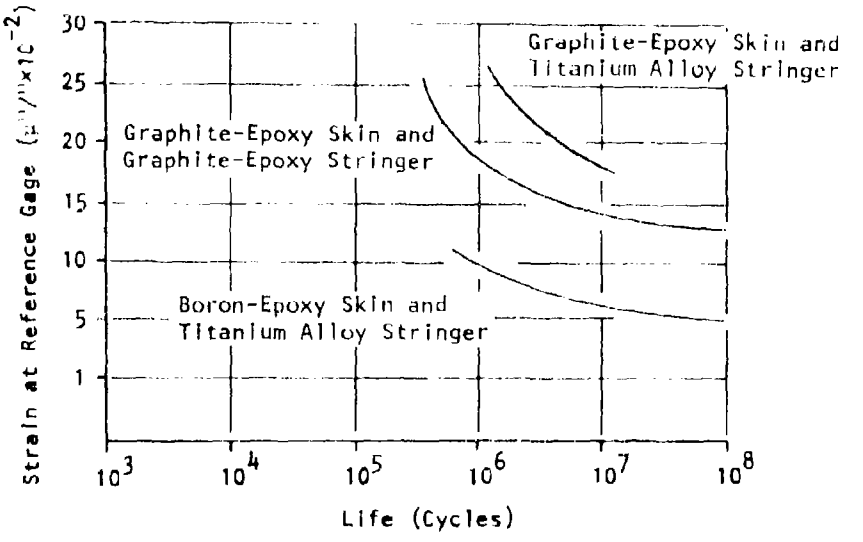

(a) Riveted Beam Shaker Specimens

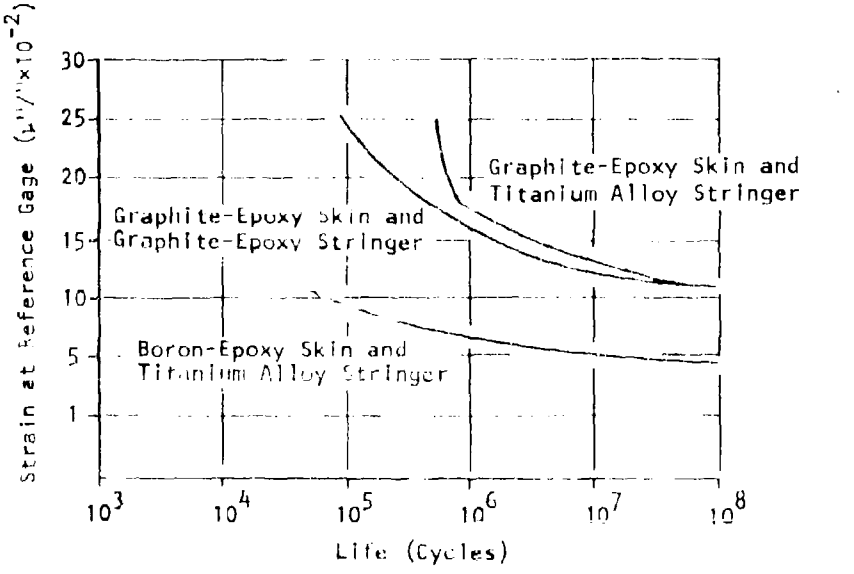

(b) Bonded Beam Shaker Specimens

FIGURE 5.3.8-4 SUMMARY OF SHAKER S-N DATA

REFERENCES FOR SECTION 5.3.8

1. Ambartsumyan, S. A.; Theory of Anisotropic Plates, Progress in Materials Science Series....Volume II, Technomic Publishing Co., Stamford, Conn., 1970.

2. Ashton, J. E., and Whitney, J. M.; Theory of Laminated Plates, Progress in Material Sciences Series.... Volume IV, Technomic Publishing Co., Stamford, Conn., 1970.

3. Ashton, J. E., Halpin, J. C., and Petit, P. H.; Primer on Composite Materials: Analysis, Progress in Material Sciences Series.... Volume III, Technomic Publishing Company, Stamford, Conn., 1969.

4. Wolf, N. D., and Jacobson, M. J.; "Design and Sonic Fatigue Characteristics of Composite Material Components," Paper No. 13, AGARD-CP-113, Advisory Group for Aerospace Research and Development, North Atlantic Treaty Organization, [illegible]., 1972.

5. Rupert, C. L.; "Sonic Fatigue and Response Tests of Boron Composite Panels," Test Report AFFDL/FYA-72-2, Air Force Flight Dynamics Laboratory, Wright Patterson Air Force Base, Ohio, 1972.

6. Jacobson, M. J.; "Advanced Composite Joints; Design and Acoustic Fatigue Characteristics," AFFDL-TR-71-126, Air Force Flight Dynamics Laboratory, Wright-Patterson Air Force Base, Ohio, 1972.

7. Jacobson, M. J.; "Acoustic Fatigue Design Information for Fiber Reinforced Structures," AFFDL-TR-68-107, Air Force Flight Dynamics Laboratory, Wright-Patterson Air Force Base, Ohio, 1968.

5.4 METHODS OF JOINING STRUCTURE

5.4.1 GENERAL CONSIDERATIONS

The application of good design practice to resist fatigue failure of structure is equally important for structure exposed to an acoustic environment. Due to the relatively high response frequencies of aircraft panels and structural components exposed to acoustic excitation and the long life requirements of these components, the designer must continuously design structure for over 10^8 cycles of applied stress. Hence, the designer must consider low applied stresses (typically less than 10 ksi rms) to achieve the desired life. This goal of long fatigue life forces the designer to consider the interaction effects of structural geometry, attachment details, material properties, testing techniques, and manufacturing processes. Hence, design experience is extremely important.

This section considers general design guidelines that relate to specific methods for joining structure. The following section discusses stress concentration factors. The topic of material properties and configuration effects as related to the fatigue characteristics of materials and joints is presented in Section 6. The interrelation of the various factors influencing fatigue life of structural assemblies is all important. The designer should consult the text books by Osgood (1) and Heywood (2) or the SAE handbook (3) for complete discussions of all aspects of fatigue design and presentations of much practical design information. The work of Harris (4) should be consulted for a discussion of the effect of standard aircraft fabrication and finishing processes upon the expected fatigue performance of structure. Finally, the designer should know the established design methods and available test data documented by his own company since much relevant information is not available in the open literature.

As indicated in Figure 5.3.2-9, the basic design concepts of symmetry, continuity, and proportion are important considerations for sonic fatigue design irrespective of the method used to join the structural components. The designer should give special attention to careful boundary design and avoid abrupt changes in stiffness. Indeed, for structural configurations and material for which sonic fatigue data exists (Section 5.3), the consideration of design details such as cutouts, clips, and various methods for joining structure are presently the most important considerations for designing sonic fatigue resistant structures.

5.4.2 MECHANICAL FASTENERS

This section contains the detail design guidelines for structural members attached using mechanical fasteners. The section is subdivided into riveted joints, bolted joints, and consideration of miscellaneous fasteners.

5.4.2.1 Riveted Joints

Undoubtedly, riveted structural connections are the most common method of joining used in aircraft construction. The designer should always aim at

providing equal strength for the rivet and the sheet material being joined. This is realized by proper spacing or pitch of the rivets in relation to the rivet diameter and material thickness. Generally, the minimum rivet pitch should never be less than three rivet diameters and should never exceed 16 to 20 times the total thickness of the material being joined. The rivet diameter should be approximately two times the thickness of the material being joined and the rivet line should never be less than three rivet diameters from the edge of a member. The recommended design practice of each company may vary from these guidelines so that the designer must always consult the appropriate design standards.

For additional guidance in determining the spacing of rivets and mechanical fasteners the designer should refer to Figure 5.3.2-10. Also, the early work of Crate (5) in establishing an optimum ratio of rivet pitch to rivet diameter is presented in Figure 5.4.1-1. This figure presents the results of a series of constant amplitude sinusoidal fatigue tests of flanged riveted joints. The curve represents an optimized value of the ratio of the alternating load per rivet for a given number of cycles to failure to the static ultimate strength per rivet. This optimum ratio was found to be essentially independent of the number of cycles to failure. This reference also presents 20 sinusoidal fatigue curves (alternating rivet load versus cycles to failure). A typical curve is presented in Figure 5.4.1-2. The material used in the tests was 24S-T (2024 heat treatable) aluminum alloy using A17S-T (2017 heat treatable) aluminum alloy rivets. The reference should be consulted for specific details as well as the data summarized by Osgood (1), Heywood (2), and Harris (4).

It is recommended that the curve presented in Figure 5.4.1-1 be considered as a minimum allowable distance between rivets and used in conjunction with Figure 5.3.2-9 to establish rivet spacing. The designer can gain additional guidance by referring to Section 8 of MIL-HDBK-5B (6) for static strength design criteria of joints for various materials and fastener combinations.

Aircraft quality blind rivets generally exhibit both static strength and fatigue characteristics similar to conventional rivets. Protruding head rivets should be used whenever possible instead of countersunk rivets. Cut countersunk riveting exhibits improved fatigue characteristics as compared to dimpled countersunk riveting. The sonic fatigue strength of a riveted joint is generally improved by using viscoelastic joining compounds, standard adhesives, and sealants between the faying surfaces. This advantage is gained at the expense of a joint that cannot be easily disassembled for repairs.

The static performance of swaged collar fasteners as compared to riveted joints is presented in Section 8 of MIL-HDBK-5B (6). These fasteners are usually required in high strength joints and as such are generally not susceptible to sonic fatigue failures (See Figure 5.3.2-9).

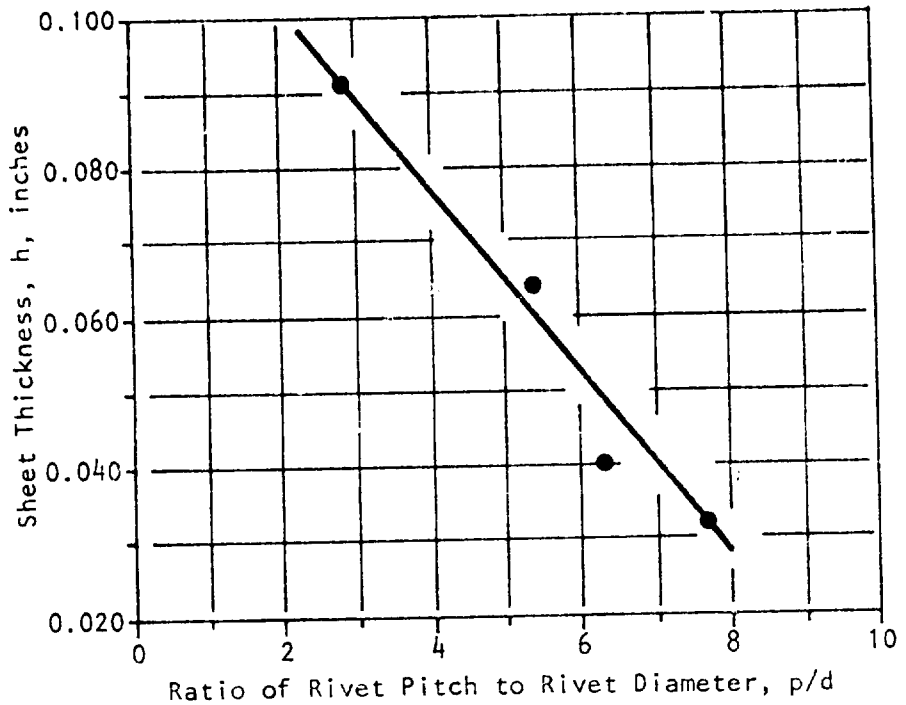

FIGURE 5.4.1-1 OPTIMUM RATIO, p/d, VERSUS SHEET THICKNESS, h, (REF.(5))

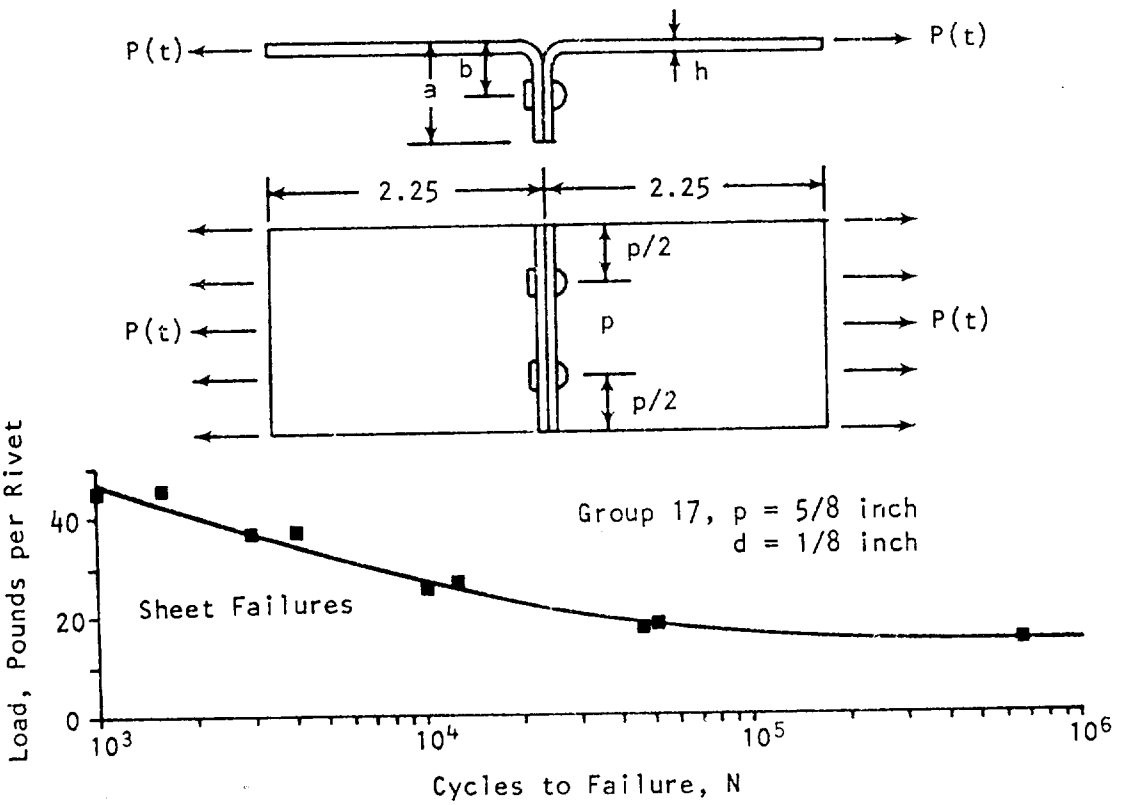

FIGURE 5.4.1-2 TYPICAL JOINT FAILURE FATIGUE CURVE (REF.(5))

5.4.2.2 Threaded Fa teners

This classification of fastener includes bolts, screws, and a wide assortment of special purpose fasteners that allow for disassembly of the components without damage to either the fastener or the components. The spacing of these fasteners generally follows the guidelines presented in Section 5.4.2.1 for riveted joints. MIL-HDBK-5B (6), Section 8, presents static strength criteria for joints fastened by threaded fasteners. This criteria should be applied to the structure with the designer taking advantage of the strength of the fastener (See Figure 5.3.2-9).

5.4.2.3 Miscellaneous Fasteners

The use of quick disconnect fasteners for attaching inspection panels to primary structure represents a potential sonic fatigue design problem. Such devices are not recommended for surface areas of an aircraft that are exposed to acoustic excitation above an overall sound pressure level of 110 dB. If such fasteners are required the designer should contemplate sonic fatigue proof testing of these components prior to accepting the design. The doubt about using such fasteners arises from the fact that they are really small structural assemblies that must be attached to the panel or substructure and, hence, defy any attempt at analysis.

5.4.3 METALLURGICAL AND ADHESIVE JOINTS

This section contains design guidelines for detail consideration of members joined by welding or brazing. The joint should be analyzed on the basis of allowable static strength, dimensions, and geometry. The allowable strength of both the adjacent parent metal and the weld metal or adhesive must be considered. Brazing, welding, and weldbonding processes are briefly discussed.

5.4.3.1 Brazed Joints

Brazing consists of joining metals by the application of heat causing the flow of a thin layer of nonferrous filler metal into the space between pieces. Bonding results from the intimate contact produced by the dissolution of a small amount of base metal in the molten filler metal without fusion of the base metal.

A comparison of welded and brazed joints for aluminum - 1½% manganese alloy (L.59) is presented by Harris (4), pages 305 to 311. The fact that brazing and welding locally cause metallurgical changes in the parent material and require special manufacturing sequences to regain the material strength has resulted in designers avoiding such fabrication techniques unless specific test data is available for the structural configuration and combination of materials being considered. Proof testing of brazed and welded structure should be seriously considered prior to acceptance of such a design if high level acoustic service environment is expected.

5.4.3.2 Welded Joints

5.4.3.2.1 Butt and Lap Welds

Superficially, consideration of welded joints as a fabrication technique for structure exposed to high level acoustic excitation should involve only the consideration of the fatigue properties of the welded joint and the application of these properties to design. However, the designer must consider the complications that arise that are peculiar to welded joints. First, the weld is essentially a cast metal with mechanical properties which may be entirely different from the parent metals being joined. Secondly, the welded components would contain geometric stress concentration characteristics due to the irregularity of the weld area and attempts to remedy this situation (i.e., machining) may not be completely successful in recovering any loss in fatigue strength. Finally, the metallurgical effects produced locally in the joint by the particular welding process may degrade the fatigue strength of the joint. Harris (3) concluded that based upon the tensile fatigue strength per inch of weld (a practical design criterion) of L.59 aluminum alloy butt welds exhibited superior fatigue strength characteristics compared to lap welds. Reversed bending fatigue tests of L.59 aluminum alloy also exhibited this tendency. Osgood (1) presents a very thorough discussion of fatigue design considerations of welded joints and a brief summary of available fatigue test data. Section 8 of MIL-HDBK-5B (6) presents static design criteria for welded joints of typical aircraft material.

5.4.3.2.2 Spot Welds

Spot welding is the most common welding process encountered in the fabrication of aircraft structural components. The ratio of the thickest sheet to the thinnest sheet in the joint should not exceed 4. Based upon static strength, the tabulated data in Section 8 of MIL-HDBK-5B (6) will provide design guidance for determining the minimum edge distances and spacing of spot welded joints. Fatigue data presented in Reference 6 indicate that for 7075-T6 and 2024-T3 aluminum alloys the endurance fatigue strength of spot welded lap joints is approximately 4% to 8% of the ultimate tensile strength of the sheet for sheet failures and approximately 10% to 20% of the static strength of the joint for shear failure of the spot weld. These results are based upon joints subjected to alternating load ratios of only 5% and, hence, do not apply for highly stressed joints. Osgood (1) presents fatigue test data and design guidelines for aluminum, titanium, and steel alloys that can be used as typical results if the designer does not have specific fatigue data available.

The designer should avoid using spot welded joints in truss structure, joints between stringers and ribs (unless a stop rivet is used), and as the last fastener at the end of a sheet-stringer joint. Spot welds should not be used as the only fastening method if tension loading of the joint is anticipated. Generally, the designer should avoid using spot welded construction in acoustic environments exceeding 165 dB overall

sound pressure level or contemplate acoustic fatigue proof testing of the design.

5.4.3.3 Bonded Joints

For bonded joints the fatigue strength due to acoustic loading is determined by the peel stresses at the edges of the joint. The peel stresses which act normal to the adhesive layer are introduced by the bending moment and are also a function of the relative stiffnesses of the two joining components.

The most prevalent application in aircraft construction is the joining of metal stiffeners to thin metal panels. Recently conducted random amplitude beam bending fatigue tests indicate that thinner beams (0.32" thick) bonded to an angle stiffener always failed in the beam close to the stiff edge, without visible damage to the bond, while thicker beams (.040" thick) excited to the same rms bending stress at the bond edge always failed in the bond at a lower number of stress cycles. Partial delamination of the bond followed by beam failure was also observed. These experiments for different bonding processes are presently continuing at AFFDL.

An important factor which influences the fatigue of bonded joints is the type of adhesive material and the surface preparation employed.

The fatigue characteristics of bonded joints of advanced composite materials and bonded panel assemblies have been reported by Wolf and Jacobson (7) and by Jacobson (8). The designer should refer to Figures 5.3.8-2 and 5.3.8-4.

5.4.3.4 Weldbonded Joints

The weldbond process is a relatively new fabrication method currently being evaluated as a standard process for joining structural members in aircraft construction (9). The fatigue aspects of weldbonded joints, employing a low grade boundary process, which allows weldability through the adhesive, have been evaluated both by random amplitude coupon fatigue tests and sonic fatigue tests of nine bay panel structures, with the weldbond joints used for skin-stiffener attachment.

The results of these tests have indicated that for flexural loading across a typical weldbonded joint the weakest element of the joint is the adhesive bond. The next strongest element of the joint is the spot weld with the skin and stringer parent material being the strongest element. Due to this progressive failure mode, it has been recommended that S-N curves be presented in pairs (one curve for bond failures and one curve for spot weld failures) for a specific joint configuration.

Due to the multiple failure mode of weldbonded joints, the definition of a joint failure is taken relative to the basis for establishing the design joint strength. If the design strength of the joint is based on

the spot weld strength only with the bond being used only to improve the joint fatigue strength, then a bond failure would not constitute a joint failure and the fatigue strength would be based upon the spot weld S-N curve of the weldbond joint. If the bond strength has been included in the design of a joint experiencing significant bond loading and a bond failure is considered as a joint failure then the fatigue strength should be based upon the bond S-N curve of the weldbond joint.

The sonic fatigue tests of six nine-bay stiffened panel test specimens utilizing weldbonded skin-stiffener attachments have been conducted (9). Four of these specimens were flat and two of these specimens were cylindrically curved panels with a radius of curvature of 85 inches. All tests utilized grazing incidence narrow band random acoustic excitation at spectrum levels from 132 to 135 dB. For all test specimens the adhesive bond delaminated first along the skin-stiffene bondline fillet. This delamination would progress along the edge of the stiffener or frame and penetrate into the weldbond joint to the row of spot welds. Continued exposure to the acoustic excitation resulted in cracks in the spot weld nuggets in the area of the bond delamination. These cracks would propagate until they interconnected causing complete failure of the joint. This failure mode essentially duplicated the failure modes observed in the coupon fatigue tests of weldbonded joints. All panel failures occurred in the center-bay of the nine-bay test specimens with the failure originating at the heel of the lengthwise stiffeners.

The failure data for the test specimens is presented in Table 5.4.3-1. Specimens 1, 2, 5, and 6 indicated in Table 5.4.3-1 were identical except that Specimens 5 and 6 were curved specimens with 85-inch radius of curvature. The specimens were manufactured from 7075-T6 aluminum alloy.

Using service life as a criteria these tests indicate that compared to countersunk riveted construction, weldbonded skin-stringer construction shows a progressive improvement over riveted structure above 10^8 or 10^9 cycles (although specific failure data was not obtained in this life range). For a design life of 10^7 cycles weldbonding does not indicate an improvement over riveted construction and below 10^6 cycles weldbonding is clearly at a disadvantage as compared to riveted construction.

TABLE 5.4.3-1

SONIC FATIGUE TEST RESULTS FOR WELDBONDED SKIN-STRINGER PANELS

Panel Number	Sound Pressure Spectrum Level	Cycles to Failure	
		Bondline	Spot Welds
1	134.5	6.05×10^4	4.66×10^5
2	135.0	5.72×10^4	2.86×10^5
3	134.5	2.05×10^5	3.14×10^6
4	135.0	6.72×10^4	6.43×10^6
5	132.0	1.10×10^5	1.20×10^6
6	134..	4.10×10^4	3.70×10^5

REFERENCES FOR SECTION 5.4

1. Osgood, C. C., Fatigue Design, Wiley-Interscience, New York, 1920.

2. Heywood, R. B.; Designing Against Fatigue of Metals, Reinhold Publishing Company, New York, 1962.

3. Graham, J. A. (Ed.); Fatigue Design Handbook, Society of Automotive Engineers, Inc., Two Pennsylvania Plaza, New York, N. Y., 10001, 1968.

4. Harris, W. J.; Metallic Fatigue, Pergamon Press, London, 1961.

5. Crate, H.; Ochiltree, D. W.; and Graves, W. T.; "Effect of Rivet Pitch to Rivet Diameter on the Fatigue Strength of Riveted Joints of 24 S-T Aluminum Alloy Sheet," NACA TN1125, National Advisory Committee for Aeronautics, Langley Field, Virginia, September 1946.

6. Anon.; Metallic Materials and Elements for Aerospace Vehicle Structures, MIL-HDBK-SB, U. S. Government Printing Office, September 1971.

7. Wolf, N. D., and Jacobson, M. J.; "Design and Sonic Fatigue Characteristics of Composite Material Components," Paper No. 13, AGARD CP-113, Advisory Group for Aerospace Research and Development North Atlantic Treaty Organization, September 1972.

8. Jacobson, M. J.; "Advanced Composite Joints; Design and Acoustic Fatigue Characteristics," AFFDL-TR-71-126, Air Force Flight Dynamics Laboratory, Wright-Patterson Air Force Base, Ohio, 1972.

9. Grosko, J. J., and Kizer, J. A.; "Weldbond Flight Component Design/Manufacturing Program," AFML-TR-74-179/AFFDL-TR-74-126, Air Force Systems Command, Wright-Patterson Air Force Base, Ohio, December 1974.

5.5 STRESS CONCENTRATION FACTORS

5.5.1 GENERAL CONSIDERATIONS

To estimate the stress response of a structure to applied loads the designer normally uses the results of a linear elasticity solution of the problem being considered to obtain estimates of the nominal stress magnitude. For example, the designer may use simple beam or plate theory to estimate stresses. Concerning the sonic fatigue problem and referring to Section 5.2, the designer estimates the stress response of the idealized structure to a unit magnitude uniform pressure (see Figure 5.2.2-24, for example). To relate the idealized structure to the actual structure, it is necessary to account for effects relating to very localized geometric discontinuities resulting from either details of joining structural components or from manufacturing processes.

Assuming elastic response of the material, it is a standard design practice to estimate the stress intensification at a particular geometric discontinuity such as a hole, fillet radii, keyway, screw thread, etc. in terms of a theoretical stress concentration factor, K_t. This theoretical factor is the ratio of the maximum stress at a point to the nominal stress at the point based upon the net cross sectional area containing the discontinuity and use of a simplified stress analysis formula. Hence, for a given loading system, the stress concentration factors describing the geometry and an assumed theory of fracture (such as maximum shear theory for ductile materials), the designer may make reliable calculations of the ultimate loads required to cause static failure of the structure.

Engineers have used the term "notch" to signify the geometric features giving rise to a stress concentration. In fatigue work, it is rarely the case that the maximum effect of the static stress concentration factor, K_t, or the fatigue strength is realized. Hence, it has been required to develop an experimental "fatigue notch factor," K_f, based upon comparing the fatigue strength of an unnotched specimen to the fatigue strength of a notched specimen. The fatigue notch factor, K_f, is defined as the ratio of the unnotched fatigue strength to the notched fatigue strength. The fatigue notch factor, K_f, does not achieve as high a value as the theoretical stress concentration factor, K_t. Since the fatigue notch factor is based upon fatigue strength, it will usually be a function of the number of cycles to failure for each material and notch configuration.

It is customary to relate the factors K_t and K_f to obtain a measure of the notch sensitivity of the material to reduction of fatigue strength. A convenient parameter is the "notch sensitivity factor," q, defined as

$$q = (K_f - 1)/(K_t - 1) . \qquad (5.5.1\text{-}1)$$

For no notch effect, $K_f = 1$ and $q = 0$. For complete realization of the theoretical stress concentration $K_f = K_t$ and $q = 1$.

For practical design, the designer must know the values for K_t and K_f or K_t and q to obtain realistic estimates for fatigue life of the structure. Hence, the designer should ideally have fatigue data available for each combination of material and notch geometry encountered in his structural design.

To appreciate the relationship between the theoretical stress concentration factor, K_t, and the material factors, K_f and q, Table 5.5.1-1 is presented (4). The results of axial load fatigue tests of aluminum riveted joints are presented in Figure 5.5.1-1 (4) as representative of typical results.

TABLE 5.5.1-1

STRESS CONCENTRATION FACTORS, K_t; FATIGUE NOTCH FACTORS, K_f; AND NOTCH SENSITIVITY FACTORS, q, FOR VARIOUS ALLOYS IN ROTATING BENDING

Alloy	K_t	K_f	q
Stainless Steel, Type 18-8	1.6	1.0	0.0
Structural Steel (BHN = 120)	1.6	1.3	0.5
Hardened Steel (BHN = 200)	1.6	1.6	1.0
Aluminum, 2024-0	1.6	1.0	0.0
Aluminum, 7075-T73	6.7	1.8	0.13
Titanium, 6Al - 4V	3.5	2.8	0.72
Magnesium, AZ80-A	1.6	1.1	0.16

This section presents a brief summary of the theoretical stress concentration factors usually encountered in sonic fatigue problems, i.e., holes in plates. The foremost compilation of theoretical stress concentration factors is that by Peterson (1). The techniques to be used to relate the static stress concentration factor, K_t, to establish fatigue life of a structure is presented in the following section and is completely described in the references (1) - (6). In particular, Heywood (5) presents an interesting analytical/empirical analysis for estimating the fatigue strength of unnotched material that applies to steels and high strength aluminum alloys and presents a detailed discussion the techniques required to relate theoretical stress concentration factors, notch sensitivity, and failure criteria to estimate the fatigue life of structure.

To estimate the effect of stress concentration on the fatigue strength of sheet material, the designer should refer to the work of Grover, et al. (7) - (9). The effect of stress concentration on the sonic fatigue failure of panels is described by Berens and West (10) and by van der Heyde and Kolb (11).

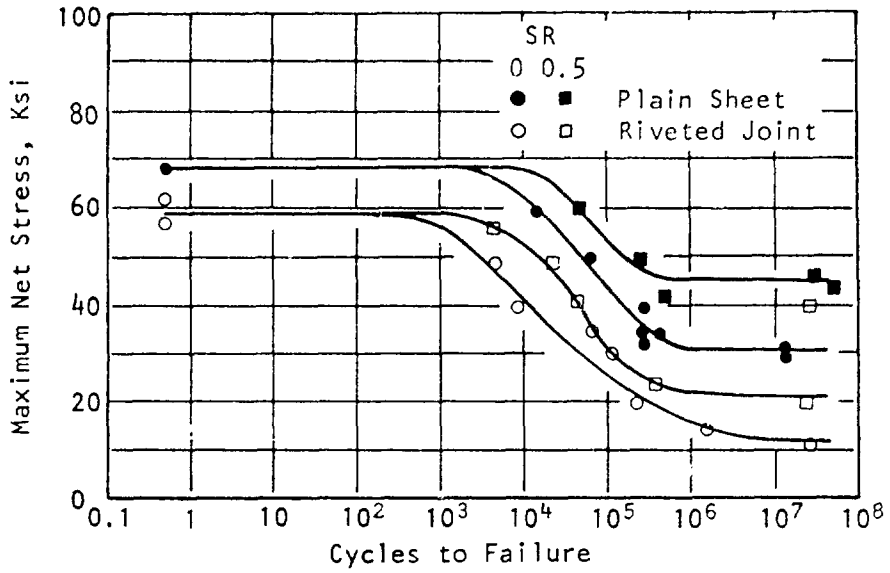

(a) Axial-Stress Fatigue Strength of 2024-T3 Plain Sheet and Riveted Joint Specimens

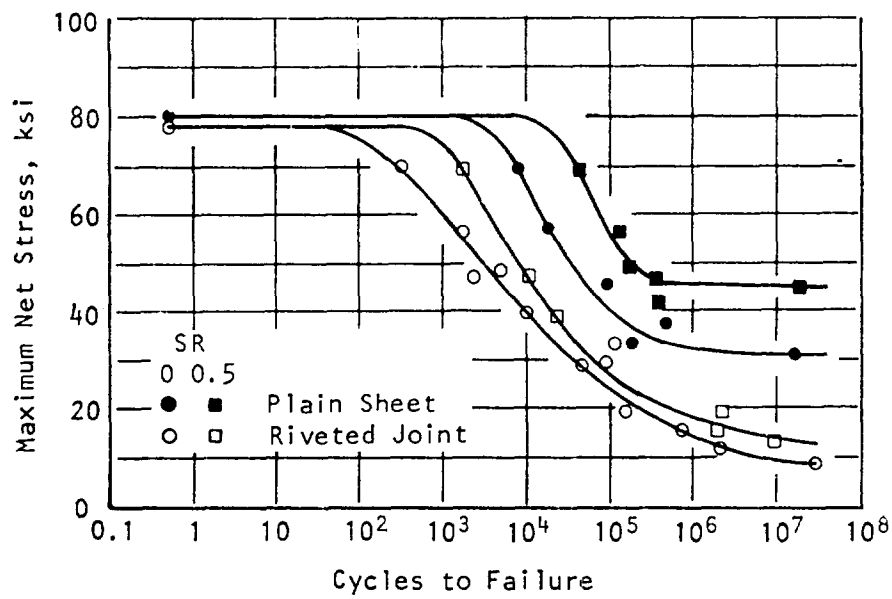

(b) Axial-Stress Fatigue Strength of 7075-T6 Plain Sheet and Riveted Joint Specimens

FIGURE 5.5.1-1 AXIAL-STRESS FATIGUE STRENGTH OF PLAIN SHEET AND RIVETED JOINT SPECIMENS

5.5.2 TYPICAL VALUES OF STRESS CONCENTRATION FACTORS

The following discussion of theoretical stress concentration factors is used to provide design guidance. The designer is advised to consult the specific references quoted. In particular, the designer should refer to the work of Peterson (1) for a thorough and complete presentation.

5.5.2.1 Welded Joints

Geometric stress concentrations are introduced into welded joints due to the irregular edges between the welded joint. The nominal stress is usually taken as the ratio of the load (either tension or shear) per unit length of the weld to the thickness of the plates being welded (2). Typical values of the stress concentration factor, $K_t = \sigma/\sigma_{nominal}$, are presented in Table 5.5.2-1 (see Section 5.4.3.2).

TABLE 5.5.2-1

STRESS CONCENTRATION FACTOR, K_t, FOR WELDS

Location	K_t
Butt Weld in Tension	1.2
Toe of Transverse Fillet Weld	1.5
End of Fillet Weld in Shear	2.7
T Butt Joint with Sharp Corners	2.0

5.5.2.2 Holes in Plates

Peterson (1) presents a very thorough collection of stress concentration factors for holes in plates. The work of Savin (12) should also be referenced by the designer to obtain estimates of the stress concentration around holes. The results presented here are taken from Peterson (1). To estimate the stress concentration effects of filled holes in plates, the designer should refer to the data and bibliography presented by Heywood (5).

Rather than to duplicate the graphs presented by Peterson (1) for general configurations of holes in plates, this section presents typical values for the stress concentration around a hole assuming that the designer follows good design practice in selecting rivet diameter, rivet pitch, and edge distance from a hole to the free edge of a plate. Based upon the discussion in Section 5.4.2.1, the following values are assumed:

Ratio: rivet diameter to edge distance = d/e = 3.0
Ratio: rivet diameter to rivet pitch = d/p = 3.0 to 6.0
Ratio: rivet diameter to plate thickness = d/h = 4.0

If the designer must use values outside of these ranges, then he should consult the references. It is common practice to assume that $K_t = 4.0$ for conventional aircraft structure.

The definition of the stress concentration factor, K_t, is

$$K_t = \sigma_{max}/\sigma_{nom} \qquad (5.5.2\text{-}1)$$

so that the designer must know both K_t and the expression for nominal stress, σ_{nom}, to calculate σ_{max}. For the assumed hole configurations, three quantities are given: K_t, σ_{nom}, and σ_{max}.

5.5.2.2.1 Axially Loaded Plates

This section presents expressions for stress concentration factors, nominal stress and maximum stress for plain holes in plates subjected to axial loading.

Single Hole in Finite Width Plate: The configuration is illustrated in Figure 5.5.2-1a (Figure 69, Ref. (1)).

$$K_t = 2.6$$

$$\sigma_{nom} = 1.2\sigma = 1.2P/wh = 0.05P/h^2 \qquad (w = 6d = 24h)$$

$$\sigma_{max} = 3.12\sigma = 0.156P/h^2$$

Eccentric Hole in Finite Width Plate: The configuration is illustrated in Figure 5.5.2-1b (Figure 71, Ref. (1)).

$$K_t = 2.6$$

$$\sigma_{nom} = 1.18\sigma/(1-0.042\ d/e);\ e \geq 3d$$

$$\sigma_{max} = 3.07\sigma/(1 - 0.042\ d/e)$$

Simple Pin Joint: The configuration is illustrated in Figure 5.5.2-1c (Figure 83, Ref. (1)).

$$K_t = 1.1$$

$$\sigma_{nom} = P/dh = P/4h^2$$

$$\sigma_{max} = 1.1\ P/dh = 0.275\ P/h^2$$

Hole Near Edge of Semi-infinite Plate: The configuration is illustrated in Figure 5.5.2-1d (Figure 70, Ref. (1)).

$$K_t = 2.7$$

$$\sigma_{nom} = 1.183\ \sigma$$

$$\sigma_{max} = 3.19\ \sigma$$

Two Holes in Infinite Plate with Tensile Loading Parallel to Hole Line: The configuration is illustrated in Figure 5.5.2-1e (Figure 75, Ref. (1)).

$$K_t = 2.82$$

$$\sigma_{nom} = \sigma$$

$$\sigma_{max} = 2.82\,\sigma$$

Two Holes in Infinite Plate with Tensile Loading Perpendicular to Hole Line: The configuration is illustrated in Figure 5.5.2-1f (Figure 76, Ref. (1)).

$K_{tA} = 3.2$ $\quad \sigma_{nom} = \sigma$ $\quad \sigma_{max} = 3.2\,\sigma$

$K_{tB} = 2.1$ $\quad \sigma_{nom} = 1.5\,\sigma$ $\quad$ $_{max} = 3.15\,\sigma$

Two Holes in Infinite Plate with Uniform Biaxial Tensile Loading: The configuration is illustrated in Figure 5.5.2-1g (Figure 77, Ref. (1)).

$K_{tA} = 2.0$ $\quad \sigma_{nom} = \sigma$ $\quad \sigma_{max} = 2.0\,\sigma$

$K_{tB} = 2.1$ $\quad \sigma_{nom} = 1.4\,\sigma$ $\quad \sigma_{max} = 2.1\,\sigma$

Row of Holes in Infinite Plate with Tensile Loading Parallel to Row: The configuration is illustrated in Figure 5.5.2-1h (Figure 78, Ref. (1)). The value of K_t is based upon an intermediate hole. See Figure 5.5.2-1c for end holes near an edge.

$$K_t = 2.8$$

$$\sigma_{nom} = \sigma$$

$$\sigma_{max} = 2.5\,\sigma$$

Row of Holes in Infinite Plate with Tensile Loading Perpendicular to Row: The configuration is illustrated in Figure 5.5.2-1i (Figure 79, Ref. (1)). The value of K_t is based upon an intermediate hole. See Figure 5.5.2-1d for end holes near an edge

$$K_t = 2.5$$

$$\sigma_{nom} = \sigma$$

$$\sigma_{max} = 2.5\sigma$$

Row of Holes in Infinite Plate with Uniform Biaxial Tensile Loading: The configuration is illustrated in Figure 5.5.2-1j (Figure 80, Ref. (1)). The value of K_t is based upon an intermediate hole.

$K_t = 1.74$

$\sigma_{nom} = \sigma$

$\sigma_{max} = 1.74\sigma$

Double Row of Holes in Infinite Plate with Tensile Loading Perpendicular to Rows: The configuration is illustrated in Figure 5.5.2-1k (Figure 82, Ref. (1)). The value of K_t is based upon intermediate holes in the rows.

θ	K_t	σ_{nom}	σ_{max}
0°	1.42	3.0 σ	4.3 σ
45°	1.95	1.9 σ	3.7 σ
60°	2.18	1.5 σ	3.3 σ
90°	2.14	1.5 σ	3.2 σ

5.5.2.2.2 Bending of Plates

This section presents expressions for stress concentration factors, nominal stress, and maximum stress for single plain holes in plates subjected to a bending moment M.

Finite Width Plate (W = 6d) with Single Hole: The configuration is illustrated in Figure 5.5.2-2a (Figure 86, Ref. (1)).

$K_t = 1.55$

$\sigma_{nom} = 1.2\ M/dh^2 \approx 0.3\ M/h^2 \quad (d = 4h)$

$\sigma_{max} = 1.9\ M/dh^2 \approx 0.47\ M/h^2$

Note: The dimensions for the bending moment are force times length.

Infinite Plate with Single Hole: The configuration is illustrated in Figure 5.5.2-2b (Figure 85, Ref. (1)).

$K_t = 1.95 \qquad 3 \leq d/h \leq 6$

$\sigma_{nom} = 6\ M/h^2$

$\sigma_{max} = 11.7\ M/h^2$

Note: The dimensions for the bending moment are force times length per unit length. When using the results of Section 5.2, σ_{nom} is computed directly (See Figure 5.2.2-24).

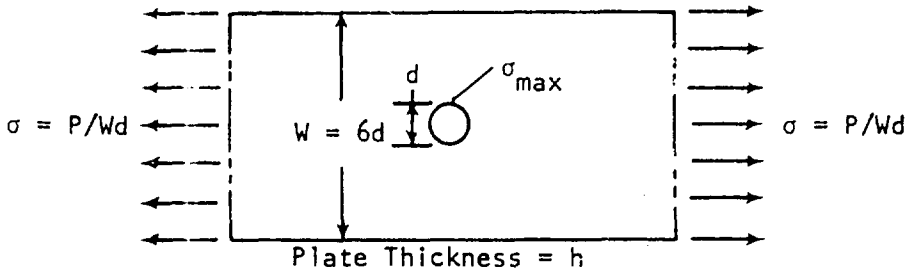

(a) Single Centered Hole in a Finite Width Plate

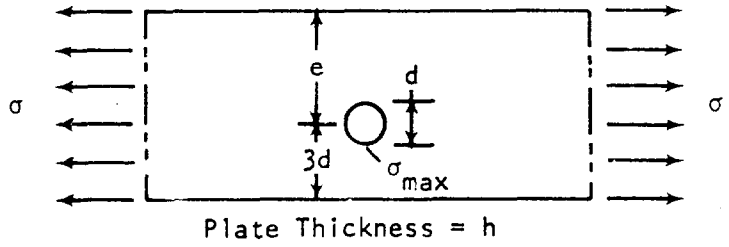

(b) Single Eccentric Hole in a Finite Width Plate

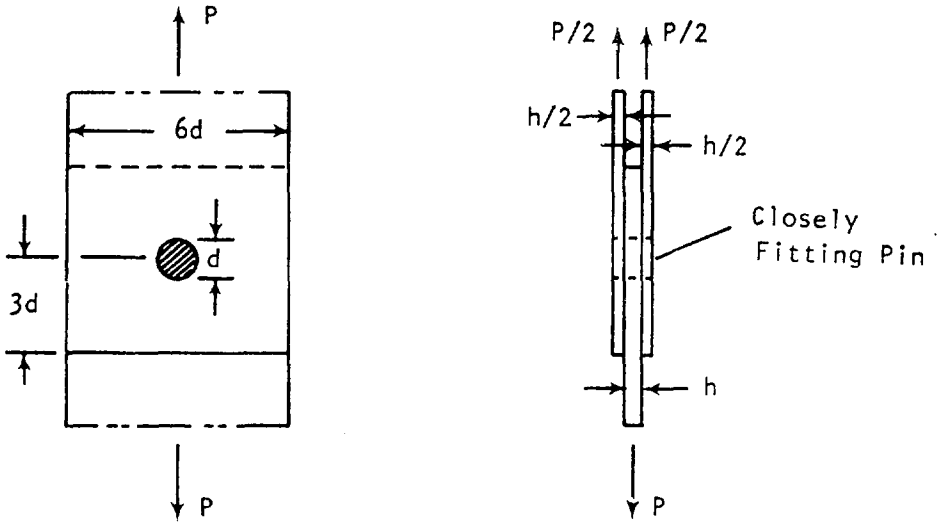

(c) Simple Pin Joint

FIGURE 5.5.2-1 CONFIGURATIONS FOR STRESS CONCENTRATION FACTORS FOR TENSILE LOADING (CONTINUED)

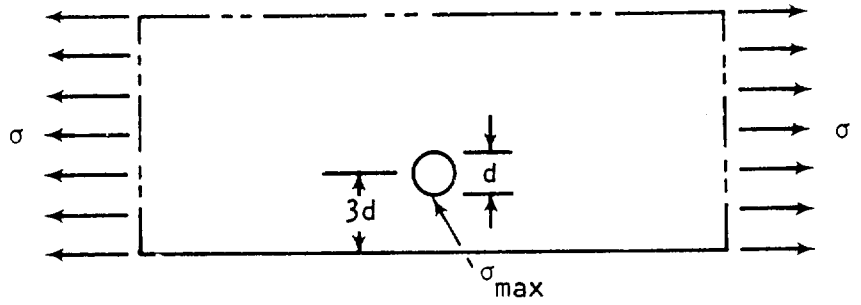

(d) Hole Near Edge of Semi-Infinite Plate

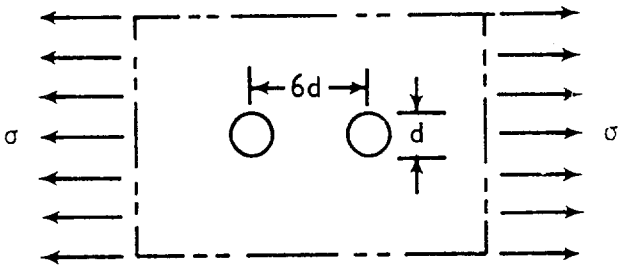

(e) Two Holes in Infinite Plate: Tension Parallel to Hole Axis

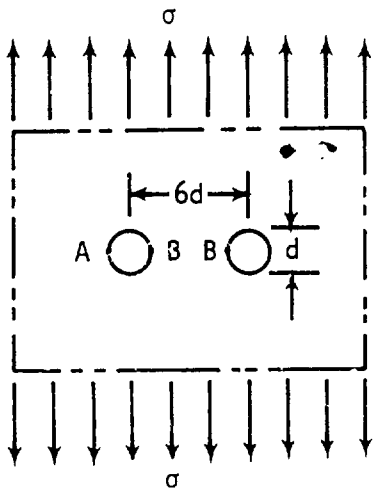

(f) Two Holes in Infinite Plate: Tension Perpendicular to Hole Axis

FIGURE 5.5.2-1 (CONTINUED)

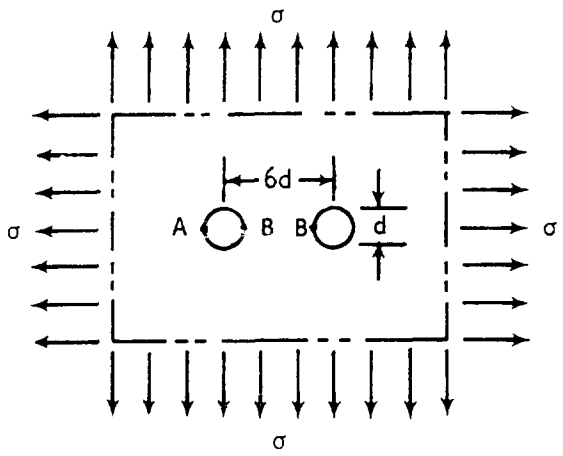

(g) Two Holes in Infinite Plate: Uniform Biaxial Tension

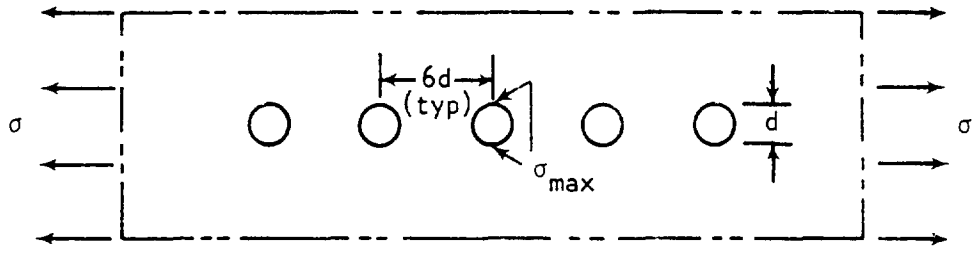

(h) Row of Holes in Infinite Plate: Tension Parallel to Row

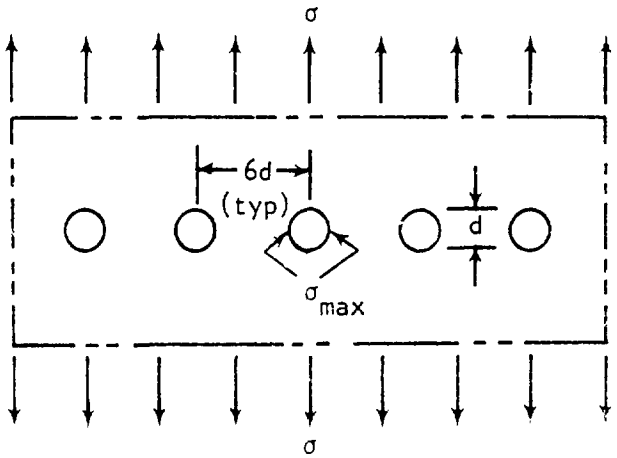

(i) Row of Holes in Infinite Plate: Tension Perpendicular to Row

FIGURE 5.5.2-1 (CONTINUED)

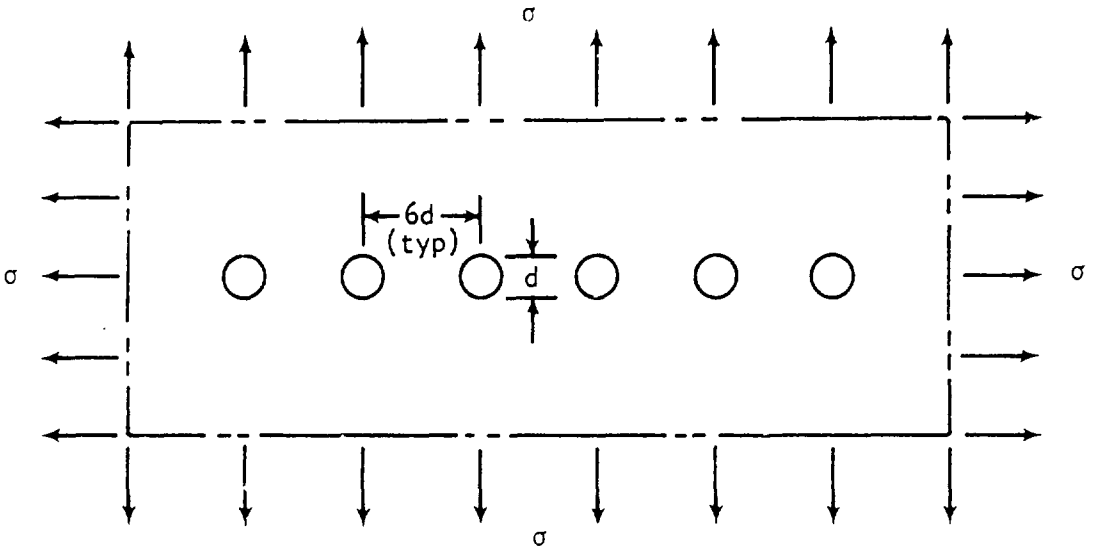

(j) Row of Holes in Infinite Plate: Biaxial Tension

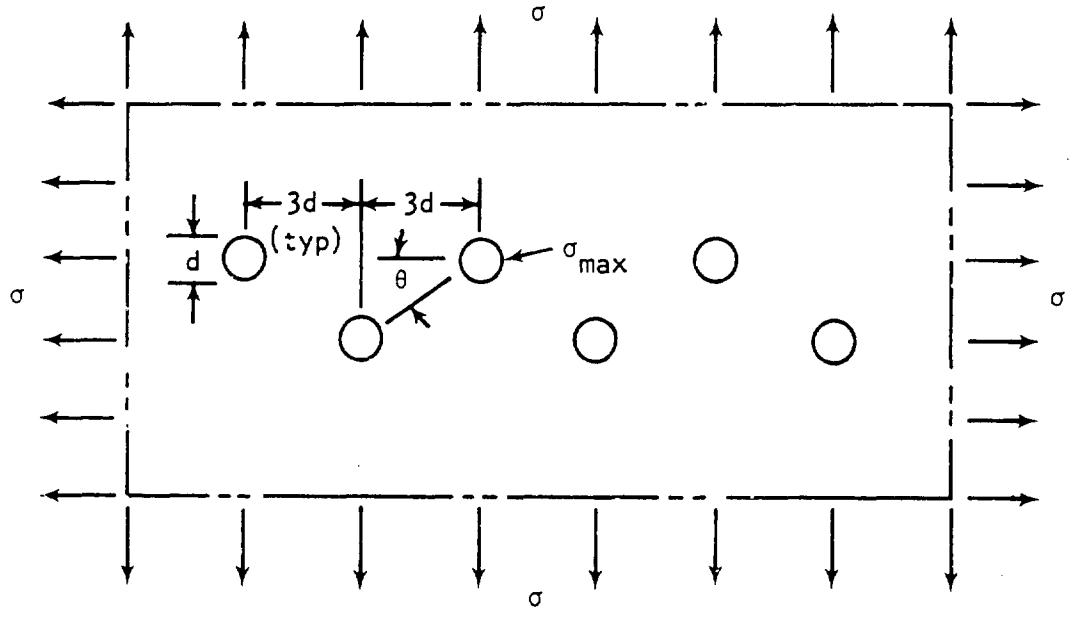

(k) Double Row of Holes in Infinite Plate: Biaxial Tension

FIGURE 5.5.2-1 (CONCLUDED)

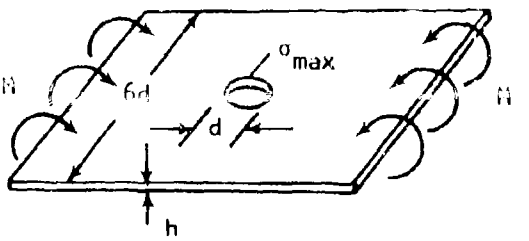

(a) Bending of Finite Width Plate with Single Hole

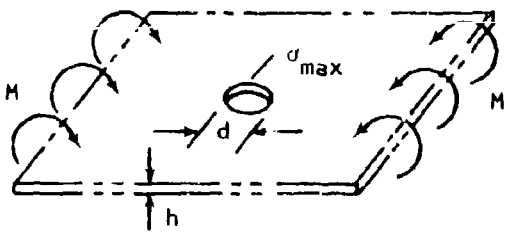

(b) Bending of Infinite Plate with Single Hole

FIGURE 5.5.2-2 CONFIGURATIONS FOR STRESS CONCENTRATION FACTORS FOR BENDING

5.5.2.2.3 Countersunk Holes

Based upon strain gage and photoelastic studies and upon fatigue tests, Whaley (13) determined that the stress concentration factors for countersunk holes were from 13% to 23% higher than the maximum values for plain holes. This maximum value is attained on the interior of the plate where the tapered countersink intersects the plain hole (approximately half to two-thirds the plate thickness for good design). In the absence of specific data, the designer can multiply the plain hole stress concentration factors given above by 1.25 to estimate the effect of a countersink on stress concentration.

5.5.2.2.4 Curved Sheet Subject to Bending

Assuming a curved beam behavior, it is possible to develop a stress concentration factor that applies to the radius bend of a sheet metal part, Reference (1), pp. 117-118. This stress concentration factor applies to the bend radius of clips and to rib flanges formed from flat sheet metal stock. The stress concentration factor for a 90° bend and a bend radius four times the sheet thickness varies inversely with the plate thickness, h, from $K_t = 1.20$ for $h = 0.125$ inches to $K_t = 2.30$ for $h = 0.020$ inches. The nominal stress is based upon the bending moment supported along one edge using the simple beam formula (Equation B.1.1-1c) with the maximum stress calculated for the opposite edge.

REFERENCES FOR SECTION 5.5

1. Peterson, R. E.; Stress Concentration Design Factors, John Wiley & Sons, New York, 953.

2. Spotts, M. F.; Design of Machine Elements (4th Ed), Prentice-Hall, Inc., Englewood Cliffs, N. J., 1971.

3. Graham, J. A. (Ed.); Fatigue Design Handbook, Society of Automotive Engineers, Inc., Two Pennsylvania Plaza, New York, N. Y. 10001, 1968.

4. Osgood, C. C.; Fatigue Design, Wiley-Interscience, New York 1970.

5. Heywood, R. B.; Designing Against Fatigue, Chapman Hall Ltd., London 1962.

6. Harris, W. J. Metallic Fatigue, Pergamon Press, London, 1961.

7. Grover, M. J., et al.; "Fatigue Strengths of Aircraft Materials - Axial Load Fatigue Tests on Notched Sheet Specimens of 24S - T3 and 75S-T6 Aluminum Alloys and of 4130 Steel with Stress Concentration Factors of 2.0 and 4.0," NACA TN 2389, National Advisory Committee for Aeronautics. June 1951.

8. Grover, H. J., et al.; "Fatigue Strengths of Aircraft Materials - Axial Load Fatigue Tests on Notched Sheet Specimens of 24S-T3 and 75S-T6 Aluminum Alloy and of SAE 4130 Steel with Stress Concentration Factor of 5.0," NACA TN 2390, National Advisory Committee for Aeronautics, June 1951.

9. Grover, M. J., et al.; "Fatigue Strengths of Aircraft Materials - Axial Load Fatigue Tests on Notched Short Specimens of 24S-T3 and 75S-T6 Aluminum Alloy and of SAE 4130 Steel with Stress Concentration Factor of 1.5," NACA TN 2639, National Advisory Committee for Aeronautics, February 1952.

10. Berens, A. P. and West B. G.; "Experimental Methods in Acoustic Fatigue," AFFDL-TR-71-113, Air Force Flight Dynamics Laboratory, Wright-Patterson Air Force Base Ohio, March 1972.

11. Van der Heyde, R. C. W. and Kolb, A. W.; "Sonic Fatigue of Light Weight Aircraft Structures," Paper No. 20, AGARD CP-113 Symposium on Acoustic Fatigue, Advisory Group for Aerospace Research and Development, North Atlantic Treaty Organization, Sept. 1972.

12. Savin, G. N.; Stress Concentration Around Holes, International Series of Monographs in Aeronautics and Astronautics, Division 1, Vol. 1, Pergamon Press, 1961.

13. Whaley, K. E.; "Stress Concentration Factors for Countersunk Holes," Proceedings of the Society for Experimental Stress Analysis, Vol. 22, No. 2, October, 1965.

INTENTIONALLY BLANK PAGE

SECTION 6

FATIGUE DESIGN

The total consideration of fatigue design covers an exceedingly wide range of topics. Fatigue failures can occur in simple plain test specimens, parts containing a discontinuity, or complex structures where both stress concentrations and load diffusions are present. Since the fatigue strength is directly influenced by the form of the loading, the designer must account for variable amplitude stress spectra and random amplitude stress spectra. Also, the designer must account for the effects of temperature and environmental factors on the fatigue life of the structure.

Two distinct areas of investigation are the development of fatigue theories concerned with predicting the fatigue mechanisms (and hence the life) of metallic materials and the accumulation and rationalization of fatigue strength data based upon experimental testing of particular specimens. The relation between theory and experiment has generally avoided a complete solution so that the designer usually relies upon available experimental data. The purpose of this section of this report is to present a basic description of design considerations and procedures required to estimate the sonic fatigue resistance of aircraft structure in the absence of specific design data such as presented in Section 5.3. Basic references describing the considerations of fatigue design are the text books by Osgood (1), Heywood (2), and Harris (3). The material data presented in MIL-HDBK-5B(4) and, in particular, the fatigue data presented in the form of constant life diagrams is an indispensible tool for use in fatigue design.

Section 6.2 describes the basic engineering parameters required to describe the fatigue strength of metallic materials. In particular, the relationship between the constant alternating stress and mean stress amplitudes to failure criteria are discussed to estimate the fatigue life of plain specimens. Additionally, introduction of the theoretical stress concentration factor and the notch sensitivity of the material allows the designer to relate the plain specimen fatigue life to the estimated fatigue life of the structure. Section 6.3 describes the statistical nature of experimental fatigue data so that the designer can appreciate the degree of confidence associated with designing for either a specified life or a range of applied loads. Section 6.4 presents a brief discussion of various cumulative damage theories so that the designer can, in the absence of specific test data, estimate the effect of variable amplitude stresses on the fatigue life of the structure. Since sonic fatigue failures result from applied stresses exhibiting random amplitudes, Section 6.5 presents a technique for converting constant amplitude S-N curves to so-called "equivalent random amplitude" S-N curves. Again, this technique will be valuable to the designer if specific test data is not available when required. Finally, Section 6.6 contains documented fatigue curves for various materials and structural configurations common to aircraft design.

6.1 NOTATION

A stress ratio = alternating stress/mean stress

A_0 ratio of alternating stress to static tensile strength of the material for zero mean stress

a	material notch alleviation factor, Table 6.2.2-1
b	material constant in Equation (6.2.2-2a), see Table 6.2.2-2
$\exp(x) = e^x$	
f_n	response frequency of a linear single degree-of-freedom system
K_F	strength reduction factor; Equation (6.2.2-1a)
K_f	atigue notch factor; determined by experiment
K_s	static strength reduction factor: ratio of the tensile strength of the plain specimen to the tensile strength of the notched specimen; σ_t/σ_{tn}
K_t	static theoretical stress concentration factor
N	cycles of alternating stress to failure, cycles
N_T	total number of cycles to failure for a spectrum of stress exposure (n_i, σ_i)
$N(\sigma_i)$	number of cycles to failure at the stress level σ_i
n	log(N)
n_i	number of cycles of alternating stress at the stress level σ_i
p(s)	Rayleigh probability density function
q	notch sensitivity factor for material; determined by experiment
R	stress ratio = minimum stress/maximum stress
r	notch radius; Equation (6.2.2-1a)
s	continuous alternating stress amplitude
T	total time of stress exposure
α_i	ratio of number of cycles of alternating stress n_i to the total number of cycles to failure N_T
γ	mean stress correction factor for fatigue strength prediction
σ_a	constant amplitude alternating stress, ksi
σ_{an}	alternating stress in a notched specimen Equation (6.2.2-1b)
σ_i	stress level associated with the i^{th} block of the stress exposure spectrum (n_i, σ_i)

σ_m constant mean stress, ksi

σ_t static ultimate tensile strength, ksi

σ_{tn} static ultimate tensile strength of notched material specimen

σ^2 mean square value of alternating stress "s"

6.2 PARAMETERS DESCRIBING FATIGUE STRENGTH

The approach taken here to describe the various parameters relating to the fatigue strength or life of a structure can be regarded as an engineer's approach. That is, the effect on the fatigue strength of a structure will be discussed in terms of engineering quantities on a phenomenological basis. Specifically, the fatigue strength will be discussed in terms of design parameters on a macroscopic scale rather than a scientific discussion of microscopic effects.

Following the work of Heywood (2), the designer should place first importance on the experimental fatigue characteristics of plain test specimens. These results can then be related to specific structural configurations by considering the "notch effects" of stress concentrations and material notch sensitivity. This approach allows the subject of fatigue to be organized on an engineering design basis. The designer does not have to be totally concerned then with the accumulation of experimental test data for all material and configuration combinations although specific test data for plain material specimens is required.

6.2.1 PLAIN SPECIMEN FATIGUE STRENGTH

Fatigue strength is a broad term implicitly relating the applied stresses and life of a material configuration. Based upon empirically derived expressions relating applied stresses and fatigue life (2), the basic material parameter can be taken as the ultimate tensile strength, σ_t, of the metallic material. The two basic loading parameters are the constant amplitude alternating stress, σ_a, and the constant mean stress, σ_m. The life of the specimen is usually measured in terms of the number of cycles to failure, N, of the alternating stress.

Heywood (2) has proposed the following relationship for plain aluminum alloys with ultimate tensile strength, σ_t in ksi, subjected to a combination of alternating stress, σ_a in ksi, and tensile mean stress, σ_m in ksi, for N cycles to failure

$$\sigma_a = \pm \sigma_t[1 - \sigma_m/\sigma_t][A_o + \gamma(1 - A_o)] \quad \text{ksi} \qquad (5.2.1\text{-}1)$$

where

$$A_o = [1 + 0.0031n^4/(1 + 0.045\sigma_t)]/(1 + 0.0031n^4)$$

$$\gamma = (\sigma_m/\sigma_t)/[1 + (\sigma_t n/320)^4]$$

$$n = \log(N)$$

It is common practice in fatigue design to combine the alternating stress, σ_a, and the mean stress, σ_m, to obtain stress ratios describing the loading condition. Two common stress ratios are the ratio of minimum stress to maximum stress in one cycle, denoted by R, and the ratio of alternating stress to mean stress, denoted by A. The specific definitions in terms of σ_a and σ_m are:

$$R = (\sigma_m - \sigma_a)/(\sigma_m + \sigma_a) \qquad (6.2.1\text{-}2a)$$

$$A = \sigma_a/\sigma_m \qquad (6.2.1\text{-}2b)$$

The most common loading condition related to sonic fatigue design is that of zero mean stress ($R = -1$, $A = \infty$) so that Equation (6.2.1-1) for aluminum alloys becomes

$$\sigma_a = \pm \sigma_t[1 + 0.0031\, n^4/(1 + 0.045\, \sigma_t)]/(1 + 0.0031\, n^4) \qquad (6.2.1\text{-}3)$$

$$n = \log(N)$$

Although Equation (6.2.1-1) was developed for tensile mean stresses, it can be used for moderate values of compressive mean stress (2). Hence, the designer can use Equations (6.2.1-1) or (6.2.1-3) to estimate the fatigue characteristics of an aluminum alloy knowing any three of the parameters σ_a, σ_m, N, or σ_t and solving for the fourth parameter. Equation (6.2.1-3) is plotted in Figure 6.2.1-1 as a σ-log(N) curve for various values of ultimate tensile strength, σ_t.

The designer may use these results in the absence of specific fatigue test data; however, he should always attempt to verify the predicted results by comparison to experimental results. The prediction formulas given in Equations (6.2.1-1) and (6.2.1-3) yield estimates of the alternating stress that are approximately 10% high for a given life as compared to values quoted in MIL-HDBK-5B(4). For estimates of fatigue life greater than $N = 10^5$ cycles to failure it is recommended that N be taken as a primary variable rather than σ_a since small changes in σ_a can result in large variations in N.

Example: Estimate the amplitude of alternating stress required to produce failure in $N = 10^7$ cycles for 2024-T3 aluminum alloy sheet (σ_t = 73 ksi) and 7075-T6 aluminum alloy sheet (σ_t = 82.5 ksi) assuming zero mean stress and no stress concentration effects. Also calculate the amplitude of alternating stress required to produce failure in $N = 10^7$ cycles for the two materials for a mean tensile stress of 20 ksi.

For $N = 10^7$, $n = \log(10^7) = 7.0$ and from Equation (6.2.1-3)

Aluminum Alloys at Zero Mean Stress

$$\sigma_a = \sigma_t\{1 + 0.003n^4/(1.0 + 0.045\sigma_t)\}/(1.0 + 0.0031n^4)$$

$$n = \log(N)$$

σ_t = Ultimate Tensile Strength

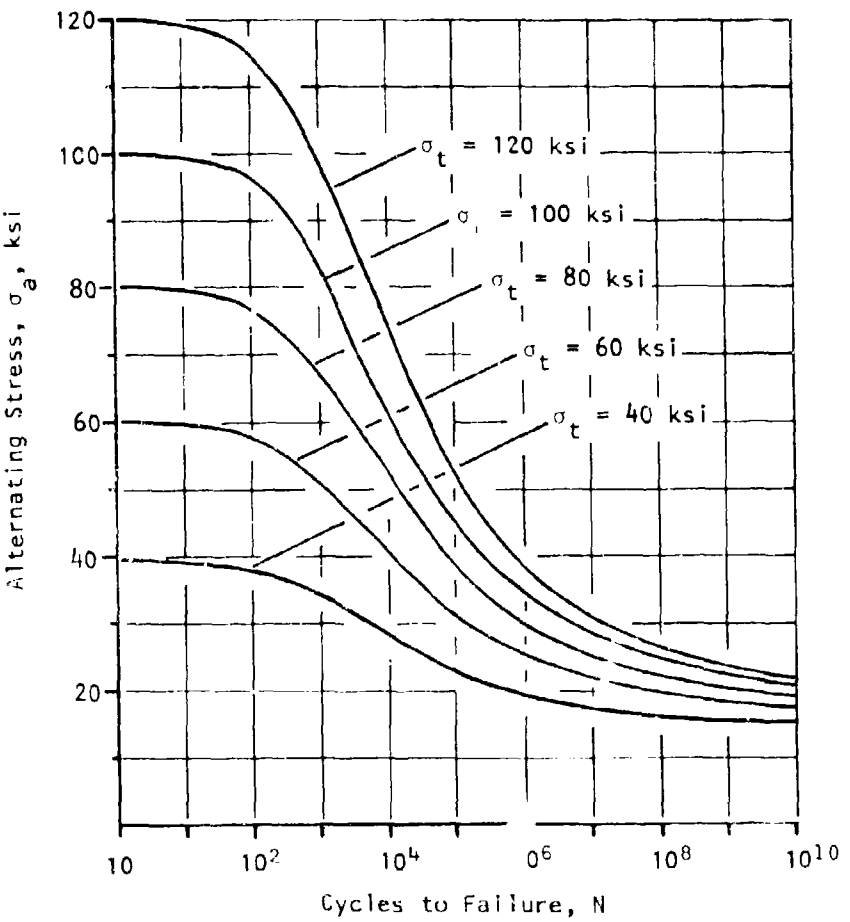

FIGURE 6.2.1-1 PREDICTED FATIGUE CHARACTERISTICS OF PLAIN SPECIMEN ALUMINUM ALLOYS AT ZERO MEAN STRESS

$$\sigma_a = \pm\ 0.1184\ \sigma_t[1.0 + 7.443(1.0 + 0.045\ \sigma_t)]\ .$$

Then for 2024-T3 alloy and zero mean stress

$$\sigma_a = \pm\ 0.1184(73)[1.0 + 7.443/(1.0 + 0.045(73))]$$

$$\sigma_a = \pm\ 23.7\ \text{ksi}$$

The value quoted in Figure 3.2.3.1.8(b) of MIL-HDBK-5B is $\sigma_a = 21.0$ ksi. Similarly, for 7075-T6 alloy ($\sigma_t = 82.5$ ksi) one calculates $\sigma_a = \pm 25.2$ ksi which compares to the value of $\sigma_a = \pm 20.0$ ksi as quoted in Figure 3.7.2.1.8(b) of MIL-HDBK-5B.

For $N = 10^7$ and $\sigma_m = 20$ ksi, one obtains from Equation (6.2.1-1) the results $\sigma_a = 18.5$ ksi for 2024-T3 alloy and $\sigma_a = \pm 20.8$ ksi for 7075-T6 alloy.

Table 6.2.1-1 presents a comparison of the predictions using Equations (6.2.1-1) and (6.2.1-3) and experimental values quoted by MIL-HDBK-5B (4) for 2024-T3 aluminum alloy. Table 6.2.1-2 presents a similar comparison for 7075-T6 aluminum alloy.

Heywood (2) presents a similar and more accurate empirical equation in the form of Equation 6.2.1-1 for high strength steel alloys. The fatigue characteristics of unnotched steel alloy specimens is approximated as

$$\sigma_a = \pm\ \sigma_t[1 - \sigma_m/\sigma_t][A_o + \gamma(1 - A_o)]\ \text{ksi} \qquad (6.2.1\text{-}4)$$

where

$$A_o = (1 + 0.0038\ n^4)/(1 + 0.008\ n^4)$$

$$\gamma = \sigma_m(2 + \sigma_m/\sigma_t)/3\sigma_t$$

$$n = \log(N)$$

6.2.2 NOTCHED SPECIMEN FATIGUE STRENGTH

In Section 5.5 the topic of stress concentration factors, K_t, fatigue notch factors, K_f, and the notched sensitivity factor q, were discussed with typical values quoted for various types of "notches" and materials. Since the stress concentration factor, K_t, is a static parameter independent of material properties, K_t is a parameter associated only with geometric effects. As indicated by Equation (5.5.1-1) the fatigue notch factor, K_f, and the notched sensitivity factor, q, are both dependent upon material properties and may vary with the life, N, of the notched specimen.

The purpose of this subsection is to indicate to the designer techniques for modifying the plain specimen fatigue strength to account for the

TABLE 6.2.1-1

COMPARISON OF PREDICTED AND EXPERIMENTAL FATIGUE STRENGTH OF UNNOTCHED 2024-T3 ALUMINUM ALLOY SHEET
Ultimate Tensile Strength: σ_t = 73 ksi

N	σ_m = 0		σ_m = 20 ksi	
	σ_a(1)	σ_a(2)	σ_a(1)	σ_a(3)
$4 \cdot 10^3$	-	53.8	-	41.7
$1 \cdot 10^4$	50	48.2	43	37.9
$4 \cdot 10^4$	41	40.4	32	32.3
$1 \cdot 10^5$	34	36.1	25	28.9
$4 \cdot 10^5$	27	30.8	21	24.7
$1 \cdot 10^6$	22	28.2	17	22.4
$1 \cdot 10^7$	21	23.7	16	18.5
$1 \cdot 10^8$	-	21.1	-	16.2
$1 \cdot 10^9$	-	19.7	-	14.8

NOTES: (1) Figure 3.2.3.1.8(b), MIL-HDBK-5B

(2) Using Equation 6.2.1-3

(3) Using Equation 6.2.1-1

TABLE 6.2.1-2

COMPARISON OF PREDICTED AND EXPERIMENTAL FATIGUE STRENGTH OF UNNOTCHED 7075-T6 ALUMINUM ALLOY SHEET
Ultimate Tensile Strength: σ_t = 82.5 ksi

N	σ_m = 0		σ_m = 20 ksi	
	σ_a(1)	σ_a(2)	σ_a(1)	σ_a(3)
$4 \cdot 10^3$	62	60.3	46.5	48.0
$1 \cdot 10^4$	58	53.7	42	43.2
$4 \cdot 10^4$	42.5	44.7	31	36.2
$1 \cdot 10^5$	34.5	39.6	23.5	32.1
$4 \cdot 10^5$	27	33.5	20.5	27.1
$1 \cdot 10^6$	23	30.5	18.5	26.2
$1 \cdot 10^7$	20	25.2	17.5	20.8
$1 \cdot 10^8$	-	22.3	-	17.9
$1 \cdot 10^9$	-	20.6	-	16.2

NOTES: (1) Figure 3.7.2.1.8(b), MIL-HDBK-5B
(2) Using Equation 6.2.1-3
(3) Using Equation 6.2.1-1

"notched" behavior. The designer should note that for the general case of alternating and mean stress loading two fatigue notch factors must be defined: one factor applying to the alternating stress and one factor applying to the mean stress. Since most sonic fatigue design problems do not require the consideration of an imposed static mean stress, the discussion here will consider only the prediction of "notched" fatigue life at zero mean stress with the consideration of mean stress effects left to the references (2). The prediction technique described here should be used by the designer only if "notched" specimen fatigue data is not available. Fortunately, much data is presented in MIL-HDBK-5B (4) and should be utilized by the designer.

6.2.2.1 Notched Specimen Fatigue Strength at Zero Mean Stress

In the absence of experimental data the "notched" fatigue strength of a material can be estimated using the concept of a "strength reduction factor," K_F, defined for a specific material at a specified life and a given "notch" configuration (2).

Following the work of Heywood (2), the strength reduction factor for a material at $N = 10^7$ cycles (taken as a limiting condition) is related to the static stress concentration factor, K_t, as

$$K_F = \sigma_a/\sigma_{an} = \frac{K_t}{1 + 2\frac{K_t - 1}{K_t}\left(\frac{a}{r}\right)^{1/2}} \qquad (6.2.2\text{-}1a)$$

where the constant "a" is termed the material "notch alleviation factor" and "r" is the radius of the notch. A high value of the material notch alleviation factor "a" implies that the stress concentration effect of a notch will be small (q is small).

The alternating stress in the notched specimen is related to the alternating stress in the plain specimen for $N = 10^7$ cycles as

$$\sigma_{an} = \left[1 + 2\frac{K_t - 1}{K_t}\left(\frac{a}{r}\right)^{1/2}\right]\sigma_a/K_t \quad \text{ksi} \qquad (6.2.2\text{-}1b)$$

Values for the notch alleviation factor "a" are given in Table 6.2.2-1 for various materials and notch configurations (2).

The above relations for a notched specimen are valid only at the life $N = 10^7$ cycles. It is now necessary to correct these estimates for an arbitrary value of N or $n = \log(N)$. Heywood (2) has continued an empirical evaluation of test data available (circa. 1962) to obtain the result

$$K_f = \sigma_a/\sigma_{an} = K_s + \frac{n^4}{b + n^4}(K_F - K_s) \qquad (6.2.2\text{-}2a)$$

where K_s is the static strength reduction factor = 1.0

K_F is obtained from Equation (6.2.2-1a)

b is a material constant evaluated in Table 6.2.2-2 for some common alloys (2)

$n = \log(N)$

The alternating stress in the notched specimen at a fatigue life of N cycles is related to the alternating stress in the plain specimen at a fatigue life of N cycles as

$$\sigma_{an} = \sigma_a / [K_s + \frac{n^4}{b + n^4} (K_F - K_s)] \quad \text{ksi} \qquad (6.2.2\text{-}2b)$$

$$n = \log(N)$$

For values of $n \geq 5$ it is permissible to set $K_s = 1.0$. If specific experimental data is not available, approximate K_s by 1.0. An example will illustrate the use of Equations (6.2.2-2) for estimating the notched fatigue strength of the material.

Example: Predict the notched fatigue life of 7075-T6 aluminum alloy sheet for the following data: $\sigma_t = 82.5$ ksi, r = 0.057 inches, $K_t = 4.0$ (values of r and K_t are selected so that predicted results can be compared to experimental results quoted in Figure 3.7.2.1.8(e) of MIL-HDBK-5B (4)).

From Tables 6.2.2-1 and 6.2.2-2 one determines the constants: $\sqrt{a} = (24/82.5)^3 = 0.0246$, $(\text{inches})^{1/2}$; b = 40.

From Equation (6.2.2-1a), one calculates $K_F = 3.464$. Supposing that the static strength reduction factor is known from experiment to be $K_s = 1.05$, then using Equation (6.2.2-2b) the alternating stress in the notched specimen, σ_{an}, at a fatigue life of N cycles is related to the alternating stress, σ_a, in the plain specimen at a fatigue life of N cycles as

$$\sigma_{an} = \sigma_a / [1.05 + (3.464 - 1.05) n^4 / (40 + n^4)] \quad \text{ksi}$$

$$\sigma_{an} = \sigma_a / [1.05 + 2.414\ n^4 / (40 + n^4)] \quad \text{ksi}$$

At $N = 10^6$ cycles, n = 6 and $\sigma_{an} = 0.295\ \sigma_a$. Now, the value of the alternating stress in the plain specimen can be taken from either the unnotched specimen experimental values or from the predicted unnotched specimen performance using the method of Section 6.2.1. From Table 6.2.1-2 at $N = 10^6$ cycles, the experimental value for σ_a is 23 ksi and the predicted value using Equation (6.2.1-3) is 30.5 ksi. Then, one obtains the predicted notch effect using experimental plain specimen data as

$$\sigma_{an} = 0.295\ (23) = 6.8 \text{ ksi} \quad \text{at } N = 10^6 \text{ cycles}$$

Using the predicted value of $\sigma_a = 30.5$ ksi, the predicted notch fatigue strength at 10^6 cycles is

$$\sigma_{an} = 0.295\ (30.5) = 9.0 \text{ ksi}$$

For comparison, the experimental value of the notched specimen of the fatigue strength at 10^6 cycles is $\sigma_{an} = 8.0$ ksi. To complete the example, the comparison is continued in Table 6.2.2-3 for fatigue strength estimate of the notched specimen of this example.

TABLE 6.2.2-1

VALUES OF NOTCH ALLEVIATION FACTOR, $\sqrt{a}$, TO BE USED WITH EQUATIONS (6.2.2-1) FROM REFERENCE 2

Notch Shape	Material	$\sqrt{a}$, (inches)$^{1/2}$
Transverse Hole	Steel	$5/\sigma_t$
Shoulder	Steel	$4/\sigma_t$
Groove	Steel	$3/\sigma_t$
All	Aluminum Alloys	$(24/\sigma_t)^3$
All	Magnesium Alloys	0.015
All	Titanium Alloys	very small (notch sensitive)

σ_t = ultimate tensile strength of the material in ksi

TABLE 6.2.2-2

VALUES OF THE CONSTANT b IN EQUATION (6.2.2-2) FROM REFERENCE 2

Steel Alloys	$(1750/\sigma_t)^2$
Aluminum Alloys: 7075-T6	25 to 40
2024-T3	60
Magnesium Alloys: (σ_t = 50 ksi)	80

σ_t = ultimate tensile strength of the material in ksi

TABLE 6.2.2-3

COMPARISON OF PREDICTED AND EXPERIMENTAL FATIGUE STRENGTH
OF NOTCHED 7075-T6 ALUMINUM ALLOY SHEET
σ_t = 82.5 ksi; K_t = 4.0; a = 0.025; b = 40

N	σ_a(1)	σ_a(2)	σ_{an}(3)	σ_{an}(4)	σ_{an}(5)
$4 \cdot 10^3$	62	60.2	20.7	20.1	20.1
$1 \cdot 10^4$	58	53.7	18.5	17.1	15.5
$4 \cdot 10^4$	42.5	44.7	13.0	13.7	12.0
$1 \cdot 10^5$	34.5	39.6	10.4	11.9	10.0
$4 \cdot 10^5$	27.0	33.5	8.0	10.0	-
$1 \cdot 10^6$	23.0	30.5	6.8	9.0	8.0
$1 \cdot 10^7$	20.0	25.2	5.8	7.4	5.0
$1 \cdot 10^8$	-	22.3	-	6.5	-
$1 \cdot 10^9$	-	20.6	-	6.0	-

NOTES: (1) From Figure 3.7.2.1.8(b), MIL-HDBK-5B

(2) Calculated using Equation (6.2.1-3)

(3) Calculated using Equation (6.2.2-2b) and σ_a from Column 1

(4) Calculated using Equation (6.2.2-2b) and σ_a from Column 2

(5) From Figure 3.2.2.1.8(e), MIL-HDBK-5B

6.2.3 OTHER FACTORS AFFECTING FATIGUE STRENGTH

The procedures described in Section 6.2.1 and 6.2.2 are presented to provide the designer techniques for predicting fatigue strength of steel and aluminum alloys in the absence of specific experimental data. The primary variables considered are the ultimate tensile strength of the material, the loading conditions described by constant amplitude alternating and mean stresses, the notch sensitivity of the material, and the fatigue life of the specimen. The accuracy of the prediction techniques is acceptable if experimental data is not available.

Other factors affecting the fatigue strength of the material include environmental factors such as thermal cycling, corrosive atmosphere, etc. For the sonic fatigue problem, the most important single factor affecting fatigue strength for long life designs (N greater than 10^7 cycles) is fretting between metal surfaces. Fretting fatigue results from a combination of stress concentration and corrosion of materials and can result in significant loss in fatigue strength. Alleviation of fretting fatigue effects has been attempted using "antifretting" compounds to decrease the fretting action between faying surfaces. Unfortunately, very little data is specifically available for design guidance so that the designer must search the literature for published results. Heywood (2) presents a basic description of fretting fatigue and early research efforts to alleviate the problem (See Section 5.4.2.1).

6.3 DATA SCATTER

The most common technique for obtaining constant amplitude fatigue data is to subject a set of test specimens to a constant amplitude alternating stress at a fixed frequency of oscillation and to observe the times at which the specimens fail. By varying the alternating stress amplitudes between sets of identical test specimens, a total set of failure points is established. For specimens tested at a constant alternating stress amplitude, the failures as described by the time of failure or more commonly the cycles to failure will not necessarily group together near a specific value of life. Hence, it is necessary to consider the statistical distribution of the failures. Unfortunately for the designer, it is very rare that a sufficient number of test specimens are available to completely define the statistics of the failure distribution.

A discussion of the consideration of data scatter and the complete statistical treatment of the subject must be left to the references (4), (5), (6). The conceptual treatment of the topic is appropriate so that the designer can appreciate the significance of fatigue data presented either as an S-N curve or a constant life diagram (4).

6.3.1 DISTRIBUTION OF FAILURES

Since data scatter in fatigue failures is a very real design consideration, the engineer must be concerned with the probability of failure associated with the determination of fatigue life of the structure. The probability of failure implies that the observed failures are scattered about some median value. Figure 6.3.1-1 illustrates, conceptually, the distribution of failures for the distribution when designing for a fatigue limit, designing for a specified life, and designing for a specified fatigue strength at a finite life (6).

When designing a structure for the fatigue limit, special considerations must be taken in the data analysis to determine the statistical aspects of the failure distribution since it is necessary to compare both the applied stress distribution to the fatigue strength distribution (5). This aspect

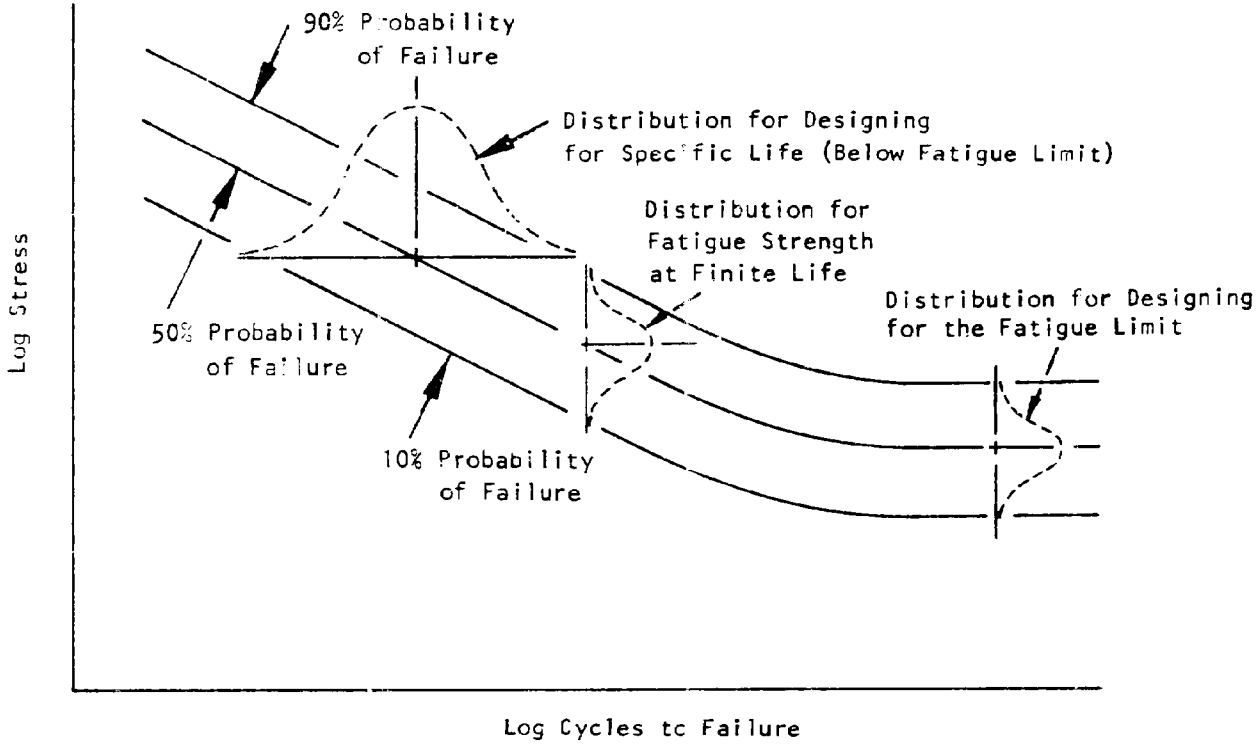

FIGURE 6.3.1-1 FATIGUE DATA SCATTER AND FAILURE DISTRIBUTIONS IMPORTANT TO FATIGUE DESIGN

of data scatter is very important to the sonic fatigue problem in that the design is almost always related to long life (N greater than 10^8 cycles). The discussion here becomes somewhat academic in that fatigue data is rarely generated beyond 10^7 cycles so that there is simply no data available to establish confidence!

It is standard practice to present only the median value of 50% probability of failure when plotting S-N data. That is, using either the prediction techniques of Section 6.2 or published fatigue data, the designer can expect, for example, that 50% of the specimens will fail before the indicated fatigue life. If enough failure data is available, it is possible to establish confidence limits (5), (7) to indicate the scatter of fatigue data (see Figures 5.3.1-2 and 5.3.1-3, for example) so that the designer can establish confidence in his design.

The distribution of fatigue failures about the mean value may not be Gaussian (5), (6), (7) so that other distributions may have to be used. One such distribution is called the Weibull distribution (8) and its use for establishing probability of failure of fatigue data is becoming more widespread. A comparison between the log-normal distribution and the Weibull distribution as the underlying distributions associated with sonic fatigue failure data is reported by Berens and West (9).

6.4 CUMULATIVE DAMAGE THEORIES

The prediction methods presented in Section 6.2 relate to the fatigue performance of either plain or notched material specimens loaded by a fixed combination of alternating and mean stress until the specimen fails. Such loading is occasionally encountered in machine design and almost never encountered in sonic fatigue design. The objective of any fatigue analysis is to determine an acceptable combination of imposed loading and structural life. To account for variable loading amplitudes and combinations or a loading spectrum, the concept of a damage function has been developed. The concept of a damage function or the term "fatigue damage" describes the gradual deterioration of a metal during cyclic straining with the damage function being zero for the virgin material and usually normalized to unit value at failure. As such, a damage function describes in a rather vague manner the fatigue characteristics of a specimen with no direct technique available to assess experimentally the "damage" between the end states.

Cumulative damage theories attempt to relate the accumulation of fatigue damage as referenced to the loading process. All methods relate to a specific set of S-N data for each specimen type with the different methods emphasizing various aspects of representing either the loading spectrum or the S-N data or both the loading spectrum and the S-N data. Osgood (1) presents a very thorough discussion of cumulative damage theories and their application to design. Osgood (1) classifies these theories as linear cumulative damage theories, nonlinear cumulative damage theories, and damage boundary techniques. Table 6.4.0-1 presents a summary of the various cumulative damage theories classified according to Osgood with the specific references

TABLE 6.4.0-1

CLASSIFICATION OF CUMULATIVE DAMAGE THEORIES
(REFERENCE 1)

LINEAR CUMULATIVE DAMAGE THEORIES	
Method or Theory	Reference
Miner's Rule	(10)
RCA Method	(1)
Lundberg's FFA Method	(11)
Shanley's IX Method	(12)
Langer's Method and Grover's Method	(13), (14)
Smith's Method	(15)
NONLINEAR CUMULATIVE DAMAGE THEORIES	
Method or Theory	Reference
Carter-Dolan Method	(6), (16)
Shanley's 2X Method	(1)
Henry's Method	(17)
DAMAGE BOUNDARY TECHNIQUES	
Stress Concentration Method	(1)
Fatigue Quality Index Method	(1)
Freudenthal and Heller Method	(18)
Mares and Starkey Method	(19)
Kommers Hypotheses	(20)
Richart and Newmark Method	(21)

quoted. The interested reader should refer to the complete discussion presented by Osgood (1) and to the specific references.

6.4.1 EVALUATION OF CUMULATIVE DAMAGE THEORIES

It is fortunate that the several methods proposed to predict the accumulation of fatigue damage have been evaluated for accuracy and ease of utilization in practical design problems (22). This evaluation was based upon comparing predicted fatigue life to experimental fatigue life to assess the degree of conservatism associated with each method. Based upon stress a similar evaluation was conducted to evaluate conservatism. The conclusions of this evaluation were that Miner's linear cumulative damage method is a very practical and versatile method at estimating fatigue life and that its accuracy was comparable to other more complicated techniques and is commensurate with uncertainties associated with the loading history and the S-N data.

6.4.2 MINER'S LINEAR CUMULATIVE DAMAGE RULE

Miner (10) proposed that fatigue damage of a metallic material under cyclic stress was related to the net work absorbed by the specimen and that the rate of damage accumulation was linearly proportional to the number of cycles at a stress level and independent of the stress level. The incremental damage resulting from n_i cycles at a stress level σ_i is then $n_i/N(\sigma_i)$ where $N(\sigma_i)$ is the number of cycles to failure at the stress level σ_i as given by a constant amplitude S-N curve or a constant life fatigue diagram.

According to Miner's rule, failure occurs when the accumulated damage is unity. Mathematically, Miner's rule is given as

$$\sum_i n_i/N(\sigma_i) = 1.0 \qquad (6.4.2\text{-}1)$$

Hence, to use Miner's rule in design practice, the designer needs to know the loading spectrum as a set of values (n_i, σ_i) and the S-N curve of the material.

An alternate form of Miner's rule, as expressed by Equation (6.4.2-1) and slightly more useful for design, is obtained by defining the total number of cycles to failure as

$$N_T = \sum_i n_i \quad \text{cycles to failure} \qquad (6.4.2\text{-}2)$$

and introducing the factor $\alpha_i = n_i/N_T$ one obtains Miner's rule in the form

$$N_T \sum_i \alpha_i/N(\sigma_i) \quad 1.0 \qquad (6.4.2\text{-}3a)$$

or

$$\sum_i \alpha_i / N(\sigma_i) = 1/N_T \qquad (6.4.2\text{-}3b)$$

The utility of Equations (6.4.2.3) as compared to Equation (6.4.3-1) is that the estimation of the number of cycles n_i at a stress level σ_i may not be conveniently determined whereas the percentage of total life at a stress level σ_i, as expressed by $\alpha_i = n_i/N_T$, may be rather easily estimated.

Additionally, the designer may introduce a "factor of safety" into Equations (6.4.2-1) and (6.4.2-3) by somewhat arbitrarily setting the value of 1.0 on the right hand side to some number less than 1.0, say 0.8. The designer must also be aware of the fact that Miner's rule is not strictly applicable for applied stresses near the fatigue limit of the material even though its use in this range is quite common (1), (10).

Example: Using Miner's cumulative damage rule estimate the fatigue life of a plain and a notched ($K_t = 2.0$) specimen of 7075-T6 aluminum alloy (ultimate tensile strength 82.5 ksi) for the following loading spectrum: $\sigma_1 = \pm 30$ ksi for 20% of the time ($\alpha_1 = 0.20$), $\sigma_2 = \pm 25$ ksi for 30% of the time, and $\sigma_3 = \pm 20$ ksi for 50% of the time.

Using the techniques of Section 6.2.2 ($K_t = 2.0$, $\sqrt{a} = (24/82.5)^3$, $b = 40$, $r = 0.057$, $K_s = 1.05$) the fatigue life for the two material conditions were predicted as follows:

Load Spectrum		Fatigue Life, $N(\sigma_i)$	
α_i	σ_i, ksi	Plain Specimen	$K_t = 2.0$
0.20	30	10^6	$1.2 \cdot 10^4$
0.30	25	10^7	$5.0 \cdot 10^4$
0.50	20	10^9	$1.4 \cdot 10^5$

Then, for the plain specimen, using Equation (6.4.2-3a)

$$N_T(0.20/10^6 + 0.30/10^7 + 0.50/10^9) = 1.0$$

$$2.305 \cdot 10^{-7} N_T = 1.0$$

$$N_T = 4.34 \cdot 10^6 \text{ cycles to failure}$$

For the notched specimen, using Equation (6.4.2-3a)

$$N_T(0.20/1.2\cdot10^4 + 0.30/5.0\cdot10^4 + 0.50/1.4\cdot10^5) = 1.0$$

$$2.64\cdot10^{-5}\ N_T = 1.0$$

$$N_T = 3.81\cdot10^4 \text{ cycles to failure}$$

Hence, the significance of a stress concentration on fatigue life is very evident since the notched specimen can be expected to exhibit less than one percent of the life of a plain specimen when exposed to the same loading environment.

6.5 RANDOM LOAD FATIGUE CURVES

Using the results of Section 6.2 or, preferably, available experimental data, the designer can determine the fatigue life of a material configuration when exposed to constant amplitude stress loading. From Section 6.3, the designer can realize that data scatter should be considered to attempt to establish some estimate for the probability of failure and the significance of this aspect to the design of his structure (1). Using Miner's rule, as described in Section 6.4, the designer can account for the effect of a loading spectrum comprised of variable amplitude stresses. This section describes techniques required to estimate the fatigue life of a material configuration exposed to a loading spectrum of random amplitude stresses as encountered in sonic fatigue design problems.

Even though this section presents analytical techniques for "converting" constant amplitude S-N curves to the so-called "equivalent random amplitude" S-N curves, the designer should always remember that - as all analytical techniques - the result is approximate (see Section 6.2). Fortunately, the approximation tends, in general, to be conservative (i.e., predict lower fatigue life than that observed by experiment). Historically, the conversion techniques described were developed in the early days of sonic fatigue design to utilize the vast quantity of constant amplitude S-N data available and to convert sonic fatigue test data obtained from discrete frequency siren testing to more realistic broad band acoustic excitation (23), (24), (25). At that time (1955-1960), the experimental facilities did not exist to generate random amplitude S-N data and the need for such data in design use was so urgent that the early investigators developed the techniques described here.

Since 1960, the experimental facilities for testing materials under random amplitude loading (both for vibratory input such as coupon testing and broad band random acoustic sources for complete structural specimen tests) have been developed. The designer should now place emphasis upon using random amplitude S-N data obtained by experiment in preference to the estimates obtained using the results of this section. Experimental random load fatigue curves that have been reported in the literature are presented in Section 6.6.

6.5.1 EQUIVALENT RANDOM LOAD FATIGUE CURVES

Two techniques have been discussed in the literature (26) that are suitable for converting S-N data obtained by conventional test techniques into equivalent random amplitude S-N curves suitable for design use. The suitability of either method is of course determined in the sense that the designer may not have the experimental random load fatigue data available when it is needed.

One technique, called the β-method, requires that the designer have available S-N data for the material obtained by testing the specimen under a two-level variable cycle block loading (1), (6). The β-method was developed by Fuller (27), and assuming the availability of basic S-N data, the method can be used to obtain rather accurate estimates of the random amplitude S-N characteristics of the material (26). Since two-level variable cycle block loading S-N data may not be readily available to the designer, the β-method has not been widely used in sonic fatigue design.

The other technique (26) was apparently initiated by Miles (28) and is briefly discussed in Section 5.1 of this report. The application of this technique in relation to sonic fatigue design by Belcher, et al. (23), McGowan (24), Fitch (25), and Cote (26) is discussed here. The utility is that the designer need only to have available conventional constant amplitude S-N data for the material and be able to perform a numerical integration. Due to the somewhat lengthy calculations, it is advisable to code the method for digital computation (24) especially if design data for several materials is required. Details of the method are not presented (25).

Assuming that random stress peaks follow a Rayleigh probability distribution (see Section 5.1) and that the fatigue damage accumulates according to Miner's cumulative damage rule (see Section 6.4), the probable number of cycles of random stress having an amplitude in the range (s, s + ds) in a time interval T for a narrow band random Gaussian stress time history is

$$n(s) = f_n T p(s) ds \qquad s \geq 0 \tag{6.5.1-1}$$

where $p(s) = \frac{s}{\sigma^2} \exp(-s^2/2\sigma^2)$ is the Rayleigh probability density function with a mean square stress, σ^2.

From Miner's cumulative damage rule, the expected or probable damage resulting from stress peaks in the range (s, s + ds) with a frequency f_n for a time period T is

$$\frac{n(s)}{N(s)} = f_n T \frac{p(s)ds}{N(s)} \tag{6.5.1-2}$$

where N(s) is the number of cycles to failure at the stress level, s, obtained from a constant amplitude S-N curve. Noting that the total number of cycles to failure at a random amplitude stress level, σ, is simply $N_r(\sigma) = f_n T$ and that the possible random amplitude stress values cover

the range ($0 \leq \sigma \leq \infty$), Miner's failure criteria becomes

$$N_r(\sigma) = \left[\int_0^\infty \frac{p(s)}{N(s)}\, ds\right]^{-1} \qquad (6.5.1\text{-}3)$$

Since N(s) is known from experiment, any convenient numerical integration of the right hand side of Equation (6.5.1-3) can be repeated for several values of the rms stress, σ, to generate a random amplitude fatigue curve. In particular, the integration in Equation (6.5.1-3) can be written in dimensionless form as

$$\int_0^\infty \frac{p(s)ds}{N(s)} = \int_0^\infty x \exp(-x^2/2)dx/N(x) \qquad (6.5.1\text{-}4)$$

where $x = s/\sigma$ is the ratio of the random amplitude stress to the rms value of the random amplitude stress. The designer will find Figure 5.1.1-8 helpful in performing hand calculations for occasional conversions of constant amplitude S-N data into equivalent random amplitude S-N data. A tabular form is presented by Fitch (25) to assist the designer in performing the numerical integration by hand.

Equivalent random amplitude fatigue curves have been obtained by McGowan (19) and are presented in Figure 6.5.1-1 in the rather unusual form of a relative strength in dB versus log cycles to failure. Figure 6.5.1-1 is presented for reference, the designer should first consult Section 6.6 or his company's data for experimental random S-N curves.

To indicate the relative differences between an equivalent random loading fatigue curve and an experimental random load fatigue curve, one of the results obtained by Phillips (29) is presented in Figure 6.5.1-2. This figure presents a comparison between constant amplitude data, random amplitude data, and predicted random load fatigue characteristics of notched Rene' 41 coupon specimens. These results are typical in that the random loading S-N curve predicts failure sooner than the constant amplitude S-N curve and that the predicted equivalent random loading S-N curves yield the most conservative results. Basing the predictions upon either the measured peak stress distribution or on an assumed Rayleigh peak stress distribution yields approximately the same results. Schjelderup and Galef (30) present an assessment of the assumption of the Rayleigh peak stress distribution for a broad set of random fatigue data concluding that the Rayleigh distribution of peak stresses is a good approximation. Phillips (29) confirms this result (See Figure 6.5.1-2) and also discusses the general experimental confirmation of the Palmgren-Miner cumulative damage rule as applied to various common aircraft materials.

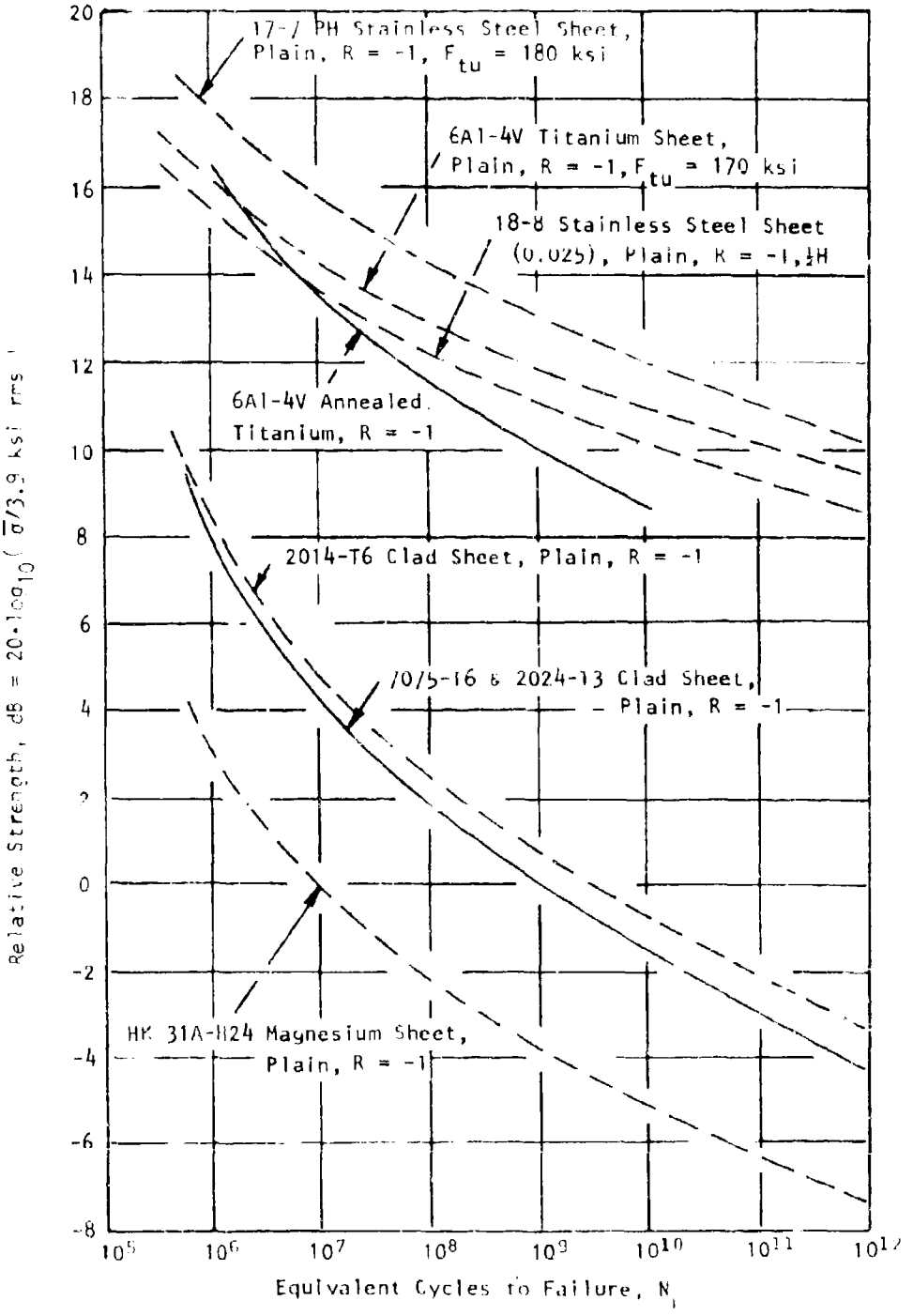

FIGURE 6.5.1-1 EQUIVALENT RANDOM LOADING FATIGUE CURVES FOR SEVERAL AIRCRAFT MATERIALS

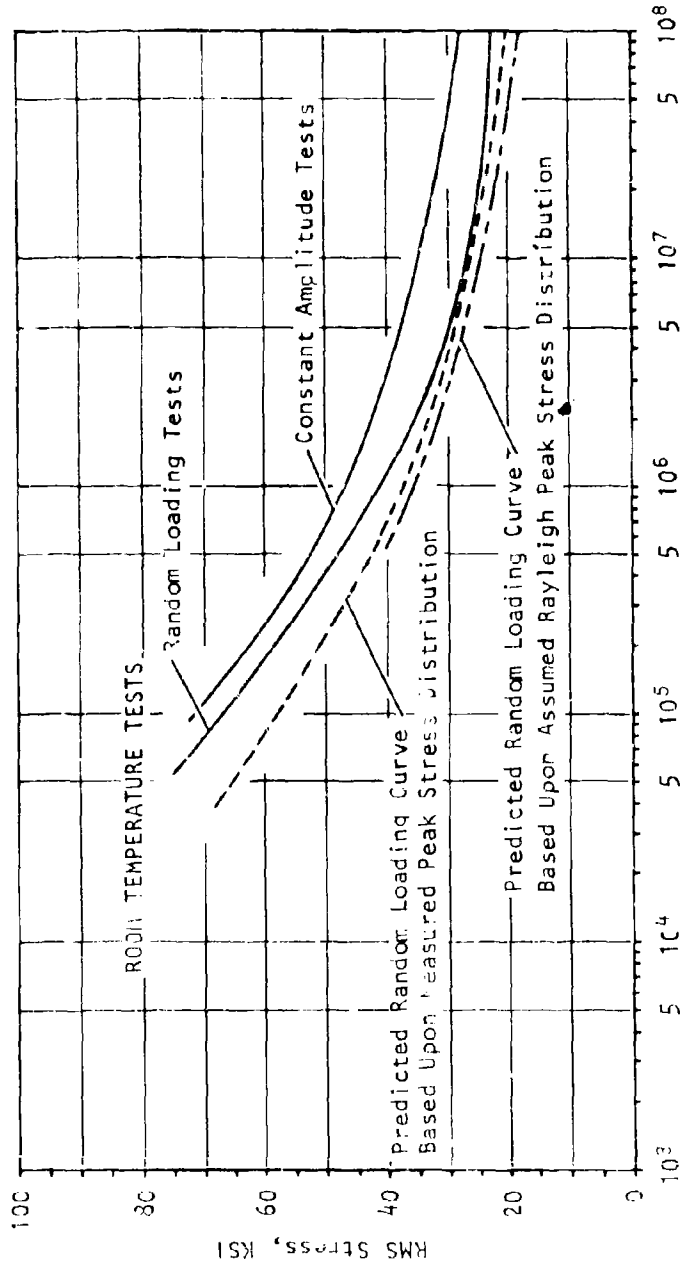

FIGURE 3.5.1-2 COMPARISON OF RESULTS OF RANDOM LOADING TESTS, CONSTANT AMPLITUDE TESTS, AND THEORETICAL PREDICTIONS: SHARPLY NOTCHED RENE' 41 SHEET

6.6 DOCUMENTED FATIGUE CURVES

The previous discussion has been focused upon the parameters describing fatigue strength, data scatter, cumulative damage theories, and equivalent random load fatigue curves. The designer will find this discussion useful for the general application of fatigue data reported in the literature to sonic fatigue design problems. If the structural configuration being considered does not correspond to the structural designs presented in Section 5.3, then the designer is forced to base the structural parameters upon the analysis techniques presented in Sections 5.1 and 5.2. The results of these two sections must be modified to account for joint design details and stress concentration factors as discussed in Sections 5.4 and 5.5. Finally, the fatigue life of the structure is estimated using available random loading fatigue curves.

The designer must always remember that two types of random loading fatigue curves are encountered in practice: equivalent random load fatigue curves obtained by converting constant amplitude sinusoidal fatigue data as described in Section 6.5 and experimental random load fatigue data. Also, the designer should verify the specimen configuration upon which the experimental data is based (i.e., configuration or stress concentration effects) before applying these results to his particular design. This section presents fatigue data reported in the literature associated with sonic fatigue tests of aircraft structural test specimens, random amplitude coupon test specimens, and equivalent random load fatigue data.

The method of presenting this documented fatigue data is to plot stress in ksi (units of 1000 psi) rms versus cycles to failure with both axes being logarithmic scales. This choice is prompted as a result of the fact that most of the experimental data is expressed in this form with a least-square linear regression line established for the data. For some of the data, confidence limits have been established by the original author and have been reproduced in the curves presented here to indicate the range of data scatter. For consistency, a format has been adopted which allows the fatigue curve and its description to be presented on one page. The reference is presented for each curve so that the designer can locate the original source if required. Generally, failure points have not been plotted.

This section is subdivided according to material type. Accordingly, some sections contain more data than others with aluminum alloys being, obviously, the most thoroughly documented section. Within each material classification the fatigue data is presented with plain specimen data, notched specimen data, and joint data being presented in that order. Due to the lack of specific data for some materials and configurations, the presentation is not complete; however, the format adopted here will allow the designer to introduce additional data as it becomes available without disrupting the main organization.

6.6.1 ALUMINUM ALLOYS

This section presents 13 random amplitude fatigue curves describing the S-N characteristics of various aluminum alloys and joint configurations. Data derived from both coupon fatigue tests and sonic fatigue tests of structural configurations are presented. Plain specimen coupon data, plain hole (mushroom head) riveted joint data and countersunk (both cut and dimpled) riveted joint data are presented. Data describing the effect of viscoelastic jointing compounds and antifretting compounds are presented. The text above each S-N curve describes the material, the specimen configuration, the test temperature, the reference for the source and notes generally cross-referencing the S-N data with other data presented in the handbook.

ALUMINUM ALLOYS

MATERIAL: 2024-T6 Clad Aluminum Sheet
VES(AL)504 Unclad Aluminum (2618-T6)

CONFIGURATION: Plain cantilever coupon test specimens with transverse random amplitude vibratory base excitation were used for the 2024-T6 clad material. Machined "T" section beams with transverse random amplitude vibratory excitation of the flange to obtain "skin" failures and tip excited free-free beam modes to obtain "flange" failures were used for the VES(AL)504 unclad material.

TEST TEMPERATURE: Room Temperature

REFERENCE: Thompson, A. R. G., and Lambert, R. F., "Acoustic Fatigue Design Data, Part II," AGARD-AG-162-Part II, 1972, Figure 1.3.

NOTES: VES(AL)504 aluminum alloy is comparable to the U. S. designation 2618-T6.

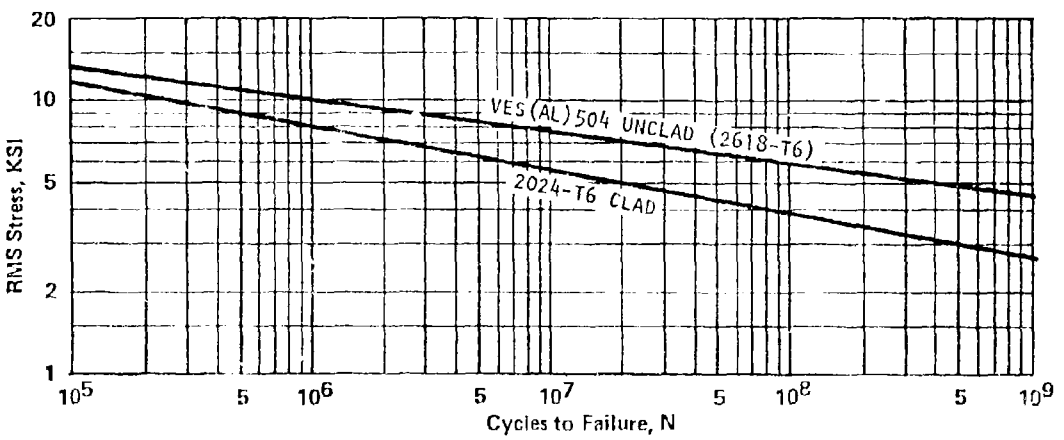

FIGURE 6.6.1-1 COUPON S-N DATA FOR PLAIN 2024-T6 CLAD SHEET AND 2618-T6 MACHINED STIFFENER SPECIMENS

ALUMINUM ALLOYS

MATERIAL: 3.1364.5 (2024-T3), Sheet
CM001-1D (2618-T6), Sheet
D.T.D. 710 (2014-T4 or 2024-T4), Sheet

CONFIGURATION: Coupon specimens with transverse random vibratory base excitation introduced to the "skin" specimen through a riveted "rib." angle ribs were used for single rivet row tests (plain holes with mushroom head rivets) and "T" section ribs were used for double rivet row tests (cut countersunk holes with flush head rivets). No jointing compounds or antifretting compounds were used.

TEST TEMPERATURE: Room Temperature

REFERENCE: Thompson, A. R. G., and Lambert, R. F., "Acoustic Fatigue Design Data, Part II," AGARD-AG-162, Part II, 1972, Figures 1.4 and 1.5.

NOTES: The British alloy designations and the comparable U. S. designations are 3.1364.5/2024-T3, CM001-1D/2618-T6, and D.T.D. 710/2014-T4 or 2024-T4.

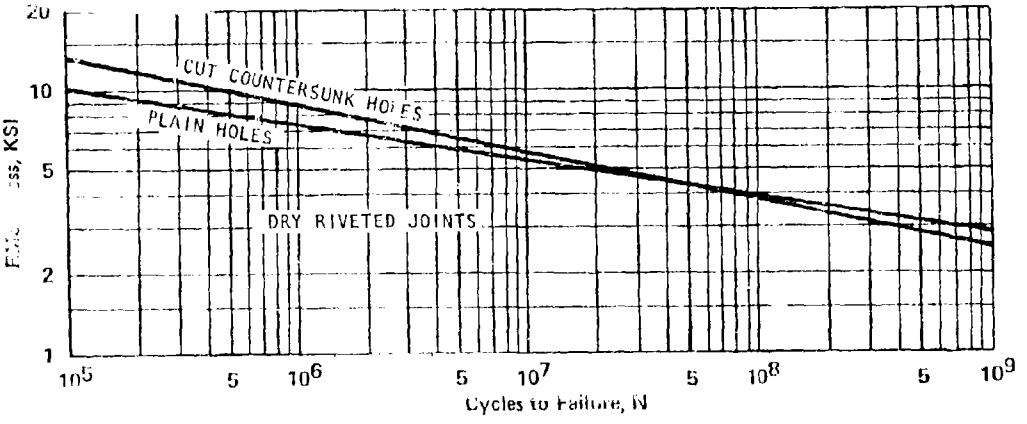

FIGURE 6.6.1-2 COUPON S-N DATA FOR DRY RIVETED JOINTS WITH PLAIN HOLES AND CUT COUNTERSUNK HOLES - VARIOUS ALUMINUM ALLOYS

ALUMINUM ALLOYS

MATERIAL: D.T.D. 5070 (2618-T6), Sheet
P.T.D. 710 (2014-T4 or 2024-T4), Sheet
3.1364.5 (2024-T3), Sheet

CONFIGURATION: Coupon specimens with transverse random vibratory base excitation introduced to the "skin" specimen through a riveted angle "rib." A single row of plain mushroom head rivets were utilized for the joint. Viscoelastic jointing compounds and antifreeting compounds were used.

TEST TEMPERATURE: Room Temperature

REFERENCE: Thompson, A. R. G., and Lambert, R. F.; "Acoustic Fatigue Design Data, Part II," AGARD-AG-162, Part II, 1972. Figures 1.6 and 1.7.

NOTES: Compare with Figures 6.6.1-4 and 6.6.1-5.

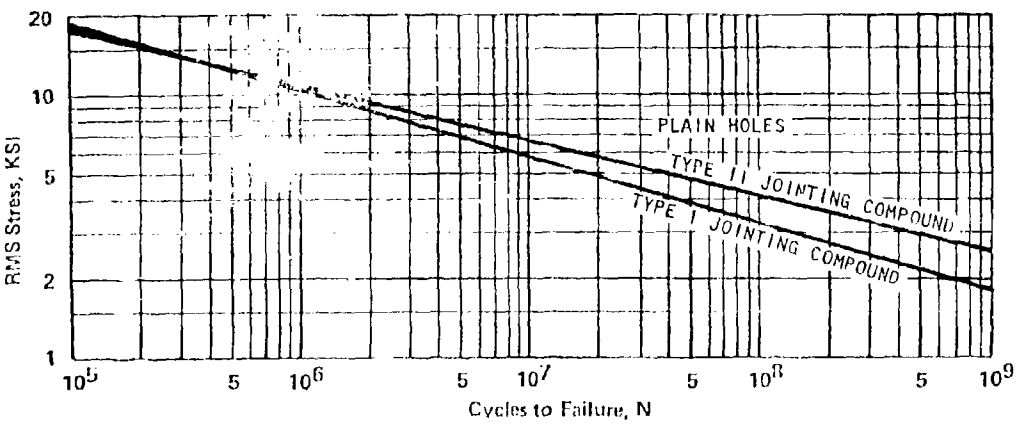

FIGURE 6.6.1-3 COUPON S-N DATA FOR RIVETED JOINTS WITH PLAIN HOLES USING VISCOELASTIC JOINTING COMPOUNDS - VARIOUS ALUMINUM ALLOYS

ALUMINUM ALLOYS

MATERIAL: D.T.D. 710 (2014-T4 or 2024-T4), Sheet
D.T.D. 746 (2014-T6 or 2024-T6), Sheet
D.T.D. 5070 (2618-T6), Sheet
CM1001-1D (2618-T6), Sheet

CONFIGURATION: Coupon specimens with transverse random vibratory base excitation introduced to the "skin" specimen through a rivited rib. Both single and double rows of cut countersunk flush head riveted joints tested using both solid and blind rivets. Viscoelastic jointing compounds and antifretting compounds were used in the tests.

TEST TEMPERATURE: Room Temperature

REFERENCE: Thompson, A. R. G., and Lambert, R. F.; "Acoustic Fatigue Design Data, Part II," AGARD-AG-162, Part II, 1972. Figures 1.8 and 1.9.

NOTES: Compare with Figures 6.6.1-3 and 6.6.1-5.

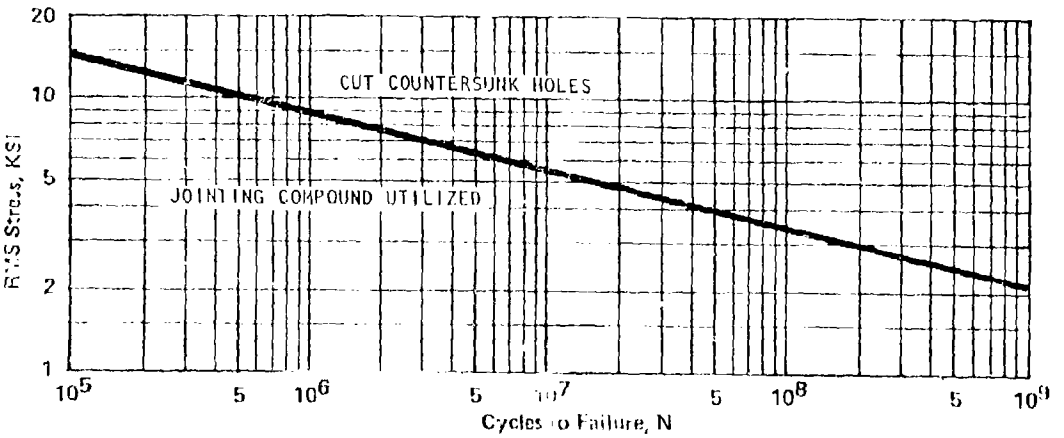

FIGURE 6.6.1-4 COUPON S-N DATA FOR RIVETED JOINTS WITH CUT COUNTERSUNK HOLES USING VISCOELASTIC JOINTING COMPOUNDS - VARIOUS ALUMINUM ALLOYS

ALUMINUM ALLOYS

MATERIAL: D.T.D. 710 (2014-T4 or 2024-T4), Sheet
3.1364.5 (2024-T3), Sheet

CONFIGURATION: Coupon specimens with transverse random vibratory base excitation introduced to the "skin" through a riveted angle "rib." A single row of hot-pressure-dimpled flush head rivets was used to form the joint. Both plain joint (3.1364.5 material) and joints with viscoelastic jointing compounds (D.T.D. 710 material) were tested.

TEST TEMPERATURE: Room Temperature

REFERENCE: Thompson, A. R. G., and Lambert, R. F.; "Acoustic Fatigue Design Data, Part II," AGARD-AG-102, Part II, 1972. Figures 1.10 and 1.11.

NOTES: Compare with Figures 6.6.1-3 and 6.6.1-4.

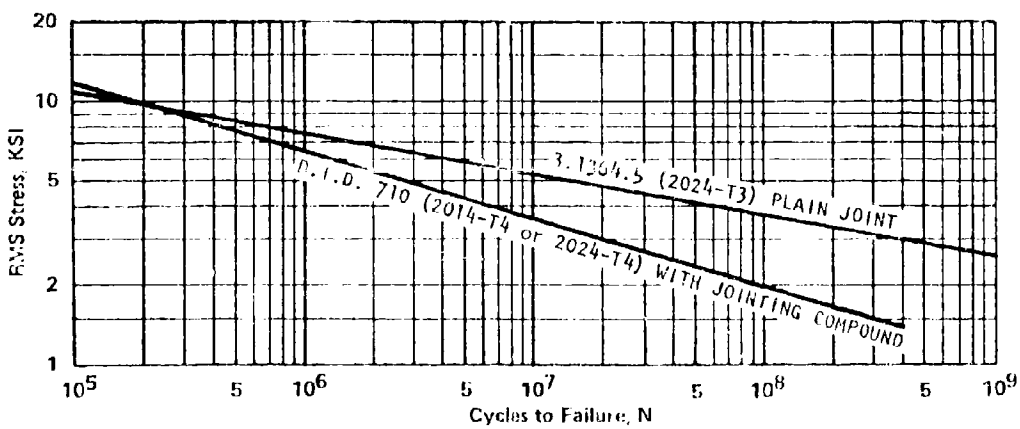

FIGURE 6.6.1-5 COUPON S-N DATA FOR RIVETED JOINTS WITH HOT-PRESSURE-DIMPLED HOLES WITH AND WITHOUT VISCOELASTIC JOINTING COMPOUNDS - VARIOUS ALUMINUM ALLOYS

ALUMINUM ALLOYS

MATERIAL: D.T.D. 710 (2014-T4 or 2024-T4), Sheet
D.T.D. 5070 (2618-T6), Sheet

CONFIGURATION: Coupon specimens with transverse random vibratory base excitation introduced to the "rib" specimen through a riveted joint with the "skin." Failure originated in the flange bend radius. S-N curves include data both for plain holes with mushroom head rivets and hot-pressure-dimpled flush head rivets and plain joints and joints with a viscoelastic jointing compound.

TEST TEMPERATURE: Room Temperature

REFERENCE: Thompson, A. R. G., and Lambert, R. F.; "Acoustic Fatigue Design Data, Part II," AGARD-AG-162, Part II, 1972. Figures 1.12 and 1.13.

NOTES: Compare with Figure 6.6.1-12.

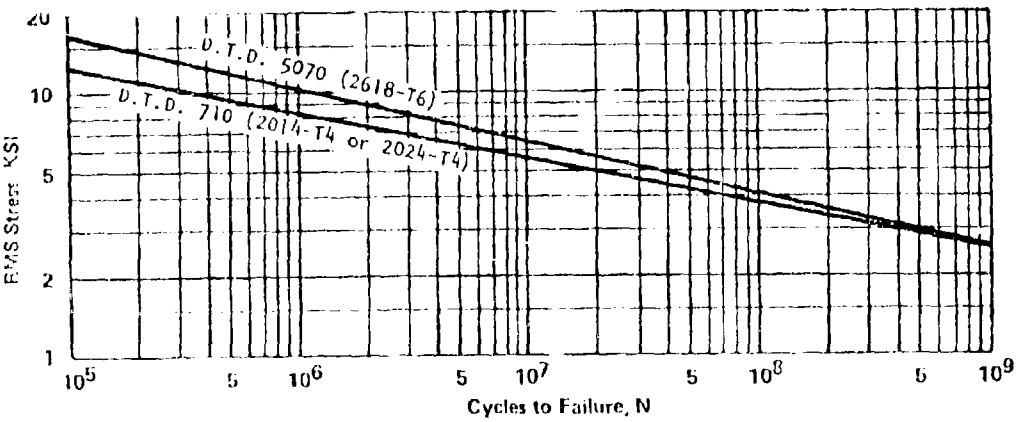

FIGURE 6.6.1-6. COUPON S-N DATA FOR RIB FLANGES - 2024-T4 AND 2618-T6 ALUMINUM ALLOYS

ALUMINUM ALLOYS

MATERIAL: 7075-T6, Sheet

CONFIGURATION: Cantilever coupon test specimens with transverse random amplitude vibratory base excitation. Both plain specimens and cut countersunk riveted specimens tested.

TEST TEMPERATURE: Room Temperature

REFERENCE: Schneider, C. W.; "Acoustic Fatigue of Aircraft Structures at Elevated Temperatures," AFFDL-TR-73-155, Part I, Air Force Flight Dynamics Laboratory, Wright-Patterson Air Force Base, Ohio, 1974. Figure 16 a), page 39.

NOTES: See Figure 5.3.1-5

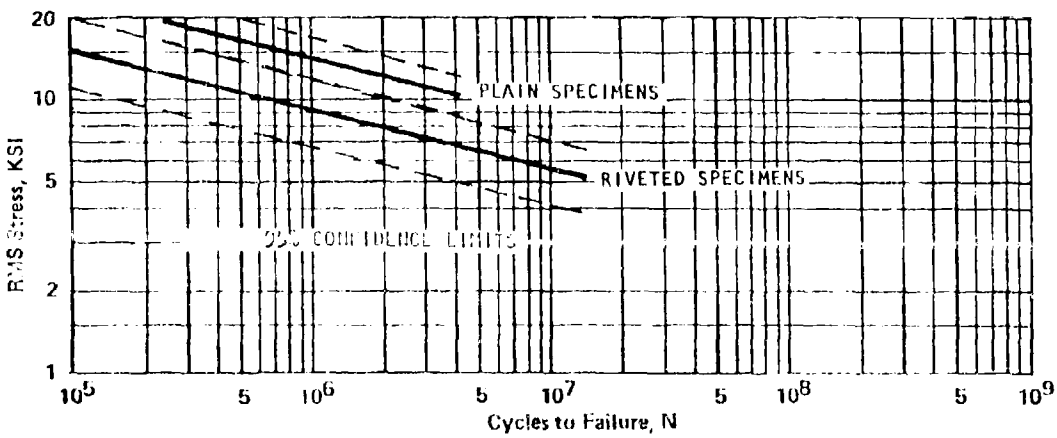

FIGURE 6.6.1-7 COUPON S-N DATA FOR PLAIN AND CUT COUNTERSUNK RIVETED 7075-T6 SPECIMENS AT ROOM TEMPERATURE

ALUMINUM ALLOYS

MATERIAL: 7075-T6, Sheet

CONFIGURATION: Cantilever coupon test specimens with transverse random amplitude vibratory base excitation. Both plain specimens and cut countersunk riveted specimens tested.

TEST TEMPERATURE: 300°F

REFERENCE: Schneider, C. W.; "Acoustic Fatigue of Aircraft Structures at Elevated Temperatures," AFFDL-TR-73-155, Part I, Air Force Flight Dynamics Laboratory, Wright-Patterson Air Force Base, Ohio, 1974. Figure 16 b), page 39.

NOTES: See Figure 5.3.1-5

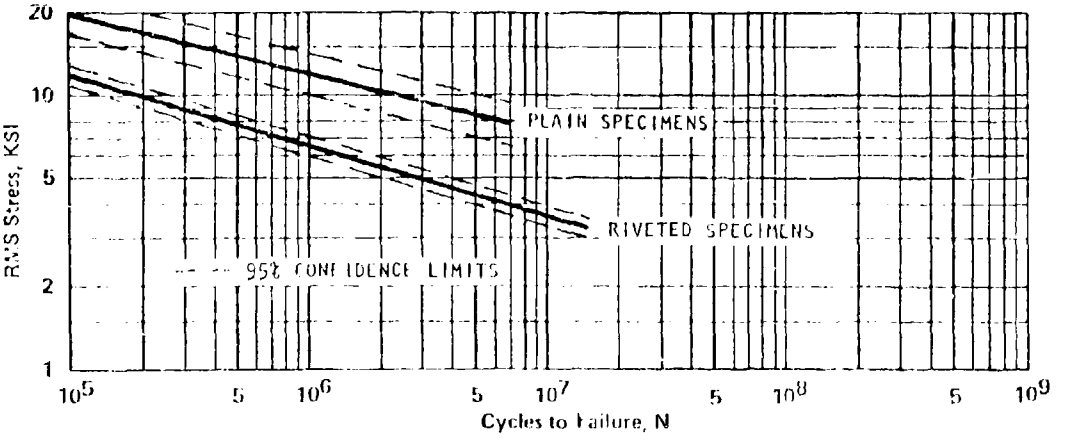

FIGURE 6.6.1-8 COUPON S-N DATA FOR PLAIN AND CUT COUNTERSUNK RIVETED 7075-T6 SPECIMENS AT 300°F

ALUMINUM ALLOYS

MATERIAL: 7075-T6, Sheet

CONFIGURATION: Coupon specimens with transverse random vibratory base excitation introduced to the "skin" specimen through an angle "rib" attached to the skin specimen by a weldbonded joint (See Section 5.4.3.4). A single row of two weldbonded spots joined the "skin" and "rib." Thickness of the coupon simulating the skin was 0.032 inch and 0.040 inch. Both bond failures and weld failures were recorded for the first two vibration modes.

TEST TEMPERATURE: Room Temperature

REFERENCE: Private communication; O. F. Mauer, Aero-Acoustics Branch, Air Force Flight Dynamics Laboratory, Wright-Patterson Air Force Base.

NOTES: See Section 5.4.3.4 for a discussion of the weldbond jointing process.

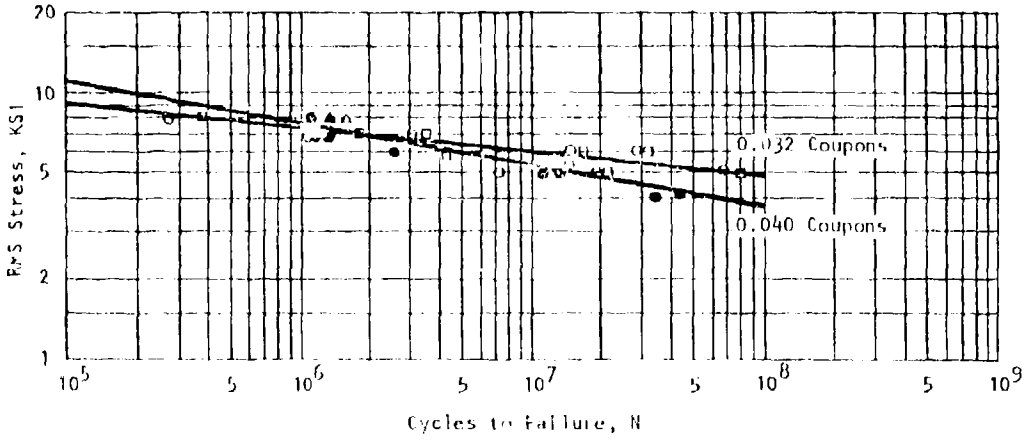

0.032 Inch Thick Specimens

- □ 1st Mode Bond Failure (30 Hz)
- △ 1st Mode Outer Skin Failure (30 Hz)
- ○ 2nd Mode Bond Failure (207 Hz)
- ▫ 2nd Mode Weld Failure (207 Hz)

0.040 Inch Thick Specimens

- ▲ 1st Mode Bond Failure (32 Hz)
- ● 2nd Mode Bond Failure (235 Hz)

FIGURE 6.6.1-9 COUPON S-N DATA FOR WELDBONDED JOINTS

ALUMINUM ALLOYS

MATERIAL: 7075-T6, Sheet

CONFIGURATION: Flat nine bay stiffened panel specimens exposed to broad band random acoustic excitation. Stress measured at the mid-span of the long side of the center bay rivet line. Cut countersunk flush head rivets used to join skin and stiffener. No jointing or anti-fretting compound used.

TEST TEMPERATURE: Room Temperature

REFERENCE: Ballentine, J. R., et. al.; "Refinement of Sonic Fatigue Structural Design Criteria," AFFDL-TR-67-156, Air Force Flight Dynamics Laboratory, Wright-Patterson Air Force Base, Ohio, Jan. 1968.

NOTES: See Figures 5.3.1-2 and 5.3.2-7

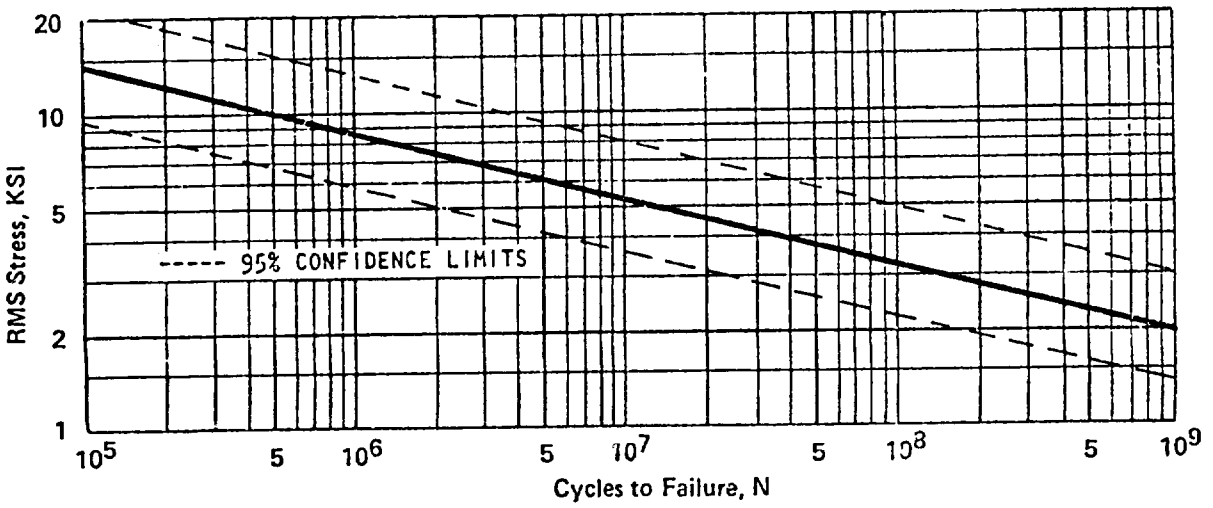

FIGURE 6.3.1-10 S-N DATA FOR 7075-T6 SHEET WITH CUT COUNTERSUNK RIVETED JOINTS - STIFFENED PANEL SONIC FATIGUE TEST SPECIMENS

ALUMINUM ALLOYS

MATERIAL: 7075-T6, Sheet

CONFIGURATION: Flat nine bay stiffened panel specimens exposed to broad band random acoustic excitation. Stress measured on stringer flange at clip connection to frame. Stringer manufactured from brake formed flat sheet stock, heat treated, and straightened using standard aircraft manufacturing practice.

TEST TEMPERATURE: Room Temperature

REFERENCE: Rudder, F. F., Jr., "Acoustic Fatigue Resistance of Aircraft Structural Component Assemblies," AFFDL-TR-71-107, Air Force Flight Dynamics Laboratory, Wright-Patterson Air Force Base, Ohio, Sept. 1971.

NOTES: See Figure 5.3.1-3

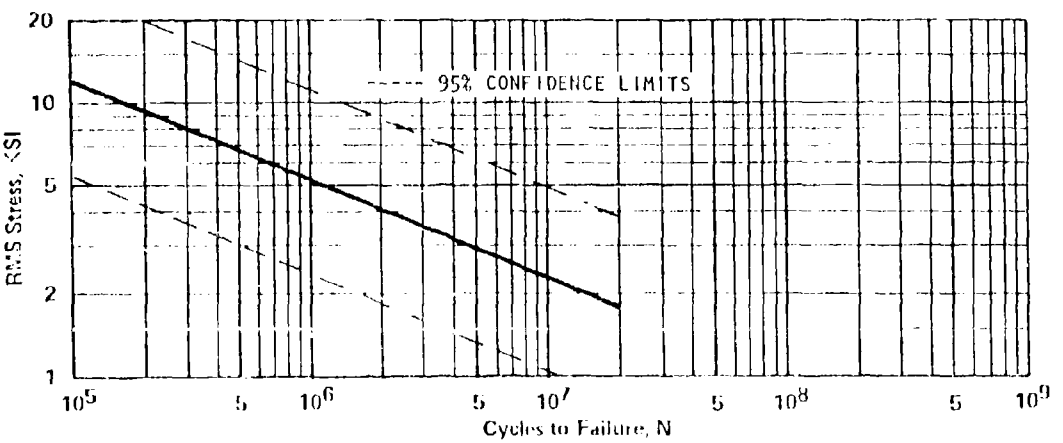

FIGURE 6.6.1-11 S-N DATA FOR 7075-T6 STIFFENER FLANGES WITH PLAIN RIVETED JOINTS - STIFFENED PANEL SONIC FATIGUE TEST SPECIMENS

ALUMINUM ALLOYS

MATERIAL: 7075-T6, Sheet

CONFIGURATION: Nine cell box structure exposed to broad band acoustic excitation on one side. Failure data representative of rib flange failures on both the exposed surface and the opposite surface. Rib flanges formed from flat sheet stock, heat treated, and straightened using standard aircraft manufacturing methods. Surface skins attached to rib flange using cut countersunk rivets on exposed surface and mushroom head rivets on the opposite flange.

TEST TEMPERATURE: Room Temperature

REFERENCE: Rudder, F. F., Jr.: "Acoustic Fatigue Resistance of Aircraft Structural Component Assemblies," AFFDL TR 71-107, Air Force Flight Dynamics Laboratory, Wright-Patterson Air Force Base, Ohio, 1972.

NOTE: See Figure 5.3.2-8

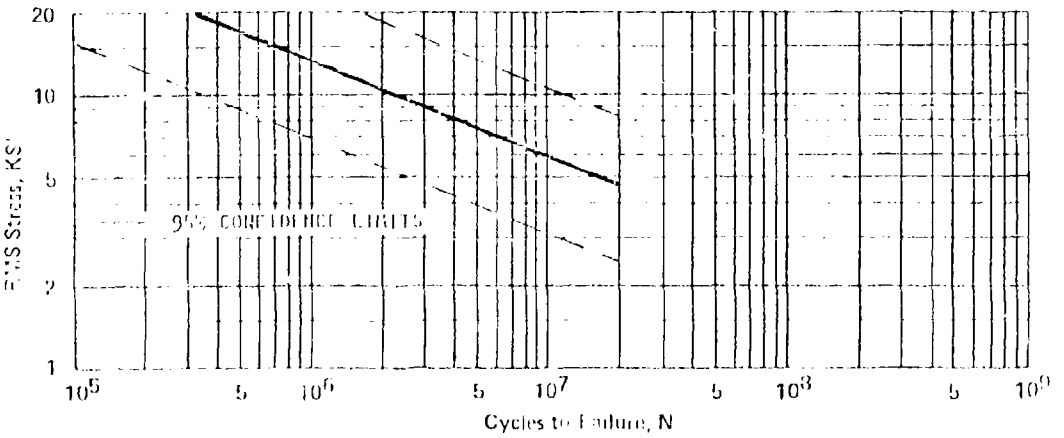

FIGURE 6.6.1-12 S-N DATA FOR 7075-T6 RIB FLANGES - BOX STRUCTURE SONIC FATIGUE TEST SPECIMENS

ALUMINUM ALLOYS

MATERIAL: 7075-T6, Sheet

CONFIGURATION: Nine bay flat and curved acoustic fatigue test specimens exposed to broadband random acoustic excitation. Weldbonded skin-stringer attachments were used. The panel configuration is described in Section 5.4.3.4.

TEST TEMPERATURE: Room Temperature

REFERENCE: Anon., "Weldbond Flight Component Design/Manufacturing Program," Ninth Quarterly Interim Technical Report Contract F33615-71-C-1716, Lockheed-Georgia Company, October 1973.

NOTES: The reference indicates that the fatigue data and S-N curves presented below are completely comparable to the axis system used in Figure 5.3.1-2. That is, Figure 5.3.1-2 can be used to predict stress levels with the S-N data presented below used to predict fatigue life.

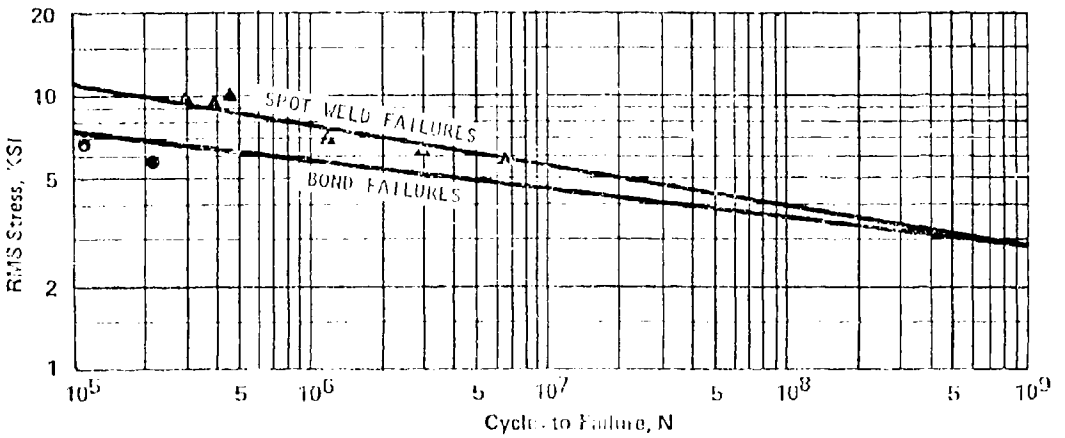

FIGURE 6.6.1-13 S-N DATA FOR 7075-T6 WELDBONDED JOINTS - NINE BAY FLAT AND CURVED SONIC FATIGUE TEST SPECIMENS

6.6.2 STAINLESS STEEL ALLOYS

This section presents equivalent random loading fatigue curves for 17-7 PH and 18- stainless steel sheet. No data reported in the literature presented experimental random amplitude fatigue data for stainless steel alloys. The designer should also see Figure 5.3.1-4 for an equivalent random loading fatigue curve for PH15-7Mo stainless steel alloy at 500°F. Other constant amplitude fatigue data is presented in MIL-HDBK-5B (4) and the "Aerospace Structural Metals Handbook" (31). The constant amplitude S-N data can be converted to equivalent random amplitude fatigue data using the method of Section 6.5.

STAINLESS STEEL ALLOYS

MATERIAL: 17-7 PH Stainless Steel Sheet

CONFIGURATION: Converted to equivalent random amplitude fatigue data from reversed bending (R = -1) constant amplitude fatigue data by the referenced source.

TEST TEMPERATURE: Room Temperature

REFERENCE: McGowan, P. R.; "Structural Design for Acoustic Fatigue," ASD-TDR-63-820, Air Force Flight Dynamics Laboratory, United States Air Force, Wright-Patterson Air Force Base, Ohio, 1963.

NOTES: The constant amplitude reversed bending data utilized was apparently data quoted in MIL-HDBK-5A. See Section 6.5.1 and Figure 6.5.1-1.

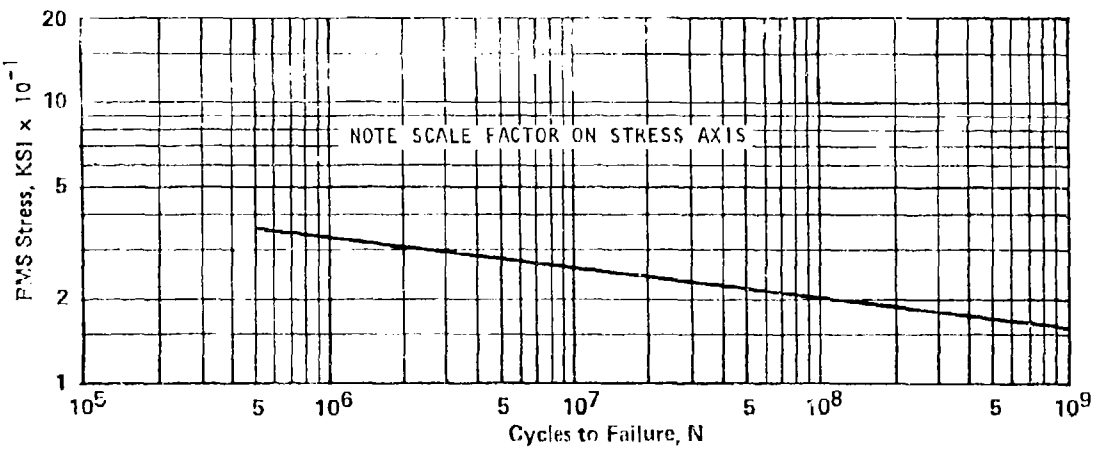

FIGURE 6.6.2-1 EQUIVALENT RANDOM LOADING S-N DATA FOR 17-7 PH STAINLESS STEEL SHEET

STAINLESS STEEL ALLOYS

MATERIAL: 18-8 Stainless Steel Sheet

CONFIGURATION: Equivalent random loading fatigue curve derived in the referenced source from constant amplitude reversed bending data (R = -1) for the material. Sheet thickness for constant amplitude data was apparently 0.025 inch.

TEST TEMPERATURE: Room Temperature

REFERENCE: McGowan, P. R.; "Structural Design for Acoustic Fatigue," ASD-TDR-63-820, Air Force Flight Dynamics Laboratory, Wright-Patterson Air Force Base, Ohio, 1963.

NOTES: See Section 6.5.1 concerning the conversion of constant amplitude fatigue data to equivalent random amplitude fatigue data. In particular, see Figure 6.5.1-1.

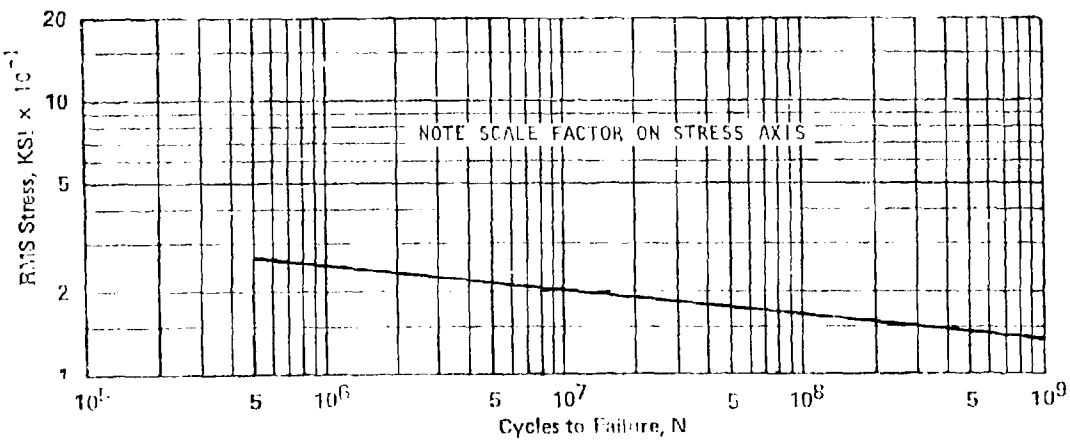

FIGURE 6.6.2-2 EQUIVALENT RANDOM LOADING S-N DATA FOR 18-8 STAINLESS STEEL SHEET

6.6.3 TITANIUM ALLOYS

This section presents random amplitude S-N data for various titanium alloys both for plain specimens, riveted specimens, and spot welded specimens. The effect of temperature on the material fatigue characteristics is also presented.

TITANIUM ALLOYS

MATERIAL: 6Al-4V Titanium, Sheet

CONFIGURATION: Cantilever coupon test specimens with transverse random amplitude vibratory base excitation. Both plain specimens and cut countersunk riveted specimens tested.

TEST TEMPERATURE: Room Temperature

REFERENCE: Schneider, C. W.; "Acoustic Fatigue of Aircraft Structures at Elevated Temperatures," AFFDL-TR-73-155, Part I, Air Force Flight Dynamics Laboratory, Wright-Patterson Air Force Base, Ohio, 1974. Figure 17 a), page 40.

NOTES: See Figure 5.3.1-5

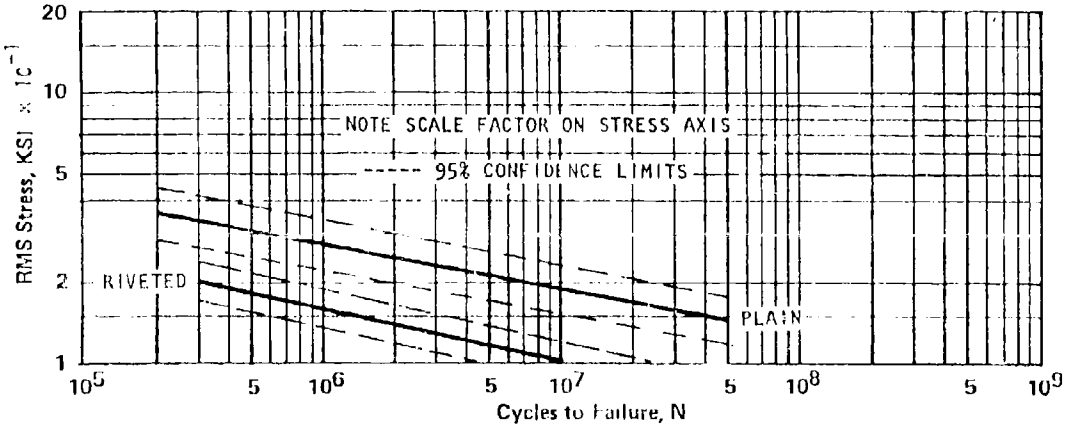

FIGURE 6.6.3-1 COUPON S-N DATA FOR 6Al-4V TITANIUM ALLOY SHEET FOR PLAIN SPECIMENS AND CUT COUNTERSUNK RIVETED SPECIMENS - ROOM TEMPERATURE

TITANIUM ALLOYS

MATERIAL: 6Al-4V Annealed Sheet

CONFIGURATION: Plain cantilever coupon specimen with transverse random amplitude vibratory base excitation. Material thickness is 0.060 inches.

TEST TEMPERATURE: Room Temperature

REFERENCE: Thompson, A. R. G., and Lambert, R. F.; "Acoustic Fatigue Design Data, Part III," AGARD-AG-162-Part III, 1973. Figure 1.2

NOTES: Compare with Figure 6.6.3-1. Limits on data scatter are based upon two standard deviations upon either side of the regression line.

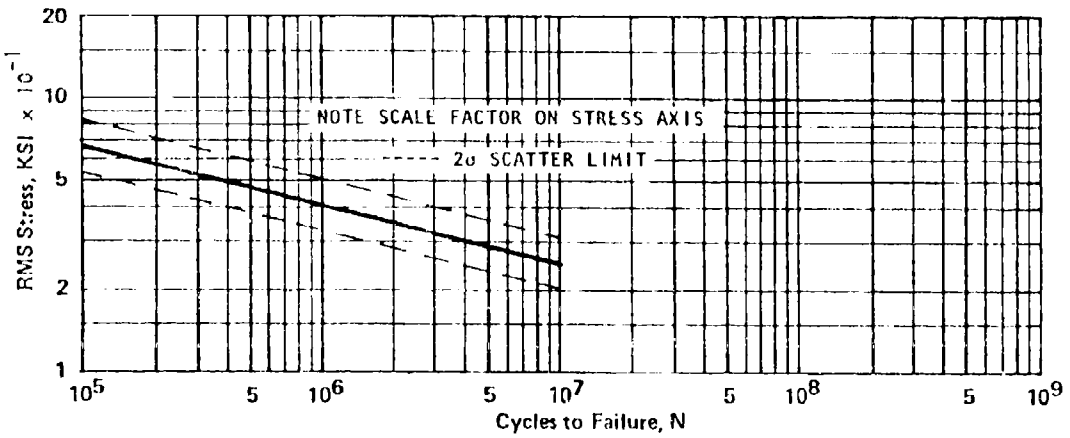

FIGURE 6.6.3-2 COUPON S-N DATA FOR 6Al-4V TITANIUM ALLOY SHEET PLAIN SPECIMENS - ROOM TEMPERATURE

TITANIUM ALLOYS

MATERIAL: 6Al-4V Titanium, Sheet

CONFIGURATION: Plain cantilever coupon test specimens with transverse random amplitude vibratory base excitation.

TEST TEMPERATURE: 600°F

REFERENCE: Schneider, C. W.; "Acoustic Fatigue of Aircraft Structures at Elevated Temperatures," AFFDL-TR-73-155, Part I, Air Force Flight Dynamics Laboratory, Wright-Patterson Air Force Base, Ohio, 1974. Figure 17 b), page 40.

NOTES: See Figure 5.3.1-5

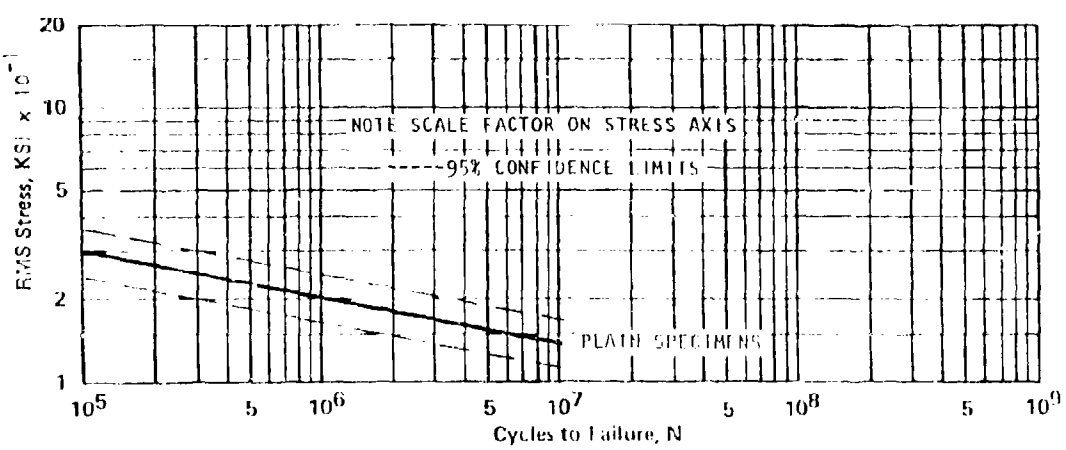

FIGURE 6.6.3-3 COUPON S-N DATA FOR 6Al-4V TITANIUM ALLOY SHEET PLAIN SPECIMENS - 600°F

TITANIUM ALLOYS

MATERIAL: 6Al-4V Titanium, Sheet

CONFIGURATION: Cut countersunk riveted cantilever coupon specimens with transverse random amplitude vibratory base excitation.

TEST TEMPERATURE: 600°F

REFERENCE: Schneider, C. W.; "Acoustic Fatigue of Aircraft Structures at Elevated Temperatures," AFFDL-TR-73-155, Part I, Air Force Flight Dynamics Laboratory, Wright-Patterson Air Force Base, Ohio, 1974. Figure 17 b), page 40.

NOTES: See Figure 5.3.1-5

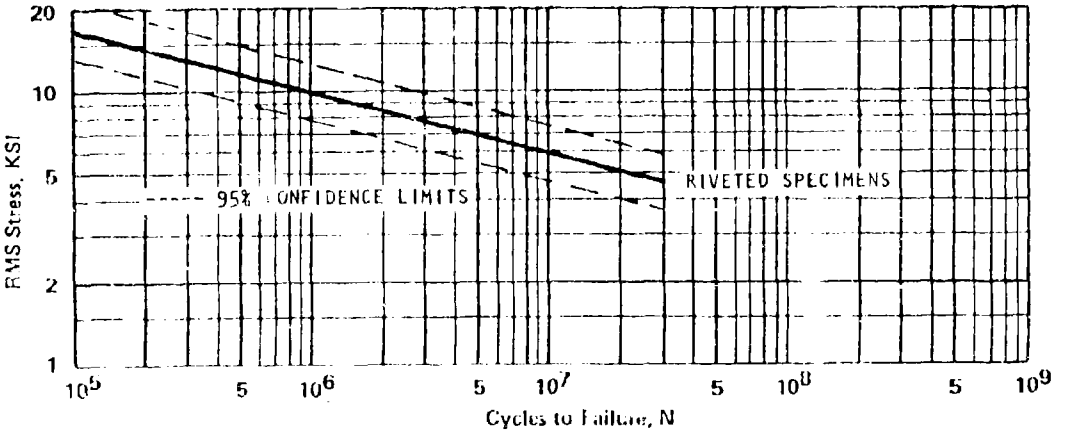

FIGURE 6.6.3-4 COUPON S-N DATA FOR 6Al-4V TITANIUM ALLOY SHEET WITH CUT COUNTERSUNK RIVETED SPECIMENS - 600°F

TITANIUM ALLOYS

MATERIAL: Ti-2Cu Aged Sheet

CONFIGURATION: Coupon specimens with transverse random vibratory base excitation introduced to the "skin" specimen through a riveted angle "rib." S-N curve is representative of both single rows of plain mushroom head rivets and flush head spin-dimpled countersunk rivets. Sheet thickness is 0.028 inches.

TEST TEMPERATURE: Room Temperature and 250°C.

REFERENCE: Thompson, A. R. G., and Lambert, R. F.; "Acoustic Fatigue Design Data, Part II," AGARD-AG-162, Part II, 1972. Figure 1.3

NOTES: Limits on data scatter are based upon two standard deviations upon either side of the regression line.

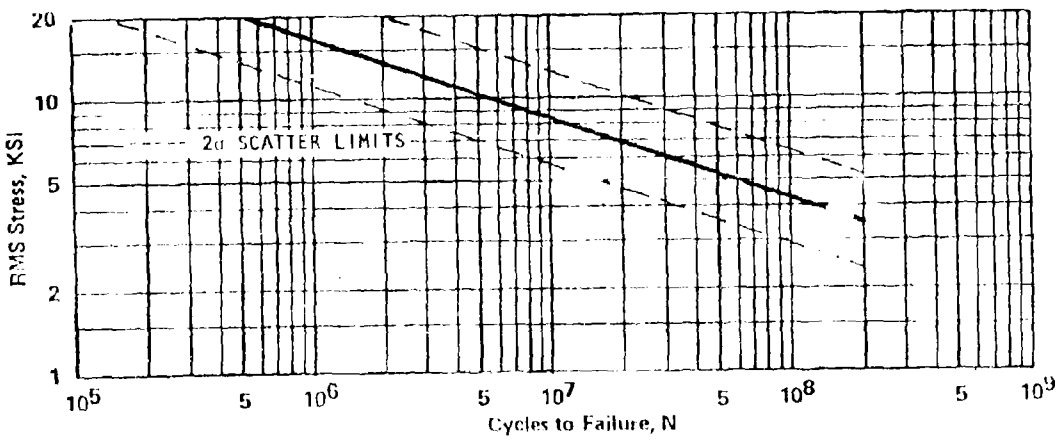

FIGURE 6.6.3-5 COUPON S-N DATA FOR Ti-2Cu TITANIUM ALLOY AGED SHEET SPECIMENS WITH PLAIN RIVETED AND SPIN-DIMPLED COUNTERSUNK HOLES

TITANIUM ALLOYS

MATERIAL: Ti-2Cu Aged Sheet

CONFIGURATION: Coupon specimens with transverse random vibratory base excitation introduced to the "skin" specimen through an angle "rib" attached to the skin by a single row of resistance spot welds. The regression line and data scatter limits are based upon specimens welded before aging and after aging and also include the effect of material grain direction. Sheet thickness is 0.028 inches.

TEST TEMPERATURE: Room Temperature

REFERENCE: Thompson, A. R. G., and Lambert, R. F.; "Acoustic Fatigue Design Data, Part III" AGARD-AG-162-Part III, 1973. Figure 1.4

NOTES: Limits on data scatter are based upon two standard deviations upon either side of the regression line.

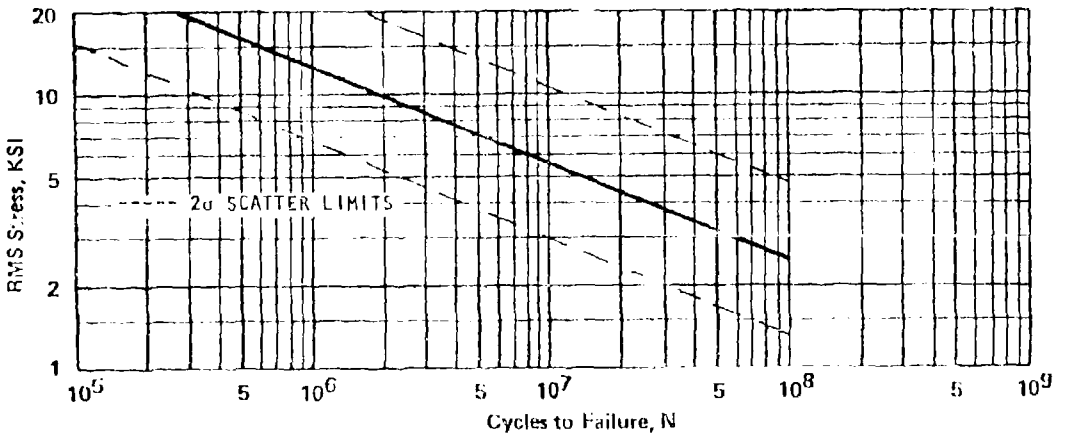

FIGURE 6.6.3-6 COUPON S-N DATA FOR Ti-2Cu TITANIUM ALLOY SHEET WITH SPOT WELDED JOINTS

TITANIUM ALLOYS

MATERIAL: Commercially Pure Titanium

CONFIGURATION: Coupon specimens with transverse random vibratory base excitation introduced to the "skin" specimen through a "T" section "rib" attached to the skin by a double row of resistance spot welds. (The reference also presents limited data for gas tungsten-arc spot welds.) The regression line and data scatter limits are based upon the resistance spot weld data only. Sheet thickness is 0.016 inches.

TEST TEMPERATURE: Room Temperature

REFERENCE: Thompson, A. R. G., and Lambert, R. F.; "Acoustic Fatigue Design Data, Part III," AGARD-AG-162-Part III, 1973. Figure 1.5

NOTES: Limits on data scatter are based upon two standard deviations upon either side of the regression line.

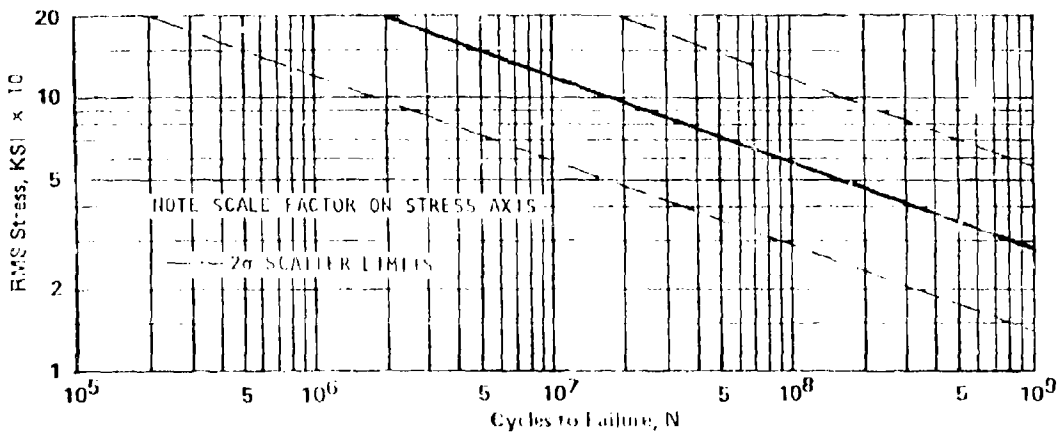

FIGURE 6.6.3-7 COUPON S-N DATA FOR COMMERCIALLY PURE TITANIUM ALLOY WITH SPOT WELDED JOINTS

6.6.4 NICKEL ALLOYS

This section presents random amplitude S-N data for sharply notched Rene' 41 coupon specimens at room temperature, 700°F, and 1400°F. Also, an equivalent random amplitude S-N curve for Inconel 718 Sheet is presented.

NICKEL ALLOYS

MATERIAL: RENE' 41, Sheet

CONFIGURATION: Cantilever sharply notched coupon specimens with random amplitude vibratory excitation of the specimen applied at the free end. The notch geometry was a symmetric 60° "V", 5/16 inch deep, with a notch radius of 0.005 ±0.001 inch. The specimen width was 1 inch, and the specimen thickness was 3/16 inch.

TEST TEMPERATURE: Room Temperature

REFERENCE: Phillips, E. P.; "Fatigue of Rene' 41 under Constant - and Random Amplitude Loading at Room and Elevated Temperatures," NASA TN D-3075, National Aeronautics and Space Administration, 1965.

NOTES: The regression line and 95% confidence limits were computed from data presented in the reference. See Figure 6.5.1-2.

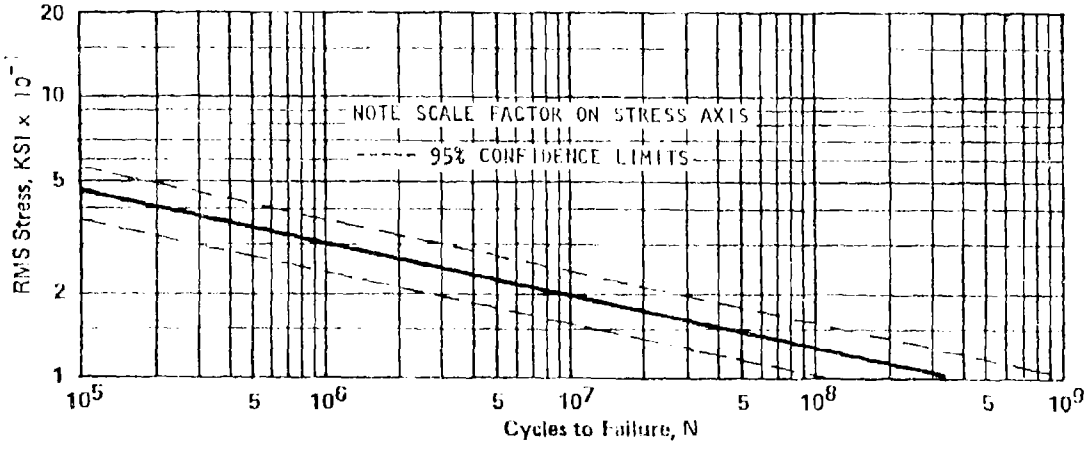

FIGURE 6.6.4-1 COUPON S-N DATA FOR SHARPLY NOTCHED RENE' 41 SHEET - ROOM TEMPERATURE

NICKEL ALLOYS

MATERIAL: RENE' 41 Sheet

CONFIGURATION: Cantilevered sharply notched coupon specimens with random amplitude vibratory excitation of the specimen applied at the free end. The notch geometry was a symmetric 60° "V", 5/16 inch deep, with a notch radius of 0.005 ±0.001 inch. The specimen width was 1 inch and the thickness was 3/16 inch.

TEST TEMPERATURE: 700°F (644°K)

REFERENCE: Phillips, E. P.; "Fatigue of Rene' 41 under Constant - and Random Amplitude Loading at Room and Elevated Temperatures," NASA TN D-3075, National Aeronautics and Space Administration, 1965.

NOTES: The regression line and the 95% confidence limits were computed from data presented in the reference.

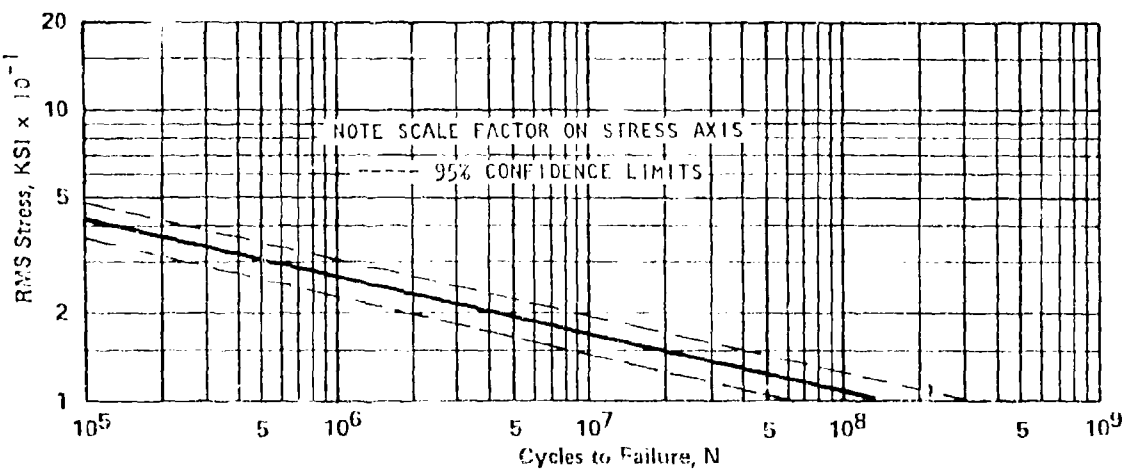

FIGURE 6.6.4-2 COUPON S-N DATA FOR SHARPLY NOTCHED RENE' 41 SHEET - 700°F

NICKEL ALLOYS

MATERIAL: RENE' 41 Sheet

CONFIGURATION: Cantilevered sharply notched coupon specimens with random amplitude vibratory excitation of the specimen applied at the free end. The notch geometry was a symmetric 60° "V", 5/16 inch deep, with a notch radius of 0.005 ±0.001 inch. The specimen width was 1 inch and the thickness was 3/16 inch.

TEST TEMPERATURE: 1400°F (1033°K)

REFERENCE: Phillips, E. P.; "Fatigue of Rene' 41 under Constant- and Random Amplitude Loading at Room and Elevated Temperatures," NASA TN D-3075, National Aeronautics and Space Administration, 1965.

NOTES: The regression line and the 95% confidence limits were computed from data presented in the reference.

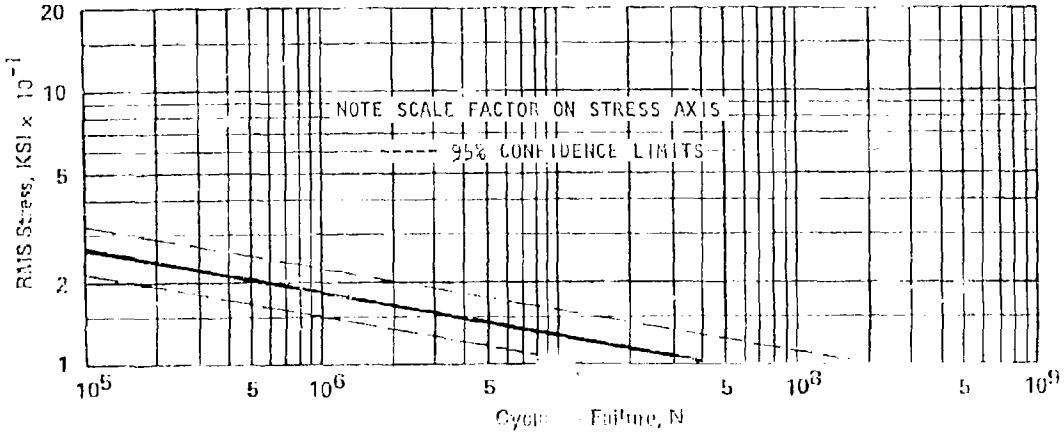

FIGURE 6.6.4-3 COUPON S-N DATA FOR SHARPLY NOTCHED RENE' 41 SHEET 1400°F

NICKEL ALLOYS

MATERIAL: INCONEL 718, Aged Sheet

CONFIGURATION: Converted to equivalent random loading fatigue curve from constant amplitude axial loading (R = -1) fatigue data for unnotched specimens presented in Figure 6.3.5.1.8 (a) of the reference.

TEST TEMPERATURE: Room Temperature

REFERENCE: Anon; Metallic Materials and Elements for Aerospace Vehicle Structures, MIL-HDBK-5B, United States Government Printing Office. September, 1971.

NOTES: See Section 6.5.1 for a discussion of the assumptions and techniques for converting constant amplitude fatigue data into equivalent random amplitude fatigue data.

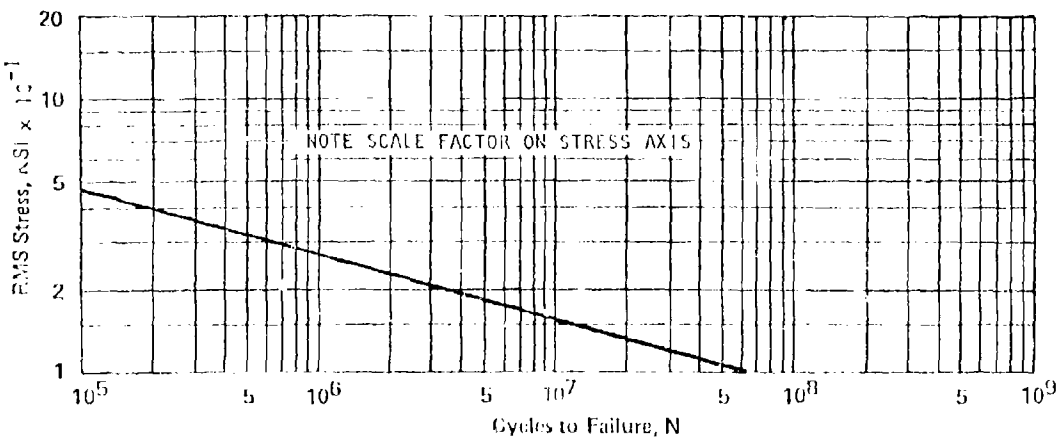

FIGURE 6.6.4-4 EQUIVALENT RANDOM LOADING S-N DATA FOR INCONEL 718 AGED SHEET

6.6.5 GLASS FIBERS

This section presents equivalent random loading fatigue curves for S901/43 and S901/81 glass fiber material illustrating the effect of warp direction upon the fatigue characteristics of the material. Also, sonic fatigue data resulting from tests of glass fiber fluted core panels is also presented for guidance. The designer is cautioned to determine the exact specimen configuration noting glass cloth type, bonding resin, curing sequence, and layer stacking sequence before relying upon data reported in the literature. The designer will find the discussions presented in Sections 5.2.2.3 and 5.3.8 useful in understanding the significance of the various parameters.

GLASS FIBERS

MATERIAL: S901/43 Longitudinal Warp Direction
S901/43 Transverse Warp Direction
S901/81 Longitudinal Warp Direction

CONFIGURATION: Equivalent random loading fatigue curves (See Section 6.5.1) were developed from constant amplitude reversed axial loading fatigue tests of 27 ply glass fiber "dog bone" test specimens. The classification of longitudinal or transverse denotes the warp direction for the specimen. All plys were laid in the same direction.

TEST TEMPERATURE: Room Temperature (Specimen heating was controlled by adjusting the loading frequency)

REFERENCE: Jacobson, M. J.; "Acoustic Fatigue Design Information for Fiber Reinforced Structures," AFFDL-TR-68-107, United States Air Force, 1968

NOTES: See Section 6.5.1 for a discussion of the assumptions and techniques associated with developing equivalent random amplitude fatigue curves from constant amplitude data.

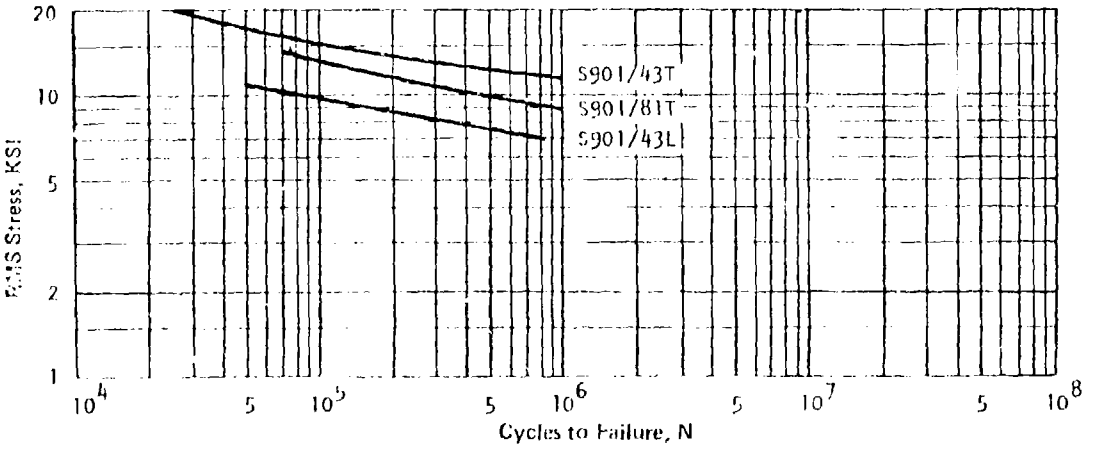

FIGURE 6.5.5.1 EQUIVALENT RANDOM LOADING S-N DATA FOR S901/43 AND S901/81 GLASS FIBER COUPON SPECIMENS

GLASS FIBERS

MATERIAL: 181-S Glass Fabric (0.010 inch/layer)
151-S Glass Fabric (0.007 inch/layer)

CONFIGURATION: Acoustic Fatigue tests of rectangular panels with tapered edges and fluted cores. Details of the panel construction are presented below:

Panel Type	Number of Plies			Notes
	Outside Face	Inside Face	Edge	
Type I	4	3	9	Empty Core
Type II	3	2	7	Foam Filled Core
Type III	4	3	9	Foam Filled Core

Panel Types I and II were manufactured using 181-S glass fabric and Type III was manufactured using 151-S glass.

TEST TEMPERATURE: Room Temperature

REFERENCE: Hayes, J. A.; "Sonic Fatigue Tolerance of Glass Filament Structure: Experimental Results," AFFDL-TR-66-78, United States Air Force, Dec. 1966.

NOTES: Original source gives no indication of ply orientation with respect to the panel layup.

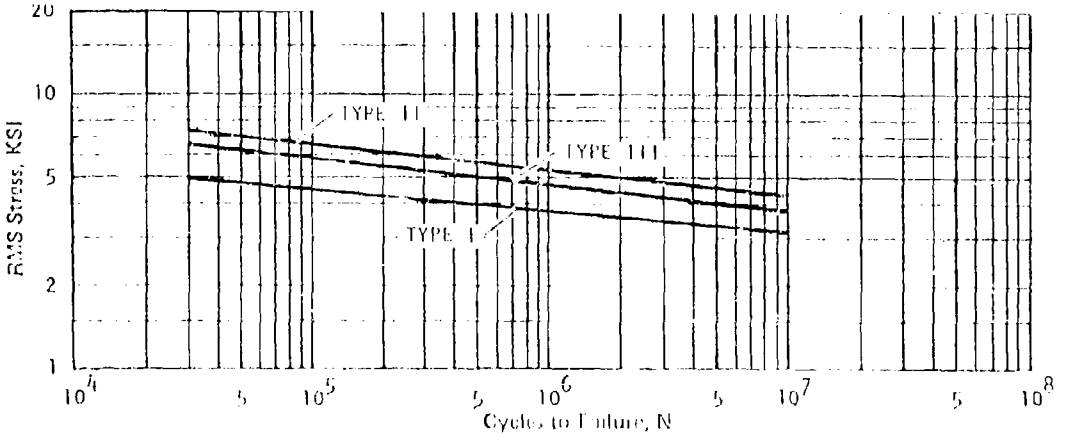

FIGURE 6.6.5-2 S-N DATA FOR 151-S and 181-S GLASS FIBER SONIC FATIGUE TEST SPECIMENS WITH FLUTED CORES

6.6.6 ADVANCED COMPOSITES

Very little random amplitude fatigue data has been reported in the literature related to the fatigue strength of advanced composite materials. Two random amplitude strain-life fatigue curves are presented in Figure 5.3.8-4 for riveted and bonded joint coupon test specimens. This section has been included so that the designer can introduce additional data as it becomes available.

REFERENCES FOR SECTION 6

1. Osgood, C. C.; Fatigue Design, Wiley-Interscience, New York, 1970.

2. Heywood, R. B.; Designing Against Fatigue, Chapman and Hall, Ltd., London 1962

3. Harris, W. J.; Metallic Fatigue, Pergamon Press, London, 1961.

4. Anon.; Metallic Materials and Elements for Aerospace Vehicle Structure, MIL-HDBK-5B, United States Government Printing Office, September, 1971

5. Anon.; A Guide for Fatigue Testing and the Statistical Analysis of Fatigue Data, ASTM Special Technical Publication No. 91-A (Second Edition), American Society for Testing and Materials, 1916 Race Street, Philadelphia, Pa., 1963.

6. Graham, J. A. (Ed.); Fatigue Design Handbook, Society of Automotive Engineers, Inc., Two Pennsylvania Plaza, New York, N. Y., 1968.

7. Bendat, J. S. and Piersol, A. G.; Measurement and Analysis of Random Data, John Wiley & Sons, Inc., New York, 1966

8. Weibull, W., Fatigue Testing and Analysis of Results, Advisory Group for Aeronautical Research and Development, North Atlantic Treaty Organization, Pergamon Press, London, 1961.

9. Berens, A. P. and West, B. S.; "Experimental Methods in Acoustic Fatigue," AFFDL-TR-71-113, Air Force Flight Dynamics Laboratory, Wright-Patterson Air Force Base, Ohio, 1972.

10. Miner, M. A.; "Cumulative Damage in Fatigue," Journal of Applied Mechanics Vol. 12, pp. 159-164, 1945.

11. Lundberg, B. K. O.; "Fatigue Life of Airplane Structures," Journal of the Aeronautical Sciences, Vol. 22, No. 6, 1955.

12. Shanley, F. R.; "A Theory of Fatigue Based upon Unbounding During Reversed Ship," Rand Corporation Report P-350-1, 1952.

13. Langer, B. F.; "Fatigue Failure from Stress Cycles of Varying Amplitude," Transactions of ASME, Vol. 59, A160, 1937.

14. Grover, H. J.; "Cumulative Damage Theories," WADC-TR-59-507, Wright Air Development Center, Wright-Patterson Air Force Base, Ohio, 1959.

15. Smith, C. R.; "Prediction of Fatigue Failures in Aluminum Alloy Structures," Proceeding of the Society for Experimental Stress Analysis, Vol. 12, No. 2, 1955.

16. Corten, H. T. and Dolan, T. J.; "Cumulative Fatigue Damage," IME and ASME, Proceedings of the International Conference on Fatigue of Metals, London, pp. 235-246, 1956.

17. Henry, D. L.; "Theory of Fatigue Damage Accumulation in Steel," Transactions of the American Society of Mechanical Engineers, Vol. 77, No. 6, 1955.

18. Freudenthal, A. M., and Heller, R. A.; "On Stress Interaction in Fatigue and a Cumulative Damage Rule," Journal of the Aero/Space Sciences, Vol. 26, No. 7, 1959.

19. Marco, S. M., and Starkey, W. L.; "A Concept of Fatigue Damage," Transactions of the American Society of Mechanical Engineers," May 1954.

20. Kommers, J. B.; "The Effect of Overstress in Fatigue on the Endurance Life of Steel, ASTM Proceedings, Vol. 45, 1945.

21. Richart, F. E., Jr. and Newmark, N. M., "A Hypothesis for Determination of Cumulative Damage in Fatigue," ASTM Proceedings, Vol. 48, 1948.

22. Crichlow, W. J., et al., "An Engineering Evaluation of Methods for the Prediction of Fatigue Life in Airframe Structures," ASD-TR-61-434, Air Force Flight Dynamics Laboratory, Wright-Patterson Air Force Base, Ohio, 1962.

23. Belcher, P. M.; Van Dyke, J. D., Jr.; and Eshleman, A. L., Jr.; "Development of Aircraft Structure to Withstand Acoustic Loads," Aero/Space Engineering, pp. 24-30, June 1959.

24. McGowan, P. R.; "Structural Design for Acoustic Fatigue," ASD-TDR-63-820, Air Force Flight Dynamics Laboratory, United States Air Force, Wright-Patterson Air Force Base, Ohio, October 1963.

25. Fitch, G. E., et al.; "Establishment of the Approach to and Development of, Interim Design Criteria for Sonic Fatigue," ASD-TDR-62-26, Air Force Flight Dynamics Laboratory, United States Air Force, Wright-Patterson Air Force Base, Ohio, June 1962.

26. Cote, M. J.; "Comparison of Approaches for Sonic Fatigue Prevention," ASD-TDR-63-704, Aeronautical Systems Division, Wright-Patterson Air Force Base Ohio, Sept. 1963.

27. Fuller, J. R.; "Research on Techniques of Establishing Random Type Fatigue Curves for Broad Band Sonic Loading," ASD-TDR-62-501, Aeronautical Systems Division.

28. Miles, John W.; "On Structural Fatigue under Random Loading," Journal of the Aeronautical Sciences, Vol. 21, No. 11, pp. 753-762, Nov. 1954.

29. Phillips, E. P.; "Fatigue of Rene' 41 under Constant and Random-Amplitude Loading at Room and Elevated Temperatures," NASA TND-3075, National Aeronautics and Space Administration, Langley Research Center, 1965.

30. Schjelderup, H. C., and Galef, A. E.; "Aspects of the Response of Structures Subject to Sonic Fatigue," WADD Technical Report 61-187, Air Force Flight Dynamics Laboratory, United States Air Force, Wright-Patterson Air Force Base, Ohio, 1961.

31. Anon., "Aerospace Structural Metals Handbook," AFFML-TR-68-115, Air Force Materials Laboratory, Wright-Patterson Air Force Base, Ohio.

APPENDIX A

NOMENCLATURES AND DEFINITIONS

This section presents basic data useful in supporting subsequent sections. Section A.1 presents basic nomenclature and definitions that are specialized as appropriate in the subsequent sections. Section A.2 presents a series of graphic scales that the designer will find useful for interpolating between the various scales presented. Section A.3 presents a brief compilation of definitions and equivalence relations between the values of engineering units commonly used in the United States and the corresponding values of the modern metric (SI) units.

A.1 BASIC NOMENCLATURE AND DEFINITIONS

The following basic nomenclature and definitions are provided for assisting the designer when using the handbook and references. For acoustic terminology the designer should consult Reference (1). For terminology relating to materials and fatigue testing References (2), (3), and (4) provide detailed lists of definitions and nomenclature. Quantities are defined in the handbook as they arise.

ACCELERATION: A vector quantity specifying the time-rate-of-change of the velocity. Self-explanatory prefixes such as peak, average, rms (root mean square) are often used.

ACOUSTIC FATIGUE: Fatigue of structure resulting from the structure being exposed repeatedly to time varying acoustic pressure waves. Also called "sonic fatigue."

AMPLITUDE DISTRIBUTION FUNCTION: A function of the amplitude of a time varying quantity expressing the fraction of time that the instantaneous value of the quantity is less than a specified level. Also called the "distribution function" or "cumulative distribution function."

AMPLITUDE DENSITY DISTRIBUTION: A function of the amplitude of a time varying quantity expressing the fraction of time that the quantity remains within a narrow amplitude interval. Also called the "probability density distribution" or simply "probability density."

AUTOCORRELATION: A measure of the similarity of a function with a displaced version of itself as a function of the displacement (usually taken as time). The value of the autocorrelation for zero displacement is the mean square value of the function.

BROAD BAND: The description of the time history of a quantity (either pressure or stress) implying that the frequency content of the time history covers a broad frequency band (usually greater than one octave). The term "wide band" is also used.

CONFIDENCE LIMITS: The upper and lower limiting values of the range of values for which a given percentage value applies. If the chances are 95 out of 100 that a sample lies between 10 and 15, the 95% confidence limits are said to be 10 and 15.

CROSSCORRELATION: A measure of the similarity of two functions with the displacement (usually time) between the two functions taken as the independent variable. If the two functions are identical, the crosscorrelation is an autocorrelation

CROSS-SPECTRUM: A frequency domain measure of the similarity of two functions.

DECIBEL (dB): One-tenth of a Bel. The decibel is a measure of level when the base of the logarithm is the tenth root of ten and the quantities concerned are proportional to power (pressure squared).

DISCRETE FREQUENCY: The description of a sound wave the instantaneous sound pressure of which is a simple sinusoidal function of time. Also called a "pure tone" or a "simple tone." When used to describe acoustic fatigue tests the excitation pressure is a random amplitude sinusoidal sound pressure.

DIRECTIVITY FACTOR: A dimensionless quantity which is a measure of the spatial variation of the sound pressure level about a sound source.

DISPLACEMENT: A vector quantity specifying the change of position of a body, a point on a body, or a particle usually measured with respect to the mean or rest position.

DISTRIBUTION FUNCTION: See Amplitude Distribution Function.

ERGODIC PROCESS (STATISTICAL) A subclass of stationary random processes for which ensemble averages (average over a set of random processes at the same instant) are equal to the corresponding temporal averages taken along any representative sample function.

FILTER(ELECTRONIC): A device for separating components of a signal on the basis of frequency. A filter is described by the frequency interval (band) for which it allows the signal to pass relatively unattenuated while it attenuates components in other frequency intervals.

FREE(SOUND FIELD: A field in a homogeneous isotropic medium that is free from boundaries. In practice, it is a field in which the effects of boundaries are negligible over the region of interest.

FREQUENCY: The repetition rate of a periodic quantity. The frequency is the reciprocal of the period and is measured in Hertz (Hz.) or in cycles per second.

FUNDAMENTAL MODE: The lowest natural frequency of a system.

g: The quantity describing the acceleration produced by the force of gravity. The standard values of the acceleration of gravity are $9.80665\ m/s^2$ = $386.087\ in/s^2$ $32.1739\ ft/s^2$.

GAUSSIAN DISTRIBUTION: A particular amplitude distribution function of fundamental importance in the theory of probability. The Gaussian distribution function is characterized by its mean value and standard deviation and describes many natural phenomena.

HISTOGRAM: The graph of an amplitude density distribution.

IMPEDANCE: The impedance of a system is a measure of the response amplitude and phase of a system in the frequency domain. Acoustic impedance at a surface is defined as the complex ratio of the sound pressure averaged over the surface to the volume velocity through it. Mechanical impedance is defined as the complex ratio of the force acting on a specified area of a mechanical device to the resulting linear velocity of that area.

LEVEL: In acoustics, the level of a quantity is defined as the logarithm of the ratio of that quantity to a reference value of that quantity.

MODE: The spatial distribution of amplitude and phase characterizing the displacement pattern of a vibrating body undergoing free undamped oscillations. A normal mode of vibration is a mode describing the relative amplitudes of various points occurring at a natural frequency of the system.

MODAL MASS: The generalized mass of a vibrating system for a specified normal mode.

MODAL STIFFNESS: The generalized stiffness of a vibrating system for a specified normal mode.

MICROBAR (μbar): A unit of pressure commonly used in acoustics. One microbar is equal to a pressure of ten micronewton per square meter.

NATURAL FREQUENCY: Any one frequency of a set of characteristic frequencies of a system at each of which the system vibrates in a normal mode.

RESONANCE: For a system in forced vibration, resonance is the description of increased response amplitude in a narrow frequency range without an increase in the magnitude of the forcing input. At resonance, the response of a mechanical system is limited only by the damping of the system.

RESONANT FREQUENCY: See Natural Frequency.

RESPONSE: The response of a system is the motion (or other output quantity) resulting from an excitation (stimulus) under specified conditions.

ROOT MEAN SQUARE (rms): The square root of the arithmetical mean of the squares of a set of instantaneous amplitudes or the square root of the time average of the square of the amplitude of a time varying quantity taken over a long interval.

SOUND: In general, an oscillation in pressure, stress, particle displacement, particle velocity, etc. in a medium with internal forces (elastic, viscous) or the superposition of such propagated alterations. For acoustic fatigue, sound is generally considered to be an airborne pressure oscillation.

OCTAVE: The interval between two sounds having a basic frequency ratio of two. The frequency interval, in octaves, between any two frequencies is the logarithm to the base 2 (or 3.322 times the logarithm to the base 10) of the frequency ratio.

POWER LEVEL: The power level of a given power is 10 times the logarithm to the base 10 of the ratio of the given power to a reference power. In acoustics the reference power is usually taken as 10^{-12} watt although 10^{-13} watt have been used in earlier work. The reference value for the power should always be stated.

PRESSURE SPECTRUM LEVEL: The pressure spectrum level of a sound at a specific frequency is the sound pressure level of that part of the signal contained within a frequency band 1 Hertz wide centered at the specific frequency. The reference pressure should be stated.

PURE TONE: See Discrete Frequency.

RANDOM: A time varying quantity whose instantaneous magnitude is not specified or cannot be predicted for any given instant of time is called a random quantity. The amplitude of a random quantity is described in terms of the probability distribution functions. (See Gaussian Distribution.)

SOUND INTENSITY: The sound intensity at a point in a specified direction is the average rate of sound energy transmitted in the specified direction through a unit area normal to this direction.

SOUND PRESSURE LEVEL: Expressed in decibels, dB, the sound pressure level is 20 times the logarithm to the base 10 of the ratio of the pressure of the sound to the reference pressure. For air the reference pressure is taken as 0.0002 microbar or 20 $\mu N/m^2$.

SPECTRUM LEVEL: Ten times the logarithm to the base 10 of the ratio of the squared sound pressure per unit bandwidth to the corresponding reference quantity. The unit bandwidth is the hertz and the corresponding reference quantity is $(20\,\mu N/m^2)^2/Hz$.

STANDARD DEVIATION: Usually denoted by "σ", the standard deviation is a linear measure of variability equal to the square root of the variance.

STATIONARY (STATISTICAL): A statistical term that describes a random process whose spectrum and amplitude distribution do not change with time.

TIME HISTORY: The variation of the amplitude of a quantity with time (usually a recorded or plotted record).

TRANSFER FUNCTION: A measure of the relation between the output signal and the input signal of a system or device usually taken as the ratio of the output signal to the input signal. See Impedance.

VARIANCE: A quadratic measure of the variability of a quantity taken as the average of the mean square value of the difference between the quantity and the arithmetic mean of the quantity.

VELOCITY: A vector quantity that specifies the time-rate-of-change of displacement with respect to a reference frame.

VIBRATION: An oscillation wherein the quantity is a parameter that defines the motion of a mechanical system.

WHITE NOISE: A description of the spectrum of a quantity whose power per unit-frequency is essentially independent of frequency over a specified frequency range.

A.2 GRAPHIC SCALES

This section presents a series of graphic scales useful for interpolating values from graphs, charts, and nomographs presented in the report. The interpolation is achieved by simply marking the divisions of the original scale on the straight edge of a piece of paper, aligning these divisions with the appropriate graphic scale presented in this section, and marking the intermediate divisions on the piece of paper. This technique allows the designer to obtain intermediate values from the charts, etc. if the original scale does not allow for the direct determination of the specific value. Graphic scales are presented for linear divisions, logarithmic divisions, and a Gaussian probability scale. Other divisions are possible; however, the scales presented here are all that one requires to utilize the graphical data and design charts presented in subsequent sections.

Figure A.2.1-1 presents a linear graphic scale for scales up to 10 divisions per inch.

Figure A.2.1-2 presents a logarithmic graphic scale for one cycle per 7.5 inches full scale.

Figure A.2.1-3 presents a logarithmic graphic scale for four cycles per 7.5 inches full scale.

Figure A.2.1-4 presents a logarithmic graphic scale for seven cycles per 8.75 inches full scale.

Figure A.2.1-5 presents a Gaussian or normal probability scale for a range of probability values between 0.01 to 99.99 per 8.25 inches full scale.

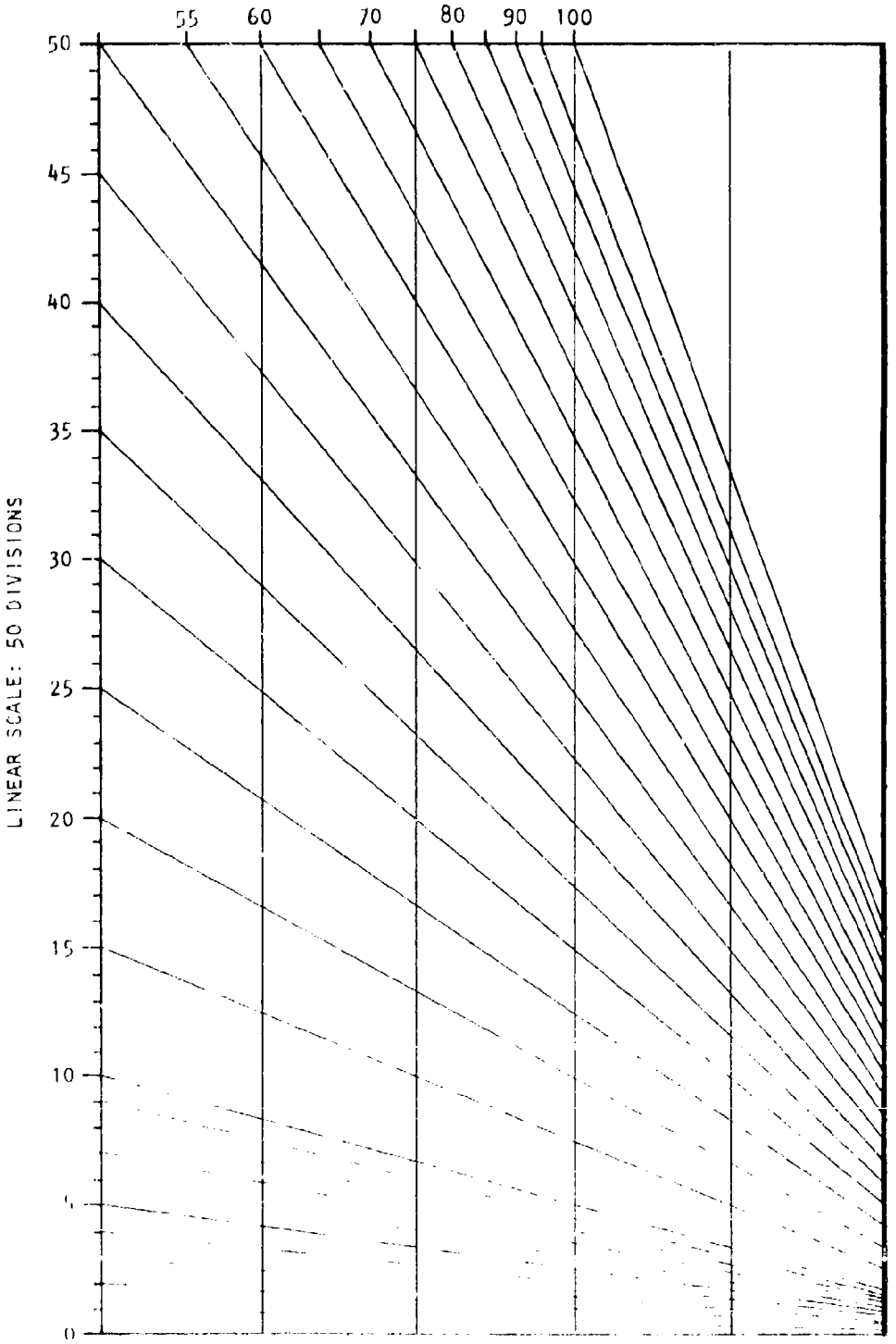

FIGURE A.2.1-1 LINEAR GRAPHIC SCALE

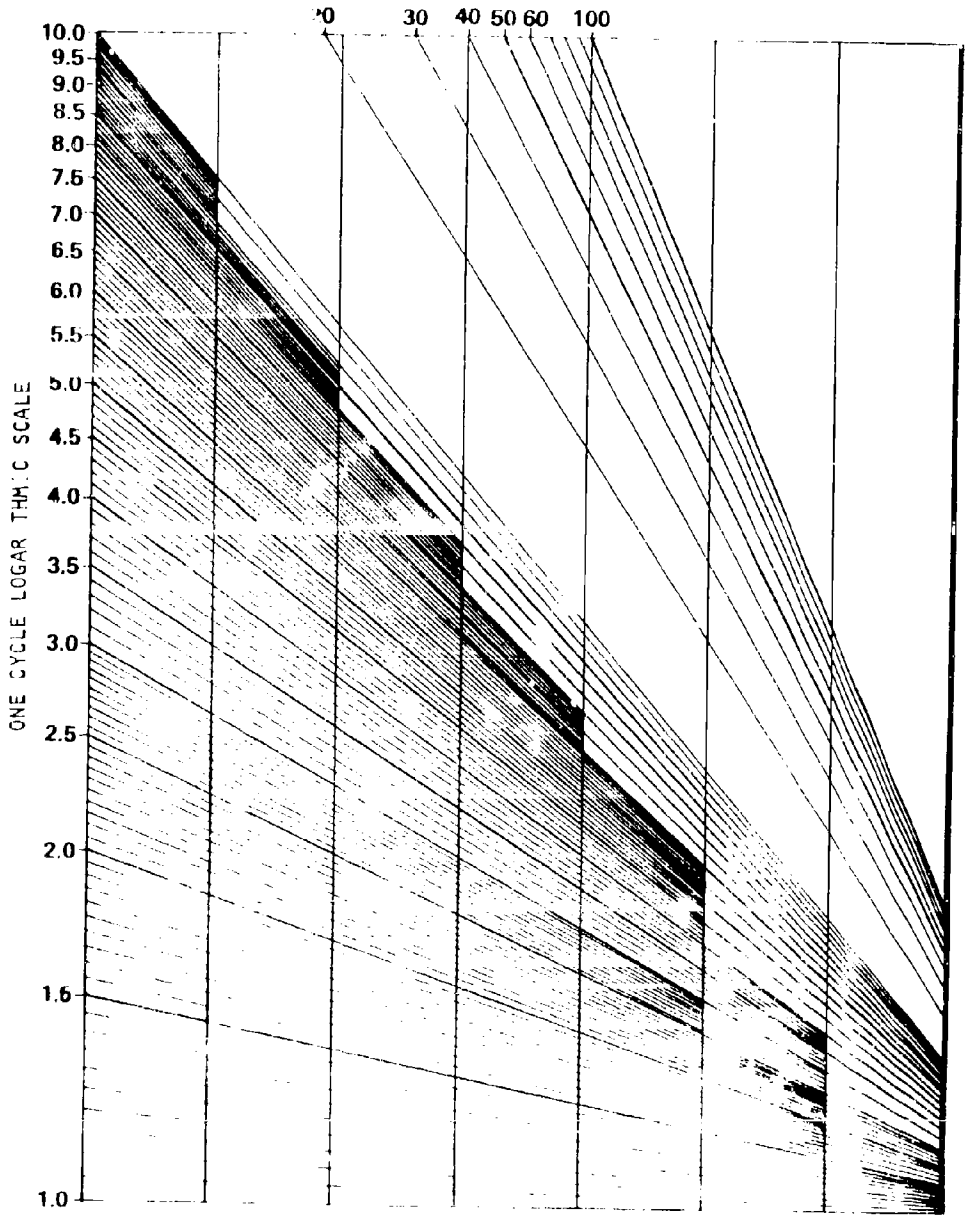

FIGURE A.7.1.2 LOGARITHMIC (CIRCUIT) SCALE

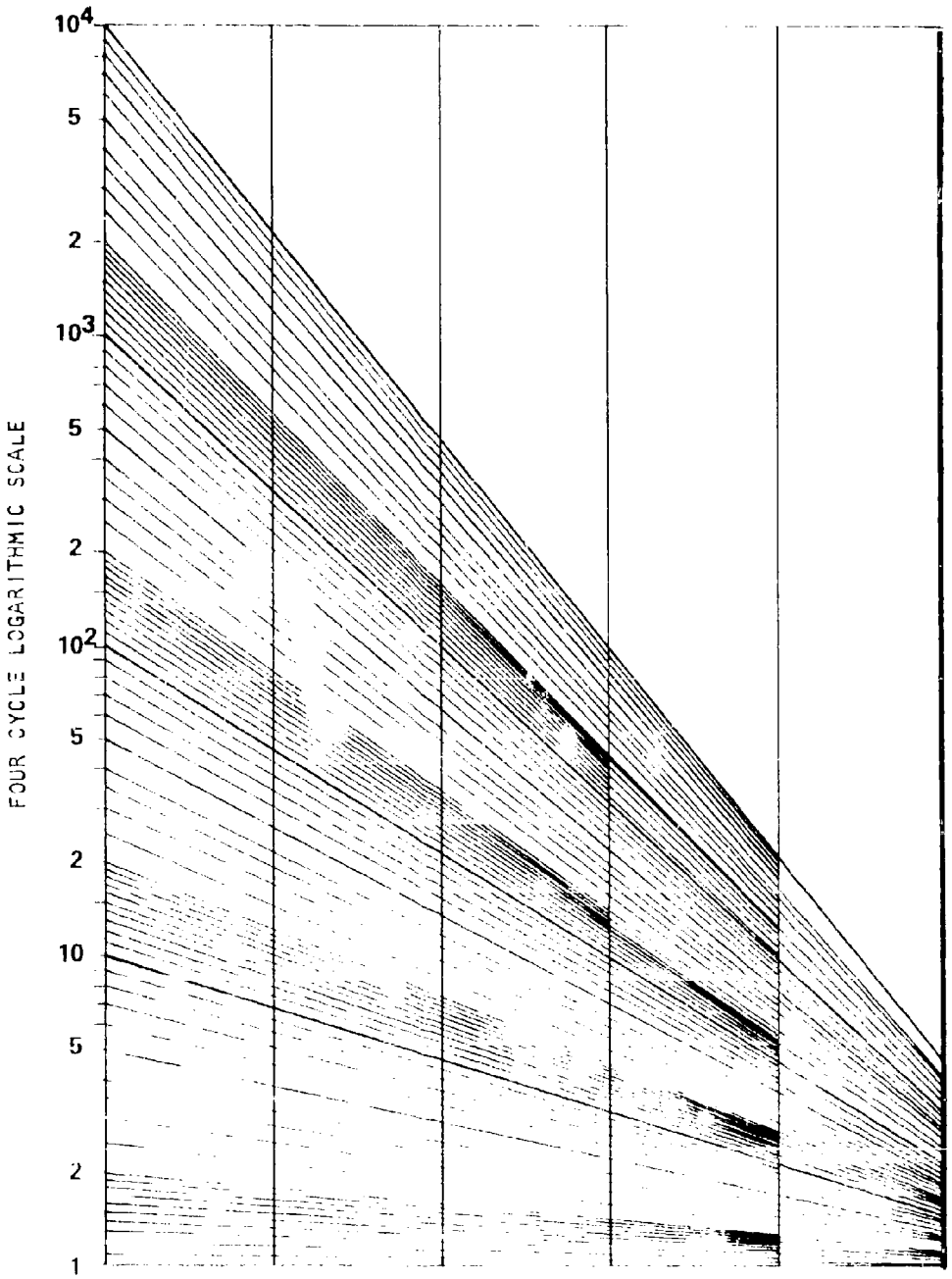

FIGURE A-2.1-3 LOGARITHMIC GRAPHIC SCALE

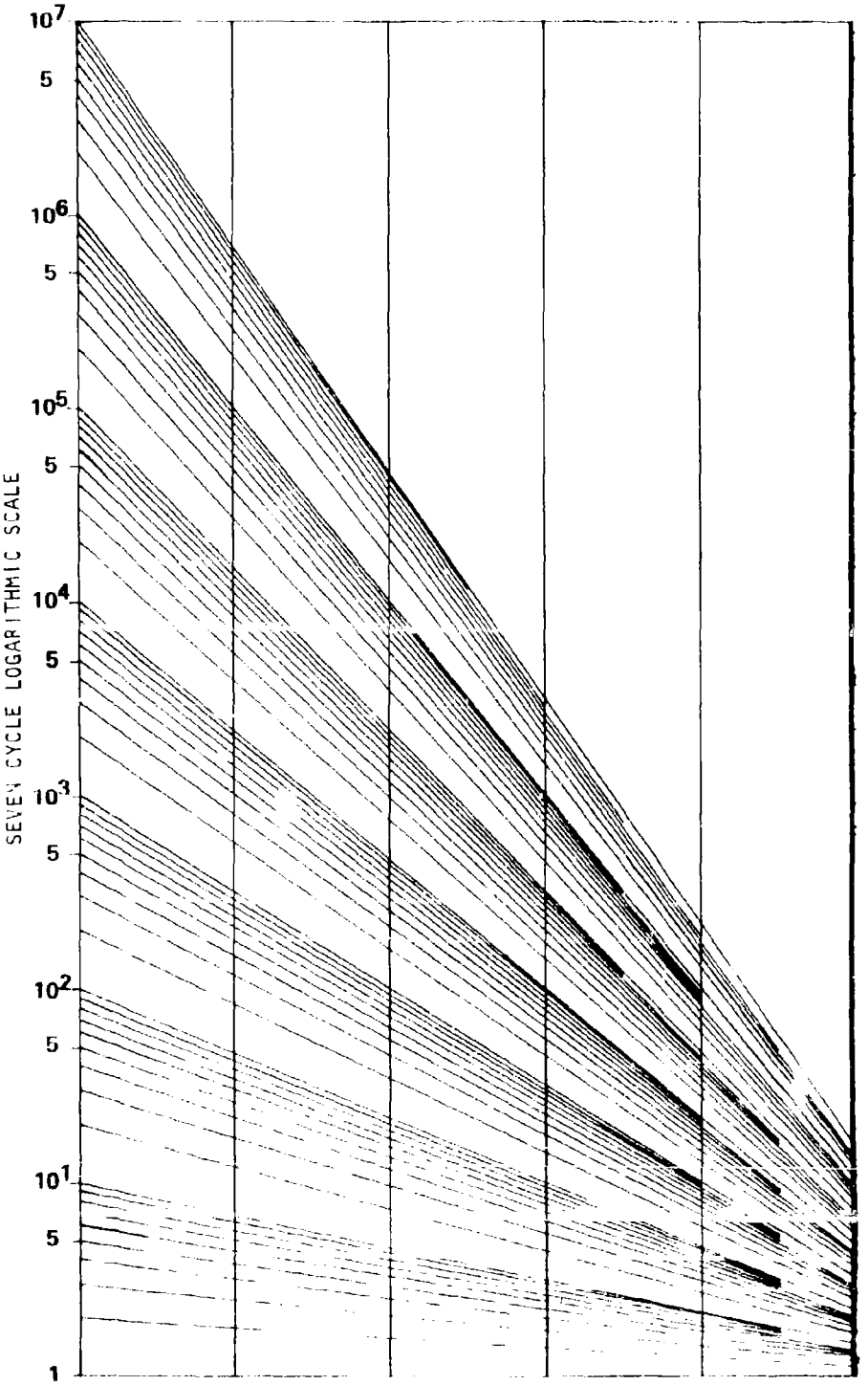

FIGURE A.2.1-4 LOGARITHMIC GRAPHIC SCALE: SEVEN CYCLES

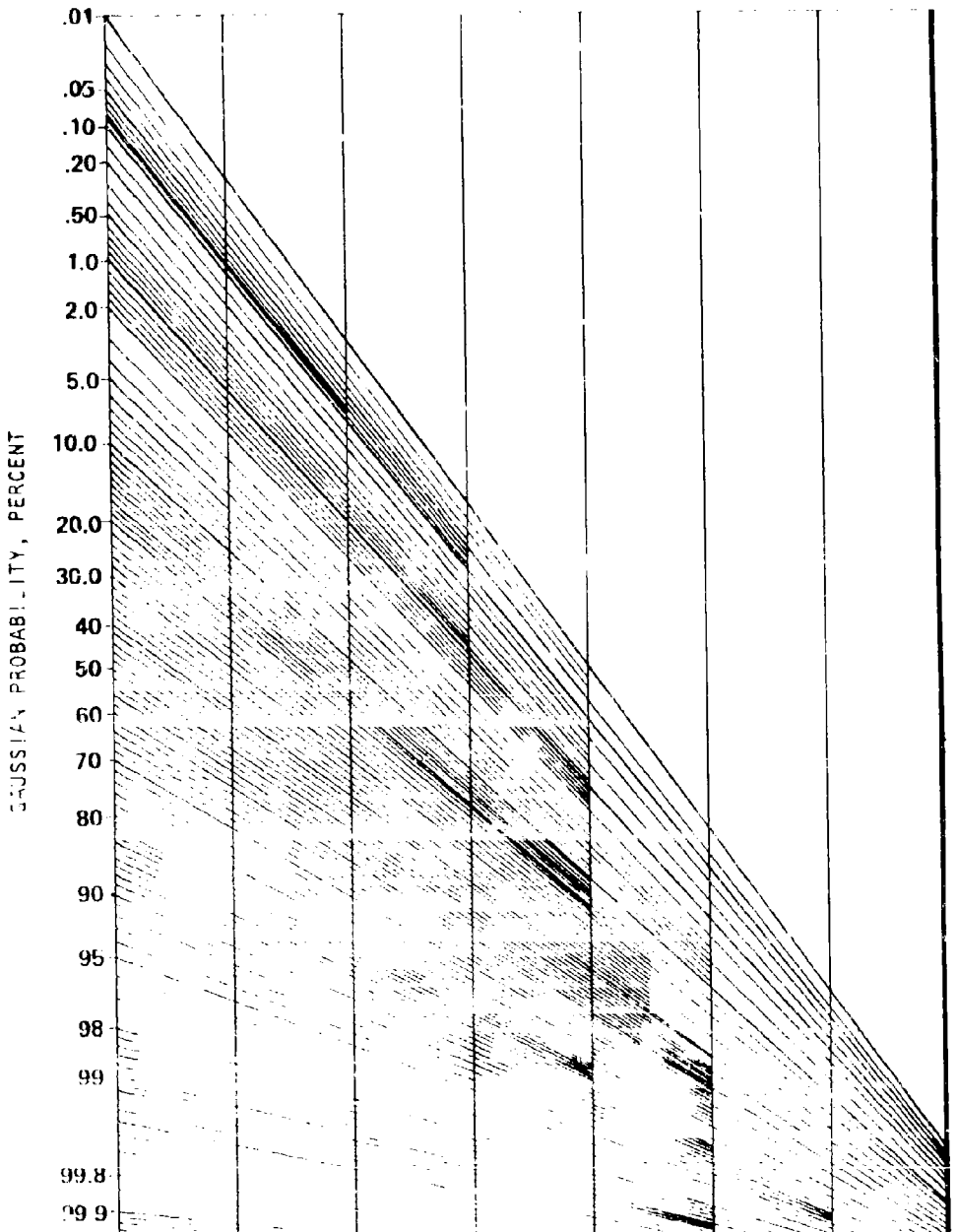

FIGURE A-2.1-5. GRAPHIC SCALE FOR GAUSSIAN PROBABILITY

A.3 CONVERSION FACTORS

This section provides summary information necessary for the conversion of values expressed in engineering units of measure commonly used in the United States to the corresponding values expressed in modern metric (SI) units. This section is not intended to be a standard, but rather a convenient source of data for use with this report. If the designer requires such a standard, it is recommended that he consult specific Government publications relating to the conversion of specific values (5), (6), (7).

Tabular data is presented here stating the relationship between units. The basic units used in this report are the inch or foot (length), the pound mass (mass), the second (time), and the degree Fahrenheit or Rankine (temperature). Table A.3.1-1 presents the basic units and the derived units for the International System of Units (SI).

The prefix nomenclature, symbols, and examples of usage for basic and derived units in the SI system are presented in Table A.3.1-2.

Table A.3.1-3 presents the equivalent value in SI units of the common engineering units used in the handbook.

Table A.3.1-4 presents the equivalence between compound or derived mass units (pound mass) as used in the handbook and the corresponding SI units.

Table A.3.1-5 presents the equivalence between compound or derived force units (pound force) as used in the handbook and the corresponding SI units.

TABLE A.3.1-1

THE INTERNATIONAL SYSTEM OF UNITS (SI)

BASIC UNITS

Quantity	Unit	Symbol
Length	meter	m
Mass	kilogram	kg
Time	second	s
Temperature	kelvin	K
Electric Current	ampere	A
Luminous Intensity	candela	cd

DERIVED UNITS

Quantity	Unit	Symbol
Area	square meter	m^2
Volume	cubic meter	m^3
Velocity	meter per second	m/s
Acceleration	meter per second squared	m/s^2
Frequency	hertz	Hz.
Density	kilogram per cubic meter	kg/m^3
Force	newton	N
Moment of Force	newton meter	N m
Pressure	newton per square meter	N/m^2
Work, Energy	joule	J, (N m)
Power	watt	W, (J/s)

TABLE A.3.1-2

SI SYSTEM OF UNITS

PREFIX NOMENCLATURE, SYMBOL AND USE

Prefix	Symbol	Multiplying Factor	Example
mega	M	10^{6}	megawatt (MW)
kilo	k	10^{3}	kilometer (km)
hecto*	h	10^{2}	
deca*	da	10^{1}	
deci*	d	10^{-1}	decimeter (dm)
centi*	c	10^{-2}	centimeter (cm)
milli	m	10^{-3}	millimeter (mm)
micro	μ	10^{-6}	microsecond (μs)

*prefixes that are multiples of 10 raised to a power that is a multiple of ± 3 is the recommended usage.

TABLE A.3.1-3

CONVERSION OF COMMON ENGINEERING UNITS TO EQUIVALENT VALUES IN SI UNITS

BASIC UNITS

Length

1 mile = 1.60934 km

1 ft = 0.3048 m = 304.8 mm

1 in = 2.54 cm = 25.4 mm

Area

1 ft^2 = 0.092903 m^2

1 in^2 = 6.4516 cm^2

Volume

1 ft^3 = 0.0283168 m^3 = $2.8317 \cdot 10^7$ mm^3

1 in^3 = 16.3871 cm^3 = $1.6387 \cdot 10^4$ mm^3

Capacity

1 gal = 4.54609 dm^3*

1 US gal = 3.78541 dm^3*

Velocity

1 mile/h = 1.60934 km/h

1 ft/s = 0.3048 m/s = 304.8 mm/s

1 in/s = 2.54 cm/s = 25.4 mm/s

Acceleration

1 ft/s^2 = 0.3048 m/s^2

1 in/s^2 = 2.54 cm/s^2

Mass **

1 lbm = 0.453592 kg

1 slug = 14.5939 kg

* The cubic decimeter equals one liter.

** The unit lbm denotes the pound mass. (a force of 1 lbf acting on a mass of 1 lbm produces an acceleration of 386.4 in/s^2)

TABLE A.3.1-4

CONVERSION OF COMMON ENGINEERING UNITS

TO

EQUIVALENT VALUES OF SI UNITS

COMPOUND MASS UNITS *

Mass Per Unit Length

1 lbm/ft = 1.48816 kg/m

1 lbm/in = 17.8580 kg/m

Mass Per Unit Area

1 lbm/ft^2 = 4.88243 kg/m^2

1 lbm/in^2 = 703.070 kg/m^2

Mass Flow Rate

1 lbm/h = 0.453592 kg/h

1 lbm/s = 0.453592 kg/s

Volume Flow Rate

1 US gal/h = 3.78541 dm^3/h

1 US gal/s = 3.78541 dm^3/s

Density

1 lbm/ft^3 = 16.019 kg/m^3

1 lbm/in^3 = 27.6799 g/cm^3

Moment of Inertia

1 lbm ft^2 = 0.042140 kg m^2

1 lbm in^2 = 2.9264×10^{-4} kg m^2

Momentum

1 lbm ft/s = 0.138255 kg m/s

Angular Momentum

1 lbm ft^2/s = 0.04214 kg m^2/s

* The unit lbm denotes the pound mass (a force of 1 lbf acting on a mass of 1 lbm produces an acceleration of 386.4 in/s^2.)

TABLE A.3.1-5

CONVERSION OF COMMON ENGINEERING UNITS

TO

EQUIVALENT VALUES IN SI UNITS

COMPOUND FORCE AND ENERGY UNITS

Force

1 lbf = 4.44822 N

Force/Unit Length

1 lbf/ft = 14.5939 N/m

1 lbf/in = 175.172 N/m

Moment of Force

1 lbf ft = 1.35582 N m

1 lbf in = 0.11298 N m

Pressure

1 lbf/ft^2 = 47.8803 N/m^2

1 lbf/in^2 = 6894.76 N/m^2

Dynamic Viscosity

1 $lbf\ s/ft^2$ = 47.8803 $N\ s/m^2$

1 lbf/ft s = 1.48816 kg/m s

1 slug/ft s = 47.8803 kg/m s

Kinematic Viscosity

1 ft^2/s = 0.092903 m^2/s

1 in^2/s = 645.16 mm^2/s

Energy

1 Btu = 1.05506 kJ

1 ft lbf = 1.35582 J

1 hp h = .00452 MJ

Power

1 hp = 745.700 W

1 ft lbf/s = 1.35582 W

Specific Energy

1 Btu/lb = 2326 J/kg

1 ft lbf/lb = 2.98907 J/kg

Specific Entropy

1 Btu/lbm°R = 4186.8 J/kg K

REFERENCES FOR SECTION A

1. Anon., "Acoustical Terminology," ANSI Standard S1.1-1960 (R 1971), American National Standards Institute; 1430 Broadway, New York, N.Y. 10018.

2. Anon., "Metallic Materials and Elements for Aerospace Vehicle Structures," MIL-HDBK-5B, Department of Defense, Washington, D.C. 20025, September 1971, Chapt. 1.

3. Anon., "A Guide for Fatigue Testing and the Statistical Analysis of Fatigue Data," ASTM Special Technical Publication No. 91-A (Second Edition), 1963.

4. Weibull, W.; Fatigue Testing and Analysis of Results, Advisory Group for Aeronautical Research and Development, North Atlantic Treaty Organization, Pergamon Press, London, 1961.

5. Mechtly, E. A.; "The International System of Units - Physical Constants and Conversion Factors," NASA SP-7012, National Aeronautics and Space Administration, Washington, D.C., 1964.

6. Anderson, P., and Bigg, P. H.; "Changing to the Metric System: Conversion Factors, Symbols, and Definitions," Third Edition, Her Majesty's Stationery Office, London, 1969.

7. Page, C. H., and Vigoureux, P. (Ed.), "SI, The International System of Units," Her Majesty's Stationery Office, London, 1973.

APPENDIX B

RELEVANT TOPICS FROM BEAM THEORY

This appendix contains relevant topics from beam theory that are necessary to support the specific design methods presented in Section 5. First, a discussion of engineering beam theory is presented that relates to slender straight beams with solid or closed cross sectional shapes. In particular, vibration of slender straight beams is discussed to acquaint the designer with the analysis methods and to introduce the eigenfunctions and eigenvalues associated with beam vibration in a logical manner. This data is useful when using the analysis techniques of Section 5.2. Next, the topic of thin-walled open section beams is presented to acquaint the designer with the design parameters encountered in stiffened aircraft structure. This data is useful in supporting Section 5.3 of this report. Finally, a discussion of the beam-like response of a row of panels is presented that illustrates the basic coupled dynamic response characteristics of structure in terms of beam vibration characteristics using a very simple - and accurate - prediction scheme.

B.1.1 BEAMS

As an isolated structural element, beams are not relatively significant with respect to sonic fatigue design problems as compared to plate-like structures. However, the use of beams to stiffen plate structures requires the designer to understand the coupling effect between beams and plates when considering structural configurations that differ significantly from those presented in Section 5.3. Additionally, results from the theory of beam vibrations have been extensively used as the basis of approximation techniques for estimating the response of plates to acoustic excitation (see Section 5.2.2). Hence, this section presents data to supplement the topic of structural vibrations and to support Section 5.2 on plate and shell vibration and Section 5.3 on built-up structure.

B.1.1.1 Notation

A	Area, point in the plane of the beam cross section shape
A_m	Amplitude coefficient for m^{th} beam vibration mode (Figure B.1.1-7)
B_m	Amplitude coefficient for m^{th} beam vibration mode
C_m	Amplitude coefficient for m^{th} beam vibration mode
C_y, C_z	Distance from centroid of beam cross section to shear center of cross section
C_r	Frequency constant for multispan beams (Tables B.1.1-7 through -9)
D	Point in the plane of the beam cross section (Figure B.1.1-7)
D_m	Amplitude coefficient for m^{th} beam vibration mode
E	Young's modulus of beam material; denotes shear center, when referenced to cross-section properties
e	Distance from centroid to shear center
f_m, f_r	Natural frequency of vibration, Hz.
G	Shear modulus of beam
I_o	Mass moment of inertia of beam
I_y, I_z, I_{yz}	Second area moments of inertia of beam cross section shape
J	St. Venant's torsion constant
L	Length of beam
M_y, M_z	Bending moments acting on beam
$p(t)$	Distributed loading on beam, bending
$q(t)$	Distributed loading on beam, torsion
R_{E_x}, R_{E_z}	Warping constants of beam, Equation (B.1.1-29c)
t	Time
u, v, w	Displacement components of beam in (x,y,z) directions, respectively
x, y, z	Coordinate directions
α_m, β_n	Numerical constants defining the vibration mode of an elementary beam (see Table B.1.1-4)
Γ	Warping constant of thin-walled open-section beam
γ	Weight per unit volume of material
$\Theta_m(x)$	Mode of vibration of beam for m^{th} torsional mode of vibration
θ	Rotation of beam cross section
ρ	Mass per unit length of beam
$\Phi_m(x), \phi_m$	Mode of vibration of beam for m^{th} bending mode of vibration
ω_m	Natural frequency of m^{th} mode, radians/sec

B.1.1.2 Slender Straight Elementary Beams

Elementary beams are taken as beams whose cross-section shape is either a solid section or a closed tube. It is assumed that the cross-section shape is symmetrical about the plane in which the loading and resulting deformation occurs. The cross-section shape is assumed to be constant along the length of the beam. For a slender beam the cross-sectional dimensions are small compared to the length of the beam. Elementary beam theory is presented in any book on structural mechanics, for example, Section 35 of Flügge (1). The basic assumption of elementary beam theory concerns the deformation of the beam cross-section during bending. Simply stated, this assumption is: "cross-sections plane and normal to the beam neutral surface before bending remain plane and normal to the neutral surface after bending".

The discussion presented here is categorized as to basic theory and section properties, bending and torsional vibrations, and useful analytical results. This data is introduced in order to support the design data of Section 5.

B.1.1.2.1 Basic Theory and Section Properties

This section provides basic design equations for relating static loading to beam deflection and stress response. It is assumed that elementary beam theory applies and that the loading acts in a plane of symmetry of the beam cross section shape.

Bending of Elementary Beams: The beam configuration and loading nomenclature are presented in Figure B.1.1-1. Assuming small transverse displacements, $w(x,t)$, and a linearly elastic material, the expressions relating the loading to the displacement and bending stresses are

$$M_{y,xx}(x,t) = -q(x,t) \qquad \text{(B.1.1-1a)}$$

$$w_{,xx}(x,t) = \frac{M_y(x,t)}{EI_y} \qquad \text{(B.1.1-1b)}$$

$$\sigma_x(x,z,t) = M_y(x,t)\cdot z/I_y \qquad \text{(B.1.1-1c)}$$

where the transverse loading, $q(x,t)$, and the bending moment, $M(x,t)$, have been assumed to vary both with position along the beam, x, and with time, t.

Alternately, the bending stresses are related to the transverse displacement as

$$\sigma_x(x,z,t) = E\cdot z\cdot w_{,xx}(x,t) \ . \qquad \text{(B.1.1-2)}$$

For a beam with an unsymmetrical cross section shape, as illustrated in Figure B.1.1-2, assuming that elementary beam theory applies, the bending stress is related to the bending moments as

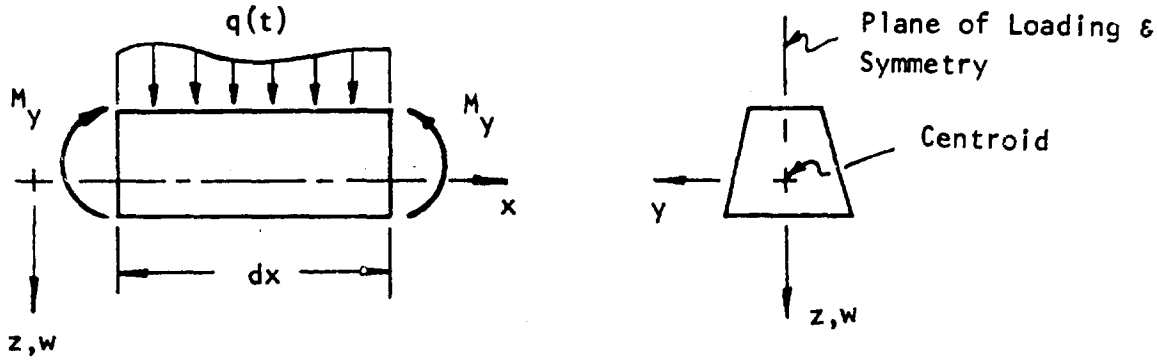

FIGURE B.1.1-1 ELEMENTARY BEAM AXIS SYSTEM, LOADING, AND GEOMETRY NOMENCLATURE

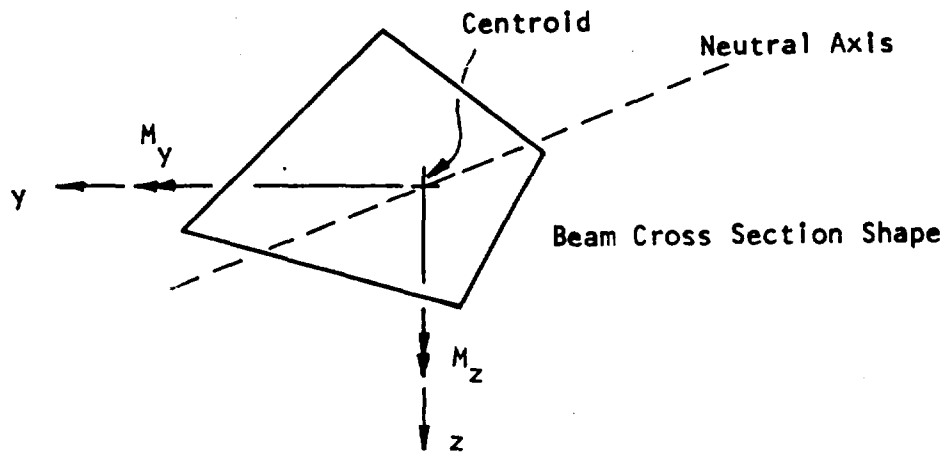

FIGURE B.1.1-2 NOMENCLATURE FOR ELEMENTARY BEAM WITH UNSYMMETRICAL CROSS SECTION

$$\sigma_x = \frac{(M_y I_z + M_z I_y)z - (M_z I_y + M_y I_z)y}{I_y I_z - I_{yz}^2} \qquad \text{(B.1.1-3)}$$

Torsion of Elementary Beams: The beam configuration and loading nomenclature are presented in Figure B.1.1-3. It is assumed that St. Venant torsion theory applies, see Timoshenko (2). In general, the relations between the twist $\theta(x)$, the shear stress, $\tau(x)$, and the torque $T(x)$, are dependent upon the cross section shape. The relationships are of the form

$$\theta_{,x}(x,t) = T(x)/GJ \qquad \text{(B.1.1-4a)}$$

$$\tau_{max}(x,t) = T(x)/k \qquad \text{(B.1.1-4b)}$$

where the torsion constant, J, and the constant, k, are functions of the beam cross section shape.

Section Properties: The section properties I_y, I_z, J and k are presented in Table B.1.1-1 for a few common shapes. Other shapes are included in the compilation by Roark (3). The following general definitions apply

$$I_y = \int_A z^2 dA; \quad I_z = \int_A y^2 dA; \quad I_{yz} = \int_A yz dA \qquad \text{(B.1.1-5)}$$

To shift the reference axis from the centroid to another set of parallel axes as indicated in Figure B.1.1-4 the following rules apply:

$$I_y^* = I_y + AC_z^2 \qquad \text{(B.1.1-6a)}$$

$$I_z^* = I_z + AC_y^2 \qquad \text{(B.1.1-6b)}$$

$$I_{yz}^* = I_y + AC_yC_z \qquad \text{(B.1.1-6c)}$$

where A is the cross section area of the uniform beam.

B.1.1.2.2 Bending and Torsional Vibrations

This section provides design equations and tabulated data for the bending and torsional vibration of beams. A beam-like structure is the most complicated structural element that is amenable, in general, to exact mathematical analysis. As such, the literature is filled with the work of numerous investigators that consider various aspects of the problem such as cross section properties that vary along the length of the beam, effect of axial loading, nonlinear response, etc. The purpose of this section is to

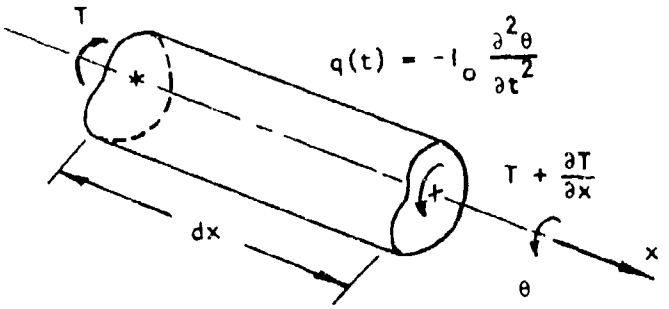

FIGURE B.1.1-3 TORSION MEMBER GEOMETRY AND NOMENCLATURE

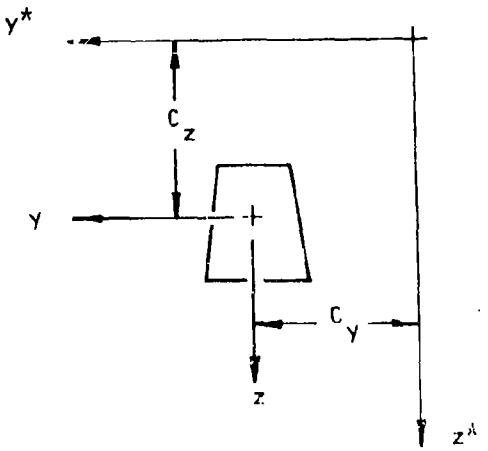

FIGURE B.1.1-4 NOMENCLATURE FOR SHIFTING BENDING AXES FROM (y,z) SYSTEM TO (y*,z*) SYSTEM

TABLE B.1.1-1

CROSS SECTION PROPERTIES OF COMMON STRUCTURAL SHAPES

Cross Section Shape	I_y	I_z	J	k
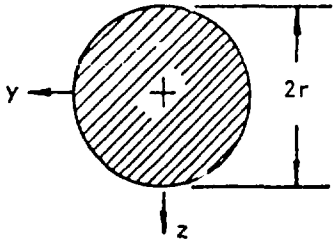	$\frac{\pi}{4} r^4$	$\frac{\pi}{4} r^4$	$\frac{\pi}{2} r^4$	$\frac{\pi}{2} r^3$
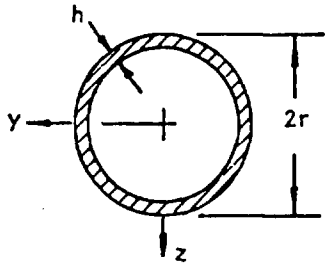	$\frac{\pi}{4}[r^4 - (r-h)^4]$	$\frac{\pi}{4}[r^4 - (r-h)^4]$	$2\pi r^3 h$	$2\pi r^2 h$
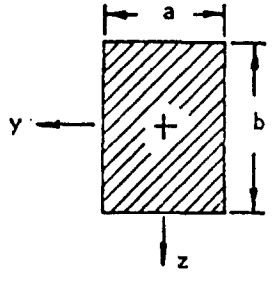	$\frac{1}{12} ab^3$	$\frac{1}{12} a^3 b$	See Tabulated Values Below	
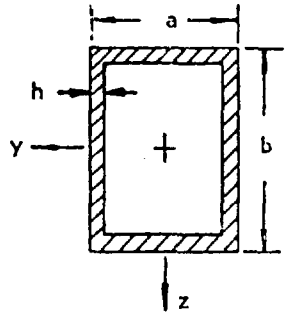	$\frac{h}{2}[b^2(a+\frac{b}{3})$ $-2h(b(a+b)$ $-2h(b+\frac{a}{3}-\frac{2}{3}h))]$	$\frac{h}{2}[a^2(b+\frac{a}{3})$ $-2h(a(a+b)$ $-2h(a+\frac{b}{3}-\frac{2}{3}h))]$	$8h^3(a+b-2h)$	$4h^2(a+b^*-2h)$

*not applicable to reentrant corners

TORSION CONSTANTS FOR SOLID RECTANGULAR SECTION

b/a	1.0	1.2	1.5	2.0	2.5	3.0	4.0	5.0	10.0	∞
J/a^3b	0.1406	0.166	0.196	0.229	0.249	0.263	0.281	0.291	0.312	0.333
k/a^2b	0.208	0.219	0.231	0.246	0.258	0.267	0.282	0.291	0.312	0.333

present basic data for uniform beams with either clamped or simply supported end conditions. A brief literature review for complicating effects is presented in Section B.1.1.4.

Bending Vibrations: The presentation here is concerned with the treatment of transverse bending vibration of straight slender beams supported at the ends. Derivation of the equation of motion and details of the method of solution can be found in almost any text on vibration, for example see Nowacki (3) or Thompson (4). For a uniform slender straight beam undergoing small amplitude free transverse vibrations the governing differential equation of motion is

$$\frac{\partial^2}{\partial x^2}\left(EI_y \frac{\partial^2 w}{\partial x^2}\right) + \rho \frac{\partial^2 w}{\partial t^2} = 0 \qquad \text{(B.1.1-7)}$$

where E is Young's modulus of the beam material

ρ is the mass density per unit length of the beam

I_y is the second area moment of the beam cross section about the neutral axis

$w(x,t)$ is the transverse displacement of the beam neutral surface

The general solution of the above governing equation is of the form (Equation (B.1.1-7) is a separable partial differential equation)

$$w(x,t) = W(x)F(t) \qquad \text{(B.1.1-8)}$$

Substituting Equation (B.1.1-8) into (B.1.1-7) performing the indicated differentiations one obtains two governing ordinary differential equations of the form

$$\ddot{F}(t) + \omega^2 F(t) = 0 \qquad \text{(B.1.1-9a)}$$

$$(EI_y W''(x))'' - \rho\omega^2 W = 0 \qquad \text{(B.1.1-9b)}$$

where the over dots denote differentiation with respect to time, t, the primes denote differentiation with respect to x, and the constant ω^2 - which physically represents frequency of vibration - is called the separation constant. The quantities ω^2 and $W(x)$ which satisfy Equation (B.1.1-9b) and the associated boundary conditions are called eigenvalues and eigenfunctions, respectively. There are, in fact, an infinite number of pairs of eigenvalues and eigenfunctions. The physical meaning is that every beam can vibrate in an infinite number of modes of vibration and each mode has a certain natural frequency. Each eigenfunction, $W_n(x)$, represents the shape of a natural mode of vibration and the corresponding eigenvalue, ω_n^2, represents the square of the natural frequency of that mode. The exact nature of $W_n(x)$ and ω_n^2 depends upon the specific boundary conditions on the beam as well as the stiffness, EI_y, and the mass distribution, ρ, of the beam.

Assuming for the moment that EI_y and ρ can vary slightly along the length of the beam, a very important characteristic of the eigenfunctions, $W_n(x)$, called an orthogonality condition will be illustrated. Consider two pairs of eigenvalues, ω_m and ω_n, and the corresponding eigenvectors $W_m(x)$ and $W_n(x)$ from Equation (B.1.1-9b) one obtains

$$(EI_y W_m'')'' - \rho\omega_m^2 W_m = 0 \qquad \text{(B.1.1-10a)}$$

$$(EI_y W_n'')'' - \rho\omega_n^2 W_n = 0 \qquad \text{(B.1.1-10b)}$$

Multiplying Equation (B.1.1-10a) by $W_n(x)$ and (B.1.1-10b) by $W_m(x)$, integrating over the length of the beam, subtracting the two resulting equations, and integrating by parts one obtains the results

$$(\omega_m^2 - \omega_n^2)\int_o^L \rho(x)W_m(x)W_n(x)dx = \left\{[W_n(EIW_m'')' - W_m(EIW_n'')'] - EI(W_n'W_m'' - W_m'W_n'')\right\}_o^L \qquad \text{(B.1.1-11)}$$

The right hand side of Equation (B.1.1-11) vanishes if at each end of the beam there is prescribed at least one of the following pairs of boundary conditions

$$W = 0 \quad \text{and} \quad W' = 0 \qquad \text{(B.1.1-12a)}$$

$$W = 0 \quad \text{and} \quad EIW'' = 0 \qquad \text{(B.1.1-12b)}$$

$$W' = 0 \quad \text{and} \quad (EIW'')' = 0 \qquad \text{(B.1.1-12c)}$$

$$EIW'' = 0 \quad \text{and} \quad (EIW'')' = 0 \qquad \text{(B.1.1-12d)}$$

Assuming that at least one of the pairs of boundary conditions given by Equations (B.1.1-12) is applied at each end of the beam, Equation (B.1.1-11) reduces to (since $\omega_n \neq \omega_m$)

$$\int_o^L \rho(x)W_m(x)W_n(x)dx = 0 \qquad m \neq n \qquad \text{(B.1.1-13)}$$

Equation (B.1.1-13) is known as the orthogonality condition for the natural mode shapes of the beam. It is important to observe that satisfaction of the orthogonality condition depends upon the existence of the boundary condition pairs prescribed by Equations (B.1.1-12). These boundary conditions have the following physical significance

Boundary Condition	Physical Meaning
$W = 0$	Zero transverse displacement at the end of the beam
$W' = 0$	Zero slope at the end of the beam
$EIW'' = 0$	Zero bending moment at the end of the beam
$(EIW'')' = 0$	Zero shear restraint at the end of the beam.

The eigenfunction or mode shape, $W_m(x)$, which is a solution to Equation (B.1.1-9b) subject to the appropriate boundary conditions of Equations (B.1.1-12) can be determined only as a relative amplitude. Hence, one may assign any convenient amplitude to $W_m(x)$ as desired. This process is called normalization of the mode shape. For example, one may desire a unit amplitude at a point $x = a$ on the beam for the m^{th} mode so that the normalized value for the m^{th} mode is given by

$$\Phi_m(x) = A_m W_m(x) \qquad \text{(B.1.1-14a)}$$

where $A_m = 1/W_m(a)$.

Another, more commonly used, normalization technique is to define A_m as

$$A_m^2 = M / \int_0^L \rho(x) W_m^2(x)\,dx \qquad \text{(B.1.1-14b)}$$

where M is taken as the total mass of the beam.

If the beam cross section and material properties are uniform along the length of the beam Equation (B.1.1-14b) becomes

$$\int_0^L \Phi_m^2(x)\,dx = 1 \qquad \text{(B.1.1-15)}$$

Combining this result with the orthogonality condition, Equation (B.1.1-13), one obtains the following very useful results.

$$\int_0^L \Phi_m(x)\Phi_n(x)\,dx = 0 \qquad \text{(B.1.1-16a)}$$

$$\int_0^L \Phi_m^2(x)\,dx = L \qquad \text{(B.1.1-16b)}$$

The solution to Equation (B.1.1-9a) requires a knowledge of the initial conditions of the beam in the form $w(x,0) = f_1(x)$ and $\dot{w}(x,0) = f_2(x)$. Except for the transient vibration response, the solution for the response time history is relatively unimportant. The main concern is to obtain the solution to equation (B.1.1-9b) subject to the appropriate boundary conditions.

Young and Felgar (5), have tabulated the numerical values for the eigenvalues, normalized eigenfunctions and derivatives of the eigenfunctions of uniform straight beams for the first five modes of vibration for the following boundary conditions: clamped-clamped, clamped-free, and clamped-supported. This nomenclature is related to the mathematical relationships of Equations (B.1.1-12) as indicated in Table B.1.1-2.

TABLE B.1.1-2
DEFINITION OF BOUNDARY CONDITIONS

Boundary Conditions	At x = 0	At x = l
Supported-Supported	(B.1.1-12b)	(B.1.1-12b)
Clamped-Clamped	(B.1.1-12a)	(B.1.1-12a)
Clamped-Free	(B.1.1-12a)	(B.1.1-12d)
Clamped-Supported	(B.1.1-12a)	(B.1.1-12b)

The general solution to Equation (B.1.1-9b) when normalized as indicated by Equation (B.1.1-15) has the form for the m^{th} mode

$$\phi_m(x) = A_m\cosh(\beta_m x) + B_m\cos(\beta_m x) + C_m\sinh(\beta_m x) + D_n\sin(\beta_m x) \qquad (B.1.1\text{-}17)$$

where the constants A_m, B_m, C_m, D_m, and β_m depend upon the boundary conditions.

The natural frequency of vibration for the m^{th} mode is related to the constant β_m as

$$\omega_m^2 = EI_y\beta_m^4/\rho \qquad (rad/sec)^2 \qquad (B.1.1\text{-}18a)$$

or

$$\omega_m^2 = EI_y(\beta_m L)^4/\rho L^4 \qquad (B.1.1\text{-}18b)$$

Values for A_m, B_m, C_m and D_n are presented in Table B.1.1-3 for the boundary conditions presented in Table B.1.1-2.

TABLE B.1.1-3

TABLE OF COEFFICIENTS FOR EQUATION (B.1.1-17)

Boundary Condition	A_m	B_m	C_m	D_n
Supported-Supported	0	0	0	α_m
Clamped-Clamped	1	-1	$-\alpha_m$	α_m
Clamped-Free	1	-1	$-\alpha_m$	α_m
Clamped-Supported	1	-1	$-\alpha_m$	α_m

For the first five modes and the various boundary conditions the numerical values for α_m and β_m are presented in Table B.1.1-4.

TABLE B.1.1-4
VALUES OF α_m AND β_m FOR NORMAL BEAM MODES

Supported-Supported

m	α_m	$\beta_m L$
1	1.4142 = $\sqrt{2}$	π
2	1.4142	2π
3	1.4142	3π
4	1.4142	4π
5	1.4142	5π

Clamped-Clamped

m	α_m	$\beta_m L$
1	0.9825	4.7300
2	1.007	7.8532
3	0.9999	10.9956
4	1.0000	14.1372
5	0.9999	17.2788

Clamped-Free

m	α_m	$\beta_m L$
1	0.7341	1.8751
2	1.0185	4.6940
3	0.9992	7.8548
4	1.0000	10.9955
5	0.9999	14.1372

Clamped-Supported

m	α_m	$\beta_m L$
1	1.0008	3.9266
2	1.0000	7.0686
3	1.0000	10.2102
4	1.0000	13.3918
5	1.0000	16.4934

The most commonly used boundary conditions are supported-supported and clamped-clamped edges. The mode shape for supported-supported condition is a sine wave and represents no difficulty in calculating results. For clamped-clamped edges, values of the mode shape, Equation (B.1.1-17), and its second derivative are presented in Table B.1.1-5 for the first mode, m = 1, and the third mode, m = 3. More extensive tabulations are presented by Young and Felgar (5). These results will prove useful when using the methods presented in Section 5.2.2

TABLE B.1.1-5

NUMERICAL VALUES FOR $\Phi_1(x)$, $\Phi_1''(x)$, $\Phi_3(x)$, $\Phi_3''(x)$

FOR A BEAM WITH CLAMPED-CLAMPED EDGES

x/L	Φ_1	$\Phi_1'' = \frac{1}{\beta_1^2}\frac{d^2\Phi_1}{dx^2}$	Φ_3	$\Phi_3'' = \frac{1}{\beta_3^2}\frac{d^2\Phi_3}{dx^2}$
0.00	0.00000	2.00000	0.00000	2.00000
0.10	0.18910	1.07433	0.77005	-0.10393
0.20	0.61939	0.19545	1.50782	-1.28572
0.30	1.09600	-0.54401	0.86864	-0.79387
0.40	1.45545	-1.04050	-0.62837	0.65569
0.50	1.58815	-1.21565	-1.40600	1.42238
0.60	1.45545	-1.04050	-0.62837	0.65569
0.70	1.09600	-0.54401	0.86864	-0.79387
0.80	0.61939	0.19545	1.50782	-1.28572
0.90	0.18910	1.07433	0.77005	-0.10393
1.00	0.00000	2.00000	0.00000	2.00000

Example: Calculate the natural frequencies of a hollow tube beam with diameter 0.25 inches, wall thickness 0.020 inch and length 12.0 inches assuming both clamped-clamped and supported-supported edge conditions. Assume $E = 10.3 \times 10^6$ psi $\gamma = 0.101$ lbs/in^3.

From Table B.1.1-1 one obtains

$$I_y = \frac{\pi}{4}\left[(0.25)^4 - (0.25 - 0.02)^4\right] = 0.000870 \text{ in}^4$$

$$EI_y = (10.3 \cdot 10^6)(0.00087) = 8.962 \cdot 10^3 \text{ in.lb.}$$

The mass per unit length of the beam is

$$\rho = \gamma A = \pi(.101)\left((.25)^2 - (.25-.02)^2\right)/386.4 = 7.88 \cdot 10^{-6}$$

From Equation B.1.1-18

$$\omega_m^2 = EI_y(\beta_m L)^4/\rho L^4 = 5.4824 \cdot 10^4 (\beta_m L)^4 \quad (\text{rad/sec})^2$$

or

$$f_m = 37.265(\beta_m L)^2 \text{ Hz.}$$

From Table B.1.1-4 one obtains the results

	Supported-Supported		Clamped-Clamped	
m	$(\beta_m L)$	f_m, Hz	$(\beta_m L)$	f_m, Hz
1	π	368.	4.7300	834.
2	2π	1,471.	7,8532	2,298.
3	3π	3,310.	10.9956	4,506.
4	4π	5,885.	14.1372	7,448.
5	5π	9,195.	17.2788	11,126.

Torsional Vibrations: The problem of twisting or torsional vibration of slender beams is treated in a manner analogous to that for bending vibrations discussed previously. For beams with a solid or closed tube cross section, the bending motion and the twisting motion are uncoupled and can be treated independently.

For torsional vibration the governing equation of motion is

$$\frac{\partial}{\partial x}\left[GJ \cdot \frac{\partial \theta}{\partial x}\right] - I_o \frac{\partial^2 \theta}{\partial t^2} = 0 \qquad \text{(B.1.1-19)}$$

where G is the shear modulus of the material

J is St. Venant's torsion constant

I_o is the moment of inertia per unit of length about the center of the twist

$\theta(x,t)$ is the twist of the beam

The general solution to Equation (B.1.2-19) has the form

$$\theta(x,t) = \Theta(x)F(t) \qquad \text{(B.1.1-20)}$$

For a uniform beam undergoing free vibration the eigenfunction must satisfy the equation of motion

$$GJ\Theta_n''(x) + \omega^2 I_o \Theta_n(x) = 0 \qquad \text{(B.1.1-21)}$$

The general solution to Equation (B.1.2-21) has the form for the m^{th} mode of vibration

$$\Theta_m(x) = A_m \sin(\gamma_m x) + B_m \cos(\gamma_m x) \qquad \text{(B.1.1-22)}$$

The boundary conditions associated with Equation (B.1.1-22) are

Clamped Edge $\Theta_m(0) = 0$ or $\Theta_m(L) = 0$ (B.1.1-23a)

Free Edge $\Theta_m'(0) = 0$ or $\Theta_m'(L) = 0$ (B.1.1-23b)

For a clamped end at $x = 0$ and a free end at $x = L$, the frequencies and mode shapes for torsional vibration of the rod are

$$\Theta_m(x) = A_m \sin(\gamma_m x) \qquad \text{(B.1.1-24)}$$

$$\omega_m^2 = \gamma_m^2 GJ/I_o = \frac{n^2\pi^2 GJ}{4I_o L^2} \quad (\text{rad/sec})^2 \qquad \text{(B.1.1-25)}$$

B.1.1.2.3 Useful Analytical Results

The main importance of studying beam vibrations in relation to the sonic fatigue problem is that the eigenfunctions given by Equation (B.1.1-17) are extensively used in approximation techniques for estimating the dynamic response of plate-like and shallow shell structures. In particular, energy methods such as the Rayleigh or Rayleigh-Ritz methods require the evaluation of integrals of the assumed modes and derivatives of the assumed modes. As a result, Felgar (6) tabulated an extensive set of these integrals, and his

work has been used by numerous investigators in the past 20 years. To facilitate the utilization of the analytical sections of this handbook and for reference, integrals of clamped-clamped beam modes are presented in Table B.1.1-6.

It should be noted that the derivatives of the eigenfunctions for a vibrating beam satisfy the following relationships

$$\phi_n''''(x) = \phi_n(x);\ \phi_n^{V}(x) = \phi_n'(x);\ \phi_n^{V\prime}(x) = \phi_n''(x)$$

where differentiation is with respect to the argument $(\beta_n x)$.

TABLE B.1.1-6 (Continued)

INTEGRALS OF CLAMPED-CLAMPED BEAM MODES
(FROM REFERENCE 6)

See Equation B.1.1-17 and Tables B.1.1-3 and -4

$$\int_0^L \phi_n(x)dx = \frac{2\alpha_n}{\beta_n}[1 - (-1)^n]$$

$$\int_0^L \phi_n^2(x)dx = L$$

$$\int_0^L \frac{d\phi_n}{dx}dx = 0$$

$$\int_0^L \left(\frac{d\phi_n}{dx}\right)^2 dx = \alpha_n\beta_n(\alpha_n\beta_n L - 2)$$

$$\int_0^L \frac{d^2\phi_n}{dx^2}dx = 0$$

$$\int_0^L \left(\frac{d^2\phi_n}{dx^2}\right)^2 dx = \beta_n^4 L$$

$$\int_0^L \frac{\phi^3\phi_n}{dx^3}dx = -2\beta_n^2[(-1)^n + 1]$$

$$\int_0^L \left(\frac{d^3\phi_n}{dx^3}\right)^2 dx = \alpha_n\beta_n^5(\alpha_n\beta_n L + 6)$$

$$\int_0^L \phi_n\frac{d\phi_n}{dx} = 0$$

$$\int_0^L \frac{d\phi_n}{dx}\frac{d^2\phi_n}{dx^2}dx = 0$$

$$\int_0^L \phi_n\frac{d^2\phi_n}{dx^2}dx = \alpha_n\beta_n(2 - \alpha_n\beta_n L)$$

$$\int_0^L \frac{d\phi_n}{dx}\frac{d^3\phi_n}{dx^3}dx = -\beta_n^4 L$$

$$\int_0^L \phi_n\frac{d^3\phi_n}{dx^2}dx = 0$$

$$\int_0^L \frac{d^2\phi_n}{dx^2}\frac{d^3\phi_n}{dx^3}dx = 0$$

$$\int_0^L \phi_m(x)\phi_n(x)dx = 0$$

TABLE B.1.1-6 (Concluded)

$$\int_0^L \frac{d\phi_m}{dx}\frac{d\phi_n}{dx}\,dx = \frac{4\beta_m^2\beta_n^2(\alpha_m\beta_m - \alpha_n\beta_n)}{\beta_n^4 - \beta_m^4}\left[(-1)^{m+n} + 1\right]$$

$$\int_0^L \frac{d^2\phi_m}{dx^2}\frac{d^2\phi_n}{dx^2}\,dx = 0$$

$$\int_0^L \frac{d^3\phi_m}{dx^3}\frac{d^3\phi_n}{dx^3}\,dx = \frac{4\beta_m^3\beta_n^3(\alpha_m\beta_m^3 - \alpha_n\beta_n^3)}{\beta_n^4 - \beta_m^4}\left[(-1)^{m+n} + 1\right]$$

$$\int_0^L \phi_n\frac{d\phi_m}{dx}\,dx = \frac{4\beta_n^2\beta_m^2}{\beta_n^4 - \beta_m^4}\left[1 - (-1)^{m+n}\right]$$

$$\int_0^L \phi_n\frac{d^2\phi_m}{dx^2}\,dx = \frac{4\beta_m^2\beta_m^3(\alpha_n\beta_n - \alpha_m\beta_m)}{\beta_n^4 - \beta_m^4}\left[1 + (-1)^{m+n}\right]$$

$$\int_0^L \phi_n\frac{d^3\phi_m}{dx^3}\,dx = \frac{4\beta_m^3\beta_n^3\alpha_m\alpha_n}{\beta_n^4 - \beta_m^4}\left[(-1)^{m+n} - 1\right]$$

$$\int_0^L \frac{d\phi_n}{dx}\frac{d^2\phi_m}{dx^2}\,dx = \frac{4\beta_m^3\beta_n^3\alpha_n\alpha_n}{\beta_n^4 - \beta_m^4}\left[1 - (-1)^{m+n}\right]$$

$$\int_0^L \frac{d\phi_n}{dx}\frac{d^3\phi_m}{dx^3}\,dx = 0$$

$$\int_0^L \frac{d^2\phi_n}{dx^2}\frac{d^3\phi_m}{dx^3}\,dx = \frac{4\beta_m^6\beta_n^2}{\beta_n^4 - \beta_m^4}\left[1 - (-1)^{m+n}\right]$$

B.1.1.3 Slender Thin-Walled Open Section Beams

This section provides a discussion of the topic of vibration of slender straight beams whose cross section shape is the form of a thin-walled open section. This form of beam is the type most commonly encountered in aircraft design. That is, the cross section shape is the form of a zee, hat, channel or other shape attached to a plate so that the cross section remains open. The deformation of such beams either as an isolated system or as a part of a built up structure is such that the bending and torsion motion is coupled.

The basic theory of thin-walled open section beams is developed by Timoshenko (7), Vlasov (8), and Oden (9). Gere (10) and Gere and Lin (11) discuss the general coupled vibrations of such beams. Lin (12) later published a note describing the application of his earlier work to consider the constrained bending-torsion vibrations when the beam is connected to a thin plate.

The basic difference between a thin-walled open section beam and a beam with a solid or closed cross section is that for nonuniform torsion of thin-walled beams, the cross section warps causing the bending and the torsion motion to be coupled.

Coupled Bending-Torsion Vibrations: The general case of coupled bending-torsion vibrations is presented by Gere and Lin (11) for the case of motion referenced to the shear center with axes taken parallel to the principal centroidal axes of the beam. The governing equations of motion are for forced vibration.

$$EI_\zeta \frac{\partial^4 v}{\partial x^4} + \rho \frac{\partial^2 v}{\partial t^2} - \rho C_z \frac{\partial^2 \theta}{\partial t^2} = p_y(t) \qquad \text{(B.1.1-26a)}$$

$$EI_\eta \frac{\partial^4 w}{\partial x^4} + \rho \frac{\partial^2 w}{\partial t^2} + \rho C_y \frac{\partial^2 \theta}{\partial t^2} = p_z(t) \qquad \text{(B.1.1-26b)}$$

$$E\Gamma \frac{\partial^4 \theta}{\partial x^4} - GJ \frac{\partial^2 \theta}{\partial x^2} - \rho C_z \frac{\partial^2 v}{\partial t^2} + \rho C_y \frac{\partial^2 w}{\partial t^2} + I_o \frac{\partial^2 \theta}{\partial t^2} = p_\theta(t) \qquad \text{(B.1.1-26c)}$$

where $v(x,t)$ is the translation of the shear center in the y direction

$w(x,t)$ is the translation of the shear center in the z direction

$\theta(x,t)$ is the rotation of the beam about the shear center

E is Young's modulus

G is the shear modulus

ρ is the mass density per unit length

I_ζ, I_η are principal centroidal moments of inertia

Γ is the warping constant of the beam cross section taken about the shear center

J is St. Venants torsion constant

I_o is the mass polar moment of inertia of the cross section about the shear center.

The axis system, displacements and geometry are presented in Figure B.1.1-5.

The twelve boundary conditions associated with Equations (B.1.1-26) are to be applied to each end of the beam and are classified as:

Supported End:

$$v = w = \theta = 0 \qquad \text{(B.1.1-27a)}$$

$$\frac{d^2v}{dx^2} = \frac{d^2w}{dx^2} = \frac{d^2\theta}{dx^2} = 0$$

Clamped End:

$$v = w = \theta = 0 \qquad \text{(B.1.1-27b)}$$

$$\frac{dv}{dx} = \frac{dw}{dx} = \frac{d\theta}{dx} = 0$$

The general solution of Equations (B.1.1-26) subject to the boundary conditions (B.1.1-27) is extremely tedious and requires a computer solution (see Gere (10)). Alternately, the Rayleigh method has been used by Gere and Lin (11) and by Lin (12) to estimate response frequencies. Even with the approximate techniques, one must solve, in general, a cubic equation for the response frequencies. The greatest simplification of Equations (B.1.1-26) occurs when the shear center and the centroid coincide such as an equal leg zee section so that $C_y = C_z = 0$ and the equations are uncoupled.

The analysis presented by Lin (12) considers the beam to be attached to a thin plate so that the beam is constrained from moving in the plane of the plate. Then, one obtains two coupled equations of motion for free vibrations as

$$EI_\zeta \frac{\partial^4 v}{\partial x^4} - EI_{\zeta\eta} S_y \frac{\partial^4 \theta}{\partial x^4} + \rho \frac{\partial^2 v}{\partial t^2} - \rho C_z \frac{\partial^2 \theta}{\partial t^2} = 0 \qquad \text{(B.1.1-28a)}$$

$$E\Gamma_s \frac{\partial^4 \theta}{\partial x^4} - GJ \frac{\partial^2 \theta}{\partial x^2} - EI_{\zeta\eta} S_y \frac{\partial^4 v}{\partial x^4} - \rho C_z \frac{\partial^2 v}{\partial t} + I_s \frac{\partial^2 \theta}{\partial t^2} = 0 \qquad \text{(B.1.1-28b)}$$

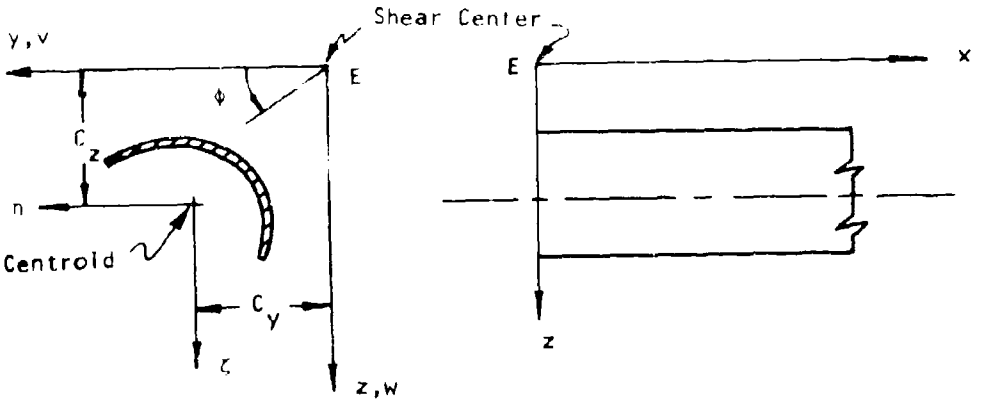

(η,ζ) is a principal axis system

FIGURE B.1.1-5 AXIS SYSTEM, GEOMETRY, AND NOMENCLATURE FOR COUPLED BENDING-TORSION VIBRATION OF THIN-WALLED OPEN SECTION BEAMS

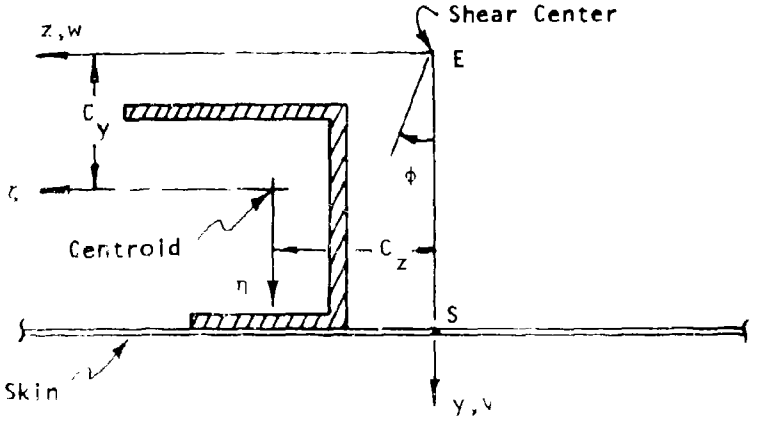

FIGURE B.1.1-6 AXIS SYSTEM, GEOMETRY, AND NOMENCLATURE FOR VIBRATION OF A THIN-WALLED OPEN SECTION BEAM ATTACHED TO A PLATE

where $I_s = I_o + \rho(S_y - C_y)^2 + \rho C_z^2$ is the mass polar moment of inertia about the point S

$\Gamma_s = \Gamma + I_{\eta} S_y^2$ is the warping constant of the section about the point S.

The displacements, v and θ are measured about the shear center as indicated in Figure B.1.1-6. The boundary conditions on v and θ are as presented in Equations (B.1.1-27).

Section Properties: The section properties for a thin-walled open section beam are defined in terms of a centroidal (x,z) axis system and a warping function $\phi(x,z)$ defined with the pole (rotation axis) taken at the shear center of the cross section. General expressions for the cross section area, area moments, torsion constant, and warping constants are presented for zee, channel, and hat cross-sectional shapes. The definition of these parameters is as follows:

$\bar{x}$, the location of the centroid, as indicated

e, the location of the shear center, as indicated

A, the cross sectional area

$$I_{xx} = \int_A x^2 dA \qquad I_{xz} = \int_A xz dA \qquad I_{zz} = \int_A z^2 dA \qquad \text{(B.1.1-29a)}$$

$$J = \int_A [(\phi_{,x} - z)^2 + (\phi_{,z} + x)^2] dA \quad \text{St. Venant's Torsion Constant} \quad \text{(B.1.1-29b)}$$

$J = \frac{1}{3} \sum_i b_i h_i^3$ b_i = mid line length of the i^{th} segment of a straight section

h_i = thickness of the i^{th} segment

$$R_{E_z} = \int_A x\phi dA \qquad R_{E_x} = \int_A z\phi dA \qquad \Gamma_e = \int_A \phi^2 dA \qquad \text{(B.1.1-29c)}$$

Note: R_{E_z} and R_{E_x} vanish if ϕ is defined relative to a mean warping of the cross section (see Timoshenko [7])

To shift the reference axis from the centroid to another set of parallel axes, the area moments transform as indicated by Equations (B.1.1-6) and Figure B.1.1-4. To shift the pole (rotation axis) from the shear center the following general rules apply

$$R_{Ax} = R_{Dx} + (d_z - a_z)I_{xz} - (d_x - a_x)I_{xx} \qquad \text{(B.1.1-30a)}$$

$$R_{Az} = R_{Dz} + (d_z - a_z)I_{zz} - (d_x - a_x)I_{xz} \qquad \text{(B.1.1-30b)}$$

$$\Gamma_A = \Gamma_D + (d_z - a_z)^2 I_{zz} + (d_x - a_x)^2 I_{xx} \qquad \text{(B.1.1-30c)}$$

$$-2(d_z - a_z)(d_x - a_x)I_{xz} + 2(d_z - z)R_{Dz} - 2(d_x - a_x)R_{Dx}$$

where (x,z) is a centroidal axis system for the cross section and the points A and D are general points in the plane of the cross section as indicated in Figure B.1.1-7.

General expressions for the various section properties for zee, channel, and hat section shapes are presented in Figures B.1.1-8, -9, and -10, respectively. These results are from Rudder (13).

B.1.1.4 Uniform Beams on Multiple Supports

The topic of vibration of uniform beams on multiple supports is relevant to the sonic fatigue problem in that the frequency response of a beam system is similar to that exhibited by an array of panels of constant width joined end to end. It is perhaps more to the point that a uniform beam system allows for a sound analytical treatment where as the plate problem does not. The beam problem can be related approximately to the plate problem with an appropriate lumping of the physical parameters of the beam (14).

One of the earliest analytical developments reported in the literature is that presented by Miles (15) in which he utilized difference equations to obtain frequency response estimates for a uniform beam on multiple interior supports that allowed only for rotation about the interior support. Mercer (16) using the normal mode method calculated the response of a multiple supported uniform beam to a random pressure field. Lin (17) considered the case of elastic interior supports. Olson (18) presents a direct technique for computing frequency response to a random pressure excitation using the finite element method with a uniform multiple supported beam as a structural model.

One of the earliest efforts in calculating the natural frequencies was developed by Ayre and Jacobsen (19) using physical reasoning to obtain simplified results for a uniform beam resting on equally spaced interior supports that allow the beam to rotate freely. For the end restraints they consider both ends simply supported, both ends clamped, and one end clamped and the other end simply supported. The response frequency spectrum for a multiple supported beam is basically different from that of a single span beam. For the multiple support case the natural frequencies appear in groups with the number of modes in each group equal to the number of spans of the beam. There are an infinite number of frequency groups.

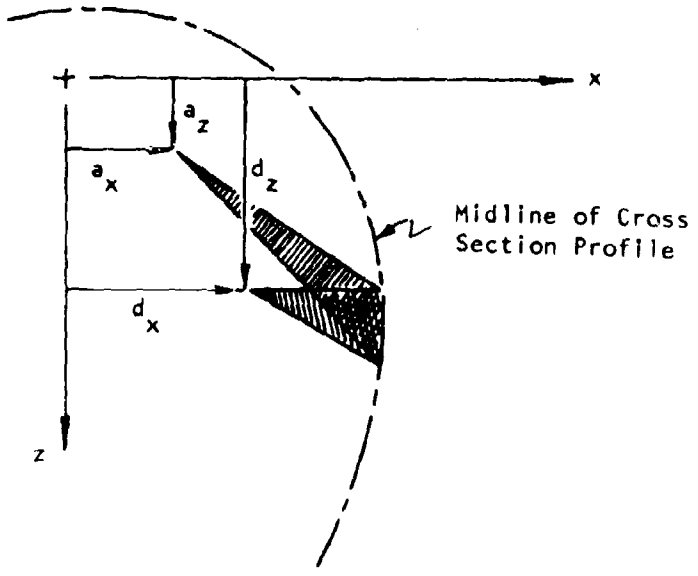

FIGURE B.1.1-7 AXIS SYSTEM AND NOMENCLATURE FOR SHIFTING THE POLE (ROTATION AXIS) OF A THIN-WALLED OPEN SECTION BEAM

GENERAL EXPRESSIONS FOR STIFFENER GEOMETRIC PARAMETERS

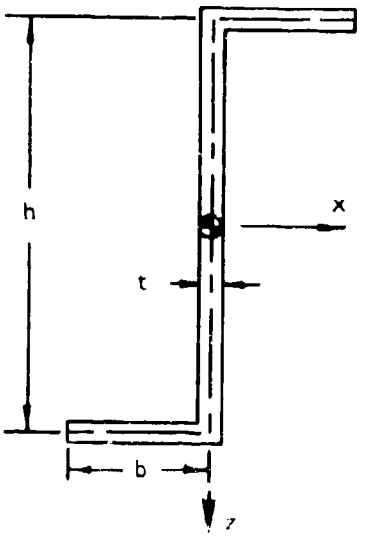

$$A = t(h + 2b)$$

$$I_{xx} = \frac{t}{12}\left[h^2(6b + h) + t^2(3h + 2b)\right]$$

$$I_{xz} = -\frac{th}{4}(2b + t)(2b - t)$$

$$I_{zz} = \frac{t}{12}\left[8b^3 + ht^2\right]$$

$$J = \frac{t^3}{3}\left[2b + h\right]$$

$$I_e = \frac{tb^3h^2(b + 2h)}{12(2b + h)}$$

FIGURE B.1.1-8. GEOMETRIC PROPERTIES - ZEE SECTION

GENERAL EXPRESSIONS FOR STIFFENER GEOMETRIC PARAMETERS

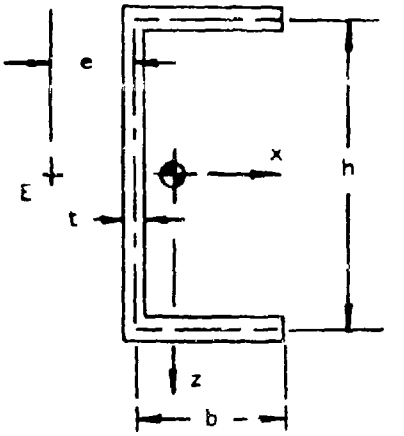

$$\bar{x} = b^2/(2b + h)$$

$$e = 3b^2/(6b + h)$$

$$A = t(h + 2b)$$

$$I_{xx} = \frac{t}{12}\left[h^2(6b + h) + t^2(3h + 2b)\right]$$

$$I_{xz} = 0$$

$$I_{zz} = \frac{t}{12}\left[12h\bar{x}^2 + 8b^3 - 24\bar{x}b(b - \bar{x}) + 12b(b - 2\bar{x})t + 6(b - \bar{x})t^2 + t^3\right]$$

$$J = \frac{1}{3}t^3(2b + h)$$

$$\Gamma_e = \frac{tb^3h^2(3b + 2h)}{12(6b + h)}$$

$$R_{Ez} = 0$$

$$R_{Ex} = 0$$

NOTE: For warping constants, the pole is taken at the shear center.

FIGURE B.1.1-9. GEOMETRIC PROPERTIES - CHANNEL SECTION

GENERAL EXPRESSIONS FOR STIFFENER GEOMETRIC PARAMETERS

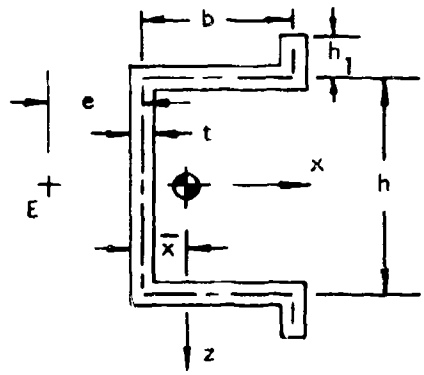

$$\bar{x} = \frac{b(b + 2h_1)}{(2b + h + 2h_1)}$$

$$e = \frac{b(3bh^2 + 2h_1(3h^2 - 4h_1^2))}{[h^2(6b + h) + 2h_1(3h^2 + 6hh_1 + 4h_1^2)]}$$

$$A = t(h + 2b + 2h_1)$$

$$I_{xx} = \frac{1}{12} t(h - t)^3 + \frac{1}{6} t(b + t)(t^2 + 3h^2) + \frac{1}{48} t(2h_1 - t)[(2h_1 - t)^2 + 12(h + h_1)^2]$$

$$I_{xz} = 0$$

$$I_{zz} = \frac{1}{12} t(h - t)(t^2 + \bar{x}^2) + \frac{2}{3} t(b + t)^3 + \frac{1}{2} t\bar{x}(b + t)[\bar{x} - 2b + 2t]$$
$$+ \frac{1}{24} t(2h_1 - t)[t^2 + 24(b - \bar{x})^2]$$

$$J = \frac{1}{3} t^3[h + 2b + 2h_1]$$

$$R_{Ex} = 0$$

$$R_{Ez} = 0$$

$$\Gamma_e = \frac{t}{12}[2b^3h^2 + 2bh^2e(e - b) + 2b^2h_1(3h^2 - 6hh_1 + 4h_1^2)$$
$$- 4bh_1e(3h^2 - 4h_1^2) + e^2(h + 2h_1)^3]$$

FIGURE B.1.1-10. GEOMETRIC PROPERTIES - HAT SECTION

Following the work of Ayre and Jacobsen, the response frequency for the r^{th} mode is given by the expression

$$f_r = \frac{C_r^2}{2L^2}\sqrt{\frac{EI_y}{\rho}} \quad \text{Hz} \qquad \text{(B.1.1-31)}$$

where the constant C_r depends upon the number of equally spaced spans of the beam and the end supports of the beam. The remaining nomenclature in Equation (B.1.1-31) is identical to that used in Equation (3.1.1-7).

To obtain estimates of the natural frequencies of a one-dimensional array of plates with width, b, length, a, and thickness, h, the frequency expression in Equations (B.1.1-31) becomes assuming a fundamental mode across the width of the panel

$$f_r = \frac{C_r^2 h}{2ab}\sqrt{\frac{E}{12(1-\nu^2)\rho}}\left[\left(\frac{b}{a}\right) + \left(\frac{a}{b}\right)\right] \quad \text{Hz} \qquad \text{(B.1.1-32)}$$

where ρ is the mass per unit volume of the plate material.

Numerical values for the constant C_r are presented in Table B.1.1-7 for both extreme ends simply supported, for the first ten modes of vibration and configurations of five spans or less. Table B.1.1-8 presents values of C_r for both extreme ends clamped and Table B.1.1-9 presents values of C_r for one end simply supported and the other end clamped. These tabulated values are from the work of Ayre and Jacobsen (19) where they present values of C_r for the first 25 frequencies and structures of up to 13 equal spans.

The beam nomenclature and geometry are presented in Figure B.1.1-11. The one dimensional panel array as characterized by Equation (B.1.1-32) is illustrated in Figure B.1.1-12. Typical mode shapes for simply supported and clamped ends are presented in Figure B.1.1-13.

Example: A piece of hydraulic tubing is supported between rigid connections at the extreme ends with intermediate supports at 18 inch intervals for three spans. The dimensions of the tubing is a diameter of 0.25 inch with a wall thickness of 0.020 inch. The material properties are $E = 16.4 \times 10^6$ psi and $\gamma = 0.16$ lbs/in^3. Calculate the first ten natural frequencies of the system.

From Table B.1.1-1 the moment of inertia of the cross section is

$$I_y = \frac{\pi}{4}\left[(0.125)^4 - (0.125 - 0.02)^4\right] = 9.628 \times 10^{-5} \quad \text{in}^4$$

The mass per unit length of the tube is

$$\rho = (0.16)\pi[(0.125)^2 - (0.125 - 0.02)^2]/386.4 = 4.988 \times 10^{-6}$$

TABLE B.1.1-7

VALUES OF C_r FOR BOTH EXTREME ENDS SIMPLY SUPPORTED
(See Equations (B.1.1-31) and (B.1.1-32))

NUMBER OF SPANS OF UNIFORM LENGTH, L

r	1	2	3	4	5
1	1.00	1.00	1.00	1.00	1.00
2	2.00	1.25	1.13	1.08	1.05
3	3.00	2.00	1.37	1.25	1.18
4	4.00	2.25	2.00	1.42	1.32
5	5.00	3.00	2.13	2.00	1.45
6	6.00	3.25	2.37	2.08	2.00
7	7.00	4.00	3.00	2.25	2.05
8	8.00	4.25	3.13	2.42	2.18
9	9.00	5.00	3.37	3.00	2.32
10	10.00	5.25	4.00	3.08	2.45

TABLE B.1.1-8

VALUES OF C_r FOR BOTH EXTREME ENDS CLAMPED
(See Equations (B.1.1-31) and (B.1.1-32))

NUMBER OF SPANS OF UNIFORM LENGTH, L

r	1	2	3	4	5
1	1.51	1.25	1.13	1.08	1.05
2	2.50	1.51	1.37	1.25	1.18
3	3.50	2.25	1.51	1.42	1.32
4	4.50	2.50	2.13	1.51	1.45
5	5.50	3.25	2.37	2.08	1.51
6	6.50	3.50	2.50	2.25	2.05
7	7.50	4.25	3.13	2.42	2.18
8	8.50	4.50	3.37	2.50	2.32
9	9.50	5.25	3.50	3.08	2.45
10	10.50	5.50	4.13	3.25	2.50

TABLE B.1.1-9

VALUES OF C_r FOR ONE END SIMPLY SUPPORTED AND ONE END CLAMPED

(See Equations (B.1.1-31) and (B.1.1-32))

	NUMBER OF SPANS OF UNIFORM LENGTH, L				
r	1	2	3	4	5
1	1.25	1.08	1.04	1.02	1.02
2	2.25	1.42	1.25	1.16	1.11
3	3.25	2.0	1.46	1.34	1.25
4	4.25	2.42	2.04	1.46	1.39
5	5.25	3.08	2.25	2.02	1.49
6	6.25	3.42	2.46	2.16	2.02
7	7.25	4.08	3.04	2.34	2.11
8	8.25	4.42	3.25	2.48	2.25
9	9.25	5.08	3.46	3.02	2.39
10	10.25	5.42	4.04	3.16	2.48

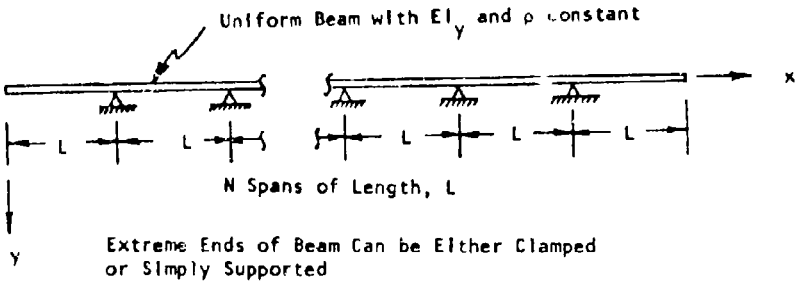

FIGURE B.1.1-11 MULTI-SPAN BEAM NOMENCLATURE

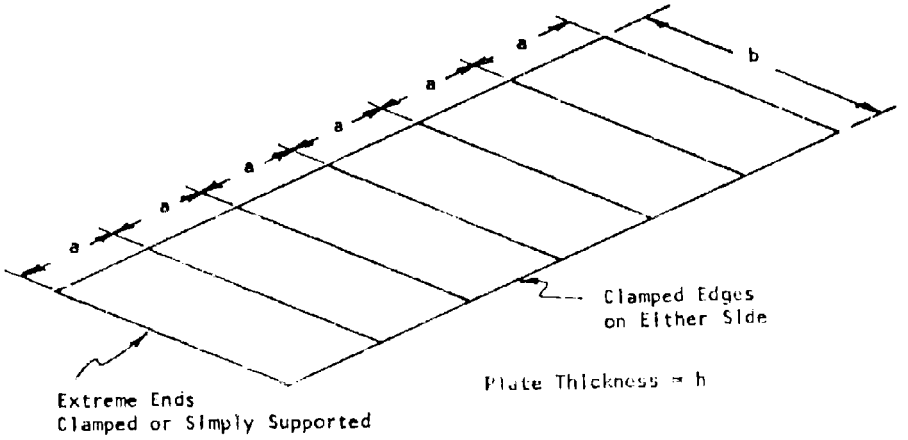

Note: Stiffeners Separating Panel Into Bays are Assumed to be Infinitely Rigid In Bending and Infinitely Flexible In Torsion. A fundamental mode is assumed across the width of the panel.

FIGURE B.1.1-12 GEOMETRY AND NOMENCLATURE FOR ONE DIMENSIONAL PANEL ARRAY

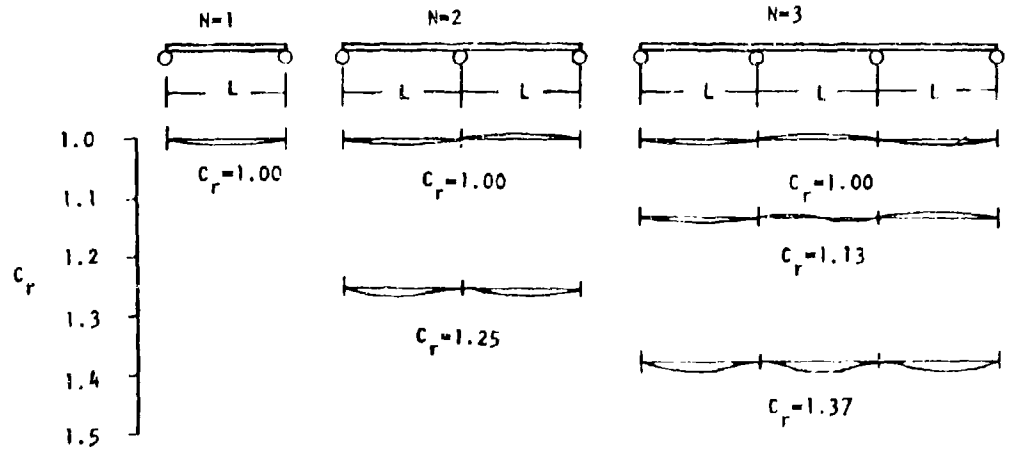

(a) Mode Group 1: Extreme Ends Simply Supported

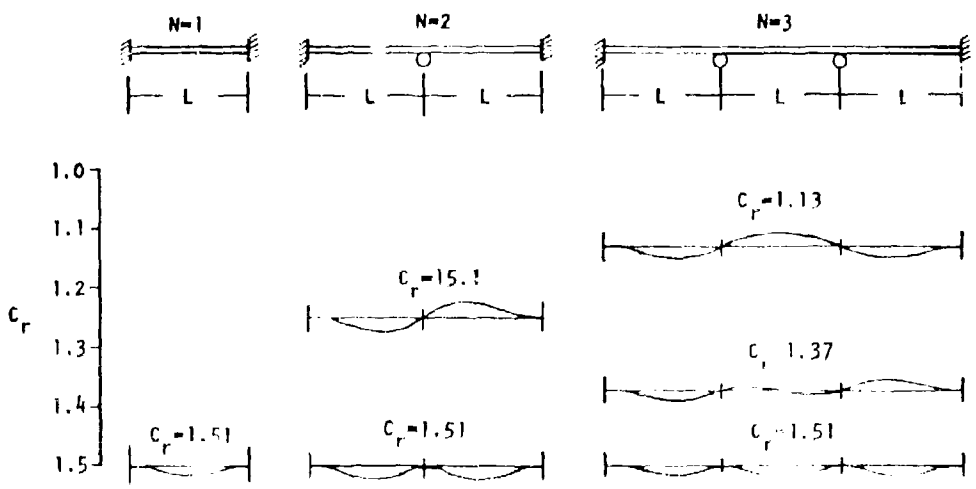

(b) Mode Group 1: Extreme Ends Clamped

FIGURE B.1.1-13 TYPICAL MODE SHAPES FOR MULTI-SPAN BEAMS

The response frequency is obtained from Equation (B.1.1-31) for the r^{th} mode as

$$f_r = 78.75\ C_r^2 \quad \text{Hz.}$$

From Table B.1.1-8 and three spans one obtains the values of C_r as shown below with the frequency calculated from the above result

Mode Number	C_r Table B.1.1-8	f_r Hz.	
1	1.13	101	mode group 1
2	1.37	148	
3	1.51	180	
4	2.13	357	mode group 2
5	2.37	442	
6	2.50	492	
7	3.13	772	mode group 3
8	3.37	894	
9	3.50	965	
10	4.13	1343	

Example: Five rectangular panels with dimensions a = 9.0 inches, b = 16.5 inches, and h = 0.052 inch are joined together with the long sides adjacent. The material properties are $E = 10^7$ psi, $\gamma = 0.10$ lbs/in^3, and h = 0.052 inch. Estimate the first five natural frequencies (mode group 1) of the panel assuming a fundamental mode across the panel width and consider the panel edges to be clamped.

From Equation (B.1.1-32) and the above data the response frequency is given by

$$f_n = 32.94C_n^2[1.833 + 0.545] = 78.33C_n^2$$

Mode Number (m,n)	C_n Table B.1.1-8	f_n Hz	f_n from Ref. 20
(1,1)	1.05	86	89
(2,1)	1.18	109	102
(3,1)	1.32	136	119
(4,1)	1.45	165	137
(5,1)	1.51	178	145

The results from Reference 20 were obtained using a 147 degree of freedom finite element analysis.

REFERENCES FOR SECTION B.1.1

1. Flugge, W. (Ed); Handbook of Engineering Mechanics, McGraw-Hill Book Company, New York, 1962.

2. Timoshenko, S. and Goodier, J. N., Theory of Elasticity, McGraw-Hill Book Company, New York, Second Edition, 1951.

3. Nowacki, W.; Dynamics of Elastic Systems John Wiley & Son, New York, 1963.

4. Thompson, W. T.; Vibration Theory and Applications, Prentice-Hall, Inc. Englewood Cliffs, N.J., 1964.

5. Young, D. and Felgar R. P.; "Tables of Characteristic Functions representing Normal Modes of Vibration of a Beam," The University of Texas Publication No. 4913, July 1949.

6. Felgar, R. P.; "Formulas for Integrals Containing Characteristic Functions of a Vibrating Beam," Circ. No. 14, Bureau of Engineering Research, University of Texas, 1950.

7. Timoshenko, S. and Gere J. M.; Theory of Elastic Stability, McGraw-Hill Book Compan-, Second Ed.; 1961.

8. Vlasov, V. Z.; Thin-Walled Elastic Beams, Second Ed., NSFTT61-1140, The Israel Program for Scientific Translations, 1961 (available from OTS, U. S. Dept. of Commerce).

9. Oden, J. T.; Mechanics of Elastic Structures, McGraw-Hill Book Co., 1967.

10. Gere, J. M.; "Bending Torsional Vibrations of Thin-Walled Bars of Open Cross Section,: Ph.D. Thesis, Stanford Univ., 1954.

11. Gere, J. M., and Lin, Y. K.; "Coupled Vibration of Thin-Walled Beams of Open Cross Section," Journal of Applied Mech., Vol. 25, Sept. 1958, pp. 373-378.

12. Lin, Y. K.; "Coupled Bending and Torsional Vibrations of Restrained Thin-Walled Beams," Journal of Applied Mechanics, Dec. 1960, pp. 739-740.

13. Rudder, F. F.; "Acoustic Fatigue of Aircraft Structural Component Assemblies,: AFFDL-TR-71-107, Air Force Flight Dynamics Laboratory, Air Force Systems Command, Wright-Patterson, Air Force Base, Ohio, Feb. 1972.

14. Rudder, F. F.; "Study of Effects of Design Details on Structural Response to Acoustic Excitation," NASA CR-1959, National Aeronautics and Space Administration, Washington, D. C., March 1972.

REFERENCES FOR SECTION B.1.1

15. Miles, J. W.; "Vibration of Beams on Many Supports,: Journal of the Engineering Mechanics Division, ASCE, EM-1 (Paper 863, January 1956).

16. Mercer, C. A.; "Response of Multi-Supported Beam to a Random Pressure Field,: ISVR Memo No. 103, Institute of Sound and Vibration Research, University of Southampton, March, 1964.

17. Lin, Y. K.; "Free Vibrations of a Continuous Beam on Elastic Supports," International Journal of Mechanical Sciences, Vol. 4, 1962.

18. Olson, M. D.; "A Numerical Approach to Random Response Problems," NRC NAE Aero. Report LR-479, National Research Council of Canada, Ottawa, Ont., Canada, April, 1967.

19. Ayre, R. S. and Jacobsen, L. S.; "Natural Frequencies of Continuous Beams of Uniform Span Length," Journal of Applied Mechanics, Vol. 17, pp. 391-395, 1950.

20. Lindberg, G. M., and Olson, M. D.; "Vibration Modes and Random Response of a Multi-Bay Panel System Using Finite Elements," NRC NAE Aero. Report LR 492, National Research Council of Canada, Ottawa, Ont., Canada, December, 1967.

U.S. Government Printing Office: 1975 — 657 022/604